CHARACTERIZING THE RELATIONSHIP BETWEEN PCSK9 AND THE ENDOPLASMIC RETICULUM (ER): IMPLICATIONS IN CARDIOMETABOLIC DISEASE

CHARACTERIZING THE RELATIONSHIP BETWEEN PCSK9 AND THE ER: IMPLICATIONS IN CARDIOMETABOLIC DISEASE

By
Paul F. Lebeau, Hons. B.Sc.

A Thesis
Submitted to the School of Graduate Studies
in Partial Fulfillment of the Requirements for the Degree of Doctor of Philosophy

PhD Thesis — Paul F. Lebeau
DOCTOR OF PHILOSOPHY (Ph.D.) (2019)
Department of Medical Sciences

McMaster University — Medical Sciences
McMaster University
Hamilton, Ontario, Canada

TITLE: CHARACTERIZING THE RELATIONSHIP BETWEEN PCSK9 AND THE ER: IMPLICATIONS IN CARDIOMETABOLIC DISEASE
AUTHOR: Paul F. Lebeau (H. B.Sc. McMaster University)
SUPERVISOR: Dr. Richard C. Austin, Ph.D.
PAGES: xii, 214.

Abstract

The proprotein convertase subtilisin/kexin type 9 (PCSK9) was first characterized in 2003 by Seidah and colleagues and marked the beginning of what is now considered by many as the greatest advancement in the field of cardiovascular disease (CVD) research since the discovery of the LDLR nearly half of a century ago. Since its discovery, PCSK9 was shown to enhance the degradation of cell-surface low-density lipoprotein (LDL) receptor (LDLR) and gain-of-function (GOF) mutations were shown to correlate with CVD risk. In contrast, patients carrying loss-of-function (LOF) mutations in *PCSK9* highlighted a novel therapeutic approach for LDL lowering as they exhibit a life-long state of hypocholesterolemia and reduced CVD risk. A decade after the cloning of the *PCSK9* gene, pharmaceutical companies have now developed a variety of PCSK9 inhibitors, ranging from monoclonal antibodies (mAbs) to small interfering RNA (siRNA) and vaccines, which have been shown to markedly reduce LDL cholesterol levels in pre-clinical models, as well as in patients at high risk of CVD. Despite these advances, there remained several unanswered questions regarding the mechanisms by which PCSK9 expression and secretion is regulated in the liver; the tissue from which the circulating pool of PCSK9 almost exclusively originates. The thought that further development of our understanding of PCSK9 biology may lead to the discovery of a signaling cascade that could be targeted by small molecules, the only class of inhibitor that has not yet been developed, has now merited additional research attention.

The focal point of my doctoral studies represents the axis between a cellular process known as endoplasmic reticulum (ER) stress and PCSK9 expression/biosynthesis. ER stress is a deleterious cellular process that is known to occur in secretory cell types, such as liver

hepatocytes, and is a well-established causative driver of an array of human diseases ranging from CVD to neurodegenerative diseases. ER stress is prevalent in the livers of patients with metabolic disease and is also known to activate the transcription factor capable of regulating PCSK9 levels, the sterol regulatory element-binding protein 2 (SREBP2). Based on this information, the first aim during the course of my PhD studies was to determine whether ER stress affected the expression and secretory status of PCSK9. In the past several years, I demonstrated that ER stress caused by ER Ca^{2+} depletion led to a marked increase in PCSK9 protein expression, but blocked its secretion as a result of its retention in the ER. Such a result was also associated with heightened hepatic LDLR expression and reduced LDL cholesterol levels in mice. Additional studies also characterized a variety of agents, including caffeine, as potent inhibitors of PCSK9 expression via increasing ER Ca^{2+} levels, which antagonized SREBP2 activity. As our initial studies revealed ER PCSK9 retention as a viable strategy for PCSK9 inhibition and LDL lowering, follow-up studies were also carried out to determine the outcome of such a strategy on liver function and injury. Given that heritable mutations in proteins that transit the ER can accumulate in this compartment and cause ER storage disease (ERSD), it was critical to further evaluate whether ER PCSK9 retention would lead to a similar outcome.

In a series of experiments with rather surprising outcomes, we observed that the retention of the LOF Q152H PCSK9 mutant in the ER failed to cause ER stress; even in mice overexpressing the protein. Interestingly, tissue culture and mouse models demonstrated that the retention of PCSK9 in this cellular compartment increased the cellular abundance of ER stress response chaperones, such as the glucose-regulated proteins of 78- and 94-kDa (GRP78 and

GRP94, respectively), but did not activate transducers of the ER stress signaling cascade. Strikingly, mice expressing the ER-retained PCSK9 Q152H mutant were protected against ER stress, suggesting a novel co-chaperone-like role of intracellular PCSK9. Collectively, the ER environment including secondary messengers like Ca^{2+} as well as its chaperones, plays a critical regulatory role on PCSK9 expression and secretion. Agents that increase ER Ca^{2+} levels can be utilized to block PCSK9 expression at the mRNA level to increase hepatic LDL clearance, and ER PCSK9 retention may also represent a safe avenue with a similar LDL lowering outcome. Beyond LDL lowering, hepatic ER PCSK9 retention may also serve as a novel strategy to enhance ER function and protect against ER stress-driven diseases of the liver.

Acknowledgements

I would like to start by thanking my friends and family for all of the support during a moment in my life that I was not able to reciprocate. The metaphorical rock under-which I lived, more commonly referred to as *the lab,* has truly highlighted your altruism.

I thank my supervisor, Rick Austin, for seeing in me the potential that others failed to see. A conversation about fishing during my interview quickly put an end to my never-ending quest for a co-op position many years ago. Most importantly, however, over the years Rick has instilled in me a deep sense of excitement for science and data; and even negative data. Nothing can turn a negative into a positive like a quick re-assessment of the hypothesis! I could not possibly have asked for a supervisor and friend better suited to my independent personality, style of learning and love for fishing and the outdoors.

I thank the many world-renowned scientists that took the time to teach me the ways of the trade. Nabil, I especially thank you for granting me the time and patience for the many fruitful discussions we have had over the years. The headway made on the topic of PCSK9 in the Austin group *literally* could not have taken place without you. Dino, I thank you for your strong sense of positive criticism, as it has undoubtedly improved the strength of my data and scientific judgement. Gui, I also thank you for maintaining a level of clinical relevance in a room filled with people that find western blots exciting; myself included of course.

I thank the two scientists that raised me, Mary and Bernard, for instilling in me a passion for science at a young age. I can't help but to think that the many microscopes, insect collections, boxes of sample tubes and chemistry sets that I was given as *gifts from Santa Claus* during my childhood ultimately led to the writing of this thesis. Growing up in the belly of the Royal Ontario Museum, surrounded by grad students and other academics, also must have contributed. I also thank my step father and hockey coach, Chuck, for teaching me perseverance: *if you can't skate faster than your opponent, you're going to skate until you vomit at the next practice.* I also thank my late brother and lifelong friend, Charlie, for reminding me of the pleasures life has to offer beyond the desk.

Finally, I thank my disputer, my challenger, my colleague, my team mate, my second half, my fiancé, Khrystyna, for compelling me to wake up every morning to do it all again. It can be hard coming home from a day filled with negative data when you're out of wine, but when you live with another grad student this tends to happen twice as often (or more…). The success that I have had as a scientist/grad student could not have happened without your seemingly endless will to help with my experiments. I hope that I will one day be able to repay you in a better way than offering you a *second author* position. Jokes aside, the papers that were published during these last few years would not have been possible without you. You have been my light at the end of the tunnel and I look forward to our life together beyond the PhD.

Preface

This is a *sandwhich*-formatted thesis as outlined in the guide for the *Preparation of Master's and Doctoral Theses* available through the School of Graduate Studies, McMaster University, Hamilton, Ontario. Chapter 1 of this thesis focuses on introductory concepts relevant to CVD, liver disease, PCSK9 biology and ER stress. The body of this thesis consists of 5 chapters (chapter 2-6), each one an independent study that is either published or in the process of being submitted to a peer-reviewed scientific journal. All scientific articles included in this manuscript were written and revised by myself and my supervisor. The preamble section proceeding each article describes the nature of the contributions made by each of the authors in the multi-authored works. The final chapters of this thesis (chapter 7-8) are comprised of discussions covering such topics as the limitations, clinical relevance and future directions of these studies.

Table of contents

List of abbreviations

ABCG1	ATP-binding cassette sub-family G member 1
APOB	apolipoprotein B
APOE	apolipoprotein E
ATF4	activating transcription factor 4
ATF6	activating transcription factor 6
ATP	adenosine triphosophate
BAK	BCL-2 homologous antagonist killer
BAX	BCL-2 associated C protein
BCL-2	B-cell lymphoma 2
BIM	BCL2-like protein
CD36	cluster of differentiation of 36
C/EBPβ/γ	CCAAT-enhancer-binding proteins
CHOP	C/EBP homologous protein
CVD	cardiovascular disease
DTT	dithiothreitol
ER	endoplasmic reticulum
ERAD	endoplasmic reticulum associated degradation
ERSD	endoplasmic reticulum storage disease
FDA	food and drug administration
FH	familial hypercholesterolemia
GADD34	growth arrest and DNA damage-inducible protein
GRP78	glucose-regulated protein of 78 kDa
GRP94	glucose-regulated protein of 94 kDa
GOF	gain of function
HAC1	bZIP transcription factor
HDL	high-density lipoprotein
HFD	high fat diet
HMGR	3-hydroxy-3-methylglutaryl-coenzyme A reductase
ICAM	intercellular adhesion molecule
INSIG1	insulin-induced gene 1
IL-1β	interleukin 1 beta
IP3R	inositol trisphosphate receptor
IRE1	inositol-requiring enzyme 1
LDL	low-density lipoprotein
LDLR	low-density lipoprotein receptor
LIPA	lipase A
LOF	loss of function
LPA	lipoprotein A
MHC-1	major histocompatibility complex
NAFLD	non-alcoholic fatty liver disease
NASH	non-alcoholic steatohepatitis

NCD	normal control diet
oxLDL	oxidized LDL
PCSK9	proprotein convertase subtilisin/kexin type 9
PERK	protein kinase R (PKR)-like endoplasmic reticulum kinase
peIF2a	phosphorylated eukaryotic initiation factor 2-α
PPARg	peroxisome proliferator-activated receptors
PUMA	P53 upregulated modulator of apoptosis
RIDD	regulated IRE1-dependent decay of mRNA
RyR	ryanodine receptor
S1/2P	site-1 and -2 protease
SCAP	SREBP cleavage activating protein
SERCA	sarco/endoplasmic reticulum ATPase
siRNA	small interfering RNA
SORT1	sortilin1
SREBP1	sterol regulatory element-binding protein 1
SREBP2	sterol regulatory element-binding protein 2
sXBP1	spliced X-box-binding protein 1
T2D	type 2 diabetes
TG	thapsigargin
TM	tunicamycin
TUDCA	tauroursodeoxycholic acid
UPR	unfolded protein response
VCAM	vascular cell adhesion molecule
VLDL	very-low-density lipoprotein
VP	vasopressin
XBP1	X-box-binding protein 1
4PBA	4-phenylbutyrate

Chapter 1: Introduction and Research Objectives

1.1 The *cholesterol theory* of CVD

In the early 1900's, Russian physicians Ignatowski and Anitschkow were the first to demonstrate that a high cholesterol diet derived from milk, eggs and meat, produced atherosclerotic lesions in rabbits [1]. Although initial studies were conducted in rodents, over a century of research now confirms that this result holds true in humans; yielding large necrotic cores with an abundant population of macrophage foam cells driving core progression [2]. These seminal studies gave rise to the *cholesterol hypothesis* of CVD and have provided the foundation on which the majority of research in the field of atherosclerosis builds upon today.

Like all theories, the cholesterol hypothesis has been the subject of criticism and rigorous testing since its conception. In recent years, alternative cholesterol-independent drivers of CVD have also been identified, such as the inflammatory mediator interleukin-1β (IL-1β) [3]. The fields of genetics, molecular biology and clinical trials, however, have produced overwhelming evidence demonstrating that cholesterol is a principal, and causative driver of CVD [4].

The LDL particle is the vehicle in which pro-atherogenic cholesterol circulates in the blood. The LDL particle is comprised of a phospholipid membrane enveloped by a single large apolipoprotein-B (ApoB) protein encasing approximately 1500 molecules of cholesterol [5]. Importantly, ApoB is present in a defined stoichiometry of 1:1 with LDL particles and provides structural integrity, as well as a ligand for receptor-mediated clearance from the blood. ApoB-derived cholesterol particles, such as the very low-density lipoprotein (VLDL) and LDL, serve as the primary means of distribution of lipid from the lipid-rich liver to peripheral tissues [6]. The ApoB-containing particle is first secreted from the liver as a triglyceride-rich VLDL. Enterocytes

from the gastrointestinal system also excrete lipid-rich chylomicrons, thereby contributing to peripheral lipid distribution. As VLDL passes through the vasculature, the ubiquitously-expressed cell-surface lipoprotein lipases extract the triglyceride from VLDL, thereby reducing VLDL particle size, but increasing of its density [7]. Finally, the newly-exposed ApoB moeity in the increasingly dense LDL particle can be readily detected by cell-surface LDLR expressed in tissues of the periphery [8]. Binding and internalization of the LDL particle by the LDLR serves to distribute cholesterol, the final payload of the LDL particle.

Because cholesterol is an essential component of the cellular lipid bilayer, *de novo* synthesis of cholesterol within the cell represents a redundant mechanism to ensure its presence in all cells [9]. Interestingly, however, recent studies have shown that *de novo* cholesterol synthesis within cells can provide up to 95% of the total required cholesterol to maintain cellular health and function [7]. In today's day and age, with a diet that provides an abundance of cholesterol, the distribution of cholesterol in the form of LDL is largely a vestigial characteristic that now promotes excess deposition and accumulation of cholesterol in tissues. Importantly, there also exists a form of retrograde cholesterol transport mediated by high-density lipoprotein (HDL) particles, which shuttle excess cholesterol from peripheral tissues back to the liver for metabolism [10, 11]. Based on this mechanism, the negative correlation between circulating HDL levels and reduced CVD risk also support the cholesterol theory of CVD (Figure 1).

Figure 1. As liver-derived VLDL particles distribute triglycerides to tissues of the periphery, they lose of there size and become increasingly dense. With the ApoB moiety exposed, LDL particles deliver the final cholesterol-rich payload to LDLR-expressing tissues of the periphery. In contrast, HDL-mediated retrograde cholesterol transport serves to remove excess cholesterol from the periphery for metabolism in the liver.

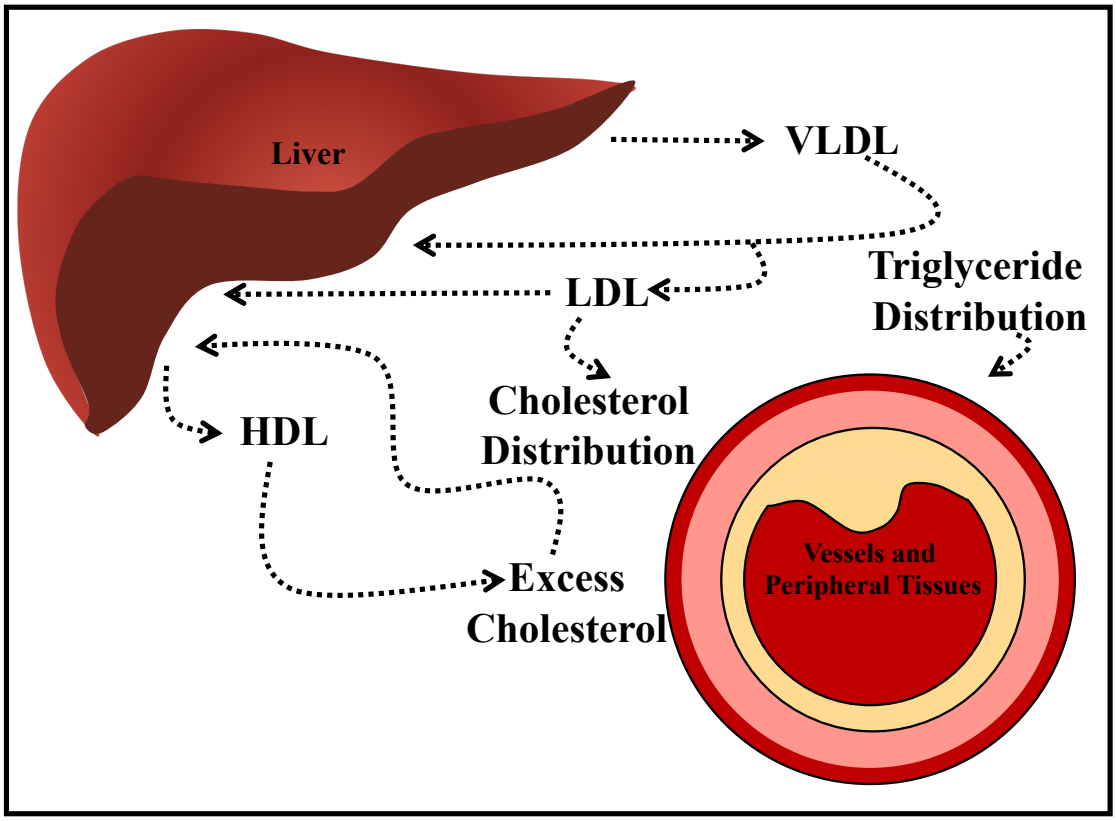
Liver
VLDL
Triglyceride
Distribution
LDL
Cholesterol
Distribution
HDL
Vessels and
Peripheral Tissues
Excess
Cholesterol

Vascular regions of non-laminar flow, such as bifurcations in the coronary arteries, are particularly prone to the penetration of LDL within the lining of the endothelial cell wall [12]. Sub-endothelial peptidoglycans interact with the positively charged domains of ApoB and hinder its exit, thereby promoting its accumulation [13]. Although LDLR-mediated clearance of LDL by macrophages within the vessel wall can reduce acute LDL buildup, long-term exposure of macrophages to cholesterol can promote an inflammatory phenotype-switch of the lipid-laden macrophages into what is commonly referred to as a foam cell [14]. Vessel-resident foam cells are known to secrete a number of bridge molecules that enhance LDL retention within the vessel wall. As LDL accumulation worsens, the oxidation status of the LDL particles also progresses. This new form of oxidized (ox)LDL exhibits diminished affinity for the LDLR but increased affinity for the abundantly-expressed scavenger receptors present on the cell-surface of foam cells [15]. Unlike the LDLR, scavenger receptors, such as the cluster of differentiation 36 (CD36), do not exhibit negative feedback characteristics and tend to increase in abundance as the cell-surface as oxLDL is absorbed by the foam cell. As this condition progresses, ever increasing amounts of LDL cholesterol accumulate in the intimal region of the vessel wall, which in turn drives foam cell formation.

Prolonged lipid accumulation in foam cells causes a change in gene expression, such that a localized pro-inflammatory milieu is created within the vessel wall. Among the pro-inflammatory mediators regulated by foam cells are ICAM and VCAM molecules on the surface of nearby endothelial cells that promote the recruitment of additional monocytes to the vessel wall [16, 17]. Exposure of the newly-recruited monocytes to lipid and pro-inflammatory mediators within the vessel wall quickly causes a phenotype switch to produce additional

macrophage foam cells. Chronic lipid overload in foam cells leads to an intracellular disturbance known as ER stress; a process ultimately known to cause apoptotic cell death of foam cells [18]. As the cycle continues, the cholesterol and matrix remnants of dead foam cells accumulate within the vessel wall, leaving behind a necrotic core. Although the necrotic core is not directly exposed to the coagulation factors present in the circulation, release of core contents into the vessel lumen via rupture of the fibrous cap causes the spontaneous formation of a thrombus [19]. Depending on the severity and size of the thrombus, reduced oxygen delivery to the downstream tissues as a result of hindered blood flow, often causes a cardiovascular event.

1.2 LDL cholesterol: an irrefutable driver of CVD

The totality of evidence demonstrating that LDL cholesterol is a causative driver of CVD stems from a wide range of fields. Most importantly, it is the sum and/or combination of these data that makes the argument irrefutable [4]. Genetic mutations that increase circulating LDL cholesterol levels increase CVD risk and in a reciprocal manner, mutations and therapeutic interventions that reduce circulating LDL cholesterol reduce CVD risk. Perhaps the most compelling evidence, however, is the consistency of this observation regardless of the mechanism by which LDL levels are affected. Our current understanding of LDL and its role in CVD progression is largely due to heritable mutations in genes that give rise to elevated circulating LDL cholesterol levels. This fairly common condition is known as familial hypercholesterolemia (FH). In its heterozygous form, FH confers a 50% chance of having a cardiovascular event before the age of 50 [20].

1.2.1 Loci involved in the pathogenesis of atherosclerosis

FH is an autosomal co-dominant disorder characterized by a marked increase in circulating LDL cholesterol levels [20, 21]. The worldwide prevalence of heterozygous FH is approximately 1:200 to 1:300 individuals and typically results in circulating LDL cholesterol levels of approximately 4.5-12 mmol/L, as well as premature atherosclerosis and coronary artery disease [22]. A gene-dose effect is also observed, as the much rarer condition known as homozygous FH produces circulating LDL cholesterol levels that can surpass 13 mmol/L [23]. Homozygous FH often results in cardiovascular complications and death within the first few years of life. FH pathogenesis was originally believed to be the consequence of excessive *de novo* cholesterol synthesis [24], however, this was shown to be incorrect by scientists Brown and Goldstein in the early 1970's. In one of the most exciting chain of discoveries in modern medicine, it was shown that cell-surface LDLR internalizes circulating LDL cholesterol to increase intracellular cholesterol levels [25, 26]. Heightened intracellular levels subsequently act as a feedback mechanism in a manner dependent on the SREBPs to attenuate further *de novo* cholesterol synthesis by 3-hydroxy-3-methylglutaryl-coenzyme A reductase (HMGR). In most patients with FH, this means that a LOF mutation in the *LDLR* gene prevents the clearance of cholesterol from the blood and also induces a constitutive state of *de novo* cholesterol synthesis. The LDLR, is now well-described and its ability to cause FH has been classified into seven groups based on mutation phenotypes [27]: (a) no detectable LDLR protein, (b) either complete (2a) or partial (2b) failure of the LDLR to traffic from the ER, (c) defective LDL binding, (d) defective clustering in clathrin-coated pits, (e) recycling-defective LDLR, (e) sorting-defective

LDLR in polarized epithelial cells, (f) increased susceptibility to degradation by circulating PCSK9 and (g) defective LDL delivery into the lysosome due to a resistance to extracellular PCSK9 [28].

It was later shown that mutations in the *APOB* gene also promote FH. Innerarity and colleagues were the first to successfully demonstrate that in certain patients with FH, failure of the interaction between the LDL particle and cell-surface LDLR was not the result of a mutation in the LDLR, but rather in the LDLR substrate, ApoB. Soria and colleagues then characterized a point mutation in *APOB,* R3500Q, as the cause of this rare form of FH [29]. Despite the significant amount of research conducted on this gene, however, only one other mutation has been shown to antagonize ApoB receptor binding, R3500W [30]. Finally, a third locus capable of causing FH was identified as the *PCSK9* gene by Abifadel & Seidah et al. in 2003 [31, 32]. *PCSK9* encodes a secretory protein that enhances the degradation of cell-surface LDLR, thereby reducing the ability of the liver to clear pro-atherogenic LDL cholesterol from the blood (Figure 2) [33]. To date, a wide variety of GOF mutations in PCSK9 have been identified, which confer elevated circulating LDL cholesterol levels, as well as increased CVD risk. In contrast to GOF mutations, LOF mutations in *PCSK9* confer significant protection against CVD risk [34, 35].

Although mutations in *LDLR*, *APOB and PCSK9* represent significant contributors, they do not account for all cases of genetic mutations resulting in increased CVD risk. Mutations in *SORT1, ABCG5/8, LPA, LIPA* and *APOE* can also increase LDL cholesterol levels and impact CVD risk [36]. Recent Mendelian randomization studies have now identified a strong positive correlation between LDL cholesterol levels and CVD risk across mutations in over 50 genes

[37-39]. Moreover, mutations in genes known to regulate triglyceride-rich lipoproteins, inflammation, vascular remodelling and vascular tone are also known to affect CVD risk [36].

Figure 2. Cell-surface LDLR interacts with the ApoB moiety of the LDL particle and subsequently removes the particle from the circulation via endocytosis. In the absence of PCSK9, LDLR is quickly recycled back to the cell surface, where it continues to clear LDL from the blood. In the presence of PCSK9, however, lysosomal degradation effectively reduces the expression of LDLR at the cell-surface, thereby increasing the abundance of LDL in the circulation.

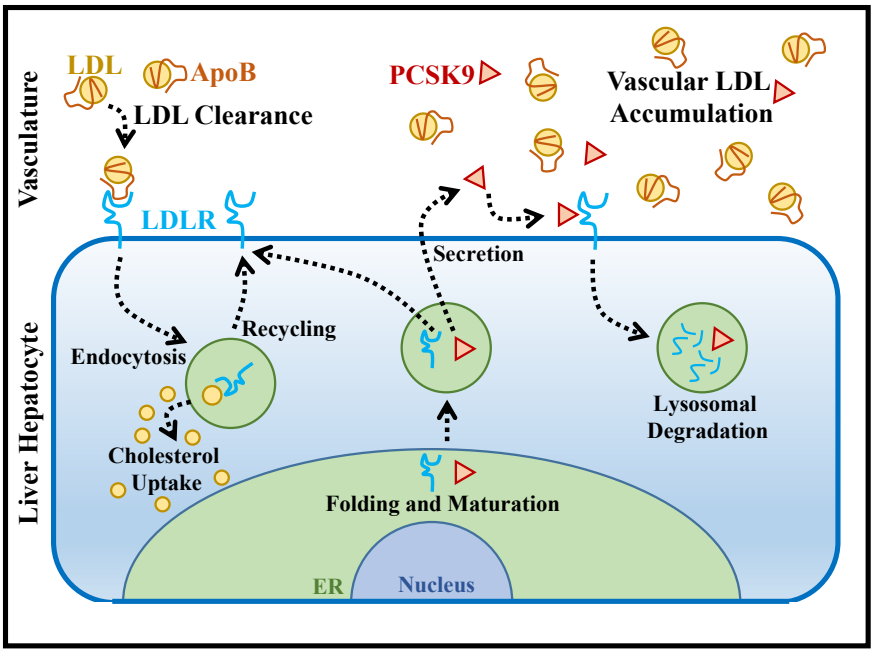
Vasculature
LDL
ApoB
LDL Clearance
PCSK9
Vascular LDL
Accumulation
LDLR
Secretion
Liver Hepatocyte
Recycling
Endocytosis
Cholesterol
Uptake
Folding and Maturation
Lysosomal
Degradation
ER
Nucleus

1.2.2 LDL-lowering therapies reduce CVD risk

Based on the discoveries made at the genetic level, or through serendipity as in the case of Akira Endo with statins [40], a variety of therapies currently exist that reduce circulating LDL cholesterol levels and CVD risk. A meta-analysis based on 26 randomized control trials involving over 170,000 patients that were treated with statin therapies, which antagonize HMGR and block *de novo* cholesterol synthesis, demonstrated an overall 22% reduction in CVD risk per mmol/L reduction in LDL cholesterol [41]. Importantly, therapies that reduce circulating LDL levels independent of HMGR, such as ezetimibe [42], bile acid sequestrantes [43], fibrates [44] and stanol esters [45] also markedly reduce CVD risk. Surgical methods that reduce cholesterol absorption from the gastro-intestinal tract, such as ileal bypass [46], also reduce LDL cholesterol levels and confer reduced CVD risk. In severe cases of FH, LDL-lowering has also been achieved via liver transplantation in order to provide FH patients with wild-type isoforms of FH-inducing genes; notably, the expression of functional LDLR in transplanted livers has been shown to significantly reduce circulating LDL cholesterol levels [47].

Overall, atherosclerosis and other forms of CVD represent a chronic illness that develops during the course of a lifetime [4]. As is the case with other chronic illnesses, the contributors of CVD are numerous and intricate. The abundance of evidence presented herein, however, strongly suggests that LDL cholesterol represents a significant driver; perhaps even accounting for the majority of disease burden. Long-term follow up studies have now demonstrated that risk of CVD posed by LDL is not only the result of absolute LDL magnitude but also of the cumulative exposure to LDL levels over a lifetime [48]. It is perhaps due to this observation that LDL-lowering therapies can yield underwhelming results on CVD risk in short-term studies. Long-

term LDL lowering from a young age, prior to the development of atherosclerosis, would likely result in a proportionately greater reduction in CVD risk [49]. In support of this notion, statin therapies have been shown to reduce CVD risk by 10% per mmol/liter of LDL lowering during the first year and by an additional 6% in the second year. By the third year of therapy, CVD risk is reduced by a total of 20%. The fourth and fifth years have been shown to yield an additional 1.5% reduction in CVD risk; a figure that appears constant during additional years of treatment as plaque burden/stability comes to equilibrium [50]. Based on these data, five years of statin treatment yields approximately 25% CVD risk reduction and therefore, 40 years should yield a CVD risk reduction of approximately 50% [4]. Strikingly, Amgen's FDA-approved human monoclonal antibodies targeted against circulating PCSK9 have been shown to reduce LDL cholesterol levels by 60% [51, 52]. This represents a marked improvement over previous statin-based therapies. Given the novelty of these antibodies, however, data supporting CVD risk in patients is currently limited. Overall, early detection of elevated LDL levels in young individuals at high risk of CVD, such as those with FH, would be beneficial as this would afford the time for LDL-lowering therapies to achieve a substantial level of risk reduction over a lifetime.

1.3.0 PCSK9: from discovery to therapeutic application

The discovery of *PCSK9* ultimately resulted in what is now widely considered as the greatest advancement in our understanding of CVD since the discovery of the *LDLR* over 40 years ago. The groundbreaking collaboration between Seidah et al. and Abifadel et al. led to back-to-back publications in early 2003, which simultaneously characterized the molecular biology of PCSK9 and identified GOF mutations as significant contributors of CVD risk [31,

32]. In the following years, it was also shown that LOF mutations in PCSK9 were associated with a lifelong state of hypocholesterolemia and a substantial reduction of CVD risk [34, 53-56].

1.3.1 PCSK9 structure and function

PCSK9 is primarily expressed in the liver, small intestine and kidney where it is synthesized as a 692 amino acid zymogen. A signal peptide spanning from amino acids 1-30 ensures that PCSK9 enters the ER via the translocon during translation. Shortly after entry, signal peptidases remove the signal peptide and nascent PCSK9 undergoes maturation via autocatalytic cleavage at position Q152↓ [32, 57]. In an event that is unique to PCSK9 within the proprotein convertase family, the cleaved pro-domain (amino acids 31-152) binds to the catalytic domain and blocks further protease functionality (Figure 3). Several studies characterizing LOF mutations in PCSK9 have shown that auto-catalytic cleavage in the ER represents the rate-limiting step of its secretion from the hepatocyte [58, 59]. A French Canadian family harboring the Q152H mutation was among the first evidence of this phenomenon, as homozygote individuals exhibit a near-complete loss of circulating PCSK9 [55]. In a reciprocal manner, artificial mutations in the catalytic domain (S386A) also demonstrate that impaired processing substantially reduces PCSK9 secretion [60]. Mutations in portions of the peptide sequence known to play a role in cellular trafficking, such as the L10 and R46L, also reduce circulating PCSK9 levels in patients [61, 62]. Overall, individuals with these mutations exhibit a lifelong state of hypocholesterolemia, which has not yet been correlated with any health complications other than a marked reduction in CVD risk.

Figure 3. Intracellular cholesterol depletion induces the activation of the transcription factor SREBP2, which translocates to the nuclease to increase the expression of PCSK9 (not shown). The signal peptide ensures that PCSK9 is translated into the ER via the translocon. PCSK9 immediately undergoes autocatalytic cleavage and maturation prior to its entry into the trans-Golgi network, where it is given a GOF phosphorylation at position Ser688 by Fam20. Finally, the proteolytically inactive and phosphorylated PCSK9 is ready for secretion from the hepatocyte.

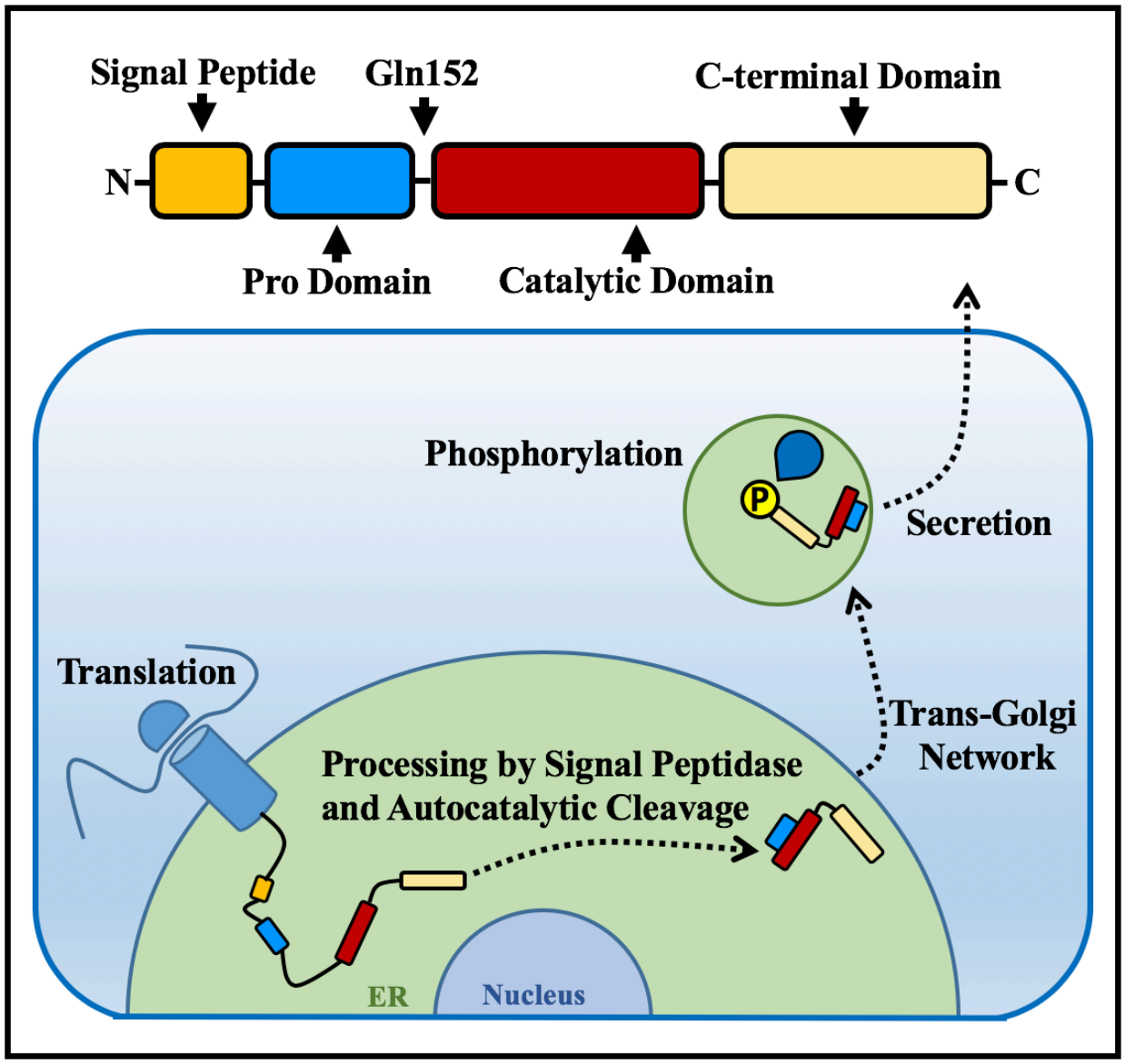
Signal Peptide
Gln152
C-terminal Domain
N
C
Pro Domain
Catalytic Domain
Phosphorylation
P
Secretion
Translation
Trans-Golgi
Network
Processing by Signal Peptidase
and Autocatalytic Cleavage
ER
Nucleus

Following cleavage and maturation of PCSK9 within the ER, PCSK9 is shuttled to the cell surface through the trans-Golgi network for secretion into the blood. Although PCSK9 is expressed in several tissues, the population of PCSK9 found in the blood originates almost exclusively from liver hepatocytes [63]. Circulating PCSK9 can then bind to cell-surface LDLR with a Kd ranging from 90-840 nmol/L. As the PCSK9-LDLR complex enters the cell via endocytosis and acidity of the lysosome increases, the Kd of PCSK9 for the LDLR also increases by approximately 20-fold [64-66]. The strength of the interaction taking place in this environment prevents release of the LDLR from PCSK9. In a series of events that are not yet understood, the PCSK9-bound LDLR is no longer recycled to the cell surface, but rather, it is degraded in the lysosome [67]. Practically speaking, the process by which PCSK9 induces the degradation of the LDLR has been shown to occur with a binding half-life of 5-10 minutes, followed by an internalization half-life of 2-3 hours. The net phenotype on total cell-surface LDLR populations can be observed 12 to 24 hours following the addition of PCSK9 to the medium, depending on experimental conditions [33].

Similar to PCSK9, the LDLR also begins its journey in the ER and requires an array of post-translational modifications [68]. Although PCSK9 and the LDLR co-exist in the cell prior to their transit to the cell-surface, PCSK9 fails to induce LDLR degradation in this compartment [69]. Paradoxically, studies have demonstrated that newly synthesized intracellular PCSK9 exhibits chaperone activity and aids in the maturation and localization of the LDLR to the cell surface [69].

1.3.2 Regulation of circulating PCSK9 levels

Like all protein species within a certain physiological compartment, PCSK9 levels in the blood represent a balance between secretion and clearance. PCSK9 synthesis is regulated by the ER-resident sterol-sensing transcription factor, known as SREBP2 [70]. Although similar to SREBP1, which regulates the expression of genes associated with triglyceride production [71], SREBP2 activation promotes cholesterol synthesis and uptake. Paradoxically, LDLR is also transcriptionally-regulated by SREBP2, which has led many to believe that PCSK9 may serve as a feedback mechanism to attenuate excessive LDLR expression/activity at the cell surface.

Induction of the PCSK9-LDLR axis begins when low intracellular cholesterol levels are detected by the sterol-sensing domain of the insulin-induced gene-1 (INSIG1); a protein charged with the task of anchoring the inactive ER-resident precursor form of SREBP2 to the luminal face of the ER. SREBP2 and its binding partner, SREBP cleavage-activating protein (SCAP), subsequently translocate to the Golgi for proteolysis and activation by site-1 and -2 proteases (S1/2P). Finally, the cleaved and activated form of SREBP2 translocates to the nucleus to increase cholesterol-regulatory gene expression, with the overall goal of increasing intracellular cholesterol levels back to the homeostatic range [72]. The addition of PCSK9 as a new member of this pathway also led to the discovery of an apparent inefficiency of LDL-lowering therapies, such as statins and ezetimibe, which inherently increase secreted PCSK9 levels by activating SREBP2 [70].

Just like PCSK9 that acts as a negative regulator of the LDLR, in a reciprocal manner, cell-surface LDLR is a negative regulator of circulating PCSK9. *Ldlr*$^{-/-}$ mice exhibit a substantial increase in circulating PCSK9 levels whereas overexpression leads to the opposite outcome [73,

74]. Likewise FH patients with LOF mutations in *LDLR* also exhibit increased plasma PCSK9 levels [75]. Beyond the LDLR, Benjannet and colleagues have demonstrated that circulating PCSK9 is cleaved by furin at the cell-surface into a truncated inactive form [76]. Because the majority of circulating PCSK9 is bound to LDL, it is no surprise that LDL also represents a strong regulator of PCSK9 half-life. Although the exact mechanism by which this process occurs is not well-understood, recent studies have shown that LDL antagonizes furin-mediated PCSK9 cleavage [77]. It is likely due to this observation that the majority of LDL-bound PCSK9 exists as the full-length protein, whereas the furin-cleaved form represents the majority of the LDL-free population. Furthermore, clinical studies have also shown that patients that undergo lipoprotein apheresis to remove LDL cholesterol from the blood, exhibited reduced PCSK9 levels [78]. Overall, PCSK9 enters the blood from liver hepatocytes and directly complexes with LDL. This interaction not only increases PCSK9 half-life by reducing furin-mediated inactivation, but also increases the affinity of PCSK9 for the LDLR by 2-fold.

1.3.3 PCSK9 inhibitors: current and future strategies

Strictly on the basis of LDL-lowering efficacy, mAbs targeted against circulating PCSK9, namely Evolocumab and Alirocumab, were approved by the FDA in 2016 [4, 79]. This event highlighted the general consensus of the scientific community, as well as regulatory agencies, with regards to the role of LDL cholesterol on CVD risk. Mechanistically, binding of the anti-PCSK9 antibody to circulating PCSK9 antagonizes further interaction between PCSK9 and cell-surface LDLR. Although this process has recently been shown to increase circulating PCSK9 levels by approximately 7-fold [80], inactivation of circulating PCSK9 leads to an increase in

cell-surface LDLR populations with a concomitant increase in LDL clearance from the blood. The story of PCSK9, from its discovery in 2003 to the recent approval of mAbs, is now widely regarded as one of the finest examples of translational bench-top to bedside research in modern medicine [81]. Clinical trials testing the efficacy of anti-PCSK9 mAbs were initiated in 2012 in patients that were at particularly high risk of CVD due to stain intolerance or FH-related complications [82]. The striking efficiency of anti-PCSK9 mAbs quickly became apparent as the results from these studies indicated a 50-60% lowering of LDL as a monotherapy and 60-70% when provided as a combination with statins and ezetimibe [52]. Belonging to the class of biologic therapies, however, PCSK9 mAbs require subcutaneous injection every two weeks and are costly to manufacture [83].

RNA silencing, using siRNA is also being explored as an avenue for PCSK9 inhibition [84, 85]. In this approach, an RNA species targeted in a complementary fashion to an mRNA of interest is delivered to a cell. The siRNA is processed by the Dicer endo-ribonuclease and conjugated to a RISC complex [86]. Using the siRNA as a guide, the RISC complex associates with the mRNA target and induces its degradation, thereby blocking the expression of the target protein. The anti-PCSK9 siRNA, inclisiran, also contains an N-acetyl galactosamine, ligand of the asialoglycoprotein receptor to ensure liver-specific delivery of the siRNA. The phase I clinical trial testing the LDL-lowering efficacy of inclisiran demonstrated a >50% inhibition 270 days following administration [84]. The long-lasting nature of siRNA is undoubtedly due to the inherent stability of the RISC complex.

Although clinical data is not yet available, anti-PCSK9 vaccines are also under development. Using the ApoE*Leiden/cholesteryl ester transfer protein mouse model, which is

susceptible to PCSK9-induced changes in atherosclerotic lesion development, the AT04A vaccine was shown to increase anti-PCSK9 antibodies well-beyond the study end-point [87]. Increased antibody titre was shown to reduce LDL cholesterol levels and atherosclerotic lesion area by 53% and and 64%, respectively. The phase I clinical trial for AT04A is currently underway. In a manner similar to inclisiran, the immune system-based anti-PCSK9 vaccine will likely yield a long-lasting LDL-lowering effect.

Anti-PCSK9 therapies prevent CVD by reducing circulating LDL cholesterol levels. Due to the complex and chronic nature of atheroscleotic lesions and other forms of CVD, risk reduction in patients taking anti-PCSK9 therapies will likely not occur until several years following initiation of the treatment. Early small-scale studies, such as the Evaluation of Cardiovascular Outcomes after an Acute Coronary Syndrome During Treatment With Alirocumab (ODYSSEY Outcomes), were among the first to provide promising results. In a cohort of 2341 high risk patients, alirocumab reduced circulating LDL cholesterol levels by 61% [88]. As a result, a lower incidence of endpoints including non-fatal miocardial infarction (MI), unstable angina and ischemic stroke was observed in alirocumab-treated patients compared to those treated with placebo (1.7% vs. 3.3%; p=0.02). Further Cardiovascular Outcomes Research with PCSK9 Inhibition in Subjects with Elevated Risk (FOURIER) was the first large-scale randomized control trial, in which 27,564 patients with established atherosclerosis were randomized to either evolocumab or placebo, to test the risk of cardiovascular outcomes [52]. Anti-PCSK9 antibody treatment in this trial was associated with a 59% reduction of LDL cholesterol levels and a modest 1.5% reduction in risk of cardiovascular endpoints at 26 months. Based on the results of this study and the high-cost associated with this therapy, addition of anti-

PCSK9 mAbs to the standard-of-care regimen has been reserved for those at particularly high-risk of cardiovascular events. Recent extrapolations in cost-benefit analyses have suggested a number needed to treat to prevent a single cardiovascular event of 74 individuals over two years in FOURIER and number needed to treat of 64 in ODYSSEY. At the current $14,400 USD/year cost of these therapies, the price of preventing a single cardiovascular event approaches the $1,000,000 USD mark [81, 89]. Overtime, however, as data on longitudinal studies are compiled and the cost of these therapies is reduced, it is likely that PCSK9 inhibitors will join statins in the standard-of-care [81].

Small molecule inhibitors represent one of the final frontiers not yet exploited for LDL-lowering via PCSK9 inhibition . The benefits of this strategy are accentuated by the exceedingly high cost associated with current strategies. The absence of small molecule antagonists of PCSK9 in today's repertoire of PCSK9 inhibitors, however, is not for the lack of trying by the scientific community [58, 59, 90]. PCSK9 proteolysis represents the rate-limiting step of PCSK9 secretion and stands as a highly sought-after and classical pharmacologic target. This process, however, follows exceedingly fast kinetics and is concealed from pharmacologic agents by two lipid bilayers. Inhibition of the binding of PCSK9 to the LDLR at the cell-surface has also proven difficult due to the flat surface of interaction between these two proteins. The appealing nature of low-cost small molecule inhibitors of PCSK9, however, far exceeds these drawbacks. A final class of small molecule inhibitors of PCSK9 that are currently gaining momentum are those that block *de novo* PCSK9 synthesis, thus leading to a reduction of its levels in the circulation. Although SREBP2 regulates the expression of PCSK9 and the LDLR, inhibition of this transcription factor commonly results in a reduction of PCSK9 and increased hepatic LDLR

levels. The difference in half-life of PCSK9 and the LDLR likely explains this paradox. With a half-life of only 5 minutes [91], circulating PCSK9 levels are closely linked to SREBP2-mediated synthesis. In contrast, with a half-life of 12 hours [92], LDLR expression is primarily regulated by factors that affect its stability at the cell surface, such as PCSK9.

1.3.4 PCSK9 beyond LDL cholesterol

Much of the research attention given to PCSK9 over the last several decades has focused on its role as a regulator of LDL cholesterol and by extension, its role as a contributor of CVD. During this period, however, a few roles beyond its ability to enhance LDLR degradation have been identified. In particular, PCSK9 has been shown to enhance the degradation of most members of the LDLR family, including LRP1, VLDLR and the ApoER2 [93, 94]. PCSK9 was also shown to enhance the degradation of the fatty acid translocase, CD36 [95]. As these receptors interact with a variety of ligands, PCSK9 has now been associated with signaling cascades, molecular mechanisms and disease states that extend beyond the realm of CVD [96]. For the same reason that PCSK9 reduces circulating lipid levels by degradation a variety of hepatic lipid receptors, accumulating evidence now demonstrates that PCSK9 can also attenuate hepatic steatosis during metabolic challenges. Replenishment of circulating PCSK9 in *E2f1* null mice, which express markedly reduced levels of PCSK9, reversed hepatic steatosis and other metabolic parameters [97]. We have also demonstrated that HFD-fed *Pcsk9* null mice exhibit increased hepatic ER stress, fibrosis and inflammation compared to controls. In *Pcsk9* knockout hepatocytes, pharmacologic and genetic antagonism of CD36 protected against palmitate-induced ER stress and lipotoxicity (see Appendix A for manuscript).

In the intestine, PCSK9 has been shown to regulate triglyceride-rich lipoprotein metabolism, as olive oil gavage led to increased lipid droplet accumulation in wild-type mice compared with *Pcsk9* knockout counterparts. Using Caco-2 cells, the authors of this study concluded that PCSK9 regulates the secretion of apoB48 [98]. This research was supported by follow-up studies demonstrating that PCSK9 knockout mice exhibit increased trans-intestinal cholesterol excretion [99]. Recent studies also demonstrate that patients carrying LOF PCSK9 mutations exhibit reduced postprandial apoB levels compared with controls [100]. In addition to the liver and the intestine, PCSK9 is also highly abundant in the kidney [32]. In this tissue, PCSK9 has been suggested to play a role in nephrogenesis [32], but its major role in this tissue remains to be determined. In immortalized embryonic kidney HEK 293 cells, PCSK9 was shown to regulate the amioride-sensitive epithelial sodium channel subunit-α (ENaC) [101], thereby increasing its degradation via the proteasomal pathway. PCSK9 deficiency in pre-clinical models, however, does not alter blood pressure as the initial *in vitro* findings had suggested [102]. Perhaps in the most elegant kidney-related study, it was discovered that nephrotic syndrome increases the hepatic expression and secretion of PCSK9 [103]. Importantly, the majority patients with kidney disease succumb to CVD due to a shift towards a pro-atherogenic lipid profile in the blood [104]. These findings identified PCSK9 as a significant contributor of CVD in patients with kidney disease.

PCSK9 was also shown to enhance the degradation of CD81, a cell surface receptor that promotes the entry of virulent particles like the hepatitis C virus [105]. This suggests that PCSK9 may protect from viral infection. Because many species of bacteria, as well as viruses, require cholesterol for host infection and proliferation [106], many have also hypothesized that PCSK9

LOF may have yielded evolutionary benefits. In support of this notion, a recent study demonstrated a marked increase in the frequency of severe malaria in Malian children carrying GOF PCSK9 mutations [107].

1.4 Liver function and CVD risk

The liver plays a central role in energy/lipid homeostasis, as well as regulating levels of secretory proteins known to contribute to a variety of disease states. Given this systemic oversight, it is not surprising that the worldwide prevalence of non-alcoholic fatty liver disease (NAFLD) is increasing along-side other metabolic complications, such as type-2 diabetes mellitus (T2D) and CVD [108-110]. NAFLD is characterized by hepatic lipid accumulation, also known as steatosis, in the absence of fibrosis and inflammation [111]. Although this condition is generally benign, it represents the gateway for a progressive fibrotic and inflammatory state known as non-alcoholic steatohepatitis (NASH). As hepatic steatosis, inflammation and fibrosis worsen, NASH can progress to cirrhosis or hepatocellular carcinoma and eventually, liver failure [109]. Although the exact mechanism by which this process occurs is not well-understood, it is now widely accepted that excess consumption of dietary fats and sugars initiates deleterious cellular processes in the liver such as ER stress, oxidative stress, Kupffer cell activation, apoptosis, fibrosis and inflammation [112]. As each of these cellular processes is known to promote the other, a net synergistic effect is often observed and is referred to as the *multiple hits hypothesis* of liver disease.

Although the role of hepatic steatosis as an independent risk factor of CVD is still under debate, it is well-established that CVD is the primary cause of mortality in patients with NAFLD

[113]. Beyond mortality, studies have shown that plasma transaminase levels correlate with incidence of stroke and myocardial infarction [114]. NAFLD is also associated with other markers of CVD such as endothelial cell dysfunction, arterial stiffness, hypertension, intima and media thickness of the carotid arteries and left ventricular diastolic dysfunction [110].

1.4.1 Molecular mechanisms by which NAFLD contributes to CVD

As one of the largest endocrine organs in the body, steatosis-driven changes in gene expression within the liver also lead to changes in the protein and lipid profiles of the blood. Increased levels of homocysteine in patients with NAFLD and NASH, a well-established driver of CVD, is perhaps one of the most well-studied examples [115, 116]. Observational studies suggest that circulating homocysteine promotes endothelial cell dysfunction, induces platelet activation and perturbs redox status. Impaired liver function was shown to cause a reduction in trans-sulfuration and re-methylation of homocysteine metabolites, thereby reducing homocysteine clearance from the blood. In this double-hit process, the accumulation of homocysteine metabolites in the liver also promotes oxidative stress and further contributes to liver disease progression. Likely as a result of this oxidative environment, recent evidence has also demonstrated a correlation between serum oxLDL levels and liver fat content [117]. A pro-atherogenic lipid profile also correlates with liver disease severity [118]. Initial studies demonstrated heightened levels of triglycerides, VLDL and LDL, as well as reduced levels of HDL in patient with NAFLD [119]. Changes in circulating levels of coagulation factors are also prevalent in patients with NAFLD, as these factors almost exclusively originate from the liver. Given that a pro-coagulative state is associated with CVD risk, this represents another

mechanism by which NAFLD may contribute to CVD progression. Finally, the liver also contains one of the largest pools of resident macrophages in the body [120]. Although causative data are currently scarce, it is conceivable and even likely, that pro-inflammatory mediators secreted by the diseased liver also contribute to CVD. Consistent with this notion, the CANTOS trial demonstrated that anti-IL-1β antibodies reduce the incidence of cardiovascular events by 15% in patients, independent of LDL lowering [3]. Studies in this field have now identified a total of 18 pro-inflammaotry mediators, increased in the blood of patients with NAFLD, that are independently known to contribute to CVD, including IL-1β (Figure 4) [110]. Increased ratio of M1/M2 macrophages, which is indicative of a pro-inflammatory state, was also observed in the venous blood of patients with NAFLD [121]. Collectively, accumulating evidence demonstrates that NAFLD represents an independent risk factor of CVD. Although causative data are currently limited, there also exists an abundance of molecular mechanisms supporting these findings.

Figure 4. The far-reaching effect of the liver, an important endocrine organ, occurs primarily via changes in the abundance of the secreted proteins and lipids that the liver regulates. In NAFLD and NASH, the liver promotes a pro-atherogenic lipid and protein profile within the circulation, thereby contributing to CVD.

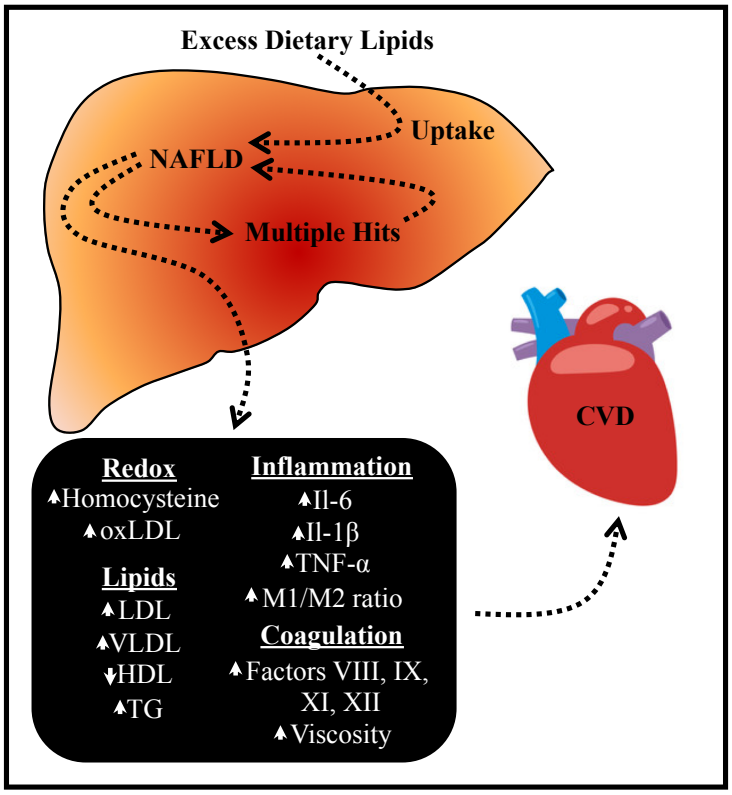
Excess Dietary Lipids
Uptake
NAFLD
Multiple Hits
CVD
Redox
Homocysteine
oxLDL
Lipids
LDL
VLDL
HDL
TG
Inflammation
Il-6
Il-1β
TNF-α
M1/M2 ratio
Coagulation
Factors VIII, IX, XI, XII
Viscosity

1.5 ER stress: a central driver of cardiometabolic disease

Hepatocytes, like all secretory cells, are rich in ER and are sensitive to disturbances that affect ER homeostasis. Because the majority of cell-surface and secretory proteins transit this organelle, it is vitally important for hepatocytes to maintain ER function [122, 123]. The ER consists interdigitated cisternae located in the perinuclear region of the cell and can be subdivided into the ribosome-enriched rough ER responsible for *de novo* protein synthesis and maturation, as well as the smooth ER responsible for the synthesis of lipids and steroids [124]. In order to carry out such a diversity of tasks, the ER contains an abundance of resident molecular chaperones within its lumen. Chaperones are charged with the task of ensuring that the constant influx of nascent proteins entering the ER are properly folded before exit and subsequent secretion from the cell. Any proteins identified as being misfolded within the ER lumen are quickly extruded through the translocon and targeted for degradation via ER-associated degradation (ERAD) [125, 126]. When the influx of newly-synthesized proteins entering the ER exceeds its protein folding capacity, an accumulation of misfolded polypeptides ensues. This state is referred to as ER stress, and often occurs when a chemical imbalance within the luminal environment reduces ER-resident chaperone protein folding efficiency. Given the importance of the ER in all secretory and metabolically active tissues, it is not surprising that ER stress has now been identified as a driver in the development of a range of human diseases including liver disease, CVD, kidney disease, T2D, as well as obesity and neurodegenerative diseases, to name a few [122, 127-129].

1.5.1 The ER environment

The lumen of the ER is a unique environment within the cell. Because most proteins that transit this compartment are eventually secreted or expressed at the cell surface, ER biochemistry very much resembles the extracellular space. Key characteristics of this biochemistry include its net oxidative potential, as well as elevated Ca^{2+} levels relative to the cytosol. This environment enhances oxidoreductase protein potential, and protein folding efficiency of Ca^{2+}-dependent chaperones located in the ER lumen [130, 131].

ER luminal Ca^{2+} levels represent a fundamental component of the environment on which the majority of ER-resident chaperones depend. To maintain elevated Ca^{2+} levels relative to the cytosol, three different classes of proteins must be expressed in the ER. These include (a) ATP-dependent pumps, such as the sarco/endoplasmic reticulum ATPase (SERCA) for pumping Ca^{2+} into the ER lumen against the electrochemical gradient [132], (b) Ca^{2+} channels, such as the ryanodine and inositol-trisphosphate receptors (RyR and IP3R), which slowly release Ca^{2+} back into the cytosol for signaling purposes [133], and (c) ER-resident Ca^{2+}-binding proteins that increase the Ca^{2+} retaining ability of the ER (Figure 5) [134]. Importantly, Ca^{2+}-binding proteins also play a dual role as chaperones to ensure the proper folding and quality control of nascent proteins. In most tissues, these chaperones include calreticulin, calnexin, GRP78 and GRP94 [135]. As Ca^{2+}-dependent chaperones, the expression and function of these proteins is directly proportional to ER Ca^{2+} levels. Given the importance of intracellular Ca^{2+} homeostasis and protein folding within the ER, it is not surprising that knockout of these chaperones leads to embryonic lethality [136]. Calreticulin and calnexin exhibit high affinity, but low-capacity Ca^{2+}-binding characteristics. The P-domain of calreticulin, for instance, can bind 1 mol of Ca^{2+}/mol

protein at Kd=1 μmol/L [134]. Calreticulin also exhibits a low-affinity high capacity domain, capable of binding 25 mol Ca^{2+} per mol protein at Kd = 2 mol/L. GRP78 and GRP94 are largely low-affinity, high capacity Ca^{2+}-binding chaperones, binding as much as 10 mol of Ca^{2+} per mol protein [135, 137]. Due to the abundance of GRP78 in the ER, however, this single chaperone is responsible for maintaining as much as 25% of total ER Ca^{2+} levels [134]. GRP78 is the most abundant and ubiquitously expressed of the chaperones and also represents the predominant ER stress marker throughout the literature as its expression increases rapidly in conditions of ER stress. GRP78 owes its role as the major regulator of ER function in mammalian cells due to its promiscuous client binding domain, which was shown to exhibit one binding site in every 36 amino acids of a randomly generated peptide [138]. Once bound to a nascent polypeptide client, GRP78 and other ER-resident chaperones undergo a series of ATP-dependent conformational changes that prevent the premature aggregation and misfolding of the polypeptides [139].

It is well-established that inducing ER Ca^{2+} depletion using SERCA pump inhibitors, like thapsigargin (TG), causes ER stress [140]. In a reciprocal manner, recent evidence also demonstrates that inhibition of channels, or promoting SERCA pump activation can also protect against ER stress [141]. Not all conditions leading to ER stress, however, function directly through Ca^{2+}-dependent mechanisms. Agents like TM can inhibit the N-glycosylation of newly synthesized proteins in the ER, a key step in the maturation of most secretory and cell-surface proteins, thus leading to their accumulation in this compartment [122, 142]. Reducing agents, like dithiotheritol (DTT), can also hinder oxidoreductase proteins that rely on the oxidative environment of the ER. This ultimately leads to an accumulation of misfolded polypeptides in need of disulfide bonds. Heritable loss-of-function mutations in the many cell-surface or

Figure 5. Extracellular Ca^{2+} is sparsely permitted to enter the cell through store-operated channels, such as the Ca^{2+} release-activated channel (CRAC). Excess cytosolic Ca^{2+} is quickly removed from the cytosol to avoid mitochondrial-induced apoptosis and activation of other undesired signaling cascades, by the SERCA pump into the ER lumen. The ER takes advantage of its abundantly-expressed Ca^{2+}-binding chaperones to buffer and maintain high levels of Ca^{2+} compared to the cytosol, thereby acting as the primary store of intracellular Ca^{2+}. ER Ca^{2+} release is tightly regulated by the IP3R and RyR for cellular signaling purposes.

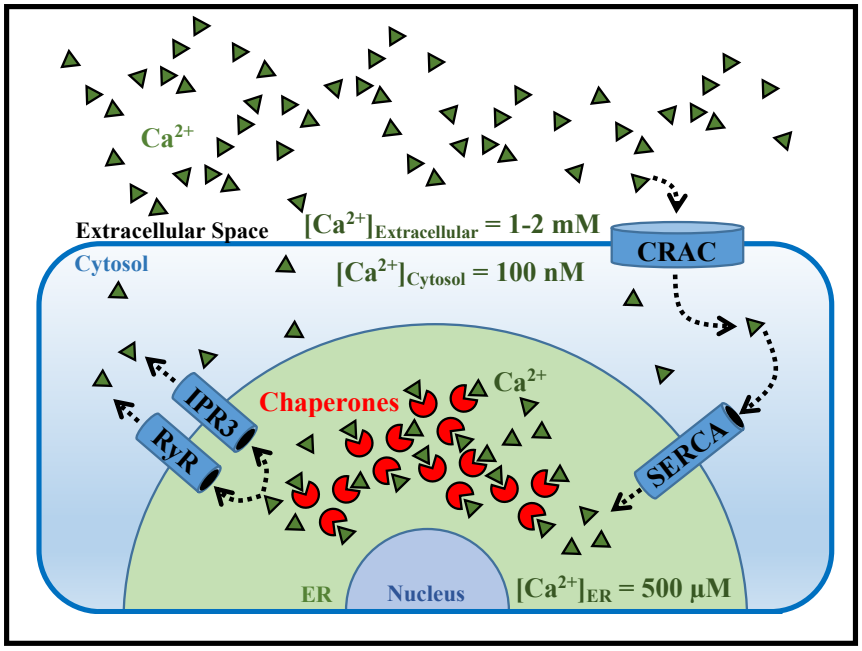
Ca2+
Extracellular Space
[Ca2+]Extracellular = 1-2 mM
CRAC
Cytosol
[Ca2+]Cytosol = 100 nM
Ca2+
Chaperones
IPR3
RyR
SERCA
ER
Nucleus
[Ca2+]ER = 500 µM

secretory proteins that transit the ER can also lead to a protein product that fails to pass ER quality controls and accumulate in the ER; a condition known to cause ERSD [143]. A well-characterized ERSD occurring in the liver results from a number of established mutations in alpha (1)-antitrypsin Z, which induce chronic ER stress and subsequent liver cirrhosis, as well as hepatocellular carcinoma [144, 145]. Additional examples include arginine-vasopressin mutations (G14R and G17V) involved in familial neurohypophyseal diabetes insipidus [146, 147], cystic fibrosis transmembrane conductance regulator-ΔF508 involved in cystic fibrosis [148], thyroglobulin mutations involved in congenital goiter and hyperthyroidism [149] and mutations in the Notch receptor known to promote cerebral autosomal-dominant arteriopathy and leukoencephalopathy [150].

1.5.2 The unfolded protein response

Acute or chronic conditions that affect the delicate environment of the ER can reduce the efficiency of ER-resident chaperones and quickly lead to an accumulation of misfolded protein in this compartment. Given that many environmental and genetic conditions can contribute to this event, cells have evolved an intricate regulatory mechanism to cope with excess misfolded proteins. Activation of this highly-conserved cascade, known as the unfolded protein response (UPR), simultaneously increases the protein folding capacity of the ER and reduces the protein folding demand by attenuating global protein synthesis (Figure 6). The UPR was first characterized in *Saccharomyces cerevisiae*, which only expresses the fundamental arm of the UPR [151]. In this system, detection of misfolded protein aggregates in the ER lumen triggers activation of the inositol-requiring enzyme-1 (IRE1). This ER stress transducer utilizes

endoribonuclease activity to cleave an inhibitory intron from the mRNA transcript of the HAC1 transcription factor. The translated and functional HAC1 protein induces the expression of ER-resident chaperones, thereby increasing ER folding capacity and restoring ER function.

Vertebrates have developed a much more complex UPR involving many arms and downstream signaling cascades. Similar to *Saccharomyces cerevisiae*, activation of the UPR promotes the dimerization and auto-transphosphorylation of IRE1 (α and β isoforms), which engages its endoribonuclease activity [151]. In this setting, however, active IRE1 splices and activates the X-box-binding protein (XBP1). Similar to HAC1, removal of the 26-nucleotide inhibitory intron causes a frame shift in the mRNA transcript resulting in its translation as an ER stress-inducible transcription factor. The activated spliced form of XBP1 (sXBP1) translocates to the nucleus where it induces the expression of genes that enhance ERAD capacity and chaperone function, among other endpoints [152]. Notably, IRE1 has been shown to increase phospholipid synthesis during conditions of ER stress, which represents an obligate component of all lipid bilayers [153]. ER expansion, a process that demands membrane production, increases luminal volume of the ER and provides advantage to ER-resident chaperones by increasing total ER volume, thus diluting the misfolded proteins [154]. Recent studies have also identified a role of IRE1 as a repressor of translation during conditions of ER stress [155]. Beyond its endoribonuclease activity on XBP1 mRNA, regulated IRE1-dependent decay (RIDD) induces the cleavage and inactivation of an array of mRNA species encoding protein products that are targeted for translation into the ER [156]. The activating transcription factor 6 (ATF6) family of proteins represent the second arm of the UPR. ER stress causes the release of ATF6 from the ER

Figure 6. During conditions of ER stress, three signaling cascades act in tandem to increase the protein folding capacity of the ER or to promote apoptosis, as a result of prolonged ER stress. Dissociation of GRP78 from the luminal domain of ATF6 causes its translocation and activation in the Golgi by S1/2P. ATF6 subsequently localizes to the nucleus where it increases chaperone expression at the ER stress response element. Dissociation of GRP78 from PERK leads to the dimerization and auto-transphosphorylation of newly-formed PERK homodimers. Activated pPERK also promotes the phosphorylation of eIF2α, which activates ATF4 in order to further increase chaperone expression. peIF2α can also directly reduce ER burden by blocking global protein translation. Lastly, dissociation of GRP78 from IRE1α also causes its dimerization and auto-transphosphorylation. Activated pIRE1α homodimers utilize endoribonuclease activity to promote the splicing of XBP1 mRNA, thereby removing an inhibitory intron from its transcript and inducing its translation. sXBP1 protein translocates to the nucleus where it increases the expression of chaperones, as well as ERAD proteins.

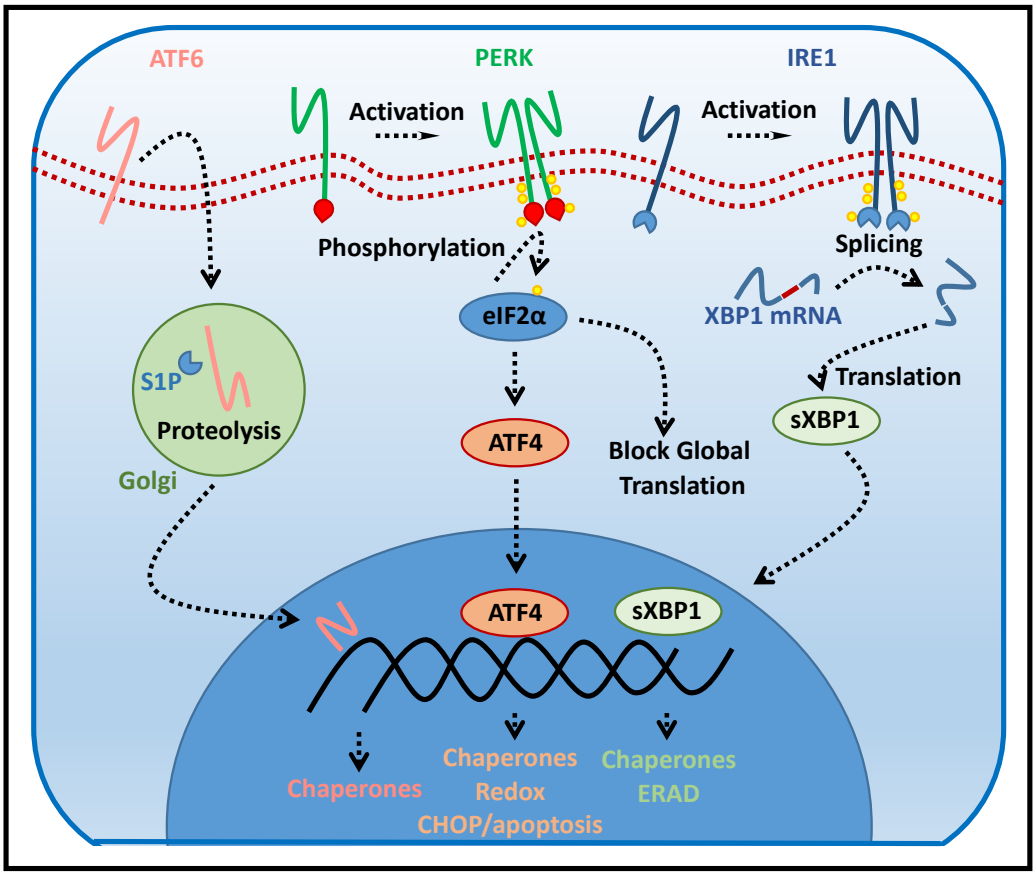
ATF6
PERK
IRE1
Activation
Activation
Phosphorylation
Splicing
XBP1 mRNA
eIF2α
S1P
Proteolysis
Golgi
Translation
sXBP1
ATF4
Block Global
Translation
ATF4
sXBP1
Chaperones
Chaperones
Redox
CHOP/apoptosis
Chaperones
ERAD

membrane resulting in its translocation to the Golgi for processing and activation by S1/2P [157]; a process of activation similar to that of the SREBPs [158]. The active ATF6 fragment then translocates to the nucleus where it increases the expression of ER chaperones, as well as ERAD machinery. In the third and final arm of the UPR, phosphorylation of the eukaryotic initiation factor 2 α (peIF2α) by the protein kinase RNA-like ER kinase (PERK) leads to an attenuation of global protein synthesis to reduce the influx of *de novo* polypeptides entering the ER lumen. PERK also induces the activating transcription factor 4 (ATF4), which in a manner similar to ATF6, increases the expression of chaperones in the ER lumen [159]. In addition to this function, ATF4 has been shown to enhance the oxidative potential of the ER as well as promote the recycling of misfolded protein aggregates in a manner dependent on autophagy [160]. Collectively, the adaptive UPR found in vertebrates acts as a pro-survival pathway; helping the cell overcome conditions of ER stress by (a) increasing folding capacity via increasing chaperone expression, (b) enhancing the degradation of misfolded proteins via ERAD and (c) reducing ER burden by blocking the influx of *de novo* proteins entering the ER.

The mechanism by which ER-luminal misfolded proteins trigger UPR activation has been a central topic of research in the field of ER stress during the past several years. Immediately following increased concentrations of misfolded proteins in the ER, the IRE1 and PERK transducers undergo a process of homodimerization and autophosphorylation [161]. Although this event is currently thought to enhance the ability of these transducers to detect misfolded proteins in the ER, data supporting this hypothesis are currently scarce. Importantly, pioneering studies in this field have demonstrated that the interaction between GRP78 and these transducers at the ER membrane serves to fine-tune UPR activation, as it represses their dimerization [162].

Furthermore, GRP78 preferentially interacts with misfolded proteins and quickly dissociates from IRE1 and PERK during conditions of ER stress; thus permitting these UPR transducers to undergo dimerization, autophosphorylation and activation. A recent study, which unequivocally confirmed this hypothesis, demonstrated that mutagenesis/deletion of the GRP78 binding domains of IRE1 and PERK led to constitutive activation of the UPR in a variety of models [163]. In the case of ATF6, interaction with GRP78 is suggested to mask the Golgi localization signal [164]. Dissociation of GRP78 from ATF6 permits ATF6 to interact with coat protein-2 at the ER membrane and to be integrated to vesicles for ER exit. Beyond the well-established role of GRP78 as the major sensor of misfolded proteins, emerging evidence has also uncovered an intrinsic capacity of the yeast IRE1 isoform to detect misfolded proteins within the ER lumen [165]. Crystallography studies have identified a peptide binding domain similar to that the of the major-histocompatibility complex class 1 (MHC-1) within the IRE1 structure [166]. This discovery led to additional studies demonstrating a two-step process of IRE1 activation in which the release of GRP78 is immediately proceeded by an interaction with misfolded protein. This hypothesis was recently confirmed in yeast models as misfolded proteins were required for IRE1 activation following its release from GRP78. Although these studies presented significant advance in the field of ER stress, other studies have now demonstrated that the MHC-1-like domain of the mammalian IRE1 isoform is theoretically incapable of interacting with protein [167]. Additionally, it is not yet known whether PERK or ATF6 are capable of interacting directly with misfolded protein. As such, in our current understanding of ER stress and UPR activation, GRP78 stands as the primary trigger for UPR activation as it releases the transducers for activation upon sequestration by misfolded protein in the ER lumen.

Although our previous understanding of the UPR suggested that ER stress caused a linear and parallel activation of all three pathways with consistent outcomes, accumulating evidence now demonstrates that there exists a variety of types UPR activation depending on the mechanism, intensity and duration of the ER stress-inducing stimulus [168]. Initial studies quickly identified ATF6 as the first of the arms activated during conditions of ER stress [169]. Additional studies demonstrated that IRE1 and PERK elicit a stronger response to ER Ca^{2+} depletion [168]. Similarly, reducing the oxidizing environment of the ER was shown to primarily trigger the IRE1 pathway [168]. Evidence also demonstrates that ATF6 is highly-sensitive to the glycosylation status of ER-resident proteins as well as the protein load of the ER membrane [170]; suggesting that this arm plays a central role in regulating the secretory pathway as well as the cargo receptors responsible for enhancing the exit of properly folded nascent proteins. Additional experiments during the course of my doctoral studies led to the observation that a significant level of cross talk occurs between the arms of the UPR. We demonstrated that pharmacologic or genetic inhibition of ATF6 led to a compensatory increase in PERK and IRE1 expression/activity in cultured cells. Such conditions were also accompanied by a marked increase in the susceptibility of cells to ER stress-induced apoptosis (see Appendix B for full publication; [171]). Collectively, although many of the functions of the arms of the UPR appear redundant (eg. increasing chaperone expression), accumulating evidence also suggests that its signaling cascades display cross-talk and specificity in response to varying conditions of ER stress.

1.5.3 Chronic UPR activation and apoptosis

In cells with a high-demand for protein folding and secretion, the UPR is constantly activated. It is important in these cells, however, not to surpass the threshold that sends the UPR from its pro-survival state into a pro-apoptotic state. In this context, apoptosis represents a well-characterized safety mechanism to remove damaged cells from the otherwise healthy tissue. Interestingly, a growing body of literature demonstrates that chronic UPR activation, and all of the protein folding benefits associated with increased chaperone expression, represents a strong contributor to tumor progression. In this context, chronic UPR activation goes unchecked as the pro-apoptotic switch of the UPR fails to trigger apoptosis [172, 173]. During the course of my PhD studies, our research group also had the opportunity to develop a novel assay for the quantification of apoptosis and other forms of cell death using a low cost dye (see Appendix C for publication).

Apoptosis under conditions of unresolved ER stress relies on the C/EBP-homologous protein (CHOP), which is responsible for fine-tuning the switch from a pro-survival to a pro-apoptotic UPR [174]. In conditions of chronic ER stress, CHOP is activated by the PERK-ATF4 axis which subsequently induces the expression of members of the B cell lymphoma family of proteins (BCL-2). These include the BAX antagonist killer (BAK), the BCL-2 homology 3 (BH3)-only protein, the BCL-2-interacting mediator of cell death (BIM), as well as other pro-apoptotic proteins, such as the p53 upregulated modulator of apoptosis (PUMA) [175]. Once activated, these proteins promote the cleavage and activation of the caspase family of proteases. In turn, caspases cleave a vast array of protein substrates including mitochondrial proteins and membrane proteins that play a role in the structural integrity of the cell [176]. Recent studies

have also highlighted the regulatory mechanism by which the UPR switches to its pro-apoptotic state. Prolonged pharmacologic insult to the ER was shown to block IRE1 activity and attenuate the pro-survival characteristics of its downstream effector, sXBP1 [177]. In this setting of long-term ER stress, the PERK-ATF4 cascade prevails, thereby increasing CHOP abundance to the point of caspase-induced apoptosis. The release of Ca^{2+} from the ER during conditions of ER stress also initiates mitochondrial-induced apoptosis [178]. Heightened levels of this secondary messenger in the cytosol are readily detected by the mitochondria, at interfaces between the ER membrane and the mitochondria that are close in proximity. In turn, the formation of cytochrome c and of the intuitively named, apoptosome complex leads to caspase activation and subsequent apoptotic cell death.

1.6.0 ER stress as a driver of liver disease

Several decades of research now demonstrate that ER stress represents a causative driver of liver disease. Increased expression of ER stress markers are observed in almost all animal models of diet-induced liver injury, including the high-fat, high-fat/high-sugar, high-cholesterol, high-cholesterol/high cholate, methionine-choline deficient as well as in genetically-induced models of injury, such as the *ob/ob* and *db/db* mouse models [179-181]. Our research group also identified GDF10 knockout mice as a novel model NASH, exhibiting hepatic ER stress, inflammation and fibrosis as a result of excessive hepatic lipid accumulation (See Appendix D for full published manuscript, [182]). The expression of ER stress markers in liver biopsies also correlates with disease grade in patients [183]. Furthermore, pre-clinical studies have demonstrated that pharmacologic inhibition of the UPR using small chemical chaperones, such

as 4-phenylbutyrate (4-PBA) and tauroursodeoxycholic acid (TUDCA), blocks the progression of liver disease in high-fat fed and *ob/ob* mice [184]. Due to their poor target specificity, however, these agents have been largely neglected in clinical practice as treatment strategies for the management of liver disease [185].

As a major metabolic and secretory organ, liver hepatocytes represent approximately 70% of total liver weight and are enriched in ER [185]. The ER of liver hepatocytes plays a central role in systemic energy homeostasis by regulating the levels of a variety of circulating proteins, as well as regulating *de novo* lipogenesis, cholesterol synthesis, glucose metabolism and exogenous drug/xenobiotic metabolism [186]. In mammals, conditions such as excessive drug consumption, hyperlipidemia, viruses and inflammation can cause imbalances in the ER environment and lead to hepatic ER stress. Although hepatic UPR cascades are perhaps more robust than those found in most cells, given their intrinsic state of activation, prolonged and/or acute severe ER stress can contribute to liver injury. As is the case with liver disease in general, hepatic lipid accumulation represents the mechanism by which ER stress first contributes to disease pathology. A systematic assessment of the livers in patients with NAFLD demonstrated that 60% of total lipid originates from adipose-derived non-esterified fatty acid overload, 25% from *de novo* lipogenesis and 15% from uptake of excess dietary fats the circulation [187]. As a strong regulator of *de novo* lipogenesis, ER stress may contribute directly to 25% of liver lipid burden. ER stress is also well-known to promote lipid overload in adipose tissue and therefore, may contribute indirectly to an additional 60% [188-190].

1.6.1 The UPR as a central regulator of *de novo* lipogenesis

Similar to the pro-apoptotic cascades of the UPR, basal signaling protects against intracellular lipid accumulation until chronic high-intensity ER stress is achieved. Although not extensively studied, the lipostatic control of the UPR was first examined under the IRE1-XPB1 axis [191, 192]. Liver-specific deletion of IRE1 in mice was found to drive TM-induced hepatic lipid accumulation [193]. To explain these findings the authors identified a reduction in the expression of lipid-regulatory genes including C/EBPβ/γ and PPARγ, as well as a reduction of lipid secretion from the liver through the VLDL. The PERK-ATF4 axis was also found to regulate hepatic lipid accumulation. Overexpression of GADD34, which induces the dephosphorylation of eIF2α, protected mice from HFD-induced hepatic steatosis and liver injury [194]. ATF4 deficient mice were also shown to be protected from high-fructose and age-onset hepatic steatosis via reduced *de novo* lipogenesis [195]. Finally, the ATF6 arm appears protective as ATF6 knockout mice exhibit heightened hepatic CHOP expression and reduced C/EBPα expression when challenged with TM [196, 197]. ATF6 is also known to antagonize the activation of SREBP1 and SREBP2, which represent well established drivers of *de novo* lipogenesis [198]. Overexpression of SREBP1 in transgenic mice led to severe hepatic steatosis and liver injury [199]. Interestingly, our research group has also characterized ER stress resulting from ER Ca^{2+} depletion as a potent activator of the SREBPs [140]. The overall contribution of the SREBPs in ER stress-induced hepatic lipid accumulation, however, is still under investigation.

1.6.2 Mechanisms of lipid-induced ER stress.

Triglycerides are the most abundant member of the lipid family in most vertebrates. Under conditions of hepatic steatosis, a subtype of lipids known as ceramides and diglycerides prevail in the liver as the dominant lipid. This outcome is not surprising, as the receptor for these saturated fatty acids, CD36, is abundantly expressed in the lipid-laden liver [200, 201]. Because changes in the lipid composition of the ER and cell membrane can be toxic to cells, intracellular lipids are quickly esterified and packaged into lipid droplets by the perilipin proteins as they accumulate in the cell. Interestingly, recent studies have shown that saturated fatty acids, such as ceramides and diglycerides, block perilipin expression and activity resulting in an accumulation of these lipids within cellular membranes [202]. Studies have also demonstrated that sudden changes in ER membrane lipid composition can antagonize the SERCA pump, thereby causing ER stress as a result of ER Ca^{2+} depletion [203, 204]. In HFD-fed mice, overexpression of SERCA, as well as correction in membrane lipid composition, attenuated ER stress and liver injury [205]. In a second recently-identified mechanism, the luminal domains of IRE1 and PERK have been shown to act as sensors of membrane lipid composition [206]. In these studies, mutagenesis was used to demonstrate that palmitate, a saturated fatty acid known to cause ER stress in a variety of cultured cell models, differentially activated downstream signaling cascades of these pathways depending on mutation types. Overall, there likely remains much to be uncovered in the relationship between ER stress and intracellular lipid accumulation. Our current understanding highlights a paradoxical relationship in which lipid overload triggers UPR activation, which in turn drives *de novo* lipogenesis to further exacerbate lipid accumulation [207]. Furthermore, several cell-surface receptors responsible for lipid uptake, such as CD36, the

VLDLR and the LDLR, are regulated by ER stress-inducible transcription factors [140, 208, 209]. Thus, ER stress also increases lipid uptake from the extracellular space by increasing the abundance of these receptors at the cell surface.

1.7.0 Research overview and objectives

While it has long been established that PCSK9 transits the ER prior to its secretion from hepatocytes, the role of ER homeostasis on this process had not been characterized prior to my doctoral studies. The SREBP2 transcription factor responsible for the regulation of PCSK9 expression, also resides in the ER as an inactive pre-cursor; this evidence represented a second line of evidence that changes in ER homeostasis could impact PCSK9 biology. Interestingly, studies from our research group, as well as others, have demonstrated that conditions of ER stress resulting from ER Ca^{2+} depletion cause the activation of the SREBPs [124, 210, 211]. These seminal discoveries led to the first hypothesis examined during my doctoral studies: *ER stress induces PCSK9 expression in hepatocytes in an SREBP2-dependent manner.*

As an established regulator of ER function, our studies had now demonstrated that ER Ca^{2+} depletion led to SREBP2 activation and PCSK9 expression. Next, we postulated in a follow-up study that *increasing ER Ca^{2+} levels may antagonize SREBP2 activity thereby blocking PCSK9 expression.*

The discoveries made during the course of these studies identified that many agents and genes capable of affecting ER Ca^{2+} levels, also affect the activation of SREBP2 and expression of PCSK9. These included (a) genetic approaches that increased ER Ca^{2+} buffering capacity, (b) genetic approaches that reduced ER Ca^{2+} leak, as well as (c) pharmacologic approaches that

increased ER Ca^{2+} uptake and/or reduced ER Ca^{2+} leak. Overall these studies identified Ca2+ as a strong regulator of the PCSK9-LDLR axis and led to the characterization of a wide variety of pharmacologic agents and proteins capable of antagonizing the expression of PCSK9.

Our next aim was to assess the impact of ER stress on PCSK9 expression in a clinical setting. Interestingly, recent studies had demonstrated that liver steatosis grade in patients correlated positively with circulating PCSK9 levels [212]. Given that secreted PCSK9 originates almost exclusively from liver hepatocytes, and that ER stress is an established driver of liver disease, this represented an ideal model to evaluate our hypothesis. Although we had previously demonstrated that ER stress affected PCSK9 expression [140], no mechanism was provided in clinical studies to explain the observed increase in circulating PCSK9 levels in patients with liver disease. With our newly-gained knowledge of the regulatory role of ER stress on PCSK9 expression, we hypothesized that *ER stress-induced de novo synthesis of PCSK9 accounted for the observed changes in circulating levels of this protein in patients with NAFLD. Furthermore, we also hypothesized that such changes could contribute to dyslipidemia in patients with NAFLD and/or in vivo models of diet-induced hepatic steatosis*.

Consistent with the previously-reported clinical observations, during the course of our studies we observed that diet-induced hepatic steatosis increased *de novo* synthesis of PCSK9, in a manner dependent on ER stress-induced SREBP2 activation. Furthermore, a marked reduction in cell-surface hepatic LDLR was also observed in wild-type mice, but not in HFD-fed *Pcsk9*$^{-/-}$ mice. Collectively, this study characterized the effect of liver function on PCSK9 and LDLR expression and also highlighted a novel mechanism by which NAFLD may contribute to CVD.

To this point, our research endeavors had focused on the effect of ER stress on PCSK9 expression. In a reciprocal manner, however, we also aimed to determine whether PCSK9 played a role in ER function. Accumulating evidence, including several of our own studies, had demonstrated that the retention of PCSK9 in the ER may represent a novel avenue for LDL-lowering. It is well established, however, that the retention of proteins in the ER can cause activation of the UPR [213]. Heritable mutations in proteins that transit the ER can cause a variety of chronic diseases, commonly referred to as ERSDs. Despite this evidence, individuals harboring the ER-retained Q152H LOF mutation in *PCSK9* appear healthy [56]. Although these findings provided promising data supporting ER PCSK9 retention as a safe therapeutic strategy, the molecular biology behind this counter-intuitive observation required further validation. In our initial studies we had the simple objective of determining whether the retention of PCSK9 in cultured liver hepatocytes caused ER stress or apoptosis. In a series of follow-up studies, the effect of ER PCSK9 retention was also characterized in mice and in members of the French Canadian families known to harbor the PCSK9-Q152H mutation. These objectives and hypotheses are discussed in further detail in the following chapters:

1.7.1 Chapter 2: Endoplasmic reticulum stress and Ca^{2+} depletion differentially modulate the sterol regulatory protein PCSK9 to control lipid metabolism

Published in The Journal of Biological Chemistry (2017), Volume 292, pages 1510-1523.

Summary — Accumulating evidence implicates endoplasmic reticulum (ER) stress as a mediator of impaired lipid metabolism, thereby contributing to fatty liver disease and atherosclerosis.

Previous studies demonstrated that ER stress can activate the sterol regulatory element-binding protein-2 (SREBP2), an ER-localized transcription factor that directly up-regulates sterol regulatory genes, including *PCSK9*. Given that PCSK9 contributes to atherosclerosis by targeting low density lipoprotein (LDL) receptor (LDLR) degradation, this study investigates a novel mechanism by which ER stress plays a role in lipid metabolism by examining its ability to modulate PCSK9 expression. Herein, we demonstrate the existence of two independent effects of ER stress on PCSK9 expression and secretion. In cultured HuH7 and HepG2 cells, agents or conditions that cause ER Ca^2 depletion, including thapsigargin, induced SREBP2-dependent up-regulation of PCSK9 expression. In contrast, a significant reduction in the secreted form of PCSK9 protein was observed in the media from both thapsigargin- and tunicamycin (TM)-treated HuH7 cells, mouse primary hepatocytes, and in the plasma of TM- treated C57BL/6 mice. Furthermore, TM significantly increased hepatic LDLR expression and reduced plasma LDL concentrations in mice. Based on these findings, we propose a model in which ER Ca^2 depletion promotes the activation of SREBP2 and subsequent transcription of PCSK9. However, conditions that cause ER stress regardless of their ability to dysregulate ER Ca^2 inhibit PCSK9 secretion, thereby reducing PCSK9- mediated LDLR degradation and promoting LDLR-dependent hepatic cholesterol uptake. Taken together, our studies provide evidence that the retention of PCSK9 in the ER may serve as a potential strategy for lowering LDL cholesterol levels.

1.7.2 Chapter 3: Caffeine Blocks SREBP2-induced Hepatic PCSK9 Expression to Enhance LDLR-Mediated Cholesterol Clearance.

Submitted to Science Translational Medicine, August (2019).

Summary — Circulating proprotein convertase subtilisin/kexin type 9 (PCSK9) has emerged as a critical regulator of low-density lipoprotein (LDL) cholesterol, an established driver of cardiovascular disease (CVD), by enhancing the degradation of hepatic LDL receptor (LDLR). The transcription factor responsible for inducing PCSK9 expression, known as the sterol regulatory element-binding protein 2 (SREBP2), also contributes to a variety of pathologies by promoting *de novo* lipogenesis in a manner dependent on genes like *HMGCR*. In the present study, we demonstrate that caffeine and other agents capable of increasing endoplasmic reticulum (ER) Ca^{2+} levels block the activation of SREBP2 and subsequent expression and secretion of PCSK9 from hepatocytes. To explain these findings, we provide evidence that caffeine and other agents that increase ER Ca^{2+} levels enhance the ability of GRP78 to sequester the ER-resident precursor form of SREBP2, thereby preventing its re-localization and activation in the Golgi. By blocking its natural inhibitor, we also provide evidence that caffeine increases the expression and activity cell-surface hepatic LDLR and improves hepatocyte-mediated LDL clearance. Collectively our findings highlight ER Ca^{2+} as a master regulator of SREBP2 activation and identify a novel mechanism by which caffeine, as well as other Ca^{2+} modulating agents, affect circulating LDL cholesterol levels.

1.7.3 Chapter 4: Diet-induced hepatic steatosis abrogates cell-surface LDLR by inducing *de novo* PCSK9 expression in mice.

Published with The Journal of Biological Chemistry (2019), Volume 294, pages 9037-9047.

Summary — The worldwide prevalence of non-alcoholic fatty liver disease (NAFLD) is increasing rapidly. Although this condition is generally benign, accumulating evidence now suggests that patients with NAFLD are also at increased risk of cardiovascular disease (CVD); the leading cause of death in developed nations. Despite the well-established role of the liver as a central regulator of circulating low-density lipoprotein (LDL) cholesterol levels, a known driver of CVD, the mechanism(s) by which hepatic steatosis contributes to CVD remains elusive. Interestingly, a recent study has shown that circulating proprotein convertase subtilisin/kexin type 9 (PCSK9) levels correlate positively with liver steatosis grade. Given that PCSK9 degrades the LDL receptor (LDLR) and prevents the removal of LDL from the blood into the liver, in the present study we examined the effect of hepatic steatosis on LDLR expression and circulating LDL cholesterol levels. We now report that in a manner consistent with findings in human patients, diet-induced steatosis increases circulating PCSK9 levels as a result of *de novo* expression in mice. We also report the novel finding that steatosis abrogates hepatic LDLR expression and increases circulating LDL levels in a PCSK9-dependent manner. These findings provide important mechanistic insights as to how hepatic steatosis modulates lipid regulatory genes like PCSK9 and the LDLR, and also highlights a novel mechanism by which liver disease may contribute to CVD.

1.7.4 Chapter 5: Loss-of-function PCSK9 mutants evade the unfolded protein response sensor GRP78 and fail to induce endoplasmic reticulum stress when retained

Published with the Journal of Biological Chemistry (2018). Volume 293, pages 7329-7343.

Summary — The proprotein convertase subtilisin/kexin type-9 (PCSK9) plays a central role in cardiovascular disease (CVD) by degrading hepatic low-density lipoprotein receptor (LDLR). As such, loss-of-function (LOF) PCSK9 variants that fail to exit the endoplasmic reticulum (ER) increase hepatic LDLR levels and lower the risk of developing CVD. The retention of misfolded protein in the ER can cause ER stress and activate the UPR. In this study, we investigated whether a variety of LOF PCSK9 variants that are retained in the ER can cause ER stress and hepatic cytotoxicity. Although overexpression of these PCSK9 variants caused an accumulation in the ER of hepatocytes, UPR activation or apoptosis was not observed. Further- more, ER retention of endogenous PCSK9 via splice switching also failed to induce the UPR. Consistent with these *in vitro* studies, overexpression of PCSK9 in the livers of mice had no impact on UPR activation. To elucidate the cellular mechanism to explain these surprising findings, we observed that the 94-kDa glucose-regulated protein (GRP94) sequesters PCSK9 away from the 78-kDa glucose-regulated protein (GRP78), the major activator of the UPR. As a result, GRP94 knockdown increased the stability of GRP78 –PCSK9 complex and resulted in UPR activation following overexpression of ER-retained PCSK9 variants relative to WT secreted controls. Given that overexpression of these LOF PCSK9 variants does not cause UPR activation under normal homeostatic conditions, thera- peutic strategies aimed at blocking the autocatalytic cleavage of PCSK9 in the ER represent a viable strategy for reducing circulating PCSK9.

1.7.5 Chapter 6: The loss-of-function PCSK9^{Q152H} mutant stabilizes GRP94 and attenuates hepatic ER stress

Submitted to the Journal of Clinical Investigation, August 2019.

Summary — Individuals harboring a loss-of-function (LOF) mutation in the gene encoding the *proprotein convertase subtilisin/kexin type-9* (*PCSK9)* at the site of autocatalytic cleavage, glutamine (Gln)^{152}, exhibit a marked reduction of circulating PCSK9 levels compared to the general population. Because circulating PCSK9 enhances the endosomal/lysosomal degradation of hepatic low-density lipoprotein (LDL) receptor (LDLR), these individuals also have reduced CVD risk and are clinically normal despite a life-long state of hypocholesterolemia. Like many secretory proteins, PCSK9 must transit the endoplasmic reticulum (ER) prior to its secretion from liver hepatocytes; the cell type from which circulating PCSK9 exclusively originates. The serine protease-mediated autocatalytic cleavage of proPCSK9 in the ER is an essential step for its exit from this compartment and secretion from the cell, and thus represents an important pharmacologic target for PCSK9 inhibition as a strategy for LDL lowering. However, heritable LOF mutations that cause secretory or cell-surface proteins to accumulate in the ER are known to cause ER stress and contribute to a variety of human pathologies. In the present studies, we examined the impact of the LOF PCSK9^{Q152H} mutation on liver function and injury in order to understand the absence of liver damage in humans with this rare *PCSK9* mutation. To achieve this goal, *Pcsk9*$^{-/-}$ mice were treated with adeno-associated virus (AAV) encoding human PCSK9^{Q152H}; a naturally occurring LOF PCSK9 mutant that fails to undergo autocatalytic

cleavage in the ER. Unexpectedly, we report here that the retention of 100-fold overexpressed PCSK9^{Q152H} in the ER does not cause conventional ER stress in liver hepatocytes compared to those expressing the ER-retained LDLR^{G544V} mutant. Furthermore, hepatic overexpression of the LDLR^{G544V} mutant, but not the PCSK9^{Q152H} mutant, caused marked liver dysfunction and injury. Strikingly, hepatic protein levels of the key stress-response chaperones, the 78- and 94-kDa glucose-regulated proteins (GRP78 and GRP94, respectively), were increased as a result of stability via direct binding to this uncleaved form of proPCSK9. In contrast to LDLR^{G544V}, PCSK9^{Q152H}-expressing hepatocytes were protected against ER stress and liver injury as a result of heightened levels of these stress-response chaperones. Our findings identify a novel intracellular role of PCSK9 as a regulator of ER chaperone abundance/activity and that promoting its retention in this organelle may represent a unique mechanism to improve the function and viability of hepatocytes. In this report, we provide molecular evidence that further describes the phenotype observed in patients harboring the PCSK9^{Q152H} mutation, demonstrating an additional clinical benefit of ER PCSK9 retention that may extend beyond dyslipidemia.

Chapter 2: Publication in the Journal of Biological Chemistry, 2017

Lebeau, P., A. Al-Hashimi, S. Sood, S. Lhotak, P. Yu, G. Gyulay, G. Pare, S. R. Chen, B. Trigatti, A. Prat, N. G. Seidah and R. C. Austin (2017). "Endoplasmic Reticulum Stress and Ca2+ Depletion Differentially Modulate the Sterol Regulatory Protein PCSK9 to Control Lipid Metabolism." J Biol Chem **292**(4): 1510-1523.

Author contributions: P. L., R. C. A., and N. G. S. conceived the studies. P. L. and S. S. performed all of the *in vitro* work, and P. L. and A. A. completed all of the *in vivo* studies. Immunohistochemical staining was completed by S. L., and fast protein liquid chromatog- raphy was performed by P. Y. and B. T. The manuscript was written by P.L. and revised by A.A., G.G., G.P., S.R.W.C., B.T., A.P., N. G. S., and R. C. A.

THE JOURNAL OF BIOLOGICAL CHEMISTRY VOL. 292, NO. 4, pp. 1510–1523, January 27, 2017

Endoplasmic Reticulum Stress and Ca^{2+} Depletion Differentially Modulate the Sterol Regulatory Protein PCSK9 to Control Lipid Metabolism*

Received for publication, June 17, 2016, and in revised form, November 8, 2016 Published, JBC Papers in Press, December 1, 2016, DOI 10.1074/jbc.M116.744235

Paul Lebeau[‡], Ali Al-Hashimi[‡], Sudesh Sood[‡], Šárka Lhoták[‡], Pei Yu[§¶], Gabriel Gyulay[‡], Guillaume Paré[‖], S. R. Wayne Chen[1], Bernardo Trigatti[§¶], Annik Prat[‡‡], Nabil G. Seidah[‡‡], and Richard C. Austin[‡§2]**

*From the [‡]Department of Medicine, Division of Nephrology, McMaster University and St. Joseph's Hamilton Healthcare and Hamilton Centre for Kidney Research, Hamilton, Ontario L8N 4A6, the [§]Thrombosis and Atherosclerosis Research Institute, Hamilton Health Sciences and McMaster University, Hamilton, Ontario L8L 2X2, the [¶]Department of Biochemistry and Biomedical Sciences, McMaster University, Hamilton, Ontario L8S 4L8, the [‖]Population Health Research Institute and the Departments of Medicine, Epidemiology and Pathology, McMaster University, Hamilton, Ontario L8L 2X2, the **Libin Cardiovascular Institute of Alberta, Department of Physiology and Pharmacology, University of Calgary, Calgary, Alberta T2N 2T9, and the [‡‡]Laboratory of Biochemical Neuroendocrinology, Clinical Research Institute of Montreal, affiliated with the University of Montreal, Montreal, Quebec H2W 1R7, Canada*

Edited by Roger J. Colbran

Accumulating evidence implicates endoplasmic reticulum (ER) stress as a mediator of impaired lipid metabolism, thereby contributing to fatty liver disease and atherosclerosis. Previous studies demonstrated that ER stress can activate the sterol regulatory element-binding protein-2 (SREBP2), an ER-localized transcription factor that directly up-regulates sterol regulatory genes, including *PCSK9*. Given that PCSK9 contributes to atherosclerosis by targeting low density lipoprotein (LDL) receptor (LDLR) degradation, this study investigates a novel mechanism by which ER stress plays a role in lipid metabolism by examining its ability to modulate PCSK9 expression. Herein, we demonstrate the existence of two independent effects of ER stress on PCSK9 expression and secretion. In cultured HuH7 and HepG2 cells, agents or conditions that cause ER Ca^{2+} depletion, including thapsigargin, induced SREBP2-dependent up-regulation of PCSK9 expression. In contrast, a significant reduction in the secreted form of PCSK9 protein was observed in the media from both thapsigargin- and tunicamycin (TM)-treated HuH7 cells, mouse primary hepatocytes, and in the plasma of TM-treated C57BL/6 mice. Furthermore, TM significantly increased hepatic LDLR expression and reduced plasma LDL concentrations in mice. Based on these findings, we propose a model in which ER Ca^{2+} depletion promotes the activation of SREBP2 and subsequent transcription of PCSK9. However, conditions that cause ER stress regardless of their ability to dysregulate ER Ca^{2+} inhibit PCSK9 secretion, thereby reducing PCSK9-mediated LDLR degradation and promoting LDLR-dependent hepatic cholesterol uptake. Taken together, our studies provide evidence that the retention of PCSK9 in the ER may serve as a potential strategy for lowering LDL cholesterol levels.

It is well established that the endoplasmic reticulum (ER)[3] plays a central role in the proper folding and maturation of cell surface and secretory proteins (1–3). The ability of the ER to mediate protein folding relies on the oxidative state and elevated Ca^{2+} concentration of the ER (≈400 μM) relative to the cytosol (≈100 nM) (4, 5). An equilibrium formed between ER Ca^{2+} uptake via sarco/endoplasmic reticulum ATPase and ER Ca^{2+} release mediated by two homologous classes of intracellular Ca^{2+} release channels, known as the ryanodine receptors (RYRs) and the inositol 1,4,5-triphosphate receptors, play a major role in the regulation of ER Ca^{2+} homeostasis (6). Additional regulators of ER Ca^{2+} homeostasis include ER luminal proteins that interact with Ca^{2+}, such as buffer proteins and chaperones. Many chaperones, such as calreticulin and the glucose-regulated proteins of 78 and 94 kDa (GRP78 and GRP94), can directly interact with Ca^{2+} due to the presence of Ca^{2+}-binding motifs (7–9). Other Ca^{2+}-dependent chaperones, such as protein-disulfide isomerase (PDI), interact with Ca^{2+}-bind-

* This work was supported in part by Heart and Stroke Foundation of Ontario Research Grant T-6146 (to R. C. A.), Canadian Institutes of Health Research Grant MOP-74477, the Ontario Research and Development Challenge Fund, the Canadian Institute of Health Research (to S. R. W. C.), Leducq Foundation Grant 13 CVD 03 (to N. G. S. and A. P.), Canada Research Chair 216684 (to N. G. S.), St. Joseph's Healthcare Hamilton and the Canadian Institutes of Health Research Team Grant in Thromboembolism FRN-79846. The authors declare that they have no conflicts of interest with the contents of this article.

[1] An Alberta Innovates-Health Solutions (AIHS) Scientist.

[2] Career Investigator of the Heart and Stroke Foundation of Ontario and holds the Amgen Canada Research Chair in the Division of Nephrology, St. Joseph's Healthcare and McMaster University. To whom correspondence should be addressed: 50 Charlton Ave. East, Rm. T-3313, Hamilton, Ontario L8N 4A6, Canada. Tel.: 905-522-1155 (Ext. 35175); Fax: 905-540-6589; E-mail: austinr@taari.ca.

[3] The abbreviations used are: ER, endoplasmic reticulum; TG, thapsigargin; TM, tunicamycin; LDLR, low density lipoprotein receptor; RYR, ryanodine receptor; qRT, quantitative RT; GOF, gain-of-function; LOF, loss-of-function; PDI, protein-disulfide isomerase; IHC, immunohistochemistry; INSIG, insulin-induced gene; PERK, (PKR)-like ER kinase; CHOP, CCAAT-enhancer-binding protein homologous protein; SCAP, SREBP cleavage activating protein; SREBP, sterol regulatory element-binding protein; AEBSF, 4-(2-aminoethyl)benzenesulfonyl fluoride; VLDLR, VLDL receptor; UPR, unfolded protein response; NT, untreated; PC, proprotein convertase; A23, A23187; PF, PF-429242; U18, U18666A; BAPTA, 1,2-bis(2-aminophenoxy)ethane-*N*,*N*,*N*′,*N*′-tetraacetic acid; LRP, LDLR-related protein.

ing proteins like calreticulin and therefore indirectly rely on ER Ca^{2+} (10). Overall, this intricately controlled system allows for Ca^{2+}-dependent chaperones to promote the proper folding of newly synthesized polypeptides. Any physiological conditions that alter the state of ER Ca^{2+} can impair chaperone activity, subsequently leading to an accumulation of misfolded proteins in the ER. This state, known as ER stress, contributes to hepatic injury in liver diseases such as cholestatic liver disease, alcoholic fatty liver disease, non-alcoholic fatty liver disease, and drug-induced liver disease (2, 11–13). In addition to liver disease, prolonged ER stress causes apoptosis of foam cell macrophages, thereby accelerating necrotic core formation, plaque rupture, and progression of atherosclerosis (14, 15).

Under normal physiological conditions, however, a moderate accumulation of ER luminal protein triggers the unfolded protein response (UPR), which in turn restores ER homeostasis. This highly conserved mechanism consists of three signaling cascades as follows: (*a*) the inositol-requiring protein-1α (IRE1α) with its intrinsic RNase activity splices and activates the X-box-binding protein-1 (XBP1); (*b*) the activating transcription factor-6 (ATF6); and (*c*) the protein kinase RNA (PKR)-like ER kinase (PERK), which induces the expression of proapoptotic CCAAT enhancer-binding protein homologous protein (CHOP) (1). Collectively, these UPR mediators alleviate ER stress by increasing the folding capacity of the ER and reducing the influx of newly synthesized peptides into the ER luminal space. In addition to the induction of these chaperones, we as well as others have reported that ER stress promotes the activation of the sterol regulatory element-binding protein-2 (SREBP2) (16–23). In its inactive state, SREBP2 resides in the ER through its interaction with the SREBP cleavage-activating protein (SCAP) (24) and the insulin-induced gene (INSIG) (25). Although the specific mechanism by which ER stress activates SREBP2 is unclear, it is established that low intracellular cholesterol concentrations cause release of the SCAP-SREBP2 complex from the ER anchor, INSIG (26). Upon translocation from the ER to the Golgi apparatus, SREBP2 is cleaved and activated by site-1 and -2 proteases (27–29). The active SREBP2 transcription factor then translocates to the nucleus where it up-regulates a number of genes that regulate *de novo* cholesterol synthesis or uptake (30). Among these genes (31) is the proprotein convertase subtilisin/kexin type-9 (*PCSK9*) (32), which plays a critical role in modulating cardiovascular disease (33) by blocking hepatic low density lipoprotein (LDL) cholesterol uptake and inducing the degradation of the LDL receptor (LDLR) (34–37). Despite its critical role in LDL cholesterol uptake, the precise mechanism by which ER stress activates SREBP2 and mediates LDLR and cholesterol uptake via PCSK9 has not yet been examined.

We now report that ER stress, specifically caused by ER Ca^{2+} depletion, leads to an SREBP2-dependent increase in PCSK9 expression in cultured HuH7 and HepG2 hepatocytes. In contrast, ER stress reduces circulating PCSK9 concentrations, thereby increasing cell surface hepatic LDLR expression and reducing circulating LDL concentrations. Collectively, our findings outline a novel mechanism by which ER stress modulates lipid metabolism through PCSK9.

Results

ER Ca^{2+} Depletion Induces de Novo PCSK9 Expression—To assess whether ER stress induces the expression of PCSK9, HuH7 and HepG2 cells were either untreated (NT) or treated with TG, A23187 (A23), TM, or dithiothreitol (DTT) for 24 h. Immunoblotting showed that HuH7 cells treated with agents that cause ER Ca^{2+} depletion, TG and A23, exhibit increased cellular abundance of the PCSK9 protein (Fig. 1*A*). This induction was not observed in cells treated with TM or dithiothreitol (DTT). As expected, UPR markers FLAG-sXBP1, GRP78, GRP94, and CHOP were up-regulated by all ER stress-inducing agents used. Similar results were observed in HepG2 cells (data not shown). Consistent with PCSK9 protein, PCSK9 mRNA levels were up-regulated by TG and A23 but not by TM or DTT (Fig. 1*B*), whereas all ER stress-inducing agents used increased the expression of UPR markers GRP78 and sXBP1 (*, $p < 0.05$ compared with NT). In addition, although GRP78 and sXBP1 mRNA were induced by TG within 6 h of treatment, we observed that TG did not significantly affect PCSK9 mRNA until 18 h following treatment (Fig. 1*C*; *, $p < 0.05$ compared with NT). To confirm induction of the UPR by these ER stress-inducing agents, HuH7 cells were transfected with FLAG-sXBP1 plasmid and visualized by labeling the FLAG antigen with Alexa 647 immunofluorescent secondary antibodies. Immunofluorescence images from this experiment illustrate that all ER stress-inducing agents used in our experiments induced the UPR marker FLAG-sXBP1 (Fig. 1*D*). To assess the role of ER Ca^{2+} release on PCSK9 expression, a Ca^{2+} release assay was completed in HuH7 cells using the cytosolic Ca^{2+} indicator Fura-2AM. Our data indicate that TG (*, $p < 0.05$ compared with NT) and A23 (**, $p < 0.05$ compared with NT) led to a significant increase in cytosolic Ca^{2+} (Fig. 1*E*).

In addition to the well established pharmacologic inducers of ER stress used in Fig. 1*A*, PCSK9 expression was examined following nutrient deprivation (Fig. 1*F*). Similar to our previous findings, although all conditions led to a state of ER stress, as indicated by the induction of GRP78, only those that caused a loss of ER Ca^{2+} resulted in increased PCSK9 expression. The absence of sterols also led to an induction of PCSK9, likely as a direct result of SREBP2 activation.

Given that RYRs are involved in ER Ca^{2+} homeostasis (38–41), we utilized HEK293 cells that stably overexpress mutant RYR2s to further assess the role of ER Ca^{2+} depletion on PCSK9 expression. Specifically, the gain-of-function (GOF) RYR2 mutants (Q4201R and V4653F) yield increased ER Ca^{2+} leakage, whereas the loss-of-function (LOF) RYR2 mutant (A4860G) exhibits reduced Ca^{2+} leak into the cytosol as compared with WT RYR2 (6, 42). Consistent with the effect of TG and A23, GOF RYR2 mutants induced PCSK9 expression (Fig. 1*G*). In addition, although GOF RYR2 mutants led to the up-regulation of the UPR marker CHOP, the LOF RYR2 mutation reduced GRP78 expression.

ER Ca^{2+} Depletion Induces PCSK9 Expression in an SREBP2-dependent Manner—Although SREBP2 is activated by ER stress and regulates PCSK9 expression, the link between ER stress and PCSK9 has not yet been reported. Immunoblot analysis was used to assess the effect of ER Ca^{2+} depletion on SREBP2 acti-

vation and on INSIG1 levels, a key regulator of SREBP2 activation. Both TG and A23 caused a reduction of INSIG1 while increasing the abundance of cleaved active nuclear SREBP2 (nSREBP2) (Fig. 2*A*). However, SREBP2 activation and PCSK9 expression were blocked by PF-429242 (PF), an inhibitor of site-1 proteases (Fig. 2*B*). Consistent with these findings, blocking the activation of SREBP2 with PF as well as fatostatin or AEBSF significantly reduced the expression of PCSK9 at the mRNA level (Fig. 2*C*; #, $p < 0.05$ compared with NT). TG-induced PCSK9 expression (*, $p < 0.05$ compared with NT) was

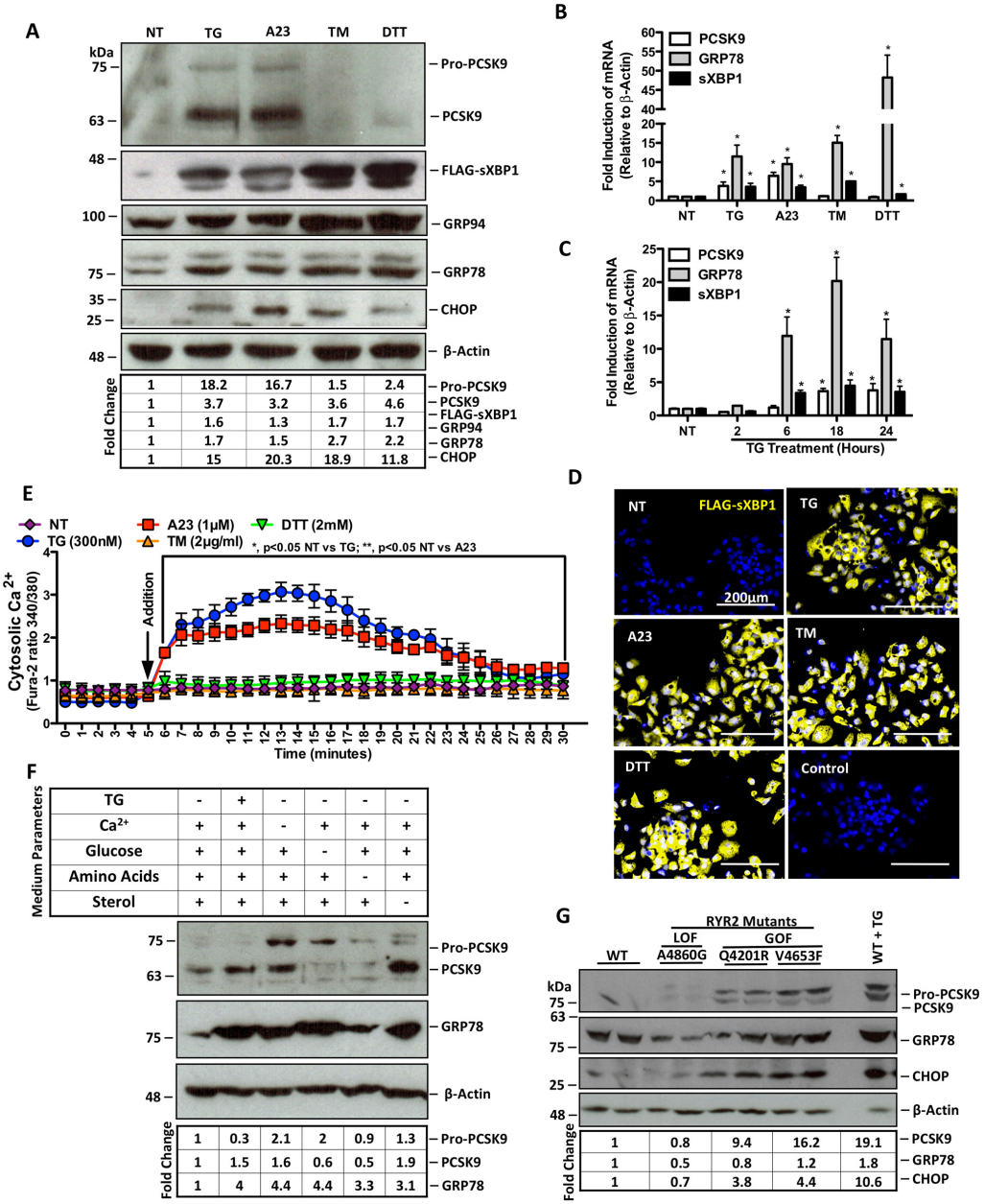

also blocked by these agents ($, $p < 0.05$ compared with TG). In a manner consistent with Fig. 2, *B* and *C*, treatment of cells with siRNA knockdown of SREBP2 blocked TG-mediated PCSK9 induction to a similar extent as that observed for U18666A (U18), a known activator of SREBP2 (Fig. 2*D*) (43).

In support of these findings, we confirmed the link between SREBP2 activation and PCSK9 expression in our model by promoting the activation of SREBP2. Similar to Fig. 2*D*, the treatment of HuH7 cells with U18 led to the activation of SREBP2 and a subsequent increase in the expression of downstream targets PCSK9 and LDLR without affecting UPR markers GRP94 and CHOP (Fig. 2*E*). Consistent with our SREBP2 inhibition studies, RT-PCR data also showed that PF (**, $p < 0.05$ compared with U18) can block U18-induced (*, $p < 0.05$ compared with NT) PCSK9 expression (Fig. 2*F*). To examine whether U18, which induces SREBP2 activation via sterol starvation, also causes ER Ca^{2+} release, a cytosolic Ca^{2+} release assay was completed. These data show that U18 causes a robust activation of SREBP2 without a spontaneous loss of ER Ca^{2+} (Fig. 2*G*).

ER Stress Reduces PCSK9 Secretion—Given that the interaction between PCSK9 and the LDLR occurs primarily in the extracellular space of the hepatocyte, we explored the effect of ER stress on PCSK9 secretion. Using ELISAs, we found that TG and TM significantly reduced the levels of secreted PCSK9 within the media from HuH7 cells (Fig. 3*A*, *, $p < 0.05$ compared with NT). Furthermore, TM reduced secreted PCSK9 concentrations to a significantly greater extent than TG (Fig. 3*A*, ±, $p < 0.05$ compared with TG). Similar results were observed in mouse primary hepatocytes (Fig. 3*B*). Given that TG increases the mRNA and cellular abundance of PCSK9, yet blocks its secretion, we next aimed to assess whether TG causes intracellular PCSK9 accumulation. HuH7 cells were pretreated with TG and subsequently permitted to rest in fresh TG-free media for 48 h. Secreted PCSK9 concentrations from the 24 to 48-h period following pretreatment were significantly greater than that of untreated cells (Fig. 3*C*). To explore the link between SREBP2 and secreted PCSK9, the media from AEBSF- and PF-treated HuH7 cells was also examined and found to contain significantly less PCSK9 than untreated controls (Fig. 3*D*, *, $p < 0.05$ compared with NT).

To determine the correlation between ER stress and PCSK9 secretion, HuH7 cells were treated with increasing concentrations of TM for 24 h. GRP78 protein expression, which served as a marker of UPR activation, was compared with the PCSK9 content in the media (Fig. 3*E*). A Pearson's correlation analysis of these data showed that the induction of the UPR inversely correlates with PCSK9 secretion ($r = -0.871$, $p = 0.0005$), which is significant (Fig. 3*E*,*, $p < 0.05$) at doses higher than 0.06 μg/ml TM.

ER Stress Retains PCSK9 in the ER—Given our previous findings that ER Ca^{2+} depletion induces *de novo* expression and cellular abundance of PCSK9, yet blocked its secretion, the cellular localization of TG- and TM-induced PCSK9 accumulation was examined. HuH7 cells transfected with V5-labeled PCSK9 were stained initially with rhodamine phalloidin and PDI to visualize the cytoskeleton and ER, respectively (Fig. 4*A*). Transfected cells were also stained for V5 and PDI (Fig. 4*B*). Upon analysis of these cells, we first observed that ER stress, whether induced by TG or TM, appeared to increase the relative size of the ER, an established phenomenon known as ER expansion (44). In addition, V5 staining revealed that PCSK9 remains confined to the ER irregardless of conditions that cause ER stress (Fig. 4). Collectively, these data indicate that regardless of the status of the UPR, exogenously expressed PCSK9 predominantly resides in the ER, as reported previously for WT PCSK9 (45).

TM Blocks PCSK9 Secretion and Induces Hepatic Cell Surface LDLR Expression in Vivo—To explore the effect of ER stress on PCSK9 secretion *in vivo*, C57BL/6 female mice were treated with increasing concentrations of TM for 24 h (Fig. 5*A*) or given a single treatment and sacrificed at 24-h intervals for a total of 120 h (Fig. 5*B*). Consistent with our *in vitro* findings, plasma PCSK9 levels were significantly reduced following TM treatment. This inhibitory effect of TM on plasma PCSK9 levels occurred at all doses of TM (*, $p < 0.05$), in a dose-dependent manner (±, $p < 0.05$) and persisted for up to 120 h following injection of TM (#, $p < 0.05$). Because of the role of PCSK9 as a major regulator of hepatic LDLR, we also examined LDLR expression. LDLR-stained liver sections from these animals show that TM induced hepatic cell surface LDLR to a similar extent as those observed in the well described PCSK9 KO mice (Fig. 5*C*) (46). The quantification of sections from multiple animals ($n = 3$) reveals similar results (Fig. 5*D*, *, $p < 0.05$). LDLR histology findings were confirmed using immunoblots, and as expected, ER stress markers GRP78 and CHOP were up-regulated by TM along with the LDLR (Fig. 5*E*). Non-permeabilized mouse primary hepatocytes were also stained for LDLR to confirm the cell surface localization of TM-dependent LDLR expression (Fig. 5*F*). Taken together, these data suggest that blockage of PCSK9 secretion, via ER stress, up-regulates hepatic LDLR expression.

TM Reduces the LDL Cholesterol Content of Plasma—Given the effect of ER stress on hepatic PCSK9 retention and

FIGURE 1. **ER Ca^{2+} depletion induces *de novo* PCSK9 expression.** HuH7 cells were seeded in DMEM and transfected with the FLAG-sXBP1 ER stress reporter plasmid. Cells were subsequently untreated (*NT*) or treated with ER stress-inducing agents TG (100 nM), A23 (1 μM), TM (2 μg/ml), or DTT (2 mM) for 24 h. *A* and *B*, following treatment, protein lysates were collected for immunoblot analysis of PCSK9 and UPR markers FLAG-sXBP1, GRP94, GRP78, and CHOP. RNA was collected for qRT-PCR analysis of PCSK9, sXBP1, and GRP78. *C*, RNA from HuH7 cells treated with TG (100 nM) for 2, 6, 18, or 24 h were also examined via qRT-PCR to determine the time dependence of TG-induced PCSK9 expression. *, $p < 0.05$. *D*, HuH7 cells, which underwent the same transfection and treatment conditions as in *A* and *B*, were also stained for FLAG to examine UPR induction via immunofluorescence microscopy. *E*, HuH7 cells were plated in clear bottom 96-well plates and incubated with Fura-2AM, a fluorescent cytosolic Ca^{2+} indicator, for 30 min. Following incubation, cytosolic Ca^{2+} of cells treated with ER stress-inducing agents was measured for 30 min. *F*, to determine the effect of ER stress-inducing conditions via non-pharmacologic means on PCSK9 expression, HuH7 cells were exposed to medium deficient in either Ca^{2+}, glucose, amino acids, or sterol for 24 h. *G*, in addition, the role of ER Ca^{2+} loss on PCSK9 expression was examined using HEK293 cells that stably overexpress tetracycline-inducible GOF or LOF RYR2 mutants using immunoblots. GOF RYR2 mutant cell lines (Q4201R and V4653F) exhibit increased ER Ca^{2+} leakage, whereas LOF RYR2 mutant (A4860G) exhibits reduced ER Ca^{2+} leak compared to WT cells (6, 42). Differences between treatments were assessed with paired Student's *t* tests, and all values are represented as mean ± S.D.

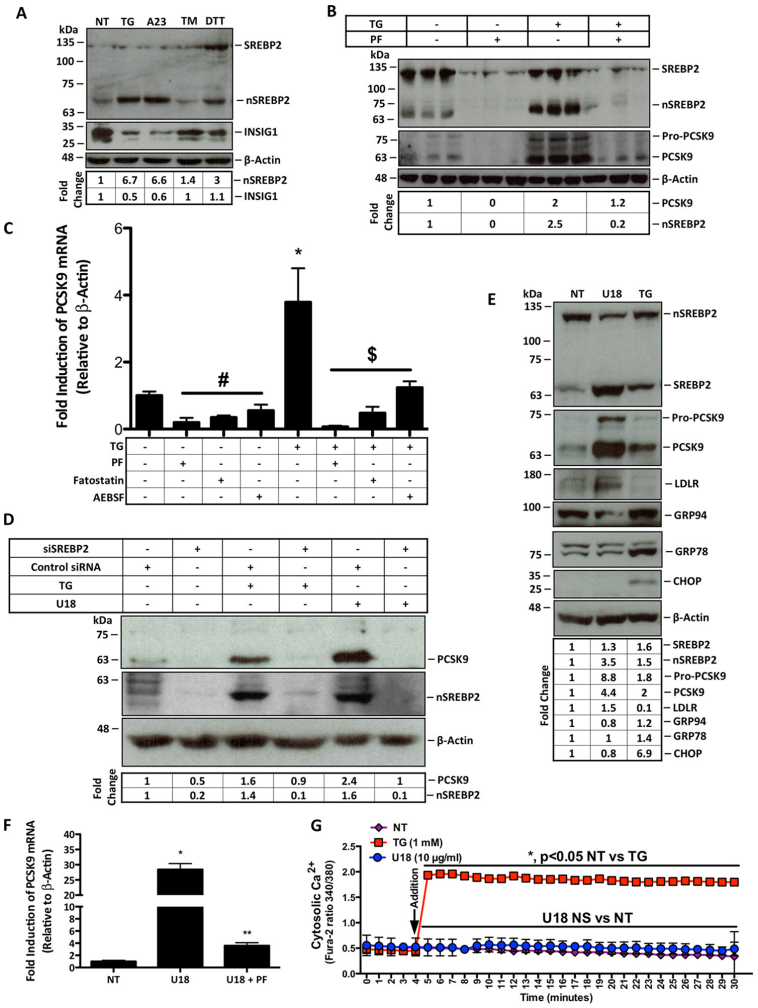

FIGURE 2. **ER Ca^{2+} depletion induces PCSK9 expression in an SREBP2-dependent manner.** *A*, protein lysates were collected from HuH7 cells either untreated (*NT*) or treated with ER stress-inducing agents TG (100 nM), A23 (1 μM), TM (2 μg/ml), or DTT (2 mM) for 24 h for immunoblot analysis. *B*, HuH7 cells were then treated with TG in the presence or absence of PF (10 μM), which inhibits SREBP2 activation, for 24 h. Immunoblot analysis was carried out as in *A* to examine the SREBP2 dependence of PCSK9 expression resulting from ER Ca^{2+} release. *C*, RNA was collected from HuH7 cells, which were treated with additional inhibitors of SREBP2 activation, including AEBSF (0.3 mM) and fatostatin (20 μM) in the presence or absence of TG (100 nM) to further elucidate the SREBP2 dependence of PCSK9 expression. #, $p < 0.05$ *versus* untreated cells (*NT*); *, $p < 0.05$ *versus* NT; $, $p < 0.05$ *versus* TG-treated cells. *D*, to confirm the link between SREBP2 activation and PCSK9 expression in our model, HuH7 cells were transfected with SREBP2 siRNA. Following transfection, cells were also treated with TG (100 nM) or U18 (1 μg/ml), an inducer of SREBP2 activation, for 24 h. *E*, to examine SREBP2 activation by U18, immunoblots were used to directly assess SREBP2 and markers of SREBP2 activation, PCSK9 and LDLR; UPR markers GRP94, GRP78, and CHOP were also evaluated to determine the influence of U18 on UPR activation. *F*, PCSK9 mRNA was also examined in HuH7 cells treated with U18 in the presence or absence of PF for 24 h. *, $p < 0.05$ *versus* NT; **, $p < 0.05$ *versus* U18-treated cells. *G*, to assess whether U18-induced PCSK9 expression occurs in a Ca^{2+}-dependent manner, HuH7 cells were incubated with fluorescent cytosolic Ca^{2+} indicator for 30 min and subsequently treated with U18 (10 μg/ml) or TG (1 mM) control. Differences between treatments were assessed with paired Student's *t* tests, and all values are represented as mean ± S.D.

increased LDLR expression, we next aimed to delineate the functional implications of these observations on circulating cholesterol levels. Our findings showed that TM treatment significantly reduces total plasma cholesterol (Fig. 6*A*, *, $p < 0.05$) and triglycerides (Fig. 6*B*, *, $p < 0.05$). Immunoblotting revealed that TM also significantly reduced the serum levels of apolipoprotein (apo) B100 and apoB48 (Fig. 6*C*) suggesting reduced abundance of very low density lipoprotein (VLDL) and LDL particles (47). Importantly, hepatic UPR markers GRP94, GRP78, and IRE1-α all confirm that TM treatment was successful in causing hepatic ER stress. Fast protein liquid chromatography (FLPC) cholesterol profile of the TM-treated mice

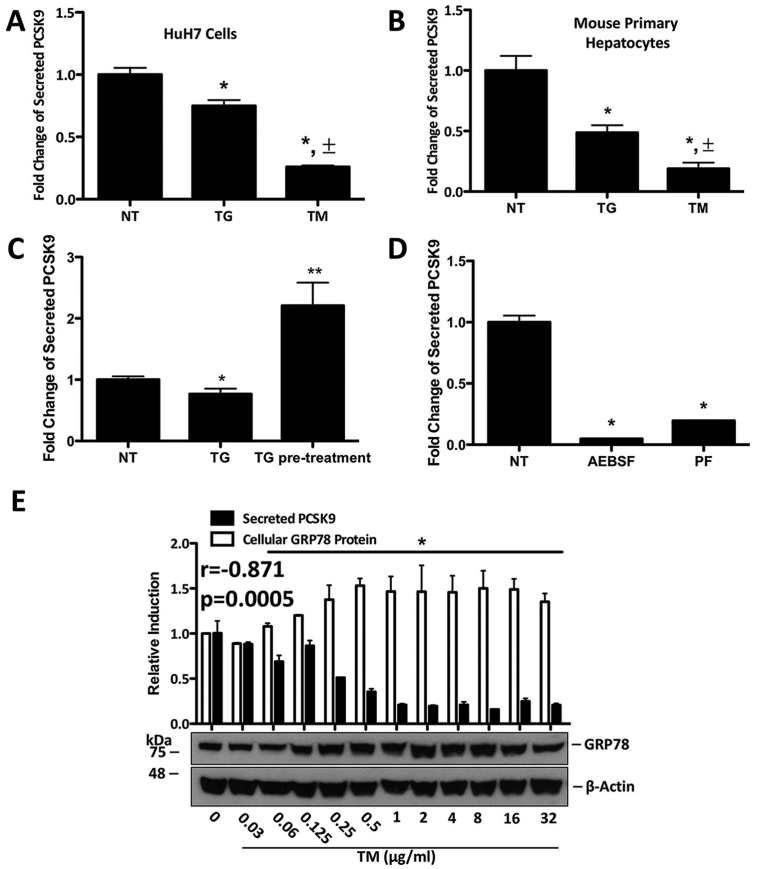

FIGURE 3. **ER stress reduces PCSK9 secretion.** *A* and *B*, HuH7 cells and primary hepatocytes were either untreated (*NT*) or treated with TG (100 nM) or TM (2 μg/ml) for 24 h. The FBS-free medium, in which these cells were cultured and treated, was collected and examined for secreted PCSK9 via ELISAs. *A* and *B*, ±, $p < 0.05$ *versus* TG-treated cells. *C*, secreted PCSK9 was then examined in the media of HuH7 cells, which were pretreated with TG (100 nM) for 4 h and permitted to rest in TG-free medium for 48 h. *D*, to examine the effect of SREBP2 inhibition on secreted PCSK9, FBS-free medium from HuH7 cells treated with AEBSF (0.3 mM) was also examined via ELISAs. *A–D*, *, $p < 0.05$ *versus* non-treated cells (*NT*). **, $p < 0.05$ *versus* TG-treated cells. *E*, correlation between UPR activation and PCSK9 secretion was assessed using a dose-response experiment in which HuH7 cells were treated with increasing concentrations of TM for 24 h. GRP78 expression, determined via immunoblots, was quantified and compared with ELISA data generated from the medium of the respective HuH7 cells. A Pearson's correlation was used to establish the relationship between cellular GRP78 expression and secreted PCSK9 ($r = -0.871$, $p = 0.0005$). *E*, $p < 0.05$ *versus* NT. Differences between treatments were assessed with paired Student's *t* tests, and all values are represented as mean ± S.D.

showed the cholesterol-lowering effect of TM (Fig. 6*D*). Quantification of these lipid profiles confirmed that TM significantly reduced plasma cholesterol concentrations in all lipoprotein classes (Fig. 6*E*; *, $p < 0.05$). These data demonstrate that TM has a potent cholesterol-lowering effect *in vivo*.

Discussion

In this study, we identify a novel role for ER stress in the modulation of hepatic PCSK9 and LDLR. We observed a striking consistency in our *in vitro* data, using a variety of cell lines, with respect to the up-regulation of PCSK9 in response to ER stress conditions that cause ER Ca^{2+} depletion (Fig. 1). In addition to the up-regulation of PCSK9 by TG and A23, a similar observation was made using sarco/endoplasmic reticulum ATPase inhibitors cyclopiazonic acid (1 μM) and cyclosporin-A (10 μg/ml) (data not shown). Previous pulse-chase studies have reported that TG- and A23-mediated ER Ca^{2+} depletion for up to 4 h had no effect on the zymogen processing or Tyr sulfonation of PCSK9 (32), which allow for its maturation and secretion, respectively. In accordance with this observation, our findings suggest that the effect of ER Ca^{2+} depletion on endogenous PCSK9 has no direct effect on PCSK9 processing. Rather, we observed a distinct effect of ER Ca^{2+} depletion on the transcriptional regulation of endogenous PCSK9 via Ca^{2+}-dependent SREBP2 activation. Notably, the observed activation of SREBP2 that we observed may be caused by the down-regulation of INSIG1 expression (Fig. 2*A*). A recent report in which copper-induced ER stress leads to ER Ca^{2+} depletion and sub-

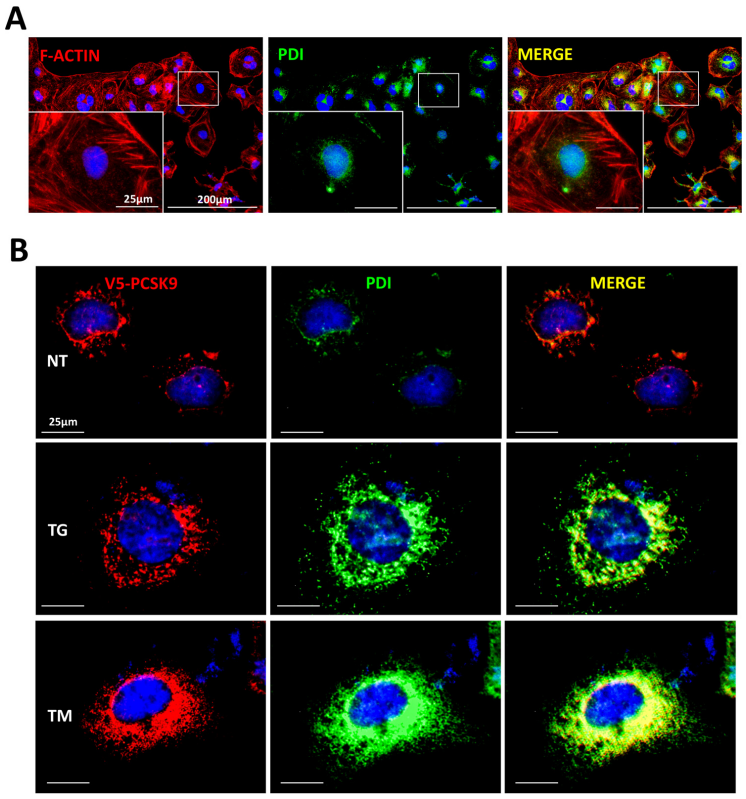

FIGURE 4. **ER stress retains PCSK9 in the ER.** HuH7 cells were plated in chamber slides and transfected with V5-PCSK9. Cells were subsequently either untreated (*NT*), treated with TG (100 nM), or TM (2 μg/ml) for 24 h. *A*, cells were then fixed and stained with rhodamine phalloidin (*red*) and ER marker PDI to allow for visualization of the cellular location of the ER relative to the cytosol. *B*, in addition, cells were also stained for V5 and PDI to identify the cellular localization of PCSK9. PCSK9 (*red*) was visualized using Alexa 594 fluorescent secondary antibodies, whereas PDI (*green*) was visualized using Alexa 647 fluorescent secondary antibodies.

sequent reduction in INSIG expression lends support to our findings (48). In addition, it has been shown that the down-regulation of an ER-resident Ca^{2+}-binding protein, calreticulin, results in ER Ca^{2+} loss and increased SREBP-1C activation (23). Finally, the direct effect of TG on the activation of SREBP-1 and -2 has also been reported previously (21). In addition to these findings, these authors also demonstrated that the TG-mediated activation of SREBP could be reversed with a 6-h treatment of the Ca^{2+}-chelating agent BAPTA (21). However, the effect of BAPTA on cellular Ca^{2+} homeostasis is subjected to temporal variations. Upon treatment of HuH7 cells with BAPTA for 24 h, we observed increased PCSK9 expression similar to that of the effect of TG (data not shown). This likely occurred due to excessive cytosolic Ca^{2+} chelation resulting in ER Ca^{2+} depletion. Furthermore, as a consequence of causing ER Ca^{2+} depletion by blocking ER Ca^{2+} uptake, TG increases cytosolic Ca^{2+} content. For this reason, the induction of PCSK9 via a 24-h treatment of BAPTA indicates that TG-mediated PCSK9 expression occurs primarily as a result of ER Ca^{2+} depletion and is not due to increased cytosolic Ca^{2+}. Collectively, our findings, as well as those of others, support a model in which a spontaneous loss of ER Ca^{2+} promotes the activation of SREBP2 and a consequent up-regulation of PCSK9. However, the specific mechanism by which ER Ca^{2+} depletion causes the down-regulation of INSIG1 and release of SREBP2 from the ER remains to be elucidated.

We also explored the effect of ER stress on PCSK9 secretion in cultured HuH7 cells and mouse primary hepatocytes. Given our previous findings that TG increased PCSK9 expression, we measured PCSK9 in the media from these cells. We found that ER stress, whether induced by TG or TM, significantly reduced the PCSK9 content of media (Fig. 4, *A* and *B*). In addition, PCSK9 appears to accumulate in the cell during conditions of stress and is subsequently processed and secreted upon alleviation of such conditions (Fig. 4*C*). Consistent with these findings, TM-treated mice also had significantly less circulating PCSK9 (Fig. 5*A*). The mechanism by which ER stress reduces PCSK9 in the media/plasma remains unclear. However, because these agents fail to block the autocatalytic cleavage of PCSK9 from its premature (75 kDa) to its mature form (68 kDa)

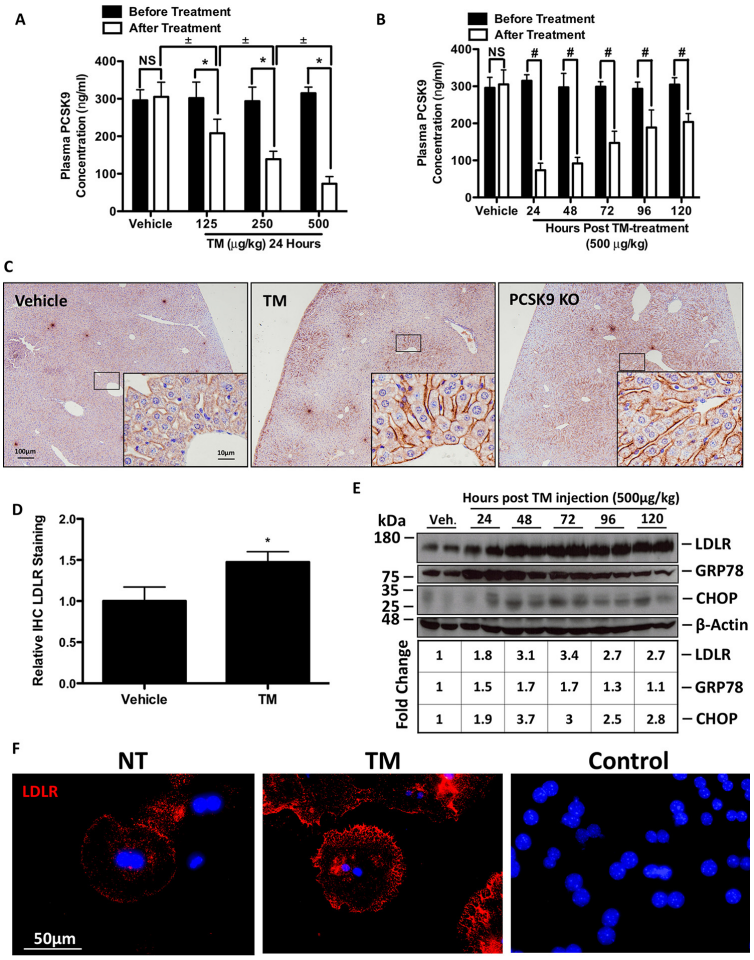

FIGURE 5. **TM blocks PCSK9 secretion and induces hepatic cell surface LDLR expression *in vivo*.** 12-Week-old C57BL/6 female mice were randomly divided into eight groups ($n = 3$) and subcutaneously injected with a single dose of PBS vehicle control or TM. Animals treated with PBS or TM (125–500 μg/kg) were sacrificed 24 h following injection. The remaining animals, belonging to groups 5–8 were treated with a single injection of TM (500 μg/kg) and sacrificed every 24 h for the following 120 h. Plasma was taken from each mouse prior to injection and after sacrifice. *A*, *, $p < 0.05$ *versus* before treatment. ±, $p < 0.05$ *versus* after treatment. *A* and *B*, plasma PCSK9 levels were quantified via ELISAs. *B*, #, $p < 0.05$ *versus* before treatment. *C* and *D*, livers from the TM-treated and untreated PCSK9 KO mice were collected, fixed in formalin, sectioned, stained for LDLR, and quantified. *E*, flash-frozen liver tissues from these animals were used to examine the expression of LDLR and of UPR markers GRP78 and CHOP using immunoblots. *, $p < 0.05$ *versus* vehicle. *F*, to elucidate whether IHC LDLR stating occurred specifically on cell surface LDLR, mouse primary hepatocytes were plated and stained for LDLR in the absence of permeabilizing agents. *Control*, HuH7 cells were also incubated with Alexa 594 secondary antibody, in the absence of primary antibody staining. Differences between treatments were assessed with unpaired Student's *t* tests, and all values are represented as mean ± S.D. *Veh*, vehicle; *NS*, not significant.

(Fig. 1*A*), our data suggest that ER stress does not directly affect PCSK9. Rather, ER stress is likely affecting other proteins in the PCSK9 secretory pathway. Recent reports have identified GRP94, an ER stress inducible protein, as an ER-resident binding partner of PCSK9 (49). Furthermore, it has been shown that the exit of PCSK9 from the ER depends on anterograde COPII vesicular trafficking (50), a process known to be impaired by ER stress (51). Taken together, these findings suggest that ER stress increases the PCSK9-retaining ability of the ER (Fig. 3) by up-regulating GRP94 (Figs. 1*A* and 6*C*), and it further hinders the exit of PCSK9 from the ER by blocking COPII vesicular transport.

Consistent with our findings, it has been reported that circulating PCSK9 levels were significantly reduced in mice fed a high cholesterol diet (52), a condition known to cause hepatic UPR activation (53). Most notably however, the reduction in circulating PCSK9 levels was linked to an increase in hepatic LDLR expression.

Similar to previous reports, we found plasma PCSK9 concentrations to be inversely related to hepatic cell surface LDLR

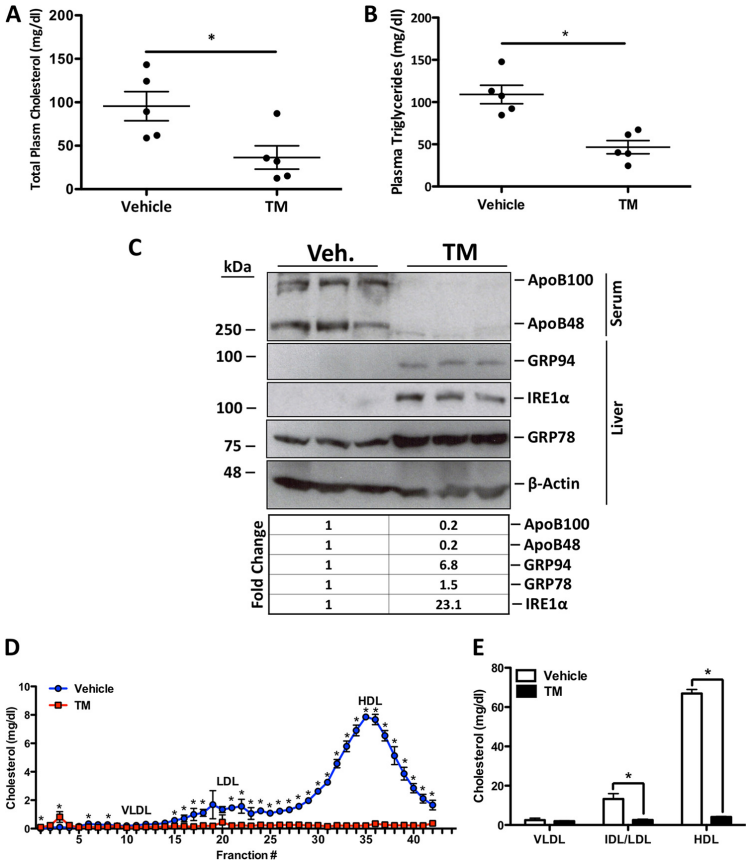

FIGURE 6. **Tunicamycin reduces the LDL cholesterol content of plasma.** 12-Week-old C57BL/6 female mice were subcutaneously injected with a single dose of TM (500 μg/kg) and sacrificed 24 h later. *A* and *B*, plasma was collected after sacrifice and total cholesterol and triglycerides were quantified using enzymatic assays. *A* and *B*, *, $p < 0.05$ *versus* vehicle. *C*, to determine the effect of TM on LDL cholesterol, plasma apoB48 and apoB100 were examined using immunoblots. Immunoblot analysis was also used to ensure TM-mediated induction of UPR markers GRP94, GRP78, and IRE1α. *D*, to further elucidate the effect of TM on all lipoprotein fractions, FPLC analysis was used to construct a lipid profile. Differences between treatments were assessed with paired Student's *t* tests, and all values are represented as mean ± S.D. *E*, *, $p < 0.05$ *versus* vehicle (NT). *Veh*, vehicle.

expression (37, 54, 55). Although it has been reported that TM induces the VLDLR via the PERK-ATF4 pathway (13), the potential mechanisms by which TM affects LDLR expression are numerous. First, because of the glycosylated nature of the LDLR, the direct impact of TM, which inhibits *N*-glycosylation, on the LDLR must be taken into consideration. Upon longer exposure of our LDLR immunoblots (Fig. 5*E*), it became apparent that TM caused a distinct accumulation of premature non-*N*-glycosylated LDLR (120 kDa, data not shown) in the livers of these mice. For this reason, the increase in LDLR expression, however, is likely a result of increased LDLR half-life due to the TM-mediated loss of PCSK9 in circulation.

Alternatively, it has been reported that newly synthesized mature ER-resident PCSK9 can act as a chaperone of the LDLR, thereby contributing to LDLR maturation and exit from the ER (56). Based on these findings, and given the effect of TM on ER PCSK9 retention (Fig. 4), it is also possible that the abundance of PCSK9 in the ER leads to a net increase in PCSK9-mediated ER LDLR processing and maturation.

Finally, although LDLR expression is transcriptionally regulated by SREBP2 (57), which can be activated by ER stress (2, 11–13), our data indicate that ER Ca^{2+} release is necessary for this process to occur (Fig. 2*A*). Based on these findings, it is unlikely that TM is directly inducing hepatic cell surface LDLR expression via SREBP2 activation. Consistent with this, others have determined that TM blocks the *N*-glycosylation and stability of SCAP, leading to a reduction of SREBP1/2 activation (58).

In addition to association between the loss of circulating PCSK9 and elevated LDLR expression, we also describe a TM-mediated ablation of circulating LDL (Fig. 6, *C–E*). Others have reported that TM blocks *de novo* cholesterol synthesis via direct inhibition of 3-hydroxy-3-methylglutaryl-coenzyme A reductase (59) and reduces cholesterol efflux (60). However, a model

in which TM reduces circulating LDL via LDLR has not been reported.

Moreover, we also observed a significant reduction in circulating HDL levels (Fig. 6, *D* and *E*). This finding has been described previously, in which lower circulating HDL levels in PCSK9$^{-/-}$ mice were shown to be dependent on LDLR-mediated uptake of HDL via apoE (61). It is also established that other ER stress-inducible members of the LDLR family, including the LDLR-related protein (LRP) (62) and VLDLR (13), can bind and internalize apoE-containing HDL (63) and be degraded by circulating PCSK9 (64–67). Consistent with these findings, the overexpression of profurin, the prodomain of a member of the proprotein convertase (PC) family, blocks PC activation and subsequently abrogates circulating HDL levels (68). Based on our findings, as well as those mentioned herein, TM may be reducing circulating HDL levels by inducing the expression of apoE-binding receptors such as the LDLR (Fig. 5*C*), VLDLR (13), and LRP. Furthermore, in a manner similar to profurin, the inhibition of *N*-glycosylation by TM may also be affecting PC activation thereby further contributing to the reduction in circulating HDL levels.

Currently, the mechanism by which PCSK9 is secreted remains unclear. However, in agreement with other studies, our findings demonstrate that PCSK9 secretion is a highly regulated process potentially involving multiple cellular pathways (63, 69–71). Our studies show that inhibition of *N*-glycosylation and induction of the UPR markedly impairs PCSK9 secretion. Our data further support the notion that reducing PCSK9 secretion, via ER retention, may contribute to a reduction in circulating LDL cholesterol (72). Overall, this study further enforces the need for additional investigations to delineate the mechanism(s) by which ER Ca^{2+} and ER stress play a role in the expression and cellular retention of PCSK9.

Experimental Procedures

Cell Culture and Cell Treatment—Human hepatocellular carcinoma HuH7 and HepG2 cells were chosen because they are known to express and secrete PCSK9 (73, 74). HuH7 cells were a generous gift from Dr. Nabil G. Seidah (University of Montreal), and HepG2 cells were purchased from American Type Culture Collection (catalog no. HB-8065). HuH7 cells and HepG2 cells were routinely grown at 37 °C with 5% CO_2 in Dulbecco's modified Eagle's medium (DMEM) (Gibco, Thermo Fisher Scientific, Waltham, MA) containing 10% fetal bovine serum (FBS, Sigma), 100 IU/ml penicillin, and 100 μg/ml streptomycin (Gibco, Thermo Fisher Scientific). HEK293 cells overexpressing RYR2 mutants (75) were used to examine PCSK9 expression. Briefly, HEK293 cells were plated to a confluence of 90% in DMEM containing 10% FBS, 100 IU/ml penicillin, 100 μg/ml streptomycin, 4 mM L-glutamine (Sigma), 0.1 mM nonessential amino acids (Gibco, Thermo Fisher Scientific), and expression of RYR2 wild type (WT) and mutants was induced via incubation with tetracycline (1 μg/ml, Sigma) for 24 h (76). Cells were subsequently treated with agents that induced varying types of ER stress for 24 h. TG (100 nM, Sigma), and Ca^{2+} ionophore A23 (1 μM, Sigma) cause ER Ca^{2+} depletion (32); TM (2 μg/ml, Sigma) inhibits *N*-glycosylation (77), and the reducing agent DTT (2 mM, Sigma) disrupts disulfide bond formation by compromising the oxidative environment of the ER lumen (18). To further examine the conditions of ER stress on PCSK9 expression, HuH7 cells were incubated in medium deficient in either Ca^{2+} (catalog no. 21068-028, Gibco, Thermo Fisher Scientific), D-glucose (catalog no. 11966-025, Gibco, Thermo Fisher Scientific), amino acids (catalog no. 24010-043, Gibco, Thermo Fisher Scientific), or sterols. With the exception of the medium deficient in sterol, which contained no FBS, all media used in these experiments were supplemented with dialyzed FBS (catalog no. 26400-036, Gibco, Thermo Fisher Scientific). To block the activation of SREBP2, cells were treated with AEBSF (20) (0.3 mM, Sigma), fatostatin (78) (20 μM, Sigma), or PF (10 μM, Sigma) (79) for 24 h. siRNA was also used to block SREBP2; briefly, HuH7 cells were transfected with SREBP2 siRNA (catalog no. 4390824, Thermo Fisher Scientific) or control siRNA (catalog no. 4390843, Thermo Fisher Scientific) using Lipofectamine RNAiMAX (catalog no. 13778030, Thermo Fisher Scientific) and incubated in the transfection mixture for 48 h. Cells were then either untreated or treated with TG (100 nM) or U18 (1 μg/ml, Sigma) for 24 h following initiation of the transfection. In addition to TG, U18 was used as an activator of SREBP2 due to its ability to promote intracellular sterol starvation (43).

Hepatocyte Isolation—Primary hepatocytes were isolated from 12-week-old male C57BL/6 mice in a two-step hepatic perfusion of prewarmed EGTA (500 μM in HEPES buffer, Sigma) and collagenase (0.05% in HEPES buffer, Sigma) solutions (80). Immediately proceeding the harvest, cells were washed, collected via low speed centrifugation with cell strainers, and plated (10^6 cells/ml) in warm William's E medium (Gibco, Thermo Fisher Scientific) supplemented with 10% FBS, 100 IU/ml penicillin, and 100 μg/ml streptomycin.

Measurement of Intracellular Ca^{2+}—Intracellular Ca^{2+} in HuH7 cells was measured using the Fura-2AM fluorescent indicator as described previously (81). Briefly, cells were plated in clear-bottom white 96-well plates (Nunc, Denmark) to a confluence of 80%. Following a 24-h resting period, cells were washed and incubated with Fura-2AM (2 μM) for 30 min. Cells were subsequently washed again and left to incubate in Hanks' balanced salt solution containing 10 mM HEPES during the course of the experiment. Fluorescence intensity measurements were taken every minute for 30 min at two distinct wavelengths (excitation 340/emission 515 and excitation 380/emission 515) using a SpectraMax Gemini EM fluorescent spectrophotometer (Molecular Devices, Sunnyvale, CA).

Plasmids, Transfections, and Immunofluorescence Microscopy—To ensure appropriate induction of the UPR by the ER stress-inducing agents used, HuH7 cells were transfected with an ER stress-activated indicator plasmid as described previously (82). Briefly, under conditions of stress, the ER stress-specific intron is spliced and removed from the ER stress-activated indicator mRNA transcript leading to a frameshift and subsequent production of functional FLAG-spliced XBP1 (sXBP1) protein. ER stress-induced FLAG-sXBP1 was visualized by staining for FLAG. To determine the cellular localization of PCSK9 in conditions of stress, HuH7 cells were transfected with WT V5-labeled PCSK9, as described previously (83), and stained for V5. Transfection of the HuH7 cells with

this plasmid was performed at 60% confluence. Briefly, a transfection mixture consisting of a 1:3 ratio (2 μg, 6 μl) of plasmid/X-tremeGENE (catalog no. 6366236001 Roche Applied Science and Sigma) and 192 μl of Opti-MEM (Thermo Fisher Scientific) were added to the HuH7 cells in 6-well culture dishes or 4-well chamber slides (catalog no.177399, Thermo Fisher Scientific) containing complete DMEM for 48 h. ER stress-inducing agents were added 24 h after the addition of the transfection mixture. Cells were either lysed for immunoblot analysis or fixed with 4% paraformaldehyde for immunofluorescence microscopy. Fixed cells were subsequently washed with PBS, either non-permeabilized or permeabilized with 0.025% Triton-X in 1× PBS, and blocked with 1% bovine serum albumin for 30 min. Cells were then stained with anti-FLAG (catalog no. F3040 Sigma), anti-V5 (catalog no. sc-83849, Santa Cruz Biotechnology), anti-LDLR (catalog no. AF2255, R&D Systems), or anti-PDI (catalog no. C81H6, Cell Signaling Technology) for 1 h in 1% BSA in 1× PBS-T. Following incubation with primary antibody, cells were washed and incubated with either Alexa 594 (catalog no. A11058, Thermo Fisher Scientific) or Alexa 647 (catalog no. 21245, Thermo Fisher Scientific) fluorescent secondary antibodies as well as DAPI. To determine the localization of the ER relative to the cytoskeleton, additional control cells were stained with rhodamine phalloidin (catalog no. R415, Thermo Fisher Scientific). Slides were then coverslipped with permafluor and visualized using the EVOS FL color imaging system at either ×20 or ×40 magnification.

Immunoblot Analysis—Cells were lysed in 4× SDS-PAGE sample buffer and separated on either 7 or 10% polyacrylamide gels in denaturing conditions, as described previously (84). Following gel electrophoresis, proteins were transferred to nitrocellulose membranes (Bio-Rad) using the Trans-Blot Semi-Dry transfer apparatus (Bio-Rad) and blocked with 5% skim milk (Compliments, Sobeys, Canada) in 1× TBS-T for 1 h at room temperature. Membranes were then incubated with primary antibodies for 18 h at 4 °C. The primary antibodies were diluted in 1× TBST with 1% skim milk. These included the following: anti-CHOP (catalog no. SC-793, Santa Cruz Biotechnology); anti-FLAG (catalog no. SC-121-G, Santa Cruz Biotechnology); anti-GRP78 (catalog no. 610979, BD Biosciences); anti-IRE1α (catalog no. 14C10 Cell Signaling Technology); anti-KDEL (catalog no. 10C3, Enzo Life Sciences); anti-PCSK9 (catalog no. NB300-959, Novus), and anti-SREBP2 (catalog no. 557037, BD Biosciences). Following the incubation with primary antibody, membranes were incubated with horseradish peroxidase-conjugated secondary antibodies diluted in 1× TBS-T with 1% milk (goat anti-mouse, catalog no. 170-6516, Bio-Rad; goat anti-rabbit, catalog no. 170-6515, Bio-Rad; and donkey anti-goat, catalog no. ab6741, Abcam). Membranes were visualized using the EZ-ECL chemiluminescent reagent (catalog no. 20-500-500, FroggaBio) on Amersham Biosciences Hyperfilm (catalog no. 28906839, GE Healthcare), which was subsequently developed on a Kodak X-Omat 1000A processor. Following exposure, band intensities were quantified using ImageJ software. Relative band intensities represent the mean of three replicate immunoblots adjusted to membranes re-probed against β-actin (catalog no. A5441, Sigma).

RT-PCR—Total RNA was isolated using RNeasy mini kits (catalog no. 74104, Qiagen) and reverse-transcribed to cDNA using SuperScript Vilo cDNA synthesis kit (catalog no. 11754050, Life Technologies, Inc.). RT-PCR was completed using Fast SYBR Green (catalog no.4385610, Life Technologies, Inc.), as described previously (83).

PCSK9 ELISA—Mouse plasma was diluted 1:200 and PCSK9 levels were determined using a mouse PCSK9 Quantikinine ELISA kit (catalog no.MCP900, R&D Systems). PCSK9 in tissue culture medium collected from cultured HuH7 cells grown in FBS-free medium was measured using the human PCSK9 quantikinine ELISA kit (catalog no. DCP900, R&D Systems).

Immunohistochemistry (IHC)—Liver tissues were collected and fixed in formaldehyde before being embedded in paraffin. Sections were subjected to antigen retrieval for 10 min at room temperature in 0.05% protease (Sigma) and stained for LDLR (catalog no. AF2255, R&D Systems), which was diluted 1:20. Quantification of LDLR staining was done using ImageJ software.

Animal Studies—Animal studies were separated into two independent experiments; the first aimed to identify the effect of ER stress on secreted PCSK9 levels, and the second was to examine the impact of ER stress on hepatic LDLR and circulating LDL levels. These experiments were completed using 12-week-old female C57BL/6 mice (strain no. 000664, Charles River, Sherbrooke, Quebec, Canada). Animals were received at 10 weeks of age and housed in 12:12 light/dark cycles and had access to rodent chow and water *ad libitum* for 2 weeks prior to studies. In our first experiment, which aimed to examine circulating PCSK9 and hepatic LDLR expression, animals were randomly divided into 8 groups (n = 3). Animals sacrificed 24 h following injection were treated with PBS vehicle control, TM 125 μg/kg, 250 μg/k, or 500 μg/kg (groups 1–4). The remaining animals were treated with TM 500 μg/kg and sacrificed every 24 h for 120 h. Plasma was collected via facial bleeds prior to the single subcutaneous injection and after sacrifice. In our second experiment, which aimed to examine circulating lipid, C57BL/6 mice were randomly divided into two groups (n = 5) and treated with either 1× PBS (n = 5) or TM 500 μg/kg (n = 5) for 24 h. In both experiments, liver tissue was flash-frozen for immunoblot and RT-PCR analyses or fixed in 4% formalin for IHC. The McMaster University Animal Research Ethics Board approved all procedures.

Plasma Lipoprotein Analysis—Total plasma cholesterol and triglycerides were determined using enzymatic kits (Wako Diagnostics, Richmond, VA). Plasma lipid profiles were generated via FPLC as described previously (85). In brief, 100 μl of plasma from each animal (n = 3) was fractioned by gel filtration FPLC using an AKTA system with a Tricorn Superose 6 HR10/300 column (GE Healthcare, Baie D'Urfe Quebec, Canada). An enzymatic assay kit was used to measure total cholesterol in fractionated plasma, following the manufacturer's instructions (catalog no. TR13421, Thermo Fisher Scientific, Ottawa, Ontario, Canada). Cholesterol from each fraction was quantified using a SpectraMax Plus384 spectrophotometer (Molecular Devices).

Statistical Analysis—Statistical analysis for differences between groups was performed using two-tailed unpaired

Student's *t* test. Comparisons between plasma PCSK9 concentrations from the same animals before and after treatment were completed using paired two-tailed Student's *t* test. Statistical tests were analyzed using Prism software (GraphPad Software, San Diego). Differences between groups were considered significant at $p < 0.05$, and all values are expressed as mean ± S.D.

Author Contributions—P. L., R. C. A., and N. G. S. conceived the studies. P. L. and S. S. performed all of the *in vitro* work, and P. L. and A. A. completed all of the *in vivo* studies. Immunohistochemical staining was completed by S. L., and fast protein liquid chromatography was performed by P. Y. and B. T. The manuscript was written by P. L. and revised by A. A., G. G., G. P., S. R. W. C., B. T., A. P., N. G. S., and R. C. A.

Acknowledgment—We thank Dr. Masayuki Miura (University of Tokyo) for the generous gift of the indicator plasmid used in this study.

References

1. Austin, R. C. (2009) The unfolded protein response in health and disease. *Antioxid. Redox Signal.* **11,** 2279–2287
2. Colgan, S. M., Hashimi, A. A., and Austin, R. C. (2011) Endoplasmic reticulum stress and lipid dysregulation. *Expert Rev. Mol. Med.* **13,** e4
3. Walter, P., and Ron, D. (2011) The unfolded protein response: from stress pathway to homeostatic regulation. *Science* **334,** 1081–1086
4. Corbett, E. F., Oikawa, K., Francois, P., Tessier, D. C., Kay, C., Bergeron, J. J., Thomas, D. Y., Krause, K. H., and Michalak, M. (1999) Ca^{2+} regulation of interactions between endoplasmic reticulum chaperones. *J. Biol. Chem.* **274,** 6203–6211
5. Tong, J., McCarthy, T. V., and MacLennan, D. H. (1999) Measurement of resting cytosolic Ca^{2+} concentrations and Ca^{2+} store size in HEK-293 cells transfected with malignant hyperthermia or central core disease mutant Ca^{2+} release channels. *J. Biol. Chem.* **274,** 693–702
6. Chen, W., Wang, R., Chen, B., Zhong, X., Kong, H., Bai, Y., Zhou, Q., Xie, C., Zhang, J., Guo, A., Tian, X., Jones, P. P., O'Mara, M. L., Liu, Y., Mi, T., *et al.* (2014) The ryanodine receptor store-sensing gate controls Ca^{2+} waves and Ca^{2+}-triggered arrhythmias. *Nat. Med.* **20,** 184–192
7. Lamb, H. K., Mee, C., Xu, W., Liu, L., Blond, S., Cooper, A., Charles, I. G., and Hawkins, A. R. (2006) The affinity of a major Ca^{2+}-binding site on GRP78 is differentially enhanced by ADP and ATP. *J. Biol. Chem.* **281,** 8796–8805
8. Biswas, C., Ostrovsky, O., Makarewich, C. A., Wanderling, S., Gidalevitz, T., and Argon, Y. (2007) The peptide-binding activity of GRP94 is regulated by calcium. *Biochem. J.* **405,** 233–241
9. Coe, H., and Michalak, M. (2009) Calcium binding chaperones of the endoplasmic reticulum. *Gen. Physiol. Biophys.* **28,** Spec. No. Focus, F96–F103
10. Corbett, E. F., and Michalak, M. (2000) Calcium, a signaling molecule in the endoplasmic reticulum? *Trends Biochem. Sci.* **25,** 307–311
11. Kaplowitz, N., Than, T. A., Shinohara, M., and Ji, C. (2007) Endoplasmic reticulum stress and liver injury. *Semin. Liver Dis.* **27,** 367–377
12. Dara, L., Ji, C., and Kaplowitz, N. (2011) The contribution of endoplasmic reticulum stress to liver diseases. *Hepatology* **53,** 1752–1763
13. Jo, H., Choe, S. S., Shin, K. C., Jang, H., Lee, J. H., Seong, J. K., Back, S. H., and Kim, J. B. (2013) Endoplasmic reticulum stress induces hepatic steatosis via increased expression of the hepatic very low density lipoprotein receptor. *Hepatology* **57,** 1366–1377
14. Lusis, A. J. (2000) Atherosclerosis. *Nature* **407,** 233–241
15. Tabas, I. (2010) Macrophage death and defective inflammation resolution in atherosclerosis. *Nat. Rev. Immunol.* **10,** 36–46
16. Pai, J. T., Brown, M. S., and Goldstein, J. L. (1996) Purification and cDNA cloning of a second apoptosis-related cysteine protease that cleaves and activates sterol regulatory element binding proteins. *Proc. Natl. Acad. Sci. U.S.A.* **93,** 5437–5442
17. Higgins, M. E., and Ioannou, Y. A. (2001) Apoptosis-induced release of mature sterol regulatory element-binding proteins activates sterol-responsive genes. *J. Lipid Res.* **42,** 1939–1946
18. Werstuck, G. H., Lentz, S. R., Dayal, S., Hossain, G. S., Sood, S. K., Shi, Y. Y., Zhou, J., Maeda, N., Krisans, S. K., Malinow, M. R., and Austin, R. C. (2001) Homocysteine-induced endoplasmic reticulum stress causes dysregulation of the cholesterol and triglyceride biosynthetic pathways. *J. Clin. Invest.* **107,** 1263–1273
19. Lee, J. N., and Ye, J. (2004) Proteolytic activation of sterol regulatory element-binding protein induced by cellular stress through depletion of Insig-1. *J. Biol. Chem.* **279,** 45257–45265
20. Colgan, S. M., Tang, D., Werstuck, G. H., and Austin, R. C. (2007) Endoplasmic reticulum stress causes the activation of sterol regulatory element binding protein-2. *Int. J. Biochem. Cell Biol.* **39,** 1843–1851
21. Lauressergues, E., Bert, E., Duriez, P., Hum, D., Majd, Z., Staels, B., and Cussac, D. (2012) Does endoplasmic reticulum stress participate in APD-induced hepatic metabolic dysregulation? *Neuropharmacology* **62,** 784–796
22. Lhoták, S., Sood, S., Brimble, E., Carlisle, R. E., Colgan, S. M., Mazzetti, A., Dickhout, J. G., Ingram, A. J., and Austin, R. C. (2012) ER stress contributes to renal proximal tubule injury by increasing SREBP-2-mediated lipid accumulation and apoptotic cell death. *Am. J. Physiol. Renal Physiol.* **303,** F266–F278
23. Vig, S., Talwar, P., Kaur, K., Srivastava, R., Srivastava, A. K., and Datta, M. (2015) Transcriptome profiling identifies p53 as a key player during calreticulin deficiency: Implications in lipid accumulation. *Cell Cycle* **14,** 2274–2284
24. Hua, X., Nohturfft, A., Goldstein, J. L., and Brown, M. S. (1996) Sterol resistance in CHO cells traced to point mutation in SREBP cleavage-activating protein. *Cell* **87,** 415–426
25. Yabe, D., Brown, M. S., and Goldstein, J. L. (2002) Insig-2, a second endoplasmic reticulum protein that binds SCAP and blocks export of sterol regulatory element-binding proteins. *Proc. Natl. Acad. Sci. U.S.A.* **99,** 12753–12758
26. Sun, L. P., Li, L., Goldstein, J. L., and Brown, M. S. (2005) Insig required for sterol-mediated inhibition of Scap/SREBP binding to COPII proteins *in vitro*. *J. Biol. Chem.* **280,** 26483–26490
27. Sakai, J., Duncan, E. A., Rawson, R. B., Hua, X., Brown, M. S., and Goldstein, J. L. (1996) Sterol-regulated release of SREBP-2 from cell membranes requires two sequential cleavages, one within a transmembrane segment. *Cell* **85,** 1037–1046
28. Nohturfft, A., Brown, M. S., and Goldstein, J. L. (1998) Sterols regulate processing of carbohydrate chains of wild-type SREBP cleavage-activating protein (SCAP), but not sterol-resistant mutants Y298C or D443N. *Proc. Natl. Acad. Sci. U.S.A.* **95,** 12848–12853
29. Nohturfft, A., DeBose-Boyd, R. A., Scheek, S., Goldstein, J. L., and Brown, M. S. (1999) Sterols regulate cycling of SREBP cleavage-activating protein (SCAP) between endoplasmic reticulum and Golgi. *Proc. Natl. Acad. Sci. U.S.A.* **96,** 11235–11240
30. Goldstein, J. L., DeBose-Boyd, R. A., and Brown, M. S. (2006) Protein sensors for membrane sterols. *Cell* **124,** 35–46
31. Horton, J. D., Shah, N. A., Warrington, J. A., Anderson, N. N., Park, S. W., Brown, M. S., and Goldstein, J. L. (2003) Combined analysis of oligonucleotide microarray data from transgenic and knockout mice identifies direct SREBP target genes. *Proc. Natl. Acad. Sci. U.S.A.* **100,** 12027–12032
32. Seidah, N. G., Benjannet, S., Wickham, L., Marcinkiewicz, J., Jasmin, S. B., Stifani, S., Basak, A., Prat, A., and Chretien, M. (2003) The secretory proprotein convertase neural apoptosis-regulated convertase 1 (NARC-1): liver regeneration and neuronal differentiation. *Proc. Natl. Acad. Sci. U.S.A.* **100,** 928–933
33. Abifadel, M., Varret, M., Rabès, J. P., Allard, D., Ouguerram, K., Devillers, M., Cruaud, C., Benjannet, S., Wickham, L., Erlich, D., Derré, A., Villéger, L., Farnier, M., Beucler, I., Bruckert, E., *et al.* (2003) Mutations in PCSK9 cause autosomal dominant hypercholesterolemia. *Nat. Genet.* **34,** 154–156
34. Benjannet, S., Rhainds, D., Essalmani, R., Mayne, J., Wickham, L., Jin, W., Asselin, M. C., Hamelin, J., Varret, M., Allard, D., Trillard, M., Abifadel, M., Tebon, A., Attie, A. D., Rader, D. J., *et al.* (2004) NARC-1/PCSK9

and its natural mutants: zymogen cleavage and effects on the low density lipoprotein (LDL) receptor and LDL cholesterol. *J. Biol. Chem.* **279,** 48865–48875
35. Lagace, T. A., Curtis, D. E., Garuti, R., McNutt, M. C., Park, S. W., Prather, H. B., Anderson, N. N., Ho, Y. K., Hammer, R. E., and Horton, J. D. (2006) Secreted PCSK9 decreases the number of LDL receptors in hepatocytes and in livers of parabiotic mice. *J. Clin. Invest.* **116,** 2995–3005
36. Zhang, D. W., Lagace, T. A., Garuti, R., Zhao, Z., McDonald, M., Horton, J. D., Cohen, J. C., and Hobbs, H. H. (2007) Binding of proprotein convertase subtilisin/kexin type 9 to epidermal growth factor-like repeat A of low density lipoprotein receptor decreases receptor recycling and increases degradation. *J. Biol. Chem.* **282,** 18602–18612
37. Maxwell, K. N., and Breslow, J. L. (2004) Adenoviral-mediated expression of Pcsk9 in mice results in a low density lipoprotein receptor knockout phenotype. *Proc. Natl. Acad. Sci. U.S.A.* **101,** 7100–7105
38. Inui, M., Saito, A., and Fleischer, S. (1987) Purification of the ryanodine receptor and identity with feet structures of junctional terminal cisternae of sarcoplasmic reticulum from fast skeletal muscle. *J. Biol. Chem.* **262,** 1740–1747
39. Inui, M., and Fleischer, S. (1988) Purification of Ca^{2+} release channel (ryanodine receptor) from heart and skeletal muscle sarcoplasmic reticulum. *Methods Enzymol.* **157,** 490–505
40. Lai, F. A., Erickson, H. P., Rousseau, E., Liu, Q. Y., and Meissner, G. (1988) Purification and reconstitution of the calcium release channel from skeletal muscle. *Nature* **331,** 315–319
41. Chen, Y. F., Chiu, W. T., Chen, Y. T., Lin, P. Y., Huang, H. J., Chou, C. Y., Chang, H. C., Tang, M. J., and Shen, M. R. (2011) Calcium store sensor stromal-interaction molecule 1-dependent signaling plays an important role in cervical cancer growth, migration, and angiogenesis. *Proc. Natl. Acad. Sci. U.S.A.* **108,** 15225–15230
42. Jones, P. P., Jiang, D., Bolstad, J., Hunt, D. J., Zhang, L., Demaurex, N., and Chen, S. R. (2008) Endoplasmic reticulum Ca^{2+} measurements reveal that the cardiac ryanodine receptor mutations linked to cardiac arrhythmia and sudden death alter the threshold for store-overload-induced Ca^{2+} release. *Biochem. J.* **412,** 171–178
43. Cenedella, R. J. (2009) Cholesterol synthesis inhibitor U18666A and the role of sterol metabolism and trafficking in numerous pathophysiological processes. *Lipids* **44,** 477–487
44. Schuck, S., Prinz, W. A., Thorn, K. S., Voss, C., and Walter, P. (2009) Membrane expansion alleviates endoplasmic reticulum stress independently of the unfolded protein response. *J. Cell Biol.* **187,** 525–536
45. Benjannet, S., Hamelin, J., Chrétien, M., and Seidah, N. G. (2012) Loss- and gain-of-function PCSK9 variants: cleavage specificity, dominant negative effects, and low density lipoprotein receptor (LDLR) degradation. *J. Biol. Chem.* **287,** 33745–33755
46. Zaid, A., Roubtsova, A., Essalmani, R., Marcinkiewicz, J., Chamberland, A., Hamelin, J., Tremblay, M., Jacques, H., Jin, W., Davignon, J., Seidah, N. G., and Prat, A. (2008) Proprotein convertase subtilisin/kexin type 9 (PCSK9): hepatocyte-specific low density lipoprotein receptor degradation and critical role in mouse liver regeneration. *Hepatology* **48,** 646–654
47. Greeve, J., Altkemper, I., Dieterich, J. H., Greten, H., and Windler, E. (1993) Apolipoprotein B mRNA editing in 12 different mammalian species: hepatic expression is reflected in low concentrations of apoB-containing plasma lipoproteins. *J. Lipid Res.* **34,** 1367–1383
48. Song, Y. F., Luo, Z., Zhang, L. H., Hogstrand, C., and Pan, Y. X. (2016) Endoplasmic reticulum stress and disturbed calcium homeostasis are involved in copper-induced alteration in hepatic lipid metabolism in yellow catfish *Pelteobagrus fulvidraco*. *Chemosphere* **144,** 2443–2453
49. Poirier, S., Mamarbachi, M., Chen, W. T., Lee, A. S., and Mayer, G. (2015) GRP94 regulates circulating cholesterol levels through blockade of PCSK9-induced LDLR degradation. *Cell Rep.* **13,** 2064–2071
50. Chen, X. W., Wang, H., Bajaj, K., Zhang, P., Meng, Z. X., Ma, D., Bai, Y., Liu, H. H., Adams, E., Baines, A., Yu, G., Sartor, M. A., Zhang, B., Yi, Z., Lin, J., *et al.* (2013) SEC24A deficiency lowers plasma cholesterol through reduced PCSK9 secretion. *eLife* **2,** e00444
51. Amodio, G., Venditti, R., De Matteis, M. A., Moltedo, O., Pignataro, P., and Remondelli, P. (2013) Endoplasmic reticulum stress reduces COPII vesicle formation and modifies Sec23a cycling at ERESs. *FEBS Lett.* **587,** 3261–3266
52. Roubtsova, A., Chamberland, A., Marcinkiewicz, J., Essalmani, R., Fazel, A., Bergeron, J. J., Seidah, N. G., and Prat, A. (2015) PCSK9 deficiency unmasks a sex- and tissue-specific subcellular distribution of the LDL and VLDL receptors in mice. *J. Lipid Res.* **56,** 2133–2142
53. Basseri, S., Lhoták, S., Sharma, A. M., and Austin, R. C. (2009) The chemical chaperone 4-phenylbutyrate inhibits adipogenesis by modulating the unfolded protein response. *J. Lipid Res.* **50,** 2486–2501
54. Park, S. W., Moon, Y. A., and Horton, J. D. (2004) Post-transcriptional regulation of low density lipoprotein receptor protein by proprotein convertase subtilisin/kexin type 9a in mouse liver. *J. Biol. Chem.* **279,** 50630–50638
55. Grefhorst, A., McNutt, M. C., Lagace, T. A., and Horton, J. D. (2008) Plasma PCSK9 preferentially reduces liver LDL receptors in mice. *J. Lipid Res.* **49,** 1303–1311
56. Strøm, T. B., Tveten, K., and Leren, T. P. (2014) PCSK9 acts as a chaperone for the LDL receptor in the endoplasmic reticulum. *Biochem. J.* **457,** 99–105
57. Horton, J. D., Goldstein, J. L., and Brown, M. S. (2002) SREBPs: activators of the complete program of cholesterol and fatty acid synthesis in the liver. *J. Clin. Invest.* **109,** 1125–1131
58. Cheng, C., Ru, P., Geng, F., Liu, J., Yoo, J. Y., Wu, X., Cheng, X., Euthine, V., Hu, P., Guo, J. Y., Lefai, E., Kaur, B., Nohturfft, A., Ma, J., Chakravarti, A., and Guo, D. (2015) Glucose-mediated *N*-glycosylation of SCAP is essential for SREBP-1 activation and tumor growth. *Cancer Cell* **28,** 569–581
59. Volpe, J. J., and Goldberg, R. I. (1983) Effect of tunicamycin on 3-hydroxy-3-methylglutaryl coenzyme A reductase in C-6 glial cells. *J. Biol. Chem.* **258,** 9220–9226
60. Röhrl, C., Eigner, K., Winter, K., Korbelius, M., Obrowsky, S., Kratky, D., Kovacs, W. J., and Stangl, H. (2014) Endoplasmic reticulum stress impairs cholesterol efflux and synthesis in hepatic cells. *J. Lipid Res.* **55,** 94–103
61. Choi, S., Aljakna, A., Srivastava, U., Peterson, B. R., Deng, B., Prat, A., and Korstanje, R. (2013) Decreased APOE-containing HDL subfractions and cholesterol efflux capacity of serum in mice lacking Pcsk9. *Lipids Health Dis.* **12,** 112
62. Tran, H., Robinson, S., Mikhailenko, I., and Strickland, D. K. (2003) Modulation of the LDL receptor and LRP levels by HIV protease inhibitors. *J. Lipid Res.* **44,** 1859–1869
63. Holtzman, D. M., Herz, J., and Bu, G. (2012) Apolipoprotein E and apolipoprotein E receptors: normal biology and roles in Alzheimer disease. *Cold Spring Harb. Perspect. Med.* **2,** a006312
64. Rashid, S., Curtis, D. E., Garuti, R., Anderson, N. N., Bashmakov, Y., Ho, Y. K., Hammer, R. E., Moon, Y. A., and Horton, J. D. (2005) Decreased plasma cholesterol and hypersensitivity to statins in mice lacking Pcsk9. *Proc. Natl. Acad. Sci. U.S.A.* **102,** 5374–5379
65. Poirier, S., Mayer, G., Benjannet, S., Bergeron, E., Marcinkiewicz, J., Nassoury, N., Mayer, H., Nimpf, J., Prat, A., and Seidah, N. G. (2008) The proprotein convertase PCSK9 induces the degradation of low density lipoprotein receptor (LDLR) and its closest family members VLDLR and ApoER2. *J. Biol. Chem.* **283,** 2363–2372
66. Roubtsova, A., Munkonda, M. N., Awan, Z., Marcinkiewicz, J., Chamberland, A., Lazure, C., Cianflone, K., Seidah, N. G., and Prat, A. (2011) Circulating proprotein convertase subtilisin/kexin 9 (PCSK9) regulates VLDLR protein and triglyceride accumulation in visceral adipose tissue. *Arterioscler. Thromb. Vasc. Biol.* **31,** 785–791
67. Canuel, M., Sun, X., Asselin, M. C., Paramithiotis, E., Prat, A., and Seidah, N. G. (2013) Proprotein convertase subtilisin/kexin type 9 (PCSK9) can mediate degradation of the low density lipoprotein receptor-related protein 1 (LRP-1). *PLoS ONE* **8,** e64145
68. Jin, W., Wang, X., Millar, J. S., Quertermous, T., Rothblat, G. H., Glick, J. M., and Rader, D. J. (2007) Hepatic proprotein convertases modulate HDL metabolism. *Cell Metab.* **6,** 129–136
69. Chorba, J. S., and Shokat, K. M. (2014) The proprotein convertase subtilisin/kexin type 9 (PCSK9) active site and cleavage sequence differentially regulate protein secretion from proteolysis. *J. Biol. Chem.* **289,** 29030–29043

70. Gustafsen, C., Kjolby, M., Nyegaard, M., Mattheisen, M., Lundhede, J., Buttenschøn, H., Mors, O., Bentzon, J. F., Madsen, P., Nykjaer, A., and Glerup, S. (2014) The hypercholesterolemia-risk gene SORT1 facilitates PCSK9 secretion. *Cell Metab.* **19,** 310–318
71. Butkinaree, C., Canuel, M., Essalmani, R., Poirier, S., Benjannet, S., Asselin, M. C., Roubtsova, A., Hamelin, J., Marcinkiewicz, J., Chamberland, A., Guillemot, J., Mayer, G., Sisodia, S. S., Jacob, Y., Prat, A., and Seidah, N. G. (2015) Amyloid precursor-like protein 2 and sortilin do not regulate the PCSK9 convertase-mediated low density lipoprotein receptor degradation but interact with each other. *J. Biol. Chem.* **290,** 18609–18620
72. Seidah, N. G. (2015) The PCSK9 revolution and the potential of PCSK9-based therapies to reduce LDL-cholesterol. *Global Cardiology Science and Practice* **59,** 1–19
73. McNutt, M. C., Kwon, H. J., Chen, C., Chen, J. R., Horton, J. D., and Lagace, T. A. (2009) Antagonism of secreted PCSK9 increases low density lipoprotein receptor expression in HepG2 cells. *J. Biol. Chem.* **284,** 10561–10570
74. Kosenko, T., Golder, M., Leblond, G., Weng, W., and Lagace, T. A. (2013) Low density lipoprotein binds to proprotein convertase subtilisin/kexin type-9 (PCSK9) in human plasma and inhibits PCSK9-mediated low density lipoprotein receptor degradation. *J. Biol. Chem.* **288,** 8279–8288
75. Jiang, D., Wang, R., Xiao, B., Kong, H., Hunt, D. J., Choi, P., Zhang, L., and Chen, S. R. (2005) Enhanced store overload-induced Ca^{2+} release and channel sensitivity to luminal Ca^{2+} activation are common defects of RyR2 mutations linked to ventricular tachycardia and sudden death. *Circ. Res.* **97,** 1173–1181
76. Jiang, D., Jones, P. P., Davis, D. R., Gow, R., Green, M. S., Birnie, D. H., Chen, S. R., and Gollob, M. H. (2010) Characterization of a novel mutation in the cardiac ryanodine receptor that results in catecholaminergic polymorphic ventricular tachycardia. *Channels* **4,** 302–310
77. Merlie, J. P., Sebbane, R., Tzartos, S., and Lindstrom, J. (1982) Inhibition of glycosylation with tunicamycin blocks assembly of newly synthesized acetylcholine receptor subunits in muscle cells. *J. Biol. Chem.* **257,** 2694–2701
78. Kamisuki, S., Mao, Q., Abu-Elheiga, L., Gu, Z., Kugimiya, A., Kwon, Y., Shinohara, T., Kawazoe, Y., Sato, S., Asakura, K., Choo, H. Y., Sakai, J., Wakil, S. J., and Uesugi, M. (2009) A small molecule that blocks fat synthesis by inhibiting the activation of SREBP. *Chem. Biol.* **16,** 882–892
79. Hawkins, J. L., Robbins, M. D., Warren, L. C., Xia, D., Petras, S. F., Valentine, J. J., Varghese, A. H., Wang, I. K., Subashi, T. A., Shelly, L. D., Hay, B. A., Landschulz, K. T., Geoghegan, K. F., and Harwood, H. J., Jr. (2008) Pharmacologic inhibition of site 1 protease activity inhibits sterol regulatory element-binding protein processing and reduces lipogenic enzyme gene expression and lipid synthesis in cultured cells and experimental animals. *J. Pharmacol. Exp. Ther.* **326,** 801–808
80. Fullerton, M. D., Galic, S., Marcinko, K., Sikkema, S., Pulinilkunnil, T., Chen, Z. P., O'Neill, H. M., Ford, R. J., Palanivel, R., O'Brien, M., Hardie, D. G., Macaulay, S. L., Schertzer, J. D., Dyck, J. R., van Denderen, B. J., *et al.* (2013) Single phosphorylation sites in Acc1 and Acc2 regulate lipid homeostasis and the insulin-sensitizing effects of metformin. *Nat. Med.* **19,** 1649–1654
81. Gonzalez-Gronow, M., Gawdi, G., and Pizzo, S. V. (1993) Plasminogen activation stimulates an increase in intracellular calcium in human synovial fibroblasts. *J. Biol. Chem.* **268,** 20791–20795
82. Iwawaki, T., Akai, R., Kohno, K., and Miura, M. (2004) A transgenic mouse model for monitoring endoplasmic reticulum stress. *Nat. Med.* **10,** 98–102
83. Mayne, J., Dewpura, T., Raymond, A., Bernier, L., Cousins, M., Ooi, T. C., Davignon, J., Seidah, N. G., Mbikay, M., and Chrétien, M. (2011) Novel loss-of-function PCSK9 variant is associated with low plasma LDL cholesterol in a French-Canadian family and with impaired processing and secretion in cell culture. *Clin. Chem.* **57,** 1415–1423
84. Al-Hashimi, A. A., Caldwell, J., Gonzalez-Gronow, M., Pizzo, S. V., Aboumrad, D., Pozza, L., Al-Bayati, H., Weitz, J. I., Stafford, A., Chan, H., Kapoor, A., Jacobsen, D. W., Dickhout, J. G., and Austin, R. C. (2010) Binding of anti-GRP78 autoantibodies to cell surface GRP78 increases tissue factor procoagulant activity via the release of calcium from endoplasmic reticulum stores. *J. Biol. Chem.* **285,** 28912–28923
85. Fuller, M., Dadoo, O., Serkis, V., Abutouk, D., MacDonald, M., Dhingani, N., Macri, J., Igdoura, S. A., and Trigatti, B. L. (2014) The effects of diet on occlusive coronary artery atherosclerosis and myocardial infarction in scavenger receptor class B, type 1/low density lipoprotein receptor double knockout mice. *Arterioscler. Thromb. Vasc. Biol.* **34,** 2394–2403

Chapter 3: Soon to be Submitted to *Science Translational Medicine*

Caffeine Blocks SREBP2-induced Hepatic PCSK9 Expression to Enhance LDLR-Mediated Cholesterol Clearance.

Author Contributions: PFL, RCA and JM conceived the study and wrote the manuscript. JHB and PFL carried out all of the *in vitro* studies. PFL, JHB and KP carried out all of the *in vivo* studies. LJJ, SRWC, NGS revised the manuscript. RCA funding acquisition.

Title: Caffeine Blocks SREBP2-induced Hepatic PCSK9 Expression to Enhance LDLR-Mediated Cholesterol Clearance.

Authors: Paul. F. Lebeau[1], Jae Hyun. Byun[1], Khrystyna. Platko[1], Luke. J. Janssen[3], S. R. Wayne Chen[4], Nabil. G. Seidah[5], Jakob. Magolan[2] and Richard. C. Austin[1]*

Affiliations:

[1]Department of Medicine, Division of Nephrology, McMaster University, St. Joseph's Healthcare Hamilton and Hamilton Center for Kidney Research, Hamilton, Ontario L8N 4A6, Canada

[2] Department of Biochemistry and Biomedical Sciences, McMaster University, Hamilton, Ontario L8S 4L8, Canada

[3] Firestone Institute for Respiratory Health, St. Joseph's Hospital, Hamilton, ON, Canada

[4] Libin Cardiovascular Institute of Alberta, Department of Physiology and Pharmacology, University of Calgary, Calgary, Alberta T2N 2T9, Canada

[5] Laboratory of Biochemical Neuroendocrinology, Clinical Research Institute of Montreal, affiliated to the University of Montreal, Montreal, Quebec H2W 1R7, Canada

* To whom correspondence should be addressed: Dr. Richard C. Austin, 50 Charlton Ave East, Room T-3313, Hamilton, Ontario, L8N 4A6. Phone: 905-522-1155 x35175; Fax: 905-540-6589; E-mail: austinr@taari.ca

One Sentence Summary: Caffeine increases the SREBP2 binding capacity of ER resident GRP78 to promote hepatic LDL cholesterol clearance through the PCSK9-LDLR axis.

Abstract: Circulating proprotein convertase subtilisin/kexin type 9 (PCSK9) has emerged as a critical regulator of low-density lipoprotein (LDL) cholesterol, an established driver of cardiovascular disease (CVD), by enhancing the degradation of hepatic LDL receptor (LDLR). The transcription factor responsible for inducing PCSK9 expression, known as the sterol regulatory element-binding protein 2 (SREBP2), also contributes to a variety of pathologies by promoting *de novo* lipogenesis in a manner dependent on genes like *HMGCR*. In the present study, we demonstrate that caffeine (CF) and other agents capable of increasing endoplasmic reticulum (ER) Ca^{2+} levels block the activation of SREBP2 and subsequent expression and secretion of PCSK9 from hepatocytes. To explain these findings, we provide evidence that CF and other agents that increase ER Ca^{2+} levels enhance the ability of GRP78 to sequester the ER-resident precursor form of SREBP2, thereby preventing its re-localization and activation in the Golgi. By blocking its natural inhibitor, we also provide evidence that CF increases the expression and activity cell-surface hepatic LDLR and improves hepatocyte-mediated LDL clearance. Collectively our findings highlight ER Ca^{2+} as a master regulator of SREBP2 activation and identify a novel mechanism by which CF, as well as other Ca^{2+} modulating agents, affect circulating LDL cholesterol levels.

Introduction

The sterol regulatory element-binding proteins (SREBPs) play a central role in cellular lipid metabolism and homeostasis. They are activated by pathological cellular processes such as ER stress (1), inflammation (2), autophagy and apoptosis (3) and have been shown to contribute to a variety of disease states including dyslipidemia, CVD, obesity, type 2 diabetes, non-alcoholic steatohepatitis, chronic kidney disease and neurodegenerative diseases (3). Conventional and/or homeostatic signaling of the SREBPs begins at the luminal face of the ER. During conditions of lowered intracellular lipids, the sterol-sensing SREBP cleavage-activating protein (SCAP) releases its ER anchor, known as the insulin induced gene 1 (INSIG1) (4). The SCAP-SREBP complex then exits the ER, subsequently leading to the cleavage and activation of pre-mature SREBP in the Golgi by site-1 and -2 proteases (S1/2P). Mature SREBP1/2 then translocate to the nucleus, where they induce the expression of fatty acid and cholesterol regulatory genes by binding to sterol-regulatory elements (5). Our group has also demonstrated that unconventional signaling triggered by the loss of ER Ca^{2+}, a process known to promote ER stress, inflammation, autophagy and apoptosis (6), can also activate the SREBPs during pathophysiological processes (1, 7-9).

The ER is located in the perinuclear region of the cell and is the largest intracellular Ca^{2+} store, yielding intra-luminal concentrations of 100-800 μM (10). Key players in the maintenance of this state include the (a) sarco/endoplasmic reticulum ATP-ase (SERCA), responsible for pumping Ca^{2+} into the ER against the chemical gradient, and (b) the ryanodine receptors (RyRs) and inositol trisphosphate receptors (IP3Rs), responsible for leaking Ca^{2+} back into the cytosol for signaling purposes, as well as (c) ER-resident Ca^{2+}-binding proteins, such as GRP78, GRP94, calnexin and calreticulin, which act as buffers to increase ER Ca^{2+} retention capacity. Given that almost all cell-surface

and secretory proteins undergo proper folding and maturation in the ER, in a manner dependent on ER-resident Ca^{2+}-dependent chaperones, the maintenance of ER Ca^{2+} homeostasis is of vital importance (11). Failure to maintain this state of homeostasis reduces the polypeptide folding efficiency of these chaperones, thus causing an accumulation of misfolded proteins in the ER lumen; a state commonly referred to as ER stress and an established driver of cardiometabolic and neurodegenerative diseases (12). Interestingly, caffeine (CF), one of the most frequently consumed drugs in the world (13), is also an established modulator of intracellular Ca^{2+} (14) and was recently shown to block SREBP expression and activation (15).

1,3,7 trimethylxanthine, or CF, is best known as a stimulant alkaloid of the central nervous system found in various plants and is commonly consumed in the form of coffee or tea. The majority of published literature demonstrates that the average adult consumes between 400 and 600 mg/day and organizations like Health Canada and the Food and Drug Administration conclude that such doses are not *negatively* associated with toxicity, cardiovascular effects, bone status, calcium imbalance, behavior, incidence of cancer or effects on male fertility (14). On the contrary, accumulating evidence now suggests that moderate to high levels of CF (400 to >600 mg/day), consumed on a daily basis in the form of non-alcoholic beverages, are associated with a protective outcome on the cardiovascular system. Although biochemical studies have shown that CF increases intracellular Ca^{2+} levels and induces vasodilation of the vascular endothelium (13, 16), a cellular process known to be cardioprotective (17), molecular mechanisms supporting clinical evidence are currently lacking.

Among the many mRNA species known to be regulated by the self-induced SREBP2 transcription factor, the isoform of SREBP implicated in cholesterol homeostasis and CVD, are PCSK9, the LDLR and HMG-CoA reductase (HMGR) (18). Recent advancements in the therapies available for the management of dyslipidemia and CVD have led to the characterization of PCSK9 as a hepatocyte-secreted circulating factor capable of enhancing the degradation of cell-surface LDLR (19-22). By extension, PCSK9 also reduces the ability of metabolically active tissues, like the liver, to remove excess LDL cholesterol (LDLc) from the blood. Based on these seminal discoveries, anti-PCSK9 antibodies are now being administered to patients at high risk of CVD with great success, yielding an unprecedented 60-70% reduction of LDLc levels (23). Although efficacious, the high cost of manufacturing fully human anti-PCSK9 antibodies poses a limit to their availability to patients worldwide (24). Such circumstances warrant the need for additional studies examining the molecular mechanisms that modulate the expression and secretion of PCSK9 from hepatocytes, in order to develop novel and more cost-effective therapies.

Our group has previously demonstrated that the expression and secretion of PCSK9 from hepatocytes is strongly influenced by changes in ER Ca^{2+} (9). We now report that heightened ER Ca^{2+} levels increase the peptide binding capacity of ER-resident Ca^{2+}-dependent chaperones, like GRP78. In turn, we observed that CF and other agents known to increase ER Ca^{2+} levels enhance the interaction taking place between GRP78 and

SREBP2, thereby preventing the exit of SREBP2 from the ER and its transit into the Golgi for activation. As such, we found that CF blocked the expression and secretion of PCSK9 from hepatocytes by enhancing its retention in the ER resulting in increased LDLR-mediated LDL clearance. Collectively our findings provide new insights into the cellular mechanisms that regulate PCSK9 expression and also highlight a novel cellular pathway by which CF and other modulators or intracellular Ca^{2+} can protect against CVD.

Results

CF blocks PCSK9 expression and secretion in hepatocytes

Previous studies have demonstrated that CF blocks SREBP2 expression and activity (15). We therefore examined whether CF would also block the expression of a downstream target of SREBP2 transcriptional activity (18), and established driver of CVD, PCSK9 (25). To initiate our studies, cultured immortalized hepatocytes known to express and secrete PCSK9 (9), including HuH7 and HepG2 cells, as well as primary mouse- and primary human-hepatocytes (PMH and PHH, respectively), were treated with CF for 24 hours and assessed for PCSK9 expression via immunoblots and real-time PCR (Fig. 1 A to D). Consistent with our hypothesis, these initial experiments revealed that CF reduced protein and mRNA transcript levels of PCSK9. CF also attenuated PCSK9 expression resulting from the SERCA antagonist and established ER stress-inducing agent, thapsigargin (TG) (9). Given that sterol deprivation represents another well-established promoter of SREBP2 activation (9), cells were also treated with CF in the presence and absence of U18666A (U18) that depletes intracellular sterols. Similar to TG-treated cells, CF attenuated U18-induced PCSK9 expression; see Table 1 in supplemental materials for a list of compounds and mechanisms of action. Importantly, CF also blocked the secretion of PCSK9 from HuH7, HepG2 cultured hepatocytes, as well as in PMH and PHH (Fig. 1E, F and G). Control experiments were performed in order to confirm that CF was not interfering with the ELISA by measuring levels of recombinant PCSK9 in the presence or absence of CF added directly to the ELISA (Fig. S1). A Coomassie stain of electrophoretically-resolved media harvested from these cells was also used to confirm that CF was not affecting global protein secretion (Fig. 1H). These data demonstrate that CF causes a marked reduction of PCSK9 expression at the mRNA and protein levels in a variety of hepatocyte models.

CF blocks SREBP2 activation in hepatocytes

Our research group has previously demonstrated that ER stress, specifically resulting from the depletion of ER Ca^{2+}, promotes the activation of SREBP2 and expression of PCSK9 (1, 7, 9). We therefore examined the effect of CF on TG-induced SREBP2 activation. Consistent with previous studies (15), we observed that CF blocked the expression of SREBP2 in PMHs and PHHs, as well as in HepG2 cells (Fig. 2A to C). CF also blocked the expression of a downstream target of SREBP2 transcriptional activity in mouse hepatocytes, HMGR (Fig. 2A), as well as SREBP1, the isoform known to regulate fatty acid synthesis (Fig. 2D). The effect of CF on the expression of hepatocyte nuclear factor 1a, a liver-expressed transcription factor also known to regulate PCSK9 expression (26) was assessed but not did not

yield a significant difference in the absence of TG (Fig. S2A). SREBP2 activation and activity was then examined at the protein level in HuH7 cells transfected with a plasmid encoding GFP driven by the sterol regulatory element (SRE-GFP; Fig 2E, F and G). Consistent with real-time PCR data, we observed that CF blocked the nuclear/ activated isoform of SREBP2 (nSREBP2; ~60kDa) and the expression of SRE-driven GFP in the presence and absence of TG. GFP expression was also visualized via immunofluorescent staining and quantified using ImageJ Software. Immunofluorescent staining of SREBP2 in cells treated with TG in the presence and absence of CF also demonstrated that CF attenuates the re-localization of SREBP2 from the perinuclear region of the cell to the nucleus (Fig. 2H; nuclei containing activated SREBP2 are indicated by white arrows). Collectively, given the well-established role of SREBP2 in the transcriptional regulation of PCSK9, our data suggested that CF reduces PCSK9 expression and secretion due to an antagonism of *de novo* synthesis. In support of this, CF did not affect the secretion of cytomegalovirus (CMV)-driven PCSK9 in cells transfected with mammalian expression vector, suggesting that PCSK9 is not affected by CF at the protein level (Fig. S2B).

Previous studies have also shown that CF can promote the phosphorylation and activation of AMPK (15, 27), a liver-expressed kinase known to induce the inhibitory phosphorylation of SREBPs (28). Despite the observed increase in hepatic pAMPK levels in response to CF treatment in the livers of mice, as well as increased levels of a marker of AMPK activation (pACC; Fig. S3A), CF also blocked PCSK9 expression and secretion in PMHs isolated from a model of hepatic AMPK deficiency (*Ampkβ1*$^{-/-}$; Fig. S3B and C) (29). A similar result was also observed in hepatocytes treated with a pharmacologic agent known to increase ER Ca^{2+} levels by inducing SERCA pump activation, CDN1163 (CDN) (Fig. S3D and E) (30). Although several studies demonstrate that AMPK is a repressor of SREBP2, and that CF can activate AMPK, our data suggest that the CF blocks SREBP2 and PCSK9 in an AMPK independent manner.

ER Ca^{2+} modulates PCSK9 expression and secretion

Among the many intracellular effects of CF on the cell, its ability to increase intracellular Ca^{2+} levels is well-studied (13). Given that we previously demonstrated that ER Ca^{2+} depletion induced SREBP2 activation, in the present study we postulated that (a) CF may increase ER Ca^{2+} levels, and (b) other agents known to increase ER Ca^{2+} levels may also block SREBP2 activation and PCSK9 expression. To test this hypothesis, we first examined cytosolic Ca^{2+} levels in CF-treated cells using the high-affinity fluorescent Ca^{2+} indicator, Fura-2-AM. Consistent with previous studies, CF significantly increased cytosolic Ca^{2+} levels in immortalized hepatocytes (Fig. S4). ER Ca^{2+} levels were then examined in cells transfected with D1ER; a genetically-encoded ER-resident fluorescence resonance energy transfer (FRET)-based calreticulin chameleon Ca^{2+} sensor, which increases in fluorescence intensity upon Ca^{2+} binding (31). The low-affinity Ca^{2+} indicator, Mag-Fluo-4, was also utilized for the direct assessment of ER Ca^{2+} and increases in fluorescence intensity upon Ca^{2+} binding (32). The fluorescence intensity of cells treated with CF and control agents, TG and CDN, was assessed using a

fluorescent spectrophotometer and also visualized using a fluorescent microscope (Fig. 3A). In addition to heightened cytosolic Ca^{2+} levels, we also observed that CF increased ER Ca^{2+} levels. As expected, control agent CDN increased ER Ca^{2+} levels, whereas TG reduced ER Ca^{2+} levels. ER Ca^{2+} content was also assessed indirectly with the high affinity Ca^{2+} dye, fura-2-AM (Fig. 3B). HuH7 cells were pretreated with CF for 24 hours and subsequently exposed to a high dose of TG, which causes a spontaneous loss of ER Ca^{2+}. In response to this treatment, we observed that cells pretreated with CF exhibited increased ER Ca^{2+} efflux compared to cells treated with the vehicle control when exposed to TG. We also observed that the expression of calnexin, an ER-resident protein with high capacity for Ca^{2+} binding (33), was induced by CF and blocked by TG (Fig. 3C).

To further test our hypothesis that increasing ER Ca^{2+} blocks PCSK9 expression, we treated cells with a variety of well-established Ca^{2+}-modulating agents. At low dose (10 nM), ryanodine is known to facilitate ER Ca^{2+} loss by enhancing RyR-mediated Ca^{2+} transients, whereas high dose ryanodine (10 μM) is known to block RyR-mediated ER Ca^{2+} leakage (34). 2 APB also blocks the exit of ER Ca^{2+} by antagonizing IP3Rs (35). In contrast to these two agents that modulate ER Ca^{2+} release, CDN is an established allosteric activator of the SERCA pump and thus increases the entry of Ca^{2+} into the ER (30). Consistent with our hypothesis, we observed that high-dose ryanodine, 2 APB and CDN, blocked SREBP2 and PCSK9 on the mRNA transcript level in the presence or absence of TG (Fig. 3D to F). These agents also blocked the TG-induced expression of the Ca^{2+}-dependent chaperone, and ER stress marker, GRP78. Consistent with our previous studies, we also observed that ER Ca^{2+} depletion via TG and CPA treatment increased PCSK9 and SREBP2 expression (Fig. 3G and H). As expected, these established ER stress-inducing agents also increased the expression of GRP78.

Secreted PCSK9 levels in the media harvested from cells treated with Ca^{2+}-modulating agents were then assessed using ELISAs. Consistent with real-time PCR findings, we observed that high-dose ryanodine, CDN and 2 APB blocked PCSK9 secretion (Fig. 3I). Overexpression of calnexin and loss-of function ryanodine receptor variants ($RyR2^{E4872A}$ and $RyR2^{A4860G}$), which were previously shown to increase ER Ca^{2+} levels (34, 36), also blocked PCSK9 secretion (Fig. 3J and K). In contrast to its effect on PCSK9 mRNA transcript levels, we also observed that TG blocked PCSK9 secretion; an observation that was consistent with our previous study (9). Sterol deprivation via treatment with U18, which is not known to affect ER Ca^{2+} levels, also yielded findings consistent with our previous observations (9) and increased PCSK9 secretion (Fig. 3M). Finally, to confirm that CF blocked PCSK9 secretion in a Ca^{2+} dependent manner, experiments were repeated in HepG2 cells incubated in Ca^{2+}-deficient medium for 48 hours. We previously demonstrated that this treatment causes robust ER stress and likely explains the observed reduction of secreted PCSK9 levels in the absence of CF. Importantly, however, these data reveal that CF failed to antagonize PCSK9 secretion in cells that have been deprived of Ca^{2+}. Overall, these data provide strong evidence that ER Ca^{2+} levels not only affect the expression of ER stress markers,

but also regulate the cholesterol-regulatory proteins, PCSK9 and SREBP2.

Ca^{2+} increases the binding capacity of GRP78 for ER-resident SREBP2 and prevents its exit from the ER

GRP78 is among a number of Ca^{2+}-dependent chaperones that play a central role facilitating a chemical equilibrium that favors elevated Ca^{2+} levels in the ER lumen relative to the cytosol via direct binding/sequestration and buffering (37). It is estimated that GRP78 increases the Ca^{2+}-retaining ability of the ER by 25% (38). Given that chaperones increase ER Ca^{2+} levels, but are also Ca^{2+}-dependent in their capacity to bind and fold polypeptides, we investigated whether ER Ca^{2+} could modulate the ability of GRP78 to interact with ER-resident pre-mature SREBP2 (~125 kDa). In support of this notion, previous studies have demonstrated that (a) GRP78 is highly promiscuous in its client specificity (39), capable of binding to one site every 36 amino acids of a randomly generated peptide (40); (b) Ca^{2+} and ATP bind to GRP78 in a cooperative manner and that ATP is necessary for the peptide binding and folding abilities of this chaperone (41); and (c) overexpression of GRP78 can attenuate the activation SREBPs in response to ER stress (1).

To test our hypothesis that increasing ER Ca^{2+} levels enhances GRP78 peptide binding capacity, HuH7 cells were treated with either CDN, which increases ER Ca^{2+} levels, or TG which causes ER Ca^{2+} depletion. Following treatment, the interaction taking place between GRP78 and SREBP2 was examined via immunoprecipitation of the former. By affecting ER Ca^{2+} levels however, these agents also directly impact the expression and abundance of GRP78 compared to untreated cells. Therefore, assessment of the relative binding capacity GRP78 for SREBP2 between treatments required normalization of immunoprecipitations to equal levels of GRP78 (Fig. 4A). Following conditions of TG-induced ER Ca^{2+} depletion and stress, GRP78 lost its intrinsic ability to interact with pre-mature SREBP2. Conversely, increasing ER Ca^{2+} levels via CDN treatment enhanced the ability of GRP78 to interact with and sequester pre-mature SREBP2. Strikingly, we observed that CF-treated cells behaved much like that of CDN-treated cells, suggesting that CF also increases the SREBP2-binding capacity of GRP78. Consistent with immunoprecipitations, immunoblots of whole-cell lysates demonstrate that CF and CDN antagonized the activation and nuclear localization of SREBP2, whereas TG had the opposite effect (Fig. 4B).

To confirm that CF blocked SREBP2 activation in a manner dependent on GRP78, cells transfected with siRNA targeted against GRP78 (siGRP78) were also treated with CF. Our findings demonstrate that siGRP78 treatment significantly increased the mRNA and secreted forms of PCSK9, as well as the mRNA levels of SREBP2 (Fig. 4C and D). Consistent with our hypothesis, we also observed that CF failed to attenuate PCSK9 and SREBP2 mRNA expression or secreted PCSK9 levels in the presence of siGRP78 (Fig. 4D and E). The siRNA-mediated knockdown of GRP78 was confirmed via immunoblotting (Fig. 4F).

Because ER Ca^{2+} depletion induces a compensatory UPR activation, we also postulated that CF may attenuate UPR marker expression by increasing ER Ca^{2+} levels. Upon assessment of PHH treated with CF, we

observed a reduction in mRNA transcript levels of ER stress markers GRP78 and the activating transcription factor 4 (ATF4; Fig. 4G). Similar experiments were also carried out in cultured HuH7 cells (Fig. S5A and S5B), in which a reduction in the expression of pPERK, IRE1α, sXBP1, ATF4 and ATF6 was also observed via immunoblotting and real-time PCR. Reactive oxygen species production, a process known to occur during conditions of ER stress, was also attenuated by CF (Fig. 5H). In support of these findings, CF blocked the accumulation of thioflavin-T-stained misfolded protein aggregates and the expression of FLAG-sXBP1 in cells transfected with the ER activated indicator plasmid (42) (Fig. 4I-K). Collectively, these data support a model in which heightened ER Ca^{2+} levels promote chaperone function and efficiency, thereby leading to a reduction in chaperone abundance. While increasing the protein binding ability of chaperones, such as GRP78, CF also attenuates SREBP2-driven gene expression (Fig. 4L).

CF blocks hepatic ER chaperone expression and attenuates PCSK9 secretion in mice

Next, we assessed the effect of CF on UPR marker and PCSK9 expression/secretion in mice. Following IP injection of CF (50 mg/kg - 8 hours) we observed a significant reduction of circulating PCSK9 and triglyceride levels (Fig. 5A and B). A time-course experiment also revealed that CF treatment required 4 hours to significantly reduce plasma PCSK9 levels in mice (Fig. 5C). The protein and mRNA expression of UPR chaperones, GRP78, GRP94, IRE1a and CHOP was also assessed via immunohistochemical staining, immunoblots and real-time PCR in the livers of these mice. Consistent with our findings in cultured cells, CF reduced the expression of UPR markers (Fig. 5D to G). Similar to previous reports, we also observed an inverse correlation between plasma PCSK9 levels and the expression of hepatic cell-surface LDLR and CD36. Immunohistochemical staining intensities were quantified using ImageJ Software (Fig. 5J). Similar to CF, we also observed that CDN increased hepatic LDLR expression in mice (Fig. S5C. 50 mg/kg; IP; 8 h).

CF increases hepatic LDL uptake

It is well-established that PCSK9 enhances the degradation of the LDLR and reduces the capacity of hepatocytes to bind and internalized extracellular LDL cholesterol (25). We therefore postulated that CF and other agents that increase ER Ca^{2+} levels, may also increase LDL clearance. We started by confirming that CF increased the expression of PCSK9-regulated receptors in our cultured cell models using immunoblots (Fig. 6A). Next, we developed an assay whereby HepG2 cells plated in black clear-bottom 96-well plates were treated with agents for 24 hours and subsequently exposed to fluorescently-labelled DiI-LDL for 5 hours in FBS-free medium prior to analysis. The uptake and accumulation of DiI-LDL was then quantified using a fluorescent spectrophotometer (Molecular Devices). Interestingly, we observed that CF increased LDL uptake and that U18, an agent that increases secreted PCSK9 levels (Fig. 3M), reduced LDL uptake (Figure 6B). To confirm that CF increased LDL uptake in cultured hepatocytes in a manner dependent on PCSK9 inhibition, this experiment was repeated in HepG2 cells stably transfected with PCSK9 shRNA. Consistent with our hypothesis, CF treatment failed to significantly increase LDL uptake in

conditions of reduced PCSK9 levels (Fig 6C). Live-cell staining of LDLR was also performed in HepG2 cells exposed to DiI-LDL. Increased cell-surface LDLR, as well as intracellular DiI-LDL, was observed in CF-treated HepG2 cells compared to vehicle-treated cells using a fluorescent microscope.

We next examined the effect of CF on hepatic LDL uptake in mice, and whether the process also occurs in a PCSK9-dependent manner. Accordingly, *Pcsk9*$^{+/+}$ and *Pcsk9*$^{-/-}$ mice were treated with either CF or PBS-vehicle for 8 hours and fluorescently-labelled DiI-LDL cholesterol during the last hour prior to sacrifice. In line with our *in vitro* studies, we observed that CF increased hepatic cell-surface LDLR expression in the *Pcsk9*$^{+/+}$ mice, but did not increase LDLR expression in *Pcsk9*$^{-/-}$ mice (Fig. 6E). CF also increased hepatic DiI fluorescence intensity and reduced serum DiI fluorescence intensity in *Pcsk9*$^{+/+}$ mice, but failed to affect these parameters in *Pcsk9*$^{-/-}$ mice (Fig 6F). Hepatic cell-surface LDLR staining and DiI-LDL uptake were also examined using a fluorescent microscope (Figure 6G). Collectively, these data suggest that CF increases hepatic LDL clearance in a manner dependent on its ability to block PCSK9 secretion from hepatocytes.

CF reduces plasma PCSK9 levels in healthy human subjects

Given that CF is among the most commonly consumed pharmacologically active compounds in the world (14), we assessed its ability to affect PCSK9 levels in fasted healthy volunteers. Serum was collected prior to, as well as 2- and 4-hours post CF treatment (400 mg orally; ~ 5 mg/kg). Consistent with our observations in cultured hepatocytes and in mice, CF reduced plasma PCSK9 levels in healthy subjects by 25% (n=12) and 21% (n=8) at the 2- and 4-hour time points, respectively (Fig. 7A and B). Plasma PCSK9 levels were also examined control subjects that did not consume CF, to verify whether the additional 2 hours of fasting during the course of the experiment would alter PCSK9 levels. No significant difference was observed in this group (n=5; Fig. 7C).

Characterization of novel CF derivatives as antagonists of PCSK9

Our data demonstrate that CF antagonizes secreted PCSK9 levels in pre-clinical models, as well as in humans. Importantly, CF is a well-characterized compound known to have several health benefits with few adverse effects. Achieving an optimal level of PCSK9 inhibition absent of the neuro-excitatory effect of CF, however, may be a challenge for the long-term clinical application of these findings. To address this issue, a variety of caffeine derivates were screened in order to identify compounds with increased efficacy for PCSK9 inhibition; with the ultimate goal of providing patients with a lower dose to achieve significant PCSK9 inhibition while avoiding the undesired neuro-excitatory effect. We started by screening a variety xanthine-derived compounds for PCSK9 inhibition. Interestingly, a variety of CF metabolites, including theobromine and paraxanthine, as well as other xanthine derived compounds, such as PSB603, 8CD and 8CC, exhibited a dose-dependent reduction of mRNA expression and secreted levels of PCSK9 (Fig. 8A and B). Xanthine derivatives with electron withdrawing groups conjugated to the carbon most susceptible to metabolism by liver CYP450 enzymes were

also developed (Fig. 8C). Experiments done in HepG2 cells demonstrate that treatment with MRLA-1812 and MRLA-1820 yield an approximate 2-fold reduction of secreted PCSK9 levels compared to CF treatment at the same dose (Fig. 8D). Moreover, at a concentration of 100 nM, these novel compounds achieved similar levels of inhibition as CF at a dose of 100 μM. Assessment at the mRNA level reveal that a similar mode of action is taking place with these novel compounds, whereby antagonism of SREBP2 reduces de novo synthesis of PCSK9 (Fig. 8E). Similar to CF, we also observed that MRLA-1812 and MRLA-1820 do not exhibit cytotoxic properties on cultured HepG2 hepatocytes (Fig. 8F). Overall, these data demonstrate that a variety of xanthine-derived compounds exhibit potency for the antagonism of PCSK9 expression. We also demonstrate that subtle changes to the chemical structure of this backbone, such as those that protect the molecule from metabolism, can significantly increase potency.

Discussion

This report provides molecular insight into the mechanism by which pathological conditions known to affect ER Ca^{2+} levels can modulate the activation of SREBP2 and expression of PCSK9 in hepatocytes. We demonstrate that agents capable of increasing ER Ca^{2+} levels, such as CF, increase the binding capacity of the ER-resident chaperone GRP78 for SREBP2, which in turn prevents the transit of SREBP2 to the nucleus. Given that conditions of ER Ca^{2+} depletion and ER stress increase chaperone expression (12), the observed reduction of chaperone expression in hepatocytes treated with agents that increase ER Ca^{2+} levels also strongly suggests that these agents promote chaperone function and protect against ER stress. Beyond the direct effect of CF on GRP78, SREBP2 and PCSK9, we observed that CF increased cell-surface hepatic LDLR and also increased LDL uptake. Given that CF did not affect LDLR expression in the livers of *Pcsk9*$^{-/-}$ mice and also failed to promote LDL uptake in PCSK9 knockdown hepatocytes, our data also demonstrate that CF-mediated upregulation of the LDLR and subsequent LDL uptake, occurs in a PCSK9-dependent manner.

The effects of CF on the vascular system and CVD, have also been examined by others in the past. Given that CF consumption occurs primarily in the form of beverages that contain inconsistent doses and that are frequently mixed with adulterants such as dairy and sugar product, results from such studies can be difficult to interpret and often vary. A recent meta-analysis provides an in-depth summary of the current body literature existing on the effects of CF consumption on cardiovascular outcomes, including total CVD (43). Interestingly, the majority of studies examined, which generally ranged from thousands to hundreds of thousands of patients, demonstrated a protective effect of CF consumption against CVD. Daily CF consumption in these studies typically ranged between 400 and 600 mg/day.

CF is known to exert its effect through a range of molecular targets, including the antagonism of adenosine receptors, GABA receptors and phosphodiesterase enzymes, as well as inducing intracellular Ca^{2+} transients by enhancing RyR-mediated calcium-induced calcium release (CICR) (13). For this reason, the identification of exact molecular mechanisms pertaining to its protective effect

on the vascular system has be challenging. In support of the aforementioned clinical observations, CF has been shown to promote vasodilation of the vascular endothelium by means of stimulating Ca^{2+} release via CICR and leading to the activation of eNOS (44). In vascular smooth muscle cells, following CICR-induced vasodilation, CF also increases intracellular Ca^{2+} levels by inducing non-selective cation channels at the cell surface (45) and has been shown to block IP3Rs (46). These studies, as well as those of others (47, 48), are consistent with our observations that CF increases intracellular Ca^{2+} levels and attenuates ER stress. Collectively, however, there exists a range of mechanisms by which CF affects intracellular Ca^{2+} levels, which tend to differ between tissue and/or cell types. In hepatocytes, our data strongly suggest that CF increases cytosolic and ER Ca^{2+} levels following a 24-hour exposure (Fig. 4A and B).

The ER serves as an important and dynamic Ca^{2+} reserve, capable extruding Ca^{2+} for signaling and/or excitatory purposes and removing excess cytosolic Ca^{2+} following periods of excitement. The Ca^{2+} sequestering capacity of the ER, which far exceeds that of the cytosol, depends on the abundance of ER-resident low-affinity/high capacity Ca^{2+}-binding proteins (49). The interaction of Ca^{2+} with these proteins also promotes chaperone function. During conditions of ER Ca^{2+} depletion, chaperones lose of their folding capacity and misfolded polypeptides accumulate in the ER. The UPR, which increases the abundance of ER-resident chaperones, is then triggered in order to restore ER folding capacity and ER Ca^{2+} levels (50). Conversely, increasing ER Ca^{2+} levels appears to have a net protective effect on ER homeostasis, given the observed reduction in UPR marker expression by agents that activate SERCA and increase ER Ca^{2+} influx or those capable of blocking leakage from either IP3R or RyR (30, 51). Consistent with this observation, we also found that CF protects against TG-induced ER stress in cultured hepatocytes and reduces the expression of a variety of ER chaperones in the livers of mice (Fig. 6).

In addition to UPR chaperones, ER stress is also known to promote the activation and expression of the self-induced transcription factors that regulate the expression of fatty acid- and cholesterol-regulatory genes, SREBP-1 and -2 (52). Although the exact mechanism by which ER stress activates the SREBPs remains elusive (7), previous studies have suggested and/or demonstrated that (a) ER stress can reduce the expression of INSIG1, a negative regulator of the SREBPs (53), (b) ER stress-induced caspases can cleave and activate the SREBPs in a manner independent of conventional S1P activation in the Golgi and (54, 55) (c), GRP78 can dissociate from the SCAP-SREBP complex thus liberating SREBP from the constraints of the ER (56). We now report the novel finding that ER Ca^{2+} levels serve to fine-tune the peptide binding capacity of GRP78, thereby affecting the exit of its binding partners — such as pre-mature SREBP2 — from the ER (Fig. 5).

In addition to blocking SREBP2-mediated PCSK9 expression, we also observed that CF induced the protein expression of the LDLR and increased LDL uptake in cultured hepatocytes. Given that SREBP2 regulates *de novo* expression of PCSK9 and the LDLR, the observed induction of cell-surface LDLR in the face of SREBP2 inhibition likely occurs in response to the loss of circulating

PCSK9 levels. Several studies have demonstrated that with a half-life of five minutes (57), PCSK9 expression closely follows that of SREBP2 (58). In contrast, with a 144-fold increased half-life compared to PCSK9 (12 hours) (59), expression of the LDLR appears less dependent on *de novo* synthesis and more on factors that influence its stability at the cell surface, like circulating PCSK9. Because SREBP2 also induces the expression of HMGR, it is also possible that CF reduces circulating LDL cholesterol levels via inhibition of HMGR-mediated *de novo* cholesterol synthesis. However, given that HMGR inhibitors like statins cause sterol deprivation and subsequently activate SREBP2 and induce PCSK9 expression (60), it is unlikely that CF effectively blocks HMGR.

PCSK9 enhances the degradation of the LDLR and promotes the onset and progression of CVD, which represents one of most challenging and costly health care problems that society faces today (61). Developing our understanding of the regulatory mechanisms that modulate the expression and secretion of PCSK9 from hepatocytes, may aid in the development of novel anti-PCSK9 therapies that are more cost-effective than those that currently exist. Overall, our study provides evidence that small molecules like CF, capable of increasing ER Ca^{2+} levels, can block the activation of SREBP2 by enhancing GRP78 chaperone function and binding capacity. We also report that CF potently blocks the expression of PCSK9, a downstream target of SREBP2 transcriptional activity, in cultured hepatocytes, in mice and in healthy human subjects. By extension, we also observed that CF induced the expression of cell-surface hepatic LDLR and increased the uptake of LDL cholesterol. Our findings delineate a novel mechanism by which ER Ca^{2+} and its modulators can affect the expression and activity of proteins that play a central role CVD.

Methods and Materials

Cell culture, treatments and transfections

HuH7 and HepG2 cells were routinely grown in complete Dulbecco's Modified Eagle's Medium (Gibco, Thermofisher Scientific) supplemented with 10% fetal bovine serum (Sigma-Aldrich) and 50 U/ml of penecilin and streptomycin (Sigma-Aldrich). CF, ryanodine, 2 APB, CDN, theobromine, paraxanthine, 8-cyclopentyl-1,3-dimethylxanthine (8CD), 8-(3-Chlorostyryl) CF (8CC), PSB603, cyclopiazonic acid and U18666A were purchased from Tocris Bioscience. All cell treatments were carried out for 24 hours unless otherwise stated. Cells were transfected with a cocktail consisting of plasmid DNA (1 µg), X-tremeGENE HP (3 µl; Thermofisher Scientific) and opti-MEM (100 µl; Thermofischer Scientific) per 1 ml complete medium containing plated cells. Human PCSK9 was overexpressed using the bicistronic pIRES-EGFP plasmid; calnexin using the mPA-GFP-N1 plasmid.

Ca^{2+} studies: fluorogenic dyes and genetically encoded FRET-based sensors

Intracellular Ca^{2+} in Huh7 and HepG2 cells was measured using a high-affinity Ca^{2+} indicator, Fura-2-AM (Thermofisher Scientific). ER Ca^{2+} levels were assessed using the low-affinity Ca^{2+} indicator, Mag-Fluo-4, and via transfection of cells with D1ER. The D1ER plasmid encodes an ER-resident calcium binding protein linked to a

fluorescent protein and increases in fluorescence intensity upon Ca^{2+} binding (31). For assessment using indicators, cells were plated in black clear-bottom 96-well plates to a confluence of 70-75% and treated with Ca^{2+} modulating agents for 24 hours (n=6). Cells were then washed and incubated with Fura-2-AM (2 µM) or Mag-Fluo-4 (2uM) for 45 minutes at 37 ˚C in HBSS containing 20mM HEPES and 2% pluronic acid v/v (Thermofisher Scientific). Fluorescence intensity of intracellular Fura-2-AM was measured at two distinct wavelengths (ex 340/em 515 and ex 380/em 515), following three consecutive washes, to assess bound and unbound states using a SpectraMax GeminiEM fluorescent spectrophotometer (Molecular Devices, Sunnyvale, California, USA). Fluorescence intensity of Mag-Fluo-4 was quantified at a single wavelength (ex 495/em 515). For assessment using D1ER, HuH7 cells were plated in black clear-bottom 96-well plates to a confluence of 70-75% and transfected (n=6). 24 hours later, cells were treated with Ca^{2+} modulating agents for an additional 24 hours and quantified (ex 495/em 515) using a SpectraMax GeminiEM fluorescent spectrophotometer.

Immunoblot Analysis

Cells were washed in phosphate-buffered saline (PBS), lysed in 4X SDS-PAGE lysis buffer and separated on 7-10% polyacrylamide gels in denaturing conditions. Gels were transferred to nitrocellulose membranes using the BioRad mini trans-blot system,blocked in 5% skim milk in tris-buffered saline (TBS) for 1h and incubated in primary antibody overnight for 16h at 4 ˚C. Membranes were then exposed to horse radish peroxidase conjugated secondary antibodies and visualized using EZ-ECL chemiluminescent reagent (Froggabio). Band intensities were quantified using ImageJ software (BioRad) against membranes reprobed for house keeping proteins.

Immunoprecipitations

Cells were grown in 10 cm dishes were resuspended in ice cold non-denaturing immunoprecipitation buffer containing 20mM tris HCL, 137mM NaCl, 1% NP-40, 2mM EDTA and protease inhibitor (Roche). Total cell protein was normalized using a protein assay (BioRad) and 1mg of protein from each sample was incubated with 2 µg of capture antibody targeted against GRP78 (Santa Cruz Biotechnology; SC-1050) and rotated on a platform for 24h at 4˚C. Following incubation, samples were exposed to 100 µl of Protein G magnetic Surebeads (BioRad) for an additional 2h on a rotating platform at 4˚C. Beads conjugated to the anti-GRP78 antibody were subsequently isolated and the remaining sample was collected and labelled "input" for use as controls. The magnetic beads underwent 4 consecutive washes using the non-denaturing IP buffer and resuspended and boiled in 100 µl of 4X SDS-PAGE sample buffer.

Immunofluorescent Staining

Cells were plated in 4-well chamber slides and incubated in complete DMEM for 24h and exposed to treatments 24 hours later for an additional 24 hours. Cells were fixed with 4% paraformaldehyde for 30 minutes and washed with either non-permeabilizing, or permeabilizing PBS containing 0.025% Triton-X. Cells were then blocked with 1% bovine serum albumin (BSA) for 30 minutes and stained with anti-GFP antibody for 1h in

phosphate-buffed saline containing 1% BSA. Afterwards, cells were washed and incubated with Alexa 488 fluorescnetly-labelled secondary antibodies, as well as the DAPI nuclear stain. Slides were then mounted with permafluor and visualized using the EVOS FL colour imaging system at either 20 or 40X magnification.

Thioflavin-T Staining

Following treatment, live cells were incubated in complete DMEM containing 5 µM Thioflavin-T (ThT; Thermofisher Scientific) for 15 minutes. Cells were then fixed in 4% paraformaldehyde and mounted with permafluor. Fluorescent staining was visualized using the EVOS FL colour system at either 20 or 40X magnification.

Immunohistochemical staining

Liver tissues were fixed in formaldehyde and subsequently embedded in paraffin for sectioning. 4 µM thick sections underwent epitope retrieval and were subsequently stained with primary antibodies for 16h at 4 ˚C. Slides were then exposed to biotin-conjugated secondary antibodies for 45 minutes and then streptavidin peroxidase for 10 minutes. Staining was visualized using the Nova Red HRP Substrate (Vector Laboratories). See supplemental Materials and Methods for a complete list of antibodies and epitope retrieval procedures.

Quantitative Real-Time PCR

RNA purification/isolation was performed using RNeasy mini kits (Qiagen) and normalized to 2 µg RNA using a NanoDrop spectrophotometer. Samples were then reverse transcribed into cDNA using Superscript Vilo cDNA Synthesis kit (Thermofisher Scientific). Real-time PCR was executed with Fast SYBR Green (Thermo Fisher Scientific) using the ΔΔct method on the ViiA7 real-time PCR platform (Thermofisher Scientific).

ELISAs

Secreted PCSK9 levels were assessed directly in cell culture medium of cells grown in FBS-free medium for 24h or in the serum isolated from either mice or human subjects. Mouse PCSK9 was measured using the Quantikinine ELISA kit (#MCP900, R&D Systems) and human PCSK9 using the PCSK9 Quantikinine ELISA kit (#DCP900, R&D Systems). Serum samples were diluted as per manufacturer's instructions.

Mouse studies and primary hepatocyte isolation

All animal studies were carried out in fasted male wild-type, *Pcsk9*$^{-/-}$ or *Ampkβ1*$^{-/-}$ mice on the C57BL/6J background and were performed in strict accordance with the McMaster University animal care guidelines. CF (25-100 mg/kg - 8 hours) and CDN (50 mg/kg) treatments were administered via intraperitoneal injection. Primary mouse hepatocytes were isolated using a two-step process with EGTA (500 M in HEPES buffer, Sigma Aldrich) and collagenase (0.05% in HEPES buffer, Sigma Aldrich) in 12-week-old male mice on the C57BL/6J background. Cells were then washed, centrifuged, and plated following isolation in cell strainers. Hepatosure 100-donor pooled primary human hepatocytes were purchased from Xenotech. Primary hepatocytes were regularly grown in William's E medium (Gibco, Thermo Fisher Scientific) containing 10% fetal bovine

serum, 100 IU/ml penicillin, and 100g/ml streptomycin.

DiI-LDL uptake assay

Cells were seeded plated in black clear-bottom 96-well plates for 24 hours and treated with experimental agents for an additional 24 hours. During the last 5 hours of treatment (hour 19 to 24) cells were exposed to DiI-LDL (10 μg/ml) and then washed with two changes of pre-warmed (37 ˚C) HBSS containing 20 mM HEPES prior to analysis. The intracellular fluorescence intensity of DiI was then quantified using the SpectraMax GeminiEM fluorescent spectrophotometer (Molecular Devices; ex 554/em 571).

CF studies in healthy human subjects

Healthy human subjects between the ages of 22 and 45 underwent fasting for 12 hours prior to oral administration of CF (5 mg/kg). Blood was collected prior to administration and at hour 2 and 4 following administration. All patients completed and signed consent forms and studies were approved by the Hamilton Integrated Research Ethics Board, project number 5805.

Statistics

Statistical analysis for differences between experimental groups was performed using two-tailed unpaired Student's *t*-test. The paired Student's *t*-test was used to compared pre- and post-treatment values in human subjects. Differences between groups were considered significant at $p<0.05$ and all values are expressed as mean ± SD.

References

1. G. H. Werstuck, S. R. Lentz, S. Dayal, G. S. Hossain, S. K. Sood, Y. Y. Shi, J. Zhou, N. Maeda, S. K. Krisans, M. R. Malinow, R. C. Austin, Homocysteine-induced endoplasmic reticulum stress causes dysregulation of the cholesterol and triglyceride biosynthetic pathways. *J Clin Invest* **107**, 1263-1273 (2001).
2. L. Plantier, V. Besnard, Y. Xu, M. Ikegami, S. E. Wert, A. N. Hunt, A. D. Postle, J. A. Whitsett, Activation of sterol-response element-binding proteins (SREBP) in alveolar type II cells enhances lipogenesis causing pulmonary lipotoxicity. *J Biol Chem* **287**, 10099-10114 (2012).
3. H. Shimano, R. Sato, SREBP-regulated lipid metabolism: convergent physiology - divergent pathophysiology. *Nature reviews. Endocrinology* **13**, 710-730 (2017).
4. J. Sakai, E. A. Duncan, R. B. Rawson, X. Hua, M. S. Brown, J. L. Goldstein, Sterol-regulated release of SREBP-2 from cell membranes requires two sequential cleavages, one within a transmembrane segment. *Cell* **85**, 1037-1046 (1996).
5. J. D. Horton, J. L. Goldstein, M. S. Brown, SREBPs: activators of the complete program of cholesterol and fatty acid synthesis in the liver. *J Clin Invest* **109**, 1125-1131 (2002).
6. D. Mekahli, G. Bultynck, J. B. Parys, H. De Smedt, L. Missiaen, Endoplasmic-reticulum calcium depletion and disease. *Cold Spring Harbor perspectives in biology* **3**, (2011).
7. S. M. Colgan, D. Tang, G. H. Werstuck, R. C. Austin, Endoplasmic reticulum stress causes the activation of sterol regulatory element binding protein-2. *Int J Biochem Cell Biol* **39**, 1843-1851 (2007).
8. S. Lhotak, S. Sood, E. Brimble, R. E. Carlisle, S. M. Colgan, A. Mazzetti, J. G. Dickhout, A. J. Ingram, R. C. Austin, ER stress contributes to renal proximal tubule injury by increasing SREBP-2-mediated lipid accumulation and apoptotic cell death. *Am J Physiol Renal Physiol* **303**, F266-278 (2012).
9. P. Lebeau, A. Al-Hashimi, S. Sood, S. Lhotak, P. Yu, G. Gyulay, G. Pare, S. R. Chen, B. Trigatti, A. Prat, N. G. Seidah, R. C. Austin, Endoplasmic Reticulum Stress and Ca2+ Depletion Differentially Modulate the Sterol Regulatory Protein PCSK9 to Control Lipid Metabolism. *J Biol Chem* **292**, 1510-1523 (2017).
10. A. Carreras-Sureda, P. Pihan, C. Hetz, Calcium signaling at the endoplasmic reticulum: fine-tuning stress responses. *Cell calcium* **70**, 24-31 (2018).
11. M. Michalak, J. M. Robert Parker, M. Opas, Ca2+ signaling and calcium binding chaperones of the endoplasmic reticulum. *Cell calcium* **32**, 269-278 (2002).
12. R. C. Austin, The unfolded protein response in health and disease. *Antioxid Redox Signal* **11**, 2279-2287 (2009).
13. D. Echeverri, F. R. Montes, M. Cabrera, A. Galan, A. Prieto, Caffeine's Vascular Mechanisms of Action. *International journal of vascular medicine* **2010**, 834060 (2010).
14. D. Turnbull, J. V. Rodricks, G. F. Mariano, F. Chowdhury, Caffeine and cardiovascular health. *Regulatory toxicology and pharmacology : RTP* **89**, 165-185 (2017).
15. H. Y. Quan, D. Y. Kim, S. H. Chung, Caffeine attenuates lipid accumulation via activation of AMP-activated protein kinase signaling pathway in HepG2 cells. *BMB reports* **46**, 207-212 (2013).

16. R. Zucchi, S. Ronca-Testoni, The sarcoplasmic reticulum Ca2+ channel/ryanodine receptor: modulation by endogenous effectors, drugs and disease states. *Pharmacol Rev* **49**, 1-51 (1997).
17. M. Khazaei, F. Moien-Afshari, I. Laher, Vascular endothelial function in health and diseases. *Pathophysiology : the official journal of the International Society for Pathophysiology* **15**, 49-67 (2008).
18. J. D. Horton, N. A. Shah, J. A. Warrington, N. N. Anderson, S. W. Park, M. S. Brown, J. L. Goldstein, Combined analysis of oligonucleotide microarray data from transgenic and knockout mice identifies direct SREBP target genes. *Proc Natl Acad Sci U S A* **100**, 12027-12032 (2003).
19. M. Abifadel, M. Varret, J. P. Rabes, D. Allard, K. Ouguerram, M. Devillers, C. Cruaud, S. Benjannet, L. Wickham, D. Erlich, A. Derre, L. Villeger, M. Farnier, I. Beucler, E. Bruckert, J. Chambaz, B. Chanu, J. M. Lecerf, G. Luc, P. Moulin, J. Weissenbach, A. Prat, M. Krempf, C. Junien, N. G. Seidah, C. Boileau, Mutations in PCSK9 cause autosomal dominant hypercholesterolemia. *Nat Genet* **34**, 154-156 (2003).
20. N. G. Seidah, S. Benjannet, L. Wickham, J. Marcinkiewicz, S. B. Jasmin, S. Stifani, A. Basak, A. Prat, M. Chretien, The secretory proprotein convertase neural apoptosis-regulated convertase 1 (NARC-1): liver regeneration and neuronal differentiation. *Proc Natl Acad Sci U S A* **100**, 928-933 (2003).
21. S. Benjannet, D. Rhainds, R. Essalmani, J. Mayne, L. Wickham, W. Jin, M. C. Asselin, J. Hamelin, M. Varret, D. Allard, M. Trillard, M. Abifadel, A. Tebon, A. D. Attie, D. J. Rader, C. Boileau, L. Brissette, M. Chretien, A. Prat, N. G. Seidah, NARC-1/PCSK9 and its natural mutants: zymogen cleavage and effects on the low density lipoprotein (LDL) receptor and LDL cholesterol. *J Biol Chem* **279**, 48865-48875 (2004).
22. K. N. Maxwell, J. L. Breslow, Adenoviral-mediated expression of Pcsk9 in mice results in a low-density lipoprotein receptor knockout phenotype. *Proc Natl Acad Sci U S A* **101**, 7100-7105 (2004).
23. M. S. Sabatine, R. P. Giugliano, A. C. Keech, N. Honarpour, S. D. Wiviott, S. A. Murphy, J. F. Kuder, H. Wang, T. Liu, S. M. Wasserman, P. S. Sever, T. R. Pedersen, F. S. Committee, Investigators, Evolocumab and Clinical Outcomes in Patients with Cardiovascular Disease. *N Engl J Med* **376**, 1713-1722 (2017).
24. D. S. Kazi, J. Penko, P. G. Coxson, A. E. Moran, D. A. Ollendorf, J. A. Tice, K. Bibbins-Domingo, Updated Cost-effectiveness Analysis of PCSK9 Inhibitors Based on the Results of the FOURIER Trial. *JAMA* **318**, 748-750 (2017).
25. N. G. Seidah, M. Abifadel, S. Prost, C. Boileau, A. Prat, The Proprotein Convertases in Hypercholesterolemia and Cardiovascular Diseases: Emphasis on Proprotein Convertase Subtilisin/Kexin 9. *Pharmacol Rev* **69**, 33-52 (2017).
26. Dong, M. Wu, H. Li, F. B. Kraemer, K. Adeli, N. G. Seidah, S. W. Park, J. Liu, Strong induction of PCSK9 gene expression through HNF1alpha and SREBP2: mechanism for the resistance to LDL-cholesterol lowering effect of statins in dyslipidemic hamsters. *J Lipid Res* **51**, 1486-1495 (2010).

27. S. Tsuda, T. Egawa, K. Kitani, R. Oshima, X. Ma, T. Hayashi, Caffeine and contraction synergistically stimulate 5'-AMP-activated protein kinase and insulin-independent glucose transport in rat skeletal muscle. *Physiological reports* **3**, (2015).
28. Y. Li, S. Xu, M. M. Mihaylova, B. Zheng, X. Hou, B. Jiang, O. Park, Z. Luo, E. Lefai, J. Y. Shyy, B. Gao, M. Wierzbicki, T. J. Verbeuren, R. J. Shaw, R. A. Cohen, M. Zang, AMPK phosphorylates and inhibits SREBP activity to attenuate hepatic steatosis and atherosclerosis in diet-induced insulin-resistant mice. *Cell metabolism* **13**, 376-388 (2011).
29. N. Dzamko, B. J. van Denderen, A. L. Hevener, S. B. Jorgensen, J. Honeyman, S. Galic, Z. P. Chen, M. J. Watt, D. J. Campbell, G. R. Steinberg, B. E. Kemp, AMPK beta1 deletion reduces appetite, preventing obesity and hepatic insulin resistance. *J Biol Chem* **285**, 115-122 (2010).
30. S. Kang, R. Dahl, W. Hsieh, A. Shin, K. M. Zsebo, C. Buettner, R. J. Hajjar, D. Lebeche, Small Molecular Allosteric Activator of the Sarco/Endoplasmic Reticulum Ca2+-ATPase (SERCA) Attenuates Diabetes and Metabolic Disorders. *J Biol Chem* **291**, 5185-5198 (2016).
31. A. E. Palmer, C. Jin, J. C. Reed, R. Y. Tsien, Bcl-2-mediated alterations in endoplasmic reticulum Ca2+ analyzed with an improved genetically encoded fluorescent sensor. *Proc Natl Acad Sci U S A* **101**, 17404-17409 (2004).
32. B. P. Diercks, R. Fliegert, A. H. Guse, Mag-Fluo4 in T cells: Imaging of intra-organelle free Ca(2+) concentrations. *Biochimica et biophysica acta. Molecular cell research* **1864**, 977-986 (2017).
33. D. B. Williams, Beyond lectins: the calnexin/calreticulin chaperone system of the endoplasmic reticulum. *J Cell Sci* **119**, 615-623 (2006).
34. W. Chen, R. Wang, B. Chen, X. Zhong, H. Kong, Y. Bai, Q. Zhou, C. Xie, J. Zhang, A. Guo, X. Tian, P. P. Jones, M. L. O'Mara, Y. Liu, T. Mi, L. Zhang, J. Bolstad, L. Semeniuk, H. Cheng, J. Zhang, J. Chen, D. P. Tieleman, A. M. Gillis, H. J. Duff, M. Fill, L. S. Song, S. R. Chen, The ryanodine receptor store-sensing gate controls Ca2+ waves and Ca2+-triggered arrhythmias. *Nat Med* **20**, 184-192 (2014).
35. M. D. Bootman, T. J. Collins, L. Mackenzie, H. L. Roderick, M. J. Berridge, C. M. Peppiatt, 2-aminoethoxydiphenyl borate (2-APB) is a reliable blocker of store-operated Ca2+ entry but an inconsistent inhibitor of InsP3-induced Ca2+ release. *FASEB journal : official publication of the Federation of American Societies for Experimental Biology* **16**, 1145-1150 (2002).
36. W. A. Wang, W. X. Liu, S. Durnaoglu, S. K. Lee, J. Lian, R. Lehner, J. Ahnn, L. B. Agellon, M. Michalak, Loss of Calreticulin Uncovers a Critical Role for Calcium in Regulating Cellular Lipid Homeostasis. *Sci Rep* **7**, 5941 (2017).
37. H. Coe, M. Michalak, Calcium binding chaperones of the endoplasmic reticulum. *General physiology and biophysics* **28 Spec No Focus**, F96-F103 (2009).
38. J. P. Lievremont, R. Rizzuto, L. Hendershot, J. Meldolesi, BiP, a major chaperone protein of the endoplasmic reticulum lumen, plays a direct and important role in the storage of the rapidly exchanging pool of Ca2+. *J Biol Chem* **272**, 30873-30879 (1997).
39. G. C. Flynn, J. Pohl, M. T. Flocco, J. E. Rothman, Peptide-binding specificity of the molecular chaperone BiP. *Nature* **353**, 726-730 (1991).

40. S. Blond-Elguindi, S. E. Cwirla, W. J. Dower, R. J. Lipshutz, S. R. Sprang, J. F. Sambrook, M. J. Gething, Affinity panning of a library of peptides displayed on bacteriophages reveals the binding specificity of BiP. *Cell* **75**, 717-728 (1993).
41. J. Yang, M. Nune, Y. Zong, L. Zhou, Q. Liu, Close and Allosteric Opening of the Polypeptide-Binding Site in a Human Hsp70 Chaperone BiP. *Structure* **23**, 2191-2203 (2015).
42. T. Iwawaki, R. Akai, K. Kohno, M. Miura, A transgenic mouse model for monitoring endoplasmic reticulum stress. *Nat Med* **10**, 98-102 (2004).
43. M. Ding, S. N. Bhupathiraju, A. Satija, R. M. van Dam, F. B. Hu, Long-term coffee consumption and risk of cardiovascular disease: a systematic review and a dose-response meta-analysis of prospective cohort studies. *Circulation* **129**, 643-659 (2014).
44. Y. Hatano, K. Mizumoto, T. Yoshiyama, M. Yamamoto, H. Iranami, Endothelium-dependent and -independent vasodilation of isolated rat aorta induced by caffeine. *Am J Physiol* **269**, H1679-1684 (1995).
45. A. Guerrero, J. J. Singer, F. S. Fay, Simultaneous measurement of Ca2+ release and influx into smooth muscle cells in response to caffeine. A novel approach for calculating the fraction of current carried by calcium. *J Gen Physiol* **104**, 395-422 (1994).
46. L. Missiaen, J. B. Parys, H. De Smedt, I. Sienaert, H. Sipma, S. Vanlingen, K. Maes, K. Kunzelmann, R. Casteels, Inhibition of inositol trisphosphate-induced calcium release by cyclic ADP-ribose in A7r5 smooth-muscle cells and in 16HBE14o- bronchial mucosal cells. *Biochem J* **329 (Pt 3)**, 489-495 (1998).
47. T. Hosoi, K. Toyoda, K. Nakatsu, K. Ozawa, Caffeine attenuated ER stress-induced leptin resistance in neurons. *Neurosci Lett* **569**, 23-26 (2014).
48. R. J. Teng, X. Jing, T. Michalkiewicz, A. J. Afolayan, T. J. Wu, G. G. Konduri, Attenuation of endoplasmic reticulum stress by caffeine ameliorates hyperoxia-induced lung injury. *American journal of physiology. Lung cellular and molecular physiology* **312**, L586-L598 (2017).
49. J. Krebs, L. B. Agellon, M. Michalak, Ca(2+) homeostasis and endoplasmic reticulum (ER) stress: An integrated view of calcium signaling. *Biochem Biophys Res Commun* **460**, 114-121 (2015).
50. A. Gorlach, P. Klappa, T. Kietzmann, The endoplasmic reticulum: folding, calcium homeostasis, signaling, and redox control. *Antioxid Redox Signal* **8**, 1391-1418 (2006).
51. D. S. Luciani, K. S. Gwiazda, T. L. Yang, T. B. Kalynyak, Y. Bychkivska, M. H. Frey, K. D. Jeffrey, A. V. Sampaio, T. M. Underhill, J. D. Johnson, Roles of IP3R and RyR Ca2+ channels in endoplasmic reticulum stress and beta-cell death. *Diabetes* **58**, 422-432 (2009).
52. S. Basseri, R. C. Austin, ER stress and lipogenesis: a slippery slope toward hepatic steatosis. *Dev Cell* **15**, 795-796 (2008).
53. E. Bobrovnikova-Marjon, G. Hatzivassiliou, C. Grigoriadou, M. Romero, D. R. Cavener, C. B. Thompson, J. A. Diehl, PERK-dependent regulation of lipogenesis during mouse mammary gland development and adipocyte differentiation. *Proc Natl Acad Sci U S A* **105**, 16314-16319 (2008).
54. X. Wang, J. T. Pai, E. A. Wiedenfeld, J. C. Medina, C. A. Slaughter, J. L. Goldstein, M. S. Brown, Purification of an interleukin-1 beta converting enzyme-related cysteine protease that

cleaves sterol regulatory element-binding proteins between the leucine zipper and transmembrane domains. *J Biol Chem* **270**, 18044-18050 (1995).
55. J. T. Pai, M. S. Brown, J. L. Goldstein, Purification and cDNA cloning of a second apoptosis-related cysteine protease that cleaves and activates sterol regulatory element binding proteins. *Proc Natl Acad Sci U S A* **93**, 5437-5442 (1996).
56. H. L. Kammoun, H. Chabanon, I. Hainault, S. Luquet, C. Magnan, T. Koike, P. Ferre, F. Foufelle, GRP78 expression inhibits insulin and ER stress-induced SREBP-1c activation and reduces hepatic steatosis in mice. *J Clin Invest* **119**, 1201-1215 (2009).
57. I. Giunzioni, H. Tavori, New developments in atherosclerosis: clinical potential of PCSK9 inhibition. *Vasc Health Risk Manag* **11**, 493-501 (2015).
58. K. K. Jensen, M. Tadin-Strapps, S. P. Wang, J. Hubert, Y. Kan, Y. Ma, D. G. McLaren, S. F. Previs, K. B. Herath, A. Mahsut, A. Liaw, S. Wang, S. J. Stout, C. Keohan, G. Forrest, D. Coelho, S. Yendluri, S. Williams, M. Koser, S. Bartz, K. O. Akinsanya, S. Pinto, Dose-dependent effects of siRNA-mediated inhibition of SCAP on PCSK9, LDLR, and plasma lipids in mouse and rhesus monkey. *J Lipid Res* **57**, 2150-2162 (2016).
59. Y. Wang, Y. Huang, H. H. Hobbs, J. C. Cohen, Molecular characterization of proprotein convertase subtilisin/kexin type 9-mediated degradation of the LDLR. *J Lipid Res* **53**, 1932-1943 (2012).
60. J. Mayne, T. Dewpura, A. Raymond, M. Cousins, A. Chaplin, K. A. Lahey, S. A. Lahaye, M. Mbikay, T. C. Ooi, M. Chretien, Plasma PCSK9 levels are significantly modified by statins and fibrates in humans. *Lipids in health and disease* **7**, 22 (2008).
61. N. G. Seidah, The PCSK9 revolution and the potential of PCSK9-based therapies to reduce LDL-cholesterol. *Global cardiology science & practice* **2017**, e201702 (2017).

Acknowledgements: pcDNA-D1ER was a gift from Amy Palmer & Roger Tsien (Addgene plasmid # 36325) and mPA-GFP-Calnexin-N-14 was a gift from Michael Davidson (Addgene plasmid # 57122). This work was supported in part by research grants to Richard C. Austin from the Heart and Stroke Foundation of Canada (G-13-0003064 and G-15-0009389), the Canadian Institutes of Health Research (74477), to Nabil G. Seidah from the Leducq Foundation (13 CVD 03), CIHR Foundation grant (148363) and Canada Research Chair (216684). Financial support from the Research Institute of St. Joseph's Healthcare Hamilton is acknowledged. Richard C. Austin is a Career Investigator of the Heart and Stroke Foundation of Ontario and holds the Amgen Canada Research Chair in the Division of Nephrology at St. Joseph's Healthcare and McMaster University.

Fig. 1. CF blocks PCSK9 expression and secretion in hepatocytes. (**A**) HuH7 cells were treated with established inducers of PCSK9 expression, TG (100 nM) or U18 (10 μM), in the presence or absence of CF (200 μM) for 24 hours. PCSK9 expression was assessed via immunoblot analysis. (**B-D**) PCSK9 expression was also assessed in PMH and PHH, as well as in HepG2 cells treated with CF and TG via real-time PCR. (**E-G**) PCSK9 ELISAs were carried on the medium harvested from CF-treated HuH7, HepG2, PMHs and PHH (*, $p<0.05$). (**H**) Coomassie blue staining of electrophoretically resolved medium harvested from CF-treated cells served to examine the effect of CF on total secreted protein levels. Values are presented as the mean and error bars as SD. *, $p<0.05$

Fig. 2. CF blocks SREBP2 activation in hepatocytes. (**A**) The effect of CF (200 μM) on SREBP2 and SREBP1 mRNA expression was examined in PMH in the presence and absence of TG (100 nM), an established activator of SREBPs. The downstream product of SREBP2 transcriptional activity, HMGR, was also examined. (**B, C**) The inhibitory effect of CF on SREBP2 was also examined in PHH and HepG2 cells. (**D**) CF-mediated SREBP1 inhibition was also examined in PMH (*, $p<0.05$). (**E-G**) HuH7 cells were transfected with a reporter construct encoding a sterol-regulatory element-driven green fluorescent protein (SRE-GFP). Cells were subsequently treated with CF (200 μM) and/or TG (100 nM) 24 hours later. GFP and nuclear (n)SREBP2 expression was examined via immunoblot analysis. GFP expression was also assessed via immunofluorescent staining, which was quantified using ImageJ. (**H**) The cellular localization of SREBP2 in CF- and TG-treated HuH7 cells was also examined via immunofluorescent staining. Nuclei containing activated SREBP2 are indicated by white arrows. Values are presented as the mean and error bars as SD. *, $p<0.05$. Scale bars; (G) 100 μm; (H) 20 μm.

Fig. 3. ER Ca^{2+} modulates PCSK9 expression and secretion. (**A**) HuH7 cells were either transfected with a FRET-based ER-resident Ca^{2+} sensor, D1ER, or pre-loaded with the low-affinity Ca^{2+} indicator, Mag-Fluo-4. Cells were subsequently treated with either TG (100 nM), CDN (100 μM) or CF (200 μM) for 24 hours. Fluorescence intensity was measured using a fluorescent spectrophotometer and visualized using a fluorescent microscope. (**B**) HuH7 cells were pre-treated with either CF or vehicle for 24 hours and loaded with the high-affinity Ca^{2+} dye, Fura-2-AM. Exposure of cells to a high dose of TG (1 mM) induced a spontaneous depletion of ER Ca^{2+} (*, $p<0.05$ vs. vehicle-treated). (**C**) The expression of an ER-resident Ca^{2+} binding protein, calnexin, was examined in CF- and TG-treated HuH7 cells using immunoblots. (**D-G**) PCSK9, SREBP2 and GRP78 mRNA expression was assessed in HuH7 cells treated with a variety of ER Ca^{2+} modulators including: ryanodine receptor agonist (ryanodine 10 nM), ryanodine receptor antagonist (ryanodine 10 μM), SERCA pump activator CDN (100 μM) and IP3R antagonist 2 APB (50 μm), in the presence and absence of TG (100 nM) for 24 hours. (**H**) mRNA transcript levels were also examined in HuH7 cells treated with SERCA pump inhibitors, TG (100 nM) and CPA (10 μM). (**I-K**) The effect of pharmacologic agents and plasmid-derived CMV-driven proteins, known to affect ER Ca^{2+} levels, on secreted PCSK9 levels was then examined using ELISAs. (**L,M**) Secreted PCSK9 levels were also examined in TG- and U18-treated cells. (**N**) The effect of CF on secreted PCSK9 levels was also examined in cells

incubated in Ca^{2+}-deficient medium. Values are presented as the mean and error bars as SD. *, $p<0.05$. Scale bars; 200 μm.

Fig. 4. ER Ca^{2+} regulates the interaction between GRP78 and SREBP2. **(A)** HuH7 cultured human hepatocytes were treated with control agents TG (100 nM), which causes ER Ca^{2+} depletion, or CDN (100 μM), a compound known to increase ER Ca^{2+} levels. The effect of CF (200 μM) was also assessed. 24 hours after treatment, a co-immunoprecipitation (IP) for GRP78 was carried out. Protein loading was normalized to GRP78 and relative co-immunoprecipitated SREBP2 was examined via immunoblots (IB). (**B**) The effect of CF, CDN and TG on the retention of ER-resident pre-mature SREBP2, and on the activated nuclear SREBP2 (nSREBP2), was also assessed via IB. (**C-E**) To confirm the role of GRP78 in CF-mediated PCSK9 inhibition, mRNA transcript and secreted protein levels were examined in HepG2 cells exposed to siRNA targeted against GRP78 (siGRP78). (**F**) Knockdown of GRP78 was confirmed via immunoblot analysis. (**G**) ER stress markers were assessed in PHH treated with CF 200 μM CDN (10 μM) via real-time PCR. (**H**) The effect of CF on reactive oxygen species production, resulting from the treatment of TG (100 nM), was also assessed in HuH7 cells (*, $p<0.05$ vs. vehicle-treated). (**I**) ER stress-induced amyloid deposition was examined using the fluorescent stain, Thioflavin-T. (**J,K**) HuH7 cells were transfected with the ER activated indicator plasmid encoding an ER stress-inducible FLAG-sXBP1. Staining intensity was using ImageJ software. (**L**) Model in which Ca^{2+} promotes the GRP78-mediated sequestration of SREBP2 in the ER. Values are presented as the mean and error bars as SD. (*, $p<0.05$).

Fig. 5. CF reduces chaperone expression and blocks hepatic PCSK9 expression in mice. 12-week-old male C57BL/6J mice were fasted and treated with CF (50 mg/kg) for 8 hours prior to sacrifice (n=6). (**A, B**) Plasma PCSK9 and triglyceride levels were measured using an ELISA and colorimetric assays, respectively. (**C**) The time-dependence of CF on plasma PCSK9 levels was also determined using an ELISA (n=5). (**D**) The livers of these mice were assessed for cell-surface expression of LDLR and CD36, as well as ER stress markers GRP78 and GRP94 via immunohistochemical staining. (**E**) Staining was quantified using ImageJ software. (**F, G**) The expression of the LDLR, as well as ER stress markers (GRP78, PERK and IRE1α) as well as cholesterol-regulatory genes (PCSK9, HMGR, SREBP1 and SREBP2) were also examined using immunoblots and real-time PCR. Values are presented as the mean and error bars as SD. (*, $p<0.05$). Scale Bars; 50 μm.

Fig. 6. CF increases hepatic LDL uptake in a PCSK9-dependent manner. (**A**) The expression of PCSK9-regulated receptors, LDLR and CD36, was examined in CF-treated cultured hepatocytes (200 μM). (**B**) The uptake and intracellular accumulation of fluorescently-labelled DiI-LDL was examined in cells treated with CF in the presence or absence of the PCSK9-inducer U18, using a fluorescent spectrophotometer. (**C**) The effect of CF treatment (200 μM) on DiI-labelled LDL uptake was also examined in PCSK9 shRNA knockdown cells (NS, non-significant). (**D**) Immunofluorescent staining of cell-surface LDLR was carried out in live CF pre-treated HepG2 cells (200 μM). Cellular DiI-LDL accumulation was also visualized in CF-treated HepG2 cells using a fluorescent microscope. *Pcsk9*$^{+/+}$ and *Pcsk9*$^{-/-}$ mice were treated with either PBS-vehicle

or CF, as well as fluorescently-labelled DiI-LDL (1 μg/kg). (**E**) Hepatic cell-surface LDLR expression was assessed via IHC and immunofluorescent staining. (**F, G**) Hepatic and serum DiI-LDL fluorescence intensity was quantified using a fluorescent spectrophotometer and visualized using a fluorescent spectrophotometer. Values are presented as the mean and error bars as SD. *, $p<0.05$; NS, non-significant. Scale bars; (D) 10 μm; (E) 50 μm; (G) 100 μm.

Fig. 7. CF reduces plasma PCSK9 levels in healthy volunteers. (**A, B**) Healthy subjects between the ages of 22 and 45 were administered 400 mg (~ 5 mg/kg) of CF following a 12-hour fasting period. Plasma PCSK9 levels were measured before administration, as well as 2- and 4-hours following administration (n=12 and n=5, respectively). (**C**) PCSK9 levels were also measure in a group of individuals (n=5) that were not administered CF to control for the 2 additional hours of fasting time during the experiment. Differences between groups were determined using a paired Student's *t*-test and error bars are presented as SD.

Fig. 8. Characterization of novel xanthine-derived compounds as PCSK9 inhibitors. (**A, B**) HepG2 cells were treated with increasing doses of CF metabolites, paraxanthine and theobromine, as well as xanthine derivatives PSB603, 8CD and 8CC. Secreted PCSK9 levels were assessed using ELISAs and mRNA transcript via real-time PCR. (**C**) A series of novel compounds were developed with the aim of increasing the inhibitory effect of CF on PCSK9 expression. Cells were treated with CF, as well as MLRA-1812 and MLRA-1820. (**D, E**) Secreted PCSK9, as well as PCSK9 mRNA and SREBP2 mRNA were assessed in these cells. (**F**) The cytotoxicity of these agents was examined using an LDH assay.

Figure 1. Lebeau et al., 2019

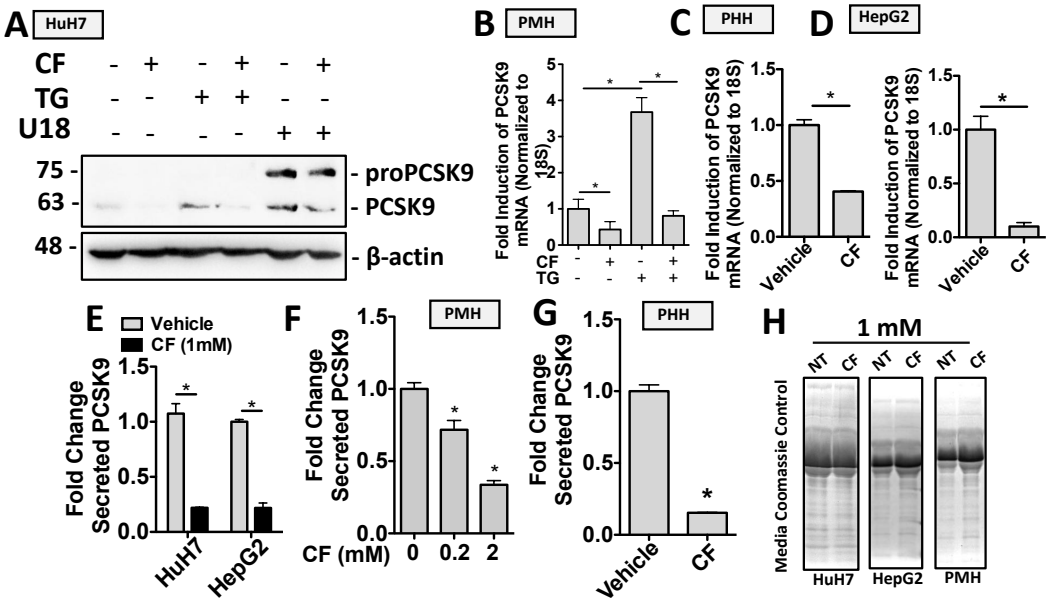

Figure 2. Lebeau et al., 2019

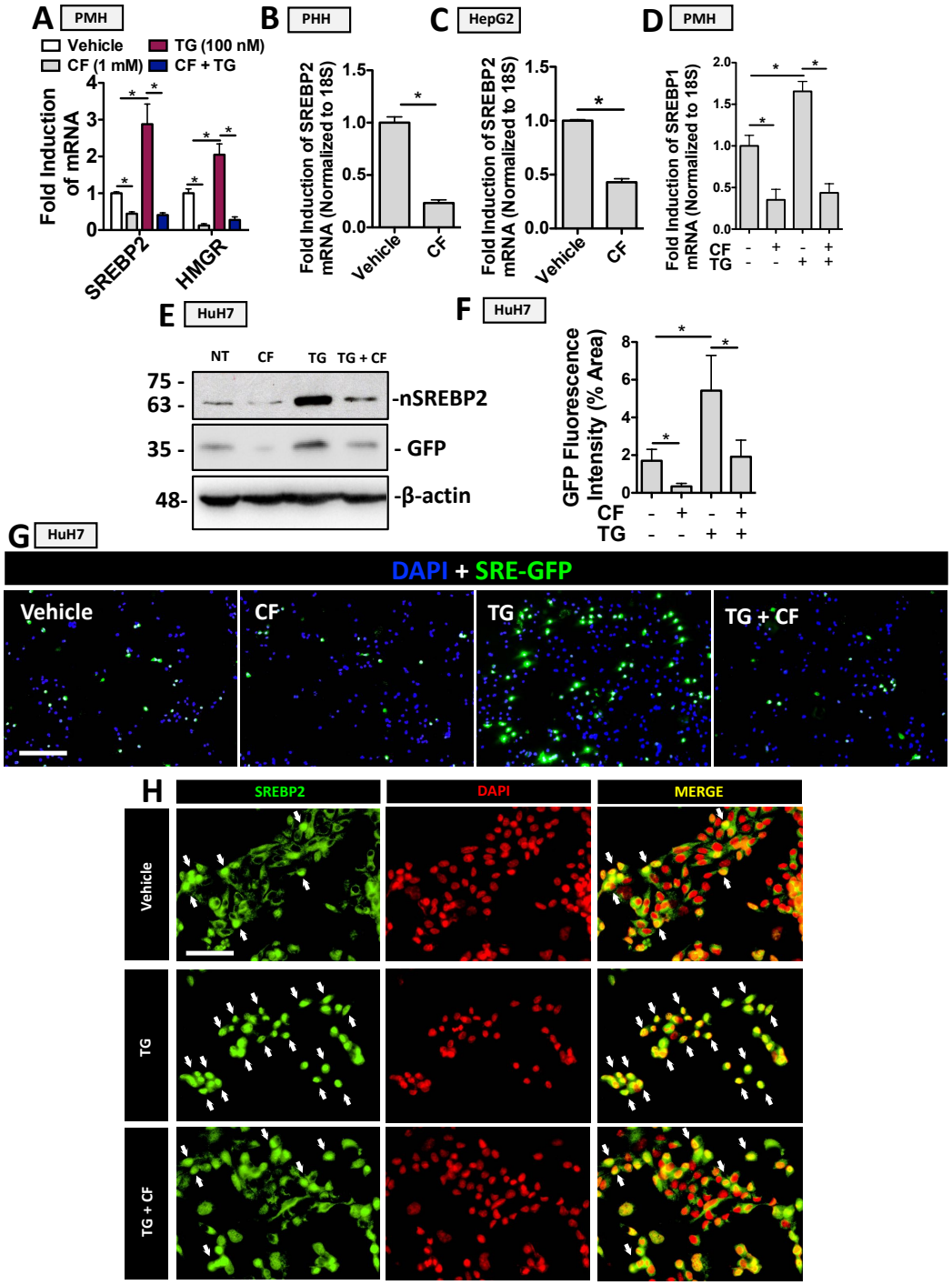

Figure 3. Lebeau et al., 2019

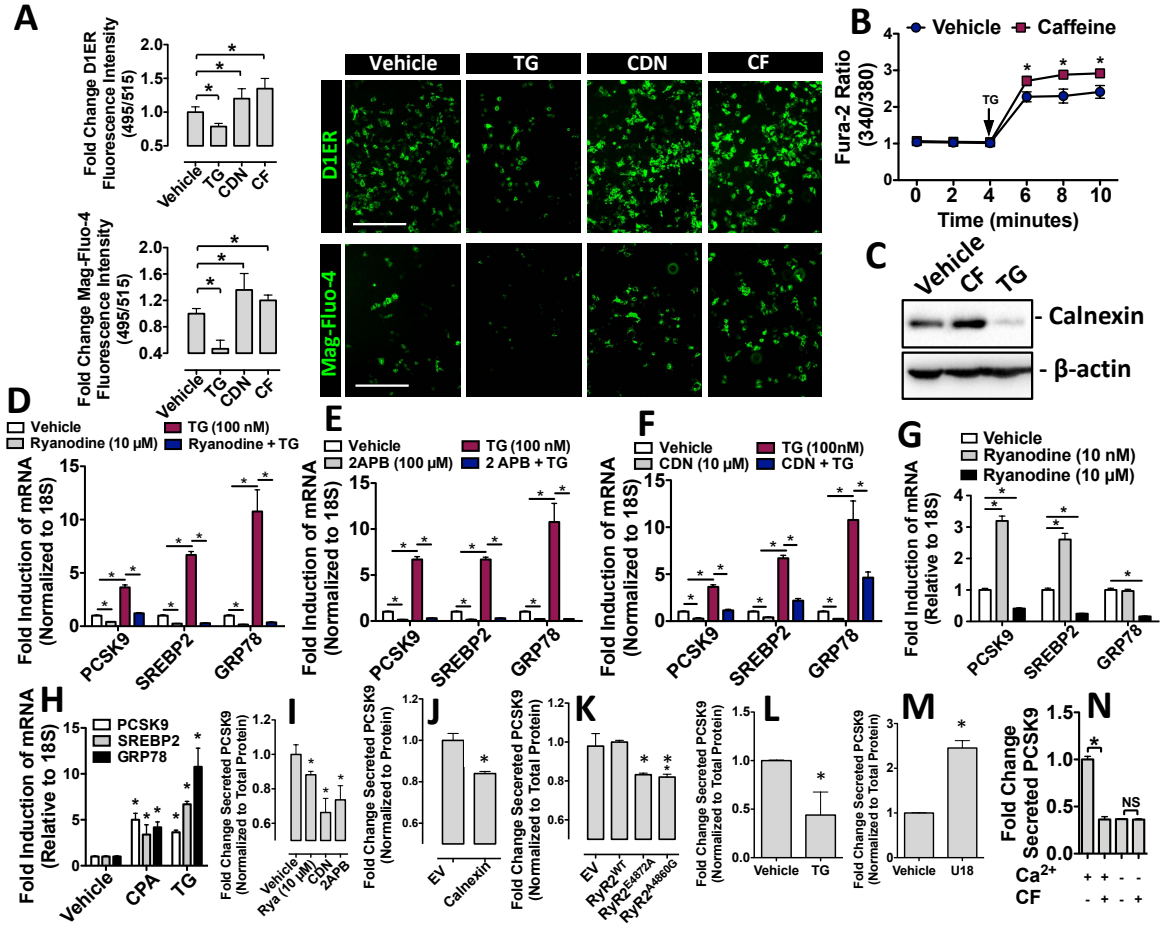

Figure 4. Lebeau et al., 2019

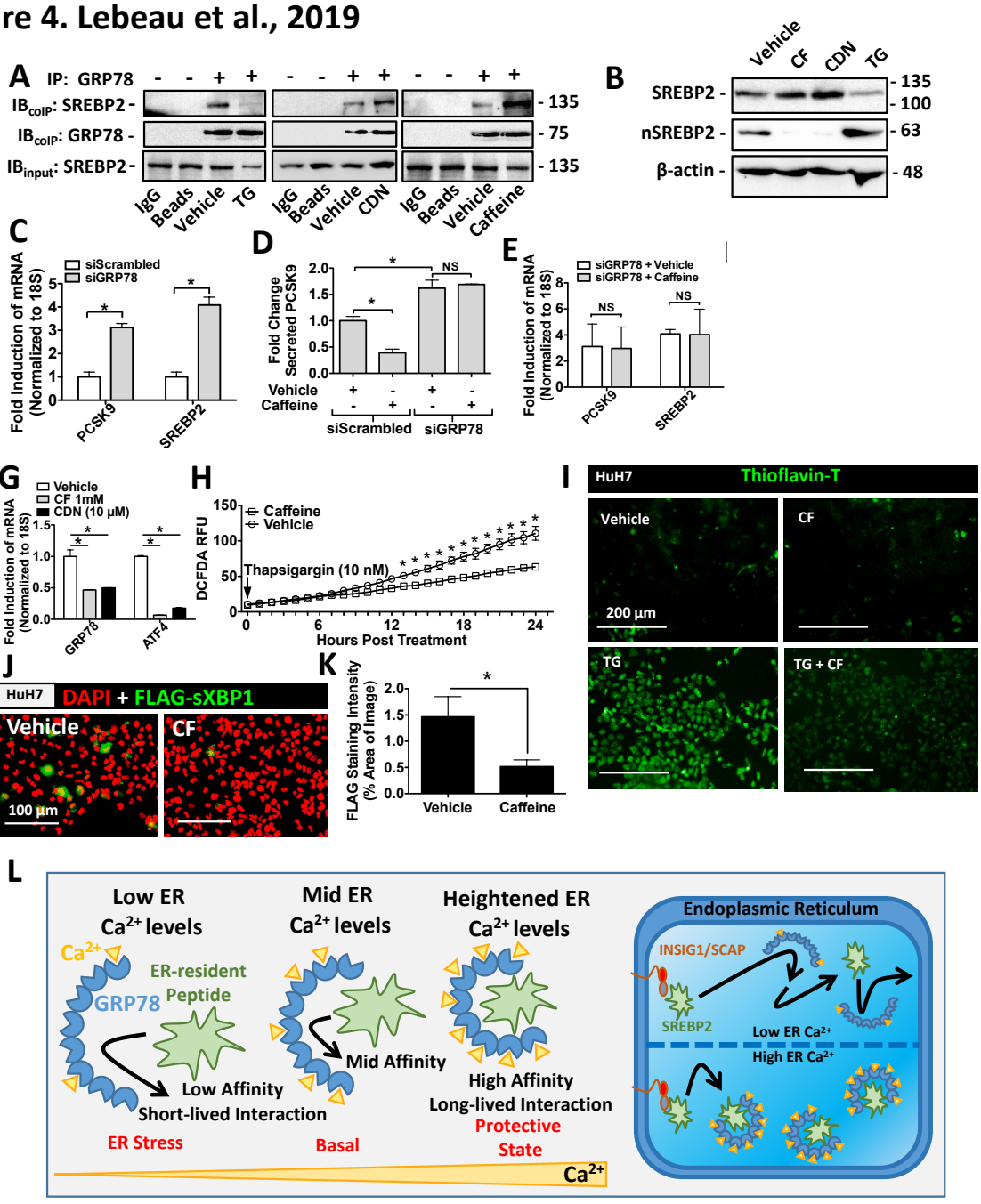

Figure 5. Lebeau et al., 2019

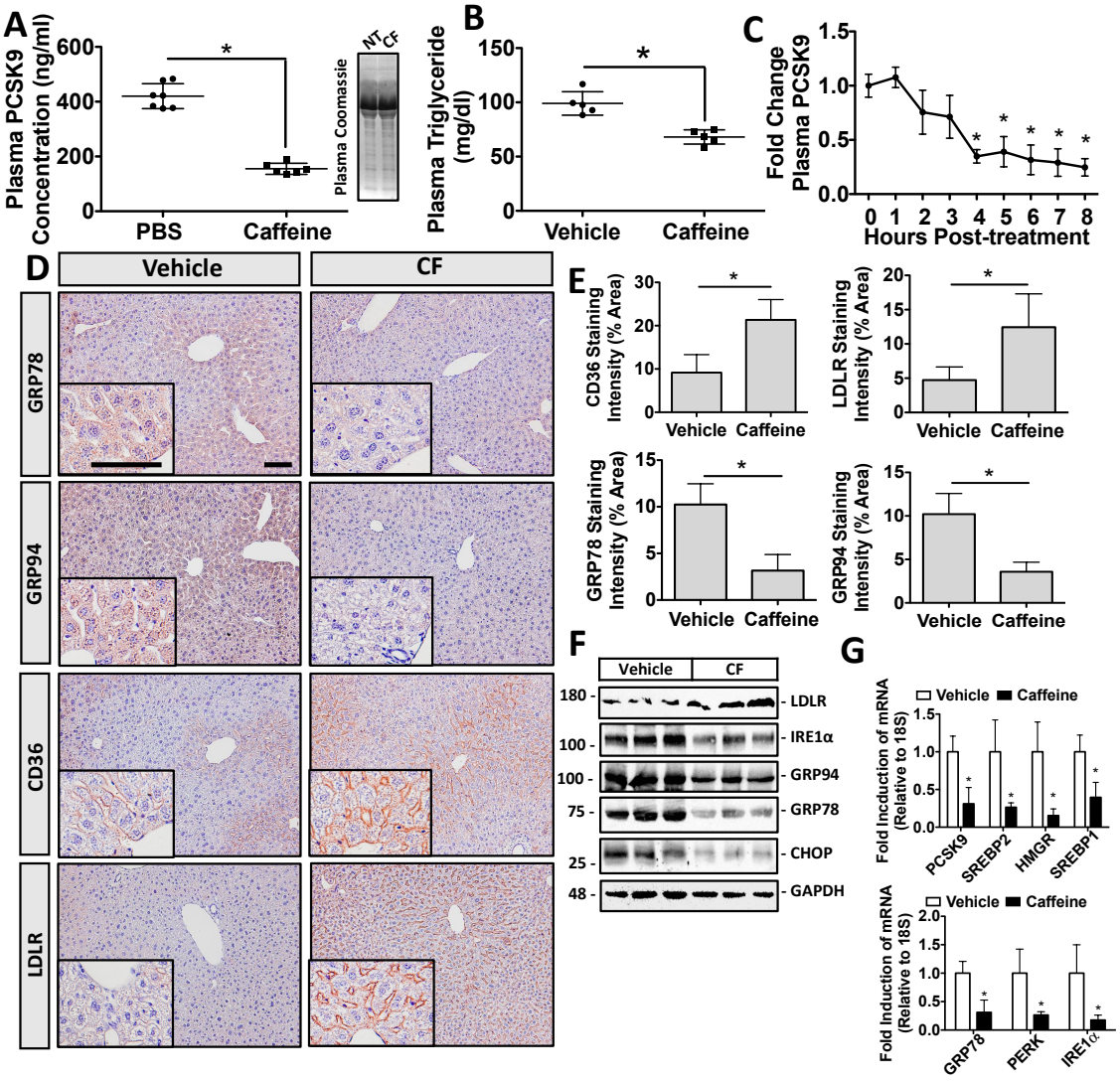

Figure 6. Lebeau et al., 2019

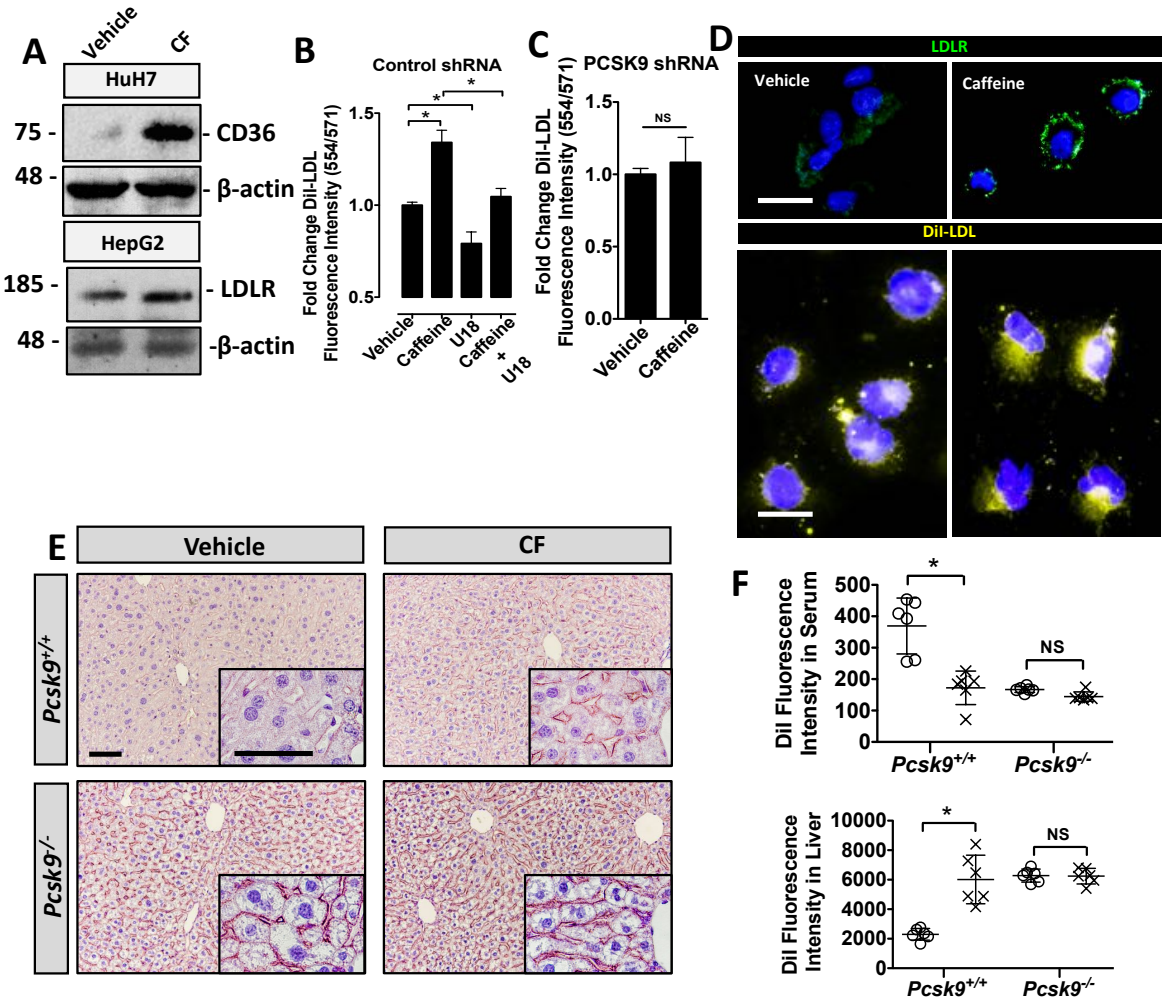

Figure 6. Lebeau et al., 2019

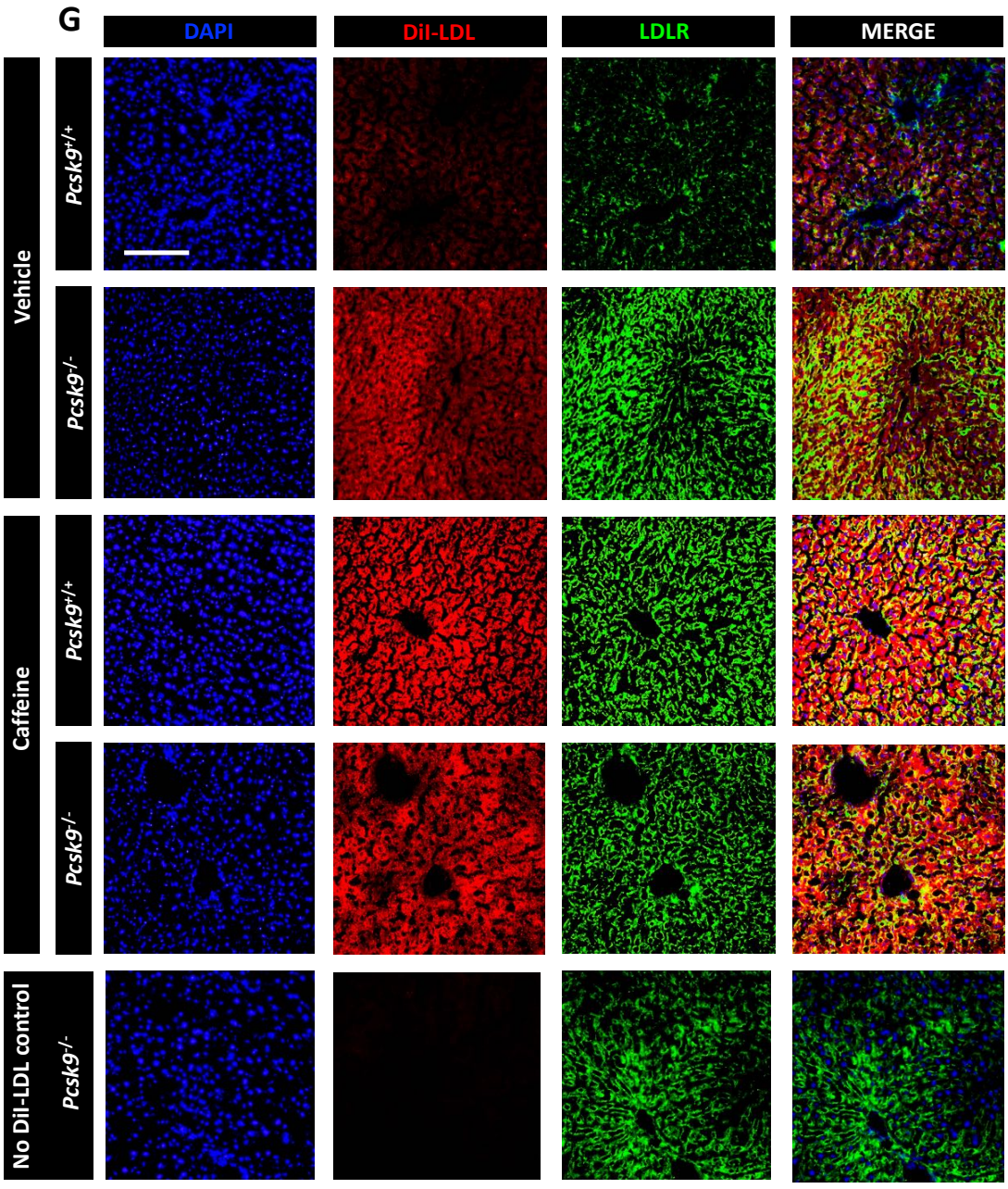

Figure 7.

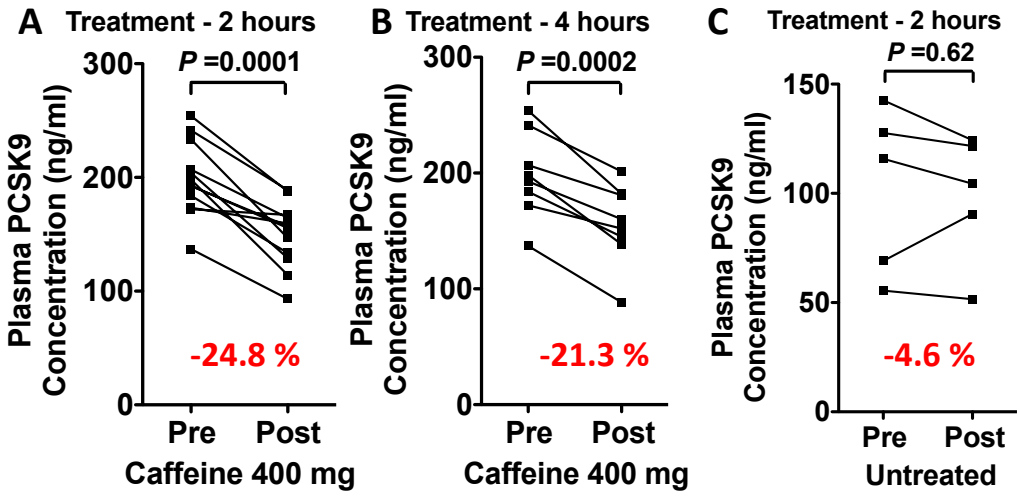
A
Treatment - 2 hours
P =0.0001
Plasma PCSK9 Concentration (ng/ml)
300
200
100
0
-24.8 %
Pre
Post
Caffeine 400 mg
B
Treatment - 4 hours
P =0.0002
Plasma PCSK9 Concentration (ng/ml)
300
200
100
0
-21.3 %
Pre
Post
Caffeine 400 mg
C
Treatment - 2 hours
P =0.62
Plasma PCSK9 Concentration (ng/ml)
150
100
50
0
-4.6 %
Pre
Post
Untreated

Figure 8. Lebeau et al., 2019

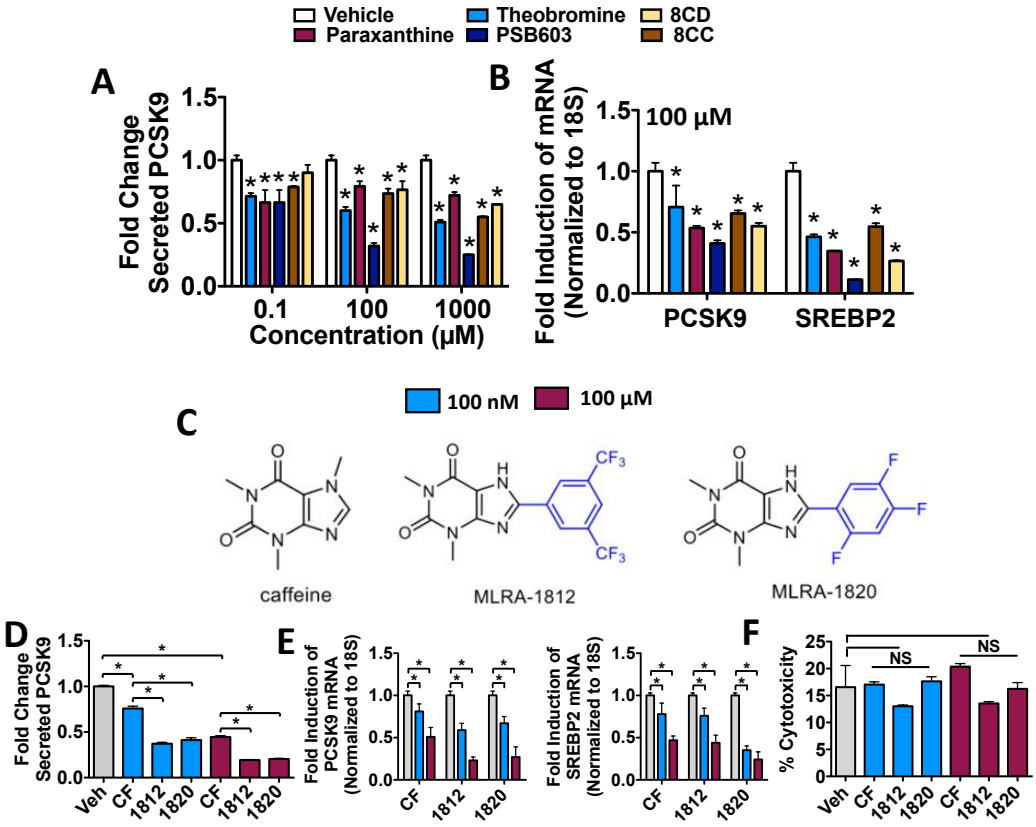

Supplementary Information

Title: Caffeine Blocks SREBP2-induced Hepatic PCSK9 Expression to Enhance LDLR-Mediated Cholesterol Clearance.

Figure Legends

Fig. S1. CF does not interfere with the PCSK9 ELISA. (A) A human PCSK9 ELISA was carried out on media harvested from HepG2 cells expressing PCSK9. CF was added directly into the ELISA at a concentration of 1 mM. NS, non-significant.

Fig. S2. CF does not affect CMV-driven PCSK9 expression. (A) The expression of the hepatocyte nuclear factor 1α was assessed in hepatocytes treated with CF in the presence or absence of the ER stress-inducing agents TG. **(B)** The effect of caffeine on secreted PCSK9 levels was examined in HepG2 cells transfected with a CMV-driven PCSK9 expression plasmid.

Fig. S3. CF blocks PCSK9 expression in a manner independent of AMPK (**A**) The livers of CF-treated mice (100 mg/kg - 8 hours) were examined for phosphorylated (p)AMPK and a downstream target of its activation, pACC. (**B,C**) CF-mediated inhibition of PCSK9 was tested in primary hepatocytes isolated from AMPKβ$^{-/-}$ via ELISA and real time PCR. (**D,E**) The effect of CDN on PCSK9 expression and secretion was also examined in AMPKβ$^{-/-}$ hepatocytes.

Fig. S4. CF increases cytosolic Ca^{2+} levels in cultured hepatocytes. Immortalized HuH7 cultured hepatocytes were loaded with the cytosolic Ca^{2+} dye, fura-2-AM, and subsequently treated with CF over a 24-hour time-course (*, $p<0.05$).

Fig. S5. CF protects against ER stress in cultured hepatocytes. (**A,B**) The effect of CF on ER stress marker expression in HuH7 cells was examined via immunoblots and real time PCR. (**C**) 12-week old C57BL/6J mice were treated with CDN 50 mg/kg and assessed for LDLR expression via immunohistochemical staining.

Table 1. Compounds used during the course of the study to block the expression and secretion of PCSK9 form hepatocytes.

Table 2. Structure activity relationship of CF and its derivatives on PCSK9 inhibition.

Fig. S1

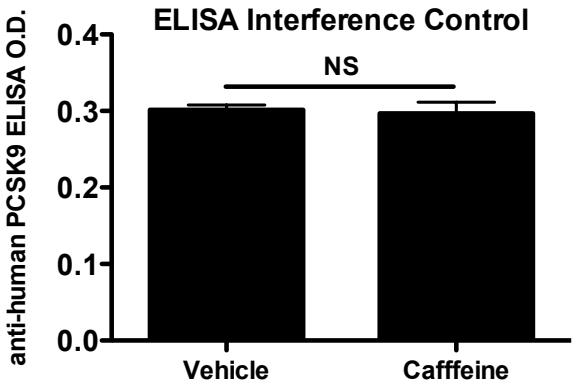
ELISA Interference Control
NS
anti-human PCSK9 ELISA O.D.
0.4
0.3
0.2
0.1
0.0
Vehicle
Cafffeine

Fig. S2.

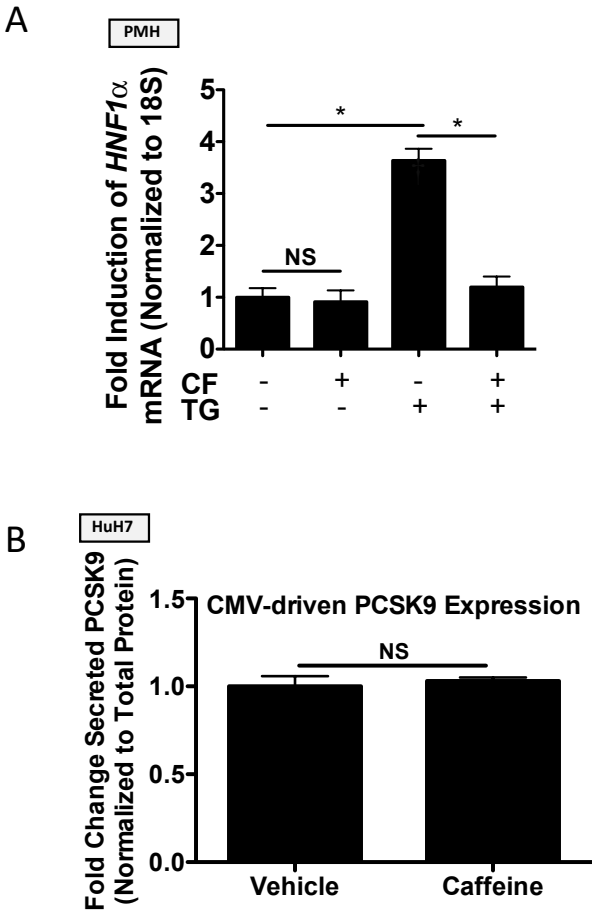
A
PMH
Fold Induction of HNF1α mRNA (Normalized to 18S)
5
4
3
2
1
0
*
*
NS
CF - + - +
TG - - + +
B
HuH7
Fold Change Secreted PCSK9 (Normalized to Total Protein)
CMV-driven PCSK9 Expression
1.5
1.0
0.5
0.0
NS
Vehicle
Caffeine

Fig. S3.

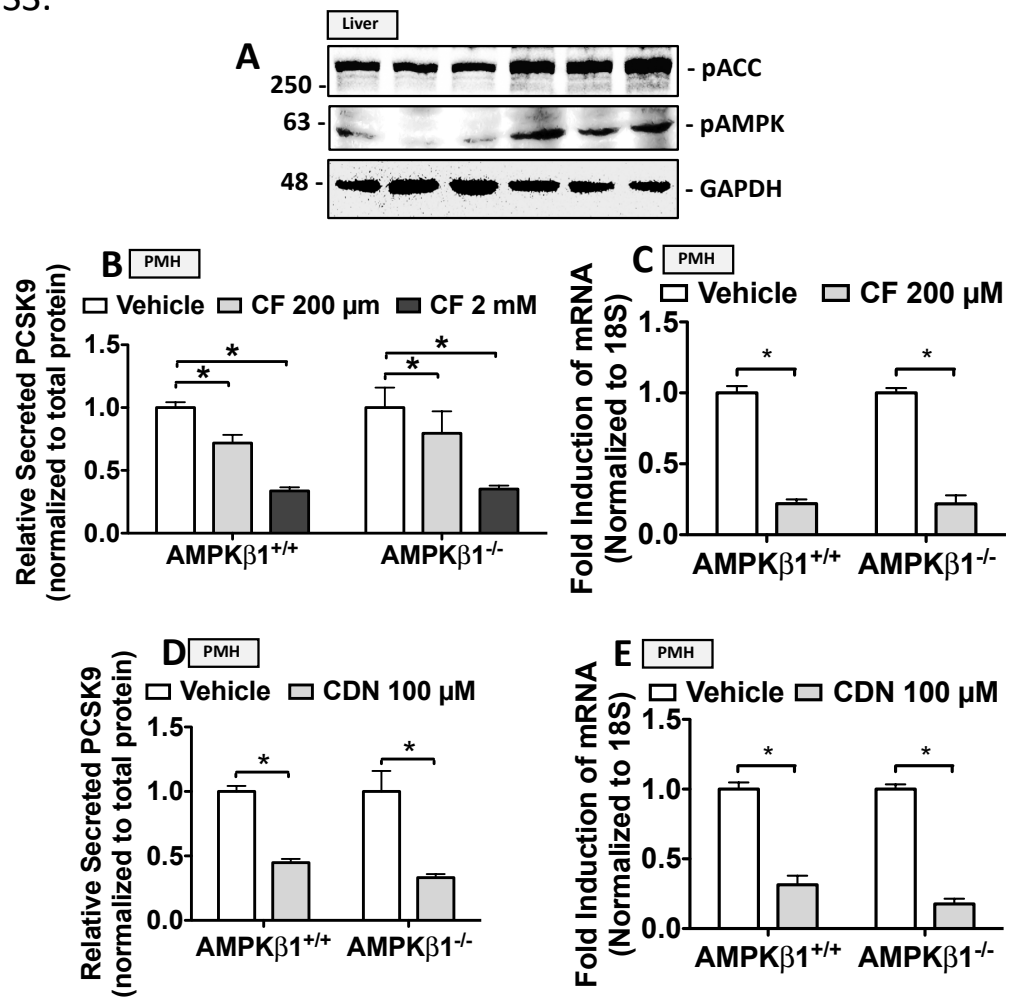
A
Liver
250 -
63 -
48 -
- pACC
- pAMPK
- GAPDH
B
PMH
Vehicle
CF 200 µm
CF 2 mM
Relative Secreted PCSK9 (normalized to total protein)
1.5
1.0
0.5
0.0
*
*
*
*
AMPKβ1+/+
AMPKβ1-/-
C
PMH
Vehicle
CF 200 µM
Fold Induction of mRNA (Normalized to 18S)
1.5
1.0
0.5
0.0
*
*
AMPKβ1+/+
AMPKβ1-/-
D
PMH
Vehicle
CDN 100 µM
Relative Secreted PCSK9 (normalized to total protein)
1.5
1.0
0.5
0.0
*
*
AMPKβ1+/+
AMPKβ1-/-
E
PMH
Vehicle
CDN 100 µM
Fold Induction of mRNA (Normalized to 18S)
1.5
1.0
0.5
0.0
*
*
AMPKβ1+/+
AMPKβ1-/-

Fig. S4.

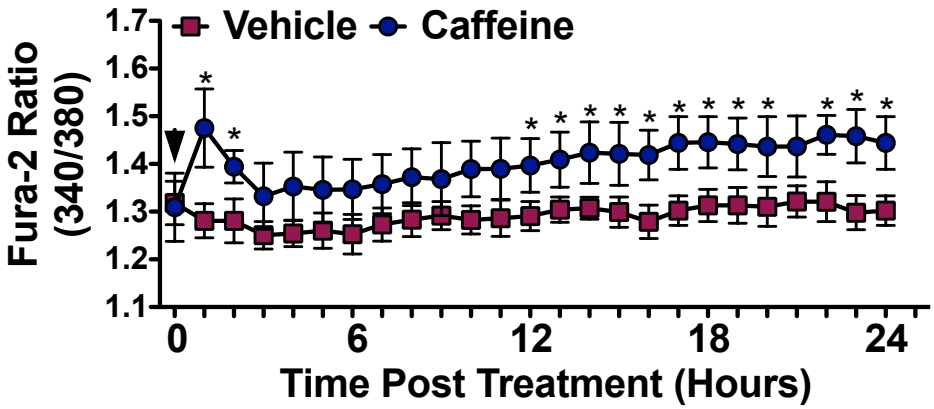
Vehicle
Caffeine
Fura-2 Ratio (340/380)
1.7
1.6
1.5
1.4
1.3
1.2
1.1
0
6
12
18
24
Time Post Treatment (Hours)

Fig. S5.

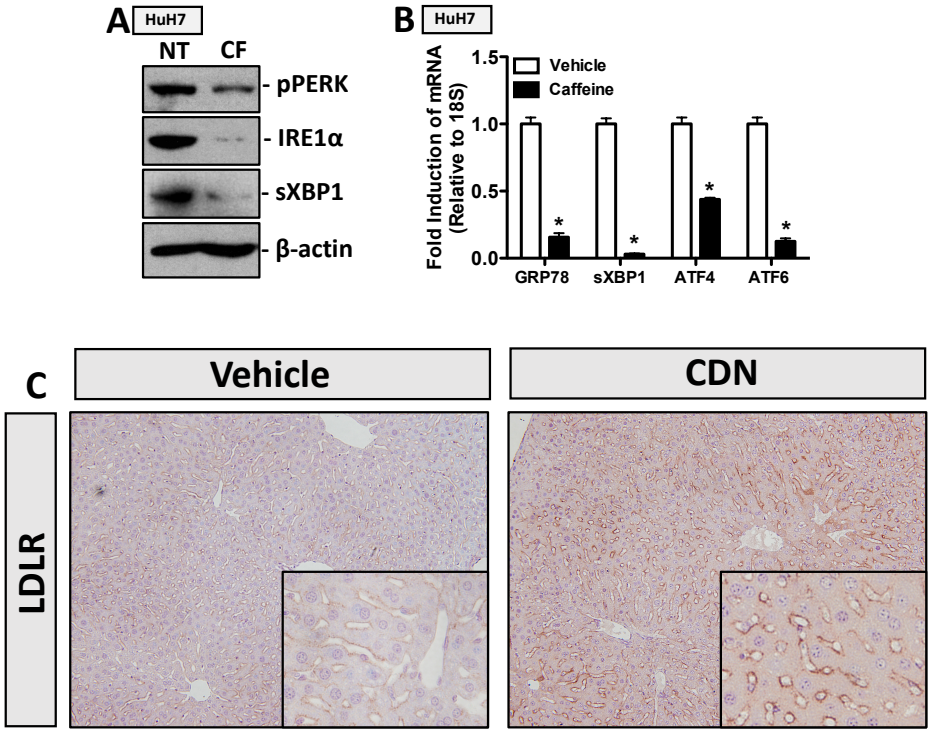
A
HuH7
NT
CF
- pPERK
- IRE1α
- sXBP1
- β-actin
B
HuH7
Fold Induction of mRNA (Relative to 18S)
Vehicle
Caffeine
1.5
1.0
0.5
0.0
GRP78
sXBP1
ATF4
ATF6
C
Vehicle
CDN
LDLR

Table 1. Compounds used during the course of these studies

Compound	Effect on ER Ca^{2+} Levels	Concentrations used	Mechanism of Action
thapsigargin (TG)	decrease	100 nM	irreversible SERCA antagonist
CDN1163 (CDN)	increase	10 µM	allosteric SERCA agonist
2 APB	increase	100 µM	IP3R antagonist
ryanodine	decrease/increase	10 nM - 10 µM	RyR agonist at nM and RyR antagonist at µM
Caffeine (CF)	hypothesized increase	10 nM – 1 mM	multiple
8CC	hypothesized increase	100 nM – 1 mM	adenosine receptor antagonist
8CD	hypothesized increase	100 nM – 1 mM	adenosine receptor antagonist
PSB 603	hypothesized increase	100 nM – 1 mM	adenosine receptor antagonist
paraxanthine	hypothesized increase	100 nM – 1mM	multiple
theophyline	hypothesized increase	100 nM – 1mM	multiple
theobromine	hypothesized increase	100 nM – 1mM	multiple
Cyclopiazonic acid (CPA)	decrease	100 µM	SERCA antagonist
U18666A	N/A	10 µM	Intracellular sterol depletion

Table 2. Structure activity relationship of CF and its derivatives on PCSK9 inhibition.

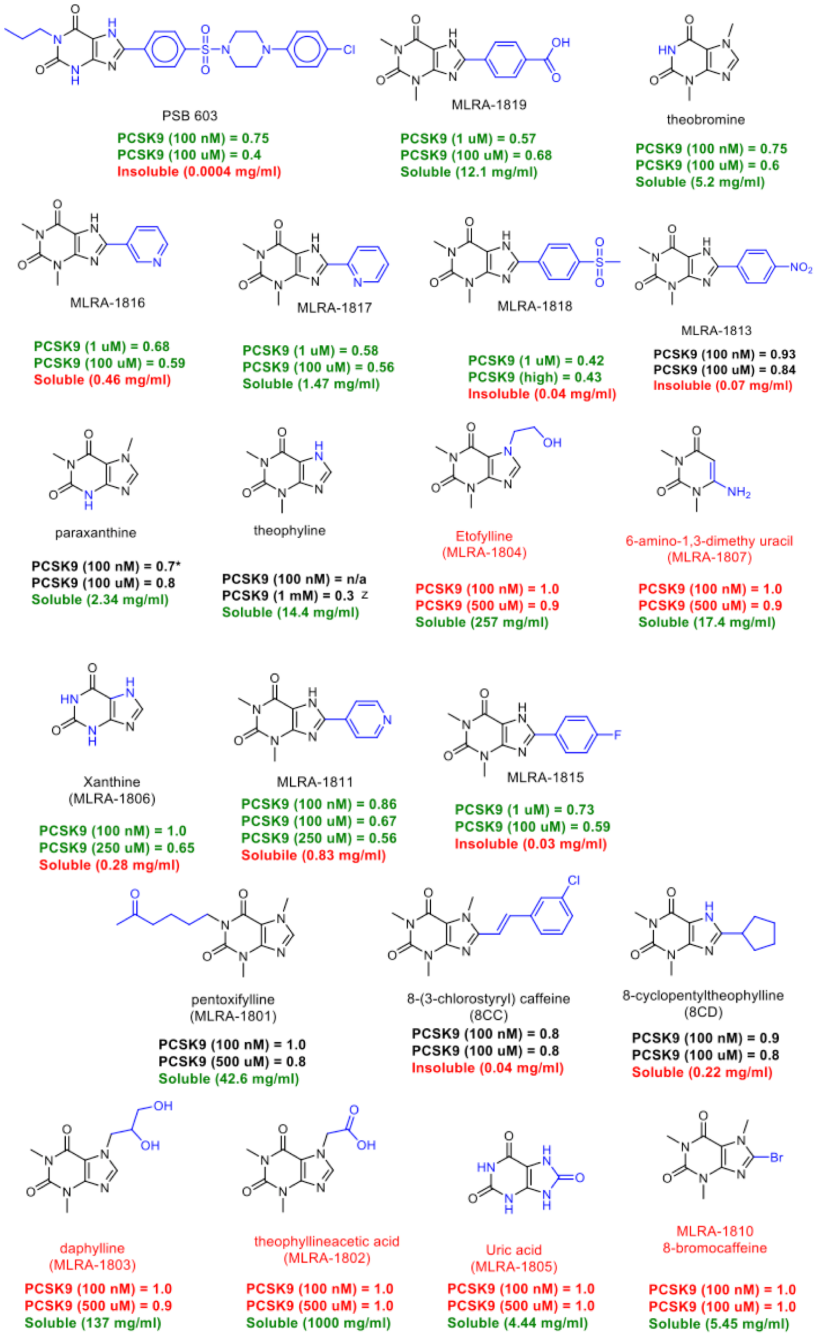

Chapter 4: Publication in the Journal of Biological Chemistry, 2019

Lebeau, P. F., Byun, J. H., Platko, K., MacDonald, M. E., Poon, S. V., Faiyaz, M., Seidah, N. G., and Austin, R. C. (2019) Diet-induced hepatic steatosis abrogates cell-surface LDLR by inducing de novo PCSK9 expression in mice. *The Journal of biological chemistry* **294**, 9037-9047

Author Contributions: P. F. L., J. H. B., K. P., N. G. S., and R. C. A. conceptualization; P. F. L., J. H. B., K. P., S. V. P., M. F., and R. C. A. data curation; P. F. L. software; P. F. L. formal analysis; P. F. L. supervision; P. F. L. validation; P. F. L., J. H. B., K. P., M. E. M., S. V. P., and R. C. A. investigation; P. F. L. visualization; P. F. L., J. H. B., K. P., M. E. M., S. V. P., and N. G. S. methodology; P. F. L. writing-original draft; P. F. L., J. H. B., and R. C. A. project administration; P. F. L., J. H. B., K. P., M. F., N. G. S., and R. C. A. writing-review and editing; R. C. A. resources; R. C. A. funding acquisition.

JBC ARTICLE

Diet-induced hepatic steatosis abrogates cell-surface LDLR by inducing *de novo* PCSK9 expression in mice

Received for publication, February 19, 2019, and in revised form, April 9, 2019 Published, Papers in Press, April 19, 2019, DOI 10.1074/jbc.RA119.008094

Paul F. Lebeau[‡1], Jae Hyun Byun[‡1], Khrystyna Platko[‡], Melissa E. MacDonald[‡], Samantha V. Poon[‡], Mahi Faiyaz[‡], Nabil G. Seidah[§], and Richard C. Austin[‡2]

From the [‡]Department of Medicine, McMaster University, The Research Institute of St. Joe's Hamilton, Hamilton, Ontario L8N 4A6 and the [§]Laboratory of Biochemical Neuroendocrinology, Montreal Clinical Research Institute, University of Montreal, Montreal, Quebec H2W 1R7, Canada

Edited by George N. DeMartino

The worldwide prevalence of non-alcoholic fatty liver disease (NAFLD) is increasing rapidly. Although this condition is generally benign, accumulating evidence now suggests that patients with NAFLD are also at increased risk of cardiovascular disease (CVD); the leading cause of death in developed nations. Despite the well-established role of the liver as a central regulator of circulating low-density lipoprotein (LDL) cholesterol levels, a known driver of CVD, the mechanism(s) by which hepatic steatosis contributes to CVD remains elusive. Interestingly, a recent study has shown that circulating proprotein convertase subtilisin/kexin type 9 (PCSK9) levels correlate positively with liver steatosis grade. Given that PCSK9 degrades the LDL receptor (LDLR) and prevents the removal of LDL from the blood into the liver, in the present study we examined the effect of hepatic steatosis on LDLR expression and circulating LDL cholesterol levels. We now report that in a manner consistent with findings in patients, diet-induced steatosis increases circulating PCSK9 levels as a result of *de novo* expression in mice. We also report the finding that steatosis abrogates hepatic LDLR expression and increases circulating LDL levels in a PCSK9-dependent manner. These findings provide important mechanistic insights as to how hepatic steatosis modulates lipid regulatory genes, including *PCSK9* and the *LDLR*, and also highlights a novel mechanism by which liver disease may contribute to CVD.

Liver fat accumulation due to reasons other than excessive alcohol consumption, or more often referred to as NAFLD,[3] currently has an estimated occurrence of 30–46% in developed nations (1). Given the current trends in global consumption of unhealthy dietary fats and sugars, it is no surprise that NAFLD is increasing in prevalence as these factors play a central role in its development (2). Although NAFLD is described as liver fat accumulation with no sign of liver injury, this initial stage often progresses to non-alcoholic steatohepatitis (NASH); a state characterized histologically by necroinflammation and hepatocyte damage (3). NAFLD and its complications are estimated to be the primary cause of liver-related mortality and liver transplantation within the next 20 years (4).

Evidence that patients with NAFLD are at higher risk of developing CVD, which is among the leading causes of death worldwide (5), is now accumulating (6–9). Given that both NAFLD and CVD share many comorbidities and frequently develop in patients at the same time, it has been a major challenge to discern the exact mechanism(s) by which one contributes to the other (10). Despite this challenge, several reports have demonstrated that NAFLD increases the expression or prevalence of factors known to contribute to CVD. These factors include circulating proinflammatory mediators, prothrombotic factors, hyperlipidemia, and risk of type-2 diabetes. Recent studies have shown a link between the presence of NAFLD and increased intima-media thickness, impaired arterial vasodilation, plaque development, as well as coronary artery calcium scores (10).

Interestingly, two independent clinical studies have also demonstrated that patients with NAFLD have increased levels of circulating PCSK9 (11, 12). PCSK9 is an established driver of atherosclerotic lesion development and CVD due to its ability to enhance the degradation of cell-surface LDLR, thereby reducing the ability of the liver to clear pro-atherogenic LDL cholesterol from the circulation (13–15). Seminal studies in this field have also shown that gain-of-function mutations in *PCSK9* correlate with increased risk of CVD in humans (16), and in a reciprocal manner, loss-of-function mutations have the opposite outcome (17). Pre-clinical data also demonstrate that

This work was supported by the Heart and Stroke Foundation of Canada Research Grants G-13-0003064 and G-15-0009389 and Canadian Institutes of Health Research Grant 74477 (to R. C. A.), Leducq Foundation Grant 13 CVD 03, CIHR Foundation Grant 148363, and Canada Research Chair Grant 216684 (to N. G. S.), and the Research Institute of St. Joe's Hamilton. The authors declare that they have no conflicts of interest with the contents of this article.

[1] Both authors contributed equally to this work.

[2] A Career Investigator of the Heart and Stroke Foundation of Ontario and holds the Amgen Canada Research Chair in the Division of Nephrology at The Research Institute of St. Joe's Hamilton and McMaster University. To whom correspondence should be addressed: 50 Charlton Ave. East, Rm. T-3313, Hamilton, Ontario L8N 4A6, Canada. Tel.: 905-522-1155 (ext. 35175); Fax: 905-540-6589; E-mail: austinr@taari.ca.

[3] The abbreviations used are: NAFLD, non-alcoholic fatty liver disease; 4PBA, 4-phenylbutyrate; ApoB, apolipoprotein-B; ATF4, activating transcription factor 4; CASP, caspase; CHOP, C/EBP homologous protein; CVD, cardiovascular disease; ER, endoplasmic reticulum; FN1, fibronectin 1; GFP, green fluorescent protein; GRP, glucose-regulated protein; H&E, hematoxylin and eosin; HFD, high-fat diet; HMG-CoA, 3-hydroxy-3-methylglutaryl-CoA; IRE1α, inositol-requiring enzyme 1α; LDL, low-density lipoprotein; LDLR, LDL receptor; Met, metformin; NASH, non-alcoholic steatohepatitis; NCD, normal control diet; ORO, Oil Red O; PA, palmitate; PCSK9, proprotein convertase subtilisin/kexin type 9; PERK, PKR-like endoplasmic reticulum kinase; SREBP, sterol regulatory element-binding protein; TBS, Tris-buffered saline; UPR, unfolded protein response; XBP1, X-box–binding protein.

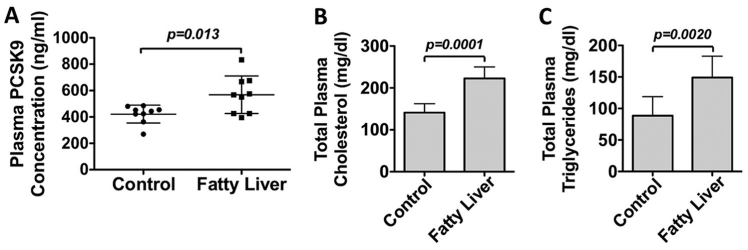

Figure 1. Circulating PCSK9 levels are increased in patients with hepatic steatosis. *A–C*, circulating PCSK9 levels, as well as total cholesterol and triglyceride levels, were assessed in patients with fatty liver ($n = 9$) and compared with healthy volunteers ($n = 9$). All samples were acquired from males over the age of 50.

adenoviral-mediated overexpression of PCSK9 in mice, or hepatocyte-specific transgenic overexpression of PCSK9 leads to a similar phenotype as that of the well-established *Ldlr*$^{-/-}$ mouse model used for the study of atherosclerosis (18, 19). In line with these data, human monoclonal antibodies targeted against PCSK9 were recently shown to reduce circulating LDL cholesterol levels by up to 60% in patients at high risk of CVD (20).

In the present study, we examined the effect of diet-induced hepatic steatosis on the expression and abundance of established drivers of CVD. Here, we show that the uptake and accumulation of the saturated fatty acid palmitate (PA), as well as high-fat diet (HFD), cause endoplasmic reticulum (ER) stress in cultured hepatocytes, and in the livers of mice, respectively. ER stress is a pathological cellular response that contributes to the development of liver disease and is also known to promote the activation of the sterol regulatory element-binding protein-2 (SREBP2); the major transcription factor responsible for the *de novo* synthesis of cholesterol regulatory proteins including PCSK9 and the LDLR. Accordingly, we also observed increased expression of PCSK9 in PA-treated hepatocytes, as well as in the livers and circulation of HFD-fed mice. Given the consistency of these data with studies done in patients with NAFLD, we next investigated the effect of this outcome on circulating LDL cholesterol and on the expression of its receptor in the liver. We also report the novel finding that HFD-induced hepatic steatosis caused a significant reduction of cell-surface LDLR expression and increased circulating LDL cholesterol levels in mice. Furthermore, because LDLR expression and serum LDL levels were unaffected by the HFD in *Pcsk9*$^{-/-}$ mice, we also identify that diet-induced hepatic steatosis affected these parameters in a PCSK9-dependent manner. Collectively, our data highlight a novel mechanism by which NAFLD may contribute to CVD by increasing PCSK9 expression to attenuate liver-mediated LDL cholesterol clearance.

Results

HFD increases circulating PCSK9 levels and attenuates hepatic cell-surface LDLR expression in mice

Consistent with previous studies (12), we first confirmed that patients with liver fat accumulation exhibit increased plasma PCSK9 levels (Fig. 1*A*; $p = 0.013$; $n = 9$), as well as circulating cholesterol (Fig. 1*B*; $p = 0.0001$; $n = 9$) and triglyceride levels (Fig. 1*C*; $p = 0.0020$; $n = 9$). Given that (*a*) PCSK9 contributes to CVD by degrading the LDLR and increasing plasma LDL levels (21), and (*b*) accumulating evidence suggests that hepatic steatosis contributes to CVD (10), we next examined the effect of steatosis on hepatic LDLR expression. Accordingly, male C57BL/6J mice were fed HFD or normal control diet (NCD) for a total of 12 weeks. Hepatic steatosis in these mice was confirmed via visualization of lipid droplets using H&E, as well as Oil Red O (ORO) (Fig. 2*A*). Strikingly, immunohistochemical staining revealed that HFD-fed mice had markedly reduced cell-surface LDLR expression compared with NCD-fed controls (Fig. 2*B*). As expected, LDLR antibody staining specificity was confirmed by the absence of staining in the livers of *Ldlr*$^{-/-}$ mice. In contrast, immunoblotting revealed a modest reduction in LDLR expression in the livers of HFD-fed mice (Fig. 2*C*). These data are representative of whole-cell LDLR abundance, however, and not strictly of the cell-surface LDLR population. Therefore, these data suggest a strong presence of an intracellular LDLR population in liver hepatocytes, which is not affected by the HFD. ORO and LDLR immunohistochemical staining intensities were also quantified using ImageJ software (Fig. 2*D*). Consistent with previous studies, we observed that hepatic LDLR expression was inversely correlated with circulating PCSK9 levels in mice (Fig. 2*D*) (14). The surrogate marker of circulating LDL cholesterol, apolipoprotein-B (ApoB) (22), as well as total cholesterol and triglyceride levels were also examined and found to be increased in HFD-fed mice compared with NCD-fed controls (Fig. 2, *E–G*). These findings demonstrate a diet-induced hepatic steatosis effect on the PCSK9-LDLR axis, which could explain the observed increase in circulating lipid levels.

Diet-induced hepatic steatosis causes hepatic ER stress and promotes de novo PCSK9 expression

Our research group has previously demonstrated that ER stress causes the activation of SREBP2 (23, 24) and expression of PCSK9 in cultured hepatocytes (25). As such, we next examined the livers of HFD-fed mice for markers of ER stress. Consistent with other reports (26, 27), increased expression of ER stress and pro-apoptotic markers, including the glucose-regulated proteins (GRP78 and GRP94), C/EBP homologous protein (CHOP), activating transcription factor 4 (ATF4), PKR-like endoplasmic reticulum kinase (PERK), as well as pro-fibrotic and apoptotic markers fibronectin 1 (FN1), Bcl-2–binding component 3 (BBC3), caspases (CASP1 and CASP3), inositol-

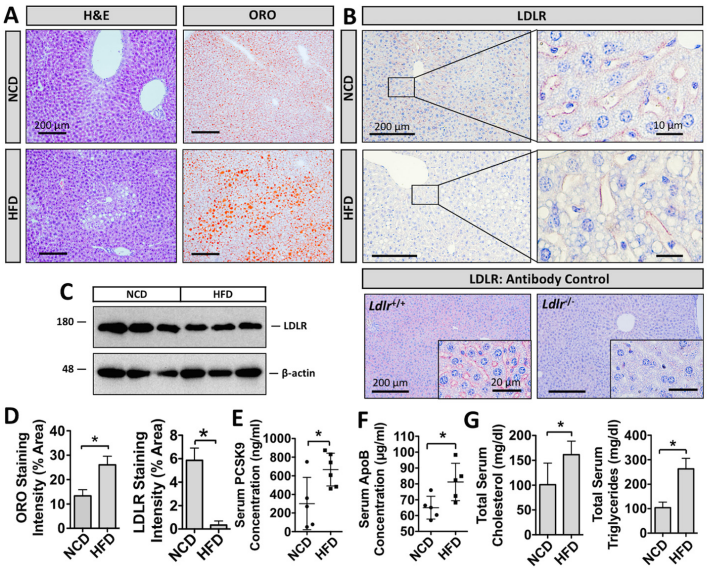

Figure 2. Diet-induced hepatic steatosis increases circulating PCSK9 levels and blocks cell-surface LDLR expression in mice. C57BL/6J mice were fed either a NCD ($n = 10$) or a HFD ($n = 10$) *ad libitum* starting at 6 weeks of age, for an additional 12 weeks. *A,* hepatic lipid droplet accumulation was confirmed using H&E as well as ORO staining. *B,* cell-surface LDLR protein expression was examined via immunohistochemical staining. LDLR antibody staining specificity was confirmed in the livers of *Ldlr*$^{-/-}$ mice. *C,* total hepatic LDLR expression was also examined via immunoblot analysis. *D,* ORO and LDLR staining intensities were quantified using ImageJ software. *E* and *F,* circulating PCSK9 and ApoB protein levels were examined using ELISAs ($n = 5$). *G,* total cholesterol and triglyceride levels were also examined in the serum of NCD- and HFD-fed mice. *, $p < 0.05$. *Error bars* represent values presented as the mean ± S.D.

requiring enzyme 1α (IRE1α), and spliced X-box–binding protein 1 (sXBP1) was observed in the livers of HFD-fed mice compared with controls via immunohistochemical staining, real-time PCR, and immunoblotting (Fig. 3, *A–C*). Furthermore, similar to our previous studies done in cultured cells (25), we observed that hepatic ER stress was associated with increased mRNA expression of SREBP2, as well as PCSK9 and the LDLR (Fig. 3*C*). Increased intracellular PCSK9 protein abundance was also observed in the livers of HFD-fed mice compared with NCD-fed controls (Fig. 3*D*). Additional modulators of cholesterol and triglyceride homeostasis, including the SREBP2-regulated HMG-CoA reductase, SREBP1, fatty acid synthase, and ApoB were examined via real-time PCR and found to be induced in the livers of HFD-fed mice (Fig. 3*F*). Overall, because circulating PCSK9 originates almost exclusively from liver hepatocytes (20, 28), these findings suggest that diet-induced hepatic ER stress represents a significant contributor in the observed increase in circulating PCSK9 levels in the context of liver fat accumulation.

Pharmacologic inhibition of ER stress, or lipid accumulation, blocks lipid-driven PCSK9 expression and restores LDLR function and expression in hepatocytes

To further examine the effect of lipid-induced ER stress on PCSK9 expression, cultured hepatocytes were treated with the fatty acid, PA. PA represents one of many saturated fatty acids that are highly abundant in animal-derived dietary fats (29) and is also a well-established inducer of ER stress in a variety of cultured cell models (30–32). Similar to the livers of mice exposed to high levels of dietary fats from the HFD, cultured human HepG2 hepatocytes treated with bovine serum albumin (BSA)-conjugated PA yielded increased mRNA expression of SREBP2, PCSK9, and LDLR compared with those treated with the BSA vehicle control (Fig. 4*A*). Because previous studies have shown that metformin (Met) and 4-phenylbutyrate (4PBA) attenuate hepatic lipid accumulation and protect against ER stress (33–35), two additional groups of cells were also pretreated with these agents for 24 h prior to PA treatment. Consistent with other studies, we observed that both agents reduced lipid accumulation (Fig. 4*B*) (36, 37) and attenuated PA-induced expression of the ER stress markers, GRP78, GRP94, and IRE1α. Furthermore, Met and 4PBA also blocked the PA-induced expression of SREBP2, PCSK9, and LDLR. SREBP2 transcriptional activity was then assessed in HuH7 cultured human hepatocytes transfected with a sterol-regulatory element (SRE)-driven GFP reporter construct (Fig. 4*C*). Similar to mRNA transcript levels of SREBP2, PA increased GFP fluorescence intensity, which was in turn blocked by Met and 4PBA. Met and 4PBA also significantly reduced PA-induced secreted PCSK9 levels in the medium harvested from HepG2 and HuH7 cells (Fig. 4*D*). To assess whether these treatments were affecting all secreted proteins, or if PCSK9 was affected with an acceptable level of specificity, medium harvested from these cells was electrophoretically resolved and stained using Coomassie Brilliant Blue protein stain. Given that the relative abundance of secreted proteins was not markedly affected by these treatments, these data suggest that PA, Met, and 4PBA-induced

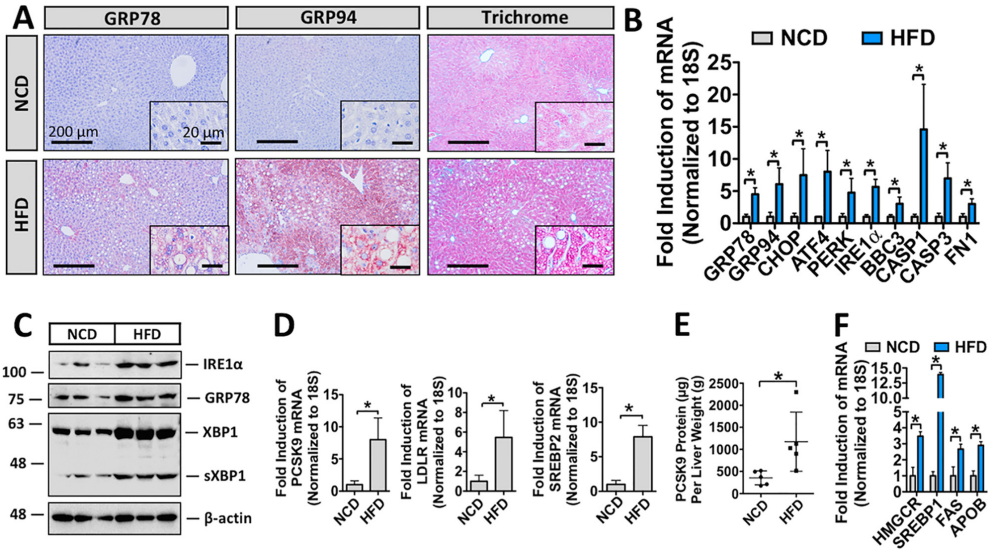

Figure 3. HFD-fed mice exhibit hepatic ER stress and increased expression of SREBP2 and PCSK9. C57BL/6J mice were fed either a *NCD* ($n = 10$) or a HFD ($n = 10$) *ad libitum* starting at 6 weeks of age, for an additional 12 weeks. *A,* immunohistochemical staining of the ER stress markers, GRP78 and GRP94, as well as Masson's trichrome staining for fibrotic collagen deposition (*blue*) in the livers of HFD-fed mice. *B,* real-time PCR analysis of hepatic ER stress marker expression (GRP78, GRP94, CHOP, ATF4, PERK, and IRE1α), apoptosis, and fibrosis markers (CASP1, CASP3, and FN1). *C,* immunoblots used to examine LDLR expression in the livers of HFD-fed mice from Fig. 2*C* were re-probed for ER stress markers GRP78, IRE1α, and XBP1. *D,* real-time PCR analysis of hepatic PCSK9, LDLR, and SREBP2 mRNA transcript levels. *E,* assessment of liver PCSK9 protein levels using an ELISA. *F,* analysis of mRNA transcript abundance of established cholesterol and triglyceride modulators HMG-CoA reductase (*HMGR*), SREBP1, fatty acid synthase (*FAS*), and ApoB via real-time PCR. *, $p < 0.05$. *Error bars* represent values presented as the mean ± S.D.

changes in secreted PCSK9 levels are not the result of changes in global protein secretion.

Next, a quantitative assessment of fluorescently-labeled DiI-LDL uptake was carried out in HepG2 cells treated with vehicle, Met, or 4PBA in the presence or absence of PA (Fig. 4*E*). Consistent with previous studies, elevated secreted PCSK9 levels were associated with a reduction of LDL uptake (38, 39). Met and 4PBA also attenuated the PA-mediated inhibition of DiI-LDL uptake observed in these cells. PCSK9 mRNA expression and secretion in response to PA treatment was also examined in primary human hepatocytes, yielding findings that were consistent with those observed in HepG2 and HuH7 cells (Fig. 4*F*).

Given our observation that 4PBA can attenuate PA-induced ER stress and PCSK9 expression in cultured cells, an additional cohort of mice was fed HFD in the presence or absence of 4PBA in the drinking water. Similar to PA-treated HepG2 cells, we observed that 4PBA attenuated the ability of the HFD to block LDLR expression (Fig. 4*G*). A reduction in the expression of the ER stress markers, GRP78 and GRP94, as well as the fibrosis marker, fibronectin, was also observed in the livers of HFD-fed mice exposed to 4PBA (Fig. 4*H*).

Diet-induced hepatic steatosis attenuates hepatic LDLR expression in a PCSK9-dependent manner

Because LDLR expression is known to be affected by other proteins and conditions (40), our final aim was to identify the extent to which PCSK9 contributed to the observed reduction of cell-surface LDLR expression in HFD-fed mice. Accordingly, *Pcsk9*$^{-/-}$ mice on a C57BL/6J background were also fed a HFD for 12 weeks starting at 6 weeks of age. Similar to wild-type C57BL/6J mice, a significant increase in hepatic lipid content was observed in HFD-fed *Pcsk9*$^{-/-}$ mice compared with those fed the NCD (Fig. 5, *A* and *B*). Strikingly, immunohistochemical staining revealed that the HFD did not significantly reduce LDLR expression in these mice. ORO and LDLR staining intensities were also quantified using ImageJ software (Fig. 5*C*). Consistent with immunohistochemical staining of cell-surface LDLR, immunoblot data also demonstrate that HFD did not markedly reduce LDLR expression in the livers of *Pcsk9*$^{-/-}$ mice (Fig. 5*D*). Furthermore, HFD also failed to increase circulating ApoB-containing LDL cholesterol in *Pcsk9*$^{-/-}$ mice (Fig. 5*E*). PCSK9 knockout in these mice was confirmed using an ELISA for circulating PCSK9 (Fig. 5*F*).

Collectively, these data suggest that intracellular lipid accumulation causes ER stress, which induces *de novo* PCSK9 expression and secretion from hepatocytes (Fig. 6). In turn, heightened circulating PCSK9 levels enhance the degradation of hepatic cell-surface LDLR and increase the levels of circulating LDL cholesterol in the context of diet-induced hepatic steatosis.

Discussion

Hepatocytes, like all secretory cells, are rich in ER and are thus susceptible to injury and damage as a result of conditions that lead to ER stress (41). It is well-established that lipid accumulation in hepatocytes can promote the activation of the

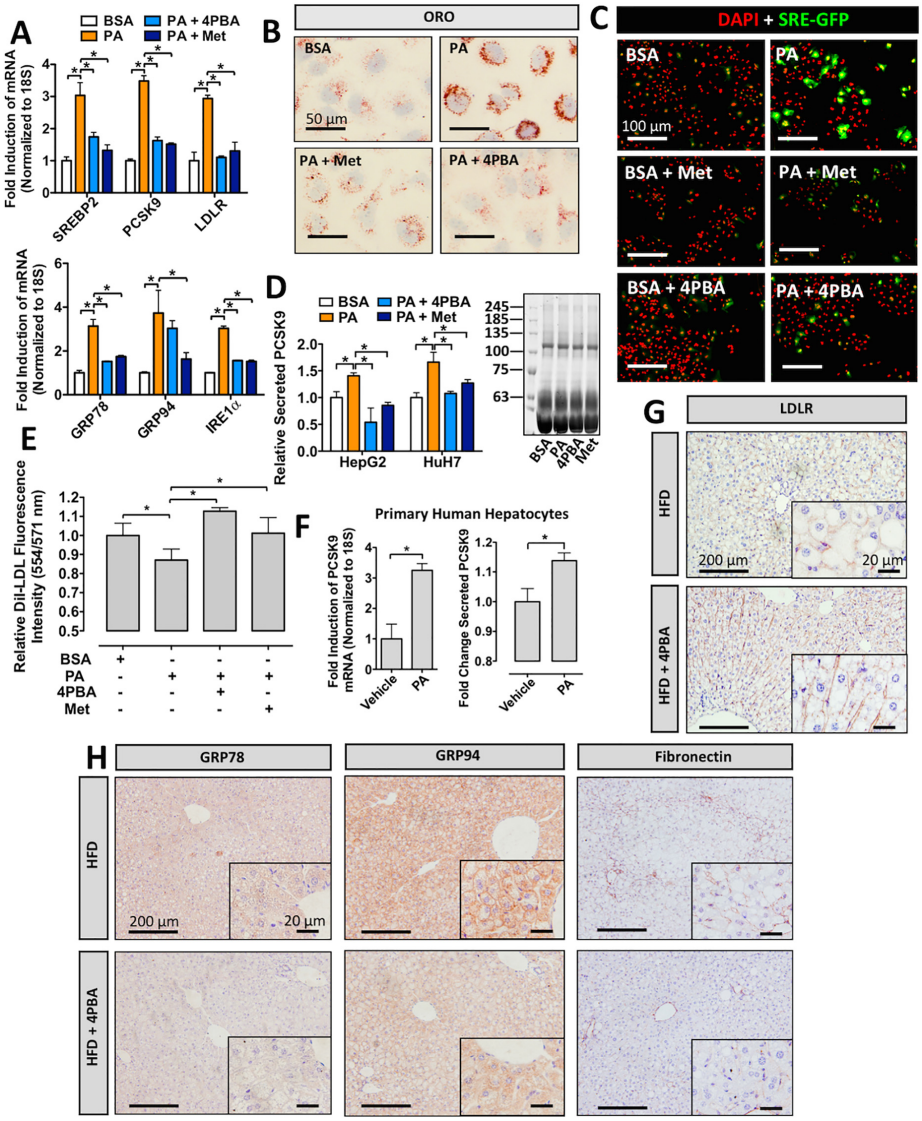

Figure 4. Blocking ER stress and lipid accumulation attenuates PCSK9 expression and restores LDLR expression and function. *A,* HepG2 cells were pre-treated with Met (1 mM) or 4PBA (1 mM) for 24 h and subsequently treated with BSA-conjugated PA (300 μM). SREBP2, PCSK9, and LDLR, as well as the ER stress markers GRP78, GRP94, and IRE1α expression was assessed using real-time PCR. *B,* lipid droplet accumulation in these cells was also assessed via ORO staining. *C,* HepG2 cells were transfected with a SRE reporter plasmid encoding GFP and subsequently pre-treated with Met (1 mM) or 4PBA (1 mM) in the presence or absence of BSA-conjugated PA (300 μM). SREBP2-mediated GFP expression was assessed using a fluorescent microscope. *D,* secreted PCSK9 levels from HepG2 and HuH7 cells grown in FBS-free medium were examined via ELISA. Coomassie staining of electrophoretically resolved medium harvested from these cells demonstrates that treatments did not affect global protein secretion. *E,* fluorescently-labeled Dil-LDL uptake was examined in treated HepG2 cells. *F,* experiments were repeated in cultured primary human hepatocytes (PA, 300 μM, 24 h). *G* and *H,* male C57BL/6J mice were fed a HFD in the presence or absence of 4PBA in the drinking water. Hepatic LDLR expression, as well as GRP78, GRP94, and fibronectin expression was examined via immunohistochemical staining. *, $p < 0.05$. *Error bars* represent values presented as the mean ± S.D.

unfolded protein response (UPR), a highly conserved signaling cascade that attempts to resolve ER stress (42). In a reciprocal manner, studies have also shown that ER stress can lead to intracellular lipid accumulation by inducing *de novo* lipid synthesis in a manner dependent on specific transcription factors, such as SREBP1 (42, 43). Given that both processes appear to

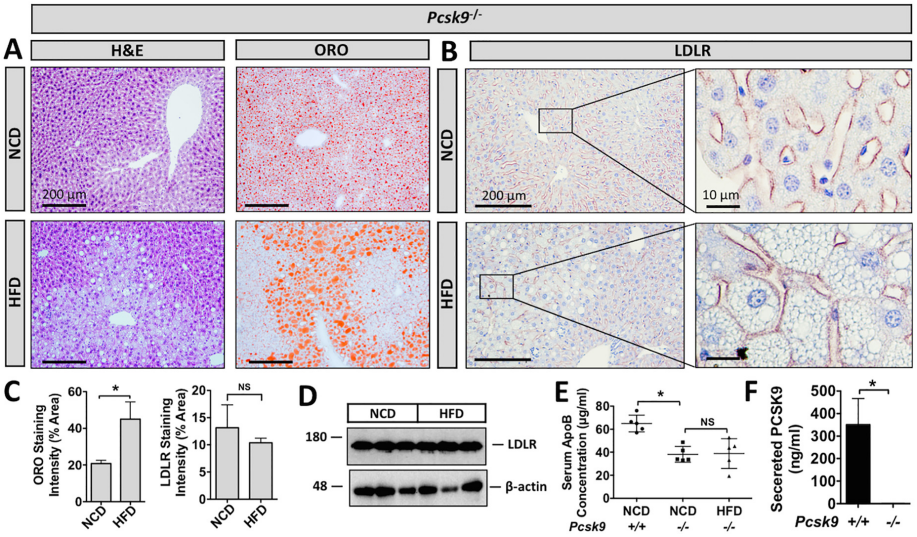

Figure 5. HFD fails to affect hepatic cell-surface LDLR and plasma LDL in *Pcsk9*$^{-/-}$ mice. *A*, *Pcsk9*$^{-/-}$ mice on a C57BL/6J background were fed either NCD ($n = 5$) or HFD ($n = 5$) *ad libitum* for 12 weeks starting at 6 weeks of age. *A* and *B*, hepatic lipid droplet accumulation was assessed via H&E and *ORO* and cell-surface LDLR expression via immunohistochemical staining. *C*, staining intensity was quantified using ImageJ Software (*, $p < 0.05$; $n = 5$). *D*, hepatic LDLR expression was also examined via immunoblot analysis. *E*, circulating ApoB levels were assessed using an ELISA. *F*, PCSK9 knockout was also confirmed via ELISA of circulating PCSK9 (*, $p < 0.05$). *Error bars* represent values presented as the mean ± S.D.

occur at the same time, however, it has been challenging to discern which of the two factors in this paradoxical relationship contributes most to the development of liver disease (10). Nonetheless, in a manner consistent with previous studies, we observed a significant increase in the expression of mediators of the UPR during conditions of hepatic steatosis in response to HFD (Fig. 3, *A* and *B*) (27). Although previous studies have demonstrated that HFD increases SREBP1 expression (44, 45), we also report the finding that diet-induced hepatic steatosis increases the expression of SREBP2 (Fig. 3*C*). Furthermore, we demonstrate that hepatic ER stress caused a significant increase in PCSK9 expression and secretion (Figs. 3*C* and 2*D*, respectively); a process that we previously demonstrated to be dependent on SREBP2 (25). We also observed that PA, a saturated fatty acid known to cause ER stress in secretory cell types (46), increased SREBP2 activity and PCSK9 expression and secretion in cultured human hepatocytes (Fig. 4). In response to elevated secreted PCSK9 levels, we observed that the livers of mice and cultured hepatocytes exhibited a significant reduction in LDLR expression and activity (Figs. 2*B* and 4*E*, respectively). Given that this phenotype was not observed in HFD-fed *Pcsk9*$^{-/-}$ mice, we conclude that the effect of diet-induced hepatic steatosis on LDLR expression occurs in a manner dependent on *de novo* SREBP2-driven PCSK9 expression and secretion (Fig. 6).

In a previous study, we observed that ER stress resulting from ER Ca^{2+} depletion, but not from the inhibition of *N*-glycosylation, caused a significant increase in SREBP2 activation and PCSK9 expression in hepatocytes (25). These findings suggest that PCSK9 expression is affected only by certain ER stress-inducing stimuli. Despite increased PCSK9 protein abundance as a result of thapsigargin treatment, we observed that thapsigargin and tunicamycin blocked the exit of PCSK9 from hepatocytes. Interestingly, in the present study we demonstrate that lipid accumulation in hepatocytes increases SREBP2 activity and promotes PCSK9 expression, suggesting that this process could occur as a result of ER Ca^{2+} depletion. Consistent with this notion, previous studies have also demonstrated that fatty acid uptake and accumulation causes ER Ca^{2+} depletion, ER stress, and apoptosis in a variety of cell lines (30, 47). In contrast to our previous study, however, diet-induced hepatic steatosis and ER stress not only increased the expression of PCSK9, but also increased its secretion from hepatocytes. Given the intricacies of the UPR and ER cargo receptors that are known to play a role in the secretion of PCSK9 and regulation of cholesterol (48, 49), it is not surprising that different conditions of ER stress affect PCSK9 in different ways. Although ER stress can increase its expression, *PCSK9* is also a lipid-responsive gene and therefore further studies are required to delineate the exact mechanism by which lipid accumulation influences PCSK9 secretion from hepatocytes.

Consistent with previous studies, we also observed that circulating PCSK9 levels were positively correlated with circulating LDL cholesterol levels, but inversely correlated with hepatic LDLR expression (Fig. 2, *B*, *D*, and *E*) (38, 50). Importantly, *de novo* synthesis of PCSK9 and the LDLR is regulated by the same transcription factor, and thus differences in the relative abundance of these proteins in the context of SREBP2 activation/inhibition can be attributed to differences in the stimuli being studied. Here, we observed that diet-induced hepatic steatosis increased *de novo* expression of the LDLR at the mRNA level (Fig. 3*C*), but blocked its expression at the protein level

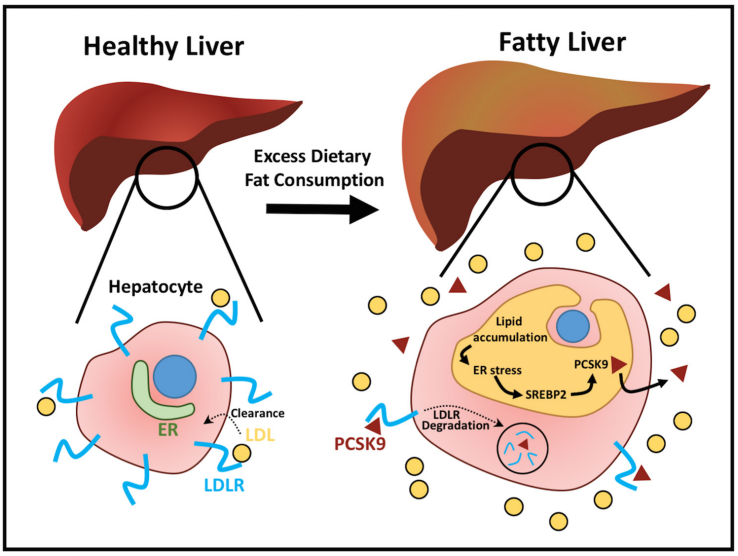

Figure 6. Fatty liver increases *de novo* PCSK9 to block cell-surface LDLR expression. The healthy liver regulates circulating LDL cholesterol levels by means of expressing high levels of cell-surface LDLR compared with most tissue types. Diet-induced hepatic steatosis, however, causes ER stress, which leads to an increase in SREBP2 activation and expression of the natural inhibitor of the LDLR, PCSK9. In this pathologic milieu, PCSK9 prevails over the LDLR and contributes to dyslipidemia and risk of CVD.

(Fig. 4*A*). Consistent with our observations, LDLR expression is inversely correlated with SREBP2 activation in naringin-treated mice and in monkeys treated with siRNA targeted against the SREBP cleavage-activating protein (51, 52); a protein known to interact with and stabilize the SREBPs (53). In contrast, it is also well-established that HMG-CoA reductase inhibitors activate SREBP2 and increase hepatic LDLR expression, as well as circulating PCSK9 levels (54, 55). Interestingly, a recent study has demonstrated that HMG-CoA reductase inhibitors can increase circulating PCSK9 levels while blocking the occurrence of a gain-of-function phosphorylation at position 688 (56). Given that HMG-CoA reductase inhibitors are well-known to reduce CVD risk (57), the aforementioned findings rectify the long-lasting PCSK9-statin anomaly. Furthermore, with a half-life of only 5 min (58), PCSK9 protein expression is more likely dependent on *do novo* synthesis than the LDLR, which has a half-life of 12 h (59).

Although we are the first to demonstrate that diet-induced liver fat accumulation increases circulating PCSK9 levels in mice, similar reports in patients have been controversial. The Dallas Heart study was the first to report a modest but significant positive correlation between hepatic steatosis and circulating PCSK9 levels (11). Ruscica and colleagues (12) also reported a statistically significant positive correlation between steatosis grade and circulating PCSK9 levels. Although our findings also demonstrate that patients with hepatic steatosis exhibit increased plasma PCSK9 levels, the statistical power of the result in this study is limited by low patient number. In contrast to the aforementioned data, a recent study by Wargny and colleagues (60) demonstrated that no significant correlation was observed between circulating PCSK9 levels and liver fat accumulation, plasma transaminase activity, NASH activity score, or lobular/portal inflammation in three patient cohorts. Inconsistencies in these data sets, however, are likely attributable to differences in liver disease severity between patient cohorts (60).

The liver is a central regulator of lipid homeostasis and yet despite the established role of lipid in the development of atherosclerosis and other cardiovascular complications, the contribution of liver disease to CVD remains elusive. Although previous studies have also demonstrated that a HFD can increase circulating LDL cholesterol levels (61), we are the first to highlight a role of the liver in this process. Because recent studies have also demonstrated that PCSK9 itself has proinflammatory properties (62), it is also possible that steatosis-driven PCSK9 expression may contribute to CVD in a manner independent of LDL cholesterol. Collectively, the present study delineates a novel mechanism by which diet-induced liver fat accumulation can influence CVD by affecting the expression of central regulators in its development, PCSK9 and the LDLR.

Experimental procedures

Patient cohort and ELISAs

Plasma samples from healthy controls and patients with fatty liver disease were acquired from Discovery Life Sciences (Huntsville, AL). All samples were acquired from males over the age of 50. PCSK9 levels in human and mouse plasma samples, as well as mouse liver lysates, were examined using commercially available ELISAs (R&D Systems). Mouse ApoB levels were also assessed using ELISAs (Abcam).

Table 1
Antibodies used for immunoblotting and immunohistochemical (IHC) staining

Antibody	Catalog No.	Application	Dilution
GRP78	SC-1050, Santa Cruz Biotechnology	IHC[a]	1:40, no retrieval
GRP94	ADI-SPA-850, Enzo Life Sciences	IHC	1:100, HIER[c]
LDLR	AF-2255, R and D Systems	IHC	1:100, HIER
Fibronectin	PA5–29578, ThermoFisher Scientific	IHC	1:200, HIER
GRP78	610979, BD Bioscience	IB[b]	1:1000
IRE1α	14C10, Cell Signaling Technologies	IB	1:500
XBP1	Sc-8015, Santa Cruz Biotechnology	IB	1:2000
β-Actin	MA5–15739, ThermoFisher Scientific	IB	1:5000
LDLR	AF2255, R and D Systems	IB	1:1000

[a] IHC, immunohistochemistry.
[b] IB, immunoblot.
[c] HIER, heat-induced epitope retrieval.

Table 2
Primers used for real-time PCR

Gene	Species	Forward	Reverse
ApoB	Mouse	AAGCACCTCCGAAAGTACGTG	CTCCAGCTCTACCTTACAGTTGA
ATF4	Mouse	ATGGCCGGCTATGGATGAT	CGAAGTCAAACTCTTTCAGATCCATT
BBC3	Mouse	TGTGGAGGAGGAGGAGTGG	TGCTGCTCTTCTTGTCTCCG
CASP1	Mouse	TCCGCGGTTGAATCCTTTTCAGA	ACCACAATTGCTGTGTGTGCGCA
CASP3	Mouse	CCTCAGAGAGACATTCATGG	GCAGTAGTCGCCTCTGAAGA
CHOP	Mouse	CTGCCTTTCACCTTGGAGAC	CGTTTCCTGGGGATGAGATA
FAS	Mouse	GCGATGAAGAGCATGGTTTAG	GGCTCAAGGGTTCCATGTT
FN1	Mouse	CGAGGTGACAGAGACCACAA	CTGGAGTCAAGCCAGACACA
GRP78	Mouse	GTCCTGCATCATCAGCGAAAG	GGTAGCCACATACTGAACACCA
GRP94	Mouse	GATGGTCTGGCAACATGGAG	CGCCTTGGTGTCTGGTAGAA
HMGCR	Mouse	CTTTCAGAAACGAACTGTAGC TCAC	CTAGTGGAAGATGAATGGACATGAT
LDLR	Mouse	GAGGAGCAGCCACATGGTAT	GCTCGTCCTCTGTGGTCTTC
PCSK9	Mouse	TTGCAGCAGCTGGGAACTT	CCGACTGTGATGACCTCTGGA
PERK	Mouse	GATGACTGCAATTACGCTATCAAGA	CCTTCTCCCGTGCCAACTC
SREBP1	Mouse	GGAGCCATGGATTGCACATT	GGCCCGGGAAGTCACTGT
SREBP2	Mouse	GCGTTCTGGAGACCATGGA	ACAAAGTTGCTCTGAAAACAAATCA

Cholesterol and triglyceride assays

Circulating plasma total cholesterol and triglyceride levels were examined using commercially available colorimetric assays and were carried out as per the manufacturer's instructions (Wako Diagnostics).

Immunohistochemical staining

Formalin-fixed paraffin-embedded liver sections were deparaffinized and stained with primary antibodies for 18 h following heat-induced epitope retrieval. Excess primary antibodies were removed via washing prior to exposure of sections to secondary antibodies conjugated to horseradish peroxidase. Staining was visualized using Nova Red (Vector Labs) and quantified using ImageJ. For quantification purposes, 20 representative images were taken from each treatment group at a magnification power of ×20. See Table 1 for antibodies used.

Cell culture studies

HepG2 cells were treated with BSA-conjugated PA (300 μM; Sigma-Aldrich) for 24 h in the presence or absence of Met (1 mM; Sigma-Aldrich) or 4PBA (1 mM; Sigma-Aldrich). Cells were fixed in 4% paraformaldehyde for the assessment of lipid droplet accumulation via ORO (Sigma-Aldrich) staining. SREBP2 transcriptional activity was assessed in HepG2 cells transfected with a reporter plasmid encoding a SRE-driven GFP (9) using X-tremeGENE HP transfection reagent (Sigma-Aldrich). PCSK9 mRNA expression and ELISAs were repeated in Hepatosure® 100-donor primary human hepatocytes purchased from Xenotech (Kansas City, KS). For the quantitative assessment of LDL uptake, HepG2 cells were seeded in black clear-bottom 96-well plates and treated with the indicated interventions for 24 h. Five hours prior to quantification using a fluorescent spectrophotometer (Molecular Devices, Gemini EM; excitation 554/emission 571), cells were treated with DiI fluorescently-labeled LDL (100 ng/ml; Alpha Aesar). Excess DiI-LDL in the medium was removed and the cell monolayer was vigorously washed with Hank's buffered saline solution containing HEPES (20 mM).

Animal studies

Pcsk9$^{-/-}$ (n = 5) and age-matched *Pcsk9*$^{+/+}$ controls on a C57BL/6J background (n = 10) were started on HFD (60% fat; Harland Tecklad) *ad libitum* at 6 weeks of age and sacrificed at 18 weeks of age. A second cohort of C57BL/6J mice were started on the HFD at 10–11 weeks of age and provided with either normal drinking water (n = 8) or water containing 4PBA (n = 9; 1 g/kg/day) for 12 weeks. Mice were fasted for 12 h prior to sacrifice. All animal studies were performed in accordance with the McMaster University animal care guidelines.

Immunoblot analysis

Cells were lysed in 4× SDS-PAGE sample buffer and separated on 10% polyacrylamide gels in reducing conditions, as described previously (63), and transferred to nitrocellulose membranes using a Trans-Blot Semi-Dry transfer apparatus (Bio-Rad). Following transfer, membranes were blocked in 1× Tris-buffered saline (TBS) and 5% BSA for 45 min. Membranes were then incubated with primary antibodies (diluted in TBS containing 1% BSA) for 18 h at 4 °C. Following primary antibody incubation, membranes were exposed to secondary antibodies conjugated to horseradish

peroxidase. EZ-ECL chemiluminescent reagent (FroggaBio) was used to visualize membranes on Amersham Biosciences Hyperfilm (GE Healthcare), which were developed using a Kodak X-Omat 1000A processor.

RNA isolation and quantitative real-time PCR

Total RNA was isolated using RNeasy Mini Kit (Qiagen) and reverse-transcribed to cDNA using High-capacity cDNA Reverse Transcription kit (Applied Biosystems). Real-time PCR was performed using Fast SYBR Green Master Mix (Applied Biosystems). Primer sequences used for real-time PCR are listed in Table 2.

Statistical analysis

Error bars represent values expressed as the mean ± S.D. Comparisons between two groups were carried out using the unpaired Student's *t* test and those involving multiple groups using a one-way analysis of variance. Differences between groups were considered significant at $p < 0.05$.

Author contributions—P. F. L., J. H. B., K. P., N. G. S., and R. C. A. conceptualization; P. F. L., J. H. B., K. P., S. V. P., M. F., and R. C. A. data curation; P. F. L. software; P. F. L. formal analysis; P. F. L. supervision; P. F. L. validation; P. F. L., J. H. B., K. P., M. E. M., S. V. P., and R. C. A. investigation; P. F. L. visualization; P. F. L., J. H. B., K. P., M. E. M., S. V. P., and N. G. S. methodology; P. F. L. writing-original draft; P. F. L., J. H. B., and R. C. A. project administration; P. F. L., J. H. B., K. P., M. F., N. G. S., and R. C. A. writing-review and editing; R. C. A. resources; R. C. A. funding acquisition.

References

1. Vernon, G., Baranova, A., and Younossi, Z. M. (2011) Systematic review: the epidemiology and natural history of non-alcoholic fatty liver disease and non-alcoholic steatohepatitis in adults. *Aliment. Pharmacol. Ther.* **34,** 274–285 CrossRef Medline
2. Sayiner, M., Koenig, A., Henry, L., and Younossi, Z. M. (2016) Epidemiology of nonalcoholic fatty liver disease and nonalcoholic steatohepatitis in the United States and the rest of the world. *Clin. Liver Dis.* **20,** 205–214 CrossRef Medline
3. Benedict, M., and Zhang, X. (2017) Non-alcoholic fatty liver disease: an expanded review. *World J. Hepatol.* **9,** 715–732 CrossRef Medline
4. Calzadilla Bertot, L., and Adams, L. A. (2016) The natural course of non-alcoholic fatty liver disease. *Int. J. Mol. Sci.* **17,** e774 Medline
5. World Health Organization (2016) *Hearts: technical package for cardiovascular disease management in primary health care*. World Health Organization, Switzerland
6. Söderberg, C., Stål, P., Askling, J., Glaumann, H., Lindberg, G., Marmur, J., and Hultcrantz, R. (2010) Decreased survival of subjects with elevated liver function tests during a 28-year follow-up. *Hepatology* **51,** 595–602 CrossRef Medline
7. Pickhardt, P. J., Hahn, L., Muñoz del Rio, A., Park, S. H., Reeder, S. B., and Said, A. (2014) Natural history of hepatic steatosis: observed outcomes for subsequent liver and cardiovascular complications. *Am. J. Roentgenol.* **202,** 752–758 CrossRef Medline
8. Ekstedt, M., Hagström, H., Nasr, P., Fredrikson, M., Stål, P., Kechagias, S., and Hultcrantz, R. (2015) Fibrosis stage is the strongest predictor for disease-specific mortality in NAFLD after up to 33 years of follow-up. *Hepatology* **61,** 1547–1554 CrossRef Medline
9. Patil, R., and Sood, G. K. (2017) Non-alcoholic fatty liver disease and cardiovascular risk. *World J. Gastrointest. Pathophysiol.* **8,** 51–58 CrossRef Medline
10. Francque, S. M., van der Graaff, D., and Kwanten, W. J. (2016) Non-alcoholic fatty liver disease and cardiovascular risk: pathophysiological mechanisms and implications. *J. Hepatol.* **65,** 425–443 CrossRef Medline
11. Lakoski, S. G., Lagace, T. A., Cohen, J. C., Horton, J. D., and Hobbs, H. H. (2009) Genetic and metabolic determinants of plasma PCSK9 levels. *J. Clin. Endocrinol. Metab.* **94,** 2537–2543 CrossRef Medline
12. Ruscica, M., Ferri, N., Macchi, C., Meroni, M., Lanti, C., Ricci, C., Maggioni, M., Fracanzani, A. L., Badiali, S., Fargion, S., Magni, P., Valenti, L., and Dongiovanni, P. (2016) Liver fat accumulation is associated with circulating PCSK9. *Ann. Med.* **48,** 384–391 CrossRef Medline
13. Benjannet, S., Rhainds, D., Essalmani, R., Mayne, J., Wickham, L., Jin, W., Asselin, M. C., Hamelin, J., Varret, M., Allard, D., Trillard, M., Abifadel, M., Tebon, A., Attie, A. D., Rader, D. J., *et al.* (2004) NARC-1/PCSK9 and its natural mutants: zymogen cleavage and effects on the low density lipoprotein (LDL) receptor and LDL cholesterol. *J. Biol. Chem.* **279,** 48865–48875 CrossRef Medline
14. Maxwell, K. N., and Breslow, J. L. (2004) Adenoviral-mediated expression of Pcsk9 in mice results in a low-density lipoprotein receptor knockout phenotype. *Proc. Natl. Acad. Sci. U.S.A.* **101,** 7100–7105 CrossRef Medline
15. Seidah, N. G., Abifadel, M., Prost, S., Boileau, C., and Prat, A. (2017) The proprotein convertases in hypercholesterolemia and cardiovascular diseases: emphasis on proprotein convertase subtilisin/kexin 9. *Pharmacol. Rev.* **69,** 33–52 Medline
16. Abifadel, M., Varret, M., Rabès, J. P., Allard, D., Ouguerram, K., Devillers, M., Cruaud, C., Benjannet, S., Wickham, L., Erlich, D., Derré, A., Villéger, L., Farnier, M., Beucler, I., Bruckert, E., *et al.* (2003) Mutations in PCSK9 cause autosomal dominant hypercholesterolemia. *Nat. Genet.* **34,** 154–156 CrossRef Medline
17. Mayne, J., Dewpura, T., Raymond, A., Bernier, L., Cousins, M., Ooi, T. C., Davignon, J., Seidah, N. G., Mbikay, M., and Chrètien, M. (2011) Novel loss-of-function PCSK9 variant is associated with low plasma LDL cholesterol in a French-Canadian family and with impaired processing and secretion in cell culture. *Clin. Chem.* **57,** 1415–1423 CrossRef Medline
18. Kumar, S., Kang, D. W., Rezvan, A., and Jo, H. (2017) Accelerated atherosclerosis development in C57Bl6 mice by overexpressing AAV-mediated PCSK9 and partial carotid ligation. *Lab. Invest.* **97,** 935–945 CrossRef Medline
19. Denis, M., Marcinkiewicz, J., Zaid, A., Gauthier, D., Poirier, S., Lazure, C., Seidah, N. G., and Prat, A. (2012) Gene inactivation of PCSK9 reduces atherosclerosis in mice. *Circulation* **125,** 894–901 CrossRef Medline
20. Sabatine, M. S., Giugliano, R. P., Keech, A. C., Honarpour, N., Wiviott, S. D., Murphy, S. A., Kuder, J. F., Wang, H., Liu, T., Wasserman, S. M., Sever, P. S., Pedersen, T. R., and FOURIER Steering Committee and Investigators. (2017) Evolocumab and clinical outcomes in patients with cardiovascular disease. *N. Engl. J. Med.* **376,** 1713–1722 CrossRef Medline
21. Seidah, N. G. (2017) The PCSK9 revolution and the potential of PCSK9-based therapies to reduce LDL-cholesterol. *Global Cardiol. Sci. Pract.* **2017,** e201702 Medline
22. Wadhera, R. K., Steen, D. L., Khan, I., Giugliano, R. P., and Foody, J. M. (2016) A review of low-density lipoprotein cholesterol, treatment strategies, and its impact on cardiovascular disease morbidity and mortality. *J. Clin. Lipidol.* **10,** 472–489 CrossRef Medline
23. Colgan, S. M., Tang, D., Werstuck, G. H., and Austin, R. C. (2007) Endoplasmic reticulum stress causes the activation of sterol regulatory element binding protein-2. *Int. J. Biochem. Cell Biol.* **39,** 1843–1851 CrossRef Medline
24. Colgan, S. M., Hashimi, A. A., and Austin, R. C. (2011) Endoplasmic reticulum stress and lipid dysregulation. *Expert. Rev. Mol. Med.* **13,** e4 CrossRef Medline
25. Lebeau, P., Al-Hashimi, A., Sood, S., Lhoták, Š., Yu, P., Gyulay, G., Paréé, G., Chen, S. R., Trigatti, B., Prat, A., Seidah, N. G., and Austin, R. C. (2017) Endoplasmic reticulum stress and Ca^{2+} depletion differentially modulate the sterol regulatory protein PCSK9 to control lipid metabolism. *J. Biol. Chem.* **292,** 1510–1523 CrossRef Medline
26. Li, J., Huang, J., Li, J. S., Chen, H., Huang, K., and Zheng, L. (2012) Accumulation of endoplasmic reticulum stress and lipogenesis in the liver through generational effects of high fat diets. *J. Hepatol.* **56,** 900–907 CrossRef Medline

27. Lee, H. Y., Lee, G. H., Bhattarai, K. R., Park, B. H., Koo, S. H., Kim, H. R., and Chae, H. J. (2016) Bax inhibitor-1 regulates hepatic lipid accumulation via ApoB secretion. *Sci. Rep.* **6,** 27799 CrossRef Medline
28. Zaid, A., Roubtsova, A., Essalmani, R., Marcinkiewicz, J., Chamberland, A., Hamelin, J., Tremblay, M., Jacques, H., Jin, W., Davignon, J., Seidah, N. G., and Prat, A. (2008) Proprotein convertase subtilisin/kexin type 9 (PCSK9): hepatocyte-specific low-density lipoprotein receptor degradation and critical role in mouse liver regeneration. *Hepatology* **48,** 646–654 CrossRef Medline
29. Carta, G., Murru, E., Banni, S., and Manca, C. (2017) Palmitic acid: physiological role, metabolism and nutritional implications. *Front. Physiol.* **8,** 902 CrossRef Medline
30. Zhang, Y., Xue, R., Zhang, Z., Yang, X., and Shi, H. (2012) Palmitic and linoleic acids induce ER stress and apoptosis in hepatoma cells. *Lipids Health Dis.* **11,** 1 CrossRef Medline
31. Cui, W., Ma, J., Wang, X., Yang, W., Zhang, J., and Ji, Q. (2013) Free fatty acid induces endoplasmic reticulum stress and apoptosis of beta-cells by Ca^{2+}/calpain-2 pathways. *PLoS ONE* **8,** e59921 CrossRef Medline
32. Zhang, Y., Miao, L., Zhang, H., Wu, G., Zhang, Z., and Lv, J. (2018) Chlorogenic acid against palmitic acid in endoplasmic reticulum stress-mediated apoptosis resulting in protective effect of primary rat hepatocytes. *Lipids Health Dis.* **17,** 270 CrossRef Medline
33. Ben Mosbah, I., Alfany-Fernandez, I., Martel, C., Zaouali, M. A., Bintanel-Morcillo, M., Rimola, A., Rodes, J., Brenner, C., Rosello-Catafau, J., and Peralta, C. (2010) Endoplasmic reticulum stress inhibition protects steatotic and non-steatotic livers in partial hepatectomy under ischemia-reperfusion. *Cell Death Dis.* **1,** e52 CrossRef Medline
34. Ford, R. J., Fullerton, M. D., Pinkosky, S. L., Day, E. A., Scott, J. W., Oakhill, J. S., Bujak, A. L., Smith, B. K., Crane, J. D., Blümer, R. M., Marcinko, K., Kemp, B. E., Gerstein, H. C., and Steinberg, G. R. (2015) Metformin and salicylate synergistically activate liver AMPK, inhibit lipogenesis and improve insulin sensitivity. *Biochem. J.* **468,** 125–132 CrossRef Medline
35. Zabielski, P., Hady, H. R., Chacinska, M., Roszczyc, K., Gorski, J., and Blachnio-Zabielska, A. U. (2018) The effect of high fat diet and metformin treatment on liver lipids accumulation and their impact on insulin action. *Sci. Rep.* **8,** 7249 CrossRef Medline
36. Woo, S. L., Xu, H., Li, H., Zhao, Y., Hu, X., Zhao, J., Guo, X., Guo, T., Botchlett, R., Qi, T., Pei, Y., Zheng, J., Xu, Y., An, X., Chen, L., *et al.* (2014) Metformin ameliorates hepatic steatosis and inflammation without altering adipose phenotype in diet-induced obesity. *PLoS ONE* **9,** e91111 CrossRef Medline
37. Nissar, A. U., Sharma, L., Mudasir, M. A., Nazir, L. A., Umar, S. A., Sharma, P. R., Vishwakarma, R. A., and Tasduq, S. A. (2017) Chemical chaperone 4-phenyl butyric acid (4-PBA) reduces hepatocellular lipid accumulation and lipotoxicity through induction of autophagy. *J. Lipid Res.* **58,** 1855–1868 CrossRef Medline
38. Khera, A. V., Qamar, A., Reilly, M. P., Dunbar, R. L., and Rader, D. J. (2015) Effects of niacin, statin, and fenofibrate on circulating proprotein convertase subtilisin/kexin type 9 levels in patients with dyslipidemia. *Am. J. Cardiol.* **115,** 178–182 CrossRef Medline
39. Gu, L., Wang, Y., Xu, Y., Tian, Q., Lei, G., Zhao, C., Gao, Z., Pan, Q., Zhao, W., Nong, L., and Tan, S. (2017) Lunasin functionally enhances LDL uptake via inhibiting PCSK9 and enhancing LDLR expression *in vitro* and *in vivo*. *Oncotarget* **8,** 80826–80840 Medline
40. Zelcer, N., Hong, C., Boyadjian, R., and Tontonoz, P. (2009) LXR regulates cholesterol uptake through Idol-dependent ubiquitination of the LDL receptor. *Science* **325,** 100–104 CrossRef Medline
41. Dara, L., Ji, C., and Kaplowitz, N. (2011) The contribution of endoplasmic reticulum stress to liver diseases. *Hepatology* **53,** 1752–1763 CrossRef Medline
42. Basseri, S., Lhoták, S., Sharma, A. M., and Austin, R. C. (2009) The chemical chaperone 4-phenylbutyrate inhibits adipogenesis by modulating the unfolded protein response. *J. Lipid Res.* **50,** 2486–2501 CrossRef Medline
43. Ruiz, R., Jideonwo, V., Ahn, M., Surendran, S., Tagliabracci, V. S., Hou, Y., Gamble, A., Kerner, J., Irimia-Dominguez, J. M., Puchowicz, M. A., DePaoli-Roach, A., Hoppel, C., Roach, P., and Morral, N. (2014) Sterol regulatory element-binding protein-1 (SREBP-1) is required to regulate glycogen synthesis and gluconeogenic gene expression in mouse liver. *J. Biol. Chem.* **289,** 5510–5517 CrossRef Medline
44. Shimomura, I., Bashmakov, Y., and Horton, J. D. (1999) Increased levels of nuclear SREBP-1c associated with fatty livers in two mouse models of diabetes mellitus. *J. Biol. Chem.* **274,** 30028–30032 CrossRef Medline
45. Jo, H. K., Kim, G. W., Jeong, K. J., Kim, D. Y., and Chung, S. H. (2014) Eugenol ameliorates hepatic steatosis and fibrosis by down-regulating SREBP1 gene expression via AMPK-mTOR-p70S6K signaling pathway. *Biol. Pharm. Bull.* **37,** 1341–1351 Medline
46. Cao, J., Dai, D. L., Yao, L., Yu, H. H., Ning, B., Zhang, Q., Chen, J., Cheng, W. H., Shen, W., and Yang, Z. X. (2012) Saturated fatty acid induction of endoplasmic reticulum stress and apoptosis in human liver cells via the PERK/ATF4/CHOP signaling pathway. *Mol. Cell. Biochem.* **364,** 115–129 CrossRef Medline
47. Xu, S., Nam, S. M., Kim, J. H., Das, R., Choi, S. K., Nguyen, T. T., Quan, X., Choi, S. J., Chung, C. H., Lee, E. Y., Lee, I. K., Wiederkehr, A., Wollheim, C. B., Cha, S. K., and Park, K. S. (2015) Palmitate induces ER calcium depletion and apoptosis in mouse podocytes subsequent to mitochondrial oxidative stress. *Cell Death Dis.* **6,** e1976 CrossRef Medline
48. Chen, X. W., Wang, H., Bajaj, K., Zhang, P., Meng, Z. X., Ma, D., Bai, Y., Liu, H. H., Adams, E., Baines, A., Yu, G., Sartor, M. A., Zhang, B., Yi, Z., Lin, J., *et al.* (2013) SEC24A deficiency lowers plasma cholesterol through reduced PCSK9 secretion. *eLife* **2,** e00444 CrossRef Medline
49. Emmer, B. T., Hesketh, G. G., Kotnik, E., Tang, V. T., Lascuna, P. J., Xiang, J., Gingras, A. C., Chen, X. W., and Ginsburg, D. (2018) The cargo receptor SURF4 promotes the efficient cellular secretion of PCSK9. *eLife* **7,** e38839 CrossRef Medline
50. Li, H., Dong, B., Park, S. W., Lee, H. S., Chen, W., and Liu, J. (2009) Hepatocyte nuclear factor 1α plays a critical role in *PCSK9* gene transcription and regulation by the natural hypocholesterolemic compound berberine. *J. Biol. Chem.* **284,** 28885–28895 CrossRef Medline
51. Jensen, K. K., Tadin-Strapps, M., Wang, S. P., Hubert, J., Kan, Y., Ma, Y., McLaren, D. G., Previs, S. F., Herath, K. B., Mahsut, A., Liaw, A., Wang, S., Stout, S. J., Keohan, C., Forrest, G., *et al.* (2016) Dose-dependent effects of siRNA-mediated inhibition of SCAP on PCSK9, LDLR, and plasma lipids in mouse and rhesus monkey. *J. Lipid Res.* **57,** 2150–2162 CrossRef Medline
52. Sui, G. G., Xiao, H. B., Lu, X. Y., and Sun, Z. L. (2018) Naringin activates AMPK resulting in altered expression of SREBPs, PCSK9, and LDLR to reduce body weight in obese C57BL/6J mice. *J. Agric. Food Chem.* **66,** 8983–8990 CrossRef Medline
53. Shao, W., and Espenshade, P. J. (2014) Sterol regulatory element-binding protein (SREBP) cleavage regulates Golgi-to-endoplasmic reticulum recycling of SREBP cleavage-activating protein (SCAP). *J. Biol. Chem.* **289,** 7547–7557 CrossRef Medline
54. Mayne, J., Dewpura, T., Raymond, A., Cousins, M., Chaplin, A., Lahey, K. A., Lahaye, S. A., Mbikay, M., Ooi, T. C., and Chrétien, M. (2008) Plasma PCSK9 levels are significantly modified by statins and fibrates in humans. *Lipids Health Dis.* **7,** 22 CrossRef Medline
55. Welder, G., Zineh, I., Pacanowski, M. A., Troutt, J. S., Cao, G., and Konrad, R. J. (2010) High-dose atorvastatin causes a rapid sustained increase in human serum PCSK9 and disrupts its correlation with LDL cholesterol. *J. Lipid Res.* **51,** 2714–2721 CrossRef Medline
56. Gauthier, M. S., Awan, Z., Bouchard, A., Champagne, J., Tessier, S., Faubert, D., Chabot, K., Garneau, P. Y., Rabasa-Lhoret, R., Seidah, N. G., Ridker, P. M., Genest, J., and Coulombe, B. (2018) Posttranslational modification of proprotein convertase subtilisin/kexin type 9 is differentially regulated in response to distinct cardiometabolic treatments as revealed by targeted proteomics. *J. Clin. Lipidol.* **12,** 1027–1038 CrossRef Medline
57. LaRosa, J. C., Grundy, S. M., Waters, D. D., Shear, C., Barter, P., Fruchart, J. C., Gotto, A. M., Greten, H., Kastelein, J. J., Shepherd, J., Wenger, N. K., and Treating to New Targets (TNT) Investigators (2005) Intensive lipid lowering with atorvastatin in patients with stable coronary disease. *N. Engl. J. Med.* **352,** 1425–1435 CrossRef Medline
58. Giunzioni, I., and Tavori, H. (2015) New developments in atherosclerosis: clinical potential of PCSK9 inhibition. *Vasc. Health Risk Manag.* **11,** 493–501 Medline

59. Wang, Y., Huang, Y., Hobbs, H. H., and Cohen, J. C. (2012) Molecular characterization of proprotein convertase subtilisin/kexin type 9-mediated degradation of the LDLR. *J. Lipid Res.* **53,** 1932–1943 CrossRef Medline
60. Wargny, M., Ducluzeau, P. H., Petit, J. M., Le May, C., Smati, S., Arnaud, L., Pichelin, M., Bouillet, B., Lannes, A., Blanchet, O., Lefebvre, P., Francque, S., Van Gaal, L., Staels, B., Vergès, B., Boursier, J., and Cariou, B. (2018) Circulating PCSK9 levels are not associated with the severity of hepatic steatosis and NASH in a high-risk population. *Atherosclerosis* **278,** 82–90 CrossRef Medline
61. Retterstøl, K., Svendsen, M., Narverud, I., and Holven, K. B. (2018) Effect of low carbohydrate high fat diet on LDL cholesterol and gene expression in normal-weight, young adults: a randomized controlled study. *Atherosclerosis* **279,** 52–61 CrossRef Medline
62. Ricci, C., Ruscica, M., Camera, M., Rossetti, L., Macchi, C., Colciago, A., Zanotti, I., Lupo, M. G., Adorni, M. P., Cicero, A. F. G., Fogacci, F., Corsini, A., and Ferri, N. (2018) PCSK9 induces a pro-inflammatory response in macrophages. *Sci. Rep.* **8,** 2267 CrossRef Medline
63. Lebeau, P., Platko, K., Al-Hashimi, A. A., Byun, J. H., Lhoták, Š., Holzapfel, N., Gyulay, G., Igdoura, S. A., Cool, D. R., Trigatti, B., Seidah, N. G., and Austin, R. C. (2018) Loss-of-function PCSK9 mutants evade the unfolded protein response sensor GRP78 and fail to induce endoplasmic reticulum stress when retained. *J. Biol. Chem.* **293,** 7329–7343 CrossRef Medline

Chapter 5: Publication in the Journal of Biological Chemistry, 2018

Lebeau, P., K. Platko, A. A. Al-Hashimi, J. H. Byun, S. Lhotak, N. Holzapfel, G. Gyulay, S. A. Igdoura, D. R. Cool, B. Trigatti, N. G. Seidah and R. C. Austin (2018). "Loss-of-function PCSK9 mutants evade the unfolded protein response sensor GRP78 and fail to induce endoplasmic reticulum stress when retained." J Biol Chem **293**(19): 7329-7343

Author Contributions: P. L., K. P., N. G. S., and R. C. A. conceptual- ization; P. L., K. P., D. C., N. G. S., and R. C. A. resources; P. L., K. P., and R. C. A. data curation; P. L. and K. P. software; P. L., K. P., J. H. B., and R. C. A. formal analysis; P. L., B. T., and R. C. A. super- vision; P. L. and R. C. A. funding acquisition; P. L., K. P., and R. C. A. validation; P. L., K. P., A. A. A.-H., J. H. B., S̆. L., N. H., G. G., D. C., and R. C. A. investigation; P. L., K. P., N. G. S., and R. C. A. visualiza- tion; P. L., K. P., D. C., N. G. S., and R. C. A. methodology; P. L., K. P., and R. C. A. writing-original draft; P. L., K. P., N. G. S., and R. C. A. project administration; P. L., K. P., A. A. A.-H., J. H. B., S̆. L., N. H., G. G., S. A. I., D. C., B. T., N. G. S., and R. C. A. writing-review and editing.

JBC ARTICLE

Loss-of-function PCSK9 mutants evade the unfolded protein response sensor GRP78 and fail to induce endoplasmic reticulum stress when retained

Received for publication, November 22, 2017, and in revised form, March 15, 2018 Published, Papers in Press, March 28, 2018, DOI 10.1074/jbc.RA117.001049

Paul Lebeau[‡], Khrystyna Platko[‡], Ali A. Al-Hashimi[‡], Jae Hyun Byun[‡], Šárka Lhoták[‡], Nicholas Holzapfel[‡], Gabriel Gyulay[‡], Suleiman A. Igdoura[§], David R. Cool[¶], Bernardo Trigatti[‖], Nabil G. Seidah[‡‡], and Richard C. Austin[‡‖1]**

*From the [‡]Department of Medicine, Division of Nephrology, McMaster University, St. Joseph's Healthcare Hamilton and Hamilton Center for Kidney Research, Hamilton, Ontario L8N 4A6, Canada, the [‖]Thrombosis and Atherosclerosis Research Institute (TaARI), Hamilton Health Sciences and McMaster University, Hamilton, Ontario L8L 2X2, Canada, the [§]Departments of Biology and Pathology, McMaster University, Hamilton, Ontario L8S 4K1, Canada, the **Departments of Biochemistry and Biomedical Sciences, McMaster University, Hamilton, Ontario L8S 4L8, Canada, the [¶]Department of Pharmacology and Toxicology, Boonshoft School of Medicine, Wright State University, Dayton, Ohio, 45435-0001, and the [‡‡]Laboratory of Biochemical Neuroendocrinology, Clinical Research Institute of Montreal, University of Montreal, Montreal, Quebec H2W 1R7, Canada*

Edited by Peter Cresswell

The proprotein convertase subtilisin/kexin type-9 (PCSK9) plays a central role in cardiovascular disease (CVD) by degrading hepatic low-density lipoprotein receptor (LDLR). As such, loss-of-function (LOF) PCSK9 variants that fail to exit the endoplasmic reticulum (ER) increase hepatic LDLR levels and lower the risk of developing CVD. The retention of misfolded protein in the ER can cause ER stress and activate the unfolded protein response (UPR). In this study, we investigated whether a variety of LOF PCSK9 variants that are retained in the ER can cause ER stress and hepatic cytotoxicity. Although overexpression of these PCSK9 variants caused an accumulation in the ER of hepatocytes, UPR activation or apoptosis was not observed. Furthermore, ER retention of endogenous PCSK9 via splice switching also failed to induce the UPR. Consistent with these *in vitro* studies, overexpression of PCSK9 in the livers of mice had no impact on UPR activation. To elucidate the cellular mechanism to explain these surprising findings, we observed that the 94-kDa glucose-regulated protein (GRP94) sequesters PCSK9 away from the 78-kDa glucose-regulated protein (GRP78), the major activator of the UPR. As a result, GRP94 knockdown increased the stability of GRP78–PCSK9 complex and resulted in UPR activation following overexpression of ER-retained PCSK9 variants relative to WT secreted controls. Given that overexpression of these LOF PCSK9 variants does not cause UPR activation under normal homeostatic conditions, therapeutic strategies aimed at blocking the autocatalytic cleavage of PCSK9 in the ER represent a viable strategy for reducing circulating PCSK9.

The discovery of PCSK9[2] has provided a novel therapeutic target for the management of CVD (1, 2). PCSK9 is mainly expressed and secreted by liver hepatocytes where it degrades the LDLR and promotes elevated circulating LDL levels (3, 4), a well-known risk factor of cardiovascular dysfunction (5, 6). Following its characterization, genetic screens revealed that gain-of-function (GOF) mutations in the *PCSK9* gene represented a third locus associated with autosomal-dominant hypercholesterolemia (7). In addition to the discovery of the first GOF variant, PCSK9^{S127R}, further investigations led to the identification of a wide range of LOF PCSK9 variants (8, 9). In contrast to GOF mutations, which enhance PCSK9-mediated LDLR degradation and promote increased circulating LDL levels, LOF mutations increase hepatic LDLR expression and reduce circulating LDL levels (10). The Atherosclerosis Risk in Communities (ARIC) study reported that nonsense (C679*X*/Y142*X*) and missense (R46L) mutations in *PCSK9* were associated with an 88 and 47% reduction in the risk of developing coronary heart

This work was supported in part by Heart and Stroke Foundation of Ontario Grant T-6146, Heart and Stroke Foundation of Canada Grants G-13-0003064 and G-15-0009389, Canadian Institutes of Health Research (CIHR) Grant 74477 (to R. C. A.); Leducq Foundation Grant 13 CVD 03, CIHR Foundation Grant 148363, and Canada Research Chair 216684 (to N. G. S.); National Institutes of Health Grant DK58111 (to D. R. C.); and St. Joseph's Healthcare Hamilton and CIHR Team Grant in Thromboembolism FRN-79846. The authors declare that they have no conflicts of interest with the contents of this article. The content is solely the responsibility of the authors and does not necessarily represent the official views of the National Institutes of Health.

[1] A career investigator of the Heart and Stroke Foundation of Ontario and holds the Amgen Canada Research Chair in the Division of Nephrology at St. Joseph's Healthcare and McMaster University. To whom correspondence should be addressed: St. Joseph's Healthcare Hamilton and Hamilton Center for Kidney Research, 50 Charlton Ave. East, Rm. T-3313, Hamilton, Ontario L8N 4A6, Canada. Tel.: 905-522-1155 (ext. 35175); Fax: 905-540-6589; E-mail: austinr@taari.ca.

[2] The abbreviations used are: PCSK9, proprotein convertase subtilisin/kexin type-9; ATF, activating transcription factor; CHOP, CCAAT/enhancer–binding protein homologous protein; CVD, cardiovascular disease; ER, endoplasmic reticulum; ERAI, ER activated indicator; ERSD, endoplasmic reticulum storage disease; EV, empty vector; GOF, gain-of-function; GRP78, 78-kDa glucose-regulated protein; GRP94, 94-kDa glucose-regulated protein; IRE1α, inositol-requiring enzyme-1α; LDLR, low-density lipoprotein receptor; LOF, loss-of-function; PERK, protein kinase RNA–like endoplasmic reticulum kinase; SSO, splice-switching oligomer; TG, thapsigargin; UPR, unfolded protein response; VP, vasopressin; XBP1, X-box–binding protein-1; PCSK9^{SV}, PCSK9 splice variant; sXBP1, spliced XBP1; PUMA, p53-up-regulated modulator of apoptosis; siGRP94, siRNA targeted against GRP94; IP, immunoprecipitation; PCSK9^{FS}, PCSK9 frameshift variant.

disease, respectively (11). Additional LOF variants such as PCSK9^{G236S}, PCSK9^{N354I}, and PCSK9^{Q152H} were subsequently identified and extensively studied *in vitro* (10, 12). The phenotype associated with such LOF mutations occurs due to the inability of the ER-resident nascent pro-PCSK9 to undergo autocatalytic cleavage and maturation in the ER, thereby leading to its retention. This was found to drive LDLR expression and accounts for the low circulating LDL levels found in patients harboring such mutations (10, 12).

There is now ample evidence supporting the notion that the retention of PCSK9 in the ER leads to a significant reduction of circulating LDL levels. In addition, we have recently demonstrated that ER stress blocks the secretion of PCSK9 in cultured hepatocytes and mice, and this was associated with increased hepatic LDLR expression and reduced circulating LDL levels (13). Furthermore, the retention of PCSK9 in the ER via GRP94 promotes elevated hepatic LDLR levels (14).

Despite the potential benefits of this strategy for reducing circulating LDL levels, ER storage diseases (ERSDs) are a common end point of ER protein retention and contribute to a wide range of human disorders (15, 16). The accumulation of retained/misfolded proteins in the ER leads to ER stress and triggers the UPR (17–19). A well-described form of ERSD occurs as a result of ER arginine vasopressin (VP) retention arising from mutations such as VP^{G14R} and VP^{G17V}. These naturally occurring mutations play a central role in the development of familial neurohypophyseal diabetes insipidus in a manner dependent on ER stress and subsequent UPR activation (20, 21). The UPR signaling cascade consists of three major transducers located at the ER membrane that are activated upon dissociation of GRP78 from their intra-ER domains. These "*arms of the UPR*" include (*a*) inositol-requiring protein-1α (IRE1α), which splices and activates X-box–binding protein-1 (XBP1), (*b*) activating transcription factor-6 (ATF6), and (*c*) protein kinase RNA (PKR)–like ER kinase (PERK), which promotes the expression of the proapoptotic CCAAT/enhancer–binding protein homologous protein (CHOP). Collectively, this cascade of UPR mediators acts to increase the folding capacity of the ER while reducing its burden by blocking global synthesis and nascent polypeptide influx (18).

Despite the well-documented phenomenon of ERSD, we now report that the ER retention of LOF PCSK9 variants does not cause UPR activation or apoptosis. This hypothesis was tested using a number of LOF PCSK9 variants, including the naturally occurring PCSK9^{Q152H}, in HuH7, HK-2, and N2a cell lines. Furthermore, ER stress and apoptosis were examined in cells treated with a splice-switching oligomer (SSO) to induce the retention of an endogenously expressed PCSK9 splice variant (PCSK9^{SV}) lacking its catalytic domain, which is required for autocatalytic cleavage (22). Finally, coimmunoprecipitation experiments show that GRP94 masks ER-resident pro-PCSK9 from GRP78, which is widely known to act as the major sensor of UPR activation (23, 24). To substantiate this observation, ER PCSK9 retention was shown to cause ER stress/UPR activation following knockdown of GRP94.

Results

Retention of PCSK9 variants in the ER does not induce the UPR

Cultured HuH7 hepatocytes, known to express PCSK9, were transiently transfected with either wildtype PCSK9 (PCSK9^{WT}) or PCSK9^{Q152H}. Endogenous PCSK9 expression was then compared with the cytomegalovirus (CMV)-driven V5-labeled PCSK9 constructs by immunoblotting using an anti-PCSK9 antibody (Fig. 1*A*). Cells transfected with PCSK9^{Q152H} exhibited 6.2-fold greater levels of ER-resident pro-PCSK9 than that of endogenously expressed PCSK9 found in empty vector (EV)–transfected controls and ~3-fold greater levels than PCSK9^{WT}-transfected controls. To confirm the cellular retention of PCSK9^{Q152H}, ELISAs were performed on the media from the PCSK9-transfected cells and demonstrated an 87% reduction in the secreted form of the protein (Fig. 1*B*). Activation of the ER stress–inducible transcription factor SREBP2 (25, 26), a regulator of PCSK9 expression (27), was also examined in PCSK9^{Q152H}-transfected HuH7 cells and found to be 5-fold down-regulated compared with PCSK9^{WT}-transfected control (Fig. 1*C*). To investigate the effect of PCSK9 variants on UPR activation, HuH7 cells cotransfected with the ER activated indicator (ERAI) plasmid in addition to plasmids encoding a variety of PCSK9 variants were examined via immunoblotting of GRP78 and CHOP. The ERAI plasmid encodes an ER stress–inducible FLAG-XBP1 and was used as an additional tool to characterize UPR activation in our model (13, 28). A group of cells were also treated with the ER stress–inducing agent thapsigargin (TG; 100 nM) to serve as a benchmark of UPR activation. PCSK9 variants examined in this experiment included PCSK9^{WT} and PCSK9^{Q152S}, which undergo autocatalytic cleavage and secretion, as well as PCSK9^{Q152H}, PCSK9^{Q152D} (29), and a C-terminal PCSK9 frameshift variant (PCSK9^{FS}),[3] all of which fail to exit the ER. Despite the retention of these PCSK9 variants in the ER, UPR activation was not observed as determined by the absence of GRP78, activated spliced XBP1 (sXBP1), and CHOP induction at the protein level (Fig. 1*D*). As expected, cells exposed to TG showed increased protein expression of these UPR markers. Furthermore, to investigate whether cells expressing variant PCSK9^{Q152H} exhibited increased susceptibility to UPR activation, transfected cells were also treated with TG. Consistent with data from HuH7 cells, immunoblots of HK-2 and N2a cell lysates confirm that retention of PCSK9^{Q152H} fails to induce UPR activation (Fig. 1*E*). Furthermore, the level of UPR induction by TG treatment was similar in cells transfected with PCSK9^{WT} and PCSK9^{Q152H}, demonstrating that ER retention of PCSK9 did not enhance the ability of TG to activate the UPR. Additionally, real-time PCR experiments demonstrated that mRNA levels of sXBP1, ATF6, and GRP78 were not significantly different (Fig. 1*F*). The temporal effect of ER PCSK9 retention on UPR activation was also examined via immunoblotting for GRP78 (Fig. 1*G*). These data demonstrate that the expression level of PCSK9^{Q152H} in the ER was greatest 48 h post-transfection. Despite this observation, GRP78 expression was not induced by PCSK9^{Q152H} at any of the time points examined. To lend sup-

[3] N. G. Seidah, unpublished data.

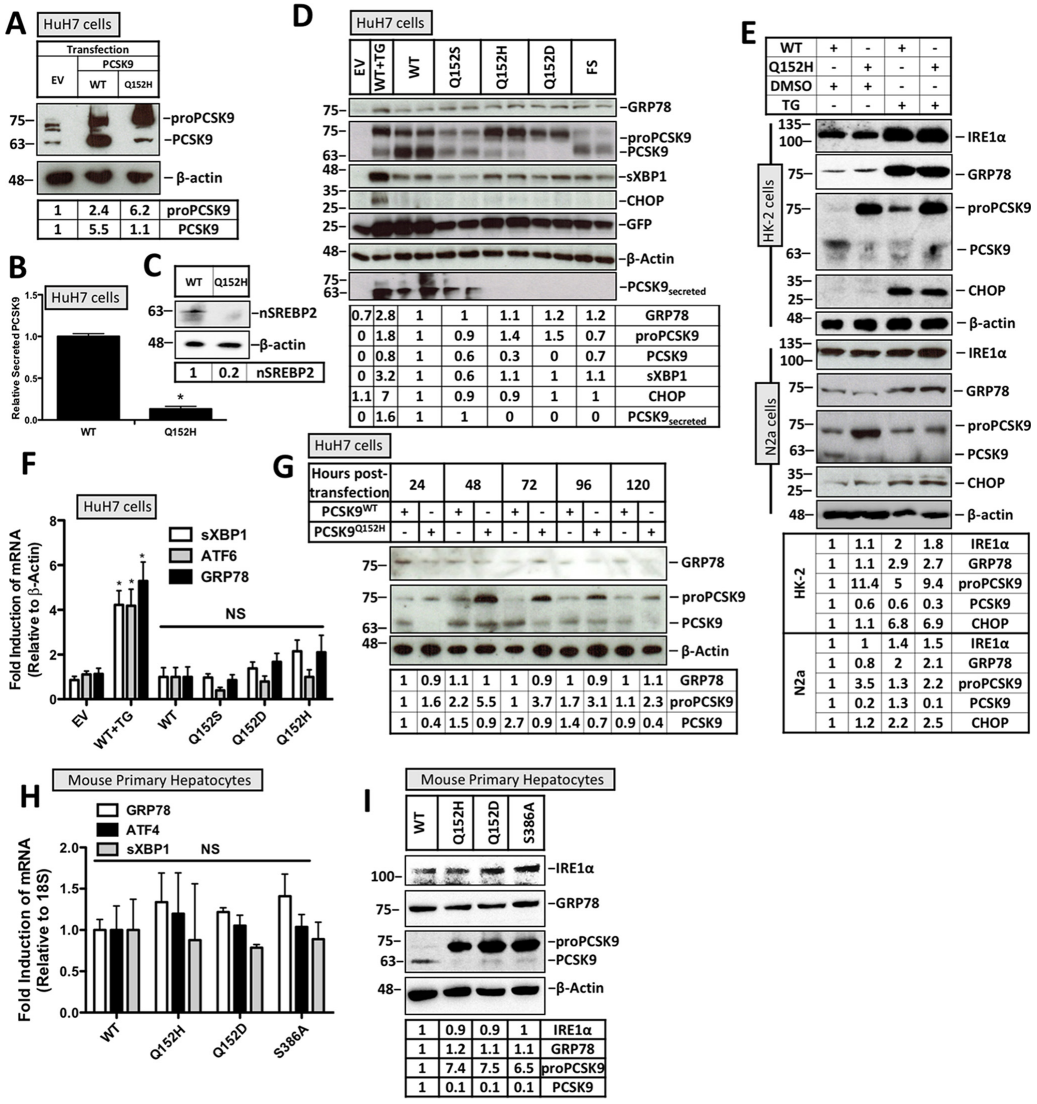

Figure 1. Retention of PCSK9 variants in the ER does not induce the UPR. HuH7 cells were seeded in DMEM and transfected with either EV control, WT, Q152H, Q152S, Q152H, Q152D, or FS V5-labeled PCSK9 variants for 48 h. Cells were also treated with TG (100 nM) for 24 h to serve as a positive control for UPR activation. In addition to V5-PCSK9 transfection, HuH7 cells were also cotransfected with the ERAI plasmid encoding FLAG-XBP1. *A*, CMV-driven PCSK9 expression was compared with endogenous PCSK9 expression in HuH7 cells. *B*, an ELISA was run on the media from HuH7 cells transfected with either $PCSK9^{WT}$ or $PCSK9^{Q152H}$. *C*, SREBP2 activation, in the form of nuclear SREBP2 (*nSREBP2*), was also examined in $PCSK9^{Q152H}$-transfected cells and compared with controls via immunoblotting. *D* and *F*, immunoblot and real-time PCR analyses of these cells were performed for ER stress markers ATF6, GRP78, sXBP1, and CHOP. Immunoblot analysis was also completed on V5-PCSK9 in whole cell lysate and medium to examine PCSK9 maturation and secretion, respectively. GFP, originating from the bicistronic pIRES2-EGFP V5-PCSK9 plasmids, served as a transfection control. *E*, HK-2 and N2a cells transfected with either $PCSK9^{WT}$ or $PCSK9^{Q152H}$ were also examined for UPR activation in the presence or absence of TG. *G*, a time course experiment was carried out in HuH7 cells transfected with either $PCSK9^{WT}$ or $PCSK9^{Q152H}$ to identify the time point yielding the greatest level of PCSK9 retention. *H* and *I*, mouse primary hepatocytes were also transfected with $PCSK9^{Q152H}$, $PCSK9^{Q152D}$, and $PCSK9^{S386A}$ and examined for ER stress marker expression of GRP78, ATF4, sXBP1, and IRE1α via real-time PCR and immunoblotting. Differences between treatments were assessed with unpaired Student's *t* tests. All values are represented as means with *error bars* representing S.D. *B*, *, $p < 0.05$ *versus* WT. *F*, *, $p < 0.05$ *versus* WT. *F* and *H*, nonsignificant (*NS*).

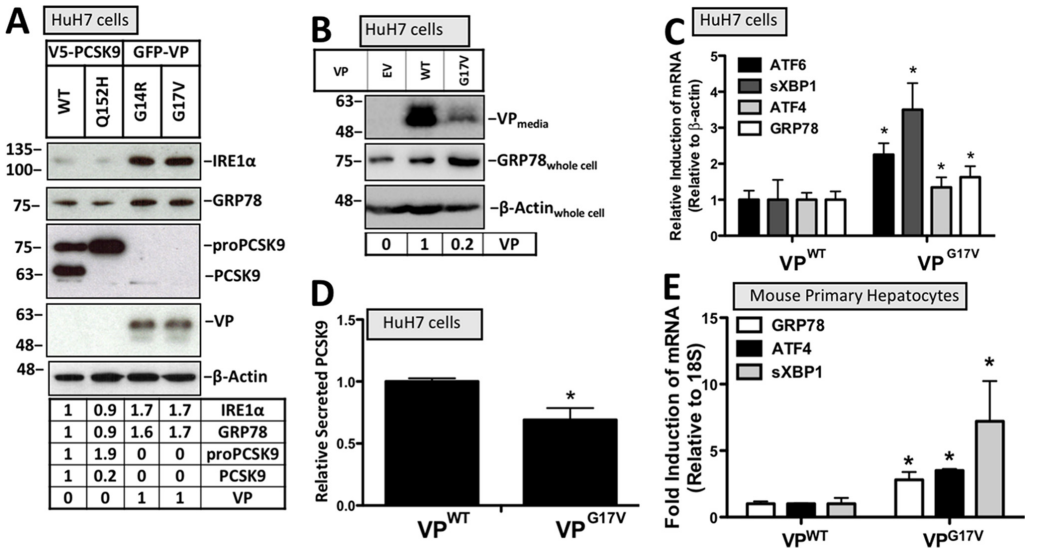

Figure 2. Retention of vasopressin variants induces the UPR. *A* and *C*, the relative expression of UPR markers IRE1α, GRP78, ATF6, sXBP1, and ATF4 were examined using immunoblotting and real-time PCR. *B*, the status of cellular VP retention was examined via immunoblotting of the media from cells transfected with VP^{WT} or VP^{G17V}. *D*, given that ER stress blocks PCSK9 secretion (13), ELISAs were also used to determine whether VP^{G17V} reduced the content of PCSK9 in the media from HuH7 cells. *E*, mouse primary hepatocytes were also transfected with VP^{WT} and VP^{G17V} and examined for UPR marker expression of GRP78, ATF4, and sXBP1 using real-time PCR. Differences between treatments were assessed with unpaired Student's *t* tests. All values are represented as means, and *error bars* represent S.D. *C* and *E*, *, $p < 0.05$ *versus* VP^{WT}.

port to our observations made in HuH7, HK-2, and N2a immortalized cell lines, freshly isolated primary mouse hepatocytes transfected with PCSK9 variants $PCSK9^{Q152H}$, $PCSK9^{Q152D}$, and $PCSK9^{S386A}$ were also examined for UPR activation. In addition to the aforementioned variants, which fail to undergo autocatalytic cleavage due to mutations at the site of cleavage, $PCSK9^{S386A}$ is an ER-retained variant that fails to undergo autocatalytic cleavage due to a point mutation in the catalytic domain (30). Consistent with our findings in immortalized cell lines, real-time PCR and immunoblot data reveal that the UPR is no more active in cells expressing ER-retained PCSK9 variants than in those expressing the WT secreted form of the protein (Fig. 1, *H* and *I*).

Retention of VP variants induces the UPR in hepatocytes

To assess whether the accumulation of misfolded proteins does indeed cause UPR activation in hepatocytes, HuH7 cells transfected with either $PCSK9^{WT}$ or its ER-retention variant $PCSK9^{Q152H}$ were compared with cells transfected with two VP variants, VP^{G14R} and VP^{G17V}, known to induce ER stress in N2a cells (20, 21). Consistent with previous reports, our data demonstrate that ER retention of VP leads to UPR activation as determined by immunoblotting for GRP78 and IRE1α (Fig. 2*A*). The secretion status of VP in these transfected cells was also examined via immunoblotting the media for VP. A greater level of VP secretion occurred in cells expressing VP^{WT} compared with cells expressing VP^{G17V}, which is consistent with increased ER retention of VP^{G17V} (Fig. 2*B*). Furthermore, increased intracellular expression of GRP78 was observed in cells expressing VP^{G17V} compared with those expressing VP^{WT} control. Similar to the immunoblot data in Fig. 2, *A* and *B*, a significant increase in mRNA levels of sXBP1, ATF4, ATF6, and GRP78 was observed in HuH7 cells transfected with the variant VP^{G17V} (Fig. 2*C*). Given that chemical ER stress blocks the secretion of PCSK9 from hepatocytes (13), ELISA was used to determine whether PCSK9 secretion status was affected in cells expressing VP^{G17V}. Consistent with the observed VP^{G17V}-induced UPR activation, these cells also secreted significantly less PCSK9 (Fig. 2*D*). In addition to HuH7 cells, the induction of UPR markers GRP78, ATF4, and sXBP1 was also observed in mouse primary hepatocytes transfected with VP^{G17V} relative to those transfected with VP^{WT} control (Fig. 2*E*).

ER retention of a PCSK9 splice variant via RNAi does not cause UPR activation

To confirm and extend our overexpression studies using exogenously expressed PCSK9 variants, UPR activation was examined in response to the retention of endogenously expressed $PCSK9^{SV}$ in HuH7 cells. To achieve this, HuH7 cells were transfected with an SSO that promotes the expression of a $PCSK9^{SV}$ lacking exon 8 that encodes the catalytic domain. This form of $PCSK9^{SV}$ fails to undergo autocatalytic cleavage and secretion as demonstrated previously (22). Our data demonstrate that sterol deprivation, which induces PCSK9 expression (13), was necessary to attain the SSO-induced formation of ER-resident $PCSK9^{SV}$ (Fig. 3*A*). Consistent with our overexpression studies using the CMV-driven PCSK9 plasmids, increasing the ER content of endogenously expressed $PCSK9^{SV}$ also did not correlate with increased expression of the ER stress

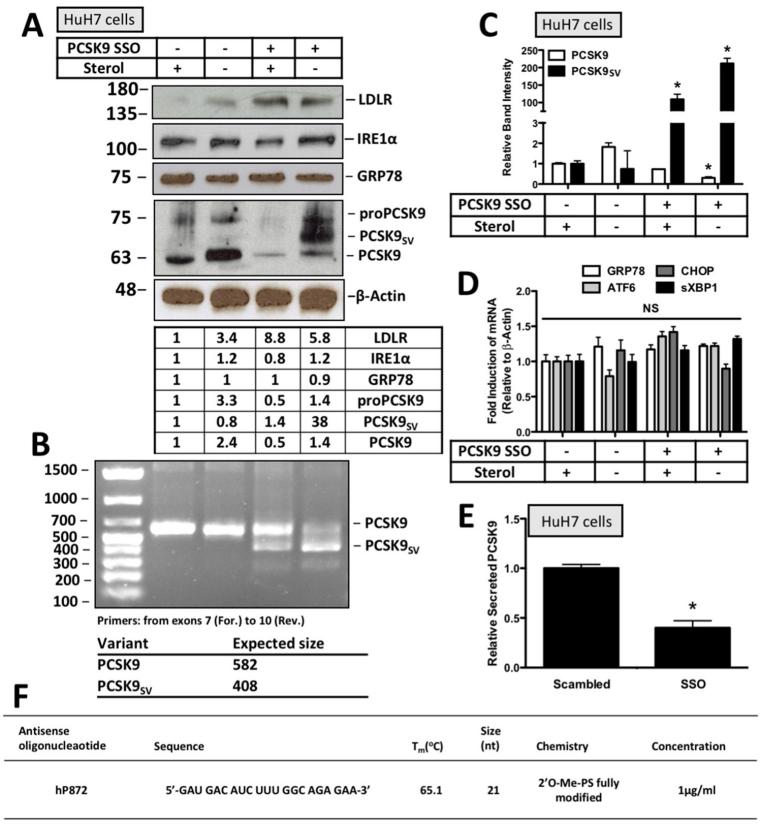

Figure 3. ER retention of a PCSK9 splice variant via RNAi does not cause UPR activation. HuH7 cells were seeded in DMEM with and without sterol and transfected with either scrambled siRNA or PCSK9 SSO (1 μM). The SSO used in these studies promotes the expression of a PCSK9^{SV} lacking exon 8 that fails to undergo autocatalytic cleavage and exit from the ER. *A*, immunoblot analysis of these cells was used to examine PCSK9 expression and the abundance of ER stress markers GRP78 and IRE1α. The status of PCSK9 secretion was also examined indirectly via LDLR immunoblotting. *B*, to confirm the formation of a PCSK9^{SV}, real-time PCR analysis was carried out for PCSK9 using a forward (*For.*) primer upstream of exon 8 and a reverse (*Rev.*) primer downstream of exon 8. The expected sizes of the PCR products from this reaction were 582 and 408 bp for full-length PCSK9 and PCSK9^{SV}, respectively. *C*, the relative band intensities of PCSK9 and its splice variant were quantified using ImageJ. *D*, mRNA analysis of ER stress markers GRP78, ATF6, CHOP, and sXBP1 using real-time PCR. *E*, retention was further confirmed using a PCSK9 ELISA to measure PCSK9 content in the media from these cells. *F*, sequence and properties of PCSK9 SSO "hP872" as described previously (22). *PS*, phosphorothioate. Differences between treatments were assessed with unpaired Student's *t* tests. All values are represented as means, and *error bars* represent S.D. *C*, *, $p < 0.05$ *versus* the respective sterol-treated controls. *E*, *, $p < 0.05$ *versus* scrambled. *NS*, nonsignificant.

markers IRE1α and GRP78. Effective alternative splicing of PCSK9 in the presence of the SSO was confirmed via real-time PCR using primers that span exon 8. Given the size of this exon, the PCR product of full-length PCSK9 had an expected size of 582 bp, whereas that of the PCSK9^{SV} lacking exon 8 was 408 bp (Fig. 3*B*). Quantification of these data shows that the SSO significantly reduced the abundance of PCSK9 mRNA (*, $p < 0.05$) while increasing the abundance of PCSK9^{SV} mRNA (*, $p < 0.05$) in the presence and absence of sterol (Fig. 3*C*). Consistent with the immunoblot data, mRNA levels of ER stress markers were not affected by the SSO (Fig. 3*D*). To confirm the cellular retention status of PCSK9 resulting from SSO treatment, secreted PCSK9 was examined via ELISA and found to be significantly reduced (*, $p < 0.05$) (Fig. 3*E*). The PCSK9 SSO used in this study, also known as hP872, was identical to that reported by Rocha *et al.* (22) (Fig. 3*F*).

ER PCSK9 retention does not induce apoptosis

It is well-established that chronic or severe ER stress can trigger apoptotic cell death (31, 32). For this reason, we examined the effect of ER PCSK9 retention on apoptosis as well as selective mediators of apoptosis. HuH7 cells transfected with PCSK9^{WT} and PCSK9^{Q152H}, in the presence or absence of TG (100 nM), were examined for apoptosis-induced DNA damage via TUNEL staining (Fig. 4*A*). No difference in TUNEL staining was observed between cells expressing PCSK9^{WT} and the PCSK9^{Q152H} retention variant. The abundance of the proapoptotic mediator PUMA was also examined in PCSK9-transfected HK-2 cells, and no significant difference was observed in the presence or absence of TG (100 nM; Fig. 4*B*). Lastly, cell viability was also assessed in PCSK9-transfected HK-2 and HuH7 cells. Although TG treatment led to a significant increase

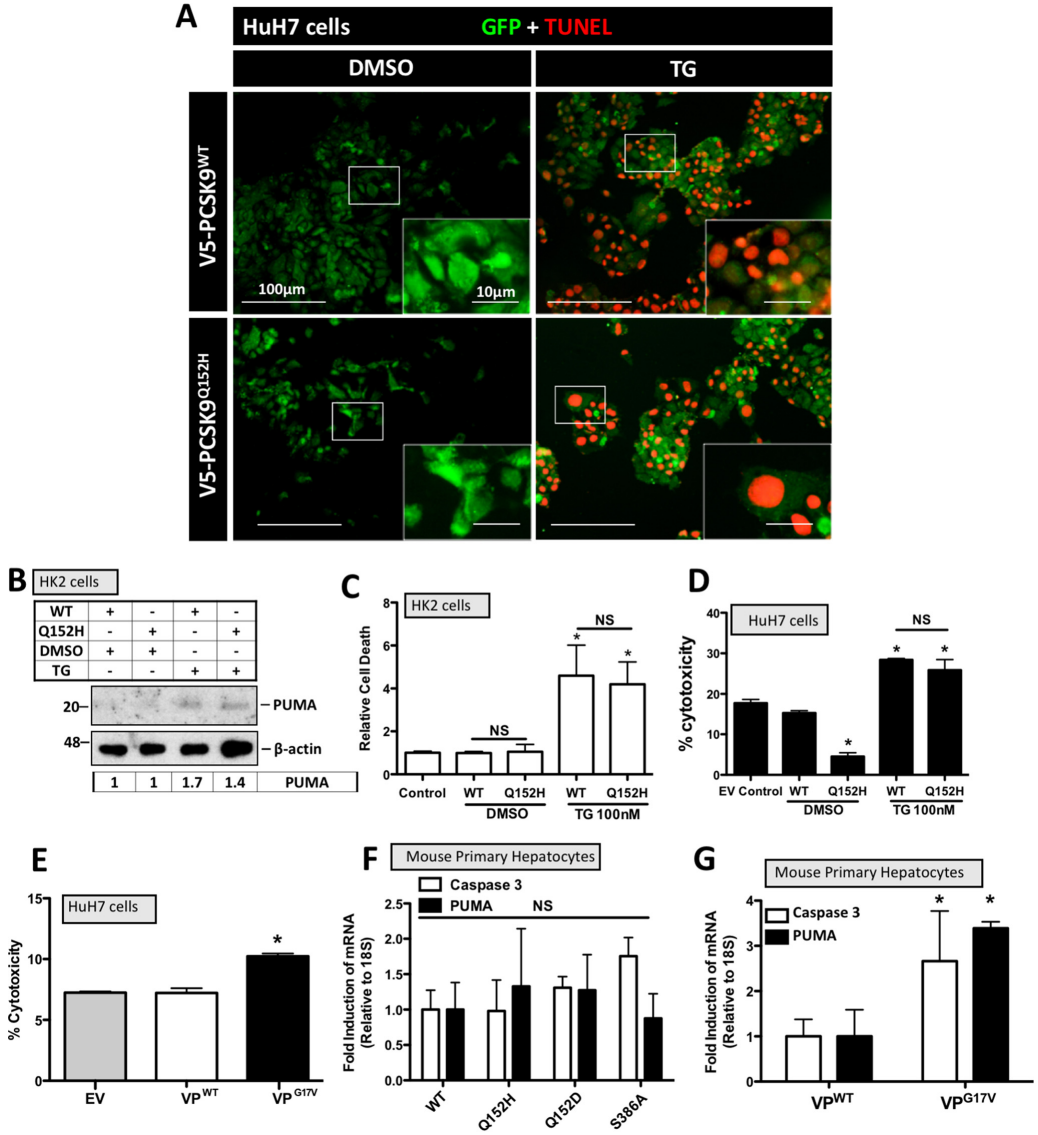

Figure 4. ER PCSK9 retention does not induce apoptosis. HuH7 and HK-2 cells were seeded in DMEM and transfected with either $PCSK9^{WT}$ or $PCSK9^{Q152H}$ for 48 h. Cells were also treated with TG (100 nM) or DMSO vehicle control for 24 h. *A*, HuH7 cells were fixed in 4% paraformaldehyde and stained for apoptosis-induced DNA damage using a 594-labeled TUNEL stain (*red*). Following TUNEL staining, cells were also stained for GFP to identify cells transfected with the bicistronic pIRES2-EGFP V5-PCSK9 plasmids (*green*). *B*, transfected HK-2 cells were also examined for the apoptosis marker PUMA via immunoblot analysis. *C* and *D*, cell viability assays were carried out on transfected HK-2 and HuH7 cells using trypan blue stain and lactate dehydrogenase assays, respectively. *E*, a lactate dehydrogenase assay was also carried out on cells transfected with VP^{G17V}, a mutant known to induce ER stress as a result of ER retention (21). *F*, freshly isolated mouse primary hepatocytes were transfected with PCSK9 variants $PCSK9^{Q152H}$, $PCSK9^{Q152D}$, and $PCSK9^{S386A}$ and examined for the apoptosis markers caspase-3 and PUMA via real-time PCR. *G*, apoptosis marker expression of caspase-3 and PUMA was also examined in VP-transfected mouse primary hepatocyte using real-time PCR. Differences between treatments were assessed with unpaired Student's *t* tests. All values are represented as means, and *error bars* represent S.D. *C*, *, $p < 0.05$ *versus* DMSO-treated WT. *D*, *, $p < 0.05$ *versus* DMSO-treated WT. *F* and *G*, *, $p < 0.05$ *versus* VP^{WT}. *C*, *D*, and *E*, nonsignificant (*NS*).

in the cytotoxicity of HK-2 and HuH7 cells (*, $p < 0.05$ and †, $p < 0.05$, respectively), ER retention of PCSK9 did not alter cell viability in either cell line (Fig. 4, *C* and *D*). In contrast to $PCSK9^{Q152H}$, the expression of VP^{G17V} significantly increased cell death compared with VP^{WT} control (Fig. 4*E*). To confirm our findings, apoptosis marker expression was also examined in

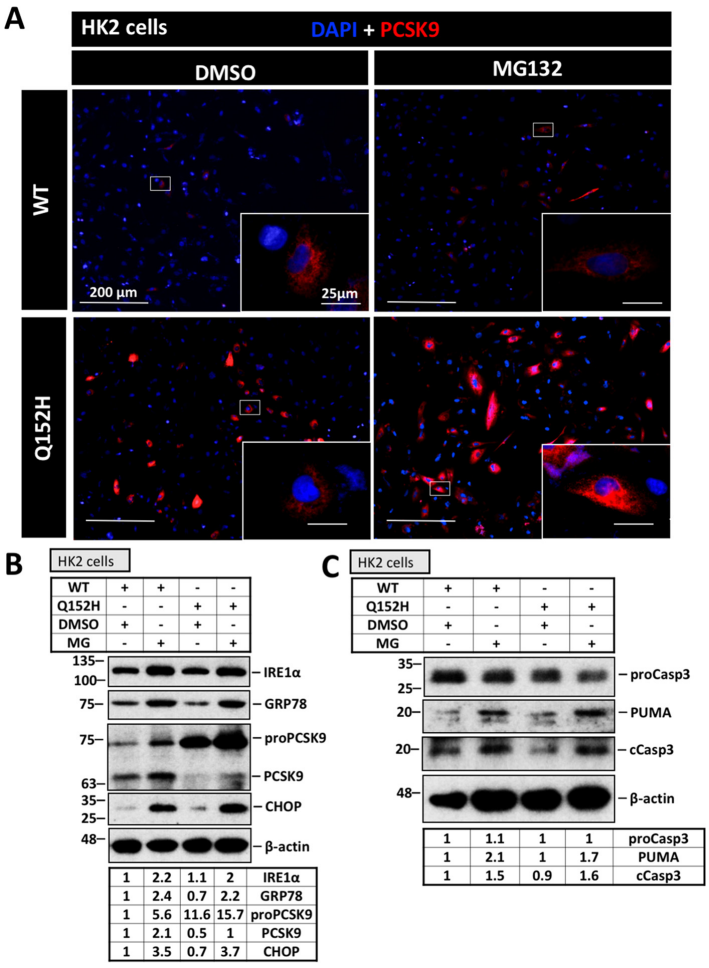

Figure 5. Proteasomal inhibition increases ER PCSK9 content. To examine the influence of the proteasome and test whether further increasing the ER content of PCSK9^{Q152H} leads to ER stress, HK-2 cells transfected with V5-labeled PCSK9 were treated with the proteasomal inhibitor MG132 (*MG*; 1 μM) for 24 h. *A*, to visualize the extent of ER PCSK9 retention, cells were fixed in 4% paraformaldehyde and stained using a V5 primary antibody and a 594-labeled secondary antibody (*red*). *B*, ER stress markers IRE1α, GRP78, and CHOP as well as ER PCSK9 content and maturation were examined via immunoblot analysis. *C*, apoptosis markers PUMA and cleaved caspase-3 (*cCasp3*) were also examined using immunoblotting.

mouse primary hepatocytes. Similar to our findings in HuH7 and HK-2 cells, real-time PCR experiments demonstrate that the retention of VP^{G17V}, but not PCSK9^{Q152H}, PCSK9^{Q152D}, or PCSK9^{S386A}, caused an induction of proapoptotic mediators caspase-3 and PUMA relative to WT secreted controls (Fig. 4, *F* and *G*).

Proteasomal inhibition increases ER PCSK9 content

ER-associated degradation, a process mediated by the proteasome, plays a major role in the removal of misfolded/accumulated proteins from the ER (33). For this reason, we investigated whether the proteasome is responsible for the removal of retained PCSK9 and elicits a protective state against UPR activation in cells transfected with PCSK9^{Q152H}. Moreover, use of the proteasome inhibitor MG132 in combination with CMV-mediated overexpression served as a tool to further enhance exogenous ER-PCSK9 content as a means of causing ER stress. Immunofluorescence staining of V5 was used to visualize the perinuclear localization and accumulation of PCSK9 (Fig. 5*A*). Representative images show that a greater intensity of staining occurred in PCSK9^{Q152H}-transfected cells than in PCSK9^{WT}-transfected controls. Furthermore, PCSK9^{Q152H}-transfected cells treated with MG132 exhibited more ER-resident PCSK9 than the respective untreated controls, suggesting that the proteasome plays a role in the degradation of PCSK9^{Q152H}. Despite a marked increase in the expression of IRE1α, GRP78, and CHOP in response to MG132, no difference was observed between PCSK9^{WT} and PCSK9^{Q152H} in the presence or

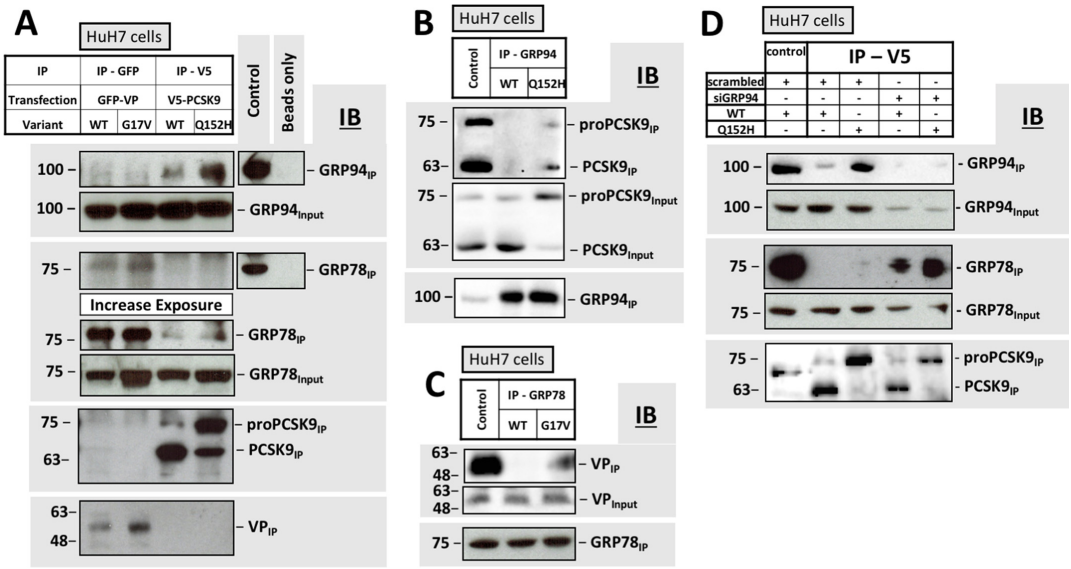

Figure 6. GRP94 masks ER-resident PCSK9 from GRP78. *A*, coimmunoprecipitation experiments were carried out on cells transfected with VP and its ER-retention variant (VP^{G17V}) and compared with that of cells transfected with PCSK9 and its ER-retention variant ($PCSK9^{Q152H}$). VP was immunoprecipitated using an anti-GFP capture antibody, whereas PCSK9 was captured using an anti-V5 antibody; effective capture was confirmed by immunoblotting (*IB*) IPs with anti-GFP and anti-PCSK9 antibodies, respectively. *B* and *C*, interactions characterized in *A* were confirmed by IP of endogenous GRP94 and GRP78 in cells transfected with V5-PCSK9 and GFP-VP, respectively. *D*, binding of GRP78 to $PCSK9^{WT}$ and $PCSK9^{Q152H}$ was also examined in the presence of siGRP94. *B*, *C*, and *D*, whole cell lysates were used as positive controls for antibody staining.

absence of MG132 (Fig. 5*B*). Consistently, MG132 treatment induced the expression of proapoptotic markers cleaved caspase-3 and PUMA, but no difference was observed as a result of $PCSK9^{Q152H}$ expression with respect to its WT counterpart (Fig. 5*C*).

GRP94 masks ER-resident PCSK9 from GRP78

Although GRP78 interacts with a diversity of client proteins (34), recent studies have demonstrated that endogenously expressed PCSK9 interacts with GRP78 to a significantly greater extent following knockdown of GRP94 (14). Given the role of GRP78 as a major trigger of UPR activation, we tested whether GRP94 could mask ER-resident PCSK9 or pro-PCSK9 from detection by GRP78. Furthermore, the interaction between $PCSK9^{Q152H}$ and GRP78 was compared with the interaction between GRP78 and VP^{G17V}. These coimmunoprecipitation experiments demonstrate that the VP retention variant interacts with GRP78 but not GRP94 (Fig. 6*A*). In contrast, PCSK9 was pulled down by GRP94 and GRP78 with the latter requiring a longer exposure of the immunoblots. Lastly, immunoprecipitation of the ER-retention variants VP^{G17V} and $PCSK9^{Q152H}$ pulled down more GRP78 and GRP94 (respectively) than their secreted WT counterparts. In a reciprocal manner, the interaction between GRP94 and PCSK9 was confirmed via immunoprecipitation of GRP94 (Fig. 6*B*), and the interaction of GRP78 with VP was confirmed via immunoprecipitation of GRP78 (Fig. 6*C*). Consistent with Fig. 6*A*, these immunoblots also demonstrate that GRP78 and GRP94 form stronger interactions with the ER-retention variants of VP and PCSK9 than their WT counterparts. Lastly, coimmunoprecipitation experiments of PCSK9-transfected cells were performed in the presence and absence of small interfering RNA (siRNA) targeted against GRP94 (siGRP94; Fig. 6*D*). As reported previously (14), we observed a significantly greater level of interaction between PCSK9 and GRP78 under conditions of GRP94 knockdown. Furthermore, we also observed more GRP78 in complex with $PCSK9^{Q152H}$ than with $PCSK9^{WT}$ under such conditions.

ER retention of PCSK9 variants leads to UPR activation in the absence of GRP94

Given that we observed a greater level of GRP78 association with the $PCSK9^{Q152H}$ variant in the absence of GRP94, our next aim was to determine whether this specific condition would lead to UPR activation. As such, UPR activation was assessed in HuH7 cells cotransfected with either $PCSK9^{WT}$ or $PCSK9^{Q152H}$ in combination with scrambled siRNA or siGRP94. Cells expressing $PCSK9^{Q152H}$, in the presence of siGRP94, exhibited increased expression of ER stress markers from all three arms of the UPR (ATF6, IRE1α, and CHOP) (Fig. 7*A*). To further substantiate the relationship between PCSK9 and GRP94, we observed a modest but consistent increase in GRP94 expression in cells transfected with $PCSK9^{Q152H}$ compared with those transfected with the $PCSK9^{WT}$ counterpart (Fig. 7, *A* and *B*). Furthermore, cells transfected with both siGRP94 and $PCSK9^{Q152H}$ showed a significant increase in cytotoxicity compared with control groups (Fig. 7, *C* and *D*; *, $p < 0.05$). The effect of GRP94 on UPR activation in response to

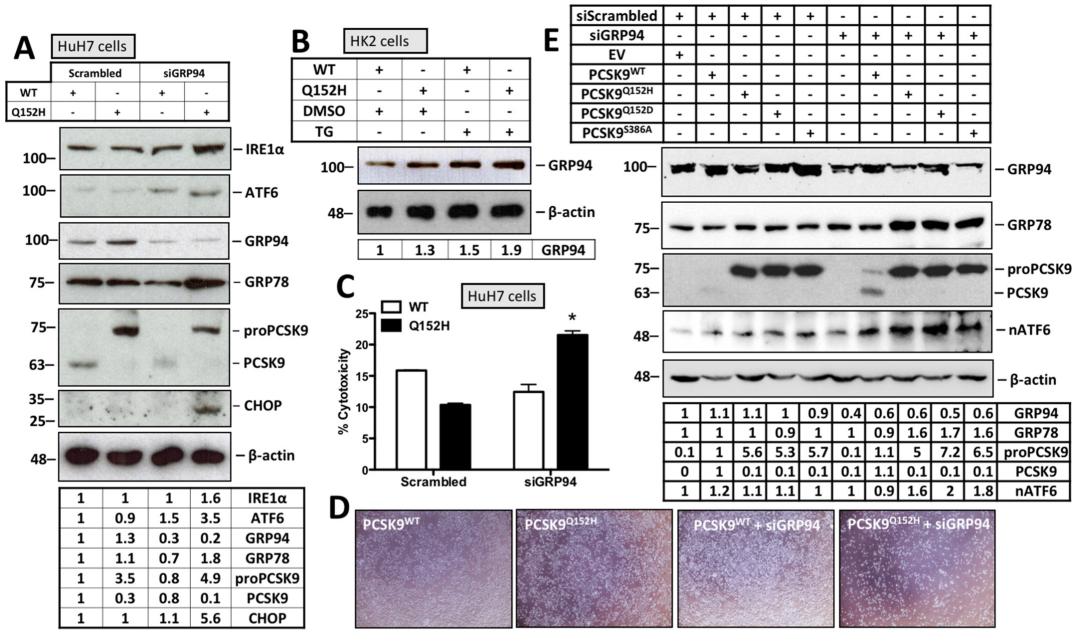

1	1	1	1.6	IRE1α
1	0.9	1.5	3.5	ATF6
1	1.3	0.3	0.2	GRP94
1	1.1	0.7	1.8	GRP78
1	3.5	0.8	4.9	proPCSK9
1	0.3	0.8	0.1	PCSK9
1	1	1.1	5.6	CHOP

1	1.1	1.1	1	0.9	0.4	0.6	0.6	0.5	0.6	GRP94
1	1	1	0.9	1	1	0.9	1.6	1.7	1.6	GRP78
0.1	1	5.6	5.3	5.7	0.1	1.1	5	7.2	6.5	proPCSK9
0	1	0.1	0.1	0.1	0.1	1.1	0.1	0.1	0.1	PCSK9
1	1.2	1.1	1.1	1	1	0.9	1.6	2	1.8	nATF6

Figure 7. ER retention of the PCSK9^{Q152H} variant leads to UPR activation in the absence of GRP94. *A*, HuH7 cells were cotransfected with PCSK9^{WT} or PCSK9^{Q152H} and siGRP94. Immunoblot analysis was carried out to examine the expression of ER stress markers IRE1α, ATF6, GRP94, GRP78, and CHOP. *B*, given that PCSK9 interacts with GRP94, the relative cellular abundance of this chaperone was also examined in HK2 cells transfected with PCSK9^{WT} and PCSK9^{Q152H}. *C*, cytotoxicity of these cells was examined using a lactate dehydrogenase cell viability assay. *D*, the relative number of live cells post-transfection was visually apparent via light microscopy. *E*, in addition to PCSK9^{Q152H}, the ability of other ER-retention PCSK9 variants PCSK9^{Q152D} and PCSK9^{S386A} to cause UPR activation in conditions of reduced GRP94 expression was examined using immunoblotting. Differences between treatments were assessed with unpaired Student's *t* tests. All values are represented as means, and *error bars* represent S.D. *C*, *, $p < 0.05$ *versus* scrambled WT control. *nATF6*, nuclear ATF6.

ER PCSK9 retention was also assessed using PCSK9 variants PCSK9^{Q152D} and PCSK9^{S386A}. Consistent with our findings in Fig. 7*A*, we observed that cotransfection of HuH7 cells with siGRP94 and ER-retained PCSK9 variants led to increased expression of UPR markers GRP78 and nuclear ATF6 relative to those transfected with siGRP94 and PCSK9^{WT} (Fig. 7*E*).

Marked overexpression of mouse PCSK9 does not induce the UPR in murine liver

Based on our cell culture studies, we examined whether transgenic mice overexpressing PCSK9 (PCSK9^{transgenic}), which increases the ER content of nascent PCSK9, would exhibit signs of ER stress. The livers from these mice were examined for UPR activation via immunoblotting for IRE1α and GRP78 (Fig. 8*A*) and real-time PCR of sXBP1 (Fig. 8*B*), which yielded no substantial difference between PCSK9^{WT} and PCSK9^{transgenic} mice. Furthermore, PCSK9 knockout (KO) mice showed no induction of the UPR compared with the other groups. LDLR immunoblotting and real-time PCR of PCSK9 served as controls for PCSK9 expression, yielding a significant increase in hepatic LDLR expression and a 100-fold increase in PCSK9 mRNA in PCSK9^{transgenic} mice compared with WT mice (Fig. 8, *A* and *C*). Lastly, ER stress was also examined via immunohistochemical staining of the livers for ER stress markers KDEL and CHOP in PCSK9^{WT} and PCSK9^{transgenic} mice as well as a control group of WT mice treated with the ER stress–inducing agent tunicamycin (500 μg/kg for 24 h). Consistent with immunoblot and real-time PCR data, no difference in KDEL or CHOP expression was observed between PCSK9^{WT} and PCSK9^{transgenic} mice (Fig. 8*D*).

Discussion

A number of ERSDs have been characterized to date (15, 16). Such diseases arise as a result of genetic mutations that lead to the synthesis of a misfolded *de novo* protein product, which fails to exit the ER (Fig. 9). Frequently, the disease phenotype occurs due to the absence of the mature functional protein at its native site of action. Another well-established mode of action for pathology in ERSDs is chronic activation of the UPR in response to ER stress. A well-characterized ERSD occurring in liver results from a number of established mutations in α_1-antitrypsin Z that induce ER stress, liver cirrhosis, and hepatocellular carcinoma (35, 36). Additional examples affecting other tissues include arginine vasopressin mutations (G14R and G17V) in familial neurohypophyseal diabetes insipidus (20, 21, 37), cystic fibrosis transmembrane conductance regulator ΔF508 in cystic fibrosis (38), thyroglobulin mutations in congenital goiter and hyperthyroidism (39), and mutations in the Notch receptor that lead to cerebral autosomal-dominant arteriopathy and leukoencephalopathy (40).

We confirm that overexpression of a mutant form of VP that is retained in the ER resulted in UPR activation and increased

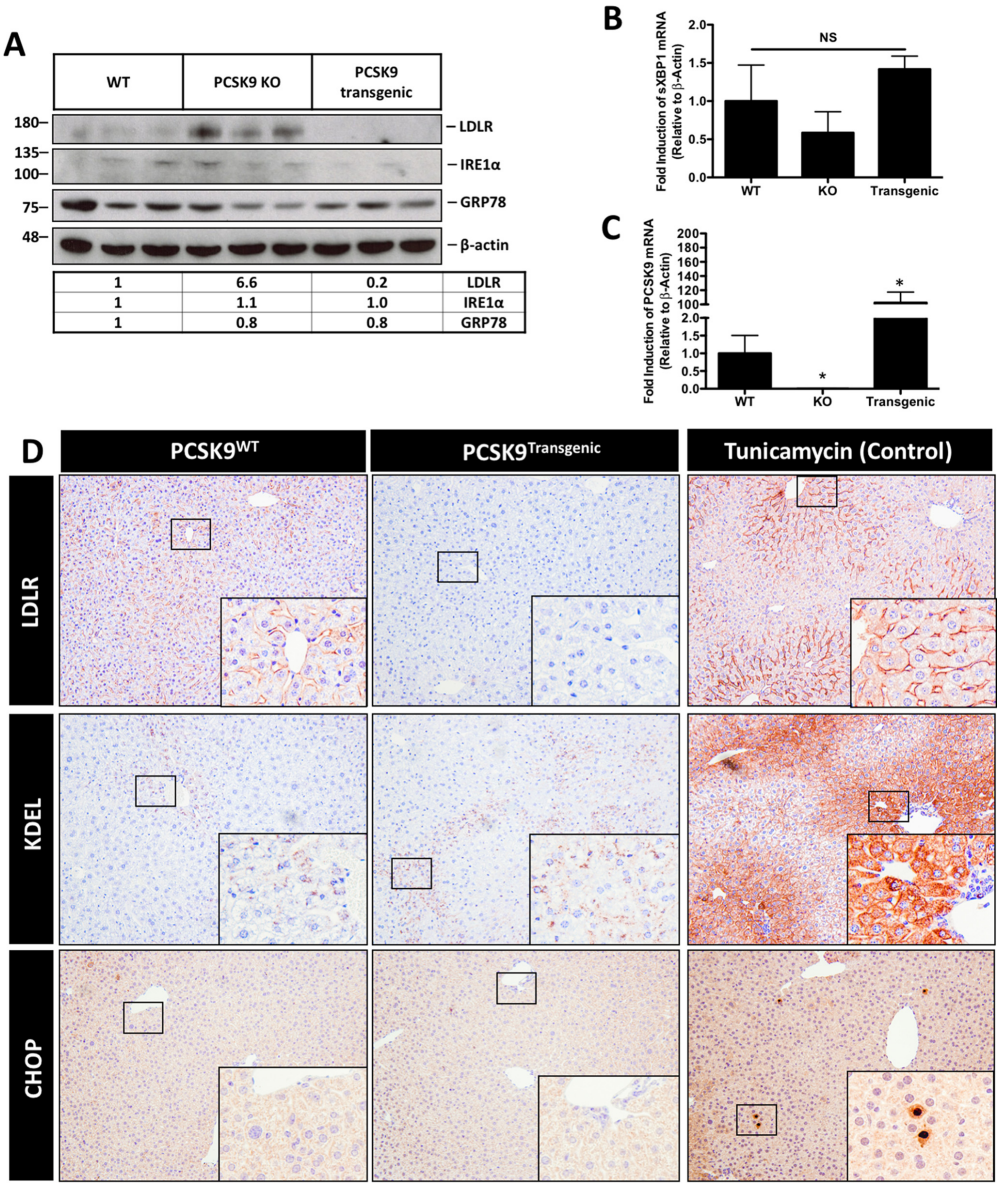

Figure 8. Marked overexpression of mouse PCSK9 does not induce the UPR in murine liver. To examine whether elevated levels of nascent ER-resident PCSK9 promote UPR activation *in vivo*, we tested the hypothesis in a transgenic murine model known to express ~40–100-fold greater levels of PCSK9 than WT controls. *A* and *B*, immunoblot and real-time PCR analyses were carried out in the livers of these mice, PCSK9 KO mice and WT controls, to characterize ER stress marker expression of IRE1α, GRP78, and sXBP1. *C*, a control real-time PCR was also done to confirm the overexpression of PCSK9 in our model. *D*, formalin-fixed paraffin-embedded liver sections from these mice in addition to mice treated with the ER stress–inducing agent tunicamycin (500 μg/kg; single injection for 24 h) were also stained for ER stress markers KDEL and CHOP. LDLR staining served as a control for the status of PCSK9 expression. Differences between treatments were assessed with unpaired Student's *t* tests. All values are represented as means, and *error bars* represent S.D. *B*, nonsignificant (*NS*). *C*, *, $p < 0.05$ *versus* WT.

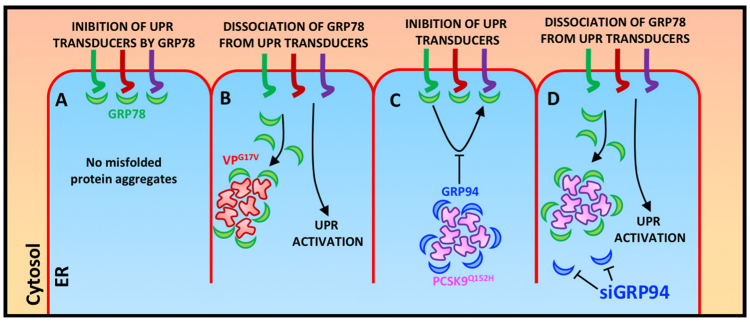

Figure 9. Model for the masking of ER-resident PCSK9 from UPR sensor GRP78. *A*, in normal homeostatic conditions, GRP78 is recruited to ER transducers ATF6, IRE1α, and PERK and acts to block UPR activation. *B*, in the presence of ER-retained protein such as VP^{G17V}, GRP78 dissociates from UPR transducers and interacts with accumulated misfolded proteins to prevent further aggregation. This process liberates ER transducers and leads to UPR activation. *C*, in contrast to VP^{G17V}, GRP78 is not recruited to ER-retained $PCSK9^{Q152H}$ due to the interaction taking place with GRP94. *D*, removal of GRP94 from PCSK9 aggregates, however, restores the function of GRP78 as a sensor of UPR activation in response to ER PCSK9 accumulation.

cytotoxicity. In contrast to these findings and with striking consistency, overexpression of LOF PCSK9 variants that accumulate in the ER did not exhibit UPR activation or apoptosis. These findings were confirmed using three cell lines (HuH7, HK-2, and N2a) originating from tissues known to express PCSK9 (liver, kidney, and brain, respectively) and with a number of PCSK9 variants ($PCSK9^{Q152H}$, $PCSK9^{Q152D}$, and $PCSK9^{FS}$) known to be retained in the ER. Despite the absence of UPR signaling, a distinct expansion of the ER was observed in HuH7 and HK-2 cells expressing $PCSK9^{Q152H}$ relative to those expressing $PCSK9^{WT}$ controls.[4] This phenomenon, which is an initial response to ER stress (41, 42), appears to occur in a manner independent of the UPR. Although the key players in this process are not yet validated, one possibility is that ER stress–inducible genes like SREBP2 promote membrane biogenesis by inducing *de novo* synthesis and uptake of lipid (43, 44). However, given that ER PCSK9 retention blocks SREBP2 activation (Fig. 1*C*), increased *de novo* synthesis is likely not the culprit. $PCSK9^{Q152H}$ expression, however, is known to result in enhanced cell surface LDLR expression (10) and likely allows the cells to acquire the ER expansion–enabling lipid from LDLR-mediated uptake of LDL.

Given that few reports have documented an absence of UPR activation resulting from ER protein retention, the remainder of this discussion will focus on the key differences between PCSK9 and other mutants known to cause ER stress when retained. An initial foundational observation stems from an epidemiological line of evidence: LOF PCSK9 mutations, including $PCSK9^{Q152H}$, are naturally occurring and confer a substantial reduction in the risk of developing CVD (11, 45, 46). As of yet, the absence/inhibition of circulating PCSK9 has not been associated with deleterious effects other than mild rashes at the site of mAb injection (47). Taken together, these factors imply a positive evolutionary selection pressure for LOF PCSK9 mutations. In support of this notion, the frequency of LOF PCSK9 mutations is relatively high, especially in Africans (48). Indeed, it was recently shown that the PCSK9 mutation C679*X*, encoding a form of PCSK9 that fails to be secreted (8), has a prevalence of 3.7% in African women (49).

It is also worth considering the implications associated with the observation that nascent $PCSK9^{WT}$ forms pro-PCSK9 oligomers while in the ER (1). Given that ER protein oligomers and/or aggregates are a principal cause of UPR activation and that ER-resident pro-PCSK9 oligomers are naturally occurring, it is therefore evident that cells expressing PCSK9 have adapted a mechanism to prevent constitutive UPR activation and cell death.

Furthermore, in contrast to a number of cell surface/secretory proteins that transit the ER, PCSK9 folding and maturation can occur in a manner independent of ER chaperones. In support of this concept, our previous studies (13) as well as those of others (45) have demonstrated that PCSK9 undergoes maturation in the presence of agents that induce ER Ca^{2+} depletion regardless of the obligate Ca^{2+} dependence of ER chaperones. In addition, endogenously expressed PCSK9 does not stably interact with endogenously expressed ER luminal GRP78 (14), which is interesting given the well-established broad client base of this chaperone (50). These findings, in addition to those highlighted in this report, suggest that ER-resident pro-PCSK9 may be undetected and unaffected by major ER chaperones like GRP78. GRP78 is a ubiquitously expressed chaperone involved in the folding of polypeptide chains, nascent chain translocation, resolving the accumulation/removal of misfolded protein in the ER, and modulating the activation of ER stress transducers (51, 52). GRP78 owes its importance in biological systems to its promiscuity, which relies on a client-binding domain known to seek 7–11-residue peptides forming β strands with alternating hydrophobic residues (53, 54). It is estimated that one GRP78-binding site would arise every 36 amino acids within a randomly generated peptide chain (54).

In addition to demonstrating that the interaction between PCSK9 and GRP78 was not as strong as that of PCSK9 and GRP94, our coimmunoprecipitation data also indicate that GRP78 forms a more abundant complex with the retained VP^{G17V} variant than with the VP^{WT} control. These data suggest that ER-retained mutant VP^{G17V} sequesters a greater amount

[4] P. Lebeau and R. C. Austin, unpublished data.

of ER-resident GRP78 (Fig. 6*A*), likely as a result of increased ER abundance relative to secreted VP^{WT} control. In turn, increased VP^{G17V}-mediated GRP78 sequestration hindered the capacity of this chaperone to act as a blocker of UPR activation and ultimately led to the observed ER stress response (Fig. 2*A*). Although a similar effect was observed with $PCSK9^{Q152H}$ interacting with GRP94 (*versus* $PCSK9^{WT}$) (Fig. 6*A*), this chaperone is not known to play a direct role as a UPR sensor or mediator of ATF6, IRE1α, and PERK activation (55). Rather, it was recently shown that PCSK9 interacts with GRP78 to a greater extent in the absence of GRP94, likely preventing early binding of PCSK9 to the LDLR in the ER (14). Our data also suggest that GRP94 masks ER-resident pro-PCSK9 oligomers from detection by GRP78. To confirm and extend these findings, we demonstrated that overexpression of the $PCSK9^{Q152H}$ variant induced the UPR following knockdown of GRP94 (Fig. 7*A*). Furthermore, the onset of ER stress in cells transfected with siGRP94 and $PCSK9^{Q152H}$ was sufficient to cause a significant increase in cytotoxicity 3 days post-transfection as compared with controls (Fig. 7, *C* and *D*).

We recently demonstrated that ER PCSK9 retention is associated with a significant reduction of circulating LDL cholesterol (13). We now also confirm that it fails to induce ER stress despite the known link among misfolded protein accumulation, UPR activation, cell death, and disease (18). Our findings demonstrate that $PCSK9^{Q152H}$ likely fails to cause ER stress as a result of a combination of efficient proteasomal degradation (Fig. 5*A*) and masking by GRP94 (Figs. 6 and 7). In support of these findings, mice expressing 100-fold greater levels of PCSK9 mRNA also failed to exhibit UPR activation (Fig. 8). We are now actively assessing whether the overexpression of LOF variants of PCSK9, including $PCSK9^{Q152H}$, in the livers of PCSK9 KO mice cause ER stress/UPR activation and/or apoptotic cell death. Taken together, our results indicate that the ER retention of mutant forms of PCSK9 unable to undergo autocatalytic cleavage does not trigger detrimental ER stress, UPR activation, and cytotoxicity. This has important implications for the design of novel therapeutics targeting PCSK9. Specifically, our findings suggest that the development of small molecule inhibitors of PCSK9 autocatalytic cleavage may serve as an effective alternative to the costly biologic PCSK9 inhibitors that are currently available.

Experimental procedures

Cell culture and transfections

HuH7, HK-2, and N2a cells were routinely grown in Dulbecco's modified Eagle's medium (DMEM; Thermo Fisher Scientific, Waltham, MA) supplemented with 10% fetal bovine serum (FBS; Sigma-Aldrich), 100 IU/ml penicillin, and 100 μg/ml streptomycin (both from Gibco, Thermo Fisher Scientific) at 37 °C with 5% CO_2. To examine the effect of ER PCSK9 retention on UPR activation, cells were seeded in 6-well plates to a confluence of 60% and transfected with plasmids encoding PCSK9 variants 24 h later. Cells were transfected in penicillin/streptomycin–free medium with Xtremegene transfection reagent (Xtremegene HP, catalogue number 6366236001, Roche Applied Science) at a 3:1 ratio with plasmid DNA (3 μl of transfection reagent/1 μg of DNA/1 ml of medium). To block GRP94 expression, siRNA targeted against GRP94 was purchased from Dharmacon (catalogue number M-006417-02-0005). RNAiMAX (catalogue number 13778030) transfection reagent was used for siRNA transfections; siRNA transfection mixtures contained 100 nM siRNA and 3 μl of RNAiMAX/ml of complete medium. Prior to treatment of cells, transfection mixtures were incubated in Opti-MEM (100 μl of Opti-MEM per treatment; Thermo Fisher Scientific) for 30 min at room temperature prior to transfection according to the manufacturer's instructions. Transfection mixture-containing medium was removed from cells after 24-h incubation and replaced with either fresh medium or medium containing the ER stress–inducing agent TG (100 nM; Sigma-Aldrich) for an additional 24 h prior to cell lysis. The plasmids used in these studies included the bicistronic pIRES2-EGFP plasmids encoding V5-$PCSK9^{WT}$ and its variants $PCSK9^{Q152S}$, $PCSK9^{Q152H}$, $PCSK9^{Q152D}$, and $PCSK9^{FS}$. VP^{WT} and its variants VP^{G14R} and VP^{G17V} were cloned into pEGFP-N1 as described previously (21), and $PCSK9^{S386A}$ was cloned into a pcDNA3.1 plasmid.

Immunoblotting

Cells were washed in phosphate-buffered saline (PBS) and resuspended in lysis buffer containing SDS and protease inhibitor (catalogue number 4693159001, Roche Applied Science). Total cell protein was normalized using a protein assay (catalogue number 5000121, Bio-Rad). Protein samples were resolved using standard Western blotting procedures on 7 or 10% acrylamide gels and subsequently transferred to nitrocellulose membranes using the Bio-Rad Mini Trans-Blot system (catalogue number 1703930). Membranes were then blocked in 5% skim milk in TBS for 1 h and then incubated in primary antibody overnight for 16 h at 4 °C. The primary antibodies used in this study include the following: anti-ATF6 (catalogue number 70B1413.1, Novus Biologicals), anti-CHOP (catalogue number SC-793, Santa Cruz Biotechnology), anti-FLAG (catalogue number F3165, Sigma-Aldrich), anti-GRP78 (catalogue number 610979, BD Biosciences), anti-IRE1α (catalogue number 3294, Cell Signaling Technology), anti-PCSK9 (catalogue number NB300-959, Novus Biologicals), anti-V5 (catalogue number sc-83849, Santa Cruz Biotechnology), anti-GFP (catalogue number sc-8334, Santa Cruz Biotechnology), anti-GFP (catalogue number NB600-308, Novus Biologicals), and anti-β-actin (catalogue number ab8227, Sigma-Aldrich). Membranes were visualized using EZ-ECL chemiluminescent reagent (catalogue number 20-500-500, Froggabio), and relative band intensities were quantified using ImageLab software (Bio-Rad). Band intensities represent the mean of three replicates adjusted to membranes reprobed for β-actin.

Coimmunoprecipitations

Cells grown in 10-cm dishes were collected in ice-cold nondenaturing IP buffer containing 20 mM Tris HCl, 137 mM NaCl, 1% Nonidet P-40, 2 mM EDTA, protease inhibitor, and phosphatase inhibitor (PhoSTOP, Roche Applied Science). Cells were further lysed by passing through an insulin syringe 20 times. Following lysis, samples were centrifuged at 4 °C for 30 min at 20,000 × *g*. Supernatants were transferred to new sam-

ple tubes, and cell debris–containing tubes were discarded. One milligram of protein from each sample was subsequently incubated with 2 μg of capture antibody targeted against V5 (catalogue number sc-83849, Santa Cruz Biotechnology) or GFP (catalogue number sc-8334, Santa Cruz Biotechnology) for V5-PCSK9– and GFP-VP–transfected cells, respectively, on a rotating platform for 24 h at 4 °C. Following this period, samples were exposed to 100 μl of Protein G magnetic Surebeads (catalogue number 1614023, Bio-Rad) for an additional 2 h on the rotating platform at 4 °C. The beads were then magnetized, and the remaining sample was placed in tubes labeled "input" to serve as controls. The magnetic bead slurry was subjected to four consecutive washes using nondenaturing IP buffer. Protein complexes bound to the beads were collected by boiling the slurry with 100 μl of 4× SDS-PAGE sample/loading buffer. Successful pulldown was confirmed by reprobing immunoblots with anti-PCSK9 antibody (catalogue number NB300-959) and anti-GFP antibody (catalogue number NB600-308).

RNA isolation and real-time PCR

RNA extraction was performed using RNeasy Mini kits (catalogue number 74104, Qiagen) as described previously (7). Total RNA was quantified, normalized, and reverse transcribed into cDNA using a Superscipt Vilo cDNA synthesis kit (catalogue number 11754050, Thermo Fisher Scientific). Real-time PCR was completed using Fast SYBR Green (catalogue number 4385610, Thermo Fisher Scientific). The relative abundance of PCSK9 and PCSK9^{SV} mRNAs from experiments involving SSO was examined via quantitative PCR and agarose gel electrophoresis as described previously (14). Quantification of the relative band intensities was done using ImageLab. DNA was quantified and normalized prior to electrophoresis using a NanoDrop^{TM} spectrophotometer.

Immunofluorescence microscopy and TUNEL assay

HuH7 and HK-2 cells were seeded in 4-well chamber slides (catalogue number 177399, Thermo Fisher Scientific) to a confluence of 50% and cultured for 24 h. Cells were then incubated in transfection mixture for 24 h and treated with MG132 (1 μM; catalogue number M8699, Sigma-Aldrich) for an additional 24 h. Following treatments, cells were washed in cold PBS, fixed in 4% paraformaldehyde, and permeabilized in 0.2% Triton X-100 (Sigma-Aldrich). Prior to the 1-h incubation with primary antibodies, cells were blocked in PBS-Tween (PBS-T) containing 5% bovine serum albumin (BSA; catalogue number 05470, Sigma-Aldrich). Primary antibodies used for immunofluorescence staining included the following: anti-V5 (catalogue number sc-83849) and anti-GFP (catalogue number NB600-308). All primary antibodies were diluted 1:100 in PBS-T containing 1% BSA. Following primary antibody incubation, cells were incubated in fluorescently labeled secondary antibodies diluted 1:200 in 1% BSA in PBS-T. These included donkey anti-goat 594 (catalogue number A11058, Thermo Fischer Scientific) and goat anti-rabbit 488 (catalogue number R37116, Thermo Fisher Scientific). Fluorescently labeled cells were then counterstained with DAPI (catalogue number D1306, Thermo Fisher Scientific). TUNEL assays were carried out according to the manufacturer's instructions using a Trevigen kit (catalogue number 4812-30-K, Trevigen).

PCSK9 ELISA

Secreted PCSK9 from cell culture models was measured using the human PCSK9 Quantikinine ELISA kit from R&D Systems (catalogue number DCP900). Briefly, FBS-free medium from transfected cells was collected and centrifuged at 1000 × *g* for 10 min to remove floating cells/debris. ELISAs were then carried out according to the manufacturer's instructions.

Cell death assays

Lactate dehydrogenase assays were completed according to the manufacturer's instructions (catalogue number 04744926001, Roche Applied Science). A novel cell death assay, based on trypan blue staining of cell debris, was also used to quantify cell death. Briefly, HK-2 cells were transfected with either EV control, PCSK9^{WT}, or PCSK9^{Q152H} in the presence or absence of TG (100 nM). The medium, which contained all cell debris, was collected 24 h later and incubated with 10% trypan blue solution (v/v) (catalogue number 15250061, Thermo Fisher Scientific) for 5 min at room temperature. Samples were then centrifuged at 10,000 × *g* to isolate the cell debris pellet. The pellet was then washed with isopropanol and subsequently incubated in Hank's balanced salt solution for 30 min at 37 °C to extract trypan blue from the debris. Optical density of trypan blue–containing Hank's balanced salt solution was then measured using a SpectraMax Plus 384 spectrophotometer at 488 nm (Molecular Devices).

Immunohistochemistry

Liver tissues were collected and fixed in formalin, embedded in paraffin, and sectioned at a thickness of 4 μm. KDEL staining was carried out using a 1:40 dilution of the primary antibody with no epitope retrieval (catalogue number ADI-SPA-827, Enzo Life Sciences). CHOP staining was carried out with heat-induced epitope retrieval using a 1:40 dilution of the primary antibody (catalogue number sc-575, Santa Cruz Biotechnology). LDLR staining was carried out using a 1:20 dilution of the primary antibody with no epitope retrieval (catalogue number AF2255, R&D Systems).

Animal studies

12-week-old PCSK9 KO mice or transgenic mice overexpressing mouse PCSK9 (3) and age-matched controls on a C57bl/6 background were housed in a 12-h light/dark cycle and fed normal chow and water *ad libitum*. Control and PCSK9 KO mice were randomly divided into four groups (n = 5 per group) and treated with either PBS vehicle control or the ER stress–inducing agent tunicamycin (500 μg/kg) for 24 h prior to sacrifice. The McMaster University Animal Research Ethics Board approved all procedures.

Primary hepatocyte isolation

A two-step hepatic perfusion of EGTA (500 M in HEPES buffer, Sigma-Aldrich) and collagenase (0.05% in HEPES buffer, Sigma-Aldrich) was used in 12-week-old male C57bl/6 mice to

isolate primary hepatocytes. Following harvest, cells were washed, separated via centrifugation and cell strainers, and plated at a confluence of 1×10^6 cells/well in William's E medium (Gibco, Thermo Fisher Scientific) supplemented with 10% fetal bovine serum, 100 IU/ml penicillin, and 100 μg/ml streptomycin.

Statistical analysis

All experiments done during these studies were carried out using a minimum of three replicates. Statistical analysis for differences between groups was performed using two-tailed unpaired Student's *t* test. Comparisons between plasma PCSK9 concentrations from the same animals before and after treatment were completed using paired two-tailed Student's *t* test. Statistical tests were completed using Prism software (GraphPad Software, San Diego, CA). Differences between groups were considered significant at $p < 0.05$, and all values are expressed as mean ± S.D.

Author contributions—P. L., K. P., N. G. S., and R. C. A. conceptualization; P. L., K. P., D. C., N. G. S., and R. C. A. resources; P. L., K. P., and R. C. A. data curation; P. L. and K. P. software; P. L., K. P., J. H. B., and R. C. A. formal analysis; P. L., B. T., and R. C. A. supervision; P. L. and R. C. A. funding acquisition; P. L., K. P., and R. C. A. validation; P. L., K. P., A. A. A.-H., J. H. B., Š. L., N. H., G. G., D. C., and R. C. A. investigation; P. L., K. P., N. G. S., and R. C. A. visualization; P. L., K. P., D. C., N. G. S., and R. C. A. methodology; P. L., K. P., and R. C. A. writing-original draft; P. L., K. P., N. G. S., and R. C. A. project administration; P. L., K. P., A. A. A.-H., J. H. B., Š. L., N. H., G. G., S. A. I., D. C., B. T., N. G. S., and R. C. A. writing-review and editing.

Acknowledgments—We thank Dr. Simon Jackson, Amgen, for constructive insights during these studies as well as Dr. Masayuki Miura, University of Tokyo, for the ERAI plasmid. We would also like to thank St. Joseph's Healthcare Hamilton for the support during the course of these studies.

References

1. Seidah, N. G., Benjannet, S., Wickham, L., Marcinkiewicz, J., Jasmin, S. B., Stifani, S., Basak, A., Prat, A., and Chretien, M. (2003) The secretory proprotein convertase neural apoptosis-regulated convertase 1 (NARC-1): liver regeneration and neuronal differentiation. *Proc. Natl. Acad. Sci. U.S.A.* **100,** 928–933 CrossRef Medline
2. Seidah, N. G., Abifadel, M., Prost, S., Boileau, C., and Prat, A. (2017) The proprotein convertases in hypercholesterolemia and cardiovascular diseases: emphasis on proprotein convertase subtilisin/kexin 9. *Pharmacol. Rev.* **69,** 33–52CrossRef Medline
3. Zaid, A., Roubtsova, A., Essalmani, R., Marcinkiewicz, J., Chamberland, A., Hamelin, J., Tremblay, M., Jacques, H., Jin, W., Davignon, J., Seidah, N. G., and Prat, A. (2008) Proprotein convertase subtilisin/kexin type 9 (PCSK9): hepatocyte-specific low-density lipoprotein receptor degradation and critical role in mouse liver regeneration. *Hepatology* **48,** 646–654 CrossRef Medline
4. Maxwell, K. N., and Breslow, J. L. (2004) Adenoviral-mediated expression of Pcsk9 in mice results in a low-density lipoprotein receptor knockout phenotype. *Proc. Natl. Acad. Sci. U.S.A.* **101,** 7100–7105 CrossRef Medline
5. Daniels, T. F., Killinger, K. M., Michal, J. J., Wright, R. W., Jr., and Jiang, Z. (2009) Lipoproteins, cholesterol homeostasis and cardiac health. *Int. J. Biol. Sci.* **5,** 474–488 Medline
6. Hooper, A. J., and Burnett, J. R. (2013) Anti-PCSK9 therapies for the treatment of hypercholesterolemia. *Expert Opin. Biol. Ther.* **13,** 429–435 CrossRef Medline
7. Abifadel, M., Varret, M., Rabès, J. P., Allard, D., Ouguerram, K., Devillers, M., Cruaud, C., Benjannet, S., Wickham, L., Erlich, D., Derré, A., Villéger, L., Farnier, M., Beucler, I., Bruckert, E., *et al.* (2003) Mutations in PCSK9 cause autosomal dominant hypercholesterolemia. *Nat. Genet.* **34,** 154–156 CrossRef Medline
8. Benjannet, S., Hamelin, J., Chrétien, M., and Seidah, N. G. (2012) Loss- and gain-of-function PCSK9 variants: cleavage specificity, dominant negative effects, and low density lipoprotein receptor (LDLR) degradation. *J. Biol. Chem.* **287,** 33745–33755 CrossRef Medline
9. Wu, N. Q., and Li, J. J. (2014) PCSK9 gene mutations and low-density lipoprotein cholesterol. *Clin. Chim. Acta* **431,** 148–153 CrossRef Medline
10. Mayne, J., Dewpura, T., Raymond, A., Bernier, L., Cousins, M., Ooi, T. C., Davignon, J., Seidah, N. G., Mbikay, M., and Chrétien, M. (2011) Novel loss-of-function PCSK9 variant is associated with low plasma LDL cholesterol in a French-Canadian family and with impaired processing and secretion in cell culture. *Clin. Chem.* **57,** 1415–1423 CrossRef Medline
11. Cohen, J., Pertsemlidis, A., Kotowski, I. K., Graham, R., Garcia, C. K., and Hobbs, H. H. (2005) Low LDL cholesterol in individuals of African descent resulting from frequent nonsense mutations in PCSK9. *Nat. Genet.* **37,** 161–165 CrossRef Medline
12. Cameron, J., Holla, O. L., Laerdahl, J. K., Kulseth, M. A., Ranheim, T., Rognes, T., Berge, K. E., and Leren, T. P. (2008) Characterization of novel mutations in the catalytic domain of the PCSK9 gene. *J. Intern. Med.* **263,** 420–431 CrossRef Medline
13. Lebeau, P., Al-Hashimi, A., Sood, S., Lhoták, Š., Yu, P., Gyulay, G., Paré, G., Chen, S. R., Trigatti, B., Prat, A., Seidah, N. G., and Austin, R. C. (2017) Endoplasmic reticulum stress and Ca^{2+} depletion differentially modulate the sterol regulatory protein PCSK9 to control lipid metabolism. *J. Biol. Chem.* **292,** 1510–1523 CrossRef Medline
14. Poirier, S., Mamarbachi, M., Chen, W. T., Lee, A. S., and Mayer, G. (2015) GRP94 regulates circulating cholesterol levels through blockade of PCSK9-induced LDLR degradation. *Cell Rep.* **13,** 2064–2071 CrossRef Medline
15. Callea, F., Brisigotti, M., Fabbretti, G., Bonino, F., and Desmet, V. J. (1992) Hepatic endoplasmic reticulum storage diseases. *Liver* **12,** 357–362 Medline
16. Rutishauser, J., and Spiess, M. (2002) Endoplasmic reticulum storage diseases. *Swiss Med. Wkly.* **132,** 211–222 Medline
17. Carlson, J. (1990) Endoplasmic reticulum storage disease. *Histopathology* **16,** 309–312 CrossRef Medline
18. Austin, R. C. (2009) The unfolded protein response in health and disease. *Antioxid. Redox Signal.* **11,** 2279–2287 CrossRef Medline
19. Wu, F. L., Liu, W. Y., Van Poucke, S., Braddock, M., Jin, W. M., Xiao, J., Li, X. K., and Zheng, M. H. (2016) Targeting endoplasmic reticulum stress in liver disease. *Expert Rev. Gastroenterol. Hepatol.* **10,** 1041–1052 CrossRef Medline
20. Birk, J., Friberg, M. A., Prescianotto-Baschong, C., Spiess, M., and Rutishauser, J. (2009) Dominant pro-vasopressin mutants that cause diabetes insipidus form disulfide-linked fibrillar aggregates in the endoplasmic reticulum. *J. Cell Sci.* **122,** 3994–4002 CrossRef Medline
21. Yan, Z., Hoffmann, A., Kaiser, E. K., Grunwald, W. C., Jr., and Cool, D. R. (2011) Misfolding of mutated vasopressin causes ER-retention and activation of ER-stress markers in Neuro-2a cells. *Open Neuroendocrinol. J.* **4,** 136–146 CrossRef Medline
22. Rocha, C. S., Wiklander, O. P., Larsson, L., Moreno, P. M., Parini, P., Lundin, K. E., and Smith, C. I. (2015) RNA therapeutics inactivate PCSK9 by inducing a unique intracellular retention form. *J. Mol. Cell. Cardiol.* **82,** 186–193 CrossRef Medline
23. Pagny, S., Lerouge, P., Faye, L., and Gomord, V. (1999) Signals and mechanisms for protein retention in the endoplasmic reticulum. *J. Exp. Bot.* **50,** 157–164 CrossRef
24. Gardner, B. M., Pincus, D., Gotthardt, K., Gallagher, C. M., and Walter, P. (2013) Endoplasmic reticulum stress sensing in the unfolded protein response. *Cold Spring Harb. Perspect. Biol.* **5,** a013169CrossRef Medline

25. Pai, J. T., Brown, M. S., and Goldstein, J. L. (1996) Purification and cDNA cloning of a second apoptosis-related cysteine protease that cleaves and activates sterol regulatory element binding proteins. *Proc. Natl. Acad. Sci. U.S.A.* **93,** 5437–5442 CrossRef Medline
26. Lhoták, S., Sood, S., Brimble, E., Carlisle, R. E., Colgan, S. M., Mazzetti, A., Dickhout, J. G., Ingram, A. J., and Austin, R. C. (2012) ER stress contributes to renal proximal tubule injury by increasing SREBP-2-mediated lipid accumulation and apoptotic cell death. *Am. J. Physiol. Renal Physiol.* **303,** F266–F278 CrossRef Medline
27. Horton, J. D., Shah, N. A., Warrington, J. A., Anderson, N. N., Park, S. W., Brown, M. S., and Goldstein, J. L. (2003) Combined analysis of oligonucleotide microarray data from transgenic and knockout mice identifies direct SREBP target genes. *Proc. Natl. Acad. Sci. U.S.A.* **100,** 12027–12032 CrossRef Medline
28. Iwawaki, T., Akai, R., Kohno, K., and Miura, M. (2004) A transgenic mouse model for monitoring endoplasmic reticulum stress. *Nat. Med.* **10,** 98–102 CrossRef Medline
29. Abifadel, M., Guerin, M., Benjannet, S., Rabès, J. P., Le Goff, W., Julia, Z., Hamelin, J., Carreau, V., Varret, M., Bruckert, E., Tosolini, L., Meilhac, O., Couvert, P., Bonnefont-Rousselot, D., Chapman, J., *et al.* (2012) Identification and characterization of new gain-of-function mutations in the PCSK9 gene responsible for autosomal dominant hypercholesterolemia. *Atherosclerosis* **223,** 394–400 CrossRef Medline
30. Cameron, J., Holla, Ø. L., Ranheim, T., Kulseth, M. A., Berge, K. E., and Leren, T. P. (2006) Effect of mutations in the PCSK9 gene on the cell surface LDL receptors. *Hum. Mol. Genet.* **15,** 1551–1558 CrossRef Medline
31. Li, J., Lee, B., and Lee, A. S. (2006) Endoplasmic reticulum stress-induced apoptosis: multiple pathways and activation of p53-up-regulated modulator of apoptosis (PUMA) and NOXA by p53. *J. Biol. Chem.* **281,** 7260–7270 CrossRef Medline
32. Sano, R., and Reed, J. C. (2013) ER stress-induced cell death mechanisms. *Biochim. Biophys. Acta* **1833,** 3460–3470 CrossRef Medline
33. Ruggiano, A., Foresti, O., and Carvalho, P. (2014) Quality control: ER-associated degradation: protein quality control and beyond. *J. Cell Biol.* **204,** 869–879 CrossRef Medline
34. Lee, A. S. (2005) The ER chaperone and signaling regulator GRP78/BiP as a monitor of endoplasmic reticulum stress. *Methods* **35,** 373–381 CrossRef Medline
35. Teckman, J. H., and Perlmutter, D. H. (2000) Retention of mutant α1-antitrypsin Z in endoplasmic reticulum is associated with an autophagic response. *Am. J. Physiol. Gastrointest. Liver Physiol.* **279,** G961–974 CrossRef Medline
36. Lin, L., Schmidt, B., Teckman, J., and Perlmutter, D. H. (2001) A naturally occurring nonpolymerogenic mutant of α_1-antitrypsin characterized by prolonged retention in the endoplasmic reticulum. *J. Biol. Chem.* **276,** 33893–33898 CrossRef Medline
37. Beuret, N., Rutishauser, J., Bider, M. D., and Spiess, M. (1999) Mechanism of endoplasmic reticulum retention of mutant vasopressin precursor caused by a signal peptide truncation associated with diabetes insipidus. *J. Biol. Chem.* **274,** 18965–18972 CrossRef Medline
38. Gilbert, A., Jadot, M., Leontieva, E., Wattiaux-De Coninck, S., and Wattiaux, R. (1998) ΔF508 CFTR localizes in the endoplasmic reticulum-Golgi intermediate compartment in cystic fibrosis cells. *Exp. Cell Res.* **242,** 144–152 CrossRef Medline
39. Kim, P. S., Lee, J., Jongsamak, P., Menon, S., Li, B., Hossain, S. A., Bae, J. H., Panijpan, B., and Arvan, P. (2008) Defective protein folding and intracellular retention of thyroglobulin-R19K mutant as a cause of human congenital goiter. *Mol. Endocrinol.* **22,** 477–484 CrossRef Medline
40. Takahashi, K., Adachi, K., Yoshizaki, K., Kunimoto, S., Kalaria, R. N., and Watanabe, A. (2010) Mutations in NOTCH3 cause the formation and retention of aggregates in the endoplasmic reticulum, leading to impaired cell proliferation. *Hum. Mol. Genet.* **19,** 79–89 CrossRef Medline
41. Schuck, S., Prinz, W. A., Thorn, K. S., Voss, C., and Walter, P. (2009) Membrane expansion alleviates endoplasmic reticulum stress independently of the unfolded protein response. *J. Cell Biol.* **187,** 525–536 CrossRef Medline
42. Schwarz, D. S., and Blower, M. D. (2016) The endoplasmic reticulum: structure, function and response to cellular signaling. *Cell. Mol. Life Sci.* **73,** 79–94 CrossRef Medline
43. Nohturfft, A., and Zhang, S. C. (2009) Coordination of lipid metabolism in membrane biogenesis. *Annu. Rev. Cell Dev. Biol.* **25,** 539–566 CrossRef Medline
44. Madison, B. B. (2016) Srebp2: a master regulator of sterol and fatty acid synthesis. *J. Lipid Res.* **57,** 333–335 CrossRef Medline
45. Benjannet, S., Rhainds, D., Essalmani, R., Mayne, J., Wickham, L., Jin, W., Asselin, M. C., Hamelin, J., Varret, M., Allard, D., Trillard, M., Abifadel, M., Tebon, A., Attie, A. D., Rader, D. J., *et al.* (2004) NARC-1/PCSK9 and its natural mutants: zymogen cleavage and effects on the low density lipoprotein (LDL) receptor and LDL cholesterol. *J. Biol. Chem.* **279,** 48865–48875 CrossRef Medline
46. Cohen, J. C., Boerwinkle, E., Mosley, T. H., Jr., and Hobbs, H. H. (2006) Sequence variations in PCSK9, low LDL, and protection against coronary heart disease. *N. Engl. J. Med.* **354,** 1264–1272 CrossRef Medline
47. Sabatine, M. S., Giugliano, R. P., Keech, A. C., Honarpour, N., Wiviott, S. D., Murphy, S. A., Kuder, J. F., Wang, H., Liu, T., Wasserman, S. M., Sever, P. S., Pedersen, T. R., and FOURIER Steering Committee and Investigators (2017) Evolocumab and clinical outcomes in patients with cardiovascular disease. *N. Engl. J. Med.* **376,** 1713–1722 CrossRef Medline
48. Sirois, F., Gbeha, E., Sanni, A., Chretien, M., Labuda, D., and Mbikay, M. (2008) Ethnic differences in the frequency of the cardioprotective C679X PCSK9 mutation in a West African population. *Genet. Test.* **12,** 377–380 CrossRef Medline
49. Hooper, A. J., Marais, A. D., Tanyanyiwa, D. M., and Burnett, J. R. (2007) The C679X mutation in PCSK9 is present and lowers blood cholesterol in a Southern African population. *Atherosclerosis* **193,** 445–448 CrossRef Medline
50. Chen, W. T., Tseng, C. C., Pfaffenbach, K., Kanel, G., Luo, B., Stiles, B. L., and Lee, A. S. (2014) Liver-specific knockout of GRP94 in mice disrupts cell adhesion, activates liver progenitor cells, and accelerates liver tumorigenesis. *Hepatology* **59,** 947–957 CrossRef Medline
51. Gidalevitz, T., Stevens, F., and Argon, Y. (2013) Orchestration of secretory protein folding by ER chaperones. *Biochim. Biophys. Acta* **1833,** 2410–2424 CrossRef Medline
52. Luo, S., Mao, C., Lee, B., and Lee, A. S. (2006) GRP78/BiP is required for cell proliferation and protecting the inner cell mass from apoptosis during early mouse embryonic development. *Mol. Cell. Biol.* **26,** 5688–5697 CrossRef Medline
53. Flynn, G. C., Pohl, J., Flocco, M. T., and Rothman, J. E. (1991) Peptide-binding specificity of the molecular chaperone BiP. *Nature* **353,** 726–730 CrossRef Medline
54. Blond-Elguindi, S., Cwirla, S. E., Dower, W. J., Lipshutz, R. J., Sprang, S. R., Sambrook, J. F., and Gething, M. J. (1993) Affinity panning of a library of peptides displayed on bacteriophages reveals the binding specificity of BiP. *Cell* **75,** 717–728 CrossRef Medline
55. Marzec, M., Eletto, D., and Argon, Y. (2012) GRP94: an HSP90-like protein specialized for protein folding and quality control in the endoplasmic reticulum. *Biochim. Biophys. Acta* **1823,** 774–787 CrossRef Medline

Chapter 6: Soon to be Submitted to *Nature Medicine*

Author Contributions: PFL, BA, SJ, MC, RP, WA, NGS and RCA contributed to study conception, experimental design and analysis. Animal studies involving AAVs were carried out by JD, SS, BA and SJ. JHB and KP contributed to data collection and interpretation. PFL, RCA and MC wrote the manuscript and JB, KP, BA, SJ, WGR, MC, HW, MB, RP, WA, and NGS assisted with manuscript editing. MC discovered the human Q152H PCSK9 mutation and initiated clinical studies, MC, HW and MM, designed the clinical protocol, directed its implementation and analyzed and interpreted the results. AT programmed the MRI, analyzed and interpreted the images.

The hypocholesterolemic loss-of-function PCSK9 Q152H mutation protects against liver injury/dysfunction by enhancing ER chaperone stabilization

Paul F. Lebeau[1], Jae Hyun Byun[1], Khrystyna Platko[1], Brandon Ason[2], Simon Jackson[2], Joshua Dobroff[3], Susan Shetterly[2], William G. Richards[4], Ali A. Al-Hashimi[1], Kevin Doyoon Won[1], Majambu Mbikay[5], Annik Prat[6], Hanny Wassef[5], An Tang[7], Guillaum Paré[8], Renata Pasqualini[9], Wadih Arap[10], Nabil G. Seidah[6], Michel Chrétien[5*] and Richard C. Austin[1*]

Authors Affiliations:
[1]Department of Medicine, McMaster University, St. Joseph's Healthcare Hamilton and Hamilton Centre for Kidney Research, Hamilton, Ontario L8N 4A6, Canada.

[2]Cardiometabolic Disorders, Amgen Research, Inc., South San Francisco, CA 94080.

[3]Bristol-Myers Squibb., Redwood City, CA 94063.

[4]Proneurotech Inc., South San Francisco, CA 94080.

[5]Laboratory of Functional Endoproteolysis, Clinical Research Institute of Montreal, affiliated to the University of Montreal, Montreal, Quebec H2W 1R7, Canada.

[6]Laboratory of Biochemical Neuroendocrinology, Clinical Research Institute of Montreal, affiliated to the University of Montreal, Montreal, Quebec H2W 1R7, Canada.

[7]Department of Radiology at the Centre Hospitalier Universitaire de Montréal, University of Montreal, Montreal, Quebec H2X 0A9, Canada.

[8]Population Health Research Institute and the Departments of Medicine, Epidemiology and Pathology, McMaster University, Hamilton, Ontario L8L 2X2,

[9]Rutgers Cancer Institute of New Jersey and Division of Cancer Biology, Department of Radiation Oncology, Rutgers New Jersey Medical School, Newark, NJ 77030.

[10]Rutgers Cancer Institute of New Jersey and Division of Hematology/Oncology, Department of Medicine, Rutgers New Jersey Medical School, Newark, NJ 77030.

*e-mail: austinr@taari.ca; michel.chretien@ircm.qc.ca

Key Words: atherosclerosis, co-chaperone, ER stress, GRP78, GRP94, LDL receptor, liver disease, PCSK9, Q152H PCSK9 mutation

Abstract

Retention of misfolded loss-of-function (LOF) proteins in the endoplasmic reticulum (ER) causes ER stress and contributes to ER storage diseases (ERSDs). Although it is well established that several LOF mutations in the human proprotein convertase subtilisin/kexin type 9 (*PCSK9*) gene are retained in the ER, their contribution to hepatic ER stress and liver injury is not known. In this study, we report that hepatic overexpression of human PCSK9^{Q152H} in *Pcsk9*$^{-/-}$ mice does not cause ER stress, liver dysfunction or injury. Strikingly, hepatic overexpression of PCSK9^{Q152H} protected against ER stress by increasing the abundance of the stress-response chaperones, GRP78 and GRP94. Finally, normal liver function was preserved and systemic ER stress, as measured by the levels of circulating anti-GRP78 autoantibodies, was unaffected in all subjects harboring the human PCSK9^{Q152H} mutation. Our findings demonstrate that ER retention of PCSK9 protects against hepatic ER stress and suggests that inhibitors of PCSK9 autocatalytic cleavage may provide benefits to the liver over and above the well-established protective role of PCSK9 inhibition on cardiovascular disease (CVD).

Introduction

Circulating low-density lipoprotein cholesterol (LDLc) is a causal factor in the development and progression of CVD[1-3]. The cloning and characterization of the *PCSK9* gene and its capacity to enhance the degradation of hepatic LDL receptor (LDLR) represents a seminal advancement in our understanding of how circulating levels of LDLc are regulated[4-6]. While gain-of-function (GOF) mutations in the *PCSK9* gene are associated with elevated serum LDLc levels and premature CVD, LOF *PCSK9* mutations confer a hypocholesterolemic phenotype with reduced CVD risk [4, 7-10]. PCSK9 protein with LOF mutations in the serine protease catalytic domain (PCSK9^{S386A}) or in the site of autocatalytic processing, Gln^{152}↓ (PCSK9^{Q152H}), do not undergo autocatalytic cleavage and maturation in the ER and thus fail to exit this cellular compartment[8,9].

The ER is the largest organelle in secretory cells and is the major site of Ca^{2+} storage, lipid and carbohydrate metabolism as well as *de novo* protein folding[11-13]. Although serine proteases like PCSK9 are common pharmacologic targets[14] and patients with LOF *PCSK9* mutations provide clinical evidence of lowered LDLc and protection against CVD[7-9], it is well-established that the retention of inactive or misfolded proteins in the ER can lead to ER stress[15-20]. A number of heritable LOF mutations in proteins that transit the ER are known to be retained in this organelle and contribute to a condition known as ERSD. The well-characterized ER-retained LOF mutations in α1-antitrypsin, for instance, cause fibrosis, toxicity and ultimately lead to liver cirrhosis as a result of prolonged hepatic ER stress[19-20]. To mitigate or resolve ER stress, canonical unfolded protein response (UPR) activation is triggered by ER-resident molecular chaperones, such as the glucose-regulated protein of 78-kDa (GRP78). When misfolded protein aggregates are detected in the ER lumen, GRP78 dissociates from the three *arms of the UPR* leading to their activation[16]. These arms/transducers include the activating transcription factor-6 (ATF6), the inositol-requiring enzyme 1α (IRE1α) and the protein kinase R-like ER kinase (PERK). IRE1α phosphorylation activates endoribonuclease activity to splice and activate XBP1 (sXBP1), which in a manner similar to ATF6, translocates to the nucleus

and induces *de novo* expression of ER chaperones via the ER stress-response element. PERK phosphorylation increases its native kinase activity and subsequently promotes the phosphorylation of the eukaryotic initiation factor 2α (p-eIF2α). The latter pathway simultaneously attenuates global protein synthesis to reduce ER burden, increases ER chaperone expression through the activating transcription factor 4 (ATF4), and during conditions of chronic or severe ER stress can promote apoptosis by inducing the expression of the CCAAT-enhancer-binding protein homologous protein (termed CHOP)[21,22].

Liver hepatocytes perform a myriad of secretory roles and are thus enriched in ER. Accumulating evidence stemming from the last two decades of research confirms that ER stress is a driver of liver disease and its complications[13,23,24]. Chronic UPR activation has been shown to promote apoptosis, inflammation and fibrosis; all of which contribute to terminal hepatic disease, commonly resulting in liver cirrhosis and cancer. Although we have recently demonstrated that the retention of a variety of LOF PCSK9 mutants in cultured hepatocyte cell lines does not cause ER stress[25], it is currently unknown whether the retention of such mutants cause hepatic ER stress or dysfunction in mice or in humans. We now demonstrate that hepatic overexpression of the PCSK9^{Q152H} mutant in *Psck9*$^{-/-}$ mice does not cause hepatic ER stress or any detectable liver dysfunction or injury, but rather acts as an ER-resident co-chaperone by enhancing the levels of GRP78 and GRP94, key ER chaperones known to protect against ER stress[26]. In support of these studies, PCSK9^{Q152H}-expressing subjects of all ages had (i) preserved liver function including normal levels of circulating liver enzymes, and (ii) no change in circulating anti-GRP78 autoantibody titres, a marker of systemic ER stress. Taken together, our findings are the first to demonstrate that the ER-retained PCSK9^{Q152H} mutant not only fails to cause ER stress, but exhibits co-chaperone-like properties by increasing the abundance of key ER chaperones that protect against hepatic dysfunction and/or liver injury. These findings provide compelling evidence that the inhibition of PCSK9 autocatalytic in the ER may confer additional health benefits to the liver over and above the well-established reduction in CVD risk.

Results

Liver function in subjects harboring the PCSK9^{Q152H} mutation

The rare LOF PCSK9^{Q152H} is limited to 4 French-Canadian families[7]. Subjects with this mutation have no defined morbid phenotype and are completely normal despite their life-long state of hypocholesterolemia[7,9]. To assess liver function, 66 subjects from 3 of the 4 families known to harbour the PCSK9^{Q152H} mutation were submitted to full medical examination. Circulating liver enzymes, LDH, AST, ALT, GGT and bilirubin were within normal range in the PCSK9^{Q152H}-expressing subjects, including those over 90 years of age (Fig. 1A). Among the older subjects, six PCSK9^{Q152H}-expressing subjects, including two homozygotes (HH; 64.7 years of age) and four heterozyotes (QH; 76.4 years of age), along with seven wild-type family controls (QQ; 67.3 years of age) were submitted for abdominal NMR-imaging. These data revealed that liver volume and fat content, which represent well-established early-stage markers of liver disease, were not different in subjects with or without the PCSK9^{Q152H} mutation (Fig. 1B).

Characterization of Pcsk9$^{-/-}$ mice overexpressing PCSK9^{Q152H} or LDLR^{G544V}

To better understand the innocuous effect on liver injury/dysfunction, PCSK9 encoding the Q152H mutation was overexpressed in the livers of male C57BL/6J *Pcsk9*$^{-/-}$ mice using the adeno-associated virus (AAV)[27]. The AAVs using in these studies encoded either human PCSK9^{WT} (AAV-hPCSK9^{WT}), human PCSK9^{Q152H} (AAV-hPCSK9^{Q152H}), human LDLR^{G544V} (AAV-hLDLR^{G544V}) or an AAV-empty-vector (EV) control. To confirm appropriate expression and localization of these proteins, livers were assessed via immunohistochemical (IHC) staining and immunoblots. Treatment with AAV-hPCSK9^{Q152H} caused an increase in ER-PCSK9 staining and induced a marked expansion of the ER compared to the AAV-hPCSK9^{WT} treatment (Fig. 2A-C). The secretory status of PCSK9 was assessed by using either human (Fig. 2D) or mouse (Fig. 2E) PCSK9 ELISAs. We observed that the treatment of AAV-hPCSK9^{WT} led to a ~15-fold increase in circulating PCSK9 levels compared to *Pcsk9*$^{-/-}$ mice treated with AAV-hPCSK9^{Q152H} (32.6 *vs*. 2.2 μg/ml) (Fig. 2D) and a ~113-fold increase compared to that of endogenously-expressed mouse PCSK9 in C57BL/6J mice (32.6 *vs*. 0.289 μg/ml) (Fig. 2E). Immunoblots were also employed to confirm the abundance of ER-retained proPCSK9 in the livers of mice treated with AAV-hPCSK9^{Q152H} and AAV-hPCSK9^{WT} (Fig. 2F). As expected, immature LDLR (LDLR-i) was abundant in the livers of mice treated with AAV-hLDLR^{G544V}. Consistent with these findings, IHC revealed increased intracellular staining for human LDLR in the livers of mice treated with AAV-hLDLR^{G544V}, compared to other groups (Fig. S1). To confirm the functionality of AAV-expressed human PCSK9 in our *Pcsk9*$^{-/-}$ mouse model, we also carried out IHC staining for endogenously expressed hepatic cell-surface mouse LDLR (Fig. 2G and H), and a quantitative assessment of plasma triglyceride (Fig. 2I) and cholesterol (Fig. 2J) levels. Consistent with the well-established role of PCSK9 as an inducer of LDLR degradation[28], *Pcsk9*$^{-/-}$ mice treated with AAV-hPCSK9^{WT} exhibited a substantial reduction in cell-surface LDLR levels, which was accompanied by an increase in plasma triglyceride and cholesterol levels, compared to AAV-EV and/or AAV-hPCSK9^{Q152H}-treated *Pcsk9*$^{-/-}$ mice. Overall, these data demonstrate that treatment with AAVs encoding hPCSK9^{Q152H} or hLDLR^{G544V} led to a marked increase in the intracellular abundance of these mutant proteins in the livers of mice.

Hepatic ER retention of PCSK9 increases the abundance of liver GRP78 and GRP94 proteins

Given that we, as well as others, have recently shown that PCSK9 can interact directly with GRP78 and GRP94[25,29], two ER-resident chaperones known to play an important role in the regulation of protein folding and UPR activation[26], we first assessed the levels and localization of these proteins via IHC staining and immunoblots (Fig. 3A-C). Similar to findings reported in cultured hepatocytes[25], the livers of mice overexpressing the PCSK9^{Q152H} mutant exhibited increased GRP94 protein compared to those of mice treated with either AAV-EV or AAV-hPCSK9^{WT}; moreover, a similar increase in GRP78 and GRP94 levels was also observed in the livers of mice treated with AAV-hLDLR^{G544V}. Increased staining with an anti-KDEL antibody, which detects both GRP94 and GRP78, was also observed in the livers of AAV-hPCSK9^{Q152H}- and AAV-

hLDLR^{G544V}-treated mice (Fig. S2). Despite having less protein abundance of GRP78 and GRP94 than the livers of mice treated with AAV-hPCSK9^{Q152H}, real-time PCR analysis revealed that only AAV-hLDLR^{G544}-treated mice had significantly increased mRNA transcript levels of these chaperones, compared to controls (Fig. 3D). A comparison of the livers of AAV-hLDLR^{G544V}-treated mice with those of C57BL/6J mice treated with ER stress-inducing agent, tunicamycin (TM; 250 μg/kg), also revealed a similar re-localization of GRP78 from the ER to the cell-surface of hepatocytes; a well-established hallmark of prolonged ER stress known to contribute to hepatocellular carcinoma as well as endothelial cell activation and atherosclerosis (Fig. S3)[30-33]. The interaction between hPCSK9 and the chaperones, GRP78 and GRP94, was also confirmed via immunoprecipitation from freshly-isolated livers (Fig. S4A). Consistent with previous studies[29], overexpression of GRP78 and GRP94, a process known to block PCSK9 secretion, increased LDL uptake of HepG2 cells (Fig. S4B).

To explore the effect of PCSK9 deficiency on hepatic GRP78 and GRP94 levels, *Pcsk9*$^{-/-}$ and age-matched *Pcsk9*$^{+/+}$ control mice were fed an ER stress-inducing high-fat diet for 12 weeks[23]. In a reciprocal manner to increased ER-PCSK9 levels, as is the case in hepatocytes exposed to AAV-hPCSK9^{Q152H}, hepatic PCSK9 deficiency led to an attenuation of HFD-induced GRP78 and GRP94 protein levels, compared to *Pcsk9*$^{+/+}$ controls (Fig. 3E, F and S5A). Similar to AAV-treated mice, real-time PCR demonstrated that changes in the expression of GRP78 and GRP94 in HFD-fed *Pcsk9*$^{-/-}$ mice were restricted to the protein level (Fig. S5B).

ER retention of PCSK9 protects cultured hepatocytes from ER stress and cytotoxicity

To explore whether increased abundance of GRP94 and/or GRP78 observed in the livers of mice expressing PCSK9^{Q152H} affects the susceptibility of cells to ER stress and cytotoxicity, HEK293 cells were transfected with mammalian expression vectors encoding either human PCSK9^{WT} or PCSK9^{Q152H} for 48 hours and treated with ER stress-inducing agents, TM (2 μg/ml) or thapsigargin (TG; 100 nM) for an additional 24 hours. In response to PCSK9^{Q152H} expression, we observed that HEK293 cells exhibited reduced expression of ER stress markers, GRP78, sXBP1, IRE1a, and ATF6 in response to ER stress-inducing agents compared to cells transfected with PCSK9^{WT} via real-time PCR (Fig. 4A). Consistent with HEK293 cells, a reduction in TG-mediated ER stress marker expression of phosphorylated (p)PERK and IRE1α was also observed at the protein level in HuH7 immortalized human hepatocytes transfected with PCSK9^{Q152H} compared to those transfected with PCSK9^{WT} (Fig. 4B). HepG2 immortalized human hepatocytes transfected with PCSK9^{Q152H} also exhibited a reduction in cytotoxicity, both in the absence and in the presence of TG or TM, compared to those transfected with PCSK9^{WT} (Fig. 4C). To confirm that the protective effect of ER-PCSK9 retention occurred in a manner dependent on GRP94, the latter experiment was repeated in HepG2 cells treated with siRNA targeted against GRP94 (siGRP94). Following reduced GRP94 expression, ER PCSK9 retention substantially increased cytotoxicity compared to cells expressing the secreted PCSK9^{WT} in the presence or absence of ER stress-inducing agents (Fig. 4D). In a reciprocal manner, siRNA-mediated

knockdown of PCSK9 also contributed to TG-induced cytotoxicity in HEK293, HepG2 and HuH7 cells (Fig. 4E).

The ability of GRP78 and GRP94 to attenuate ER stress-induced cytotoxicity was also examined in HepG2 cells by means of overexpression using mammalian expression plasmids (Fig. 4F and G). Consistent with cells overexpressing PCSK9^{Q152H}, we observed that cells overexpressing GRP78 or GRP94 also were protected against TG- and TM-induced cell death. Finally, to determine whether the expression of PCSK9^{Q152H} confers general protection against ER stress-induced cytotoxicity as a result of a misfolded protein mutant, HepG2 cells were co-transfected with native secreted WT vasopressin (VP^{WT}) or an ER-retained VP^{G17V} mutant that was previously shown to cause ER stress and cytotoxicity in a variety of cell lines[17,25]. Consistent with previous studies, we observed that the retention of VP^{G17V} in the ER markedly increased cytotoxicity; an effect that was attenuated by the co-expression of ER-retained PCSK9^{Q152H} (Fig. 4H), suggesting that PCSK9^{Q152H} could protect against ER stress induced by another misfolded protein. These findings were also confirmed using a TUNEL assay, which stains damaged DNA resulting from apoptosis (Fig. 4I and J). The expression/inhibition of proteins of interest in HepG2 cells transfected with mammalian expression vectors or siRNA was confirmed via immunoblot analysis (Fig. 4K).

ER retention of LDLR^{G544V}, but not PCSK9^{Q152H}, causes robust UPR activation, apoptosis and fibrosis in the livers of Pcsk9$^{-/-}$ mice.

Given that GRP78 and GRP94 were upregulated at the protein and mRNA levels in mice treated with AAV-hLDLR^{G544V}, a result limited to protein level in mice treated with AAV-hPCSK9^{Q152H}, we reasoned that (1) ER retention of PCSK9^{Q152H} increases the stability of these chaperones via protein-protein interaction, and that (2) ER retention of LDLR^{G544V} increases the expression of these chaperones as a result of an ER stress-induced increase in mRNA transcript. IHC staining revealed a marked increase in pPERK and pIRE1α in the livers of AAV-hLDLR^{G544V}-treated mice compared to AAV-EV (Fig. S6A). Immunoblots also demonstrated increased expression of UPR markers pPERK, IRE1α, sXBP1 and p-eIF2α in the livers of AAV-hLDLR^{G544V}-treated mice, compared to controls (Fig. 5A). Increased expression of UPR markers ATF4, sXBP1, PERK, CHOP and IRE1α was also observed in AAV-hLDLR^{G544V}-treated mice via real-time PCR (Fig. 5B). In contrast to mice treated with AAV-hLDLR^{G544V}, those treated with AAV-hPCSK9^{Q152H} did not exhibit increased protein or mRNA levels of these UPR markers, compared to controls. Misfolded protein aggregates or amyloid accumulation resulting from ER stress was also examined via Thioflavin-S staining (Fig. S6B). Consistent with ER stress marker expression, an increase in amyloid accumulation was observed in the livers of mice treated with AAV-hLDLR^{G544V}, compared to other groups. Overall, these results are consistent with previous tissue culture studies demonstrating that ER retention of LDLR^{G544V} causes robust UPR activation, whereas ER retention of PCSK9^{Q152H} fails to do so[25,35].

To further examine the role of PCSK9 on ER stress and liver injury, AAV experiments were repeated in *Pcsk9*$^{+/+}$ mice (n=5). Interestingly, in a manner similar to previous reports[8,9], the

expression of ER-retained PCSK9^{Q152H} caused the retention of endogenously-expressed mouse PCSK9 (Fig. 5C), likely via oligomerization of ER retained proPCSK9[5]. We also observed that *Pcsk9*$^{+/+}$ mice treated with AAV-hLDLR^{G544V} exhibited a marked reduction in endogenously-expressed circulating PCSK9 levels compared to AAV-EV-treated *Pcsk9*$^{+/+}$ controls. Based on our previous studies demonstrating that ER stress causes the retention of PCSK9 within the ER[35], we postulated that ER stress resulting from of LDLR^{G544V} expression was antagonizing the secretion PCSK9 from the livers of these mice. Consistent with this hypothesis, an increase in hepatic PCSK9 protein was also observed in the livers of AAV-hLDLR^{G544V}-treated *Pcsk9*$^{+/+}$ mice as determined by ELISA (Figure 5D). Importantly, no change was observed in PCSK9 mRNA transcript levels (Fig. S7), thus suggesting that increased PCSK9 protein abundance did not occur as a result of *de novo* synthesis. Next, we tested whether the accumulation of PCSK9 in the ER could protect against ER stress. Comparison between AAV-hLDLR^{G544V}-treated *Pcsk9*$^{-/-}$ and *Pcsk9*$^{+/+}$ mice revealed that the presence of PCSK9, which had accumulated in the livers of the AAV-hLDLR^{G544V}-treated *Pcsk9*$^{+/+}$ mice, attenuated the hLDLR^{G544V}-induced expression of ER stress markers (Fig. 5E). Finally, liver injury in these mice was assessed via quantification of circulating ALT activity. Similar to ER stress marker expression, a marked increase in serum ALT activity was observed in AAV-hLDLR^{G544V}-treated mice, but not those treated with AAV-hPCSK9^{Q152H} (Fig. 5F). Furthermore, a substantial reduction in ALT activity was observed in AAV-hLDLR^{G544V}-treated *Pcsk9*$^{+/+}$ compared to AAV-hLDLR^{G544V}-treated *Pcsk9*$^{-/-}$ mice (Fig. 5G).

In the context of prolonged and/or chronic UPR activation, the associated apoptosis is an established contributor to pathology in a variety of ERSD states[21,22]. Therefore, we next examined the expression of pro-apoptotic markers in livers of AAV-treated *Pcsk9*$^{-/-}$ mice. Consistent with the observed UPR activation, increased cleaved caspase-3 staining was observed in the livers of AAV-hLDLR^{G544V}-treated mice, compared to other groups (Fig. S8A and B). Additional pro-apoptotic mediators including PARP, cleaved (c)PARP, caspases (Casp) and cleaved caspases (cCasp)-1, -3, -7 and -9 were also assessed via immunoblot (Fig. S8C) and real-time PCR (Fig. S8D) and were exclusively upregulated in the livers of AAV-hLDLR^{G544V}-treated mice.

In addition to apoptotic cell death, the complex interplay of cellular events known to take place during conditions of hepatic ER stress also includes fibrosis and inflammation[13,23]. As such, the livers of AAV-treated mice were examined for fibrosis via staining of picrosirius-red (PSR), α-smooth muscle actin (αSMA), and fibronectin (FN1). The infiltration of CD20-positive inflammatory macrophages was also assessed via IHC staining. Similar to the observed increase in UPR activation and expression of pro-apoptotic mediators, we observed an increase in the staining of fibrotic and inflammatory markers in the livers of AAV-hLDLR^{G544V}-treated mice compared to controls (Fig. S9A,B). Heightened expression of fibrotic markers αSMA, FN1, TGFβ, as well as inflammatory markers CD4, IL6, IL1β and TNFα was also observed in this treatment group via immunoblot (Fig. S9C) and real-time PCR (Fig. S9D). Collectively, these data demonstrate that ER retention of misfolded

proteins, such as the LDLR, can cause severe hepatic ER stress, as well as liver injury. Furthermore, these data also imply that PCSK9 is retained in the ER during conditions of ER stress in order to attenuate UPR activation and subsequent liver injury.

NASH patients, but not PCSK9^{Q152H}-expressing subjects, exhibit elevated levels of anti-GRP78 autoantibodies

During conditions of prolonged ER stress, ER-resident GRP78 can localize to the cell-surface, where it plays a variety of roles as a pro-survival signaling molecule with implications in cancer progression and atherosclerosis [30-33]. Hepatocytes in the livers of AAV-hLDLR^{G544V}-treated mice, as well as hepatocytes in the livers of TM-treated mice, exhibited increased cell-surface GRP78 expression (Fig. S2). Following the expression of this neoantigen at the cell-surface, the immune system can generate autoantibodies targeted against GRP78[30,33]. Because this process is dependent on ER stress, we utilized circulating anti-GRP78 autoantibodies as a surrogate marker of systemic ER stress in subjects harboring the PCSK9^{Q152H} mutation. Interestingly, a modest but significant increase in autoantibody titres was observed in patients with NASH; a progressive form of liver disease in which ER stress is a well-established and causative driver[13,23,36]. However, individuals expressing ER-retained PCSK9^{Q152H} did not exhibit increased levels of anti-GRP78 autoantibodies (Fig. 6). Overall, these data demonstrate that ER stress driven liver disease can increase circulating levels of anti-GRP78 autoantibodies and suggests that patients expressing ER-retained PCSK9^{Q152H} do not exhibit hepatic ER stress.

Discussion

Individuals harboring the LOF PCSK9^{Q152H} mutation present with reduced or absent circulating PCSK9 levels and hypocholesterolemia due to the synthesis of a cleavage-resistant form of proPCSK9 that fails to exit the ER[5,8,9]. Despite the beneficial reduction in CVD risk, it is currently unknown whether the retention and accumulation of these uncleavable forms of PCSK9 within the ER leads to a form of ERSD. Our results demonstrate that hepatic overexpression of the PCSK9^{Q152H} mutant in *Psck9*$^{-/-}$ mice does not cause hepatic ER stress or any detectable liver dysfunction or injury. Our findings also demonstrate that ER PCSK9 retention in mice can increase the protein abundance of GRP78 and GRP94, key ER chaperones known to protect against ER stress and liver disease[26], without affecting the remainder of UPR signaling cascades. Similarly, PCSK9^{Q152H}-expressing subjects had (i) preserved liver function, including normal levels of circulating liver enzymes, and (ii) no increase in circulating anti-GRP78 autoantibody titres, a marker of systemic ER stress[30-33].

Assessment of UPR signaling cascades in this study also identified the ER-retained LDLR^{G544V} mutant as a potent inducer of hepatic ER stress in mouse models; a finding consistent with cultured human hepatocyte cell lines[34]. Although increased protein abundance of GRP78 and GRP94 was observed in the livers of AAV-hPCSK9^{Q152H} and AAV-hLDLR^{G544V}-treated mice, increased mRNA levels of these chaperones was restricted to LDLR^{G544V}-expressing mice. Conventional UPR activation, including elevated expression of a breadth of UPR chaperones at the protein and mRNA transcript levels, was only observed in the livers of AAV-hLDLR^{G544V}-treated and not

AAV-hPCSK9^{Q152H}-treated mice. Taken together, these data strongly suggest that by interacting with GRP78 and GRP94, ER-resident PCSK9 increases their stability without affecting their transcriptional status or inducing UPR activation.

In accordance with these observations, *Pcsk9*$^{-/-}$ mice exhibited reduced GRP78 and GRP94 protein levels in response to the ER stress-inducing HFD compared to *Pcsk9*$^{+/+}$ counterparts. A marked reduction in the protein abundance of GRP94 was also observed in the livers of *Pcsk9*$^{-/-}$ mice fed NCD compared to controls, suggesting a strong PCSK9-dependence of hepatic GRP94. The observed increase in GRP94 expression in AAV-hPCSK9^{Q152H}-treated mice (8-fold *vs*. AAV-EV) compared to that of GRP78 (3-fold vs AAV-EV) also suggests that the interaction between PCSK9 and GRP94 exceeds that of PCSK9 and GRP78.

Given the observed increase in the expression of GRP78 and GRP94, two chaperones known to play protective roles against ER stress and cytotoxicity in a variety of pathologies, the protective role of PCSK9^{Q152H} also became a primary objective of our study. Accordingly, we observed that PCSK9^{Q152H}-expressing cultured cells were protected from pharmacologically-induced ER stress, as well as cell death resulting from the retention of an ER-retained VP mutant that was previously shown to cause ER stress[17,37]. Although our study provides evidence of a novel role of intracellular PCSK9, it is not the first to identify ER-resident proteins capable of increasing the stability of ER chaperones to protect against ER stress. Previous studies have identified Bag5 as an ER-resident GRP78 binding partner capable of increasing its stability and expression at the protein level in cardiomyocytes[38]. Consistent with our observations, overexpression of Bag5 reduced cell death whereas siRNA-mediated knockdown had the opposite effect. GALNT6 was also identified as an O-type glycosyltransferase capable of increasing the protein stability of GRP78 and suppressing ER stress-induced apoptosis[39].

Given the well-established pro-survival/ protective role of GRP78, it is not surprising that proteins that increase its stability also confer protection against ER stress-inducing stimuli. Similar to GRP78, however, accumulating evidence now suggests that GRP94 also plays a significant protective role[40,41]. In support of this, recent evidence has demonstrated that (a) the knockdown of GRP94 is embryonic lethal[26], that (b) GRP94 knockout in embryonic stem cells leads to compensatory changes in UPR signaling/ activation[41], which commonly leads to increased susceptibility to cytotoxicity[43], and that (c) liver-specific deletion of GRP94 leads to liver injury and spontaneous hepatocellular carcinoma in aged mice[44]. Likewise, overexpression of these chaperones is also known to protect against ER stress[40,45].

Our previous findings demonstrated that conditions of ER stress, via pharmacologic intervention, causes the retention of PCSK9 in the ER of hepatocytes and reduces its levels in circulation[35]. Consistent with this observation, we now report that expression of LDLR^{G544V} — which causes severe ER stress and liver injury in *Pcsk9*$^{-/-}$ mice — also abolished the circulating levels of endogenously-expressed mouse PCSK9. Given that hepatic PCSK9 protein levels are increased in AAV-hLDLR^{G544V}-treated mice compared to AAV-EV-treated controls, and

that mRNA transcript levels are not affected, these data suggest that PCSK9 is being retained in the livers of these mice as a result of ER stress. Given the use of a liver-targetted AAV serotype in our studies, these data are also consistent with liver-specific *Pcsk9* ablation studies demonstrating that circulating PCSK9 originates almost exclusively from liver hepatocytes[46]. The previously-documented dominant negative effect of ER-retained PCSK9^{Q152H} on secreted levels of endogenously-expressed mouse wild-type PCSK9 was also observed in our studies[8,9]. Finally, in a manner consistent with our findings in cultured cells, the cellular retention of PCSK9 in the livers of AAV-hLDLR^{G544V}-treated *Pcsk9*$^{+/+}$ mice caused a reduction of ER stress marker expression in comparison to mice expressing the same LDLR mutant that lack PCSK9 (AAV-hLDLR^{G544V}-treated *Pcsk9*$^{-/-}$). Collectively, these results demonstrate that retention of PCSK9 in hepatocytes during conditions of ER stress leads to an attenuation of UPR activation and liver injury.

The clinically approved anti-PCSK9 antibody therapeutics markedly reduce plasma LDLc in patients at high-risk of cardiovascular events[47]. Given the impressive efficacy of PCSK9 reduction, and the prevalence of the underlying disease against which it is targeted, the need for additional PCSK9 inhibitory treatment modalities is well-justified[48-50]. Currently, pharmacologic inhibition of PCSK9 proteolysis to induce its retention in the ER has proven to be a major biochemical challenge[51,52]. Although PCSK9 auto-endoproteolysis represents the rate-limiting step of PCSK9 secretion and stands as a highly sought-after and classical pharmacologic target, this process follows exceedingly fast kinetics and is concealed from pharmacologic agents by two lipid bilayers[50]. The appealing nature of low-cost small molecule inhibitors of PCSK9, however, far exceeds these drawbacks. Beyond the novel role of proPCSK9 as a putative co-chaperone of hepatic GRP78 and GRP94, our findings provide biochemical and genetic evidence that the inhibition of proPCSK9 autocatalytic cleavage in the ER, may represent a safe and unique approach for the management of hyperlipidemia as well as having the added benefit of preventing liver dysfunction. The experimental findings and the clinical observations described in this study suggests that the naturally-occurring LOF PCSK9^{Q152H} mutant is an important player in ER stress response. This is the first example that a single mutation of a human gene, already beneficial against CVD risk, may also offer additional protection against a major group of liver-related diseases[53,54].

Acknowledgments: The authors thank Dr. David R. Cool (Department of Pharmacology and Toxicology, Boonshoft School of Medicine, Wright State University) for the vasopressin expression plasmids and Gavin Wright (Addgene plasmid #111008) for the GRP94 expression plasmid. This work was supported in part by research grants to Richard C. Austin from the Heart and Stroke Foundation of Ontario (T-6146), the Heart and Stroke Foundation of Canada (G-13-0003064 and G-15-0009389), the Canadian Institutes of Health Research (FRN 74477, 148539), to Nabil G. Seidah from the Leducq Foundation (13 CVD 03), CIHR Foundation grant (148363) and Canada Research Chair (216684) and to Michel Chrétien from La Fondation J-Louis Lévesque and the Richard and Edith Straus-Aclon Foundations. Financial support from St. Joseph's Healthcare Hamilton is also acknowledged. Richard C. Austin is a Career Investigator of the Heart and Stroke Foundation of Ontario and holds the Amgen Canada Research Chair in the Division of Nephrology at St. Joseph's Healthcare and McMaster University.

Author Contributions: PFL, BA, SJ, AP, MC, RP, WA, NGS and RCA contributed to study conception, experimental design and analysis. Animal studies involving AAVs were carried out by JD, SS, BA and SJ. JHB and KP contributed to data collection and interpretation. PFL, RCA and MC wrote the manuscript and JB, KP, BA, SJ, WGR, MC, HW, MB, RP, WA, and NGS assisted with manuscript editing. MC discovered the human Q152H PCSK9 mutation and initiated clinical studies, MC, HW and MM, designed the clinical protocol, directed its implementation and analyzed and interpreted the results. AT programmed the MRI, analyzed and interpreted the images.

Competing Interests: Authors from McMaster University, the Clinical Research Institute of Montreal, Rutgers Cancer Institute of New Jersey and Rutgers New Jersey Medical School declare that no conflicts of interest exist. B.A., S.S. and S.J. are employees of Amgen and hold Amgen Stock. R.C.A. is on the scientific advisory board of Precision BioLogic Inc.

References

1. Ference, B.A.*, et al.* Low-density lipoproteins cause atherosclerotic cardiovascular disease. 1. Evidence from genetic, epidemiologic, and clinical studies. A consensus statement from the European Atherosclerosis Society Consensus Panel. *Eur Heart J* **38**, 2459-2472 (2017).
2. Huynh, K. Lipids: Very low achieved LDL-cholesterol levels improve cardiovascular outcomes. *Nature reviews. Cardiology* **14**, 630-631 (2017).
3. Fernandez-Ruiz, I. Atherosclerosis: Should we redefine the 'normal' LDL-cholesterol range? *Nature reviews. Cardiology* **15**, 68-69 (2018).
4. Abifadel, M.*, et al.* Mutations in PCSK9 cause autosomal dominant hypercholesterolemia. *Nat Genet* **34**, 154-156 (2003).
5. Seidah, N.G.*, et al.* The secretory proprotein convertase neural apoptosis-regulated convertase 1 (NARC-1): liver regeneration and neuronal differentiation. *Proc Natl Acad Sci U S A* **100**, 928-933 (2003).
6. Maxwell, K.N. & Breslow, J.L. Adenoviral-mediated expression of Pcsk9 in mice results in a low-density lipoprotein receptor knockout phenotype. *Proc Natl Acad Sci U S A* **101**, 7100-7105 (2004).
7. Cohen, J.C., Boerwinkle, E., Mosley, T.H., Jr. & Hobbs, H.H. Sequence variations in PCSK9, low LDL, and protection against coronary heart disease. *N Engl J Med* **354**, 1264-1272 (2006).
8. Mayne, J.*, et al.* Novel loss-of-function PCSK9 variant is associated with low plasma LDL cholesterol in a French-Canadian family and with impaired processing and secretion in cell culture. *Clin Chem* **57**, 1415-1423 (2011).
9. Benjannet, S., Hamelin, J., Chretien, M. & Seidah, N.G. Loss- and gain-of-function PCSK9 variants: cleavage specificity, dominant negative effects, and low density lipoprotein receptor (LDLR) degradation. *J Biol Chem* **287**, 33745-33755 (2012).
10. Chretien, M. & Mbikay, M. 60 YEARS OF POMC: From the prohormone theory to pro-opiomelanocortin and to proprotein convertases (PCSK1 to PCSK9). *Journal of molecular endocrinology* **56**, T49-62 (2016).
11. Kim, I., Xu, W. & Reed, J.C. Cell death and endoplasmic reticulum stress: disease relevance and therapeutic opportunities. *Nat Rev Drug Discov* **7**, 1013-1030 (2008).
12. Oakes, S.A. & Papa, F.R. The role of endoplasmic reticulum stress in human pathology. *Annual review of pathology* **10**, 173-194 (2015).
13. Lebeaupin, C.*, et al.* Endoplasmic Reticulum stress signaling and the pathogenesis of Non-Alcoholic Fatty Liver Disease. *J Hepatol* (2018).
14. Walker, B. & Lynas, J.F. Strategies for the inhibition of serine proteases. *Cell Mol Life Sci* **58**, 596-624 (2001).
15. Carlson, J. Endoplasmic reticulum storage disease. *Histopathology* **16**, 309-312 (1990).
16. Austin, R.C. The unfolded protein response in health and disease. *Antioxid Redox Signal* **11**, 2279-2287 (2009).
17. Yan, Z., Hoffmann, A., Kaiser, E.K., Grunwald, W.C., Jr. & Cool, D.R. Misfolding of Mutated Vasopressin Causes ER-Retention and Activation of ER-Stress Markers in Neuro-2a Cells. *Open neuroendocrinology journal* **4**, 136-146 (2011).

18. Rutishauser, J. & Spiess, M. Endoplasmic reticulum storage diseases. *Swiss medical weekly* **132**, 211-222 (2002).
19. Teckman, J.H. & Perlmutter, D.H. Retention of mutant alpha(1)-antitrypsin Z in endoplasmic reticulum is associated with an autophagic response. *Am J Physiol Gastrointest Liver Physiol* **279**, G961-974 (2000).
20. Lin, L., Schmidt, B., Teckman, J. & Perlmutter, D.H. A naturally occurring nonpolymerogenic mutant of alpha 1-antitrypsin characterized by prolonged retention in the endoplasmic reticulum. *J Biol Chem* **276**, 33893-33898 (2001).
21. Hetz, C. The unfolded protein response: controlling cell fate decisions under ER stress and beyond. *Nat Rev Mol Cell Biol* **13**, 89-102 (2012).
22. Faitova, J., Krekac, D., Hrstka, R. & Vojtesek, B. Endoplasmic reticulum stress and apoptosis. *Cellular & molecular biology letters* **11**, 488-505 (2006).
23. Dara, L., Ji, C. & Kaplowitz, N. The contribution of endoplasmic reticulum stress to liver diseases. *Hepatology* **53**, 1752-1763 (2011).
24. Malhi, H. & Kaufman, R.J. Endoplasmic reticulum stress in liver disease. *J Hepatol* **54**, 795-809 (2011).
25. Lebeau, P.*, et al.* Loss-of-function PCSK9 mutants evade the unfolded protein response sensor GRP78 and fail to induce endoplasmic reticulum stress when retained. *J Biol Chem* **293**, 7329-7343 (2018).
26. Zhu, G. & Lee, A.S. Role of the unfolded protein response, GRP78 and GRP94 in organ homeostasis. *Journal of cellular physiology* **230**, 1413-1420 (2015).
27. Fang, C.C.*, et al.* AAV serotype 8-mediated liver specific GNMT expression delays progression of hepatocellular carcinoma and prevents carbon tetrachloride-induced liver damage. *Sci Rep* **8**, 13802 (2018).
28. Poirier, S.*, et al.* The proprotein convertase PCSK9 induces the degradation of low density lipoprotein receptor (LDLR) and its closest family members VLDLR and ApoER2. *J Biol Chem* **283**, 2363-2372 (2008).
29. Poirier, S., Mamarbachi, M., Chen, W.T., Lee, A.S. & Mayer, G. GRP94 Regulates Circulating Cholesterol Levels through Blockade of PCSK9-Induced LDLR Degradation. *Cell reports* **13**, 2064-2071 (2015).
30. Al-Hashimi, A.A.*, et al.* Binding of anti-GRP78 autoantibodies to cell surface GRP78 increases tissue factor procoagulant activity via the release of calcium from endoplasmic reticulum stores. *J Biol Chem* **285**, 28912-28923 (2010).
31. Zhang, Y., Liu, R., Ni, M., Gill, P. & Lee, A.S. Cell surface relocalization of the endoplasmic reticulum chaperone and unfolded protein response regulator GRP78/BiP. *J Biol Chem* **285**, 15065-15075 (2010).
32. Zhang, X.X.*, et al.* The cell surface GRP78 facilitates the invasion of hepatocellular carcinoma cells. *BioMed research international* **2013**, 917296 (2013).
33. Crane, E.D.*, et al.* Anti-GRP78 autoantibodies induce endothelial cell activation and accelerate the development of atherosclerotic lesions. *JCI insight* **3**(2018).
34. Sorensen, S., Ranheim, T., Bakken, K.S., Leren, T.P. & Kulseth, M.A. Retention of mutant low density lipoprotein receptor in endoplasmic reticulum (ER) leads to ER stress. *J Biol Chem* **281**, 468-476 (2006).

35. Lebeau, P.*, et al.* Endoplasmic Reticulum Stress and Ca2+ Depletion Differentially Modulate the Sterol Regulatory Protein PCSK9 to Control Lipid Metabolism. *J Biol Chem* **292**, 1510-1523 (2017).
36. Wree, A., Broderick, L., Canbay, A., Hoffman, H.M. & Feldstein, A.E. From NAFLD to NASH to cirrhosis-new insights into disease mechanisms. *Nat Rev Gastroenterol Hepatol* **10**, 627-636 (2013).
37. Birk, J., Friberg, M.A., Prescianotto-Baschong, C., Spiess, M. & Rutishauser, J. Dominant pro-vasopressin mutants that cause diabetes insipidus form disulfide-linked fibrillar aggregates in the endoplasmic reticulum. *J Cell Sci* **122**, 3994-4002 (2009).
38. Gupta, M.K.*, et al.* GRP78 Interacting Partner Bag5 Responds to ER Stress and Protects Cardiomyocytes From ER Stress-Induced Apoptosis. *J Cell Biochem* **117**, 1813-1821 (2016).
39. Lin, J.*, et al.* GALNT6 Stabilizes GRP78 Protein by O-glycosylation and Enhances its Activity to Suppress Apoptosis Under Stress Condition. *Neoplasia* **19**, 43-53 (2017).
40. Vitadello, M.*, et al.* Overexpression of the stress protein Grp94 reduces cardiomyocyte necrosis due to calcium overload and simulated ischemia. *FASEB journal : official publication of the Federation of American Societies for Experimental Biology* **17**, 923-925 (2003).
41. Marzec, M., Eletto, D. & Argon, Y. GRP94: An HSP90-like protein specialized for protein folding and quality control in the endoplasmic reticulum. *Biochim Biophys Acta* **1823**, 774-787 (2012).
42. Mao, C.*, et al.* Targeted mutation of the mouse Grp94 gene disrupts development and perturbs endoplasmic reticulum stress signaling. *PLoS One* **5**, e10852 (2010).
43. Lebeau, P., Byun, J.H., Yousof, T. & Austin, R.C. Pharmacologic inhibition of S1P attenuates ATF6 expression, causes ER stress and contributes to apoptotic cell death. *Toxicology and applied pharmacology* **349**, 1-7 (2018).
44. Chen, W.T.*, et al.* Liver-specific knockout of GRP94 in mice disrupts cell adhesion, activates liver progenitor cells, and accelerates liver tumorigenesis. *Hepatology* **59**, 947-957 (2014).
45. Suyama, K.*, et al.* Overexpression of GRP78 protects glial cells from endoplasmic reticulum stress. *Neurosci Lett* **504**, 271-276 (2011).
46. Zaid, A.*, et al.* Proprotein convertase subtilisin/kexin type 9 (PCSK9): hepatocyte-specific low-density lipoprotein receptor degradation and critical role in mouse liver regeneration. *Hepatology* **48**, 646-654 (2008).
47. Sabatine, M.S.*, et al.* Evolocumab and Clinical Outcomes in Patients with Cardiovascular Disease. *N Engl J Med* **376**, 1713-1722 (2017).
48. Latimer, J., Batty, J.A., Neely, R.D. & Kunadian, V. PCSK9 inhibitors in the prevention of cardiovascular disease. *Journal of thrombosis and thrombolysis* (2016).
49. Sabatine, M.S., Underberg, J.A., Koren, M. & Baum, S.J. Focus on PCSK9 Inhibitors: From Genetics to Clinical Practice. *Postgraduate medicine* **128 Suppl 1**, 31-39 (2016).
50. Seidah, N.G., Prat, A., Pirillo, A., Catapano, A.L. & Norata, G.D. Novel strategies to target proprotein convertase subtilisin kexin 9: beyond monoclonal antibodies. *Cardiovasc Res* **115**, 510-518 (2019).

51. Chorba, J.S. & Shokat, K.M. The proprotein convertase subtilisin/kexin type 9 (PCSK9) active site and cleavage sequence differentially regulate protein secretion from proteolysis. *J Biol Chem* **289**, 29030-29043 (2014).
52. Chorba, J.S., Galvan, A.M. & Shokat, K.M. Stepwise processing analyses of the single-turnover PCSK9 protease reveal its substrate sequence specificity and link clinical genotype to lipid phenotype. *J Biol Chem* **293**, 1875-1886 (2018).
53. Mbikay, M., Mayne, J. & Chretien, M. Proprotein convertases subtilisin/kexin type 9, an enzyme turned escort protein: hepatic and extra hepatic functions. *Journal of diabetes* **5**, 391-405 (2013).
54. Williams, S.C. Genetic mutations you want. *Proc Natl Acad Sci U S A* **113**, 2554-2557 (2016).
55. Xiong, Y.*, et al.* Long-acting MIC-1/GDF15 molecules to treat obesity: Evidence from mice to monkeys. *Sci Transl Med* **9**(2017).

Figure Legends

Figure. 1. Liver function in PCSK9 Q152H-expressing subjects and family controls. (A) Correlations between age and the circulating liver enzymes lactate dehydrogenase (LDH), aspartate aminotransferase (AST), alanine aminotransferase (ALT) and gamma-glutamyl transferase (GGT) for Q152H subjects (-/-,+/-) and (+/+) family controls. Squares represent men, circles represent women. Homozygous Q152H (-/-) subjects are coloured in red, heterozygous Q152H (+/-) subjects are half black and family controls (+/+) are in white. Second order quadratic correlation is shown for the entire cohort. (**B)** Age, BMI, percent liver fat fraction and liver volume of Q152H subjects (-/-,+/-) and non-carrier family subjects (+/+). All data are presented as mean ± s.d.All data were analyzed by unpaired student t-test.

Figure 2. Characterization of PCSK9/LDLR AAV-treated mice. *Pcsk9*$^{-/-}$ mice (n=5) were treated with adeno-associated virus (AAV) encoding empty vector (EV), human (h)PCSK9 wild-type (WT) and ER-retained variants hPCSK9^{Q152H} and hLDLR^{G544V}. (**A,B**) Intracellular PCSK9 expression and retention was assessed via immunohistochemical staining and quantification using ImageJ software. (**C**) Immunofluorescent staining of PCSK9 and ER marker, PDI, was also used to visualize ER PCSK9 retention and expansion (ER area depicted as yellow dotted line). Secreted PCSK9 levels were examined using human (**D**) and mouse (**E**) PCSK9 ELISAs. (**F**) Liver expression of immature LDLR (LDLR-i; 100 kDa) and proPCSK9 (75 kDa) was confirmed via immunoblots. Additional parameters known to be modulated by secreted PCSK9, including (**G,H**) cell-surface hepatic LDLR expression, (**I**) plasma triglyceride levels and (**J**) plasma cholesterol levels, were also examined. Values are represented as mean and error bars as S.D. *, $P < 0.05$. ANOVA and *t* test were used for all statistical comparisons. Scale bars, Fig. 1A and G, 200 µm; Fig. 1C, 10 µm.

Figure 3. ER retention of PCSK9 increases the stability of UPR chaperones, GRP78 and GRP94. (**A**) The livers of *Pcsk9*$^{-/-}$ mice (n=5) treated with adeno-associated virus (AAV) encoding empty vector (EV), human (h)PCSK9 wild-type (WT) and ER-retained variants

hPCSK9^{Q152H} and hLDLR^{G544V} were examined for expression of ER-resident chaperones GRP78 and GRP94 *via* immunohistochemical staining. (**B**) Relative staining intensities were quantified using ImageJ software. (**C,D**) GRP78 and GRP94 mRNA protein and mRNA levels were also assessed using immunoblots and real time PCR. (**E,F**) *Pcsk9*$^{-/-}$ and age-matched *Pcsk9*$^{+/+}$ controls (n=5) were fed either normal chow diet (NCD) or high-fat diet (HFD) for 12 weeks and examined for GRP78 and GRP94 expression via immunohistochemical staining and immunoblots. Values are represented as mean and error bars as S.D. ANOVA and *t* test were used for all statistical comparisons. *, $P < 0.05$. Scale bars, 200 μm.

Figure 4. ER PCSK9 retention reduces ER stress-induced cytotoxicity in cultured immortalized hepatocytes. (A) Hek293 cells were transfected with plasmids encoding either human PCSK9 wild-type (PCSK9^{WT}) or the ER-retained variant PCSK9^{Q152H} for 48 hours and subsequently treated with ER stress-inducing agents thapsigargin (TG; 100 nM) or tunicamycin (TM; 2 μg/ml) for an additional 24 hours. ER stress marker expression was assessed via real-time PCR. (**B**) The expression of ER stress markers pPERK, IRE1α and GRP94 were also assessed in HuH7 immortalized hepatocytes transfected with either PCSK9^{WT} or PCSK9^{Q152H} in the presence and absence of TG using immunoblots. Cytotoxicity was examined in PCSK9-transfected HepG2 cells in the absence (**C**) or in the presence (**D**) of siRNA targeted against GRP94 (siGRP94) using a Lactate dehydrogenase (LDH) assay. (**E**) Cytotoxicity was also examined in Hek293, HuH7 and HepG2 cells transfected with siRNA targeted against PCSK9 (siPCSK9) in the presence and absence of TG. (**F,G**) The effect of increased GRP78 and GRP94 expression on cytotoxicity caused by ER stress-inducing agents, thapsigargin (TG; 100nM) and tunicamycin (TM; 2 μg/ml) was also examined. (**H**) LDH assays were carried out in HepG2 cells co-transfected with wild-type arginine-vasopressin (VP) or a naturally occurring variant known to cause ER stress and cytotoxicity (VP^{G17V}; 23) in the presence or absence of ER-retained PCSK9^{Q152H}. (**I,J**) These findings were confirmed via staining of apoptotic DNA damage using a TUNEL assay. (**K**) Effective transfection in HepG2 cells was confirmed using immunoblots. Values are represented as mean and error bars as S.D. *, $P < 0.05$. ANOVA and *t* test were used for all statistical comparisons. Scale bars; 200 μm.

Figure 5. ER retention of LDLR^{G544V}, but not PCSK9^{Q152H}, causes a robust UPR activation in liver. (**A,B**) The livers of *Pcsk9*$^{-/-}$ mice (n=5) treated with adeno-associated virus (AAV) encoding empty vector (EV), human (h)PCSK9 wild-type (WT) and ER-retained variants hPCSK9^{Q152H} and hLDLR^{G544V} were examined for expression of UPR markers pPERK, IRE1α, sXBP1, peIF2α, ATF4 and CHOP *via* immunoblotting and real-time PCR. (**C,D**) Serum and hepatic PCSK9 levels were examined in *Pcsk9*$^{+/+}$ mice treated with AAV encoding either ER, hPCSK9^{Q152H} or hLDLR^{G544V}. (**E**) ER stress marker expression in the livers of *Pcsk9*$^{-/-}$ expressing hLDLR^{G544V} were compared to *Pcsk9*$^{+/+}$ mice expressing hLDLR^{G544V} via immunoblotting. (**F,G**) Liver injury was examined in these mice via quantification of serum ALT activity. Values are represented as mean and error bars as S.D. *, $P < 0.05$. ANOVA and *t* test were used for all statistical comparisons.

Fig. 6. Anti-GRP78 autoantibody titres in the plasma of Q152H subjects and non-carrier family controls. ELISAs were used to measure plasma levels of anti-GRP78 autoantibodies in patients with NASH; a progressive form of liver disease, in which ER stress is an established driver. Anti-GRP78 autoantibodies were next examined in the plasma of $PCSK9^{Q152H}$-expressing subjects (-/-,+/-) and non-carrier family siblings (+/+). Values are represented as mean and error bars as S.D. *, $P < 0.05$. *t*-tests were used for all statistical comparisons.

Lebeau et al., 2019. Figure 1.

A

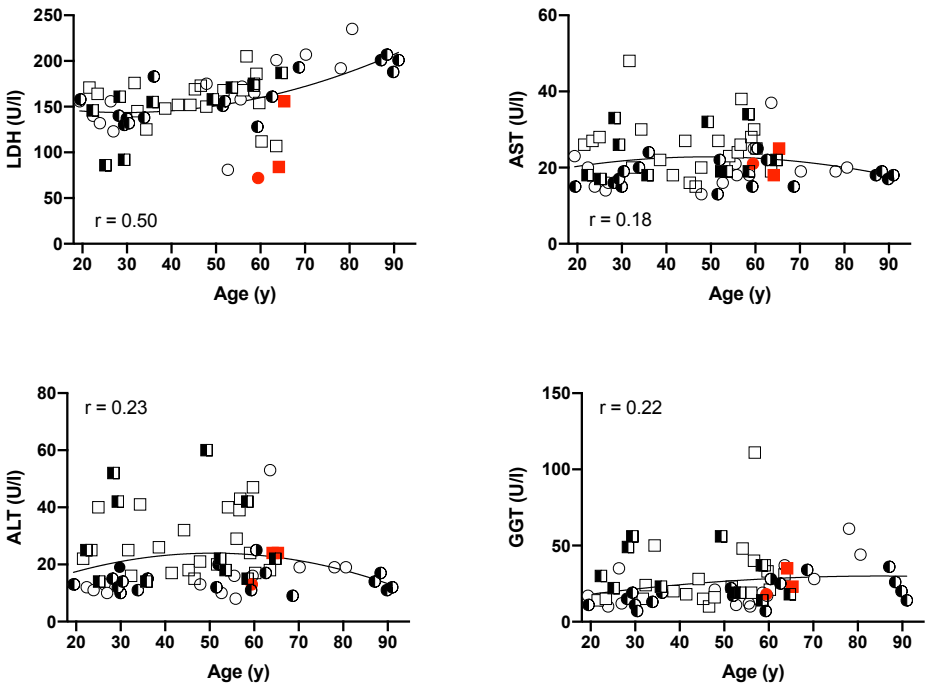

B

#	PCSK9-Q152H	Age	BMI	Liver fat fraction, %	Liver Volume, ml
1	-/-	64.2	30.2	10.40	1835.00
2	-/-	65.3	24.8	4.00	1371.00
Mean	**-/-**	**64.7**	**27.5**	**7.2**	**1603**
SD	**-/-**	**0.8**	**3.8**	**4.5**	**328.1**
3	+/-	89.8	24.6	3.20	1023.00
4	+/-	88.4	23.7	4.10	1113.00
5	+/-	64.7	22.2	4.70	1780.00
6	+/-	62.6	21.2	4.00	1134.00
Mean	**+/-**	**76.4**	**22.9**	**4**	**1262.5**
SD	**+/-**	**14.7**	**1.5**	**0.6**	**348.3**
7	+/+	80.6	32.0	8.70	1493.00
8	+/+	78.0	28.1	22.80	1206.00
9	+/+	70.2	24.8	2.80	1318.00
10	+/+	63.6	27.7	16.20	1598.00
11	+/+	63.5	26.0	4.90	1744.00
12	+/+	56.9	40.4	10.40	1875.00
13	+/+	58.6	26.7	1.50	1217.00
Mean	**+/+**	**67.3**	**29.4**	**9.6**	**1493**
SD	**+/+**	**9.2**	**5.4**	**7.7**	**261.1**

Lebeau et al., 2019. Figure 2.

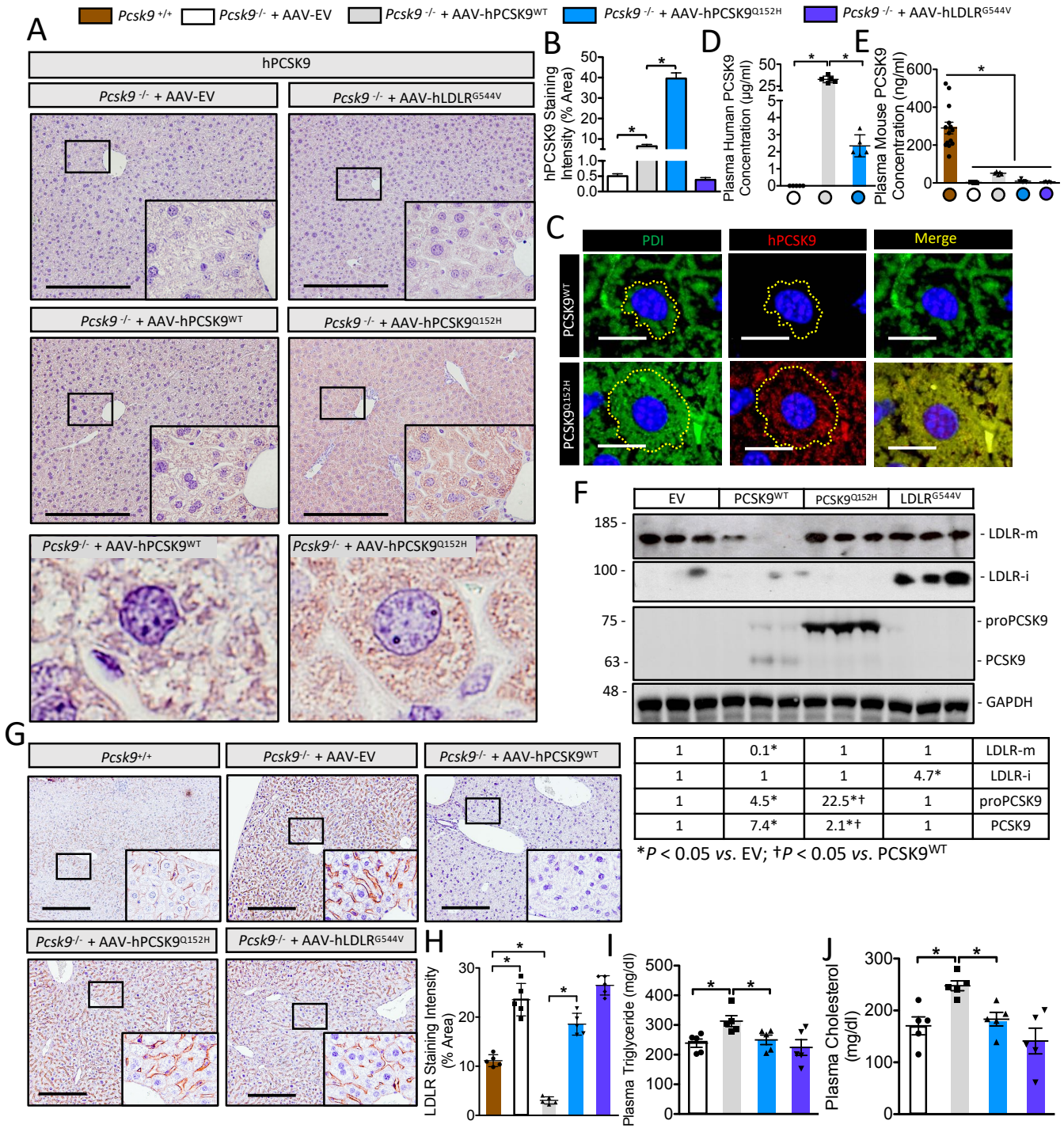

1	0.1*	1	1	LDLR-m
1	1	1	4.7*	LDLR-i
1	4.5*	22.5*†	1	proPCSK9
1	7.4*	2.1*†	1	PCSK9

*$P < 0.05$ *vs.* EV; †$P < 0.05$ *vs.* PCSK9^{WT}

Lebeau et al., 2019. Figure 3.

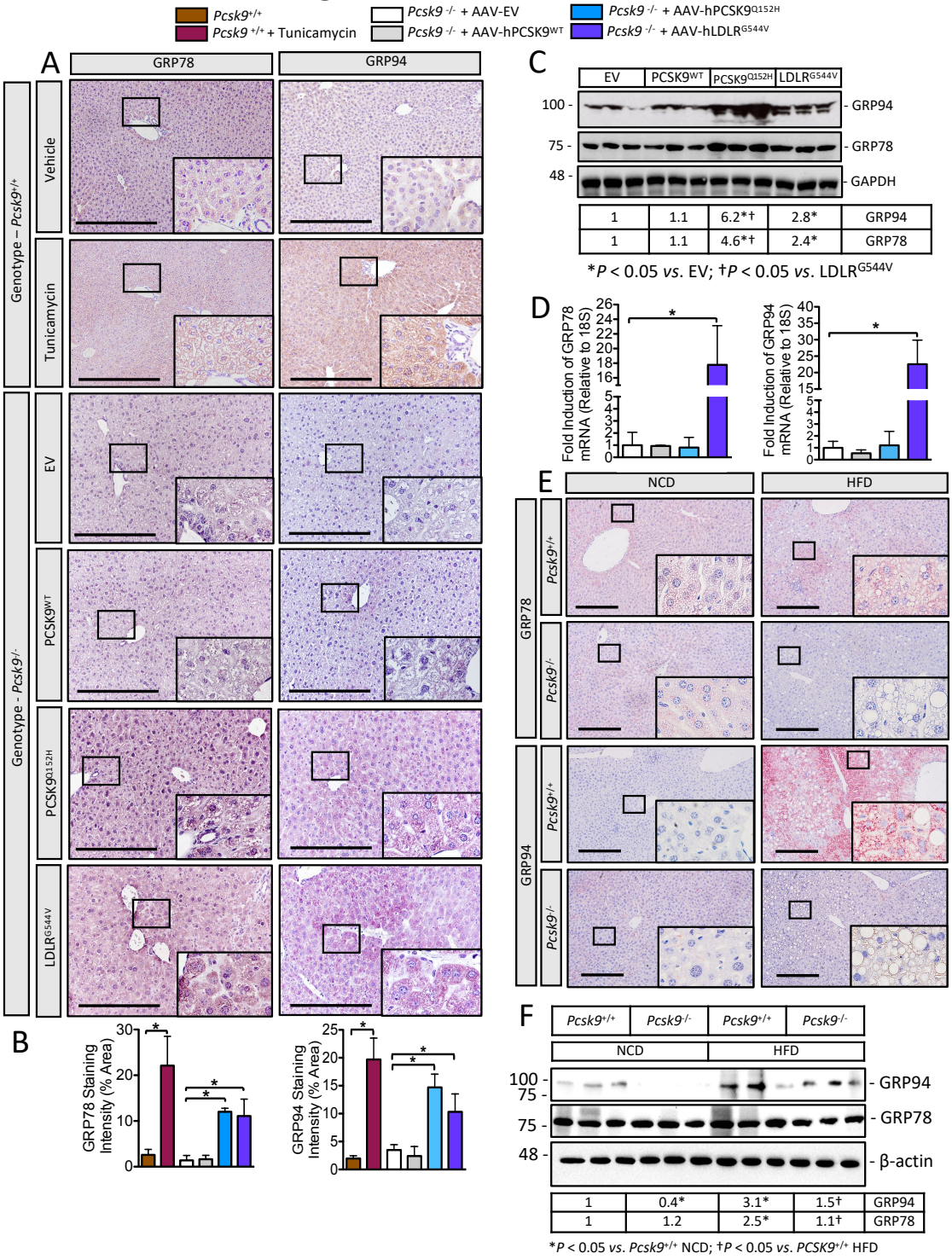

Lebeau et al., 2019. Figure 4.

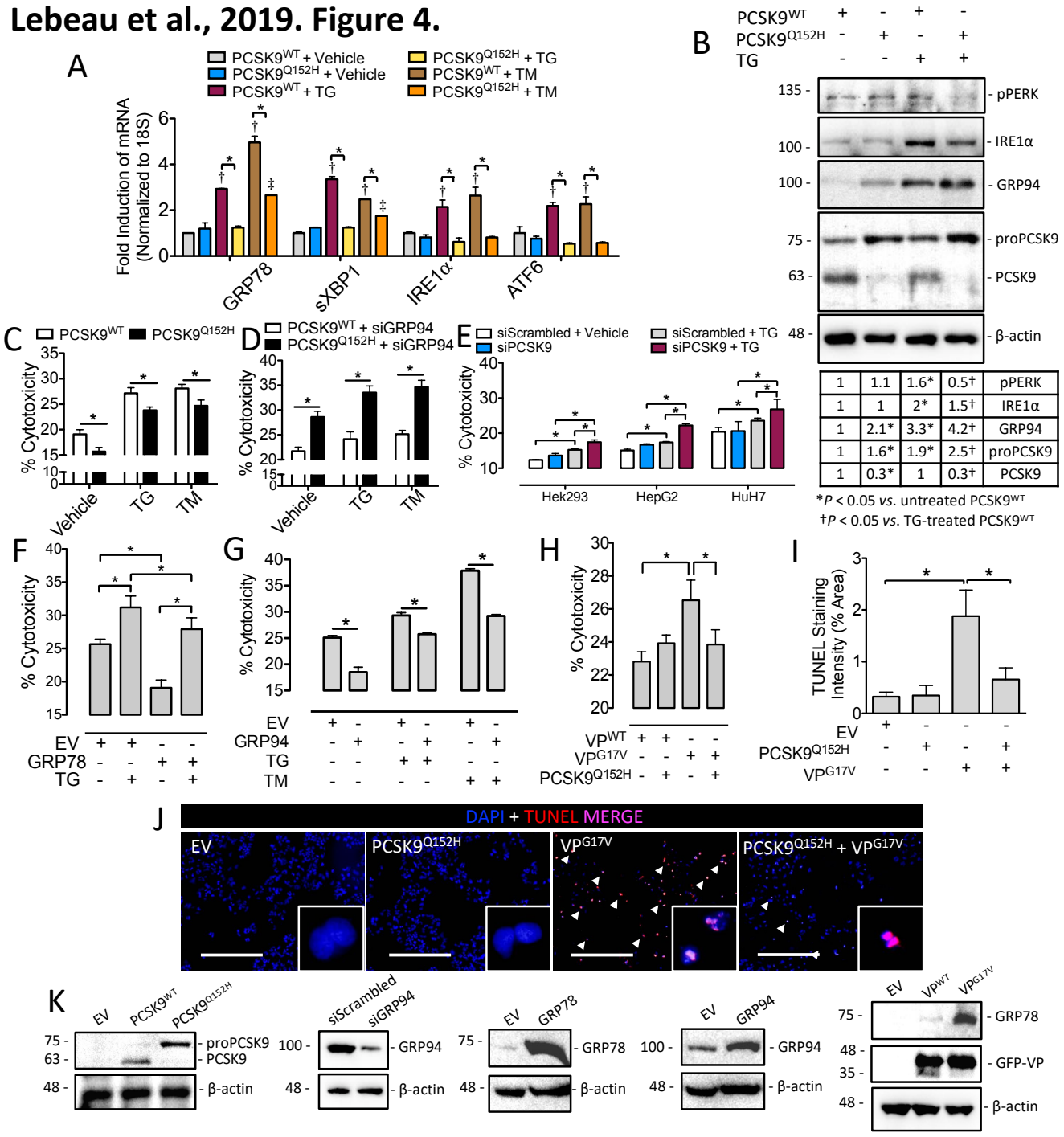

Lebeau et al., 2019. Figure 5.

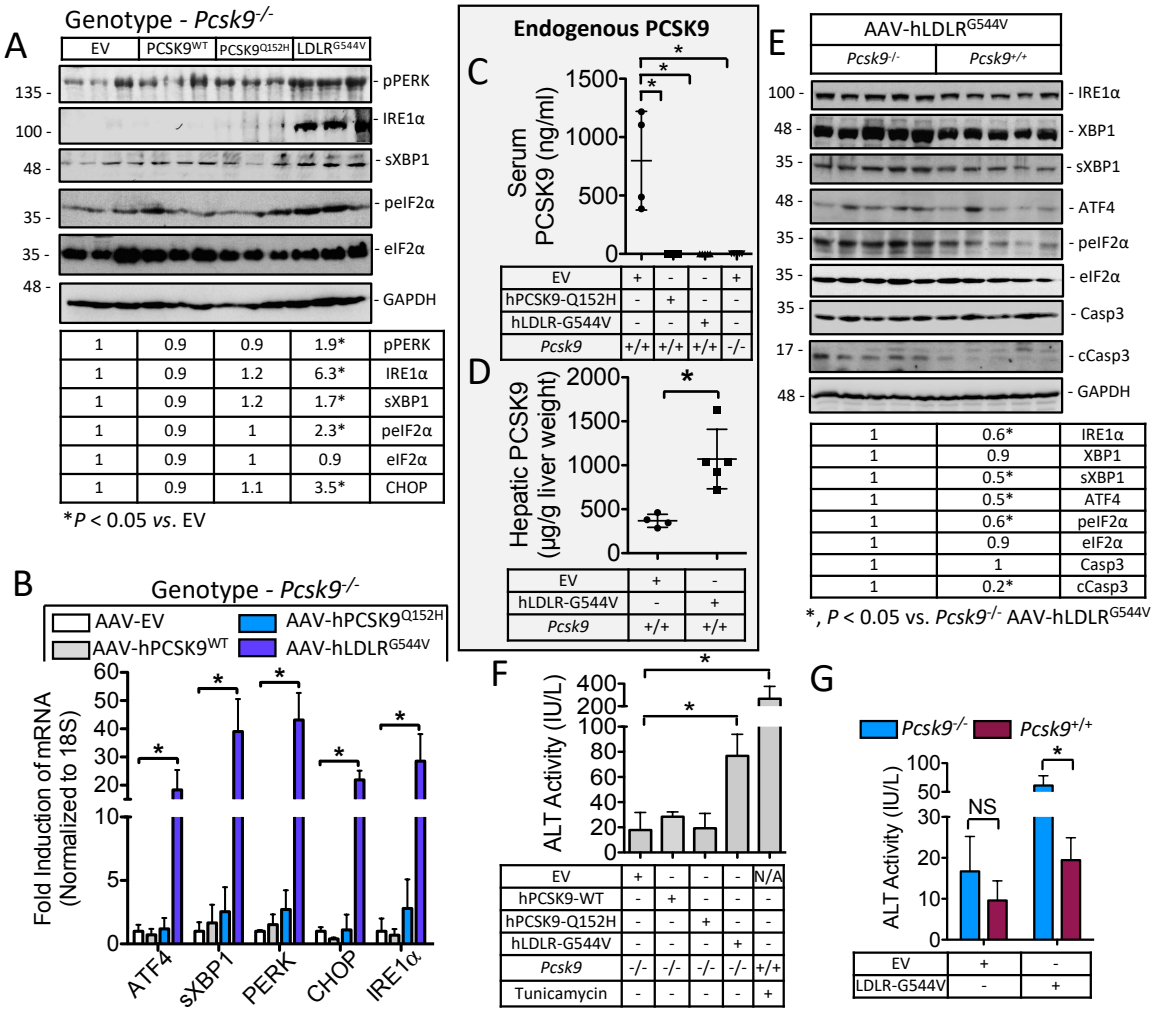

Lebeau et al., 2019. Figure 6.

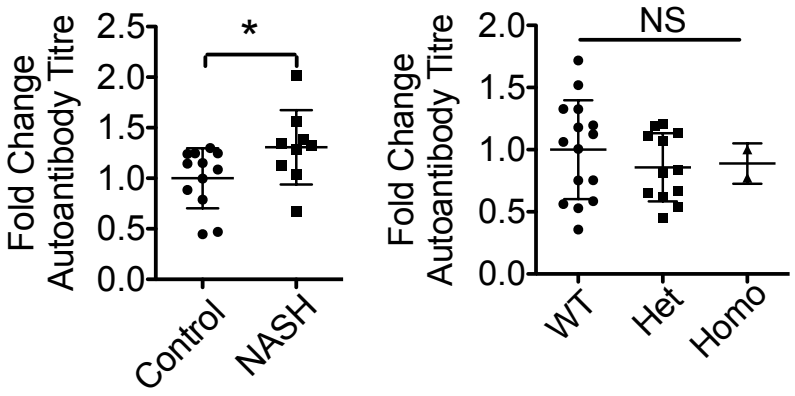

Online Methods and Supplementary Information

The hypocholesterolemic loss-of-function PCSK9 Q152H mutation protects against liver injury/dysfunction by enhancing ER chaperone stabilization

Human studies

Samples were collected after participants were fasted 12h and had abstained from consuming alcohol for 48h. Plasma samples were separated by ultracentrifugation; aliquoted and stored at -80 C. Standard assays of plasma biochemistry were performed by a certified private laboratory (Biron Health Group, Quebec, Canada).

Liver MRI

Magnetic resonance imaging (MRI) was performed on a 3T system (Magnetom Skyra; Siemens, Erlangen, Germany). Three-dimensional (3D) dual-echo spoiled gradient-recalled echo (VIBE) phase-sensitive two-point Dixon sequences were acquired for separation of whole-body water and fat. Two-dimensional (2D) multi-echo spoiled gradient-recalled echo sequences with seven-echo readout were acquired during a single breath-hold to cover the entire liver for calculation of fat fraction along a dynamic scale from 0 to 50% (34-37).

Mouse studies and AAV administration

Mouse AAV injections in male *Pcsk9*$^{-/-}$ (n=5) mice on the C57BL/6J background and in *Pcsk9*$^{+/+}$ on the C57BL/6J background (n=5) were conducted at Amgen Inc. and were approved by Amgen Institutional Animal Care and use Committee (IACUC). Mice had access to water and NCD *ad libitum* and were maintained in rooms with 12-hour light/dark cycles. Mice were injected with AAV at 6 weeks of age and killed at 12 weeks of age. The four AAV treatment groups included AAV-hPCSK9^{WT}, AAV-hPCSK9^{Q152H}, AAV-hLDLR^{G544V} and AAV-EV control.

Mouse studies involving the feeding of HFD were carried out at McMaster University and performed in strict accordance with the McMaster University animal ethics guidelines. Male *Pcsk9*$^{-/-}$ mice on a C57BL/6J background and age-matched C57BL/6J *Pcsk9*$^{+/+}$ controls (n=5; Jackson Laboratories) were started on either HFD, or NCD control, at 6 weeks of age for the duration of 12 weeks. These mice were also housed in rooms with 12-hour light/dark cycles.

AAV vector generation

PCSK9 and LDLR mutant cDNA were inserted between a bovine growth hormone poly A and an elongation factor 1a promoter. A mammalian expression cassette was subsequently inserted and flanked by inverted terminal repeats of AAV. Human embryonic kidney-293 T cells were then transfected with the resulting construct and recombinant AAV was collected, as described previously[55]. Briefly, 8×10^8 cells were lysed in 8 ml of serum-free DMEM through 3 rounds of freeze/thaw. AAV-containing lysate was then treated and loaded onto AVB Sepharose columns. Following elution with pH 3.0 glycine HCl, acidic pH was promptly neutralized with 1M tris-HCl and dialyzed using phosphate-buffered saline (PBS) containing 1 mM $MgCl_2$ and 2.5 mM KCl.

Slid-A-Lyzer Concentration Solution (Thermofisher Scientific) was then used to concentrate the isolated AAV in the dialysis cassette. The QuickTiter AAV Quantification Kit (Cell Biolabs Inc.) was then used to titer and quantify purified AAV particles.

Cell culture, treatments and transfections

HepG2 cells were grown in Dulbecco's Modified Eagle's Medium (DMEM; Gibco, Thermofisher Scientific) supplemented with 10% (v/v) fetal bovine serum (FBS; Sigma-Aldrich) and 50 U/ml of penicillin and streptomycin (Sigma-Aldrich). Cells were seeded in 6-well cell culture dishes to a confluence of 60% and transfected 24 hours later. Transfection cocktail consisted of 1 µg DNA:3 µl X-tremeGENE HP DNA reagent (Sigma-Aldrich): 100 µl Opti-MEM (Gibco, Thermofisher Scientific) per well of cells containing 1 ml complete DMEM. The cDNA of human PCSK9 and its mutant, Q152H, was cloned into pIRES-EGFP (Clontech) and a V5-tag was inserted between the N-terminal signal peptide (residues 1-30) and the start of the prosegment, as described (7). Human GRP78 cDNA was cloned into pcDNA3.1. siRNA targeted against GRP94 (SMARTpool siGenome HSP90B1) and PCSK9 (SMARTpool siGenome PCSK9) were purchased from Dharmacon and transfected by using RNAiMAX (Thermofisher Scientific). Cells were incubated in transfection cocktail for 24 hours and media was subsequently replaced with fresh DMEM containing 1% FBS for an additional 48 hours prior to lysis or assessment of cytotoxicity with lactate dehydrogenase (LDH) assays. For assessment of ER stress and/or ER stress-induced cytotoxicity, cells were treated with either vehicle (containing equimolar DMSO), thapsigargin (300 nM) or tunicamycin (2 µg/ml) 24 hours prior to lysis.

Immunoblots and quantification

Small fragments of mouse liver (~0.05g) were lysed in SDS-containing buffer and normalized to total protein before being electrophoretically resolved on polyacrylamide gels. Resolved proteins were then transferred to nitrocellulose membranes, blocked in skim milk and exposed to primary antibodies overnight (18 hours) on a rocker at 4 ºC. Unbound primary antibodies were subsequently removed via tris-buffered saline (TBS) washes. Immunoblots were then incubated in HRP-conjugated secondary antibodies and developed by using chemiluminescent reagent (Froggabio) and quantified by using a BioRad Imaging system with immunoblots reprobed against β-actin or GAPDH. See Table 1 for a list of antibodies used for immunoblots.

Real-time PCR

Liver RNA was collected by using RNeasy mini kits (Qiagen) and normalized to 2 µg before being reverse-transcribed to cDNA by using SuperScript Vilo cDNA synthesis kit (Life Technologies). The viia7 system (Thermofisher Scientific) in conjunction with FAST SYBR Green (Life Technologies) was used for quantitative real-time PCR assessment of mRNA species in each sample (see Table 2 for a list of primers used).

LDH and TUNEL assays in cultured cells

Transfected cells were incubated in DMEM containing 1% FBS 24 hours prior to LDH cytotoxicity assays. Assay was carried out as per manufacturer's instructions (Roche). TUNEL staining of apoptotic nuclei in transfected HuH7 cells was also carried out as per manufacturer's instructions (Trevigen). Briefly, HuH7 cells were fixed in paraformaldehyde and permeabilized in TBS

containing 0.02% Triton-X. Cell were then incubated with the TDT-labelling enzyme at 37 ºC for one hour, which biotinylates damaged DNA, and subsequently incubated in 594-labelled streptavidin. Cells were visualized in a fluorescent microscope (EVOS, Life Technologies) and quantified by using ImageJ Software (NIH).

Quantitative assessment of plasma ALT activity, triglycerides/cholesterol levels and circulating PCSK9

Examination of plasma ALT (Cayman Chemical), triglyceride (Wako Dignostics) and cholesterol (Wako Dignostics) was carried by using colorimetric assays and serum/hepatic PCSK9 levels via ELISAs (R and D Systems).

Quantification of serum GRP78 autoantibodies

Autoantibodies were detected using ELISAs, as described previously[33]. Briefly, 96-well plates coated with a KLH-conjugated GRP78-specific peptide (CNVSKDSC) were blocked in PBS-Tween containing 3% BSA. Serum samples diluted 1:100 were added to the plates and incubated for 18h. Excess sample was then removed via washing and the plate was subsequently exposed to alkaline phosphatase-conjugated anti-human IgG and developed using alkaline phosphatase substrate at a wavelength of 405 nm using a spectrophotometer (Molecular Devices).

IHC and immunofluorescent staining of paraffin-embedded tissue

IHC was conducted as described previously[25,35]. Briefly, 4 μm thick paraffin-embedded mouse liver or adipose tissue sections were stained with primary antibodies overnight (18 hours). Sections were then stained with biotinylated secondary antibodies and streptavidin-HRP. Exposure to NovaRED peroxidase kit for five minutes or less then permitted for the visualization of analyte antibody complexes. Thioflavin-S staining was also carried out in paraffin-embedded tissues. Following deparaffinization, sections were exposed to a 1% filtered aqueous solution of Thioflavin-S (Sigma-Aldrich) for 10 minutes and subsequently washed in 80% ethanol. Slides were mounted in aqueous mount and imaged immediately to avoid photobleaching. All images were taken with a high-powered light microscope and processed and/or quantified by using ImageJ software. For quantification purposes, several images were taken from the livers of each mouse by using a 20× objective and staining intensity measured with a fixed pixel-density threshold between groups. See Table 1 for a list of antibodies used for IHC.

Statistics

All values are expressed as mean with error bars expressed as SD. Statistical analysis for two-group comparisons were done by using the unpaired Student's *t*-test and comparisons involving multiple groups by using one-way ANOVA. Differences between groups were considered significant at $P < 0.05$.

Supplementary Figure Legends

Fig. S1. Liver-expressed LDLR^{G544V} fails to be expressed at the cell surface. The expression and cellular localization of the human isoform of AAV-expressed LDLR^{G544V} was examined in the livers of *Pcsk9*$^{-/-}$ mice (n=5) and compared to wild-type mouse LDLR using two different antibodies targeted against human and mouse LDLR, respectively. Scale bars; 50 μm.

Fig. S2. ER PCSK9 retention increases the abundance of hepatic chaperones containing the KDEL ER-localization peptide. The expression of ER-localized chaperones containing the KDEL sequence was assessed in *Pcsk9*$^{-/-}$ mice (n=5) treated AAVs encoding either empty vector (EV), wild-type (WT) secreted PCSK9 or the ER-retained variants PCSK9^{Q152H} and LDLR^{G544V} via immunohistochemical staining. Values are represented as mean and error bars as S.D. Scale bars; 200 μm.

Fig. S3. ER PCSK9 retention induces ER expansion but fails to promote cell-surface localization of GRP78. The livers of *Pcsk9*$^{-/-}$ mice (n=5) treated with AAVs encoding human wild-type PCSK9 (PCSK9^{WT}), as well as two variants that fail to exit the ER, PCSK9^{Q152H} and LDLR^{G544V}, were examined for cellular localization of GRP78 via immunohistochemical staining. The livers of tunicamycin (TM)-treated *Pcsk9*$^{+/+}$ mice served as positive controls for ER stress-induced cell-surface localization of GRP78. Scale bars; 50 μm.

Fig. S4. ER-retained PCSK9 interacts directly with GRP78 and GRP94. The interaction between ER-resident PCSK9 and chaperones GRP78 and GRP94 was assessed via immunoprecipitation of human (h)PCSK9 from the livers mice treated with either AAV-hPCSK9 wild-type (PCSK9^{WT}) or ER-retained variant AAV-hPCSK9^{Q152H}. Additional immunoblots of input lysates for GRP94 and GRP78 confirm the increased abundance of these chaperones in the livers of PCSK9^{Q152H} AAV-treated mice; β-actin serves as a control for immunoblot loading. (**B**) The interaction between GRP78/GRP94 and PCSK9 was further examined via analysis of LDLR activity; a well-established target of secreted PCSK9 (23). shRNA control or PCSK9 shRNA knockdown HepG2 cells were transfected with mammalian expression vectors encoding either GRP78 or GRP94. The uptake and accumulation of exogenously added fluorescently-labelled DiI-LDL was examined using a fluorescent spectrophotometer (Molecular Devices). Values are represented as mean and error bars as S.D. *, $P < 0.05$ *vs*. Control shRNA. ANOVA and *t* test were used for all statistical comparisons.

Fig. S5. *Pcsk9*$^{-/-}$ mice exhibit reduced GRP78 and GRP94 expression in response to diet-induced ER stress. (**A**) Hepatic GRP78 and GRP94 protein levels in *Pcsk9*$^{-/-}$ and age-matched *Pcsk9*$^{+/+}$ controls fed either high-fat diet (HFD, n=5) or normal control diet (NCD, n=5) from 6 weeks of age to 18 weeks of age were assessed by immunohistochemical staining and quantified

using ImageJ Software. (**B**) Hepatic GRP78 and GRP94 mRNA expression was also examined via real time PCR. *, $P < 0.05$. ANOVA and *t* test were used for all statistical comparisons.

Fig. S6. ***Expression of hLDLR^{G544V} induces the expression of ER stress markers, pPERK and pIRE1α, as well as amyloid accumulation in the livers of mice.*** The livers of *Pcsk9*$^{-/-}$ mice (n=5) treated with AAVs encoding human wild-type PCSK9 (PCSK9^{WT}), as well as two variants that fail to exit the ER, PCSK9^{Q152H} and LDLR^{G544V}, were examined for the expression of ER stress markers pPERK and pIRE1α via IHC. IHC staining intensities were quantified using ImageJ Software. (**B**) Misfolded protein amyloid was also examined in the livers of these mice via thioflavin-S staining. Values are expressed as the mean and error bars as SD. *, $P < 0.05$. ANOVA and *t* test were used for all statistical comparisons. Scale bars, 200 μm.

Fig. S7. ***The expression of hLDLR^{G544V} does not affect de novo PCSK9 expression.*** PCSK9 mRNA transcript in the livers of mice treated with AAV-EV and AAV-hLDLR^{G544V} was assessed via real-time PCR. Values are expressed as the mean and error bars as SD. *, $P < 0.05$. The *t* test was used for statistical comparison.

Fig. S8. ER retention of two protein variants, LDLR^{G544V} and PCSK9^{Q152H}, differentially affects apoptosis. (**A,B**) The livers of *Pcsk9*$^{-/-}$ mice (n=5) treated with adeno-associated virus (AAV) encoding empty vector (EV), human (h)PCSK9 wild-type (WT) and ER-retained variants hPCSK9^{Q152H} and hLDLR^{G544V} were examined for expression of cleaved (c)Caspase-3 via immunohistochemical staining, which was quantified using ImageJ software. (**C,D**) Additional pro-apoptotic markers including, PARP, cleaved PARP (cPARP), caspase 1 (CASP1), caspase 3 (CASP3), caspase 7 (CASP7), cleaved caspase-3 (cCasp-3), cleaved caspase-7 (cCasp7) and PUMA were also examined using immunoblots and real-time PCR. (**E**) Liver toxicity was assessed via measurement of plasma alanine transaminase (ALT) activity. Values are represented as mean and error bars as S.D. *, $P < 0.05$. ANOVA and *t* test were used for all statistical comparisons. Scale bars; 50 μm.

Fig. S9. ER retention of LDLR^{G544V} promotes fibrosis and increases the abundance of CD20-positive inflammatory macrophages. (**A**) The livers of *Pcsk9*$^{-/-}$ mice (n=5) treated with adeno-associated virus (AAV) encoding empty vector (EV), human (h)PCSK9 wild-type (WT) and ER-retained variants hPCSK9^{Q152H} and hLDLR^{G544V} were examined for fibrotic collagen deposition using picrosirius-red (PSR) staining. Immunohistochemical staining was used to assesses hepatic deposition of α-smooth muscle actin (αSMA) and fibronectin (FN1) and infiltration of CD20-positive inflammatory macrophages. (**B**) Staining was quantified using ImageJ software. (**C,D**) Additional pro-fibrotic markers, including αSMA, FN1 and TGFβ, as well as pro-inflammatory markers including CD4, IL6, IL1β were examined using immunoblots and real-time PCR. Values are represented as mean and error bars as S.D. *, $P < 0.05$ *vs*. EV. ANOVA and *t* test were used for all statistical comparisons. Scale bars; 200 μm.

Lebeau et al., 2019. Supplemental Figure 1.

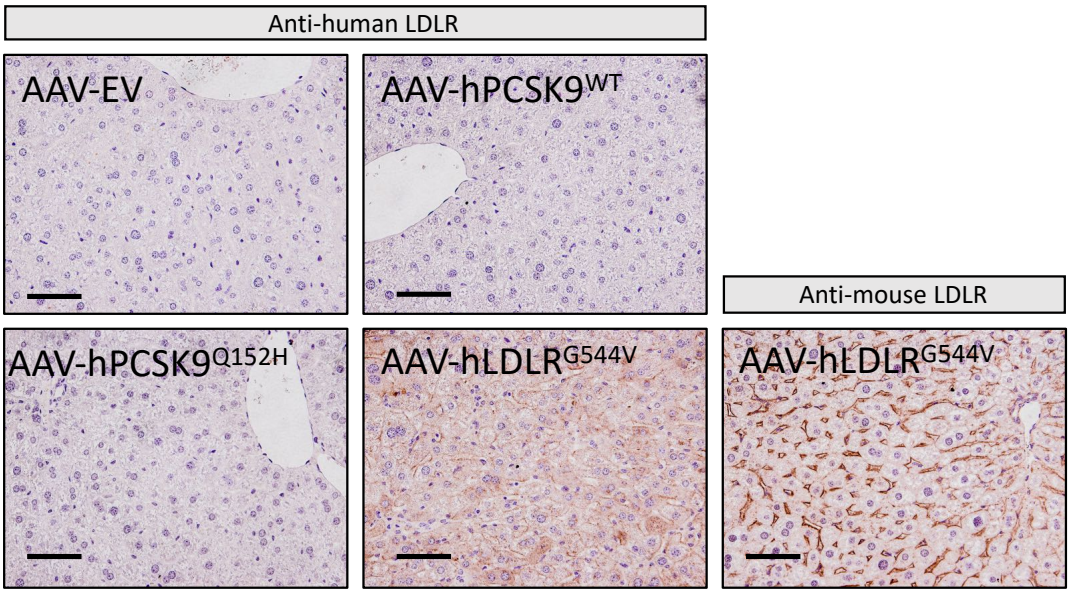

Lebeau et al., 2019. Supplemental Figure 2.

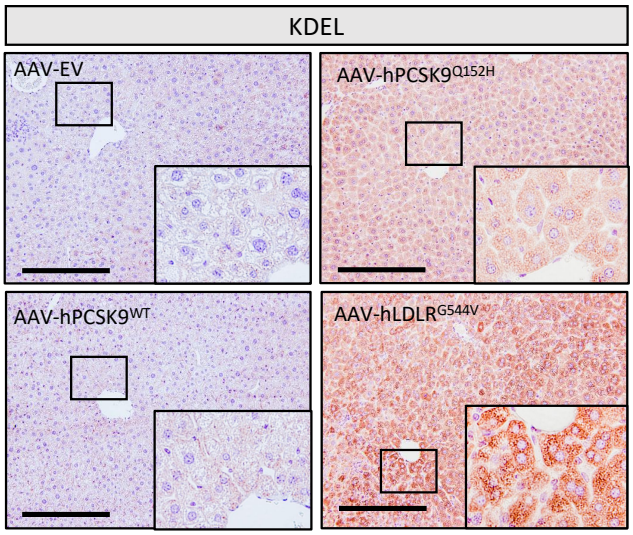

Lebeau et al., 2019. Supplemental Figure 3.

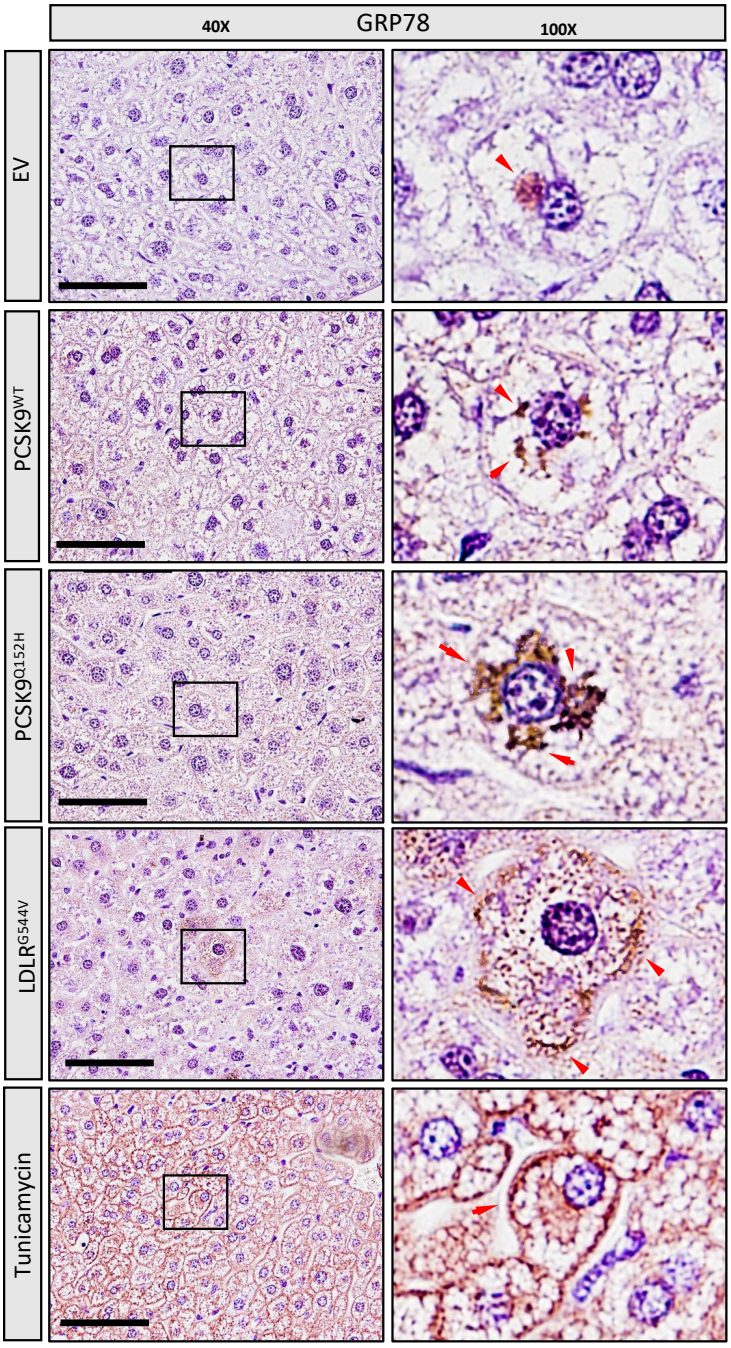

Lebeau et al., 2019. Supplemental Figure 4.

A

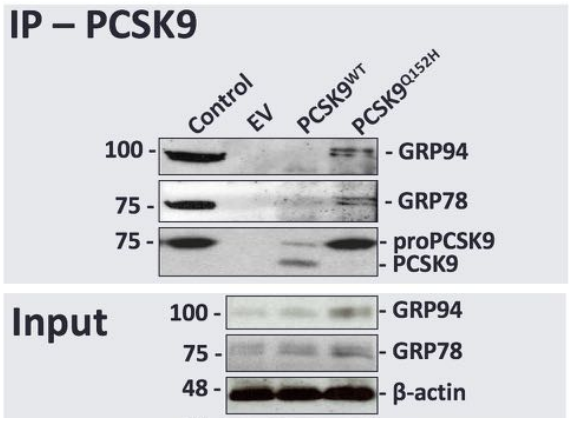

B

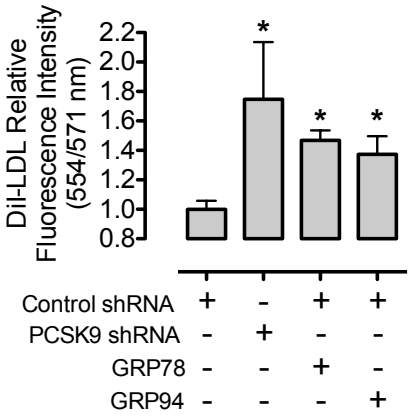

Lebeau et al., 2019. Supplemental Figure 5.

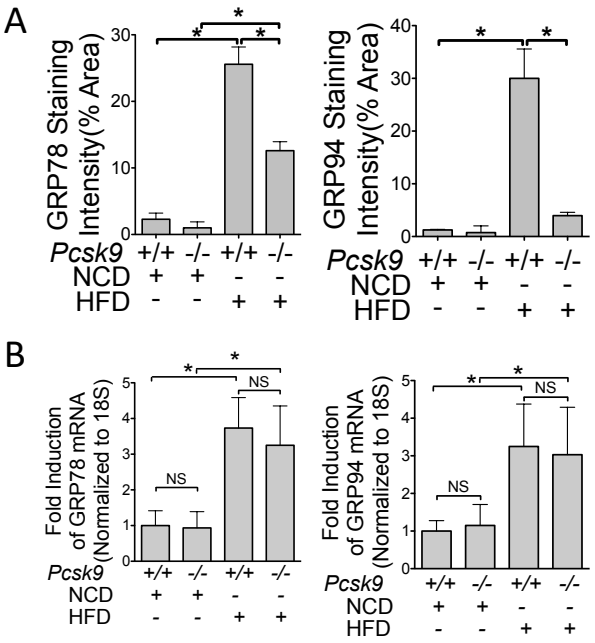

Lebeau et al., 2019. Supplemental Figure 6.

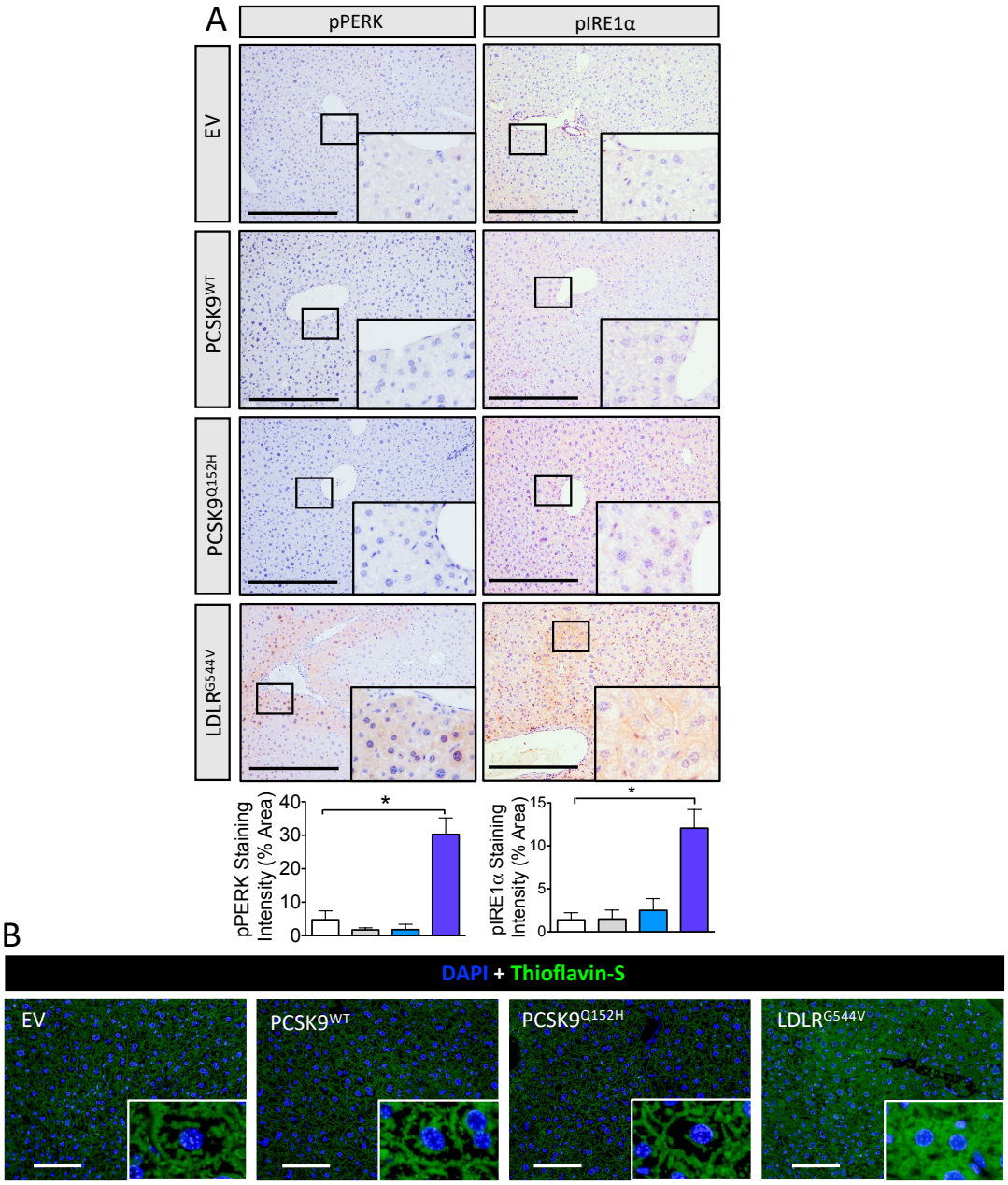

Lebeau et al., 2019. Supplemental Figure 7.

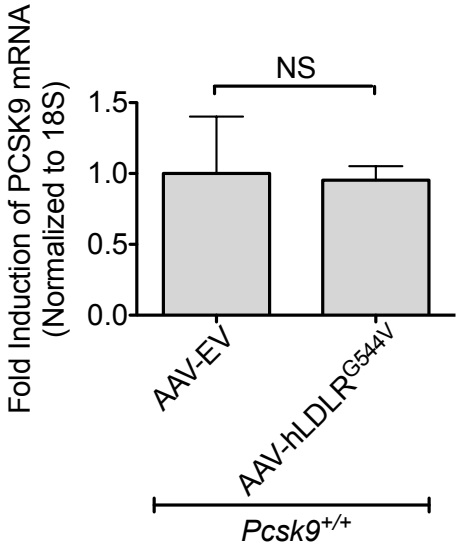

Lebeau et al., 2019. Supplemental Figure 8.

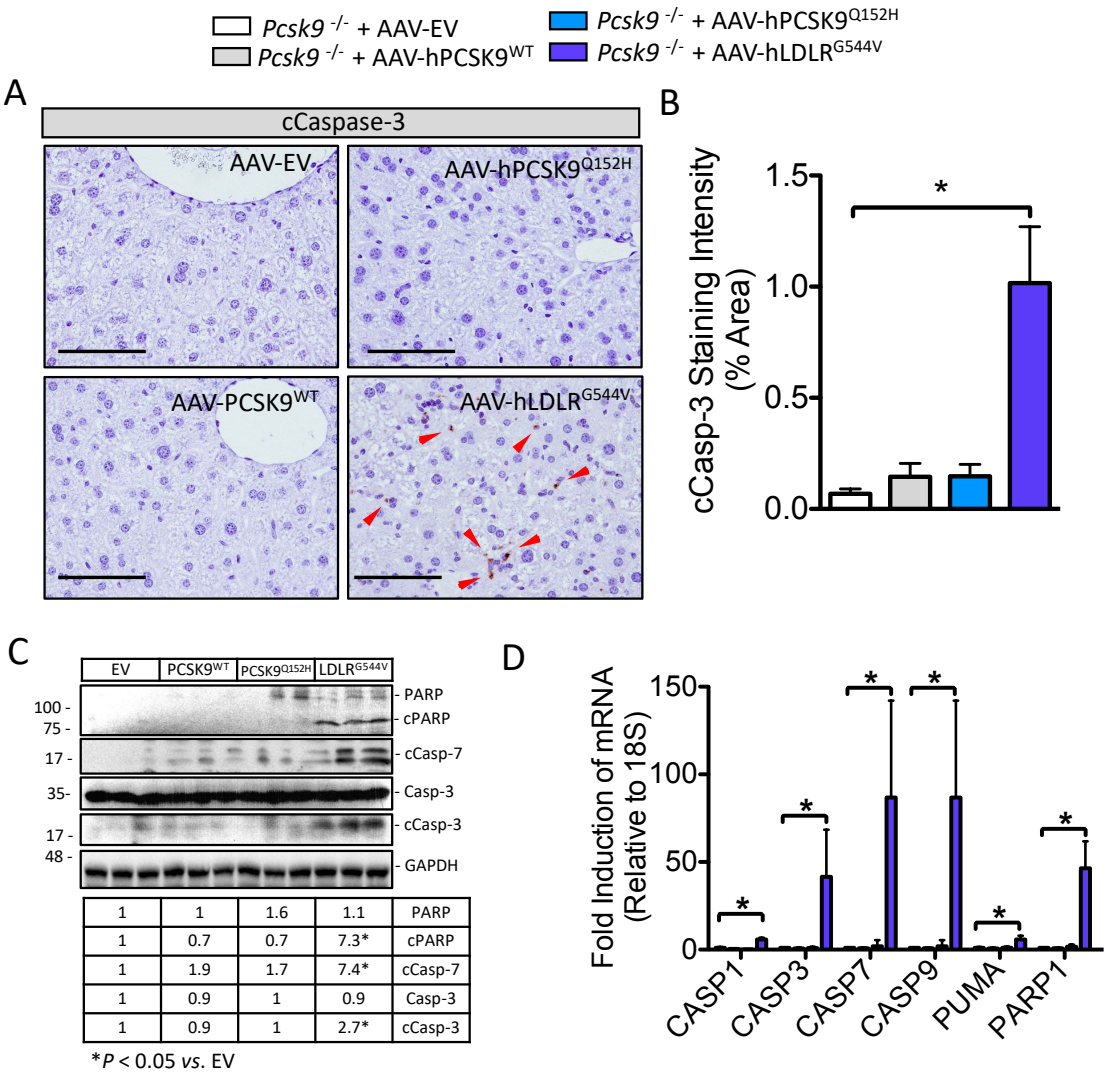

1	1	1.6	1.1	PARP
1	0.7	0.7	7.3*	cPARP
1	1.9	1.7	7.4*	cCasp-7
1	0.9	1	0.9	Casp-3
1	0.9	1	2.7*	cCasp-3

*$P < 0.05$ *vs.* EV

Lebeau et al., 2019. Figure 9.

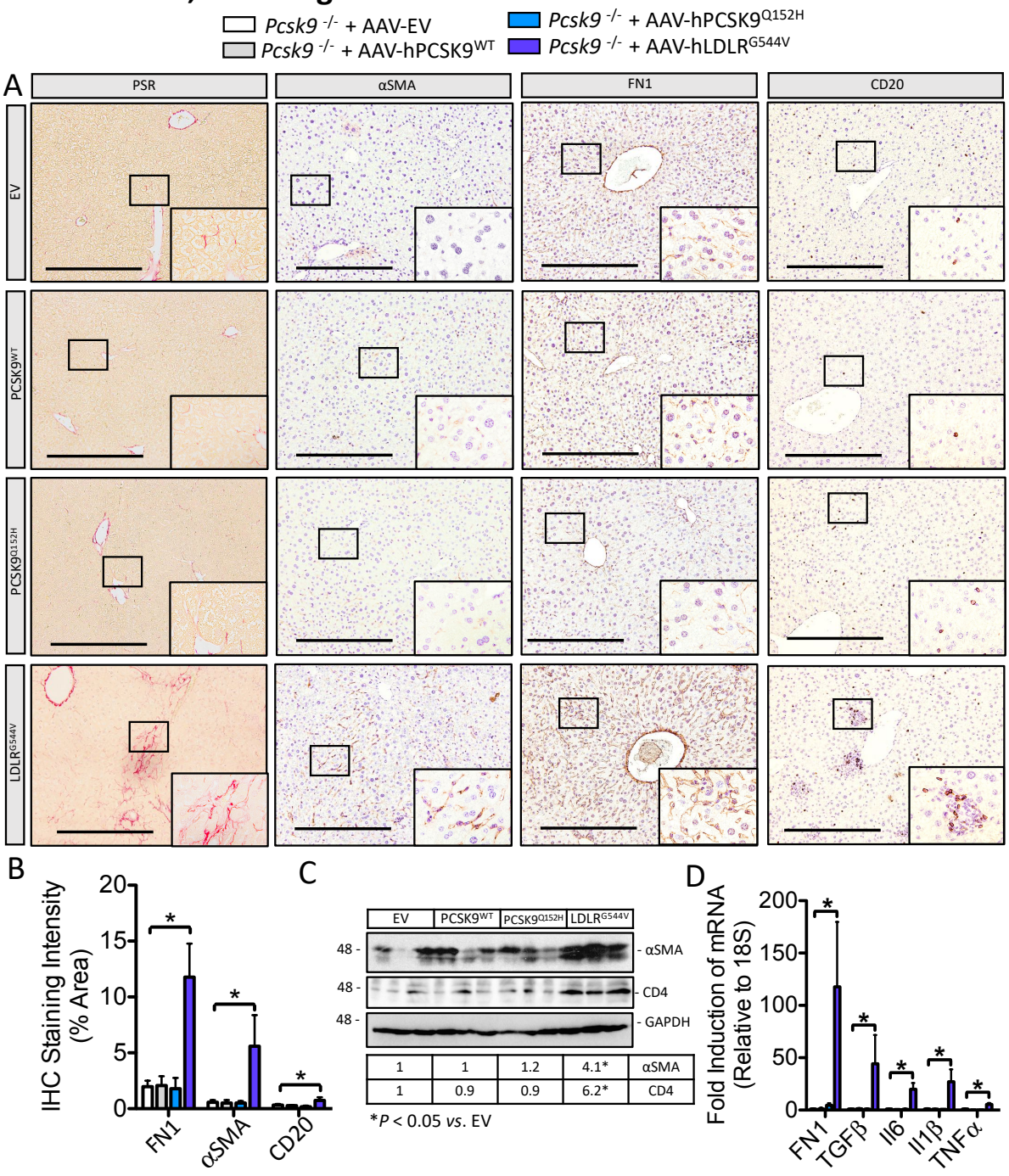

Chapter 7: Discussion

The identification of PCSK9 as a liver-secreted factor with a prominent affinity for LDLR degradation firmly positioned PCSK9 as a target for the management of LDL cholesterol levels [214]. Given the clinical importance of this discovery, much about PCSK9 biology had been characterized from the time of its original discovery in 2003 to the time my doctoral studies had begun in 2016. There remained important gaps, however, pertaining to the regulation of PCSK9 levels in the blood by the liver; the tissue from which the circulating pool of PCSK9 almost exclusively originates [63]. ER stress, a fundamental cellular process known to occur in the livers of patients with a variety of metabolic diseases, was known to activate the transcription factor that regulates PCSK9 expression [211]. Because metabolic disease and CVD commonly present in patients as comorbidities [215], this hypothesis and newly gained insight provided our research group with the opportunity to shed light on the possible link between PCSK9 and ER stress in the context of cardiometabolic disease. Lastly, the identification of ER-retained variants of PCSK9 in hypocholesterolemic patients left many inconsistencies with our current understanding of ER stress biology [55]. As the retention of mutant and misfolded proteins is known to cause ER stress and disease [213], the healthy state of patients harboring the PCSK9 Q152H mutation posed several unanswered questions.

Assessment of our first hypothesis led to the observation that SREBP2 was activated by ER Ca^{2+} depletion. Interestingly, our *in vitro* models also demonstrated that other types of ER stress did not activate this transcription factor [140]. In contrast to intracellular expression levels, cultured hepatocyte cell lines and mice treated with ER stress-inducing agents exhibited a

reduction in the secreted levels of PCSK9. Additional studies were then carried out to identify the cellular compartment in which PCSK9 was being retained in hepatocytes. Not surprisingly, ER stress was causing the retention of PCSK9 in the ER. Because these conditions were also associated with increased hepatic LDLR expression and reduced circulating LDL cholesterol levels, these data supported ER PCSK9 retention as a viable strategy for LDL lowering [140]. As a deleterious cellular process, however, mechanisms other than ER stress would have be utilized to block PCSK9 secretion from hepatocytes in a clinical setting. Since the completion of this research project in 2017, other research groups have also confirmed ER Ca^{2+} as a strong regulator of cholesterol regulatory genes [216]. Furthermore, in striking consistency with our animal studies, a recent study has also demonstrated that patients with ER stress-inducing glycosylation disorders exhibit increased LDLR expression as well as low circulating LDL cholesterol levels [217].

In line with our initial findings, further studies led to the discovery that agents known to increase ER Ca^{2+} levels potently blocked SREBP2 activation and *de novo* PCSK9 expression. As expected, this result was also accompanied by a reduction in secreted PCSK9 levels. Interestingly, although a variety of agents that are known to affect ER Ca^{2+} levels were tested for PCSK9 inhibition, caffeine was among the first compounds examined. As an agent capable of increasing ER Ca^{2+} levels, its ability to attenuate ER stress in hepatocytes was also confirmed. The association between caffeine and/or coffee consumption and CVD risk had been intensively studied for several decades at the time of our studies [218, 219]. Although such correlations can be difficult to discern due to the large variety of confounding variables in patient populations,

recent meta-analyses support a net protective effect of caffeine on CVD risk [218, 220]. The mechanism by which this process occurs, however, remains poorly understood.

Pharmacologic ER stress in hepatocytes, using agents such as TM and TG, caused a reduction in PCSK9 secretion. Likewise, we demonstrated that caffeine protects against ER stress and also blocks PCSK9 secretion from hepatocytes. Clearly, these data suggest that ER stress*, per se,* encompasses too many intricate signaling cascades to serve as a viable model/ mechanism to account for changes in PCSK9 secretory status. Ca^{2+} signaling within the cell, however, a process heavily associated with ER function, stood out as a potent regulator of PCSK9 biology and also accounted for the differences between our observations. Utilizing this model, a number of additional agents that were not previously known to affect genes associated with CVD, were identified as regulators of PCSK9 expression and secretion. Additional studies also led to the observation that caffeine increased cell-surface hepatic LDLR expression and reduced LDL cholesterol levels in a PCSK9-dependent manner. Overall, these data suggested that PCSK9 inhibition may represent a molecular mechanism to explain the cardioprotective effect of caffeine consumption.

Although previous studies had demonstrated that conditions of ER stress can cause activation of the SREBPs and subsequent intracellular lipid accumulation as a result of *de novo* lipogenesis, the mechanism by which this process occurred also remained obscure. Previous evidence suggested that (1) ER stress-induced activation of the SREBPs required S1/2P [211] and that, (2) attenuation of ER stress via overexpressing GRP78 could block SREBP activation [210]. Upon further assessment of the mechanism by which caffeine blocked SREBP2 activation in our studies, we observed that heightened ER Ca^{2+} levels increased the abundance of the ER

resident form of SREBP2 and reduced its nuclear/active form. Immunoprecipitation studies revealed that caffeine, and other agents that increased ER Ca^{2+} levels, enhanced the ability of GRP78 to sequester pre-mature SREBP2 in the ER. This finding is consistent with previous studies demonstrating the Ca^{2+} is required for GRP78 to form interactions with, and properly fold nascent polypeptides [221]. In contrast, ER Ca^{2+} depletion via TG treatment reduced the frequency of the interaction taking place between GRP78 and SREBP2, resulting in increased nuclear abundance of SREBP2. Overall, during the course of our studies examining the effect of caffeine and other ER Ca^{2+} modulating agents on the expression of genes associated with CVD, many interesting observation were made. The mechanism by which caffeine and other xanthine-derived compounds increase ER Ca^{2+} levels, however, is not yet clear. Interestingly, a recent study demonstrated that caffeine intercalates into the ER lumen and acts as a Ca^{2+} chelator to increase its levels in this cellular compartment [222]. Although these data suggest that caffeine could increase ER Ca^{2+} levels in a similar manner as Ca^{2+}-binding chaperones of the ER, further studies are needed to elucidate these findings in hepatocytes.

Beyond our studies examining the effects of pharmacologic agents that enhance or impair the ER environment, our next aim was to assess the effect of a naturally occurring form of hepatic ER stress on PCSK9 expression and secretion. ER stress is a common observation and well-established driver of liver disease in patients with NAFLD and NASH [186]. Similar to the available literature on the topic of caffeine and its impact on CVD risk, accumulating evidence now suggests that liver disease also correlates with CVD risk [223]; albeit as a driver of disease and not as a protective agent. Also similar was the apparent lack of mechanistic evidence supporting its association with CVD in patient cohorts. Strikingly, two independent studies have

now demonstrated that liver steatosis grade correlates positively with circulating PCSK9 levels [212, 224]. Given the role of ER stress in liver disease progression, and in the regulation of PCSK9 expression/secretion, a number of *in vivo* experiments were carried out with the goal of (a) characterizing the mechanism by which this process occurred and (b) to determine whether the observed change in PCSK9 levels affected hepatic cell-surface LDLR and circulating LDL cholesterol levels.

Consistent with findings in patients, our studies revealed that mice exposed to a HFD for 12 weeks exhibited a significant increase in circulating, as well as hepatic PCSK9 protein levels [225]. Importantly, PCSK9 and SREBP2 mRNA levels were also elevated, suggesting that heightened PCSK9 protein abundance occurred as a result of SREBP2-driven *de novo* synthesis. *In vitro* studies, in which cultured HepG2 and primary human hepatocytes treated with the saturated fatty acid, palmitate, yielded similar findings. Interestingly, the HFD as well as palmitate reduced cell-surface LDLR expression, despite increasing the abundance of its mRNA transcript levels. These findings, however, are consistent with several other studies in which SREBP2 activation correlates positively with circulating PCSK9 levels and inversely with cell-surface LDLR levels [226, 227]. Although the exact mechanism behind this observation is not yet confirmed, one possibility is that the short PCSK9 half-life renders the circulating pool of this protein dependent on replenishment via *de novo* synthesis. In contrast, with a half-life of 12 hours, cell-surface LDLR is perhaps more dependent on factors that affect its stability at the cell surface, such as PCSK9. Although numerous studies are consistent with this hypothesis, there remains a well-known example in which it does not hold true. Statins activate SREBP2 to increase LDLR expression and reduce circulating LDL cholesterol levels. To activate SREBP2,

however, this class of compounds antagonizes HMGR, thereby reducing intracellular cholesterol levels [72]; as a downstream product of SREBP2 activity, statin-induced PCSK9 expression was thought to represent an inefficiency of this mechanism of action. Until recently, this created a paradox because statins are well-known to reduce circulating LDL cholesterol levels [228]. Importantly, it has now been demonstrated that under such circumstances, statins antagonize a GOF phosphorylation on PCSK9 by the Fam20 kinase. As a result, statins increase the expression of PCSK9, but it represents a LOF form PCSK9 with diminished efficacy for LDLR inhibition [229].

An interesting inconsistency in the observations made during the course of our studies was the ability of the HFD and palmitate to increase PCSK9 secretion from hepatocytes, whereas other ER stress-inducing agents reduced its levels. Given that intracellular lipid dysregulation is well-known to cause ER stress via ER Ca^{2+} depletion [188], however, it is not surprising that the HFD and palmitate increased intracellular PCSK9 expression. Differences in the secretory status of the protein between these treatments may have occurred due to a variety of reasons. First, although we have characterized PCSK9 as an ER stress-inducible gene [140], PCSK9 is also a lipid-responsive gene [70, 230]. Because palmitate is simultaneously a lipid that induces ER stress, it becomes difficult to discern which aspect of this form of stimulus has a greater effect on PCSK9 biology. Answering this question would require additional studies characterizing the precise mechanism by which conventional, or pharmacologic, ER stress induces the cellular retention of PCSK9. A possibility that has not yet been confirmed stems from the apparent increase in ER PCSK9 abundance during conditions of ER stress. Given that we, as well as others, have demonstrated that PCSK9 can interact directly with chaperones, such as GRP78 and

GRP94, the possibility that PCSK9 is being retained as a result of direct interaction with these chaperones during conditions of ER stress is likely. As strong inducers of ER stress, pharmacologic agents such as TG and TM, may increase ER chaperone abundance to a significantly greater extent than the HFD or palmitate. Heightened chaperone expression as a result of TG or TM treatment relative to lipid-induced ER stress, which only modestly increases chaperone abundance, may contribute to the net reduction in secreted PCSK9 levels via increased sequestration in the ER. Overall, ER stress in the lipid-laden liver increases PCSK9 expression and secretion whereas pharmacologically-induced severe ER stress also increases its expression but causes its retention. Perhaps, increased PCSK9 secretion during conditions of diet-induced hepatic steatosis represents a protective negative feedback loop to prevent further lipid uptake and liver injury, however, additional studies are required to confirm this reasoning. Additionally, although the retention of PCSK9 during conditions of severe ER stress may be a coincidental event, it is also possible that PCSK9 serves a purpose in this compartment under such conditions.

The retention of misfolded proteins in the ER is the underlaying cause of ER stress. Heritable mutations that lead to the production of misfolded protein are also known to contribute to a variety of human diseases. Not all proteins that are retained in the ER, however, cause ER stress and disease. The overexpression of ER-resident chaperones, such as GRP78 and GRP94 for instance, is well-known to alleviate ER stress and protect against metabolic disease [136, 231-233]. Likewise liver-specific knockout of these chaperones was shown to cause liver injury, metabolic abnormalities and hepatocellular carcinoma [234, 235]. Interestingly, the data accumulated during the course of my studies suggest that certain characteristics of intracellular

PCSK9 parallel those of ER chaperones. Although PCSK9 knockout mice have not been shown to develop severe phenotypes like those deficient in chaperones, our studies suggest that several similarities exist between these mice. Consistent with chaperone deficient mice, PCSK9 knockout mice exhibit increased activation of UPR signaling cascades and liver injury in response to the ER stress-inducing HFD (Lebeau and Austin, unpublished data) and the methionine/choline deficient diet compared to controls (Lebeau and Austin, unpublished data). Increased UPR activation and liver injury is also observed in the livers of PCSK9 KO mice 72 hours post TM treatment compared to controls (Lebeau and Austin, unpublished data). Collectively, experiments in which PCSK9 knockout mice are challenged with ER stress-inducing stimuli demonstrate that intracellular PCSK9 plays a role in ER homeostasis.

The apparent lack of UPR activation in cultured hepatocytes overexpressing ER-retained LOF PCSK9 variants was among our first clues as to the potential role of PCSK9 in ER function [236]. Additional studies led to the observation that prolonged overexpression of ER-retained PCSK9 increased the abundance of the chaperones, GRP78 and GRP94 at the protein level, but did not affect their mRNA transcript abundance. Furthermore, cultured hepatocytes overexpressing ER-retained PCSK9 were protected from ER stress and cytotoxicity in a manner dependent on these chaperones. In contrast, overexpression of ER retained PCSK9 Q152H in cells treated with siRNA targeted against GRP94, induced ER stress and cytotoxicity. Overall, these data as well as those characterizing the physical interaction taking place between PCSK9 and GRP78/GRP94, strongly suggest that ER-resident PCSK9 increases the stability of these chaperones; which in turn, confers protection against ER stress. This notion is also supported by *in vivo* studies in which overexpression of ER retained PCSK9 Q152H increased the protein

abundance of GRP78 and GRP94, but did not affect the expression of UPR transducers, ATF6, IRE1α or PERK. In contrast, overexpression of the ER-retained LDLR G544V variant caused marked ER stress, characterized by increased expression of a variety of ER stress markers at the mRNA and protein level. Interestingly, expression of the LDLR G544V abolished secreted PCSK9 levels. These findings were consistent with our previous studies in which ER stress was causing the retention of PCSK9 in the ER. In follow up studies, we observed that PCSK9-expressing wild-type mice exhibited less ER stress than PCSK9 knockout counterparts in response to LDLR G544V. These findings are also in line with our observations in PCSK9 knockout mice treated with ER stress-inducing stimuli. The deficiency of GRP78/GRP94 in the PCSK9 knockout mice likely reduces protein folding capacity of the ER and increases their susceptibility to ER stress and liver injury.

In conclusion, the studies conducted during my doctoral studies characterized an array of regulatory processes and molecular mechanisms that affect the biology of PCSK9 and LDL cholesterol metabolism. As a secretory protein, we have identified that the transit of PCSK9 through the ER represents a major regulator of its secretion during conditions of stress. Furthermore, ER stress and ER Ca^{2+} homeostasis can regulate PCSK9 expression at the mRNA level via GRP78-mediated sequestration of its transcription factor, SREBP2. Additional studies in this area of research may uncover agents, such as caffeine and/or its derivatives, that may potently increase ER Ca^{2+} levels to simultaneous protect against hepatic ER stress, as well as block PCSK9-mediated CVD risk. Further studies are also required to identify the exact mechanism by which caffeine and its derivatives increase ER Ca^{2+} levels. The discovery that hepatic ER stress contributes to elevated circulating PCSK9 levels in models of diet-induced

NAFLD and that such PCSK9 levels also increase LDL cholesterol levels may prove beneficial in the years to come. Pharmacologic agents that block ER stress signaling cascades could be utilized to reduce the hepatic burden on CVD risk, as well as attenuate ER stress-driven liver disease progression in patients with cardiometabolic disease. Finally, despite the abundance of evidence suggesting that ER protein retention can lead to chronic ER stress, we have clearly demonstrated that hepatic PCSK9 retention fails to yield this outcome. Our studies in this area have demonstrated that ER-resident PCSK9 interacts directly with GRP94, and that in the absence of this chaperone can cause ER stress in hepatocytes. Consistent with these findings, expression of the ER-retained PCSK9 Q152H mutant also failed to cause ER stress in mice or in human subjects harbouring the mutation. Strikingly, by increasing the abundance of ER stress response chaperones, we observed that ER-retained PCSK9 protected against ER stress in mice rather than induce it. These final data suggest that causing the ER retention of PCSK9 may simultaneously reduce LDL cholesterol and CVD risk while protecting against ER stress driven liver disease and injury. The identification of small molecules capable of inhibiting PCSK9 synthesis, processing and/or secretion from the ER is a major objective of future studies in the Austin Laboratory.

Chapter 8: Overall Contribution and Future Directions

In the field of molecular biology and genetics, when a new protein is described as being a contributor of a certain disease state, the majority of research efforts are aimed at identifying ways to block it's activity. In the case of PCSK9 and its ability to enhance the degradation of the LDLR and contribute to a disease widely known as the leading cause of death worldwide, it was no different. To date, inhibitory strategies that have been successful in pre-clinical models include (a) clustered regularly interspaced short palindromic repeats, (b) siRNA, (c) translation inhibitors (PF-06446846), (d) adnectins, (e) ABD-fused anticalin, (f) mAbs against the CHRD of PCSK9, (g) mAbs against EGFa-binding domain of PCSK9, (h) vaccines and (e) sdAbs. As is the case with any therapeutic, however, many of these strategies are limited in the clinical space due to undesired off-target effects or high cost. Although siRNAs and vaccines have been shown to markedly reduce circulating LDL cholesterol levels, FDA/Health Canada approval has only been granted to mAbs against the EGFa-binding domain of PCSK9 [85].

The original intent on PCSK9 research in the Austin Laboratory was not necessarily to follow this research paradigm. Over the course of several research projects, however, ER Ca^{2+} emerged as a novel and potent regulator of lipid-responsive genes. As such, one of my major contributions to the field of PCSK9 biology has been the identification that agents capable of increasing ER Ca^{2+} levels and protecting against ER stress tend to block SREBP2-mediated PCSK9 expression and also increase hepatic LDLR expression to reduce circulating LDL cholesterol levels. Much progress has been made in this area, including the identification of novel xanthine derivatives that are capable of antagonizing PCSK9, as well as proof of principle studies demonstrating efficacy in healthy volunteers (Lebeau et al., 2019). Future endeavors in

this area of research will focus on expanding our library of novel xanthine derivatives with increased potency as inhibitors of PCSK9, as well as proof of principle studies characterizing the effect of caffeine on atherosclerotic lesion development in mice. See Table 1 for a list of future experiments in this area of research in the Austin Laboratory.

Table 1. Future directions in research on the topic of ER Ca^{2+} as a regulator of PCSK9.

Research Question	Experiment(s)
Does caffeine (or its derivatives) protect against ER stress *in vivo*?	1. Pre-treat mice with caffeine and then expose to pharmacologic ER stress-inducing agents (e.g. tunicamycin or thapsigargin). 2. Treat mice with caffeine in the drinking water and expose to ER stress-inducing metabolic challenge (e.g. 60% HFD or *ob/ob* or *db/db*). Assess ER stress marker expression in the liver and kidney. Assessment of metabolic function via GTT/ITT and glucose production would also be of interest.
Does caffeine (or its derivatives) protect against atherosclerosis *in vivo*?	1. Expose APOE*3 leiden mice to atherogenic diet in the presence or absence of caffeine in the drinking water and assess lesion development. Lesion development in this model occurs in a PCSK9-dependent manner. 2. Expose *Apoe*$^{-/-}$ or *Ldlr*$^{-/-}$ mice to atherogenic diet in the presence or absence of caffeine in the drinking water and assess lesion development. Lesion development in these models does not occurs in a PCSK9-dependent manner.

The remainder of the research in the field of PCSK9 biology has aimed to identify roles of PCSK9 beyond LDL metabolism and CVD risk. Based on our current understanding of evolution, it would make no sense that natural selection would favour the propagation of a gene that only promotes CVD and reduces overall fitness. In this landscape of research the studies conducted during the course of my PhD have led to the identification of two benefits incurred by the presence of PCSK9 in a biological system. First, we have demonstrated that PCSK9 plays a role as a co-chaperone in the ER of metabolically active tissues, such as liver and kidney, to protect against ER stress. Using a variety of *in vivo* and *in vitro* models, we have observed that PCSK9 deficiency leads to heightened injury when challenged with ER stress-inducing stimuli.

Likewise, overexpression of PCSK9 increases chaperone expression and lends further protection against injury. In the context of metabolic diseases in which ER stress is an established driver of progression, such findings have clear and important implications. See Table 2 for a list of future experiments in this area of research in the Austin Laboratory.

Table 2. Future directions in research on the topic of ER-retained LOF PCSK9 variants and ER stress.

Research Question	Experiment(s)
Does endogenously-expressed PCSK9^{Q152H} protect against ER stress?	1. Express PCSK9^{Q152H} in mice using CRISPR via the sterol regulatory element and challenge with ER stress-inducing stimulus. Assess liver and kidney for ER stress marker expression.
Do other forms of ER-retained LOF PCSK9 variants protect against ER stress?	1. Express PCSK9^{S386A} (catalytic inactive) and/or PCSK9^{679X} (cleaved but not secreted) and examine whether this protects against ER stress in a similar manner as PCSK9^{Q152H}.
Does PCSK9^{Q152H} protect against liver injury in response to a metabolic challenge?	1. Express ER-retained LOF PCSK9 variants and challenge mice with a 60% HFD for 12 weeks. Assess hepatic ER stress marker expression and injury. 2. Express ER-retained LOF PCSK9 variants in *ob/ob* or *db/db* mouse models. Assess livers for ER stress marker expression and injury. 3. In both of the above cases, assess parameters of insulin resistance and diabetes. This includes ITTs/GTTs, glucose production, hepatic gluconeogenic gene expression.

A second evolutionary benefit offered by circulating PCSK9 will likely come into play in modern society where excess dietary lipid is frequently consumed on a daily basis. Based on research demonstrating that PCSK9 reduces the expression of CD36, a fatty acid translocase known to uptake circulating free fatty acids, we demonstrated that PCSK9 knockout mice are more susceptible to ER stress, inflammation and injury of the liver in response to a HFD. Furthermore, during early stages of NAFLD, we as well as others have demonstrated that circulating PCSK9 levels in the blood are also increased; likely as a result of lipid-induced ER stress and activation of SREBP2. As such, my research in this area has suggested that the fatty

liver secretes elevated levels of PCSK9 in order to enhance the degradation of cell-surface receptors, such as CD36, to reduce the uptake and accumulation of free fatty acids.

Elevated LDLR expression is desired due to its protective outcome on CVD, whereas elevated CD36 expression is associated with a variety of lipid-driven disorders. Because of this fact, a thought that will come to the mind of any molecular biologist is that mAbs that *block* PCSK9 may reduce circulating LDL cholesterol levels via their effect on the LDLR, but that they may also promote hepatic and peripheral lipid accumulation by increasing the expression of CD36. In recent months, we have set out to answer this burning question and have encountered very interesting and counter-intuitive results. First, it is important to understand that the primary route of PCSK9 clearance from the blood is via interaction with the LDLR; as such, mAbs against PCSK9 have been shown to increase the circulating pool of PCSK9 by approximately 7-fold. Second, it is important to note that PCSK9 interacts with the LDLR and CD36 via two different domains. This is supported by evidence demonstrating that mutations in PCSK9 that enhance its affinity for the LDLR (e.g. D377Y) do not enhance its affinity for CD36 [95]. Based on this evidence, we have recently postulated that circulating PCSK9 bound to mAbs targeted against the EGFa-binding domain may retain a certain level of activity against CD36. For this reason it becomes important to make the distinction that mAbs like Evolocumab and Alirocumab do not *block* PCSK9, but rather prevent its association with the LDLR. By reducing LDLR-mediated clearance of circulating PCSK9, such mAbs may increase the rate at which PCSK9 antagonizes CD36. Based on this reasoning, the currently FDA-approved mAbs against PCSK9 may simultaneously protect against CVD by increasing LDLR expression and protect against NAFLD by reducing CD36 expression. Although many more experiments are required before

firm conclusions can be made in this area, our preliminary findings strongly suggest that this is indeed the case (Lebeau and Austin, unpublished data). See Table 3 for a list of future experiments in this area of research in the Austin Laboratory.

Table 3. Future directions in research on the topic of PCSK9 and NAFLD.

Research Question	Experiment(s)
Do Alirocumab/Evolocumab affect hepatic or renal CD36 expression?	1. Treat mice with Alirocumab or Evolocumab for one week and examine circulating PCSK9 levels, as well as hepatic LDLR and CD36 expression.
Do Alirocumab/Evolocumab protect against diet-induced NAFLD?	1. Expose mice to a HFD for 12 weeks in the presence or absence of Alirocumab or Evolocumab (bi-weekly injection). Assess hepatic steatosis, ER stress and liver injury at endpoint. 2. Similar experiments can be repeated in other models known to develop diet-induced liver injury, such as the *ob/ob* or *db/db* mouse models. 3. In both of the above cases, assess parameters of insulin resistance and diabetes. This includes ITTs/GTTs, glucose production, hepatic gluconeogenic gene expression.

Overall, the findings made over the course of my doctoral studies have aided in our understanding of PCSK9 biology on two fronts. In the first, the therapeutically relevant discovery that caffeine and other xanthine derivatives potently antagonize *de novo* PCSK9 expression add to our knowledge of small molecule inhibitors of PCSK9. It is not necessarily the idea that caffeine *per se* leads to a reduction of PCSK9 expression that is important, but rather the discovery of the mechanism by which this phenomenon takes place. We have observed that not only caffeine, but a variety of agents known to increase ER Ca^{2+} levels, markedly reduce SREBP2 activity, PCSK9 expression and circulating LDL cholesterol levels. Although much work remains to be done in order to identify novel compounds with increased liver specificity as compared with caffeine, it remains that this work has provided scientists with a first stepping stone. Moreover, we have also characterized two distinct molecular pathways, or answers for the

age-old question of “why does a protein like PCSK9 exist in biological systems if only to promote disease?”. To this question, I now add to the work of Nabil G. Seidah who demonstrated an important role of PCSK9 in liver regeneration [63]. Here, we show that (a) PCSK9 also plays a key role as a co-chaperone of the ER, incurring increased resilience to cells against environmental or genetic toxins and (b) protection of the liver against lipotoxicity by fine-tuning the uptake and accumulation of free fatty acids from the circulation. New and exciting research from the Austin Laboratory will likely continue to advance our understanding, as well as the applicability of these concepts, for years to come.

Appendix A: Manuscript Accepted in JHEP Reports

PCSK9 knockout exacerbates diet-induced non-alcoholic steatohepatitis, fibrosis and liver injury in mice.

Paul F. Lebeau[1], Jae Hyun Byun[1], Khrystyna Platko[1], Ali A. Al-Hashimi[1], Šárka Lhoták [1], Melissa E. MacDonald[1], Aurora Mejia-Benitez[1], Annik Prat[2], Suleiman A. Igdoura[3], Bernardo Trigatti[4,5], Kenneth N. Maclean[6], Nabil G. Seidah[2], Richard C. Austin*[1]

Authors Affiliations: [1]Department of Medicine, McMaster University, St. Joseph's Healthcare Hamilton, Ontario L8N 4A6, Canada, the [2] Laboratory of Biochemical Neuroendocrinology, Clinical Research Institute of Montreal, affiliated to the University of Montreal, Montreal, Quebec H2W 1R7, Canada, the [3]Department of Biology and Pathology, McMaster University, Hamilton, Ontario, L8S 4K1, Canada, the [4]Thrombosis and Atherosclerosis Research Institute (TaARI), Hamilton Health Sciences and McMaster University, Hamilton, Ontario L8L 2X2, Canada, the [5]Department of Biochemistry and Biomedical Sciences, McMaster University, Hamilton, Ontario L8S 4L8, Canada, and [6]the Department of Pediatrics, University of Colorado School of Medicine, Aurora, Colorado. USA.80045.

***Corresponding Author:** To whom correspondence should be addressed: Dr. Richard C. Austin, 50 Charlton Ave East, Room T-3313, Hamilton, Ontario, L8N 4A6. Phone: 905-522-1155 x35175; Fax: 905-540-6589; E-mail: austinr@taari.ca

Conflict of interest: The authors do not have competing interests to declare.

Financial Support: This work was supported in part by research grants to Richard C. Austin from the Heart and Stroke Foundation of Canada (G-13-0003064 and G-15-0009389), the Canadian Institutes of Health Research (74477), to Nabil G. Seidah and Annik Prat from the Leducq Foundation (13 CVD 03), CIHR Foundation grant (148363) and Canada Research Chair (216684). Kenneth N. Maclean gratefully acknowledges financial support from the William R. Hummel Homocystinuria Research Fund and holds the Ehst-Hummel-Kaufmann Family Endowed Chair in Inherited Metabolic Disease. Financial support from the Research Institute of St. Joseph's Healthcare Hamilton is acknowledged. Richard C. Austin is a Career Investigator of the Heart and Stroke Foundation of Ontario and holds the Amgen Canada Research Chair in the Division of Nephrology at St. Joseph's Healthcare and McMaster University.

Author Contributions: PL, NGS and RCA conceived the studies. PL, JHB, AAA, KP, SL, and MEM performed all of the *in vitro* and *in vivo* studies. The manuscript was written by PL and RCA and revised by AMB, AP, SAI, KNM, BT and NGS.

Key Words: ER stress, CD36, HFD, NAFLD, Liver disease, Cardiometabolic disease, CVD.

List of Abbreviations: ABCA1, ATP-binding cassette subfamily A member 1; ACOX1, acyl-coA Oxidase 1; AKT, protein kinase B; ALT, alanine transaminase; APOC2, apolipoprotein C2; ApoE, apolipoprotein E; ATF6, Activating transcription factor-6; cCasp3, cleaved-caspase 3;

cCasp12, cleaved caspase 12; CD36, cluster of differentiation 36; CHOP, CCAAT/enhancer-binding protein homologous protein; CPA, cyclopiazonic acid; CTGF, connective tissue growth factor, CVD, cardiovascular disease; eIF2, eukaryotic initiation factor 2; ELISA, enzyme-linked immunosorbent assay; ER, endoplasmic reticulum; FA, fatty acid; FAS, fatty acid synthase; FMO2, flavin containing monooxygenase 2; GRP78, 78-kDa glucose regulated protein; GRP94, 94-kDa glucose regulated protein; GTT, glucose tolerance tests; G6P, glucose 6-phosphate; H&E, hematoxylin and eosin; HDL, high-density lipoprotein; HFD, high-fat diet; IL, interleukin; IRE1α, Inositol-requiring enzyme-1 alpha; ITT, insulin tolerance tests; JNK, c-Jun N-terminal kinase; LA, linoleate; LDL, low density lipoprotein; LDLR, LDL receptor; LOF, loss-of-function; MCP-1, monocyte chemoattractant protein-1; NAFLD, non-alcoholic fatty liver disease; NASH, non-alcoholic steatohepatitis; NCD, normal control diet; NS, non-significant; OA, oleate; ORO, Oil Red O; oxLDL, oxidized LDL; PA, palmitate; PCSK9, proprotein convertase subtilisin/kexin type 9; PDK1, pyruvate dehydrogenase kinase 1; PDK4, pyruvate dehydrogenase kinase 4; PERK, Protein kinase RNA-like endoplasmic reticulum kinase; PGC1α, PPAR gamma coactivator 1-alpha; PPAR, peroxisome proliferator-activated receptors; PPARγ, peroxisome proliferator-activated receptor gamma; PRK, protein kinase RNA; PSR, Picrosirius Red; ROS, reactive oxygen species; SA, stearate; SCD1, stearoyl-coA desaturase-1; SD, standard deviation; SERCA, sarco/endoplasmic reticulum ATPase; shRNA, short hairpin RNA; siRNA, small interfering RNA; αSMA, alpha smooth muscle actin; SREBP, sterol regulatory element-binding protein; SSO, sulfosuccinimidyl oleate; STAT3, signal transducer and activator of transcription 3; T2D, type 2 diabetes; TBS, tris-buffered saline; TLR, toll-like receptor; TM, tunicamycin; TNFα, tumour necrosis factor alpha; UPR, unfolded protein response; VCAM, vascular cell adhesion protein 1; VLDLR, very low-density lipoprotein receptor; WT, wild-type; XBP1, X-box-binding protein.

Lay Abstract: The proprotein convertase subtilisin/kexin type 9 (PCSK9) is a circulating protein known to reduce the abundance of receptors on the surface of liver cells charged with the task of lipid uptake/removal from the blood. Although PCSK9 deficiency is known to cause lipid accumulation in mice and in cultured cells, the toxicological implications of this observation have not yet been reported. In this study, we demonstrate that PCSK9 can protect against cytotoxicity in cultured liver cells treated with a saturated fatty acid and we also show that PCSK9 knockout mice develop increased liver injury in response to a high fat diet.

Abstract:

Background & Aims: The fatty acid translocase, also known as the cluster of differentiation 36 (CD36), is a well-established scavenger receptor for fatty acid (FA) uptake and is abundantly expressed in many metabolically active tissues. In the liver, CD36 is known to contribute to the progression of non-alcoholic fatty liver disease (NAFLD), to the more severe non-alcoholic steatohepatitis (NASH), by promoting triglyceride accumulation and subsequent lipid-induced endoplasmic reticulum (ER) stress. Given the recent discovery that the hepatocyte-secreted proprotein convertase subtilisin/kexin type 9 (PCSK9) blocks CD36 expression, we sought to investigate the role of PCSK9 in liver fat accumulation and injury in response to saturated FAs and in a mouse model of diet-induced hepatic steatosis.

Methods: In this study, the role of PCSK9 on the uptake and accumulation of FAs, as well as FA-induced toxicity, was examined in a variety of cultured hepatocytes. Diet-induced hepatic steatosis and liver injury was also assessed in *Pcsk9*$^{-/-}$ mice.
Results: Our results indicate that PCSK9 deficiency in cultured hepatocytes increased the uptake and accumulation of saturated and unsaturated FAs. In the presence of saturated FAs, PCSK9 also protected cultured hepatocytes from ER stress and cytotoxicity. In line with these findings, a metabolic challenge using a high fat diet (HFD) caused severe hepatic steatosis, ER stress inflammation and fibrosis in the livers of *Pcsk9*$^{-/-}$ mice compared to controls. Given that inhibition of CD36 ablated the observed accumulation of lipid *in vitro* and *in vivo*, our findings also highlight CD36 as a strong contributor of steatosis and liver injury in the context of PCSK9 deficiency.
Conclusions: Collectively, our findings demonstrate that PCSK9 regulates hepatic triglyceride content in a manner dependent on CD36. In the presence of excess dietary fats, PCSK9 can also protect against hepatic steatosis and liver injury.

Introduction

Given that the liver plays a central role in glucose and lipid metabolism, it is no surprise that NAFLD has emerged as a contributor of other chronic diseases, such as type 2 diabetes (T2D) and cardiovascular disease (CVD) [1, 2]. Severity ranges from simple steatosis to progressive stages of NASH, depending on the presence or absence of inflammation, fibrosis and hepatocyte injury. Excessive consumption of dietary saturated fats and sugars is widely accepted as the primary driver of NAFLD and its prevalence is currently on the rise; affecting 30 to 46% of individuals in Western societies [3].

Although the exact mechanisms by which NAFLD progresses to NASH are not well understood, an accumulation of events including oxidative stress, mitochondrial dysfunction, adipokine alteration, lipid peroxidation and Kupffer cell activation are all believed to contribute to the currently accepted *multiple hit* hypothesis [4]. Chief among these *hits* is the process by which misfolded polypeptides accumulate in the ER and cause ER stress. Paradoxically, this cellular stress pathway is also known to promote oxidative stress, mitochondrial dysfunction and Kupffer cell-mediated inflammation [5, 6]. In a manner similar to other secretory cells, hepatocytes are rich in ER and the signaling cascades associated with its state of stress have been shown to promote apoptotic cell death, lipotoxicity, inflammation and insulin resistance; all of which are commonly observed in patients with obesity, NAFLD and NASH [4].

In response to ER stress, the unfolded protein response (UPR) is activated *via* three signaling cascades that include (a) the highly conserved inositol-requiring 1α (IRE1α)-X-box-binding protein 1 (XBP1) pathway required for hepatic lipid regulation during conditions of ER stress [7], (b) the protein kinase RNA (PRK)-like ER kinase (PERK)-Activating transcription factor-4 (ATF4) pathway known to modulate *de novo* lipogenesis through fatty acid synthase (FAS) and the sterol regulatory element-binding protein-1C (SREBP1-C) [8], and (c) activating transcription factor-6 (ATF6), which in its nuclear active form interacts

directly with nuclear SREBP-2, thereby attenuating the expression of lipid regulatory genes [9]. Overall, canonical UPR activation increases the folding capacity of the ER and blocks global protein synthesis in order to reduce ER burden. In a manner similar to NAFLD, ER stress and ER stress-induced apoptosis are also well-established contributors of CVD [10].

In recent years, CVD is considered the leading cause of death in the USA, accounting for 34% of total deaths in individuals <75 years of age [11]. The discovery of PCSK9 [12] and its ability to induce the degradation of the low-density lipoprotein (LDL) receptor (LDLR) once secreted from the liver, firmly positioned PCSK9 as a target for the management of CVD [13]. These seminal discoveries have since led to the development of human anti-PCSK9 monoclonal antibodies capable of reducing circulating LDL levels by 60% in patients at high risk of CVD [14]. In addition to its ability to induce the degradation of cell-surface LDLR, secreted PCSK9 was recently shown to promote the degradation of several other receptors known to uptake lipid from the circulation into the liver, such as the very low-density lipoprotein receptor (VLDLR) [15, 16], LDLR-related protein-1 [17], the apolipoprotein E (ApoE) receptor-2 [15] and CD36 [18]. Based on these studies, inhibiting circulating PCSK9 may impact the levels of these receptors on the cell-surface of hepatocytes, thereby increasing liver burden via enhanced hepatic lipid uptake and accumulation.

The purpose of this study was to determine whether the previously reported increase in hepatic lipid content observed in *Pcsk9*$^{-/-}$ mice [18] correlated with the hallmark features of NASH, such as ER stress, apoptosis, inflammation and fibrosis. Accordingly, primary human hepatocytes, as well as cultured HepG2 and HuH7 hepatocyte cell lines, were treated with a variety of lipoproteins and dietary FAs known to cause ER stress. Our data demonstrate that PCSK9 strongly regulates the lipid content of cultured hepatocytes and in the presence of saturated FA, can protect against ER stress, reactive oxygen species (ROS) production and lipotoxicity. Consistently, a significant increase in triglyceride content in the livers of normal control diet (NCD)-fed *Pcsk9*$^{-/-}$ mice compared to *Pcsk9*$^{+/+}$ was also observed. Feeding of a HFD for 12 weeks, however, led to a more severe fatty liver phenotype; yielding increased expression of ER stress, apoptotic and fibrotic markers, as well as elevated serum alanine transaminase (ALT) levels in *Pcsk9*$^{-/-}$ mice compared to *Pcsk9*$^{+/+}$ counterparts. Based on these observations, our data suggest that PCSK9 can act as a modulator of hepatic lipid content, capable of protecting against hepatic steatosis and liver injury in response to a metabolic challenge.

Materials and Methods

Cell culture and free FA treatments. HuH7 and HepG2 immortalized human hepatocytes were cultured at 37°C with 5% CO_2 in complete Dulbecco's Modified Eagle's Medium (Gibco, Thermorfisher Scientific) containing 10% fetal bovine serum (Sigma-Aldrich) and 50 U/ml of penicillin and streptomycin (Sigma-Aldrich). HepatoSure 100-donor primary human hepatocytes were purchased from Xenotech and cultured in complete William's E medium as per manufacturer's instructions. FAs used for cell treatment such as oleate (OA; Sigma-Aldrich), linoleate (LA; Sigma-Aldrich),

stearate (SA; Sigma Aldrich) and palmitate (PA; Sigma-Aldrich) were conjugated to FA-free bovine serum albumin (BSA; Sigma Aldrich), as previously described [19], to a stock concentration of 1 mM. Cells were also treated with LDL (Lee Biosolutions), high-density lipoprotein (HDL; Alpha Aesar) and oxidized (ox)LDL (Alpha Aesar). Additional treatments used in cell culture studies included recombinant human (rh)PCSK9 (Cayman Chemical), DiI-LDL (Alpha Aesar) and sulfo-N-succinimidyl oleate (SSO). All cell treatments were carried out for 24 hours, unless specified otherwise. Small interfering RNA (siRNA) targeted against PCSK9 (siPCSK9) and CD36 (siCD36) were purchased from siGenome, Dharmacon, and transfections were carried out as per manufacturer's instructions using RNAiMAX (ThermoFisher Scientific). The overexpression of human wild-type $PCSK9^{(WT)}$ and the secretion-deficient $PCSK9^{Q152H}$, as well as human CD36 (Addgene, # 52025) was achieved using X-tremeGENE transfection reagent as per manufacturer's instructions.

Animal studies. Hepatic lipid accumulation was first examined in 12-week-old male *Pcsk9*$^{-/-}$ mice (n=10) on a C57BL/6J background and age-matched C57BL/6J controls (*Pcsk9*$^{+/+}$; n=10) fed NCD. Experiments were then repeated in a second cohort of *Pcsk9*$^{-/-}$ mice (n=5) on a C57BL/6J background and age-matched *Pcsk9*$^{+/+}$ controls (n=5), which were fed either NCD or HFD (60% fat/Kcal, ENVIGO #TD.06414), starting at 6 weeks of age for an additional 12 weeks prior to sacrifice. A final cohort of 12-week-old male *Pcsk9*$^{-/-}$ mice on a C57BL/6J background (n=6) were treated with SSO (10 mg/kg; intraperitoneal injection) and one hour later with OA (1g/kg, intraperitoneal injection) for an additional two hours prior to study endpoint. All animals were housed in a vented rack system, had access to food and water *ad libitum* and were exposed to 12h light:dark cycles. Animal experiments were performed in strict accordance with the McMaster University animal care guidelines.

Statistical analysis: All data are presented as the mean and error bars as SD. Statistical differences between two groups were determined using the unpaired *t* test. For analysis of experiments involving multiple groups, the one-way ANOVA was performed. All comparisons were considered statistically significant when $p<0.05$.

See *Supplemental Materials and Methods* for additional information.

Results

PCSK9 reduces lipid accumulation in cultured hepatocytes treated with FAs and lipoproteins.

The effect of PCSK9 on cellular lipid accumulation was first examined in cultured HepG2 hepatocytes stably transfected with short hairpin RNA (shRNA) targeted against PCSK9 or control shRNA. Knockdown of PCSK9 in these cells was first confirmed via enzyme-linked immunosorbant assay (ELISA) for secreted PCSK9 and immunoblotting of PCSK9-regulated receptors, LDLR and CD36 (Fig. 1A and B). Consistent with previous studies, PCSK9 expression was inversely correlated with LDLR and CD36 expression [13,18]. Increased uptake of fluorescently-labelled DiI-LDL cholesterol was also observed in PCSK9 shRNA knockdown cells compared to shRNA controls (Fig. S1A and S1B). Staining with Oil-red-O (ORO), as well as triglyceride

extraction and quantification, revealed a marked increase in triglyceride accumulation in PCSK9 shRNA cells treated with dietary saturated FAs (PA and SA), unsaturated FAs (OA and LA) and lipoproteins (LDL and HDL) (Fig. 1C and D). The dose-dependent effect of exogenously-added extracellular PCSK9 on intracellular lipid accumulation was also examined in OA-treated HepG2 cells using rhPCSK9 (Fig. 1E). A modest but significant reduction in CD36 expression and in OA-induced lipid accumulation was also observed in HepG2 cells and primary mouse hepatocytes transfected with wild-type (WT) PCSK9 compared to those transfected with a loss-of-function (LOF) Q152H-PCSK9 variant that fails to be secreted (Fig. S1C to S1F) [20]. Transfection efficiency in these cells was confirmed via immunoblotting for PCSK9 and GFP encoded by the bicistronic plasmid utilized in these studies (Fig. S1G). Lipid uptake and accumulation was also assessed in primary human hepatocytes that were exposed to medium harvested from HuH7 cells transfected with either WT-PCSK9 or the secretion-deficient Q152H-PCSK9 variant (Fig. 1F). Consistent with cultured HepG2 cells, secreted WT-PCSK9 significantly reduced OA-induced lipid accumulation in primary human hepatocytes.

The CD36 inhibitor, SSO, reduces OA-induced lipid droplet accumulation in PCSK9 knockdown hepatocytes.

Our next aim was to assess the recently described inhibitory role of PCSK9 on CD36 as the mechanism by which PCSK9 regulates hepatic lipid levels using a pharmacologic antagonist of CD36, SSO [21]. Consistent with PCSK9 shRNA knockdown HepG2 cells, the knockdown of PCSK9 in HepG2 and HuH7 cells using siRNA increased intracellular lipid content; a result that was further exacerbated via incubation of the cells in OA (Fig. 2A and B). No such increase in lipid accumulation, however, was observed in cells pre-treated with SSO. Consistently, SSO pre-treatment also attenuated hepatic lipid accumulation in *Pcsk9*$^{-/-}$ mice exposed to a bolus injection of OA (Fig. 2C). The knockdown of CD36 using siRNA (siCD36) also reduced lipid accumulation in HepG2 cells challenged with OA (Fig. 2D and E). Lastly, to confirm the role of CD36 as a driver of lipid accumulation in the context of PCSK9 deficiency, experiments were repeated in cells co-transfected with siPCSK9 and siCD36. ORO extract and quantification from these cells demonstrates that ablation of CD36 expression markedly reduced lipid accumulation occurring as a result of PCSK9 knockdown in the presence or absence of OA (Fig. 2F). Similar findings were observed in HuH7 cells (Fig. S2A). The difference in lipid accumulation between control and PCSK9 shRNA cells was also lost in cells overexpressing CD36 (Fig. 2G). Effective knockdown of PCSK9 and CD36, as well as overexpression of CD36 in HepG2 cells, was confirmed via immunoblotting (Fig. S2B to S2D). Collectively, these data suggest that increased expression of CD36 strongly contributes to the heightened levels of intracellular lipids observed in hepatocyte cell lines with reduced PCSK9 expression.

PCSK9 protects cultured hepatocytes from palmitate-induced ER stress and cytotoxicity.

To substantiate our findings, we next investigated whether PCSK9 would protect from the well-established ER stress-associated effects of increased CD36 expression, such as ER Ca^{2+} depletion, ROS production and cytotoxicity [22]. First, increased expression of the ER stress markers

IRE1α, glucose-regulated protein of 78-kDa (GRP78), the pro-apoptotic marker CCAAT/ enhancer-binding protein homologous protein (CHOP), ATF6 and sXBP1 was observed in PCSK9 shRNA compared to control shRNA HepG2 cells treated with PA via immunoblotting and quantitative real time PCR (Fig. 3A and B). Similarly, primary human hepatocytes exposed to medium harvested from HuH7 cells transfected with a secretion-defective Q152H-PCSK9 also yielded increased PA-induced expression of ER stress markers compared to those exposed to medium containing WT-PCSK9 (Fig. 3C). Consistent with previous studies [19], treatment with OA and lipoproteins did not cause ER stress in HepG2 cells (Fig. S3A, S3B and S3C).

PCSK9 shRNA HepG2 cells also exhibited increased cytotoxicity in response to PA relative to controls (Fig. 3D and S3D). Interestingly, although SSO-mediated CD36 inhibition failed to reduce PA-induced cytotoxicity in shRNA control cells, the CD36 inhibitor attenuated cytotoxicity in PCSK9 shRNA knockdown cells (Fig. 3D). Given the role of ER stress in the production of ROS, the ability of PCSK9 to protect from PA-induced ROS was also examined in HepG2 cells (Fig. 3E). We observed that PA treatment led to a significant increase in ROS production in PCSK9 shRNA HepG2 cells compared to shRNA controls during the course of the experiment.

Next, we assessed ER Ca^{2+} depletion, which represents another established outcome of ER stress in cells treated with PA [23]. The fluorometric cytosolic Ca^{2+} indicator utilized in these studies, Fura-2-AM, increases in fluorescence intensity as Ca^{2+} exits the ER into the cytosol [24]. To measure relative ER Ca^{2+} content, HepG2 cells pre-treated with PA (5 hours; 500 μM) were exposed to a potent sarco/endoplasmic reticulum ATPase (SERCA) pump inhibitor, cyclopiazonic acid (CPA; 50 μM; Fig. 3F). In response to CPA, we observed that PA-treated shRNA control cells exhibited ER Ca^{2+} loss to a similar extent as that of untreated controls. In contrast to this result, PA pre-treated PCSK9 shRNA knockdown cells failed to exhibit loss of ER Ca^{2+} in response to CPA, suggesting that PA induced ER Ca^{2+} depletion during pre-treatment in these cells. Consistently, a time-course study in which ER Ca^{2+} depletion was monitored over a 210-minute period yielded similar findings (Fig. S3E). Increased ER expansion, another hallmark feature of ER stress, was also observed in HepG2 cells transfected with a splice-switching oligomer that causes ER retention of PCSK9 in response to PA (Fig. S4A and S4B). Appropriate splice-switching and ER retention of PCSK9 in these cells was confirmed via immunoblotting (Fig. S4C).

***Pcsk9*$^{-/-}$ mice exhibit compensatory changes in biliary cholesterol excretion and in the expression of hepatic lipid regulatory proteins**.

Given the observed increase in lipid droplet content in cultured hepatocytes, PCSK9-dependent changes in hepatic lipid content were also examined *in vivo*. The livers of NCD-fed 12-week-old *Pcsk9*$^{-/-}$ mice exhibited increased ORO-staining of lipid droplets and protein levels of the lipid droplet marker perilipin (Fig. 4A) compared to controls. Consistent with previous reports, immunohistochemical staining also demonstrated a marked increase in cell-surface levels of LDLR, VLDLR and CD36 expression in the livers of *Pcsk9*$^{-/-}$ compared to controls [13, 16, 18]. We also report the

novel finding that *Pcsk9*$^{-/-}$ mice exhibit increased levels of the cholesterol efflux transporter ABCA1 when compared to controls (Fig. 4A and S5A). In contrast to the LDLR, CD36 and the VLDLR, changes in hepatic ABCA1 expression in *Pcsk9*$^{-/-}$ mice likely occurred as a result of increased mRNA transcript expression (Fig. S5B). Elevated expression of hepatic PCSK9-regulated receptors, LDLR, VLDLR and CD36 was also confirmed using immunoblots (Fig. 4B). Given that hepatic biliary secretion or trans-intestinal cholesterol excretion are established mechanisms of cholesterol clearance [25, 26], fecal cholesterol content was also assessed (Fig. 4C). The feces of *Pcsk9*$^{-/-}$ mice contained increased levels of cholesterol compared to controls. The positive correlation between PCSK9 and circulating cholesterol and triglycerides was also confirmed *via* colorimetric assays (Fig. 4D). Consistent with our hypothesis that elevated hepatic lipid content in *Pcsk9*$^{-/-}$ occurs as a result of increased lipid uptake, no difference was observed in the FA oxidation marker, β-hydroxybutyrate (Fig 4E). Furthermore, we observed that the livers of *Pcsk9*$^{-/-}$ mice exhibited (a) a significant reduction in peroxisome proliferator-activated receptor gamma (PPARγ) co-activator 1-alpha (PGC1α), a protein commonly associated with *de novo* cholesterol synthesis and PPARγ-mediated NAFLD; (b) a modest but significant increase in mRNA levels of the lipolysis markers ACOX1 and APOC2; and (c) no change in the expression of the FA oxidation marker PPARα (Fig. 4F). Consistent with IHC data, a significant increase at the mRNA level of perilipin was also observed in *Pcsk9*$^{-/-}$ mice relative to controls (Fig. 4F). Although additional studies are required to confirm that *de novo* lipogenesis and lipid oxidation do not contribute to the observed phenotype, our data suggest that lipid accumulation in the livers of *Pcsk9*$^{-/-}$ mice occurs largely as a result of increased lipid uptake at the cell surface.

PCSK9 knockout exacerbates diet-induced hepatic steatosis in mice.

Although we did not observe profound differences in gross liver morphology or injury in NCD-fed *Pcsk9*$^{-/-}$ mice compared to *Pcsk9*$^{+/+}$ counterparts, this diet is not lipid-rich or used for the study of hepatic steatosis. Therefore, our next aim was to assess the effect of a HFD on liver function and injury in the context of PCSK9 deficiency and increased hepatic CD36 expression. Accordingly, 6-week-old *Pcsk9*$^{-/-}$ mice and *Pcsk9*$^{+/+}$ controls were fed either NCD or HFD for 12 weeks. Upon removal of the liver from these animals during sacrifice, an apparent increase in size and change in colour was observed in the HFD-fed *Pcsk9*$^{-/-}$ mice compared to controls (Fig. 5A). Assessment of hepatic lipid droplets via ORO and H&E staining also yielded an increase in lipid droplets in the livers of HFD-fed *Pcsk9*$^{-/-}$ mice compared to HFD-fed controls (Fig. 5B). Although total body weight was not affected by PCSK9 (Fig. 5C) in these experiments, a significant increase in liver weight (Fig. 5D) and liver triglyceride and cholesterol content (Fig. 5E) was also observed in HFD-fed *Pcsk9*$^{-/-}$ compared to controls. A trend was also apparent for elevated gonadal, inguinal and brown adipose tissue weights in the *Pcsk9*$^{-/-}$ mice on HFD, but the differences between genotypes were not statistically significant in this experiment (Fig. 5F).

PCSK9 knockout mice exhibit increased diet-induced liver injury and insulin resistance.

We next examined hepatic ER stress in these mice; a process well known to contribute to hepatic steatosis [4-6]. Increased expression of ER stress markers pPERK, pIRE1α, IRE1α, sXBP1, peIF2α, GRP78, GRP94 and CHOP; pro-apoptotic markers cleaved caspase-3 and -12 (cCasp3 and cCasp12); and pro-fibrotic markers α smooth muscle actin (αSMA) and connective tissue growth factor (CTGF) were observed in the livers of HFD-fed *Pcsk9*$^{-/-}$ mice compared to HFD-fed *Pcsk9*$^{+/+}$ control mice (Fig. 6A, B and C). Increased staining of F4/80, a marker of pro-inflammatory Kupffer cells, as well as hepatic mRNA expression of pro-inflammatory markers tumor necrosis factor α (TNFα), interleukin (IL) 1β, IL6, IL12, toll-like receptor (TLR) 1, TLR2, TLR4, intercellular adhesion molecule (ICAM), vascular cell adhesion protein (VCAM) and monocyte chemoattractant protein (MCP1) mRNA was also observed in the livers of HFD-fed *Pcsk9*$^{-/-}$ mice compared to controls. A modest increase in fibrosis was also observed in these mice via Mason's trichrome staining of collagen (blue), as well as immunohistochemical staining of fibronectin. Assessment of plasma ALT activity, as well as apoptosis using a TUNEL assay, also revealed that *Pcsk9*$^{-/-}$ mice were more prone to diet-induced hepatic injury compared to controls (Fig. 6D and E). Similarly, an increase in protein aggregate accumulation was observed in HFD-fed *Pcsk9*$^{-/-}$ mice compared to controls using thioflavin-T (Fig. S6)

Hepatic steatosis is also an established driver of insulin resistance and diabetes as it tends to promote chronically elevated circulating glucose levels resulting from constitutively activated gluconeogenic pathways [27]. For this reason, our last aim was to examine the effect of PCSK9 knockout on markers of hepatic insulin resistance in HFD-fed mice. First, however, assessment of glucose production in PCSK9 shRNA HepG2 cells revealed that PA treatment induced glucose production to a greater extent in PCSK9 knockdown cells than in control cells (Fig. 7A). Further, exposure of naive HepG2 cells to medium harvested from HuH7 cells transfected with either PCSK9^{WT} or the secretion-defective PCSK9^{Q152H} also demonstrated that PCSK9 protected against PA-induced gluconeogenesis (Fig. 7B).

In mice, glucose and insulin tolerance tests (GTT and ITT, respectively) revealed that HFD-fed *Pcsk9*$^{-/-}$ mice exhibited a reduction in glucose uptake in response to a bolus injection of glucose or insulin (Fig. 7C), indicative of resistance to insulin [28, 29]. A significant increase in resting glucose levels, which represents another characteristic of insulin resistance, was also observed in HFD-fed *Pcsk9*$^{-/-}$ mice compared to HFD-fed controls (Fig. 7D). In contrast to other models of diet-induced insulin resistance [30], plasma insulin levels were reduced in *Pcsk9*$^{-/-}$ mice compared to controls, but this likely involving pancreatic islet abnormalities, as reported previously (Fig. 7E) [28, 29]. Mice were also injected with insulin one hour prior to sacrifice in order to examine the phosphorylation/activation status of protein kinase B (AKT); a central regulator and strong promoter of hepatic glucose uptake and metabolism (Fig. 7F) [30]. As expected, insulin treatment led to the phosphorylation of AKT in the livers of NCD-fed mice, but no difference was observed between *Pcsk9*$^{-/-}$ and *Pcsk9*$^{+/+}$ mice. In HFD-fed mice, however,

the ability of insulin to activate hepatic AKT was reduced to a greater extent in *Pcsk9*$^{-/-}$ mice than in the *Pcsk9*$^{+/+}$ control mice. Consistent with other studies, hepatic steatosis severity in the mice was positively correlated with the mRNA abundance of hepatic gluconeogenic markers, including signal transducer and activator of transcription 3 (STAT3), glucose 6 phosphatase (G6P), stearoyl-CoA desaturase-1 (SCD1), pyruvate dehydrogenase kinase 4 (PDK4) and the Dimethylaniline monooxygenase [N-oxide-forming] 2 (FMO2) (Fig. 7G) [31]. In line with the other endpoints examined in these mice, increased gluconeogenic marker expression was observed in the livers of *Pcsk9*$^{-/-}$ compared to *Pcsk9*$^{+/+}$ mice. Collectively, these data suggest that PCSK9 can reduce liver lipid accumulation and protect against ER stress, hepatic insulin resistance and glucose production in response to a HFD.

Discussion

Previous studies have demonstrated that the equilibrium of hepatic lipid levels can favor hepatic steatosis during conditions of (a) increased *de novo* lipogenesis, (b) heightened lipid uptake (c) reduced lipid efflux and (d) reduced lipid oxidation [31]. In the case of *Pcsk9*$^{-/-}$ mice, our studies as well as those of others [18], suggest that PCSK9 prevents the uptake of lipid into the liver by down-regulating the expression of CD36. Consistent with our observations, previous studies have also shown that increased expression of CD36 can promote fatty liver disease and contribute to hepatic insulin resistance [32]. Furthermore, CD36-mediated FA uptake is known to promote ER stress and lipotoxicity in cells types with high capacity for FA metabolism including adipocytes, cardiomyocytes, hepatocytes, endothelial cells, macrophages, pancreatic β cells, podocytes and neurons [22]. Here we demonstrate that PCSK9 prevents CD36-mediated FA uptake and accumulation in cultured hepatocytes. We also show that under normal dietary conditions, several compensatory mechanisms in the livers of *Pcsk9*$^{-/-}$ mice may act to suppress hepatic steatosis. During a HFD metabolic challenge, however, we observed a significant increase in the expression of markers of ER stress, fibrosis, inflammation and apoptosis as well as plasma levels of ALT in *Pcsk9*$^{-/-}$ mice compared to *Pcsk9*$^{+/+}$ controls.

The current landscape of studies examining the role of PCSK9 in hepatic steatosis in humans remains controversial. Pre-clinical data however, have been largely consistent; demonstrating that circulating PCSK9 can prevent hepatic lipid uptake and accumulation in mice. Demers and coworkers were the first to demonstrate that PCSK9 negatively regulates the expression of CD36 and also reported a 3-4 fold increase in hepatic triglyceride levels in NCD-fed *Pcsk9*$^{-/-}$ [18]. Recent studies have also identified *E2f1* as a major regulator of hepatic lipid homeostasis in a manner dependent on PCSK9 [33]. Lai and colleagues reported increased hepatic lipid content in *E2f1*$^{-/-}$ mice and also discovered that these mice exhibit significantly reduced circulating PCSK9 levels. Upon re-expression of PCSK9 in these mice, the fatty liver phenotype was lost. Consistent with this growing body of literature, a recent network analysis done in primary human hepatocytes identified PCSK9 as a gene linked to liver fat content and NAFLD [34].

Two independent clinical studies have now demonstrated consistent findings with regards to the association between liver fat content and circulating PCSK9 levels. The Dallas heart study reported a modest but significant positive correlation between liver fat content and circulating PCSK9 levels (n=2027 subjects; $p<0.0001$) [35]. Ruscica and colleagues have now also reported a positive correlation between circulating PCSK9 and liver steatosis grade ($p=0.0011$) as well as necroinflammation, ballooning and fibrosis stage (n=201) [36]. Consistent with these findings our research group has observed that diet-induced steatosis promotes *de novo* hepatic PCSK9 expression and increases circulating PCSK9 levels in mice (Lebeau, Byun and Austin, unpublished data). In contrast to these data, Wargny and colleagues failed to observe a significant correlation between circulating PCSK9 levels and plasma transaminases, liver fat content, histological liver lesions, steatosis severity, NASH activity score, lobular and/or portal inflammation or ballooning in three patient cohorts with advanced stages of NASH (n=478) [37]. Given the severity of steatosis in the patients from this study, however, the authors highlight that variations between studies suggest that in humans, PCSK9 likely plays a role in the early development of NAFLD and not in late stages of NASH.

Beyond liver fat content, Mbikay and colleagues have reported abnormalities in pancreatic islets of *Pcsk9*$^{-/-}$ mice, which were shown to contribute to insulin resistance [28]. Consistent with these findings, we also report the novel finding that diet-induced hepatic steatosis attenuates insulin-induced phosphorylation and activation of AKT in the livers of *Pcsk9*$^{-/-}$ mice to a significantly greater extent than in controls. Consistently, here we show that HFD-fed *Pcsk9*$^{-/-}$ mice exhibit reduced rates of glucose uptake and insulin sensitivity; all of which represent hallmark features of hepatic insulin resistance. In line with these findings, a recent study also identified a positive correlation between LOF PCSK9 mutations and increased fasting glucose, body weight, waist-to-hip ratio and odds ratio of T2D in patients [38].

Accumulating evidence demonstrates that PCSK9 regulates the uptake and accumulation of lipid in the livers of mice. Given the current inconsistencies in clinical data sets, additional studies are required before strong conclusions can be made in the context of human disease. Interestingly, recent studies have demonstrated that FDA-approved monoclonal antibodies targeted against the LDLR-binding domain of circulating PCSK9 increase its concentrations 7-fold as a result of antagonizing LDLR-mediated clearance [39]. Given that the domain utilized by PCSK9 to interact with CD36 differs from its LDLR binding domain [18], it remains possible and even likely that such antibodies may also reduce CD36 expression as a byproduct of increasing the circulating pool of PCSK9. Additional studies are required to answer this important question and to determine whether anti-PCSK9 antibodies could be utilized to protect against CD36-driven diseases like NAFLD and NASH.

Overall, the abundance of data characterizing PCSK9 as a modulator of circulating cholesterol strongly suggest that its influence on the latter exceeds that of its effect on circulating and peripheral triglyceride levels. Nonetheless, our findings as well as those discussed herein, suggest that hepatic PCSK9

expression is upregulated during conditions of steatosis to prevent further lipid uptake and accumulation in the liver, thus acting as a classical feedback modulator of hepatic lipid levels. Moreover, our data demonstrate that in mice, PCSK9 can protect against ER stress, fibrosis and injury of the liver in response to conditions of excessive fat consumption.

Acknowledgements
The mammalian expression plasmid encoding His-CD36 was a gift from Gavin Wright (Addgene plasmid # 52025).

References

[1] Francque SM, van der Graaff D, Kwanten WJ. Non-alcoholic fatty liver disease and cardiovascular risk: Pathophysiological mechanisms and implications. J Hepatol 2016;65:425-443.
[2] Patil R, Sood GK. Non-alcoholic fatty liver disease and cardiovascular risk. World journal of gastrointestinal pathophysiology 2017;8:51-58.
[3] Vernon G, Baranova A, Younossi ZM. Systematic review: the epidemiology and natural history of non-alcoholic fatty liver disease and non-alcoholic steatohepatitis in adults. Aliment Pharmacol Ther 2011;34:274-285.
[4] Zhang XQ, Xu CF, Yu CH, Chen WX, Li YM. Role of endoplasmic reticulum stress in the pathogenesis of nonalcoholic fatty liver disease. World journal of gastroenterology 2014;20:1768-1776.
[5] Puri P, Mirshahi F, Cheung O, Natarajan R, Maher JW, Kellum JM, et al. Activation and dysregulation of the unfolded protein response in nonalcoholic fatty liver disease. Gastroenterology 2008;134:568-576.
[6] Rinella ME, Elias MS, Smolak RR, Fu T, Borensztajn J, Green RM. Mechanisms of hepatic steatosis in mice fed a lipogenic methionine choline-deficient diet. J Lipid Res 2008;49:1068-1076.
[7] Zhang K, Wang S, Malhotra J, Hassler JR, Back SH, Wang G, et al. The unfolded protein response transducer IRE1alpha prevents ER stress-induced hepatic steatosis. EMBO J 2011;30:1357-1375.
[8] Bobrovnikova-Marjon E, Hatzivassiliou G, Grigoriadou C, Romero M, Cavener DR, Thompson CB, et al. PERK-dependent regulation of lipogenesis during mouse mammary gland development and adipocyte differentiation. Proc Natl Acad Sci U S A 2008;105:16314-16319.
[9] Zeng L, Lu M, Mori K, Luo S, Lee AS, Zhu Y, et al. ATF6 modulates SREBP2-mediated lipogenesis. EMBO J 2004;23:950-958.
[10] Minamino T, Kitakaze M. ER stress in cardiovascular disease. Journal of molecular and cellular cardiology 2010;48:1105-1110.
[11] Mozaffarian D, Benjamin EJ, Go AS, Arnett DK, Blaha MJ, Cushman M, et al. Heart disease and stroke statistics--2015 update: a report from the American Heart Association. Circulation 2015;131:e29-322.
[12] Seidah NG, Benjannet S, Wickham L, Marcinkiewicz J, Jasmin SB, Stifani S, et al. The secretory proprotein convertase neural apoptosis-regulated convertase 1 (NARC-1): liver regeneration and neuronal differentiation. Proc Natl Acad Sci U S A 2003;100:928-933.
[13] Maxwell KN, Breslow JL. Adenoviral-mediated expression of Pcsk9 in mice results in a low-density lipoprotein receptor knockout phenotype. Proc Natl Acad Sci U S A 2004;101:7100-7105.
[14] Sabatine MS, Giugliano RP, Keech AC, Honarpour N, Wiviott SD, Murphy SA, et al. Evolocumab and Clinical Outcomes in Patients with Cardiovascular Disease. N Engl J Med 2017;376:1713-1722.

[15] Poirier S, Mayer G, Benjannet S, Bergeron E, Marcinkiewicz J, Nassoury N, et al. The proprotein convertase PCSK9 induces the degradation of low density lipoprotein receptor (LDLR) and its closest family members VLDLR and ApoER2. J Biol Chem 2008;283:2363-2372.
[16] Roubtsova A, Munkonda MN, Awan Z, Marcinkiewicz J, Chamberland A, Lazure C, et al. Circulating proprotein convertase subtilisin/kexin 9 (PCSK9) regulates VLDLR protein and triglyceride accumulation in visceral adipose tissue. Arterioscler Thromb Vasc Biol 2011;31:785-791.
[17] Canuel M, Sun X, Asselin MC, Paramithiotis E, Prat A, Seidah NG. Proprotein convertase subtilisin/kexin type 9 (PCSK9) can mediate degradation of the low density lipoprotein receptor-related protein 1 (LRP-1). PLoS One 2013;8:e64145.
[18] Demers A, Samami S, Lauzier B, Des Rosiers C, Ngo Sock ET, Ong H, et al. PCSK9 Induces CD36 Degradation and Affects Long-Chain Fatty Acid Uptake and Triglyceride Metabolism in Adipocytes and in Mouse Liver. Arterioscler Thromb Vasc Biol 2015;35:2517-2525.
[19] Wei Y, Wang D, Topczewski F, Pagliassotti MJ. Saturated fatty acids induce endoplasmic reticulum stress and apoptosis independently of ceramide in liver cells. American journal of physiology Endocrinology and metabolism 2006;291:E275-281.
[20] Lebeau P, Platko K, Al-Hashimi AA, Byun JH, Lhotak S, Holzapfel N, et al. Loss-of-function PCSK9 mutants evade the unfolded protein response sensor GRP78 and fail to induce endoplasmic reticulum stress when retained. J Biol Chem 2018;293:7329-7343.
[21] Kuda O, Pietka TA, Demianova Z, Kudova E, Cvacka J, Kopecky J, et al. Sulfo-N-succinimidyl oleate (SSO) inhibits fatty acid uptake and signaling for intracellular calcium via binding CD36 lysine 164: SSO also inhibits oxidized low density lipoprotein uptake by macrophages. J Biol Chem 2013;288:15547-15555.
[22] Park YM. CD36, a scavenger receptor implicated in atherosclerosis. Experimental & molecular medicine 2014;46:e99.
[23] Xu S, Nam SM, Kim JH, Das R, Choi SK, Nguyen TT, et al. Palmitate induces ER calcium depletion and apoptosis in mouse podocytes subsequent to mitochondrial oxidative stress. Cell death & disease 2015;6:e1976.
[24] Samtleben S, Jaepel J, Fecher C, Andreska T, Rehberg M, Blum R. Direct imaging of ER calcium with targeted-esterase induced dye loading (TED). Journal of visualized experiments : JoVE 2013:e50317.
[25] Le May C, Berger JM, Lespine A, Pillot B, Prieur X, Letessier E, et al. Transintestinal cholesterol excretion is an active metabolic process modulated by PCSK9 and statin involving ABCB1. Arterioscler Thromb Vasc Biol 2013;33:1484-1493.
[26] Su K, Sabeva NS, Wang Y, Liu X, Lester JD, Liu J, et al. Acceleration of biliary cholesterol secretion restores glycemic control and alleviates hypertriglyceridemia in obese db/db mice. Arterioscler Thromb Vasc Biol 2014;34:26-33.
[27] Capeau J. Insulin resistance and steatosis in humans. Diabetes Metab 2008;34:649-657.
[28] Mbikay M, Sirois F, Mayne J, Wang GS, Chen A, Dewpura T, et al. PCSK9-deficient mice exhibit impaired glucose tolerance and pancreatic islet abnormalities. FEBS Lett 2010;584:701-706.
[29] Da Dalt L, Ruscica M, Bonacina F, Balzarotti G, Dhyani A, Di Cairano E, et al.

PCSK9 deficiency reduces insulin secretion and promotes glucose intolerance: the role of the low-density lipoprotein receptor. European heart journal 2019;40:357-368.
[30] Guo S. Insulin signaling, resistance, and the metabolic syndrome: insights from mouse models into disease mechanisms. The Journal of endocrinology 2014;220:T1-T23.
[31] Song S, Andrikopoulos S, Filippis C, Thorburn AW, Khan D, Proietto J. Mechanism of fat-induced hepatic gluconeogenesis: effect of metformin. Am J Physiol Endocrinol Metab 2001;281:275-282.
[32] Wilson CG, Tran JL, Erion DM, Vera NB, Febbraio M, Weiss EJ. Hepatocyte-Specific Disruption of CD36 Attenuates Fatty Liver and Improves Insulin Sensitivity in HFD-Fed Mice. Endocrinology 2016;157:570-585.
[33] Lai Q, Giralt A, Le May C, Zhang L, Cariou B, Denechaud PD, et al. E2F1 inhibits circulating cholesterol clearance by regulating Pcsk9 expression in the liver. JCI insight 2017;2.
[34] Lee S, Zhang C, Liu Z, Klevstig M, Mukhopadhyay B, Bergentall M, et al. Network analyses identify liver-specific targets for treating liver diseases. Molecular systems biology 2017;13:938.
[35] Lakoski SG, Lagace TA, Cohen JC, Horton JD, Hobbs HH. Genetic and metabolic determinants of plasma PCSK9 levels. The Journal of clinical endocrinology and metabolism 2009;94:2537-2543.
[36] Ruscica M, Ferri N, Macchi C, Meroni M, Lanti C, Ricci C, et al. Liver fat accumulation is associated with circulating PCSK9. Annals of medicine 2016;48:384-391.
[37] Wargny M, Ducluzeau PH, Petit JM, Le May C, Smati S, Arnaud L, et al. Circulating PCSK9 levels are not associated with the severity of hepatic steatosis and NASH in a high-risk population. Atherosclerosis 2018;278:82-90.
[38] Schmidt AF, Swerdlow DI, Holmes MV, Patel RS, Fairhurst-Hunter Z, Lyall DM, et al. PCSK9 genetic variants and risk of type 2 diabetes: a mendelian randomisation study. The lancet Diabetes & endocrinology 2017;5:97-105.
[39] Shapiro MD, Miles J, Tavori H, Fazio S. Diagnosing resistance to a proprotein convertase subtilisin/kexin type-9 inhibitor. Annals of internal medicine 2018;168:376-379.

Figure Legends

Fig. 1. PCSK9 reduces the triglyceride content of HepG2 cells and primary human hepatocytes. (A,B) PCSK9 knockdown in PCSK9 shRNA HepG2 cells was confirmed *via* ELISA for secreted PCSK9 (*, $p<0.05$) and immunoblots for PCSK9-regulated receptors LDLR and CD36. (C) ORO lipid droplet staining of HepG2 control cells (shRNA control) and PCSK9 knockdown cells (PCSK9 shRNA) in the presence or absence of OA (200 μm) and LDL (50 μg/ml). (D) Intracellular triglyceride content was also quantified in cells treated with either OA (200 μM), LA (200 μM), PA (200 μM), SA (200 μM) and lipoproteins LDL (50 μg/ml) and HDL (50 μg/ml) for 24 hours (*, $p<0.05$; †, $p<0.05$ vs. vehicle-shRNA control; ‡, $p<0.05$ vs. vehicle-PCSK9 shRNA). (E) The effect of rhPCSK9 on OA uptake was examined in HepG2 cells via quantification of the density of ORO extracts (*, $p<0.05$). (F) ORO staining was carried out in primary human hepatocytes that were exposed to medium harvested from HuH7 cells transfected with either secreted wild-type (WT)-PCSK9 or a PCSK9 variant that fails to exit the cell [20], Q152H-PCSK9, and

treated with OA (200 μM) for 24 hours. ORO extracts from primary human hepatocytes were also quantified (*, $p<0.05$). Results are shown as the mean and error bars as S.D. Differences between groups were determined via Student's *t* test or one-way ANOVA. Scale bars, 50 μm.

Fig. 2. PCSK9 regulates FA uptake in immortalized hepatocytes through CD36. (A,B) HepG2 and HuH7 cells were transfected with siPCSK9 targeted against or scrambled control siRNA. Cells were subsequently treated with OA and or SSO (10 μM), a well-established blocker of CD36 (23), for an additional 24 hours (*, $p<0.05$). (C) 12-week-old male C57BL/6J mice were pre-treated with SSO (50 μg/kg) for 1 hour and subsequently administered with OA for an additional 2 hours. Hepatic lipid accumulation was visually examined via ORO staining and quantified using a triglyceride assay. (D,E) The effect of CD36 inhibition on OA uptake was also assessed using siRNA targeted against CD36 (siCD36) (*, $p<0.05$). Finally, intracellular lipid accumulation was examined in HepG2 cells co-transfected with siPCSK9 and siCD36, via ORO extract and quantification using a spectrophotometer (*, $p<0.05$). (G) The effect of CD36 overexpression on lipid accumulation was examined in HepG2 cells via quantification of ORO extract (*, $p<0.05$; †, $p<0.05$ vs. control shRNA; ‡, $p<0.05$ vs. PCSK9 shRNA). Results are shown as the mean and error bars as S.D. Differences between groups were determined via Student's *t* test or one-way ANOVA. Scale bars, (A) 50 μm, (C) 200 μm.

Fig. 3. PCSK9 blocks palmitate-induced ER stress in HepG2 cells. (A,B), Immunoblot and real time PCR analysis of ER stress marker expression in shRNA control and PCSK9 shRNA HepG2 cells treated with vehicle (BSA) or PA (100 or 500 μM) for 24 hours (*, $p<0.05$). (C) Primary human hepatocytes were exposed to medium harvested from HuH7 cells transfected with either WT-PCSK9 or a Q152H-PCSK9 variant that fails to be secreted. Hepatocytes were then treated with PA (500 μM) for 24 hours and assessed for ER stress marker expression via real time PCR (*, $p<0.05$). (D) Cytotoxicity of PA-treated HepG2 cells was also examined using a lactate dehydrogenase assay in the presence or absence of CD36 inhibitor, SSO (10 μM; *, $p<0.05$; †, $p<0.05$ vs. PA). (E) ROS production was assessed by pre-loading cells with DCF, a ROS-sensitive fluorogenic dye, at 1, 2 and 3 hours in HepG2 cells following PA treatment (*, $p<0.05$). (F) The Fura-2-AM Ca^{2+} indicator was used to examine PA-induced ER Ca^{2+} release. Following the incubation of HepG2 cells with PA for 5 hours (500 μM), the SERCA blocker CPA (50 μM) was used to promote the spontaneous release of ER Ca^{2+} to examine total ER Ca^{2+} content (*, $p<0.05$). Results are shown as the mean and error bars as S.D. Differences between groups were determined via Student's *t* test or one-way ANOVA.

Fig. 4. *Pcsk9*$^{-/-}$ mice exhibit compensatory changes in the expression of lipid regulatory proteins. (A) Representative ORO staining of hepatic lipid droplets in *Pcsk9*$^{+/+}$ and *Pcsk9*$^{-/-}$ mice (n=10; C57BL/6J). Protein levels of the lipid droplet marker, perilipin, as well as LDLR, VLDLR and CD36 and the cholesterol efflux transporter, ABCA1, were also examined via immunohistochemistry. (B) Hepatic expression of LDLR, VLDLR and CD36 was also examined using immunoblots. (C,D,E) Fecal cholesterol, total plasma cholesterol and

triglycerides as well as a circulating marker of FA oxidation, β-hydroxybutyrate, were measured using colorimetric assays (n=5). (F) mRNA levels of genes known to play a role in FA metabolism (n=5). Results are shown as the mean and error bars as S.D. *, $p<0.05$ by Student's *t* test or one-way ANOVA. Scale bars, 200 μm.

Fig. 5. PCSK9 reduces ER stress-induced hepatic lipid accumulation. (A) Changes in liver size and gross morphology were first visualized and imaged following the sacrifice of NCD- and HFD-fed *Pcsk9*$^{-/-}$ and *Pcsk9*$^{+/+}$ mice (n=5). (B) Hepatic lipid accumulation was then examined via ORO and H&E. Changes in body and liver weight (C and D), as well as liver triglycerides and cholesterol levels (E) and adipose weights (F) were also examined. Results are shown as the mean and error bars as S.D. *, $p<0.05$ by Student's *t* test or one-way ANOVA. Scale bars, 200 μm.

Fig. 6. PCSK9 knockout exacerbates diet-induced ER stress and inflammation in the livers of mice. (A, B and C) Markers of ER stress (pPERK, pIRE1α, IRE1α, pJNK, sXBP1, peIF2α and CHOP), inflammation (F4/80, TNFα, IL1β, IL6, IL12, TLR1, TLR2, TLR4, ICAM, VCAM and MCP1), fibrosis (fibronectin, αSMA, CTGF) and apoptosis (cCasp12 and Casp12) were examined in the livers of NCD- and HFD-fed mice via immunohistochemical staining, immunoblotting and real time PCR. Hepatic collagen deposition (blue) was also examined via Masson's Trichrome. (D,E) Liver injury was examined via assessment of plasma ALT activity, as well as liver TUNEL staining of apoptotic cells. Results are shown as the mean and error bars as S.D. *, $p<0.05$ by Student's *t* test or one-way ANOVA. Scale bars, 100 μm.

Fig. 7. PCSK9 knockout contributes to gluconeogenesis and diet-induced insulin resistance.
(A) Gluconeogenesis was first examined in PCSK9 shRNA and control shRNA HepG2 cells. Cells incubated in glucose free-medium were treated with either vehicle or the saturated free FA, PA. Glucose content of the medium, occurring as a result of cellular gluconeogenesis, was subsequently quantified using a colorimetric assay (*, $p<0.05$). (B) Gluconeogenesis was also examined in wild-type HepG2 cells exposed to medium harvested from HuH7 cells transfected with either the secreted PCSK9^{WT} or the secretion-defective PCSK9^{Q152H} variant (*, $p<0.05$). (C) One week prior to sacrifice, mice were injected with either insulin (1 IU/kg) or glucose (0.8g/kg) (ITT and GTT, respectively) to assess insulin resistance in NCD- and HFD-fed *Pcsk9*$^{+/+}$ and *Pcsk9*$^{-/-}$ mice (*, $p<0.05$ vs. *Pcsk9*$^{+/+}$). (D) Resting glucose levels were also assessed prior to injections. (E) Resting plasma insulin levels in these mice were examined using an ELISA. (F) Mice were injected with insulin one hour prior to sacrifice to assess hepatic insulin resistance via phosphorylation of AKT via immunoblotting. (G) The expression of pro-gluconeogenic markers (STAT3, G6P, SCD1, PDK1, PDK4 and FMO2) was examined in the livers of HFD-fed mice via real time PCR (*, $p<0.05$. vs. HFD-fed *Pcsk9*$^{+/+}$). Results are shown as the mean and error bars as S.D. *, $p<0.05$. NCD, normal control diet; HFD, high-fat diet; PA, palmitate; ITT, insulin tolerance test; GTT, glucose tolerance test. Differences between groups were determined via Student's *t* test or one-way ANOVA.

Figure 1. Lebeau et al., 2019

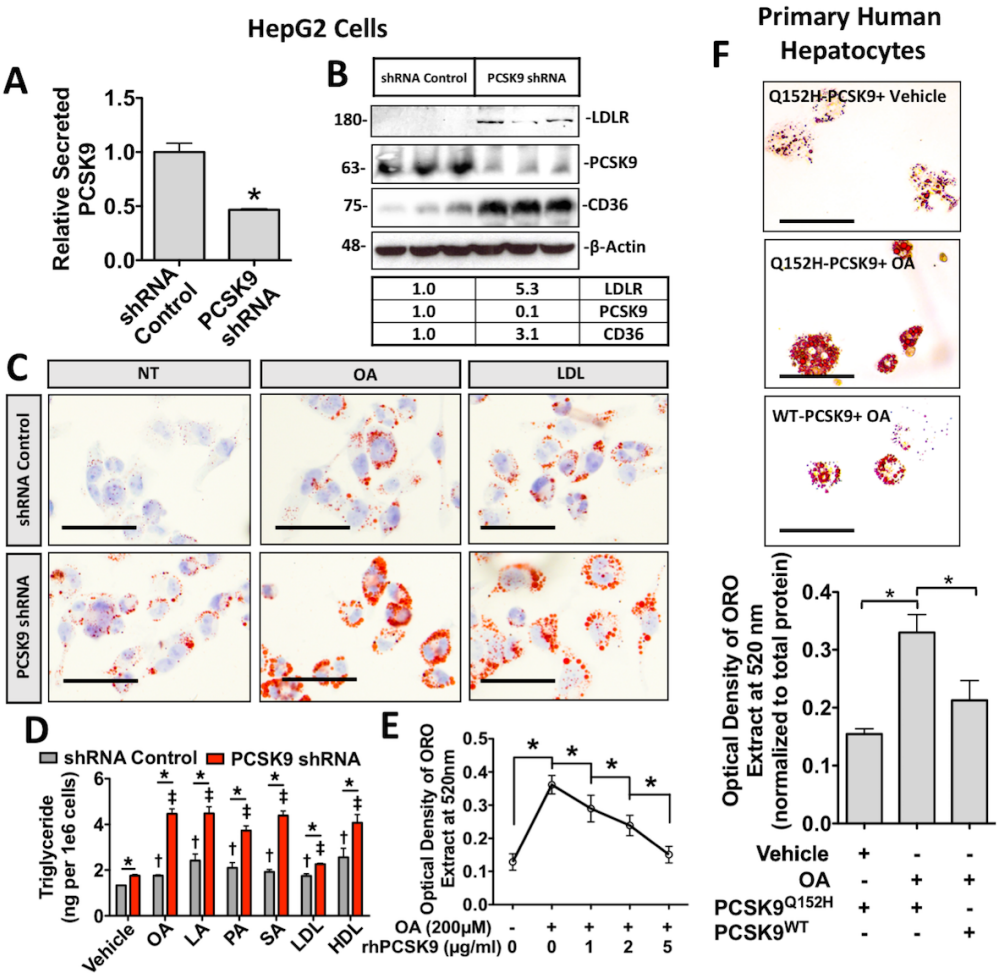

Figure 2. Lebeau et al., 2019

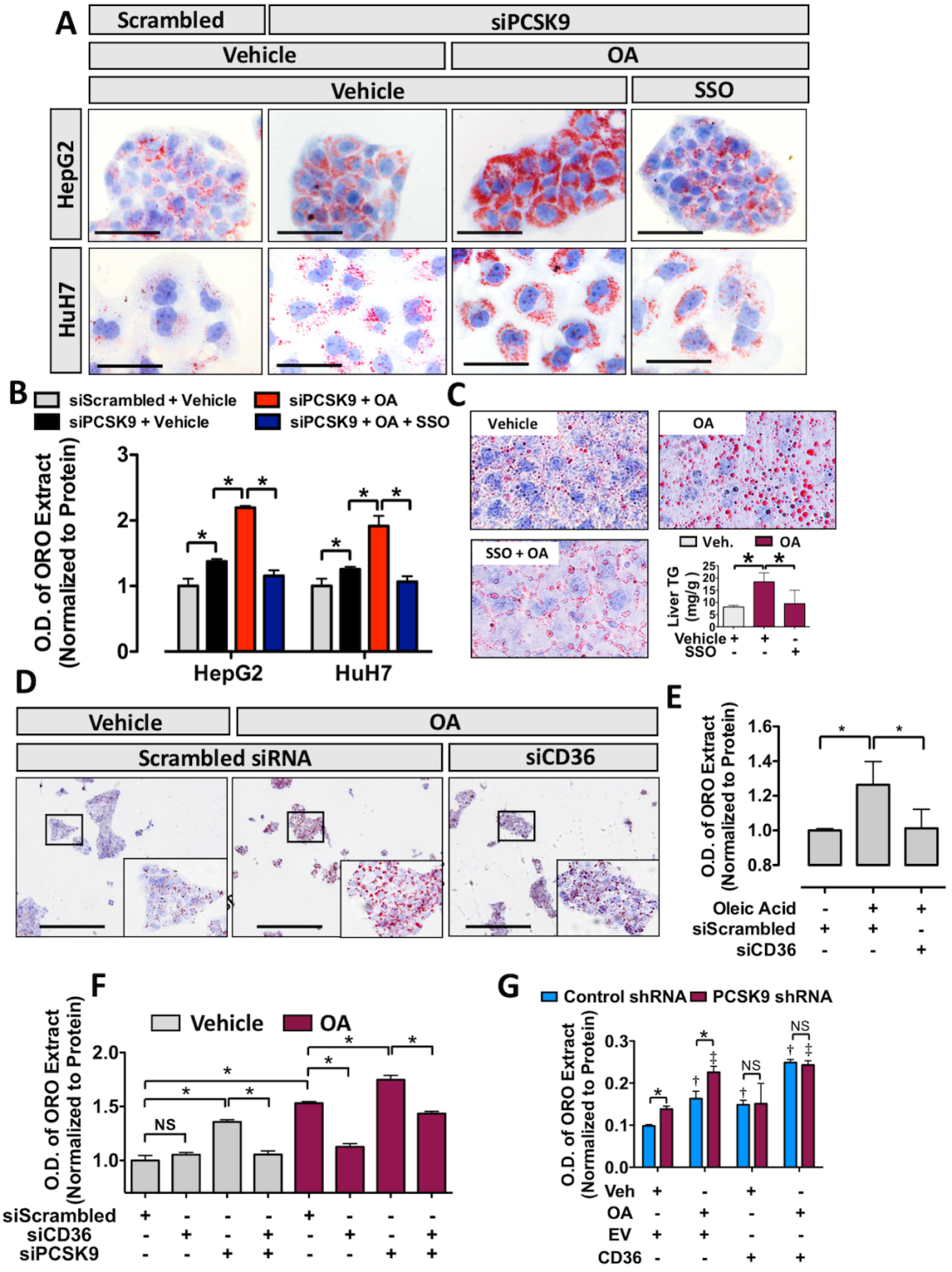

Figure 3. Lebeau et al., 2019

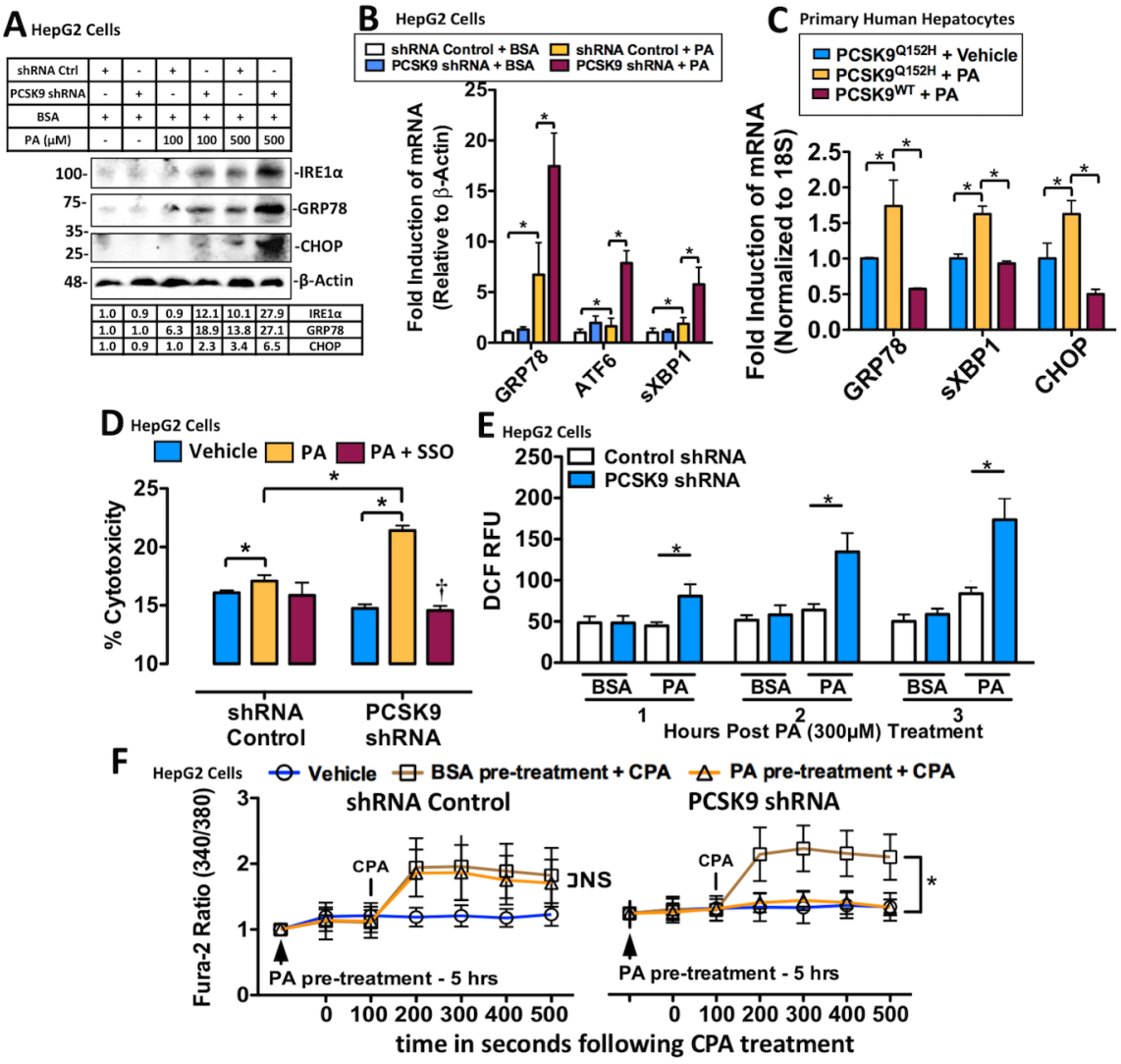

Figure 4. Lebeau et al., 2019

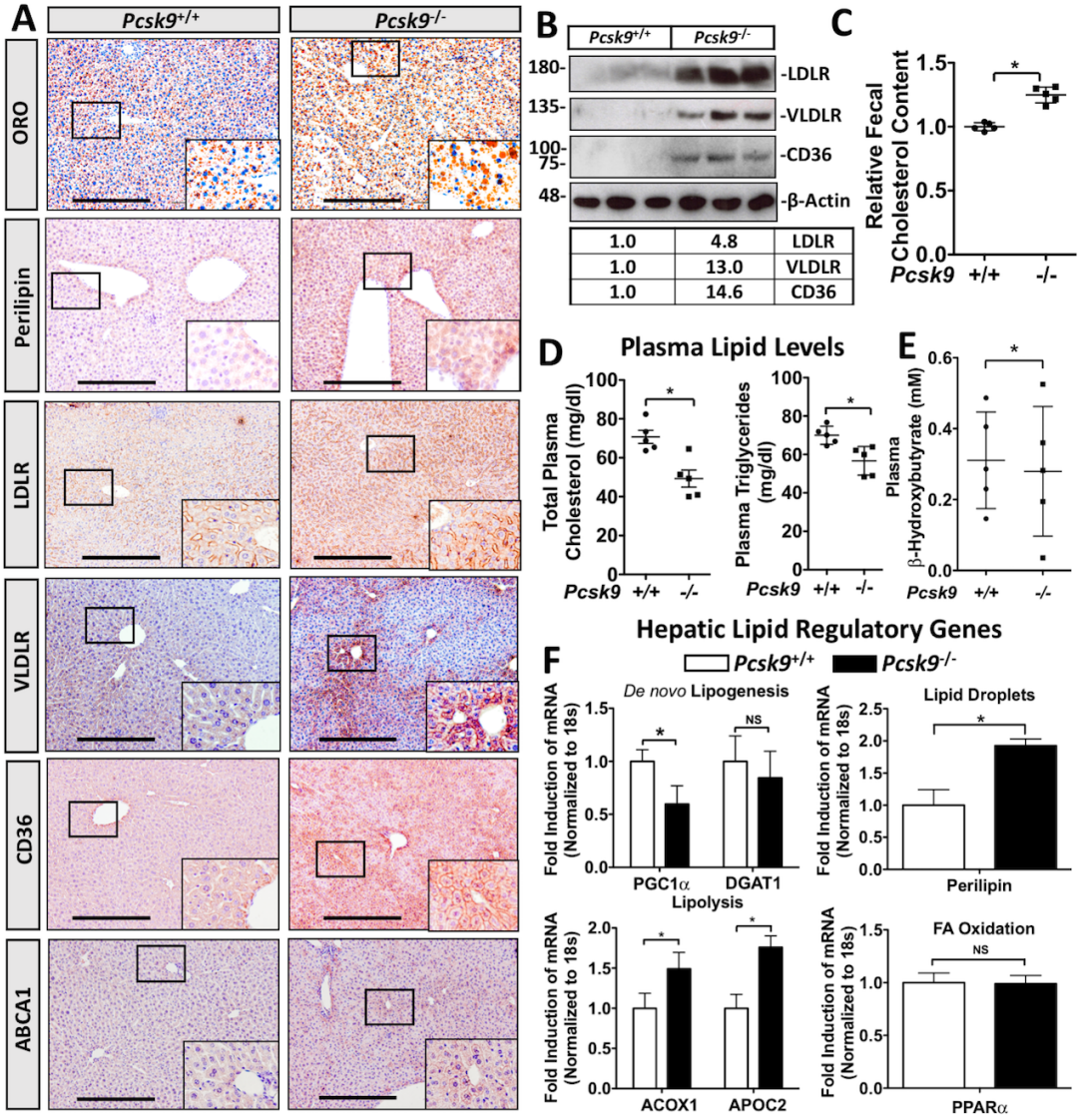

Figure 5. Lebeau et al., 2019

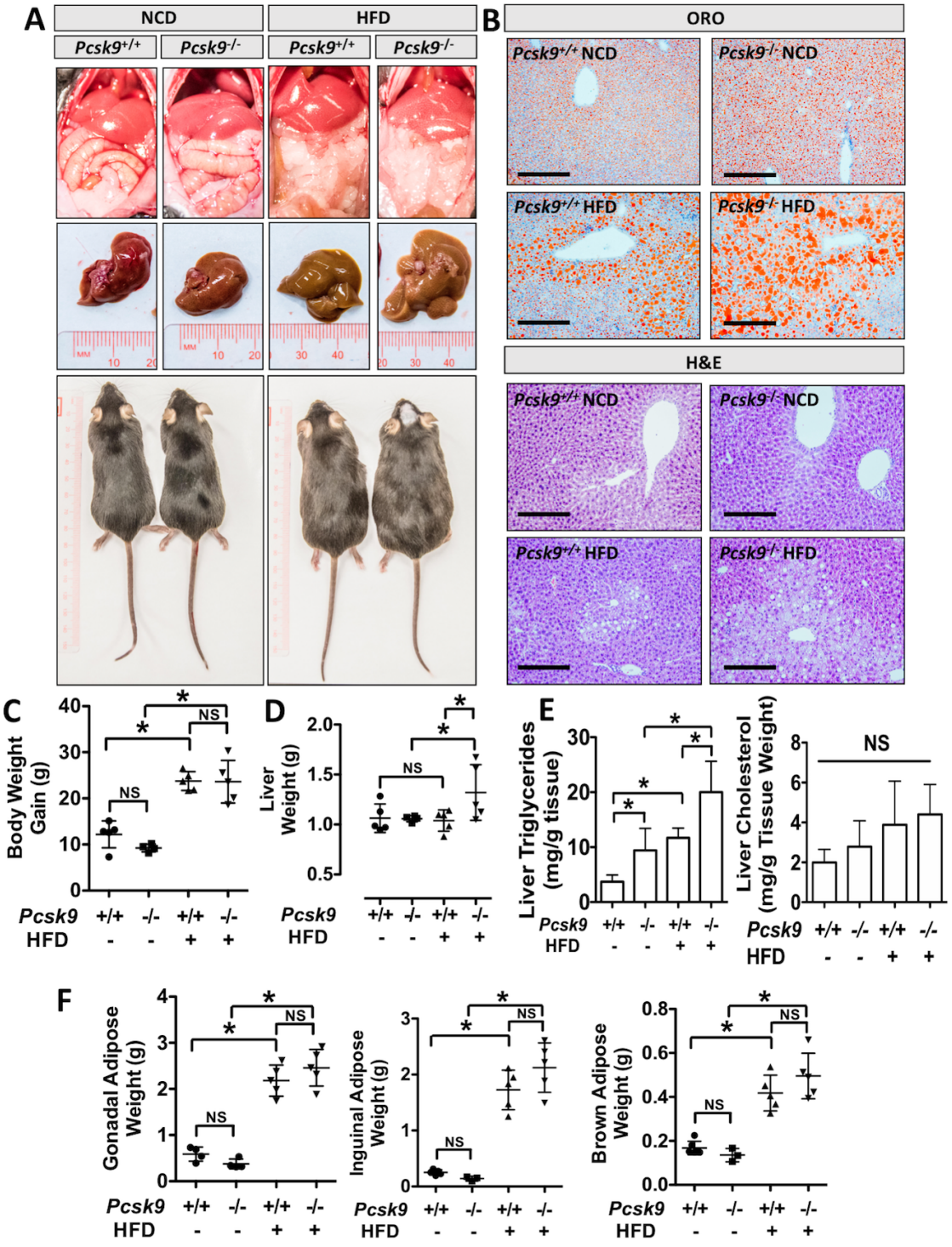

Figure 6. Lebeau et al., 2019

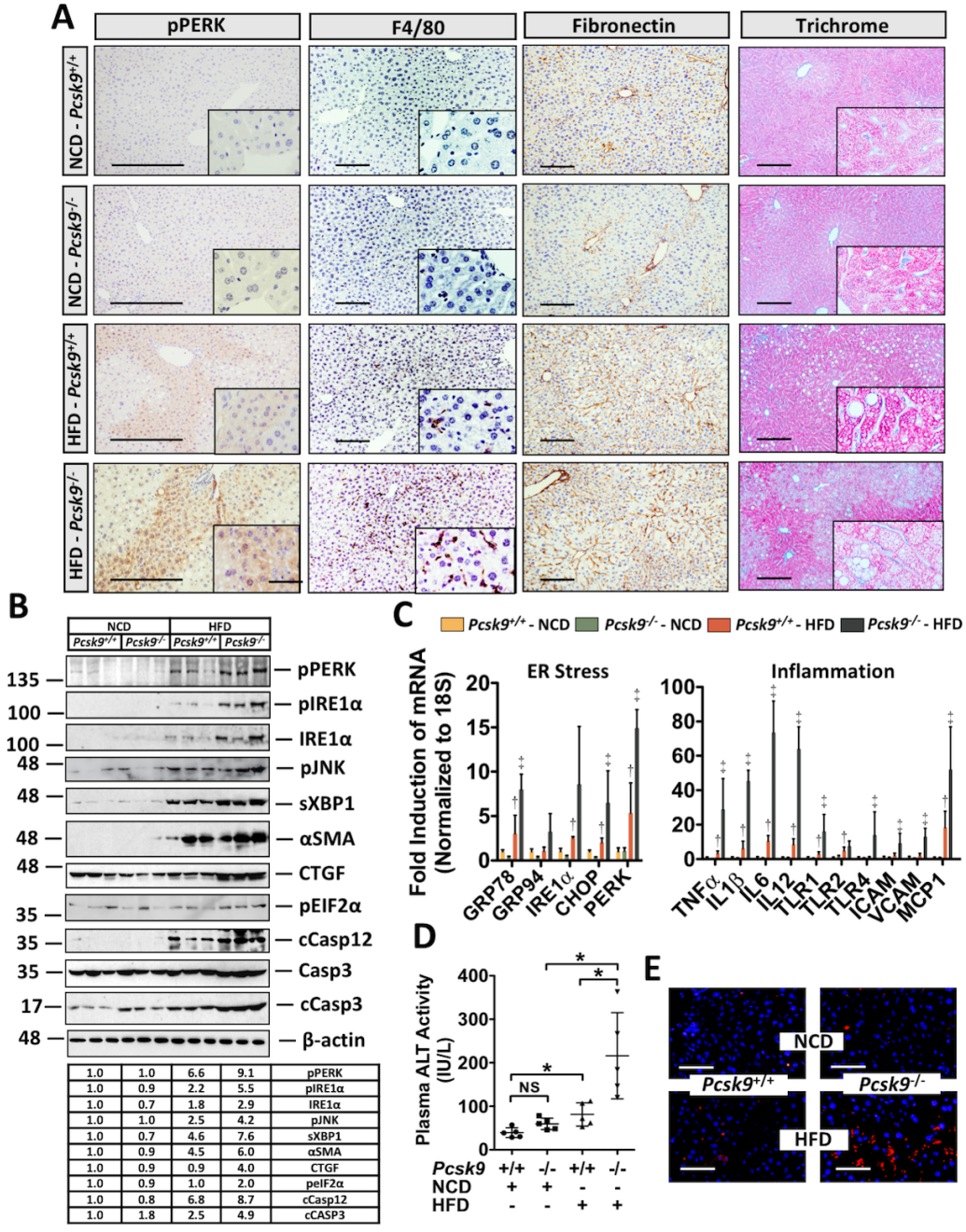

Figure 7. Lebeau et al., 2019

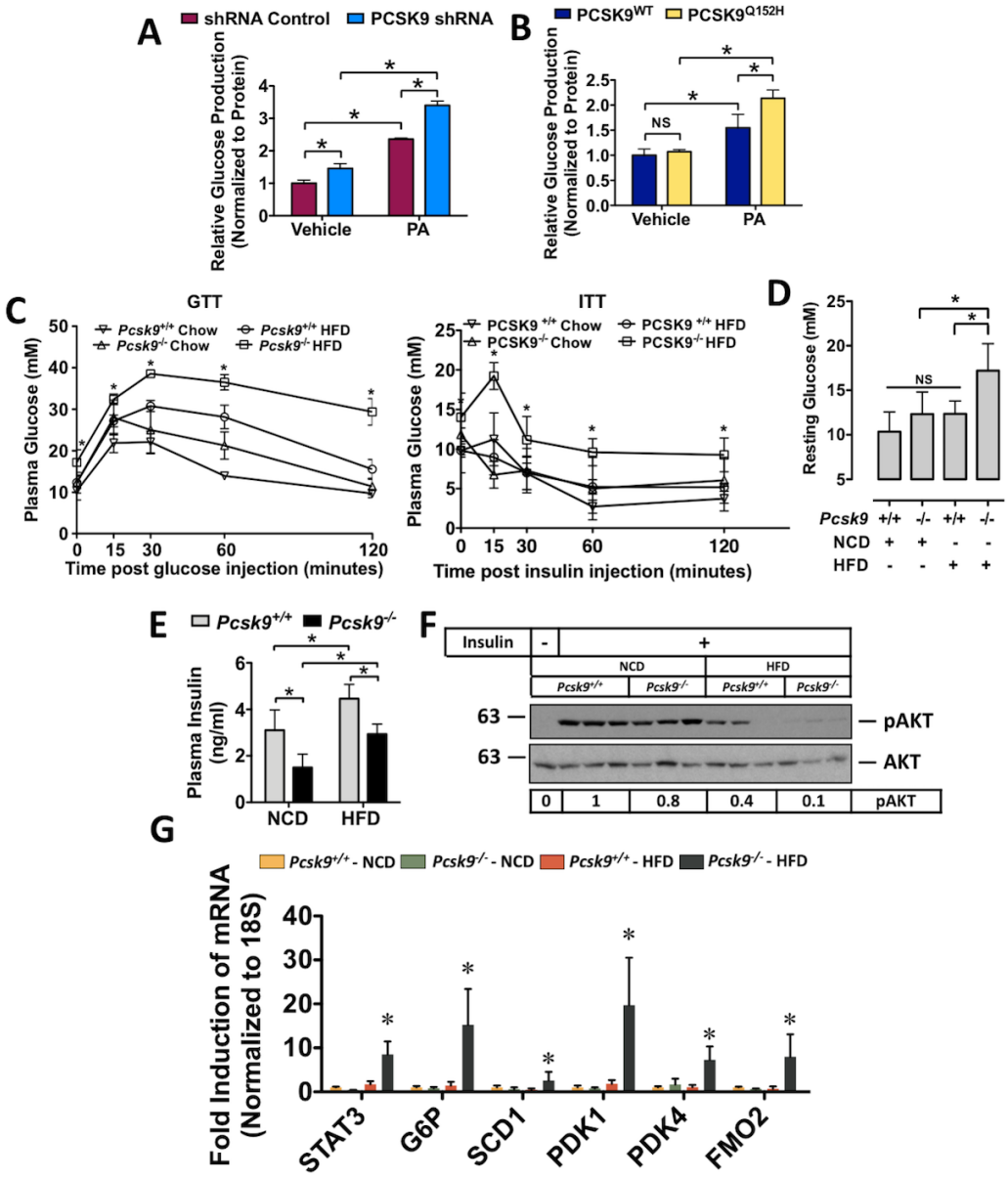

Appendix B: Publication in the Journal of Toxicology and Applied Pharmacology

Toxicology and Applied Pharmacology 349 (2018) 1–7

Contents lists available at ScienceDirect

Toxicology and Applied Pharmacology

journal homepage: www.elsevier.com/locate/taap

High impact short article

Pharmacologic inhibition of S1P attenuates ATF6 expression, causes ER stress and contributes to apoptotic cell death

Paul Lebeau[1], Jae Hyun Byun[1], Tamana Yousof, Richard C. Austin*

Department of Medicine, Division of Nephrology, McMaster University, St. Joseph's Healthcare Hamilton, Hamilton Centre for Kidney Research, Hamilton, Ontario L8N 4A6, Canada

ARTICLE INFO

Keywords:
S1P inhibition
SREBP
ATF6
PF-429242
ER stress
UPR inhibition

ABSTRACT

Mammalian cells express unique transcription factors embedded in the endoplasmic reticulum (ER) membrane, such as the sterol regulatory element-binding proteins (SREBPs), that promote *de novo* lipogenesis. Upon their release from the ER, the SREBPs require proteolytic activation in the Golgi by site-1-protease (S1P). As such, inhibition of S1P, using compounds such as PF-429242 (PF), reduces cholesterol synthesis and may represent a new strategy for the management of dyslipidemia. In addition to the SREBPs, the unfolded protein response (UPR) transducer, known as the activating transcription factor 6 (ATF6), is another ER membrane-bound transcription factor that requires S1P-mediated activation. ATF6 regulates ER protein folding capacity by promoting the expression of ER chaperones such as the 78-kDa glucose-regulated protein (GRP78). ER-resident chaperones like GRP78 prevent and/or resolve ER polypeptide accumulation and subsequent ER stress-induced UPR activation by folding nascent polypeptides. Here we report that pharmacological inhibition of S1P reduced the expression of ATF6 and GRP78 and induced the activation of UPR transducers inositol-requiring enzyme-1α (IRE1α) and protein kinase RNA-like ER kinase (PERK). As a consequence, S1P inhibition also increased the susceptibility of cells to ER stress-induced cell death. Our findings suggest that S1P plays a crucial role in the regulation of ER folding capacity and also identifies a compensatory cross-talk between UPR transducers in order to maintain adequate ER chaperone expression and activity.

1. Introduction

The ER is the intracellular compartment that plays a central role in the synthesis and folding of nascent polypeptides (Austin, 2009). One third of the proteome originates in the ER, consisting primarily of cell-surface and secretory proteins, which undergo post-translational modifications, including disulfide bond formation, *N*-linked glycosylation and proline *cis-trans* isomerization (Schwarz and Blower, 2016; Vincenz-Donnelly and Hipp, 2017).

Due to the constant influx of newly synthesized polypeptides entering the ER, the expression of ER-resident chaperones burdened with the task of protein folding is tightly regulated. GRP78 is a ubiquitously expressed ER chaperone known to promote polypeptide folding, enhance nascent polypeptide chain translocation and resolve the accumulation of misfolded proteins. Perhaps its most well-studied role is its ability to prevent constitutive activation of the UPR by blocking the release of ATF6, IRE1α and PERK at the ER luminal surface (Shen et al., 2002; Lee, 2005; Gardner et al., 2013). Conditions that cause the protein folding requirements of the cell to exceed the protein folding capacity of the ER lead to an accumulation of misfolded polypeptides in the ER lumen. This state of ER stress is associated with numerous human diseases including heritable ER storage diseases, cardiovascular disease, neurodegenerative disease and metabolic disorders (Rutishauser and Spiess, 2002; McAlpine et al., 2010; Xiang et al., 2017).

In order to prevent further misfolding of *de novo* polypeptide chains, GRP78 dissociates from the ER luminal domain of ATF6, IRE1α and PERK, thereby leading to the release of these transducers from the ER and causing UPR activation. Among these “arms of the UPR” is the ATF6 transcription factor; IRE1α which utilizes intrinsic endoribonuclease activity to cleave the X-box-binding protein-1 (XBP1) mRNA to form the active spliced-XBP1 (sXBP1) transcription factor; as well as PERK, which promotes the expression of the pro-apoptotic CCAAT-enhancer-binding protein homologous protein (CHOP). Collectively, this UPR signaling cascade increases the protein folding capacity of the ER, while reducing its burden by blocking global *de novo* protein synthesis (Basseri and Austin, 2008).

Chief among the transcription factors capable of binding to the

* Corresponding author at:50 Charlton Ave East, Room T-3313, Hamilton, Ontario L8N 4A6, Canada.
E-mail address: austinr@taari.ca (R.C. Austin).
[1] Co-first authors.

https://doi.org/10.1016/j.taap.2018.04.020
Received 19 December 2017; Received in revised form 12 April 2018; Accepted 16 April 2018
Available online 22 April 2018
0041-008X/

CCAAT consensus sequence of the ER stress element, is the basic leucine zipper protein ATF6 (Okada et al., 2003). Upon its release from the ER by GRP78, ATF6 translocates to the Golgi complex where it undergoes proteolytic activation by S1P. Other ER stress-inducible transcription factors known to reside in the ER and to be cleaved and activated by S1P are the SREBPs (Brown and Goldstein, 1999); isoforms of the SREBPs consist of SREBP1 and SREBP2, which regulate triglyceride and cholesterol synthesis, respectively. Because SREBPs play a central role in *de novo* lipogenesis, S1P has recently been identified as a putative therapeutic target for the management of dyslipidemia (Hay et al., 2007; Hawkins et al., 2008; Basu et al., 2015).

In the present study we used a pharmacological approach to examine whether blocking S1P would reduce ATF6 expression and lead to UPR activation. Due to the well-established role of the liver in cholesterol synthesis, these studies were carried-out in HuH7 cultured human hepatocytes. S1P was blocked using the aminopyrrolidineamide small-molecule reversible inhibitor, PF, which was first characterized for its hypolipidemic properties from a high throughput screen done in a Pfizer compound library (Hay et al., 2007; Hawkins et al., 2008; Uchida et al., 2016). We show here for the first time that reducing the activation of ATF6, *via* PF-mediated S1P inhibition, is associated with an induction of IRE1α and increased phosphorylation of PERK. We also observed that S1P inhibition increased the susceptibility of cells to cytotoxicity in the presence of ER stress-inducing agent thapsigargin (TG). Because ATF6 is a major regulator of GRP78 expression, which modulates the activation of the UPR, the observed downregulation of GRP78 is a likely cause of IRE1α and PERK induction. Indeed, a compensatory UPR activation to account for reduced ATF6 activity may represent another explanation for these observations. Upon inhibition of IRE1α activity *via* STF-083010 (STF), which did not reduce GRP78 expression, we also observed that cells were more susceptible to TG-induced UPR activation and apoptosis. Taken together, our findings demonstrate that S1P plays a critical role in maintaining the protein folding capacity of the ER and that there exists a compensatory cross-talk between UPR transducers.

2. Materials and methods

2.1. Cell culture and reagents

HuH7, HepG2, HEK293 and DU145 cells were routinely grown in Dulbecco's Modified Eagle's Medium (Gibco, Thermofisher Scientific) supplemented with 10% (v/v) fetal bovine serum (Sigma-Aldrich) and 50 U/ml of penicillin and streptomycin (Sigma-Aldrich). TG, AEBSF, PF, STF and 4-phenylbutyrate (4PBA) were purchased from Sigma-Aldrich (St. Louis, MO, USA). Cells were treated with TG (100 nM), AEBSF (300 μM), PF (10 μM), STF (60 μM) and/or 4PBA (1 mM) for 24 h prior to lysis.

2.2. Transfection and plasmids

Transfection of HuH7 cells was carried-out using XtremeGene HP (Roche Applied Sciences) at a 3:1 ratio with plasmid DNA (3 μl transfection reagent, 1 μg DNA per ml media). The ER stress-activated indicator (ERAI) plasmid used in our studies encodes XBP1 that displays a FLAG antigen upon splicing and removal of the ER stress-specific intron by IRE1α (Iwawaki et al., 2004). This form of FLAG-sXBP1 is lacking its DNA-binding domain and serves strictly as a marker of IRE1α activity with no transcriptional capacity. Inhibition of SREBP2 was achieved using siRNA (200 nM, #4390824, Thermofisher Scientific), which was transfected into HuH7 cells using Lipofectamine RNAiMAX (X13778-030, Invitrogen).

2.3. Immunoblotting and antibodies

Cells were lysed in 4× SDS-PAGE lysis buffer and protein lysates were resolved on 10% polyacrylamide gels in denaturing conditions, as described previously (Lebeau et al., 2017). Following gel electrophoresis, resolved proteins were transferred to nitrocellulose membranes. Membranes were then blocked in 5% skim milk dissolved in 1× Tris-buffered saline with 1% Tween-20 (TBS-T). Incubation of membranes with primary antibodies was carried-out for 18 h at 4 °C. Primary antibodies were diluted in TBS-T containing 1% skim milk, which included the following: anti-ATF6, (70B1413.1, Novus Biologicals), anti-CHOP (#SC-793, Santa Cruz Biotechnology), anti-GRP78 (#610979, BD Bioscience), anti-GRP94 (#ADI-SPA-850, Enzo Life Sciences), anti-IRE1α (#14C10 Cell Signaling Technology), anti-pPERK (#3179S, Cell Signaling Technology) and anti-SREBP2 (#557037, BD Bioscience). Membranes were visualized using the EZ-ECL chemiluminescent reagent (#20-500-500, FroggaBio) and quantified using ImageLab software (BioRad). Quantification of band intensities represent the mean of three replicates, normalized against membranes re-probed for β-actin.

2.4. Reverse transcription and quantitative real-time PCR

Total RNA was extracted using RNeasy Mini kits (#74104, Qiagen) and reverse transcribed to cDNA using Superscript Vilo cDNA Synthesis kit (#11754050, Life Technologies). Real-time PCR was completed using Fast SYBR Green (#4385610, Life Technologies), as described previously (Al-Hashimi et al., 2010).

2.5. Immunofluorescent staining

HuH7 cells were seeded in 4-well chamber slides, transfected with the ERAI plasmid for 48 h and treated with PF or TG 24 h prior to fixation in 4% paraformaldehyde. Following fixation, cells were permeabilized with phosphate-buffered saline (PBS) containing 0.025% Triton-X, blocked in PBS containing 1% bovine serum albumin and incubated in primary antibodies targeted against FLAG (1:100; F3165, Sigma Aldrich) for 1 h. Cells were then washed in PBS containing 1% tween and incubated with Alexa 488 fluorescently-labelled secondary antibody (1:200; #A32723, ThermoFisher Scientific) for 45 min. Actin and nuclei were stained using rhodamine phalloidin (#R415, ThermoFisher Scientific) and DAPI (Sigma-Aldrich), respectively. Immunofluorescent staining of ATF6 was carried-out with the same protocol as mentioned above using an anti-ATF6 antibody (1:100; Enzo Life Sciences, 70B1413.1). TUNEL assays, which stain DNA damage, were used to assess cell apoptosis. After fixation of cells in 4% paraformaldehyde, TUNEL assays were carried-out as per manufacturer's instructions (#4810–30-CK, Trevigen). Briefly, HuH7 cells were incubated with terminal deoxynucleotidyl transferase, which biotinylates damaged DNA, for 1 h at 37 °C. Biotinylated DNA was then labelled *via* incubation with streptavidin-594 (1:200 in PBS) for an additional hour at room temperature. 5 representative images of TUNEL-stained cells from each treatment group were quantified using ImageJ software (U. S. National Institute of Health).

2.6. Lactate dehydrogenase cytotoxicity assay

Lactate dehydrogenase cytotoxicity assays were performed as per manufacturer's instructions (#04744926001, Roche Applied Sciences).

2.7. Measurement of cellular reactive oxygen species

HuH7 cells were seeded in a black clear-bottom 96-well plate and permitted to adhere for 24 h. Live cells were then washed with Hank's Balanced Salt Solution (HBSS) containing 20 mM HEPES and loaded with DCFDA (25 μM, #D6883, Sigma-Aldrich) *via* incubation for 1 h at 37 °C. DCFDA-containing HBSS was then washed off and an additional 100 μl of HBSS and treatments were added to each well. DCFDA relative fluorescence units (RFU) were measured using the Gemini EM Microplate Reader at 37 °C for 18 h with the excitation and emission

wavelengths of 480 and 515 nm, respectively.

2.8. Isolation of primary hepatocytes

A two-step hepatic perfusion of collagenase (0.05% in HEPES buffer, Sigma) and EGTA (500 M in HEPES buffer, Sigma) was used in 12-week-old male C57bl/6 mice to isolate fresh primary hepatocytes. Following harvest, cells were washed, separated *via* centrifugation and cell strainers and plated at a confluence of 1×10^6 cells/well in William's E medium (Gibco, Thermo Fisher Scientific) supplemented with 10% fetal bovine serum, 100 IU/ml penicillin, and 100 g/ml streptomycin.

2.9. Statistical analysis

Error bars are represented as standard deviation of the mean. Statistical significance was calculated using unpaired Student's *t*-tests. Comparisons between means of immunoblot quantifications was done using one-way ANOVA.

3. Results

3.1. PF blocks ATF6 activation and GRP78 expression

The role of S1P in the activation of ATF6 and expression of GRP78 was explored in HuH7 cells *via* treatment with PF for 24 h. Our data demonstrate that PF significantly reduced the abundance of nuclear ATF6 (nATF6; Fig. 1A) and expression of GRP78, whether in the presence or absence of the ER stress-inducing agent TG (Fig. 1B). Consistent with our previous findings (Lebeau et al., 2017), we observed that PF blocked SREBP2 activation and reduced the abundance of a downstream target of SREBP2 transcriptional activity, the proprotein convertase subtilisin/kexin type-9 (PCSK9). Immunoblot findings were confirmed *via* real-time PCR of cells treated with PF as well as the serine protease inhibitor AEBSF (Fig. 1C). The effect of PF on GRP78 and ATF6 expression was also examined in HepG2 immortalized human hepatocytes *via* real-time PCR (Fig. 1D). Given that PF blocks the S1P-mediated proteolytic cleavage of ATF6 in the Golgi complex, we also examined the effect of PF on TG-induced nuclear localization of ATF6 *via* immunofluorescence staining (Fig. 1E). Our findings demonstrate that upon treatment of HuH7 cells with TG, ATF6 localizes to the nucleus, as well as the perinuclear region of the cell. In the presence of PF, however, TG-induced nuclear localization of ATF6 was not observed; rather a distinct accumulation of ATF6 was observed in the perinuclear compartments of the cell (white arrows), likely the ER or Golgi.

3.2. Pharmacologic inhibition of S1P induces UPR activation

Given the well-established role of GRP78 as a sensor/repressor of UPR transducers, and that inhibition of S1P downregulates GRP78 (Okada et al., 2003), we investigated whether treatment of PF would lead to UPR activation. After a 24 h treatment with PF, a significant upregulation of the remaining two arms of the UPR, PERK and IRE1α, was observed in HuH7 cells (Fig. 2A). We also observed a marked increase in the expression of GRP94; another member of the heat-shock protein (HSP) family of proteins, which in contrast to GRP78 was not downregulated by S1P inhibition. Given the significant induction of IRE1α by PF, the splicing of XPB1 was also examined in HuH7 cells transfected with the ERAI plasmid *via* immunofluorescence staining. Consistent with the observed PF-mediated increase in IRE1α expression was a concomitant increase in cells that stained positive for sXBP1 (Fig. 2B and C). The effect of PF on UPR activation was also confirmed in freshly isolated primary mouse hepatocytes (Fig. 2D), human embryonic kidney (HEK293) and HepG2 cells *via* real-time PCR (Fig. 2E and F) and immunoblots (Fig. 2G and H). Consistent with our observations in immortalized cultured human hepatocytes (HuH7), we

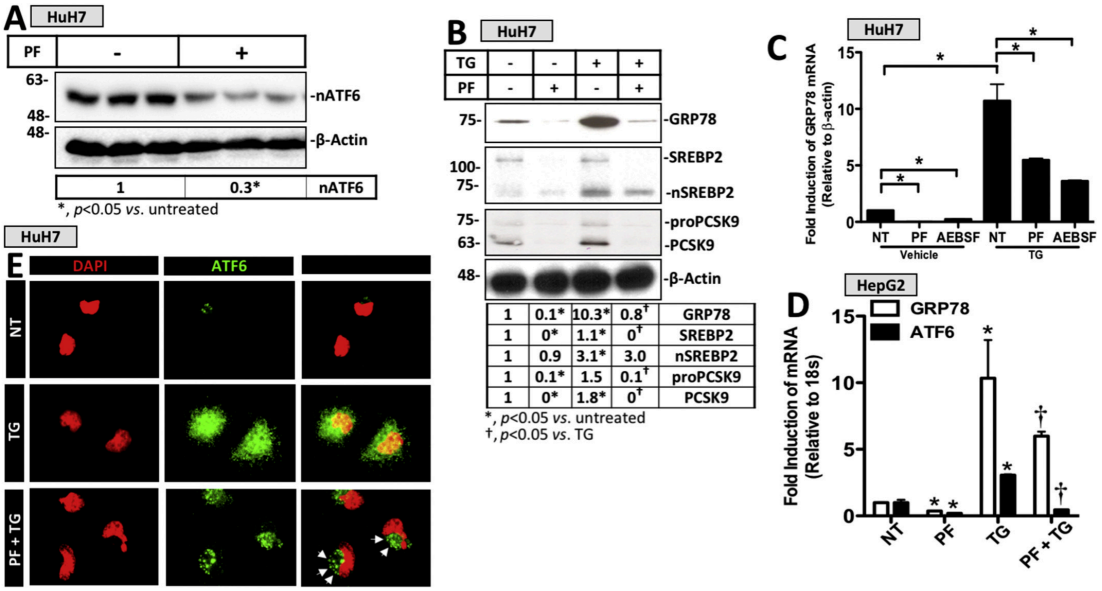

Fig. 1. PF-429242 (PF) blocks ATF6 activation and GRP78 expression. (a and b) Immunoblots of HuH7 cells incubated with PF (10 μM) in the presence or absence of thapsigargin (TG; 100 nM) for 24 h show that PF blocks nuclear ATF6 (nATF6), GRP78, nuclear SREBP2 (nSREBP2) and PCSK9 expression. (c) Transcriptional repression of GRP78 mRNA by S1P inhibitors AEBSF and PF was also examined using real-time PCR 8 h post-treatment (*, $p < 0.05$). (d) PF-mediated inhibition of GRP78 and ATF6 was also examined in HepG2 cells *via* real-time PCR (*, $p < 0.05$ *vs.* NT; †, $p < 0.05$ *vs.* TG). (e) PF-mediated inhibition of ATF6 nuclear localization was also observed in HuH7 cells treated with TG *via* immunofluorescence staining.

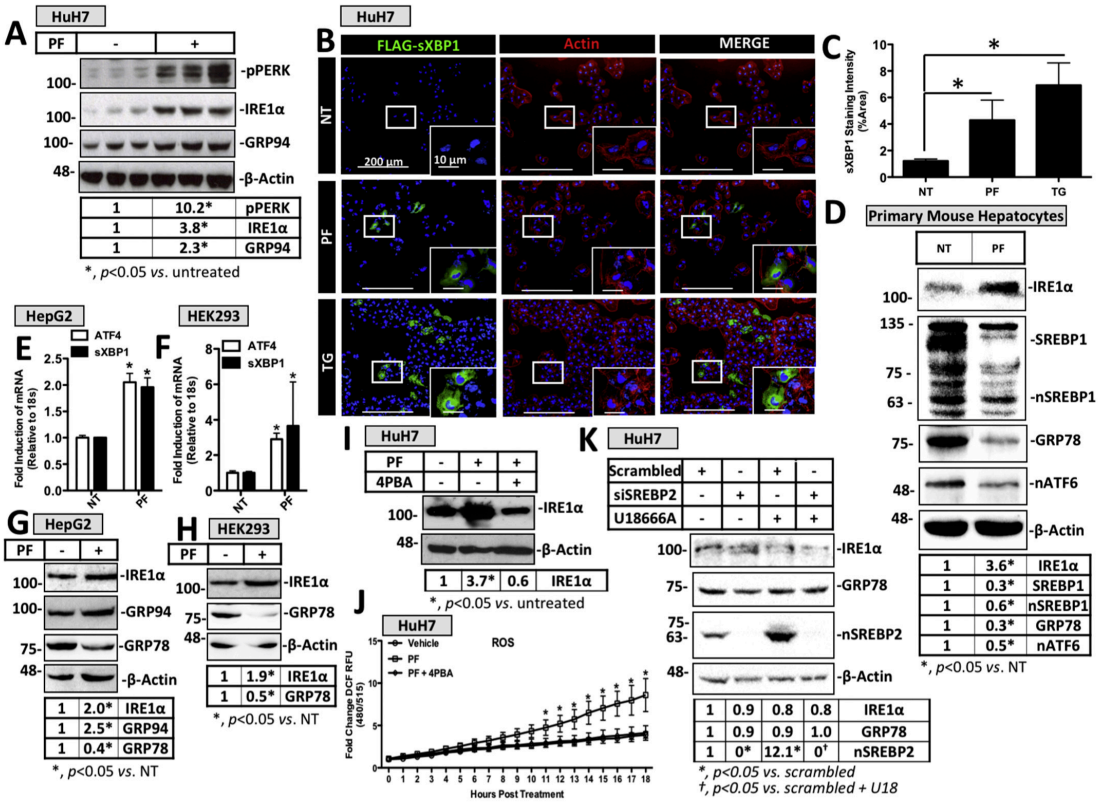

Fig. 2. Pharmacologic inhibition of S1P induces UPR activation. (a) UPR markers phospho-PERK (pPERK), IRE1α and GRP94 were examined in HuH7 cells incubated with PF-429242 (PF; 10 μM), *via* immunoblots. (b) The PF-mediated splicing of XBP1 (sXBP1) was examined in HuH7 cells transfected with the ER-activated indicator (ERAI) plasmid using immunofluorescence staining. ERAI-transfected cells were also treated with ER stress-inducing agent thapsigargin (TG; 100 nM) to serve as a positive control. (c) Quantification of ERAI positive staining using ImageJ (*, $p < 0.05$ *vs.* NT). (d, e, f, g and h) The effect of PF on UPR marker expression was confirmed *via* real-time PCR and immunoblots in mouse primary hepatocytes, HepG2 and HEK293 cells. (i) The reversibility of PF-induced ER stress was also examined *via* pre-treatment of cells with the small chemical chaperone 4-phenylbutyrate (4PBA, 1 mM) using immunoblots. (j) PF-mediated cellular reactive oxygen species (ROS) production was also examined in HuH7 cells in the presence and absence of 4PBA using a DCF assay during an 18 h treatment time-course (*, $p < 0.05$ *vs.* Vehicle). (k) The effect of SREBP2 inhibition on UPR marker expression was examined in HuH7 cells transfected with siRNA targeted against SREBP2 (siSREBP2) in the presence and absence of an agent that induces SREBP2 activation, U18666A (Basu et al., 2015).

observed that a 24 h treatment of PF (10 μM) blocked the expression of GRP78 but increased the expression of UPR markers ATF4, sXBP1, IRE1α and GRP94. SREBP1 expression was also examined in PF-treated primary hepatocytes and found to be significantly reduced, which is consistent with that of the other S1P-regulated transcription factors, ATF6 and SREBP2.

To confirm that the PF-mediated induction of IRE1α occurred in a manner dependent on ER stress, HuH7 cells were treated with 4PBA; a small chemical chaperone well-known to alleviate ER stress (Basseri et al., 2009; Liu et al., 2016). Consistent with our findings in Fig. 2A, we observed that PF increased the cellular abundance of IRE1α and that this increase was blocked in the presence of 4PBA (Fig. 2I). The production of reactive oxygen species (ROS), a process closely related to ER stress (Zeeshan et al., 2016), was also examined in PF-treated HuH7 cells (Fig. 2J). Our data show that PF caused a significant increase in cellular ROS starting at the 11 h time point, which persisted until the 18 h endpoint. Consistent with findings in Fig. 2I, we also observed that 4PBA abolished PF-mediated ROS production, likely due to its ability to attenuate ER stress. Because of the dual role of S1P in activation of the SREBPs and ATF6, we next examined whether the inhibition of SREBP2 would lead to UPR activation. Despite the significant siRNA-mediated reduction in the nuclear form of SREBP2 (nSREBP2), immunoblots reveal that GRP78 and IRE1α were not affected (Fig. 2K). Furthermore, the expression of UPR markers was not altered upon induction of SREBP2 *via* U18666A, an agent that causes intracellular sterol deprivation (Basu et al., 2015).

3.3. Inhibition of S1P leads to ER stress-induced cell death

It is well-established that prolonged ER stress promotes programmed cell death in a manner dependent on the UPR mediator CHOP (Szegezdi et al., 2006). Despite the observed UPR activation in response to PF, our findings demonstrate that an additional stimulus by the ER stress-inducing agent TG was required for PF to elicit an effect on CHOP expression (Fig. 3A) and cytotoxicity (Fig. 3B) in HuH7 cells. Given that a number of inhibitors of the UPR have been shown to reduce the onset and progression of a variety of cancer types, the pro-apoptotic effect of PF-mediated ATF6 inhibition was also examined in a well-established prostate cancer cell line DU145 (Fig. 3C). Consistent with our previous observation that 4PBA attenuated PF-induced UPR activation, we also

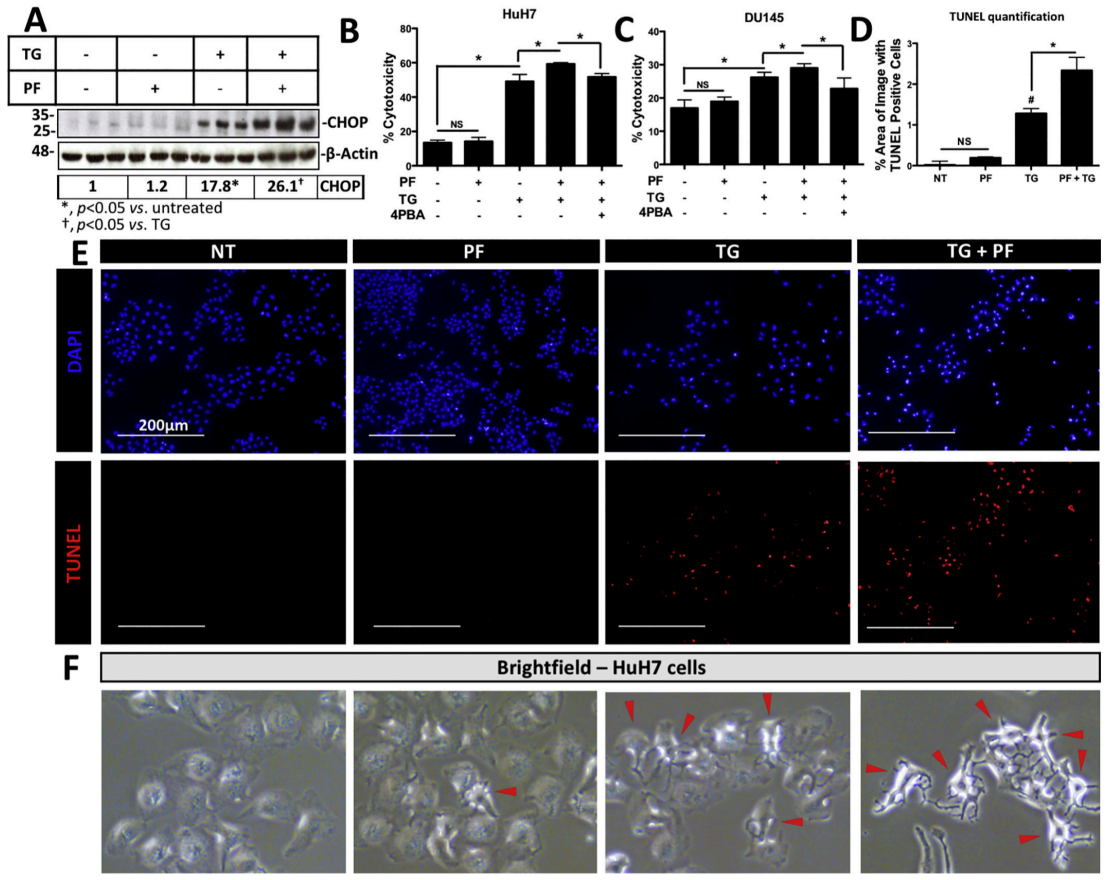

Fig. 3. Inhibition of S1P leads to ER stress-induced cell death. (a) Expression of the pro-apoptotic UPR marker, CHOP, was examined in HuH7 cells treated with PF-429242 (PF, 10 µM) in the presence and absence of ER stress-inducing agent thapsigargin (TG; 100 nM) using immunoblots. (b and c) Cell death was assessed in these cells, as well as DU145 prostate cancer cells, *via* lactate dehydrogenase cytotoxicity assays (*, $p < 0.05$). The role of ER stress in the observed cell death was confirmed *via* pre-treatment of cells with the small chemical chaperone 4-phenylbutyrate (4PBA; 1 mM), which significantly reduced cytotoxicity. (d and e) Apoptosis was also examined in PF-treated HuH7 cells in the presence and absence of TG using a TUNEL assay (red) (#, $p < 0.05$ *vs.* NT; *, $p < 0.05$). (f) PF-mediated changes in cell morphology were examined in the presence and absence of TG using light microscopy. (For interpretation of the references to colour in this figure legend, the reader is referred to the web version of this article.)

observed that 4PBA reduced PF-induced cytotoxicity in HuH7 and DU145 cells. To examine apoptosis specifically, a TUNEL assay was carried-out and also revealed that TG is required to attain a PF-mediated increase in cell death (Fig. 3D and E). Furthermore, we observed an increase in the TG-mediated shrinking and budding of cells (red arrows) in the presence of PF; a well-established morphological hallmark of apoptosis (Fig. 3F).

3.4. Inhibition of IRE1α, via STF, exacerbates TG-mediated UPR activation but does not block GRP78 expression

To investigate whether PF-mediated UPR activation occurred solely as a result of reduced GRP78 expression, or also as a result of a compensatory response of the UPR, cells were treated with an inhibitor of IRE1α that fails to reduce GRP78 expression. To confirm effective STF-mediated inhibition of IRE1α activity, sXBP1 was examined *via* real-time PCR. These data demonstrate that STF significantly reduced the cellular abundance of sXBP1, the downstream marker of IRE1α activity, whether in the presence or absence of TG (Fig. 4A). The STF-mediated effect on UPR marker expression was then examined *via* real-time PCR and immunoblot analysis (Fig. 4B and C). In a consistent manner, these data demonstrate that STF treatment failed to induce GRP78 and CHOP expression; however, in the presence of TG, STF significantly increased the cellular abundance of both UPR markers. In support of the PF findings, TUNEL assay data also demonstrate that STF treatment required an additional ER stress-inducing stimulus to elicit a significant increase in cell death (Fig. 4D and E).

4. Discussion

Accumulating evidence implicates S1P as a major regulator of cholesterol due to its role in the activation of SREBP1/2 (Brown and Goldstein, 1999; Hawkins et al., 2008; Hyrina et al., 2017). In support of this, we have recently demonstrated that inhibition of S1P, *via* AEBSF and PF, blocks the activation of SREBP2 and PCSK9 expression (Lebeau et al., 2017). In addition to the SREBPs, S1P is also known to mediate

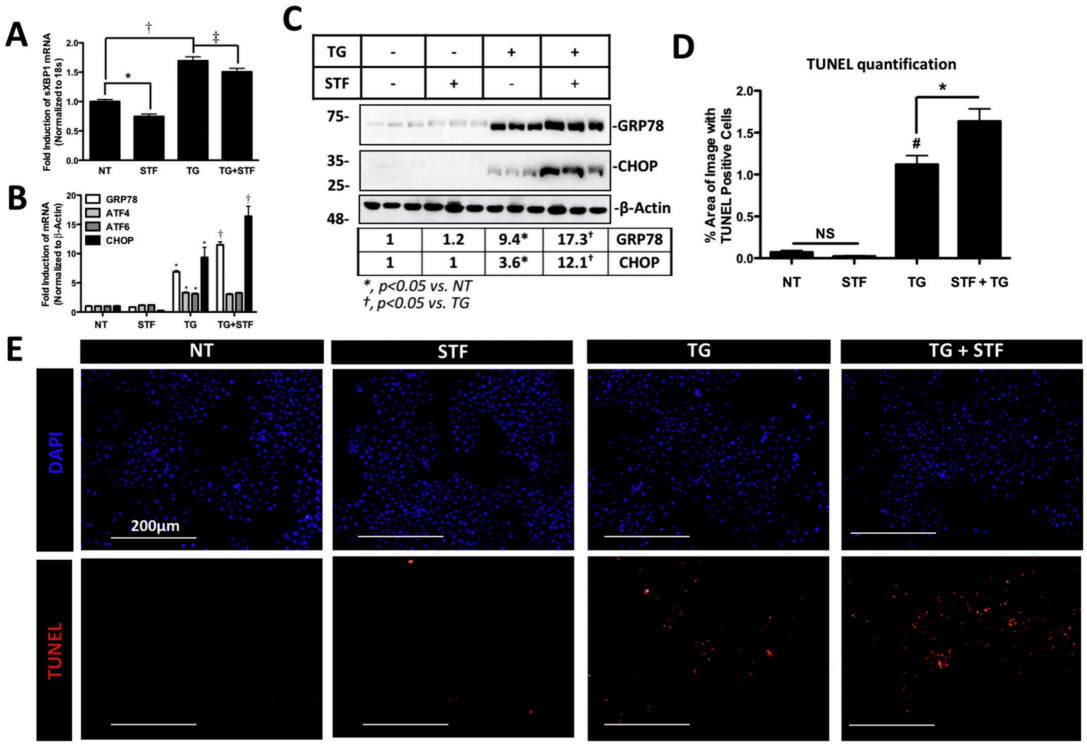

Fig. 4. Inhibition of IRE1α, *via* STF-083010 (STF), exacerbates thapsigargin (TG)-mediated UPR activation but does not block GRP78 expression. (a) STF-mediated IRE1α inhibition was assessed *via* analysis of mRNA levels of spliced-XBP1 (sXBP1); a downstream target of IRE1α endoribonuclease activity. (b and c) Real-time PCR and immunoblots of UPR markers GRP78, ATF4, ATF6 and CHOP in HuH7 cells incubated with STF in the presence or absence of ER stress-inducing agent TG (100 nM; *, $p < 0.05$ *vs.* NT; †, $p < 0.05$ *vs.* TG). (d and e) Apoptosis in STF/TG-treated cells was also examined *via* TUNEL assay (red). (For interpretation of the references to colour in this figure legend, the reader is referred to the web version of this article.)

the activation of the ATF6 transcription factor that plays a central role in the transcriptional regulation of ER chaperones, such as GRP78 (Li et al., 2000). Given that GRP78 promotes the folding and maturation of nascent polypeptides and acts as a repressor of ATF6, IRE1α and PERK function, we investigated whether S1P inhibition would lead to UPR activation.

Despite the potential benefits associated with S1P inhibitor-mediated cholesterol lowering (Hawkins et al., 2008; Basu et al., 2015), the major finding of this study suggests that S1P plays a crucial role in maintaining ER chaperone expression and ER folding capacity. Our findings demonstrate that inhibition of S1P leads to UPR activation in the absence of additional ER stress-inducing stimuli (Fig. 2). While S1P inhibition did not induce a significant level of cytotoxicity, a significant increase in cytotoxicity was observed in the presence of TG (Fig. 3).

Given that S1P regulates the activation of SREBP1/2 and ATF6 (Velho et al., 2017), which are both ER stress-inducible proteins (Colgan et al., 2007), we also examined whether inhibition of SREBP2 corresponded with UPR activation using small-interfering RNA (Fig. 2K). We observed that inhibition of SREBP2 expression did not yield UPR activation, suggesting that S1P inhibition promotes UPR activation in a manner dependent on ATF6 and/or GRP78. Because GRP78 has intrinsic chaperone activity and plays a major role in the repression of UPR activation, it remains unclear whether PF-mediated downregulation of GRP78 contributes to UPR activation *via* liberation of the UPR transducers from the ER or as a compensatory response to reduced ATF6 and GRP78 chaperone activity.

In support of the notion by which S1P inhibition promotes UPR activation as a compensatory response, we also observed that IRE1α inhibition increased the susceptibility of cells to TG-induced ER stress despite not having an effect on GRP78 expression (Fig. 4C). Accumulating evidence suggests that the three arms of the UPR work in concert to maintain ER folding capacity and cellular homeostasis. ATF6$^{-/-}$ mice exhibit increased hepatic lipid accumulation and UPR activation in response to ER stress-inducing agent tunicamycin (Yamamoto et al., 2010). Similarly, liver-specific PERK$^{-/-}$ mice exhibit increased tunicamycin-mediated hepatic apoptosis (Teske et al., 2011). Inhibition of the UPR was also shown to cause severe atrophy in cultured myotubules, a process known to contribute to skeletal muscle wasting in cancer patients (Bohnert et al., 2016).

The UPR is emerging as a therapeutic target due to its well-established role in the onset and progression of a variety of human diseases (Maly and Papa, 2014; Nagelkerke et al., 2014). Inhibitors of IRE1α activity and PERK have been shown to reduce the progression of atherosclerosis and various cancers including multiple myeloma and pancreatic cancer (Atkins et al., 2013; Chien et al., 2014; Feng et al., 2017; Tufanli et al., 2017). The present study supports the notion that networks of the UPR are fully integrated and act in concert to maintain ER chaperone activity. Inhibitors of S1P and the UPR may confer significant protection against dyslipidemia or disease in tissues laden by chronic UPR activation. However, given that blocking ATF6 and IRE1α can promote cell death in conditions that increase ER burden, the long-term systemic effect of such inhibitors remains to be elucidated.

Funding

This work was supported in part by research grants to Richard C. Austin from the Heart and Stroke Foundation of Ontario (T-6146), the Heart and Stroke Foundation of Canada (G-13-0003064 and G-15-0009389) and the Canadian Institutes of Health Research (74477).

Conflicts of interest

The McMaster University Animal Research Ethics Board approved all procedures used for primary hepatocyte isolation.

Acknowledgements

We would like to thank Dr. Masayuki Miura, University of Tokyo, for the ERAI plasmid. "Dr. Richard C. Austin is a career investigator of the Heart and Stroke Foundation of Ontario" and that "this research was made possible by the generous support of St. Joseph's Healthcare Hamilton."

References

Al-Hashimi, A.A., Caldwell, J., Gonzalez-Gronow, M., Pizzo, S.V., Aboumrad, D., Pozza, L., Al-Bayati, H., Weitz, J.I., Stafford, A., Chan, H., Kapoor, A., Jacobsen, D.W., Dickhout, J.G., Austin, R.C., 2010. Binding of anti-GRP78 autoantibodies to cell surface GRP78 increases tissue factor procoagulant activity via the release of calcium from endoplasmic reticulum stores. J. Biol. Chem. 285, 28912–28923.

Atkins, C., Liu, Q., Minthorn, E., Zhang, S.Y., Figueroa, D.J., Moss, K., Stanley, T.B., Sanders, B., Goetz, A., Gaul, N., Choudhry, A.E., Alsaid, H., Jucker, B.M., Axten, J.M., Kumar, R., 2013. Characterization of a novel PERK kinase inhibitor with antitumor and antiangiogenic activity. Cancer Res. 73, 1993–2002.

Austin, R.C., 2009. The unfolded protein response in health and disease. Antioxid. Redox Signal. 11, 2279–2287.

Basseri, S., Austin, R.C., 2008. ER stress and lipogenesis: a slippery slope toward hepatic steatosis. Dev. Cell 15, 795–796.

Basseri, S., Lhotak, S., Sharma, A.M., Austin, R.C., 2009. The chemical chaperone 4-phenylbutyrate inhibits adipogenesis by modulating the unfolded protein response. J. Lipid Res. 50, 2486–2501.

Basu, D., Huq, A., Iqbal, J., Hussain, M.M., Jiang, X.C., Jin, W., 2015. Hepatic S1P deficiency lowers plasma cholesterol levels in apoB-containing lipoproteins when LDLR function is compromised. Nutr. Metab. (Lond.) 12, 35.

Bohnert, K.R., Gallot, Y.S., Sato, S., Xiong, G., Hindi, S.M., Kumar, A., 2016. Inhibition of ER stress and unfolding protein response pathways causes skeletal muscle wasting during cancer cachexia. FASEB J. 30, 3053–3068.

Brown, M.S., Goldstein, J.L., 1999. A proteolytic pathway that controls the cholesterol content of membranes, cells, and blood. Proc. Natl. Acad. Sci. U. S. A. 96, 11041–11048.

Chien, W., Ding, L.W., Sun, Q.Y., Torres-Fernandez, L.A., Tan, S.Z., Xiao, J., Lim, S.L., Garg, M., Lee, K.L., Kitajima, S., Takao, S., Leong, W.Z., Sun, H., Tokatly, I., Poellinger, L., Gery, S., Koeffler, P.H., 2014. Selective inhibition of unfolded protein response induces apoptosis in pancreatic cancer cells. Oncotarget 5, 4881–4894.

Colgan, S.M., Tang, D., Werstuck, G.H., Austin, R.C., 2007. Endoplasmic reticulum stress causes the activation of sterol regulatory element binding protein-2. Int. J. Biochem. Cell Biol. 39, 1843–1851.

Feng, Y.X., Jin, D.X., Sokol, E.S., Reinhardt, F., Miller, D.H., Gupta, P.B., 2017. Cancer-specific PERK signaling drives invasion and metastasis through CREB3L1. Nat. Commun. 8, 1079.

Gardner, B.M., Pincus, D., Gotthardt, K., Gallagher, C.M., Walter, P., 2013. Endoplasmic reticulum stress sensing in the unfolded protein response. Cold Spring Harb. Perspect. Biol. 5, a013169.

Hawkins, J.L., Robbins, M.D., Warren, L.C., Xia, D., Petras, S.F., Valentine, J.J., Varghese, A.H., Wang, I.K., Subashi, T.A., Shelly, L.D., Hay, B.A., Landschulz, K.T., Geoghegan, K.F., Harwood Jr., H.J., 2008. Pharmacologic inhibition of site 1 protease activity inhibits sterol regulatory element-binding protein processing and reduces lipogenic enzyme gene expression and lipid synthesis in cultured cells and experimental animals. J. Pharmacol. Exp. Ther. 326, 801–808.

Hay, B.A., Abrams, B., Zumbrunn, A.Y., Valentine, J.J., Warren, L.C., Petras, S.F., Shelly, L.D., Xia, A., Varghese, A.H., Hawkins, J.L., Van Camp, J.A., Robbins, M.D., Landschulz, K., Harwood Jr., H.J., 2007. Aminopyrrolidineamide inhibitors of site-1 protease. Bioorg. Med. Chem. Lett. 17, 4411–4414.

Hyrina, A., Meng, F., McArthur, S.J., Eivemark, S., Nabi, I.R., Jean, F., 2017. Human Subtilisin Kexin Isozyme-1 (SKI-1)/Site-1 protease (S1P) regulates cytoplasmic lipid droplet abundance: a potential target for indirect-acting anti-dengue virus agents. PLoS One 12, e0174483.

Iwawaki, T., Akai, R., Kohno, K., Miura, M., 2004. A transgenic mouse model for monitoring endoplasmic reticulum stress. Nat. Med. 10, 98–102.

Lebeau, P., Al-Hashimi, A., Sood, S., Lhotak, S., Yu, P., Gyulay, G., Pare, G., Chen, S.R., Trigatti, B., Prat, A., Seidah, N.G., Austin, R.C., 2017. Endoplasmic reticulum stress and Ca2+ depletion differentially modulate the sterol regulatory protein PCSK9 to control lipid metabolism. J. Biol. Chem. 292, 1510–1523.

Lee, A.S., 2005. The ER chaperone and signaling regulator GRP78/BiP as a monitor of endoplasmic reticulum stress. Methods 35, 373–381.

Li, M., Baumeister, P., Roy, B., Phan, T., Foti, D., Luo, S., Lee, A.S., 2000. ATF6 as a transcription activator of the endoplasmic reticulum stress element: thapsigargin stress-induced changes and synergistic interactions with NF-Y and YY1. Mol. Cell. Biol. 20, 5096–5106.

Liu, S.H., Yang, C.C., Chan, D.C., Wu, C.T., Chen, L.P., Huang, J.W., Hung, K.Y., Chiang, C.K., 2016. Chemical chaperon 4-phenylbutyrate protects against the endoplasmic reticulum stress-mediated renal fibrosis in vivo and in vitro. Oncotarget 7, 22116–22127.

Maly, D.J., Papa, F.R., 2014. Druggable sensors of the unfolded protein response. Nat. Chem. Biol. 10, 892–901.

McAlpine, C.S., Bowes, A.J., Werstuck, G.H., 2010. Diabetes, hyperglycemia and accelerated atherosclerosis: evidence supporting a role for endoplasmic reticulum (ER) stress signaling. Cardiovasc Hematol Disord Drug Targets 10, 151–157.

Nagelkerke, A., Bussink, J., Sweep, F.C., Span, P.N., 2014. The unfolded protein response as a target for cancer therapy. Biochim. Biophys. Acta 1846, 277–284.

Okada, T., Haze, K., Nadanaka, S., Yoshida, H., Seidah, N.G., Hirano, Y., Sato, R., Negishi, M., Mori, K., 2003. A serine protease inhibitor prevents endoplasmic reticulum stress-induced cleavage but not transport of the membrane-bound transcription factor ATF6. J. Biol. Chem. 278, 31024–31032.

Rutishauser, J., Spiess, M., 2002. Endoplasmic reticulum storage diseases. Swiss Med. Wkly. 132, 211–222.

Schwarz, D.S., Blower, M.D., 2016. The endoplasmic reticulum: structure, function and response to cellular signaling. Cell. Mol. Life Sci. 73, 79–94.

Shen, J., Chen, X., Hendershot, L., Prywes, R., 2002. ER stress regulation of ATF6 localization by dissociation of BiP/GRP78 binding and unmasking of Golgi localization signals. Dev. Cell 3, 99–111.

Szegezdi, E., Logue, S.E., Gorman, A.M., Samali, A., 2006. Mediators of endoplasmic reticulum stress-induced apoptosis. EMBO Rep. 7, 880–885.

Teske, B.F., Wek, S.A., Bunpo, P., Cundiff, J.K., McClintick, J.N., Anthony, T.G., Wek, R.C., 2011. The eIF2 kinase PERK and the integrated stress response facilitate activation of ATF6 during endoplasmic reticulum stress. Mol. Biol. Cell 22, 4390–4405.

Tufanli, O., Telkoparan Akillilar, P., Acosta-Alvear, D., Kocaturk, B., Onat, U.I., Hamid, S.M., Cimen, I., Walter, P., Weber, C., Erbay, E., 2017. Targeting IRE1 with small molecules counteracts progression of atherosclerosis. Proc. Natl. Acad. Sci. U. S. A. 114, E1395–E1404.

Uchida, L., Urata, S., Ulanday, G.E., Takamatsu, Y., Yasuda, J., Morita, K., Hayasaka, D., 2016. Suppressive effects of the site 1 protease (S1P) inhibitor, PF-429242, on dengue virus propagation. Viruses 8.

Velho, R.V., De Pace, R., Klunder, S., Di Lorenzo, G., Schweizer, M., Braulke, T., Pohl, S., 2017. Site-1 protease and lysosomal homeostasis. Biochim. Biophys. Acta 1864 (, 2162–2168.

Vincenz-Donnelly, L., Hipp, M.S., 2017. The endoplasmic reticulum: a hub of protein quality control in health and disease. Free Radic. Biol. Med. 108, 383–393.

Xiang, C., Wang, Y., Zhang, H., Han, F., 2017. The role of endoplasmic reticulum stress in neurodegenerative disease. Apoptosis 22, 1–26.

Yamamoto, K., Takahara, K., Oyadomari, S., Okada, T., Sato, T., Harada, A., Mori, K., 2010. Induction of liver steatosis and lipid droplet formation in ATF6alpha-knockout mice burdened with pharmacological endoplasmic reticulum stress. Mol. Biol. Cell 21, 2975–2986.

Zeeshan, H.M., Lee, G.H., Kim, H.R., Chae, H.J., 2016. Endoplasmic reticulum stress and associated ROS. Int. J. Mol. Sci. 17, 327.

Appendix C: Publication in MethodsX Journal

MethodsX 6 (2019) 1174–1180

Contents lists available at ScienceDirect

MethodsX

journal homepage: www.elsevier.com/locate/mex

Method Article

The trypan blue cellular debris assay: a novel low-cost method for the rapid quantification of cell death

Paul F. Lebeau, Jack Chen, Jae Hyun Byun, Khrystyna Platko, Richard C. Austin*

Department of Medicine, Division of Nephrology, McMaster University, St. Joseph's Healthcare Hamilton and Hamilton Centre for Kidney Research, Hamilton, Ontario L8N 4A6, Canada

A B S T R A C T

Cell death is a common driver of human disease and is frequently studied in a variety of *in vitro* settings. There currently exists a range of commercially available assays to examine cell death, however, most are costly and require assay-specific experimental conditions that may not be suitable for many cell types. Here, we show that cellular debris occurring as a result of cell death can be used to quantify cell death using trypan blue. Furthermore, we demonstrate that the data generated using this technique are comparable to the widely-used lactate dehydrogenase (LDH) assay. Overall, we describe a novel application for trypan blue, a stain found in most biology laboratories, as a novel and cost-effective method for the quantification of cell death via staining of cell debris.

A R T I C L E I N F O

Method name: Trypan blue cellular debris assay

Keywords: Cell death, Assay, Trypan blue, LDH assay, Cytotoxicity, Dye, Cell viability, 96-well plate, Apoptosis

Article history: Received 19 December 2018; Accepted 9 May 2019; Available online 15 May 2019

- The technique is quick and affordable.
- No manipulation of experimental conditions, such as low FBS, are required to accommodate the assay.
- Data generated using the assay are consistent with the widely-used LDH release assay.

* Corresponding author at: 50 Charlton Ave. E., Rm. T-3313, Hamilton, Ontario L8N 4A6, Canada.
E-mail addresses: lebeaup@mcmaster.ca (P.F. Lebeau), chenj63@mcmaster.ca (J. Chen), austinr@taari.ca (R.C. Austin).

https://doi.org/10.1016/j.mex.2019.05.010

Specifications Table

Subject Area:	Biochemistry, Genetics and Molecular Biology
More specific subject area:	Molecular Biology
Method name:	Trypan Blue Cellular Debris Assay
Name and reference of original method:	W. Strober, Trypan blue exclusion test of cell viability, Curr Protoc Immunol Appendix 3 (2001) Appendix 3B.
Resource availability:	• 6-well tissue culture dish • 96-well plate • Complete cell culture medium • Phosphate-buffered saline (PBS), pH 7.4 • 99% v/v Isopropanol • 0.4% w/v Trypan blue solution (ThermoFisher Scientific, Cat. no. 15250061) - Alternatively, dissolve 400 μg of trypan blue powder (Sigma- Aldrich, Cat. no. T6146) in 100 mL of distilled water • Microcentrifuge • Dry block heater • 1.5 mL Microcentrifuge tubes • Spectrophotometer

Method details

Here, we describe a non-invasive method, referred to as the trypan blue cellular debris (TBCD) assay, to examine media content of cell debris occurring as a result of cell death. Following the harvest of debris, live adherent cells can continue to be grown or be utilized for additional assays. Although the following protocol was optimized using 6-well tissue culture dishes, the protocol can also be optimized for use with other culture dish formats.

Equipment and reagents

- 6-well tissue culture dish
- 96-well plate
- Complete cell culture medium
- Phosphate-buffered saline (PBS), pH 7.4
- 99% v/v Isopropanol
- 0.4% w/v Trypan blue solution (ThermoFisher Scientific, Cat. no. 15250061)
  - Alternatively, dissolve 400 μg of trypan blue powder (Sigma-Aldrich, Cat. no. T6146) in 100 mL of distilled water
- Microcentrifuge
- Dry block heater
- 1.5 mL Microcentrifuge tubes
- Spectrophotometer

Seeding and treatment of cells

1 Centrifuge complete medium at 15,000 × *g* for 5 min to remove any particulates found in the FBS and warm medium to the desired temperature prior to seeding. This can be done using sterile microcentrifuge tubes in a table-top microcentrifuge.
2 Seed cells in 6-well tissue culture dishes containing the appropriate volume of medium. We recommend using 1 mL of complete medium per well and a seeding density of approximately 8×10^5 cells per well or 80% confluency. Ensure that each well contains an equal number of cells.
3 Treat cells with appropriate drugs/interventions.

Staining of cell debris

1 Following the desired treatment period, carefully harvest cell debris by collecting all of the medium from each well using a pipette without disturbing cells attached to the bottom of the plate. The

medium containing cell debris should be placed in pre-labelled microcentrifuge tubes. Continue to grow the cells by adding fresh pre-warmed medium or collect lysate for analysis of protein or mRNA using the appropriate lysis buffer.
2 Pellet cell debris via centrifugation at 10,000 × *g* for 2 min at room temperature. Although not necessary for most cell types, live weakly adherent cells must be cleared from the media prior to isolation of cell debris via low-speed centrifugation at 500 × *g* for 1 min. Remove the cell debris-containing supernatant and continue the standard protocol; be careful not to agitate the pellet of live cells from the bottom of the tube.
3 Discard the medium by inverting the tube or collect medium for other assays using a pipette. Be careful not to agitate the cell debris pellet.
4 Add 100 μL of trypan blue solution to each tube and re-suspend the pellet using a vortex. Allow cell debris to stain on the bench top for 5 min at room temperature.
5 Centrifuge the samples at 12,000 × *g* for 2 min at room temperature and discard excess trypan blue stain by inverting the tube. Be careful not to disturb the pellet.
6 Wash the pellet by adding 500 μL of 99% isopropanol. Slowly invert the tube and open the lid to remove the wash (Fig. 1). Remove any excess isopropanol using a pipette while being careful not to disturb the trypan blue-stained cell debris pellet.

Extraction and quantification

1 Add 100 μL of PBS to each of the tubes in order to extract the stain from the pellet. Agitate the pellet using a vortex and heat the tubes using a dry block heater for 10 min at 80 °C.
2 Centrifuge the samples to remove cell debris from the blue-coloured PBS extract.
3 Load the blue-coloured PBS extract into a 96-well plate as technical duplicates of 45 μL and measure the optical density of the extract using a spectrophotometer at a wavelength of 590 nm.

Data analysis and recommended controls

Similar to many assays, data generated using the TBCD assay described in this report can be presented as (a) relative or fold changes in cell death or (b) absolute cell death. To present data in a manner relative to an untreated or vehicle control group, no assay controls are required; simply normalize the mean optical density value obtained from each treatment group to the mean value obtained for the untreated/vehicle control. Error values should be treated in the same manner as the means. To illustrate absolute cell death, blank and 100% cell death controls are required. The blank can be generated by adding 100 μL of trypan blue to a new microcentrifuge tube containing no cell debris (starting at step 4 of Staining of cell debris). A small amount of stain will adhere to the plastic and

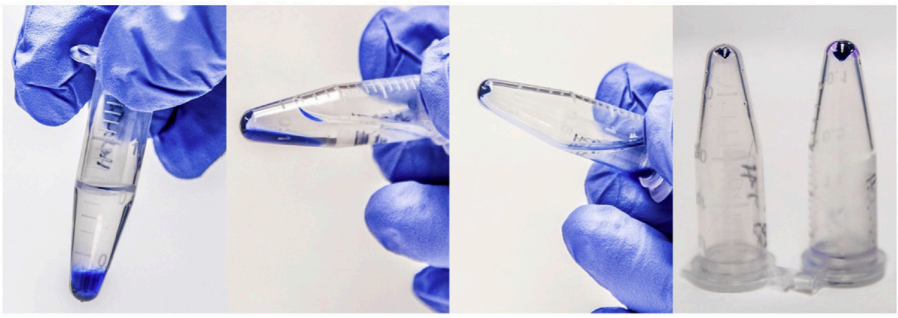

Fig. 1. Isolate and wash the trypan blue-stained cell debris pellet by adding 500 μL of isopropanol and gently inverting the tube. The isopropanol will displace the aqueous trypan blue fraction and leave behind a clean blue pellet.

generate non-specific signal. Optical density generated from the blank should be subtracted from the mean value of each treatment group during data processing. To generate a 100% cell death control, place a culture dish containing the same total number of cells as those used for the treatment groups into a freezer for 20 min; remove medium from these cells prior to freezing. Following freezing, resuspend cell debris in PBS. Ensure that all cells/debris are collected by scraping the bottom of the well with a cell scrapper. Collect and stain these cell debris using the protocol described above. To calculate percent cell death, use the optical density values obtained from experimental and controls groups in Eq. (1).

$$\%\text{Cell Death} = \frac{\text{Experimental Value} - \text{Blank Value}}{100\%\,\text{Cell Death Value} - \text{Blank Value}} \times 100 \quad (1)$$

Method validation

To ensure the validity and sensitivity of the TBCD assay, HuH7 immortalized human hepatocytes were seeded in 6-well culture dishes at a confluency of 80%. The following day, cell debris was generated by freezing the cells at -80 °C for 20 min. Serial two-fold dilutions of cell debris were carried out prior to staining in order to mimic incremental changes in cell death.

Quantification of the optical density of the PBS extracts using a spectrophotometer (Molecular Devices) demonstrates that changes in cell debris concentration can be detected using trypan blue (n = 3 wells) (Fig. 2). HuH7 cells were then treated with increasing concentrations of a pharmacologic agent known to cause cell death in a manner dependent on endoplasmic reticulum stress, thapsigargin (Tg) (Fig. 3A) [1]. Data generated using the TBCD assay were compared to data generated using an LDH release assay (Roche); both assays were carried out on the same experiments using the same medium. Qualitative assessment of apoptosis was also carried out in Tg-treated cells using a terminal deoxynecleotidyl transferase dUTP nick end labeling (TUNEL) assay (Trevigen). TUNEL-positive apoptotic cells were visualized using a fluorescent microscope (EVOS, ThermoFisher Scientific). Quantification of TUNEL staining intensity of 5 separate wells of cells per treatment using ImageJ software (NIH) also reveals that findings are consistent with the LDH and TBCD assays (Fig. 3B and C). Our research group has also used the TBCD assay described in this report to demonstrate changes in cell death in HK2 cells transfected with mammalian expression plasmids [2].

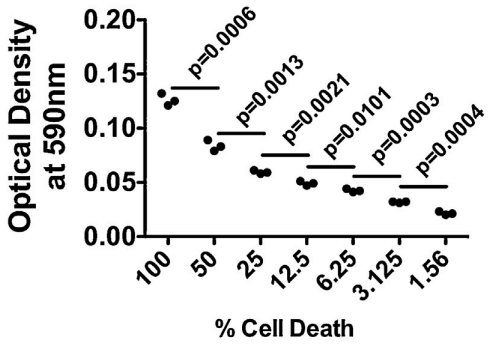

Fig. 2. Cell debris was generated by freezing cell monolayers for 20 min (n = 3). Debris was resuspended, underwent two-fold serial dilutions and was stained using the trypan blue debris assay protocol. Statistical analysis was carried out using the unpaired Student's *t*-test.

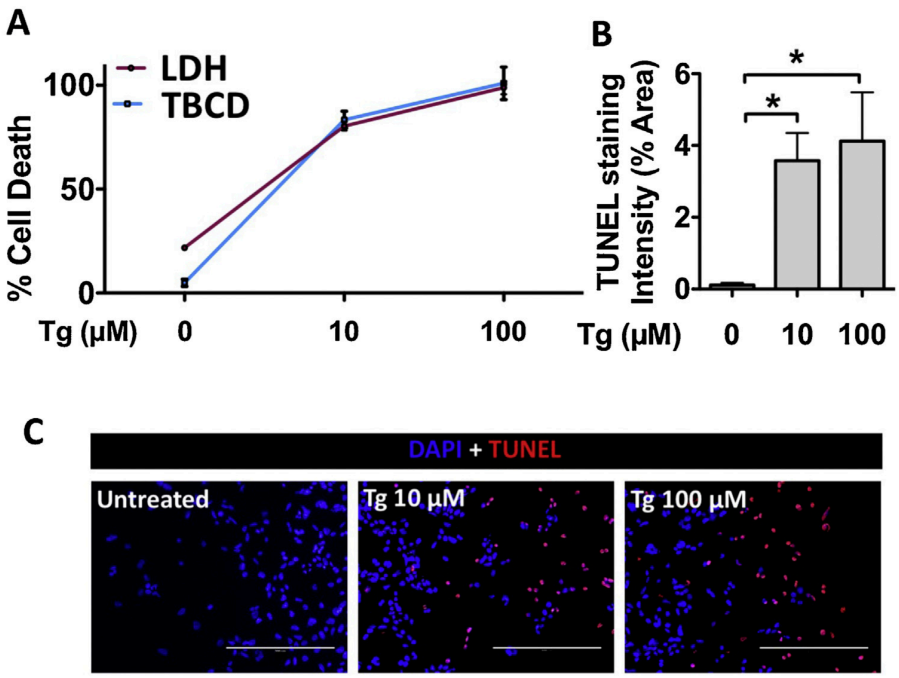

Fig. 3. (A) A comparison of data generated using a lactate dehydrogenase (LDH) release assay and the trypan blue cellular debris assay (TBCD) in HuH7 immortalized human hepatocytes treated with thapsigargin (Tg). (B) Apoptotic cells were also visualized by staining for DNA damage using a TUNEL assay, which was quantified using ImageJ Software. Error bars are represented as SD. Scale bars, 200 μm. *, $p < 0.05$. Statistical analysis was carried out using the unpaired Student's *t*-test.

Supplementary material and/or additional information

Trypan blue is a widely-available low-cost dye used to distinguish between intact live cells and permeable dead cells and debris [3]. Although this dye is commonly used to stain and exclude dead cells for the quantification of live cells using a hemocytometer, to the best of our knowledge the quantification of cell debris found in the medium using trypan blue has not yet been described. The use of cell debris, a component that is generally discarded in most experiments, to generate data on cell viability status represents the first advantage of this method. Because debris is isolated from the sample, all of the media and cell monolayer remains available for additional experiments.

Other common cell death assays include (a) intracellular protein release assays, such as the LDH release assay, and (b) metabolism-based assays [4,5]. The former relies upon the release of proteins that are normally expressed in cells into the medium as a result of cytotoxicity-induced perturbations in membrane integrity. Activity is then measured in the medium by providing the enzyme with detectable substrate. Because ATP production is reduced in dying cells, metabolism-based assays can also be used to quantify ATP levels in cells using a firefly-luciferase system [6]. Each of these enzyme-dependent classes of cell death assays, however, share a common limitation. The expression of such enzymes can be affected by certain treatments thus leading to either over- or under-estimations of true cell death. Because the TBCD assay relies on damaged cell membrane, which represents a more direct marker of cell viability, this assay is not affected by alterations in enzyme expression and/or activity.

Another common method to quantify cell death in a manner dependent on cell membrane integrity involves a fluorescent dye, known as propidium iodide (PI) [7]. Similar to trypan blue, PI does not

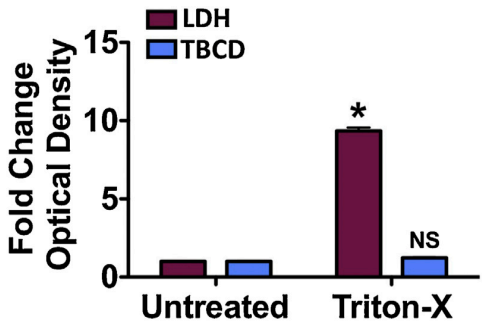

Fig. 4. To determine the limitations of the trypan blue cellular debris (TBCD) assay in comparison to the lactate dehydrogenase (LDH) release assay, HuH7 immortalized human hepatocytes were treated with a detergent capable of dissolving cell membrane. Representative images of cells treated with Triton-X were taken with a light microscope. *, $p < 0.05$ vs. LDH assay - untreated; NS, non-significant vs. TBCD assay untreated. Statistical analysis was carried out using the unpaired Student's *t*-test. Error bars are presented as SD.

readily pass through intact membrane in live cells. In damaged cells, PI passes through pores of the cell membrane and intercalates with DNA; therefore, PI is generally used to visualize and quantify cell death using fluorescence microscopy and/or flow cytometry [8]. High-throughput PI-based fluorometric assays have also been developed, however, these are often expensive and laborious processes that are known to produce false-positive results. Furthermore, as PI-based assay rely on intact nuclei of damaged cells within the cell monolayer, PI assays also fail to detect dead floating cells that have lifted from the monolayer [9]. In this regard, the because the LDH and TBCD assays quantify a by-product of cell death found in the medium, these assays may represent better tools to assess total cell death.

The dependence on cell membrane, however, also has its limitations. Detergent-based treatments known to dissolve cell membrane significantly reduce the ability of the TBCD assay to detect changes in media debris content. To test this, a side-by-side comparison was made between the TBCD assay and the LDH release assay using HuH7 cells treated with Triton-X; a harsh detergent commonly used to generate positive control values for the LDH release assay (Fig. 4). Although nearly 100% cell death occurred as a result of this treatment, which was confirmed using a light microscope, media debris content did not accurately reflect cell death.

In conclusion, there exists many assays for the assessment of cytotoxicity and cell death and each has its limitations. The assay described in this report adds to the repertoire of techniques available to examine cell death and may offer significant advantage over enzyme-based assays in certain circumstances.

Acknowledgements

We would like to thank students of the Honours Biology and Pharmacology Co-op program at McMaster University, Lisa Cheng, Natalka Parzei and Haley Yun, who contributed to assay optimization during their Discovery Project. This work was supported in part by research grants to Richard C. Austin from the Heart and Stroke Foundation of Ontario (T-6146), the Heart and Stroke Foundation of Canada (G-13-0003064 and G-15-0009389), the Canadian Institutes of Health Research (74477).

References

[1] C.M. Oslowski, F. Urano, Measuring ER stress and the unfolded protein response using mammalian tissue culture system, Methods Enzymol. 490 (2011) 71–92.
[2] P. Lebeau, K. Platko, A.A. Al-Hashimi, J.H. Byun, S. Lhotak, N. Holzapfel, G. Gyulay, S.A. Igdoura, D.R. Cool, B. Trigatti, N.G. Seidah, R.C. Austin, Loss-of-function PCSK9 mutants evade the unfolded protein response sensor GRP78 and fail to induce endoplasmic reticulum stress when retained, J. Biol. Chem. 293 (2018) 7329–7343.

[3] W. Strober, Trypan blue exclusion test of cell viability, Curr. Protoc. Immunol. 21 (1) (2001) A.3B.1–A.3B.2 Appendix 3, Appendix 3B.
[4] O. Kepp, L. Galluzzi, M. Lipinski, J. Yuan, G. Kroemer, Cell death assays for drug discovery, Nat. Rev. Drug. Discov. 10 (2011) 221–237.
[5] B. Mery, J.B. Guy, A. Vallard, S. Espenel, D. Ardail, C. Rodriguez-Lafrasse, C. Rancoule, N. Magne, In vitro cell death determination for drug discovery: a landscape review of real issues, J. Cell Death 10 (2017) 1179670717691251.
[6] S.P. Crouch, R. Kozlowski, K.J. Slater, J. Fletcher, The use of ATP bioluminescence as a measure of cell proliferation and cytotoxicity, J. Immunol. Methods 160 (1993) 81–88.
[7] C. Riccardi, I. Nicoletti, Analysis of apoptosis by propidium iodide staining and flow cytometry, Nat. Protoc. 1 (2006) 1458–1461.
[8] W.A. Dengler, J. Schulte, D.P. Berger, R. Mertelsmann, H.H. Fiebig, Development of a propidium iodide fluorescence assay for proliferation and cytotoxicity assay, Anti Cancer Drugs 6 (1995) 522–532.
[9] A.M. Rieger, B.E. Hall, L.T. Luong, L.M. Schang, D.R. Barreda, Conventional apoptosis assays using propidium iodide generates a significant number of false positives that prevent accurate assessment of cell death, J. Immunol. Methods 358 (2010) 81–92.

Appendix D: Publication in Molecular Metabolism

Original Article

MOLECULAR METABOLISM

GDF10 blocks hepatic PPARγ activation to protect against diet-induced liver injury

Khrystyna Platko [1,4], Paul F. Lebeau [1,4], Jae Hyun Byun [1], Samantha V. Poon [1], Emily A. Day [2], Melissa E. MacDonald [1], Nicholas Holzapfel [1], Aurora Mejia-Benitez [1], Kenneth N. Maclean [3], Joan C. Krepinsky [1], Richard C. Austin [1,*]

ABSTRACT

Objective: Growth differentiation factors (GDFs) and bone-morphogenic proteins (BMPs) are members of the transforming growth factor β (TGFβ) superfamily and are known to play a central role in the growth and differentiation of developing tissues. Accumulating evidence, however, demonstrates that many of these factors, such as BMP-2 and -4, as well as GDF15, also regulate lipid metabolism. GDF10 is a divergent member of the TGFβ superfamily with a unique structure and is abundantly expressed in brain and adipose tissue; it is also secreted by the latter into the circulation. Although previous studies have demonstrated that overexpression of GDF10 reduces adiposity in mice, the role of circulating GDF10 on other tissues known to regulate lipid, like the liver, has not yet been examined.

Methods: Accordingly, GDF10$^{-/-}$ mice and age-matched GDF10$^{+/+}$ control mice were fed either normal control diet (NCD) or high-fat diet (HFD) for 12 weeks and examined for changes in liver lipid homeostasis. Additional studies were also carried out in primary and immortalized human hepatocytes treated with recombinant human (rh)GDF10.

Results: Here, we show that circulating GDF10 levels are increased in conditions of diet-induced hepatic steatosis and, in turn, that secreted GDF10 can prevent excessive lipid accumulation in hepatocytes. We also report that GDF10$^{-/-}$ mice develop an obese phenotype as well as increased liver triglyceride accumulation when fed a NCD. Furthermore, HFD-fed GDF10$^{-/-}$ mice develop increased steatosis, endoplasmic reticulum (ER) stress, fibrosis, and injury of the liver compared to HFD-fed GDF10$^{+/+}$ mice. To explain these observations, studies in cultured hepatocytes led to the observation that GDF10 attenuates nuclear peroxisome proliferator-activated receptor γ (PPARγ) activity; a transcription factor known to induce *de novo* lipogenesis.

Conclusion: Our work delineates a hepatoprotective role of GDF10 as an adipokine capable of regulating hepatic lipid levels by blocking *de novo* lipogenesis to protect against ER stress and liver injury.

Keywords BMP-3b; ER stress; Hepatic steatosis; HFD; NAFLD; NASH; TGFβ

1. INTRODUCTION

Obesity is considered by many as the epidemic of the 21st century, affecting over 2 billion individuals worldwide and still increasing in frequency [1]. Although obesity is commonly thought of as a disease characterized by excess adipose tissue, other hallmark characteristics are also common in obese individuals. Non-alcoholic fatty liver disease (NAFLD) affects approximately 75% of obese individuals and contributes to other comorbidities associated with obesity, such as type 2 diabetes mellitus, hypertension, heart disease and ischemic stroke [2,3]. NAFLD is defined as an accumulation of triglyceride in the liver in excess of 5% of total liver weight and is commonly referred to as steatosis. Simple steatosis is largely benign; however, NAFLD can progress to life-threatening non-alcoholic steatohepatitis (NASH) or liver cirrhosis. Although the precise mechanism of progression remains poorly understood, the well-accepted *multiple-hits hypothesis* suggests that cellular events including oxidative stress, lipid peroxidation, Kupffer cell activation, and adipocytokine alterations play a central role [1,4]. Numerous studies have also demonstrated that ER stress plays a key role in the development of NAFLD and NASH by promoting Kupffer cell activation, oxidative stress and mitochondrial dysfunction [5–7]. Given that secretory cells like adipocytes and hepatocytes are rich in ER, the role of ER stress has become a topic of considerable interest in the development of metabolic diseases. ER stress is characterized by an overwhelming of ER-resident chaperones by misfolded *de novo* polypeptides in the ER lumen. This event triggers the unfolded protein response (UPR) in order to increase ER protein folding capacity and restore homeostatic conditions. The signaling cascades of the UPR are comprised of (a) the activating transcription factor 6 (ATF6) pathway, which modulates sterol regulatory element-binding protein (SREBP)-2

[1]Department of Medicine, McMaster University, The Research Institute of St. Joe's Hamilton, Hamilton Centre for Kidney Research, Hamilton, Ontario, L8N 4A6, Canada [2]The Division of Endocrinology and Metabolism, Department of Medicine, McMaster University, 1280 Main Street West, Hamilton, Ontario, L8N 4A6, Canada [3]The Department of Pediatrics, University of Colorado School of Medicine, Aurora, CO, 80045, USA

[4] Khrystyna Platko and Paul F. Lebeau contributed equally to this work.

*Corresponding author. 50 Charlton Ave East, Room T-3313, Hamilton, Ontario, L8N 4A6, Canada. Fax: +905 540 6589. E-mail: austinr@taari.ca (R.C. Austin).

Received April 9, 2019 • Revision received June 14, 2019 • Accepted June 24, 2019 • Available online xxx

https://doi.org/10.1016/j.molmet.2019.06.021

Original Article

Abbreviations

ANGPTL4	angiopoietin-like 4
ACOX1	acyl-coenzyme A oxidase 1
ACOT2	acyl-coenzyme A thioesterase 2
ACADM	acyl-coenzyme A dehydrogenase, C-4 to C-12 straight chain
ATF4	activating transcription factor 4
ATF6	activating transcription factor 6
ALT	alanine-L transaminase
BMP	bone morphogenic protein
BAT	brown adipose tissue
BSA	bovine-serum albumin
C/EBPα	CCAAT-enhancer-binding protein α
CD36	cluster of differentiation 36
CGTZ	ciglitizone
CLAMS	Columbus Instruments Comprehensive Lab Animal Monitoring System
CRTC2	CREB-regulated transcription cofactor 2
CHOP	C/EBP homologous protein
DMEM	Dulbecco's Modified Eagle's Medium
ER	endoplasmic reticulum
FBS	fetal bovine serum
FATP5	fatty acid transport protein 5
FSP27	fat-specific protein 27
FOXO1	forkhead box protein O1
FN1	fibronectin 1
FFPE	formalin-fixed paraffin-embedded
GDF10	growth differentiation factor 10
GAT	gonadal adipose tissue
GRP78	glucose-regulated protein of 78 kDa
GRP94	glucose-regulated protein of 94 kDa
β-HB	β-hydroxybutyrate
HFD	high-fat diet
IHC	immunohistochemistry
IAT	inguinal adipose tissue
IRE1α	inositol-requiring 1α
LPL	lipoprotein lipase
IL1β	interleukin 1β
LDH	lactate dehydrogenase
NAFLD	non-alcoholic fatty liver disease
NASH	non-alcoholic steatohepatitis
NCD	normal control diet
ORO	Oil Red O
OA	oleate
PFA	paraformaldehyde
PPARγ/α	peroxisome proliferator-activated receptor γ/α
PGC1β	peroxisome proliferator-activated receptor gamma coactivator 1-β
PPRE	peroxisome proliferator response element
PSR	Picrosirius red
PDK4	pyruvate dehydrogenase lipoamide kinase isozyme 4
PERK	protein kinase RNA (PKR)-like ER kinase
PA	palmitate
PCK1	phosphoenolpyruvate carboxykinase 1
PBS	phosphate-buffered saline
rhGDF10	recombinant human growth differentiation factor 10
si	small interfering
STAT3	signal transducer and activator of transcription 3
SREBP-1/-2	sterol regulatory element-binding protein-1/-2
TGFβ	transforming growth factor β
TGFβR1	TGFβ receptor subtype-1
TG	thapsigargin
TM	tunicamycin
TNFα	tumor necrosis factor alpha
UPR	unfolded protein response
XBP1	X-box-binding protein 1

mediated *de novo* lipogenesis [8]; (b) the highly conserved inositol-requiring 1α (IRE1α) - X-box-binding protein 1 (XBP1) pathway, which is required for the regulation of hepatic lipids during conditions of stress [9]; as well as (c) the protein kinase RNA (PKR)-like ER kinase (PERK) - activating transcription factor 4 (ATF4) pathway capable of regulating *de novo* lipogenesis via fatty acid synthase and SREBP-1 [10]. Previous studies have also demonstrated that ATF4 can induce the expression and activation of PPARγ, a transcription factor known to promote the expression of pro-adipogenic mediators including fatty acid transport protein 5 (*FATP5*), angiopoietin-like 4 (*ANGPTL4*), lipoprotein lipase *(LPL), Perilipin,* cluster of differentiation 36 (*CD36*) and fat-specific protein 27 (*FSP27*) [11,12]. Clinical studies have also characterized increased PPARγ expression in the livers of patients with NAFLD [13]. Although pro-survival at its core, chronic or severe ER stress can induce the expression of lipid-regulatory genes that promote *de novo* lipogenesis, as well as drive inflammation, fibrosis, and apoptosis in the liver [14].

GDF10, also known as BMP-3b, is an atypical member of the TGFβ superfamily capable of inhibiting osteoblast differentiation by antagonizing BMP-2 and -4 -mediated osteogenesis [15]. To date, over 30 members of the superfamily have been described, and all share common features. They are synthesized as precursor proteins containing N-terminal signal peptide sequences and pro-regions. Once secreted, the mature, biologically active molecule is believed to consist of a homodimer originating from proteolytically-cleaved precursors [16]. In recent years, accumulating evidence has shown that these factors play a central role in the regulation of energy balance and homeostasis. BMP-2 and -4 promote white adipogenesis while BMP-7 promotes brown adipogenesis [17–19]. Studies have also demonstrated that *in vitro* knockdown of GDF10 enhances adipogenesis and that transgenic mice overexpressing GDF10 are protected against diet-induced obesity and insulin resistance [20,21]. GDF15 has also been shown to regulate feeding and fatty acid oxidation and to protect against steatosis, insulin resistance, obesity, and ER stress in the livers of mice fed a HFD [22–24].

It is well-established that adipokines can modulate obesity and a variety of its comorbidities, including NAFLD [25]. However, little is known about the role of circulating GDF10 on liver health/function and injury in the face of diet-induced obesity. Here, we report that pharmacologic and diet-induced ER stress increases the expression of GDF10 in cultured pre-adipocytes and in white adipose tissue. We also show that GDF10$^{-/-}$ mice exhibit increased nuclear PPARγ expression and activity coupled with hepatic steatosis on the NCD and develop a severe NASH-like phenotype on the HFD. Collectively, our findings suggest that circulating GDF10 plays a critical role as a regulator of hepatic PPARγ during conditions of dietary stress and that GDF10 is capable of attenuating the progression of steatosis to NASH.

MOLECULAR METABOLISM

2. MATERIALS AND METHODS

2.1. Animal studies

GDF10$^{-/-}$ mice were a generous gift from Dr. Se-Jin Lee (Johns Hopkins University) [16]. Animals were housed in 12 h light cycles and controlled temperature and humidity conditions and had access to standard NCD (2918, Envigo) and water *ad libitum* (n = 10). In experiments designed to study diet-induced hepatic steatosis, male GDF10$^{-/-}$ mice and age-matched GDF10$^{+/+}$ controls were provided with HFD (60% Kcal; TD.06414, Envigo) *ad libitum* starting at 6 weeks of age for an additional 12 weeks prior to sacrifice (n = 5). Measurements of metabolic parameters were performed using the Columbus Instruments Comprehensive Lab Animal Monitoring System (CLAMS) one week prior to sacrifice. A cohort of 12-week-old male C57BL/6J mice were also treated with phosphate-buffered saline (PBS) vehicle control or with the ER stress-inducing agent, tunicamycin (TM; 500 μg/kg), for 24 h via intraperitoneal injection in the left flank (n = 5). All mice were fasted for 6 h and anesthetized using isoflurane prior to sacrifice. Experimental procedures were approved by the McMaster University Animal Research Ethics Board.

2.2. Cell culture and treatment

Huh7 and HepG2 immortalized human hepatocyte cell lines as well as primary human hepatocytes were maintained in 5% CO_2 at 37 °C and cultured in Dulbecco's Modified Eagle's Medium (DMEM) or Willams' E medium, supplemented with 10% v/v fetal bovine serum (FBS), 100 IU/ml penicillin and 100 μg/ml streptomycin. For experimental procedures designed to examine the effect of GDF10 on lipid accumulation, cells were pre-treated with rhGDF10 (250 ng/mL, R&D Systems) for 24 h and then treated with agents known to stimulate lipid droplet accumulation, such as oleate (OA; 200 μM, Sigma–Aldrich), palmitate (PA; 200 μM, Sigma–Aldrich), thapsigargin (TG; 100 nM, Sigma–Aldrich) and TM (2 μg/mL, Sigma–Aldrich) for an additional 24 h. Similarly, for studies examining the effect of GDF10 on PPARγ-mediated lipid accumulation, hepatocytes were pre-treated with rhGDF10 and then treated with PPARγ agonist, ciglitizone (CGTZ; 10 μM, Tocris Bioscience), for 24 h prior to analysis. For experiments designed to examine the effect of GDF10 on PPARγ cellular localization and promoter binding, cells were pre-treated with rhGDF10 for 24 h, and subsequently treated with CGTZ for 1 h prior to analysis. All cell culture experiments were repeated a minimum of 3 times. To block Smad3 expression, siGENOME SMARTpool siRNA targeted against Smad3 (UCAAGAGCCUGGUCAAGAA, GAGUUCGCCUUCAAUAUGA, GGACGCAGGUUCUC-CAAAC, GGACGAGGUCUGCGUGAAU) was purchased from Dharmacon (SO-2782081G). 100 nM of siRNA targeted against Smad3 or scrambled siRNA control was transfected using RNAiMAX (ThermoFisher Scientific) as described previously [26].

2.3. Cell fractionation and transcriptional activity studies

Huh7 and HepG2 cells were seeded into 100 mm dishes and allowed to grow to confluency of 80%. Following treatment, nuclear and cytosolic fractions were isolated using an extraction kit (Abcam) according to the manufacturer's instructions. For experiments designed to examine the effect of GDF10 on PPARγ transcriptional activity, HepG2 cells were pre-treated with rhGDF10 for 24 h, and subsequently treated with CGTZ for 1 h prior to cellular fractionation. PPARγ transcription factor assay kit (Abcam) was carried out according to manufacturer's instructions. Briefly, 120 μg of protein isolated from nuclear extracts was added to each well of a 96-well plate coated with a double-stranded DNA sequence containing peroxisome proliferator response element (PPRE). Following an over-night incubation, anti-PPARγ primary antibody was added, followed by an HRP-conjugated secondary antibody. PPARγ binding to the PPRE was detected using a spectrophotometer at a wavelength of 450 nm.

2.4. Histological and immunohistochemical staining

Histological analysis was carried out in formalin-fixed paraffin-embedded (FFPE) tissues that were cut into 4 μm thick sections. Gross pathological changes were first examined with hematoxylin and eosin (H&E) and collagen accumulation was examined using Mason's Trichrome (Sigma–Aldrich). Analysis of intracellular triglyceride accumulation was carried out in OCT-embedded liver sections (10 μm) and in cultured cells fixed in 4% paraformaldehyde (PFA) using Oil Red O (ORO). The ORO content of isopropanol extracts was measured using a spectrophotometer (Molecular Devices) at a wavelength of 520 nm [27]. Immunohistochemical (IHC) staining was also carried out in 4 μm thick FFPE sections. Briefly, deparaffinized sections were blocked in 5% serum, incubated in primary antibody for 18 h at 4 °C, and exposed to biotin-labeled secondary antibody (Vector Laboratories; for a complete list of antibodies and working dilutions, please refer to Supplemental Table 1). Streptavidin-labeled HRP solution (Vector Laboratories) and the developing solution (Vector Laboratories) were used to visualize staining. Slides were examined using a Nikon microscope and images were quantified using ImageJ Software (NIH).

2.5. Quantitative real time PCR

Total RNA was isolated using RNA purification kits (ThermoFisher Scientific). A total of 2 μg of RNA was reverse transcribed to cDNA using the High-Capacity cDNA Reverse Transcription Kit (Applied Biosystems). PCR amplification was performed using the Fast SYBRGreen PCR master mix (Applied Biosystems) according to the manufacturer's instructions. All primer sequences are listed in Supplemental Table 2.

2.6. Immunoblots

Whole cell and tissue lysates were prepared using SDS lysis buffer containing a protease inhibitor cocktail (Roche), and protein concentration was measured as described previously [26]. The samples were resolved using SDS-PAGE and subsequently transferred to nitrocellulose membranes. Nitrocellulose membranes were then incubated in 5% w/v skimmed milk and primary antibody followed by the respective secondary antibody. The signal was detected using a Konica Minolta X-Ray film processor.

2.7. Immunofluorescent staining

Following treatment, Huh7 and primary human hepatocytes were fixed in 4% PFA and permeabilized in 0.025% Triton X-100 for 15 min. After blocking in 5% bovine-serum albumin (BSA), cells were stained with primary antibody, washed, and subsequently stained with fluorescently-labeled secondary antibodies and DAPI nuclear stain. Slides were then mounted using an aqueous mounting medium (ThermoFisher Scientific) and visualized using the EVOS FL (ThermoFisher Scientific) imaging system.

2.8. Plasma β-hydroxybutyrate (β-HB), ELISA, lactate dehydrogenase (LDH) and alanine-L transaminase (ALT) assays

Plasma levels of the ketone body β-HB were measured using a colorimetric assay (Cayman). Circulating GDF10 levels were measured using a mouse GDF10 ELISA kit (Elabscience). Plasma ALT was measured using a commercially available colorimetric assay (Abcam). Cytotoxicity was examined using a LDH colorimetric assay kit (Roche). All assays were performed according to the manufacturer's instructions.

Original Article

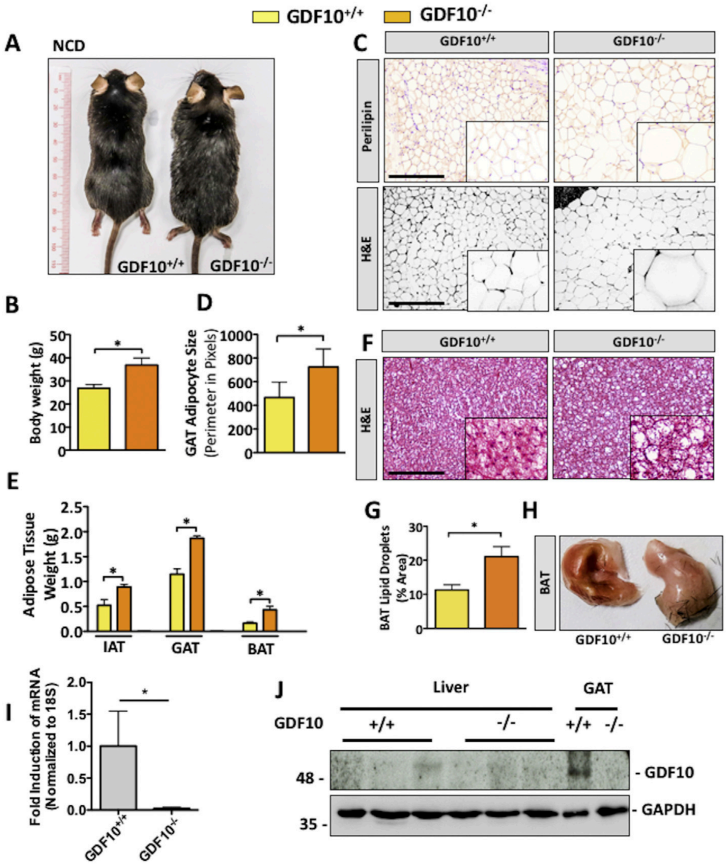

Figure 1: GDF10$^{-/-}$ mice have increased body weight and adiposity. (A) Macroscopic appearance and (B) body weights of 30 week old GDF10$^{+/+}$ and GDF10$^{-/-}$ mice fed NCD (n = 5). (C) IHC staining of the adipocyte marker perilipin and H&E staining of the GAT. (D) Average adipocyte size in GAT. (E) Weights of the IAT, GAT, and BAT. (F) H&E staining of the BAT. (G) Quantification of lipid droplets in BAT using ImageJ software. (H) Macroscopic appearance of the BAT from GDF10$^{+/+}$ and GDF10$^{-/-}$ mice at 30 weeks of age. (I) Real time PCR analysis of mRNA abundance of GDF10 in the GAT to confirm knockout (n = 5). (J) Immunoblots of the liver and GAT from GDF10$^{+/+}$ and GDF10$^{-/-}$ mice. Scale bars, 100 μm. All data are shown as the mean ± S.D. *, $p < 0.05$ by unpaired two-tailed Student's *t*-test.

2.9. Quantification of plasma, hepatic, and fecal lipid

Equal amounts of liver tissues were lysed in a mixture of hexane/2-propanol and incubated on an orbital shaker at 37 °C for 5 h. Samples were then subjected to centrifugation for 5 min (12,000 rpm) in order to isolate the lipid-containing liquid phase. Lipid content was quantified using a colorimetric triglyceride assay (Wako Diagnostics) according to the manufacturer's instructions. In a similar manner, fecal cholesterol content was measured directly from feces normalized to dry weight. Hepatic cholesterol content was measured using a commercially available colorimetric kit (Abcam) according to the manufacturer's instructions.

2.10. Statistical analysis

Data are reported as the mean ± SD. Statistical analysis was performed using GraphPad Prism. For comparison between two groups, an unpaired two-tailed Student's *t*-test was used. For analysis of three or more groups, a one-way ANOVA followed by Tukey's HSD multiple comparison test was performed. Differences between groups were considered statistically significant when $p < 0.05$.

3. RESULTS

3.1. GDF10$^{-/-}$ mice exhibit increased body weight gain and adiposity

Increased body weight gain in our GDF10$^{-/-}$ mouse colony was among our initial observations and was consistently observed in mice fed NCD (Figure 1A,B; *, $p < 0.05$, n = 5). Following this observation, adiposity was examined via IHC staining for the adipocyte marker, perilipin, as well as H&E of the gonadal adipose tissue (GAT). Consistent with gross morphological observations, GDF10$^{-/-}$ mice had increased mean adipocyte size (Figure 1C,D; *, $p < 0.05$, n = 5) and weight of the inguinal adipose tissue (IAT), GAT and brown adipose tissue (BAT) (Figure 1E; *, $p < 0.05$, n = 5). BAT from GDF10$^{-/-}$ mice also appeared lighter in color and revealed increased lipid droplets

MOLECULAR METABOLISM

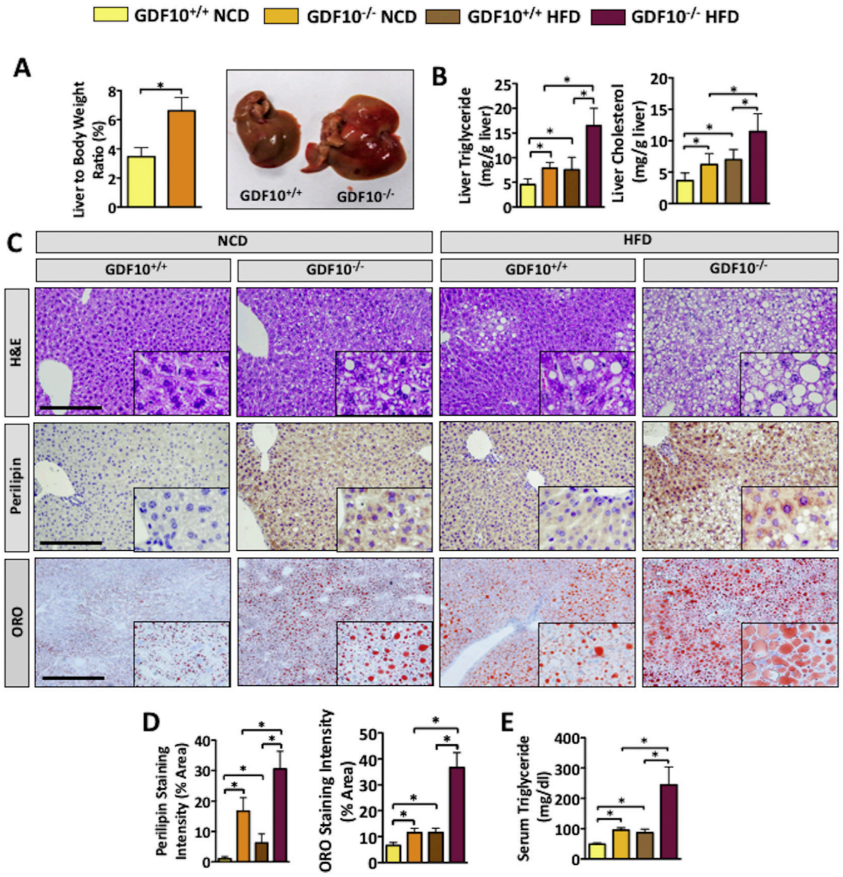

Figure 2: GDF10 deficiency leads to hepatic lipid accumulation. (A) Weights and macroscopic appearance of the livers from NCD-fed GDF10$^{+/+}$ and GDF10$^{-/-}$ mice (n = 5). (B) Hepatic triglyceride and cholesterol content (n = 5). (C) H&E, perilipin and ORO staining of livers from GDF10$^{+/+}$ and GDF10$^{-/-}$ mice fed NCD or HFD. (D) Quantification of perilipin and ORO staining using ImageJ Software (n = 5). (E) Serum triglyceride content. Scale bar, 100 μm. All data are shown as the mean ± S.D. *, $p < 0.05$ by unpaired two-tailed Student's *t*-test or one-way ANOVA.

compared to BAT from control mice (Figure 1F,G and H; *, $p < 0.05$, n = 5). GDF10 knockout was confirmed in these mice via real time PCR in GAT (Figure 1I; *, $p < 0.05$) and immunoblot (Figure 1J). Immunoblot analysis also revealed that GDF10 is expressed in GAT, but not in the livers of healthy wild-type mice (Figure 1J).

3.2. GDF10$^{-/-}$ mice exhibit hepatic lipid accumulation

Given that steatosis is commonly observed in obese patients as well as in rodent models of obesity [1,4], we next examined the livers of GDF10$^{-/-}$ mice fed NCD and HFD. Consistent with our observations in adipose tissue, liver weight was increased in GDF10$^{-/-}$ mice compared to controls on the NCD (Figure 2A; *, $p < 0.05$, n = 5). Analysis of hepatic triglyceride and cholesterol content yielded findings that were consistent with liver weights (Figure 2B; *, $p < 0.05$, n = 5). Similarly, H&E, perilipin and ORO staining also revealed increased lipid accumulation in the livers of NCD- and HFD-fed GDF10$^{-/-}$ mice compared to wild-type counterparts (Figure 2C). To confirm our visual observations, perilipin and ORO staining was quantified using ImageJ software (Figure 2D; *, $p < 0.05$, n = 5). In line with increased hepatic lipid accumulation, an increase in plasma triglyceride content was also observed in GDF10$^{-/-}$ compared to GDF10$^{+/+}$ mice (Figure 2E; *, $p < 0.05$). The ability of GDF10 to modulate lipid droplet accumulation was then examined in immortalized human HepG2 cells. Consistent with *in vivo* findings, exogenously added rhGDF10 markedly reduced lipid accumulation in hepatocytes, resulting from exposure to the fatty acid, PA, and to the ER stress-inducing agent, TG (Fig. S1A; *, $p < 0.05$). Exogenously added rhGDF10 also reduced cytotoxicity resulting from the treatment of cells with ER stress-inducing agents known to cause *de novo* lipogenesis [28], TG and TM (Fig. S1B; *, $p < 0.05$).

Original Article

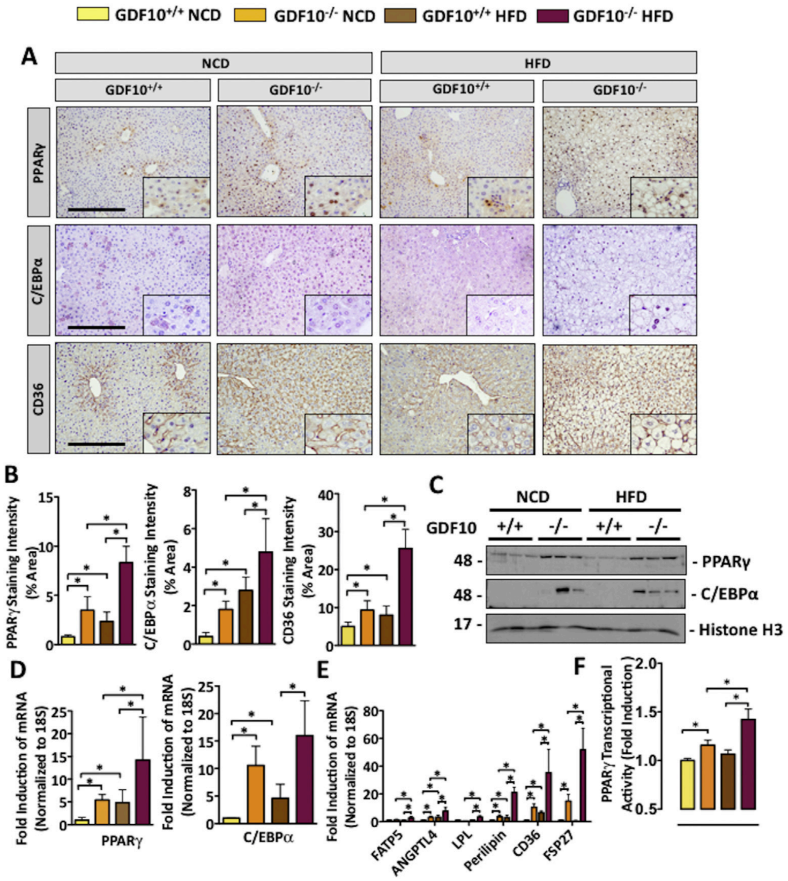

Figure 3: GDF10 deficiency increases the nuclear abundance of hepatic PPARγ and C/EBPα. (A) IHC staining of PPARγ, C/EBPα and CD36 in the livers of mice fed NCD or HFD. (B) Quantification of indicated histological staining. (C) Immunoblots of the nuclear subcellular fraction from livers of the mice fed NCD or HFD. (D) Real time PCR analysis of hepatic mRNA abundance of PPARγ, C/EBPα and (E) mRNA abundance of PPARγ-regulated genes. (F) PPARγ transcription factor activity assay. Scale bar, 100 μm. All data are shown as the mean ± S.D. *, $p < 0.05$ by one-way ANOVA.

3.3. GDF10 reduces PPARγ expression via the TGFβR1-Smad3 pathway in hepatocytes

Given the abundance of triglyceride observed in the livers of GDF10$^{-/-}$ mice, we next assessed the expression of established modulators of *de novo* lipogenesis and lipid uptake.

Previous studies have demonstrated that mouse models of steatosis exhibit increased PPARγ expression and activity [29]; thus, it was among the first markers examined. It is also well-known that naturally occurring derivatives of long-chain polyunsaturated fatty acids, including palmitic, linoleic, linolenic, and arachidonic acids, can activate PPAR receptor transcriptional activity [30,31]. Upon assessment of these mice, IHC staining revealed an increase in PPARγ expression in the livers of NCD- and HFD-fed GDF10$^{-/-}$ mice compared to controls. The expression of pro-adipogenic PPARγ-responsive proteins, including C/EBPα and CD36, were also increased (Figure 3A,B; *, $p < 0.05$, n = 5). Immunoblot analysis of nuclear fractions from the livers of NCD- and HFD-fed mice revealed consistent findings, whereby an increase in PPARγ and C/EBPα was observed in GDF10$^{-/-}$ compared to GDF10$^{+/+}$ mice (Figure 3C; n = 3). The mRNA transcript abundance of PPARγ and C/EBPα was also increased in the livers of NCD- and HFD-fed GDF10$^{-/-}$ (Figure 3D; *, $p < 0.05$, n = 5), as was the expression of CD36 and other PPARγ-responsive targets including FATP5, ANGPTL4, LPL, Perilipin and FSP27 (Figure 3E; *, $p < 0.05$, n = 5). Further examination of PPARγ using an ELISA-based transcription factor assay [32,33] revealed a concomitant increase in the binding of PPARγ to its PPRE, indicative of increased transcriptional activity in the livers of GDF10$^{-/-}$ mice compared to controls (Figure 3F; *, $p < 0.05$, n = 5). Given its established role in the regulation of feeding and metabolism, circulating leptin was also examined in a cohort of 30 week old NCD-fed GDF10$^{-/-}$ mice and age-matched controls. Consistent with previous reports in which PPARγ activation was inversely correlated with leptin, we observed leptin levels to be approximately 2-fold lower in GDF10$^{-/-}$ mice (Fig. S2; *, $p < 0.05$; n = 7) [34].

MOLECULAR METABOLISM

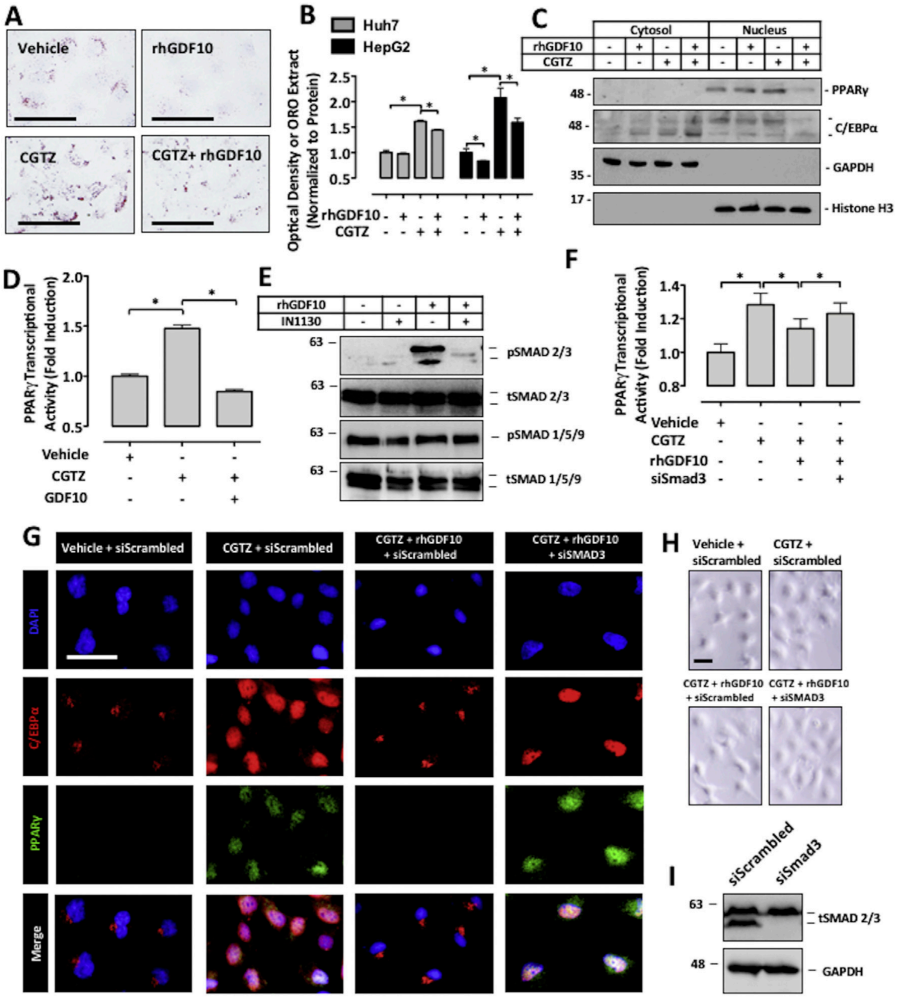

Figure 4: GDF10 modulates PPARγ nuclear abundance and transcriptional activity. (A) ORO staining and (B) extract quantification of HepG2 cells treated with PPARγ agonist, CGTZ (10 μM), or rhGDF10 (250 ng/mL) for 24 h. (C) Immunoblots of the nuclear and cytosolic subcellular fractions of Huh7 cells treated with CGTZ or rhGDF10. (D) PPARγ transcription factor activity assay after treatment with rhGDF10 or CGTZ for 1 h. (E) Immunoblots of HepG2 cells treated with IN1130 (100 nM) or rhGDF10. (F) PPARγ transcription factor activity assay in HepG2 cells transfected with either siRNA targeted against Smad3 or scrambled control siRNA and subsequently treated with CGTZ or rhGDF10. (G) Immunofluorescent staining of PPARγ and C/EBPα in Huh7 cells transfected with siRNA targeted against Smad3 and treated with rhGDF10 or CGTZ. (H) Morphology of the Huh7 cells was examined using a light microscope. (I) Immunoblots of HepG2 cells transfected with either siRNA targeted against Smad3 or scrambled control siRNA to confirm knockdown. Scale bars, 50 μm. All data are shown as the mean ± S.D. *, $p < 0.05$ by one-way ANOVA.

To substantiate our findings on the inhibitory effect of GDF10 on PPARγ-mediated lipid droplet accumulation, cultured HepG2 and Huh7 immortalized human hepatocytes were pre-treated with rhGDF10 and exposed to CGTZ, an established glitazone agonist of PPARγ. Representative images of HepG2 cells, as well as quantification of ORO isopropanol extracts of HepG2 and Huh7 cells, demonstrate that GDF10 reduced cellular lipid content in response to CGTZ treatment (Figure 4A,B; *, $p < 0.05$).

To follow up with our *in vivo* observations, we next examined the ability of GDF10 to modulate the nuclear abundance of C/EBPα as well as PPARγ in Huh7 cells. Consistent with the livers of GDF10$^{-/-}$ mice, immunoblot analysis of subcellular fractions in cultured hepatocytes revealed that GDF10 blocked the CGTZ-mediated nuclear localization of C/EBPα, and abundance of PPARγ (Figure 4C). In line with subcellular fraction data, immunofluorescent staining of HepG2 and primary human hepatocytes also demonstrated that GDF10 blocked the

Original Article

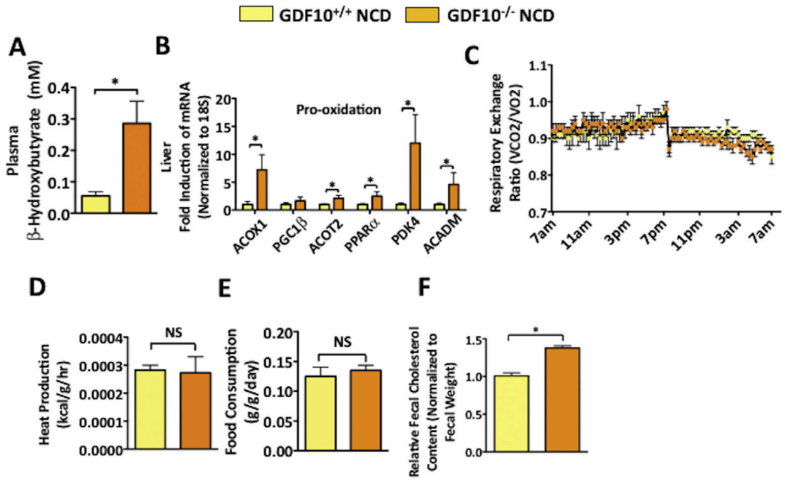

Figure 5: GDF10$^{-/-}$ mice exhibit compensatory changes in lipid homeostasis. (A) Plasma β-HB content (n = 5). (B) Real time PCR analysis of hepatic mRNA abundance of the indicated genes. (C) Respiratory exchange ratio (D) heat production and (E) food consumption in GDF10$^{+/+}$ and GDF10$^{-/-}$ mice fed NCD (n = 5). (F) Biliary cholesterol excretion in GDF10$^{+/+}$ and GDF10$^{-/-}$ mice fed NCD. All data are shown as the mean ± S.D. *, $p < 0.05$ by unpaired two-tailed Student's *t*-test.

CGTZ-mediated nuclear localization of these transcription factors (Fig. S3A,S3B). Finally, the antagonistic effect of GDF10 on PPARγ transcriptional activity was also confirmed in HepG2 cells using the transcription factor activity assay (Figure 4D; *, $p < 0.05$).

We next utilized this cultured hepatocyte model to determine the mechanism by which GDF10 affects PPARγ expression and activity. Importantly, previous studies have demonstrated that (a) signaling of TGFβ through TGFβ receptor subtype-1 (TGFβR1) induces the phosphorylation of Smad3, which (b) leads to the suppression of PPARγ expression and activity [35,36]. Furthermore, recent studies have also shown that (c) in a manner similar to TGFβ, GDF10 induces the phosphorylation of Smad3 [35]. Similar to previous studies, we observed that exogenously-added rhGDF10 induced the phosphorylation of Smad3, but only in the absence of the TGFβR1 antagonist, IN1130. Also consistent with previous studies, rhGDF10 and/or IN1130 did not affect the phosphorylation of Smad1/5/9 (Figure 4E). Using the PPARγ transcription factor assay, we next observed that rhGDF10 failed to antagonize CGTZ-mediated PPARγ activity in cells transfected with small interfering (si)RNA targeted against Smad3 (siSmad3; Figure 4F; *, $p < 0.05$). This observation was also confirmed via immunofluorescent staining of PPARγ and C/EBPα in Huh7 cells (Figure 4G). No marked change in cytotoxicity or cell morphology was observed in these cells (Figure 4H) and effective knockdown of Smad3 was confirmed via immunoblotting (Figure 4I). Finally, in line with these findings, we also observed that IN1130 attenuated the lipid-lowering effect of rhGDF10 in the presence of CGTZ (Fig. S4). Taken together, our results indicate that GDF10 acts to oppose PPARγ-mediated lipid accumulation in cultured hepatocyte models via TGFβR1-induced Smad3 phosphorylation.

3.4. GDF10$^{-/-}$ mice exhibit compensatory changes in fatty acid oxidation

Other parameters known to contribute to fatty liver and/or obesity, such as changes in lipid oxidation, biliary cholesterol excretion, energy expenditure and food consumption were also examined in GDF10$^{-/-}$ mice. To examine the possibility of lipid accumulation occurring as a result of reduced fatty acid oxidation, the ketogenic marker β-HB, was measured in the plasma. Interestingly, the elevated levels of β-HB observed in NCD-fed GDF10$^{-/-}$ mice are indicative of increased global fatty acid oxidation (Figure 5A; *, $p < 0.05$), likely working as a compensatory mechanism to oppose further lipid accumulation. Consistent with this result, increased hepatic mRNA transcript levels of a number of known drivers of fatty acid oxidation, including acyl-coenzyme A oxidase (ACOX1), peroxisome proliferator-activated receptor gamma coactivator 1- β (PGC1β), acyl-coenzyme A thioesterase 2 (ACOT2), peroxisome proliferator-activated receptor α (PPARα), pyruvate dehydrogenase lipoamide kinase isozyme 4 (PDK4) and acyl-coenzyme A dehydrogenase, C-4 to C-12 straight chain (ACADM) were also observed in the livers of NCD-fed GDF10$^{-/-}$ mice (Figure 5B; *, $p < 0.05$). However, no difference in respiratory exchange ratio and heat production was detected between GDF10$^{+/+}$ and GDF10$^{-/-}$ mice (Figure 5C,D. *, $p < 0.05$). In addition, no difference in food consumption was observed between GDF10$^{+/+}$ and GDF10$^{-/-}$ mice (Figure 5E. *, $p < 0.05$). Increased fecal cholesterol content was also observed in the GDF10$^{-/-}$ mice, suggesting heightened biliary cholesterol excretion (Figure 5F; *, $p < 0.05$). Collectively, these data suggest that despite increased liver fat content observed in GDF10$^{-/-}$ mice, a variety of compensatory mechanisms act in tandem to attenuate further lipid accumulation.

3.5. GDF10$^{-/-}$ mice exhibit increased UPR activation, fibrosis and liver injury

ER stress is a well-established early initiator of hepatic steatosis and is known to contribute to the progression of liver disease [7,37,38]. Therefore, our next aim was to assess the expression of ER stress markers in the livers of NCD- and HFD-fed GDF10$^{-/-}$ mice. Consistent with the observed increase in hepatic triglyceride levels, histological analysis revealed increased expression of ER stress markers, glucose regulated protein of 78 and 94 kDa (GRP78, GRP94) as well as phosphorylated (p)PERK in response to a HFD in the livers GDF10$^{-/-}$

MOLECULAR METABOLISM

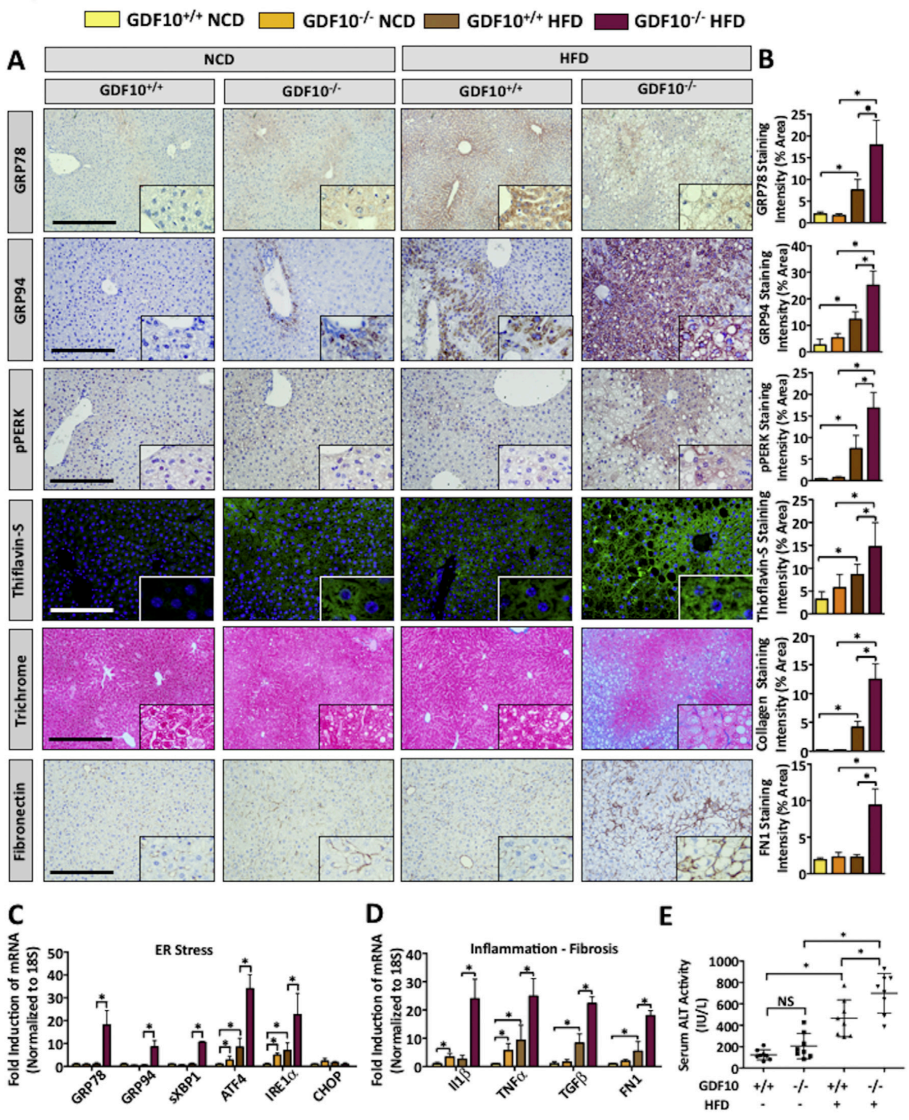

Figure 6: Livers from GDF10$^{-/-}$ mice exhibit increased UPR activation, fibrosis, and inflammation. (A) IHC staining of GRP78, GRP94, pPERK and fibronectin, as well as Masson's Trichrome and Thioflavin-S in the livers of NCD- and HFD-fed mice. (B) Quantification of indicated histological staining (n = 5). Real time PCR analysis of hepatic mRNA abundance of the indicated genes involved in (C) ER stress, (D) inflammation, and fibrosis. (E) Analysis of serum ALT activity, a marker of liver injury (n = 8). Scale bars, 100 μm. All data are shown as the mean ± S.D. *, $p < 0.05$ by one-way ANOVA.

mice (Figure 6A,B; *, $p < 0.05$). Thioflavin-S staining of misfolded protein amyloid, known to occur as a result of prolonged ER stress [9] was also increased in HFD-fed GDF10$^{-/-}$ mice compared to controls. Further assessment of the livers via IHC staining of fibronectin and Masson's Trichrome also revealed increased fibrosis in HFD-fed GDF10$^{-/-}$ mice (Figure 6A,B; *, $p < 0.05$, n = 5). Increased fibrosis in the livers of HFD-fed GDF10$^{-/-}$ mice was also independently confirmed via Picrosirius red (PSR) staining of fibrotic collagen deposition (Fig. S5A). Although a marked increase in ER stress and fibrosis markers was observed in the livers of HFD-fed GDF10$^{-/-}$ mice, no substantial difference was observed in the NCD-fed cohort. mRNA transcript abundance of ER stress, fibrotic, inflammatory, and

Original Article

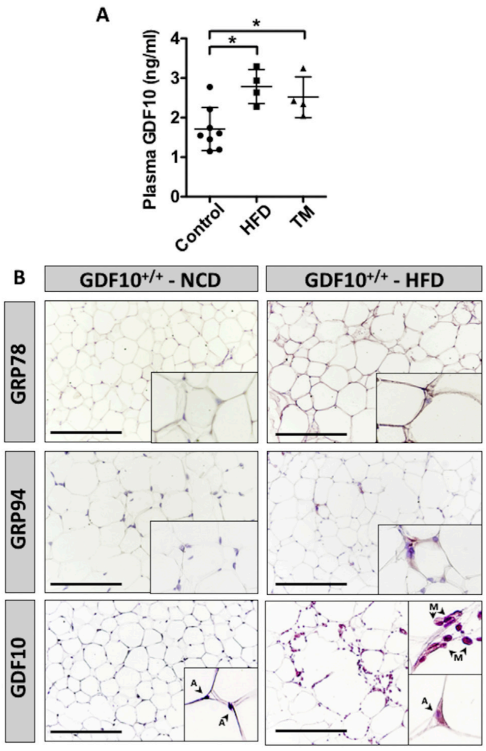

Figure 7: ER stress increases GDF10 abundance in GAT and in circulation. (A) Plasma content of circulating GDF10 in mice fed NCD or HFD for 12 weeks (n = 5), and mice treated with a bolus injection of TM (250 μg/kg - 24 h; n = 5). (B) IHC staining of GRP78, GRP94 and GDF10 in the GAT of mice fed NCD or HFD. Scale bars, 100 μm. A and M indicate adipocytes and macrophages, respectively. All data are shown as the mean ± S.D. *, $p < 0.05$ by one-way ANOVA.

apoptotic markers was also examined by real time PCR and yielded consistent findings with histological analysis (Figure 6C, D and Fig. S5B; *, $p < 0.05$, n = 5).

Hepatic insulin resistance represents another hallmark feature of liver disease. Thus, markers of hepatic gluconeogenesis were assessed via real time PCR. Interestingly, the glucoconeogenic markers induced in the livers GDF10$^{-/-}$ mice, including signal transducer and activator of transcription 3 (STAT3), CREB-regulated transcription cofactor 2 (CRTC2), forkhead box protein O1 (FOXO1) and phosphoenolpyruvate carboxykinase 1 (PCK1) are also known to be upregulated by conditions of ER stress (Fig. S5C; *, $p < 0.05$) [39]. Finally, the enzymatic activity of circulating ALT was increased in the HFD-fed GDF10$^{-/-}$ mice compared to NCD-fed controls, which is indicative of liver injury (Figure 6E; *, $p < 0.05$). Collectively, these data provide compelling evidence of heightened ER stress in the livers GDF10$^{-/-}$ mice and highlight the ability of GDF10 to attenuate diet-induced liver injury.

3.6. ER stress increases circulating and adipose GDF10 levels

Given the role of GDF10 in the regulation of hepatic triglyceride levels and injury, our final aim was to assess the effect of diet-induced stress on GDF10 expression in GDF10$^{+/+}$ mice. Similar to findings demonstrating a positive correlation between circulating GDF15 levels and hepatic ER stress [24], we also observed increased plasma GDF10 levels in HFD-fed GDF10$^{+/+}$ and in wild-type mice injected with the ER stress-inducing agent, TM (Figure 7A; *, $p < 0.05$, n = 7). Because GDF10 is primarily expressed in adipose tissue, we also examined whether TM affects GDF10 expression in 3T3-L1 adipocytes at day 10 of differentiation (Fig. S6; *, $p < 0.05$, n = 5) and in GAT from HFD-fed mice (Figure 7B; n = 7). Similar to secreted levels, an increase in GDF10 expression was observed in response to TM in 3T3-L1 adipocytes and in the GAT from HFD-fed GDF10$^{+/+}$ mice. We also report the surprising finding that GAT-resident macrophages in HFD-fed mice express abundant levels of GDF10 (Figure 7B); an observation that was not present in GAT from NCD-fed mice. Collectively, these data suggest that during conditions of diet-induced stress, adipose tissue promotes the expression of GDF10 to attenuate further triglyceride accumulation in the liver as a response to injury.

4. DISCUSSION

A growing body of evidence suggests that GDF10, in addition to being a key modulator of osteogenesis, also plays a critical role in adipose lipid metabolism [20,21]. To the best of our knowledge, however, the functional importance of GDF10 in liver lipid metabolism has not yet been evaluated. Here, we demonstrate that GDF10$^{-/-}$ mice exhibit increased adiposity, as well as increased body weight and hepatic triglyceride and cholesterol levels; an early feature in the development of diet-induced liver disease [3]. We also observed that severe lipid accumulation in the livers of HFD-fed GDF10$^{-/-}$ mice was associated with a substantial induction of a variety of ER stress markers and concomitant liver injury. Additional hallmark characteristics of liver disease, such as apoptosis, inflammation, fibrosis and changes in gluconeogenic gene expression, were also observed in the livers of HFD-fed GDF10$^{-/-}$ mice.

To explain these findings, we examined a number of metabolic parameters and expression of genes known to alter lipid metabolism. Despite elevated body weight and adiposity, an increase in global fatty acid oxidation was observed in GDF10$^{-/-}$ mice. Given that this finding is in mechanistic contrast to the obese phenotype in the mice, these findings suggest that heightened fatty acid oxidation likely occurred as a compensatory response to attenuate further fat accumulation. In line with these data, an increase in biliary cholesterol excretion was also identified. To this end, we observed an increase in the expression of key modulators of adipogenesis and well-known drivers of NAFLD, such as PPARγ and C/EBPα, in the livers of GDF10$^{-/-}$ mice. Upon further analysis using cultured hepatocytes, exogenously added rhGDF10 reduced the abundance and transcriptional activity of PPARγ, and also blocked PPARγ agonist-driven lipid accumulation. Lastly, we have also demonstrated that GDF10 inhibits PPARγ transcriptional activity via the conventional TGFβR1-Smad3 signaling cascade. Collectively, these data suggest that GDF10 is a potent antagonist of PPARγ and can protect from diet-induced hepatic steatosis.

Several groups have recently demonstrated the involvement of multiple TGFβ superfamily members in the pathogenesis of obesity-related diseases such as type 2 diabetes and NAFLD [40–42]. In clinical studies, GDF15 expression correlates with a variety of metabolic disorders, including obesity, insulin resistance and the risk of cardiovascular events [43]. GDF15$^{-/-}$ mice also exhibit increased body weight and peripheral lipid accumulation following a metabolic challenge, whereas overexpression of this protein led to reduced body weight and improved metabolic parameters [44,45]. Similar to GDF15$^{-/-}$ mice, GDF10$^{-/-}$ mice have increased body weight and

MOLECULAR METABOLISM

adiposity, a phenotype that unlike GDF15$^{-/-}$ mice, does not require a metabolic stimulus such as a HFD. Our findings are also consistent with studies in which overexpression of GDF10 in mice led to a reduction in adiposity and improved metabolic outcomes [21].

Activation of the TGFβ signaling cascade has been shown to differentially modulate the expression of lipogenic markers, based on tissue/cell-specific expression, and unique molecular interactions with a variety of inhibitory molecules and receptor—ligand complexes. TGFβ signaling has been shown to induce lipogenesis, inflammation and cell death via Smad2/3 [42], while also blocking PPARγ expression, activity and lipogenesis in a manner dependent on β-catenin [46]. Overexpression of Smad3 and its partner Smad4 has been shown to reduce PPARγ promoter activity in aortic smooth muscle cells [47]. Furthermore, TGFβ suppresses PPARγ expression and activity via Smad3/4 binding to the inhibitory element in the PPAR promoter region in lung fibroblasts [36]. Given that GDF10 can induce the phosphorylation and activation of Smad3, but also block the transcriptional activation of PPARγ, our data suggest that in a manner similar to TGFβ, GDF10 reduces PPARγ activity in a Smad3-dependent manner.

PPARγ activation is necessary and sufficient to induce adipocyte differentiation. Studies have demonstrated that (a) selective ablation of PPARγ, using a tamoxifen-dependent recombination system in mice, led to the death of adipocytes only a few days following treatment [48], and (b) AAV-mediated hepatic overexpression of PPARγ$_2$ in mice promoted an adipose-like phenotype in hepatocytes by inducing the expression of pro-adipogenic mediators, such as adipsin, adiponectin, and aP2, which resulted in severe steatosis [49]. Moreover, previous studies have also demonstrated that hepatic PPARγ is robustly induced in the livers of patients, as well as in pre-clinical models of NAFLD [13,49]. Conversely, PPARγ deletion in mouse hepatocytes has been shown to attenuate intracellular lipid accumulation [50]. Consistent with our studies, it is also well-established that exposure of mice to a HFD promotes the expression of hepatic PPARγ and a variety of its downstream targets [51]. In addition to PPARγ, we also observed increased expression and nuclear localization of C/EBPα in the livers of GDF10$^{-/-}$ mice compared to the GDF10$^{+/+}$ controls. C/EBPα is also known to play a crucial role in adipocyte differentiation, and similar to PPARγ, its expression is both necessary and sufficient for adipogenesis [52]. Studies also demonstrate that C/EBPα can directly regulate PPARγ promoter activity [53] and has been described as a critical and obligate regulator of PPARγ expression [54]. Furthermore, PPARγ and C/EBPα mutually induce each other's expression in order to promote adipogenesis [53,55,56] Given the cross-talk that occurs between these two master regulators of adipogenesis, it remains unclear which of the two, or whether both are directly affected by GDF10.

In summary, we demonstrate that GDF10 is an essential modulator of hepatic lipid homeostasis and is crucial for the maintenance of hepatic lipid turnover. GDF10 knockout leads to hepatic steatosis in NCD-fed mice, as well as severe steatosis, inflammation, fibrosis, and ER stress in response to a HFD. Given that most diet-induced models of liver disease fail to recapitulate fibrosis, a key marker of NASH, in this report we also describe a new genetic model for the study of liver disease. Furthermore, conditions that cause hepatic and/or adipocyte lipid accumulation also induced a compensatory increase in circulating GDF10 levels in GDF10-expressing control mice. Additional tissue-specific knockdown studies, however, are required to confirm the origin of circulating GDF10 in the context of diet-induced NAFLD. Future studies examining the correlation between polymorphisms in the *GDF10* gene and the prevalence of obesity and/or NAFLD may also yield interesting findings. Overall, we identify circulating GDF10 as a novel regulator of liver lipid metabolism and demonstrate that in a manner similar to GDF15, this adipokine could be utilized for the management of metabolic disorders.

FINANCIAL SUPPORT

This work was supported in part by research grants to Richard C. Austin from the Heart and Stroke Foundation of Canada (G-13-0003064 and G-15-0009389) and the Canadian Institutes of Health Research (74477, 111239). Financial support from the Research Institute of St. Joe's Hamilton is acknowledged. Richard C. Austin is a Career Investigator of the Heart and Stroke Foundation of Ontario and holds the Amgen Canada Research Chair in the Division of Nephrology at St. Joseph's Healthcare Hamilton and McMaster University. Kenneth N. Maclean gratefully acknowledges financial support from the William R. Hummel Homocystinuria Research Fund and holds the Ehst-Hummel-Kaufmann Family Endowed Chair in Inherited Metabolic Disease.

AUTHOR CONTRIBUTIONS

KP, PL, and RCA conceived the studies and wrote the manuscript. KP, PL, JHB, SVP, EAD, MEM, and AMB performed all of the *in vitro* and *in vivo* studies. The manuscript was revised by KNM and JCK.

CONFLICT OF INTEREST

The authors declare that they have no conflicts of interest with the contents of this article.

APPENDIX A. SUPPLEMENTARY DATA

Supplementary data to this article can be found online at https://doi.org/10.1016/j.molmet.2019.06.021.

REFERENCES

[1] Gonzalez-Muniesa, P., Martinez-Gonzalez, M.A., Hu, F.B., Despres, J.P., Matsuzawa, Y., Loos, R.J.F., et al., 2017. Obesity. Nature Reviews Disease Primers 3:17034.

[2] Perry, R.J., Samuel, V.T., Petersen, K.F., Shulman, G.I., 2014. The role of hepatic lipids in hepatic insulin resistance and type 2 diabetes. Nature 510:84—91.

[3] Brunt, E.M., Wong, V.W., Nobili, V., Day, C.P., Sookoian, S., Maher, J.J., et al., 2015. Nonalcoholic fatty liver disease. Nature reviews Disease primers 1:15080.

[4] Angulo, P., 2002. Nonalcoholic fatty liver disease. New England Journal of Medicine 346:1221—1231.

[5] Kim, J.Y., Garcia-Carbonell, R., Yamachika, S., Zhao, P., Dhar, D., Loomba, R., et al., 2018. ER stress drives lipogenesis and steatohepatitis via caspase-2 activation of S1P. Cell 75:133—145 e115.

[6] Ashraf, N.U., Sheikh, T.A., 2015. Endoplasmic reticulum stress and oxidative stress in the pathogenesis of non-alcoholic fatty liver disease. Free Radical Research 49:1405—1418.

[7] Puri, P., Mirshahi, F., Cheung, O., Natarajan, R., Maher, J.W., Kellum, J.M., et al., 2008. Activation and dysregulation of the unfolded protein response in nonalcoholic fatty liver disease. Gastroenterology 134:568—576.

[8] Zeng, L., Lu, M., Mori, K., Luo, S., Lee, A.S., Zhu, Y., et al., 2004. ATF6 modulates SREBP2-mediated lipogenesis. The EMBO Journal 23:950—958.

[9] Zhou, H., Liu, R., 2014. ER stress and hepatic lipid metabolism. Frontiers in Genetics 5:112.

[10] Bobrovnikova-Marjon, E., Hatzivassiliou, G., Grigoriadou, C., Romero, M., Cavener, D.R., Thompson, C.B., et al., 2008. PERK-dependent regulation of lipogenesis during mouse mammary gland development and adipocyte differentiation. Proceedings of the National Academy of Sciences of the United States of America 105:16314–16319.

[11] Matsusue, K., Kusakabe, T., Noguchi, T., Takiguchi, S., Suzuki, T., Yamano, S., et al., 2008. Hepatic steatosis in leptin-deficient mice is promoted by the PPAR gamma target gene Fsp27. Cell Metabolism 7:302–311.

[12] Lee, Y.J., Ko, E.H., Kim, J.E., Kim, E., Lee, H., Choi, H., et al., 2012. Nuclear receptor PPARγ-regulated monoacylglycerol O-acyltransferase 1 (MGAT1) expression is responsible for the lipid accumulation in diet-induced hepatic steatosis. Proceedings of the National Academy of Sciences of the United States of America 109:13656–13661.

[13] Pettinelli, P., Videla, L.A., 2011. Up-regulation of PPAR-γ mRNA expression in the liver of obese patients: an additional reinforcing lipogenic mechanism to SREBP-1c induction. Journal of Clinical Endocrinology & Metabolism 96: 1424–1430.

[14] Zhang, X.Q., Xu, C.F., Yu, C.H., Chen, W.X., Li, Y.M., 2014. Role of endoplasmic reticulum stress in the pathogenesis of nonalcoholic fatty liver disease. World Journal of Gastroenterology 20:1768–1776.

[15] Matsumoto, Y., Otsuka, F., Hino, J., Miyoshi, T., Takano, M., Miyazato, M., et al., 2012. Bone morphogenetic protein-3b (BMP-3b) inhibits osteoblast differentiation via Smad2/3 pathway by counteracting Smad1/5/8 signaling. Molecular and Cellular Endocrinology 350:78–86.

[16] Zhao, R., Lawler, A.M., Lee, S.J., 1999. Characterization of GDF-10 expression patterns and null mice. Developmental Biology 212:68–79.

[17] Tseng, Y.H., Kokkotou, E., Schulz, T.J., Huang, T.L., Winnay, J.N., Taniguchi, C.M., et al., 2008. New role of bone morphogenetic protein 7 in brown adipogenesis and energy expenditure. Nature 454:1000–1004.

[18] Schulz, T.J., Tseng, Y.H., 2009. Emerging role of bone morphogenetic proteins in adipogenesis and energy metabolism. Cytokine & Growth Factor Reviews 20:523–553.

[19] Zamani, N., Brown, C.W., 2011. Emerging roles for the transforming growth factor-β superfamily in regulating adiposity and energy expenditure. Endocrine Reviews 32:387–403.

[20] Hino, J., Miyazawa, T., Miyazato, M., Kangawa, K., 2012. Bone morphogenetic protein-3b (BMP-3b) is expressed in adipocytes and inhibits adipogenesis as a unique complex. International Journal of Obesity 36:725–734.

[21] Hino, J., Nakatani, M., Arai, Y., Tsuchida, K., Shirai, M., Miyazato, M., et al., 2017. Overexpression of bone morphogenetic protein-3b (BMP-3b) in adipose tissues protects against high-fat diet-induced obesity. International Journal of Obesity 41:483–488.

[22] Chrysovergis, K., Wang, X., Kosak, J., Lee, S.H., Kim, J.S., Foley, J.F., et al., 2014. NAG-1/GDF-15 prevents obesity by increasing thermogenesis, lipolysis and oxidative metabolism. International Journal of Obesity 38:1555–1564.

[23] Li, D., Zhang, H., Zhong, Y., 2018. Hepatic GDF15 is regulated by CHOP of the unfolded protein response and alleviates NAFLD progression in obese mice. Biochemical and Biophysical Research Communications 498:388–394.

[24] Tsai, V.W.W., Husaini, Y., Sainsbury, A., Brown, D.A., Breit, S.N., 2018. The MIC-1/GDF15-GFRAL pathway in energy homeostasis: implications for obesity, cachexia, and other associated diseases. Cell Metabolism 28:353–368.

[25] Polyzos, S.A., Kountouras, J., Mantzoros, C.S., 2016. Adipokines in nonalcoholic fatty liver disease. Metabolism Clinical and Experimental 65:1062–1079.

[26] Lebeau, P., Platko, K., Al-Hashimi, A.A., Byun, J.H., Lhotak, S., Holzapfel, N., et al., 2018. Loss-of-function PCSK9 mutants evade the unfolded protein response sensor GRP78 and fail to induce endoplasmic reticulum stress when retained. Journal of Biological Chemistry 293:7329–7343.

[27] Lebeau, P.F., Byun, J.H., Platko, K., MacDonald, M.E., Poon, S.V., Faiyaz, M., 2019. Diet-induced hepatic steatosis abrogates cell-surface LDLR by inducing de novo PCSK9 expression in mice. Journal of Biological Chemistry 294: 9037–9047.

[28] Lee, J.S., Zheng, Z., Mendez, R., Ha, S.W., Xie, Y., Zhang, K., 2012. Pharmacologic ER stress induces non-alcoholic steatohepatitis in an animal model. Toxicology Letters 211:29–38.

[29] Gross, B., Pawlak, M., Lefebvre, P., Staels, B., 2017. PPARs in obesity-induced T2DM, dyslipidaemia and NAFLD. Nature Reviews Endocrinology 13:36–49.

[30] Bocos, C., Göttlicher, M., Gearing, K., Banner, C., Enmark, E., Teboul, M., et al., 1995. Fatty acid activation of peroxisome proliferator-activated receptor (PPAR). The Journal of Steroid Biochemistry and Molecular Biology 53:467–473.

[31] Krey, G., Braissant, O., L'Horset, F., Kalkhoven, E., Perroud, M., Parker, M.G., et al., 1997. Fatty acids, eicosanoids, and hypolipidemic agents identified as ligands of peroxisome proliferator-activated receptor by coactivator-dependent receptor ligand assay. Molecular Endocrinology 6:779–791.

[32] Ahmad, I., Mui, E., Galbraith, L., Patel, R., Tan, E.H., Salji, M., et al., 2016. Sleeping beauty screen revealed pparg activation in metastatic prostate cancer. Proceedings of the National Academy of Sciences 29:8290–8295.

[33] Jiang, Y., Thakran, S., Bheemreddy, R., Ye, E.A., He, H., Walker, R.J., et al., 2014. Pioglitazone normalizes insulin signaling in the diabetic rat retina through reduction in tumor necrosis factor α and suppressor of cytokine signaling 3. Journal of Biological Chemistry 289:26395–26405.

[34] De Vos, P., Lefebvre, A.M., Miller, S.G., Guerre-Millo, M., Wong, K., Saladin, R., et al., 1996. Thiazolidinediones repress ob gene expression in rodents via activation of peroxisome proliferator-activated receptor gamma. Journal of Clinical Investigation 98:1004–1009.

[35] Upadhyay, G., Yin, Y., Yuan, H., Derynch, R., Glazer, R.I., 2011. Stem cell antigen-1 enhances tumorigenicity by disruption of growth differentiation factor-10 (GDF10)-dependent TGF-β signaling. Proceedings of the National Academy of Sciences of the United States of America 108:7820–7825.

[36] Lakshmi, S.P., Reddy, A.T., Reddy, R.C., 2017. Transforming growth factor β suppresses peroxisome proliferator-activated receptor γ expression via both SMAD binding and novel TGF- β inhibitory elements. Biochemical Journal 474: 1531–1546.

[37] Wang, D., Wei, Y., Pagliassotti, M.J., 2006. Saturated fatty acids promote endoplasmic reticulum stress and liver injury in rats with hepatic steatosis. Endocrinology 147:943–951.

[38] Bashiri, A., Nesan, D., Tavallaee, G., Sue-Chu-Lam, I., Chien, K., Maguire, G.F., et al., 2016. Cellular cholesterol accumulation modulates high fat high sucrose (HFHS) diet-induced ER stress and hepatic inflammasome activation in the development of non-alcoholic steatohepatitis. Biochemica et Biophysica Acta 1861:594–605.

[39] Kim, O.K., Jun, W., Lee, J., 2015. Mechanism of ER Stress and inflammation for hepatic insulin resistance in obesity. Annals of Nutrition & Metabolism 67: 218–227.

[40] Yadav, H., Quijano, C., Kamaraju, A.K., Gavrilova, O., Malek, R., Chen, W., et al., 2011. Protection from obesity and diabetes by blockade of TGF-β/Smad3 signaling. Cell Metabolism 14:67–79.

[41] Margoni, A., Fotis, L., Papavassiliou, A.G., 2012. The transforming growth factor-beta/bone morphogenetic protein signalling pathway in adipogenesis. The International Journal of Biochemistry & Cell Biology 44:475–479.

[42] Yang, L., Roh, Y.S., Song, J., Zhang, B., Liu, C., Loomba, R., et al., 2014. Transforming growth factor beta signaling in hepatocytes participates in steatohepatitis through regulation of cell death and lipid metabolism in mice. Hepatology 59:483–495.

[43] Kempf, T., Guba-Quint, A., Torgerson, J., Magnone, M.C., Haefliger, C., Bobadilla, M., et al., 2012. Growth differentiation factor 15 predicts future insulin resistance and impaired glucose control in obese nondiabetic individuals: results from the XENDOS trial. European Journal of Endocrinology 167:671–678.

[44] Macia, L., Tsai, V.W., Nguyen, A.D., Johnen, H., Kuffner, T., Shi, Y.C., et al., 2012. Macrophage inhibitory cytokine 1 (MIC-1/GDF15) decreases food intake,

MOLECULAR METABOLISM

body weight and improves glucose tolerance in mice on normal & obesogenic diets. PLoS One 7:e34868.

[45] Kim, J.M., Kosak, J.P., Kim, J.K., Kissling, G., Germolec, D.R., Zeldin, D.C., et al., 2013. NAG-1/GDF15 transgenic mouse has less white adipose tissue and a reduced inflammatory response. Mediators of Inflammation 2013:641851.

[46] Qian, J., Niu, M., Zhai, X., Zhou, Q., Zhou, Y., 2012. Beta-catenin pathway is required for TGF-β1 inhibition of PPARγ expression in cultured hepatic stellate cells. Pharmacological Research 66:219—225.

[47] Fu, M., Zhang, J., Lin, Y., Zhu, X., Zhao, L., Ahmad, M., et al., 2003. Early stimulation and late inhibition of peroxisome proliferator-activated receptor gamma (PPAR gamma) gene expression by transforming growth factor beta in human aortic smooth muscle cell: role of early growth-response factor-1 (Egr-1), activator protein 1 (AP1) and Smads. Biochemical Journal 370:1019—1025.

[48] Imai, T., Takakuwa, R., Marchand, S., Dentz, E., Bornert, J.M., Messaddeq, N., et al., 2004. Peroxisome proliferator-activated receptor gamma is required in mature white and brown adipocytes for their survival in the mouse. Proceedings of the National Academy of Sciences of the United States of America 101:4543—4547.

[49] Yu, S., Matsusue, K., Kashireddy, P., Cao, W.Q., Yeldandi, V., Yeldandi, A.V., et al., 2003. Adipocyte-specific gene expression and adipogenic steatosis in the mouse liver due to peroxisome proliferator-activated receptor γ1 (PPARγ1) overexpression. Journal of Biological Chemistry 278:498—505.

[50] Moran-Salvador, E., Lopez-Parr, M., Garcia-Alonso, V., Titos, E., Martinez-Clemente, M., Gonzalez-Periz, A., et al., 2011. Role of PPARγ in obesity-induced hepatic steatosis as determined by hepatocyte- and macrophage-specific conditional knockouts. Federation of American societies of Experimental Biology 25:2538—2550.

[51] Inoue, M., Ohtake, T., Motomura, W., Takahashi, N., Hosoki, Y., Miyoshi, S., et al., 2005. Increased expression of PPARγ in high fat diet-induced liver steatosis in mice. Biochemical and Biophysical Research Communications 336:215—222.

[52] Lane, M.D., Tang, Q.Q., Jiang, M.S., 1999. Role of the CCAAT enhancer binding proteins (C/EBPs) in adipocyte differentiation. Biochemical and Biophysical Research Communications 3:677—683.

[53] Clarke, S.L., Robinson, C.E., Gimble, J.M., 1997. CAAT/enhancer binding proteins directly modulate transcription from the peroxisome proliferator-activated receptor γ2 promoter. Biochemical and Biophysical Research Communications 1:99—103.

[54] Madsen, M.S., Siersbaek, R., Boergesen, M., Nielsen, R., Mandrup, S., 2014. Peroxisome proliferator-activated receptor gamma and C/EBPalpha synergistically activate key metabolic adipocyte genes by assisted loading. Molecular and Cellular Biology 34:939—954.

[55] Wu, Z., Rosen, E., Brun, R., Hauser, S., Adelmant, G., Troy, A., 1999. Cross regulation of C/EBPα and PPARγ controls the transcriptional pathway of adipogenesis and insulin sensitivity. Molecular Cell 3:151—158.

[56] Elberg, G., Gimble, J., Tsai, S., 2000. Modulation of the murine peroxisome proliferator-activated receptor γ2promoter activity by CCAAT/enhancer-binding proteins. Journal of Biological Chemistry 275:27815—27822.

Chapter 9: References

[1] Virchow R. Gesammelte Abhandlungen zur wissenschaftlichen Medizin. Frankfurt: Phlogose und Thrombose im Gefäßsystem; 1856.

[2] Rafieian-Kopaei M, Setorki M, Doudi M, Baradaran A, Nasri H. Atherosclerosis: process, indicators, risk factors and new hopes. International journal of preventive medicine 2014;5:927-946.

[3] Ridker PM, Everett BM, Thuren T, MacFadyen JG, Chang WH, Ballantyne C, et al. Antiinflammatory Therapy with Canakinumab for Atherosclerotic Disease. N Engl J Med 2017;377:1119-1131.

[4] Ference BA, Ginsberg HN, Graham I, Ray KK, Packard CJ, Bruckert E, et al. Low-density lipoproteins cause atherosclerotic cardiovascular disease. 1. Evidence from genetic, epidemiologic, and clinical studies. A consensus statement from the European Atherosclerosis Society Consensus Panel. Eur Heart J 2017;38:2459-2472.

[5] Shapiro MD, Fazio S. Apolipoprotein B-containing lipoproteins and atherosclerotic cardiovascular disease. F1000Research 2017;6:134.

[6] Ikonen E. Mechanisms for cellular cholesterol transport: defects and human disease. Physiological reviews 2006;86:1237-1261.

[7] Daniels TF, Killinger KM, Michal JJ, Wright RW, Jr., Jiang Z. Lipoproteins, cholesterol homeostasis and cardiac health. Int J Biol Sci 2009;5:474-488.

[8] Huang S, Henry L, Ho YK, Pownall HJ, Rudenko G. Mechanism of LDL binding and release probed by structure-based mutagenesis of the LDL receptor. Journal of lipid research 2010;51:297-308.

[9] van Meer G, Voelker DR, Feigenson GW. Membrane lipids: where they are and how they behave. Nat Rev Mol Cell Biol 2008;9:112-124.

[10] Hewing B, Moore KJ, Fisher EA. HDL and cardiovascular risk: time to call the plumber? Circ Res 2012;111:1117-1120.

[11] Rader DJ, Hovingh GK. HDL and cardiovascular disease. Lancet 2014;384:618-625.

[12] Prado CM, Ramos SG, Elias J, Jr., Rossi MA. Turbulent blood flow plays an essential localizing role in the development of atherosclerotic lesions in experimentally induced hypercholesterolaemia in rats. International journal of experimental pathology 2008;89:72-80.

[13] Bentzon JF, Otsuka F, Virmani R, Falk E. Mechanisms of plaque formation and rupture. Circ Res 2014;114:1852-1866.

[14] Yu XH, Fu YC, Zhang DW, Yin K, Tang CK. Foam cells in atherosclerosis. Clin Chim Acta 2013;424:245-252.

[15] Park YM. CD36, a scavenger receptor implicated in atherosclerosis. Experimental & molecular medicine 2014;46:e99.

[16] Bobryshev YV. Monocyte recruitment and foam cell formation in atherosclerosis. Micron 2006;37:208-222.

[17] Woollard KJ, Geissmann F. Monocytes in atherosclerosis: subsets and functions. Nature reviews Cardiology 2010;7:77-86.

[18] Tabas I. The role of endoplasmic reticulum stress in the progression of atherosclerosis. Circ Res 2010;107:839-850.

[19] Cardoso L, Weinbaum S. Changing views of the biomechanics of vulnerable plaque rupture: a review. Ann Biomed Eng 2014;42:415-431.
[20] Defesche JC, Gidding SS, Harada-Shiba M, Hegele RA, Santos RD, Wierzbicki AS. Familial hypercholesterolaemia. Nature reviews Disease primers 2017;3:17093.
[21] McCrindle BW. Familial hypercholesterolemia in children and adolescents. Curr Opin Lipidol 2012;23:525-531.
[22] Singh S, Bittner V. Familial hypercholesterolemia--epidemiology, diagnosis, and screening. Curr Atheroscler Rep 2015;17:482.
[23] Cuchel M, Bruckert E, Ginsberg HN, Raal FJ, Santos RD, Hegele RA, et al. Homozygous familial hypercholesterolaemia: new insights and guidance for clinicians to improve detection and clinical management. A position paper from the Consensus Panel on Familial Hypercholesterolaemia of the European Atherosclerosis Society. Eur Heart J 2014;35:2146-2157.
[24] Soutar AK, Naoumova RP. Mechanisms of disease: genetic causes of familial hypercholesterolemia. Nat Clin Pract Cardiovasc Med 2007;4:214-225.
[25] Brown MS, Goldstein JL. Familial hypercholesterolemia: defective binding of lipoproteins to cultured fibroblasts associated with impaired regulation of 3-hydroxy-3-methylglutaryl coenzyme A reductase activity. Proc Natl Acad Sci U S A 1974;71:788-792.
[26] Goldstein JL, Brown MS. The LDL receptor. Arterioscler Thromb Vasc Biol 2009;29:431-438.
[27] Hobbs HH, Russell DW, Brown MS, Goldstein JL. The LDL receptor locus in familial hypercholesterolemia: mutational analysis of a membrane protein. Annu Rev Genet 1990;24:133-170.
[28] Susan-Resiga D, Girard E, Kiss RS, Essalmani R, Hamelin J, Asselin MC, et al. The Proprotein Convertase Subtilisin/Kexin Type 9-resistant R410S Low Density Lipoprotein Receptor Mutation: A NOVEL MECHANISM CAUSING FAMILIAL HYPERCHOLESTEROLEMIA. J Biol Chem 2017;292:1573-1590.
[29] Soria LF, Ludwig EH, Clarke HR, Vega GL, Grundy SM, McCarthy BJ. Association between a specific apolipoprotein B mutation and familial defective apolipoprotein B-100. Proc Natl Acad Sci U S A 1989;86:587-591.
[30] Gaffney D, Reid JM, Cameron IM, Vass K, Caslake MJ, Shepherd J, et al. Independent mutations at codon 3500 of the apolipoprotein B gene are associated with hyperlipidemia. Arterioscler Thromb Vasc Biol 1995;15:1025-1029.
[31] Abifadel M, Varret M, Rabes JP, Allard D, Ouguerram K, Devillers M, et al. Mutations in PCSK9 cause autosomal dominant hypercholesterolemia. Nat Genet 2003;34:154-156.
[32] Seidah NG, Benjannet S, Wickham L, Marcinkiewicz J, Jasmin SB, Stifani S, et al. The secretory proprotein convertase neural apoptosis-regulated convertase 1 (NARC-1): liver regeneration and neuronal differentiation. Proc Natl Acad Sci U S A 2003;100:928-933.
[33] Maxwell KN, Breslow JL. Adenoviral-mediated expression of Pcsk9 in mice results in a low-density lipoprotein receptor knockout phenotype. Proc Natl Acad Sci U S A 2004;101:7100-7105.

[34] Benjannet S, Hamelin J, Chretien M, Seidah NG. Loss- and gain-of-function PCSK9 variants: cleavage specificity, dominant negative effects, and low density lipoprotein receptor (LDLR) degradation. J Biol Chem 2012;287:33745-33755.
[35] Wu NQ, Li JJ. PCSK9 gene mutations and low-density lipoprotein cholesterol. Clin Chim Acta 2014;431:148-153.
[36] Khera AV, Kathiresan S. Genetics of coronary artery disease: discovery, biology and clinical translation. Nature reviews Genetics 2017;18:331-344.
[37] Linsel-Nitschke P, Gotz A, Erdmann J, Braenne I, Braund P, Hengstenberg C, et al. Lifelong reduction of LDL-cholesterol related to a common variant in the LDL-receptor gene decreases the risk of coronary artery disease--a Mendelian Randomisation study. PLoS One 2008;3:e2986.
[38] Ference BA, Yoo W, Alesh I, Mahajan N, Mirowska KK, Mewada A, et al. Effect of long-term exposure to lower low-density lipoprotein cholesterol beginning early in life on the risk of coronary heart disease: a Mendelian randomization analysis. J Am Coll Cardiol 2012;60:2631-2639.
[39] Willer CJ, Schmidt EM, Sengupta S, Peloso GM, Gustafsson S, Kanoni S, et al. Discovery and refinement of loci associated with lipid levels. Nat Genet 2013;45:1274-1283.
[40] Endo A. A historical perspective on the discovery of statins. Proceedings of the Japan Academy Series B, Physical and biological sciences 2010;86:484-493.
[41] Cholesterol Treatment Trialists C, Baigent C, Blackwell L, Emberson J, Holland LE, Reith C, et al. Efficacy and safety of more intensive lowering of LDL cholesterol: a meta-analysis of data from 170,000 participants in 26 randomised trials. Lancet 2010;376:1670-1681.
[42] Cannon CP, Blazing MA, Giugliano RP, McCagg A, White JA, Theroux P, et al. Ezetimibe Added to Statin Therapy after Acute Coronary Syndromes. N Engl J Med 2015;372:2387-2397.
[43] Ross S, D'Mello M, Anand SS, Eikelboom J, Consortium CAD, Stewart AF, et al. Effect of Bile Acid Sequestrants on the Risk of Cardiovascular Events: A Mendelian Randomization Analysis. Circulation Cardiovascular genetics 2015;8:618-627.
[44] Jakob T, Nordmann AJ, Schandelmaier S, Ferreira-Gonzalez I, Briel M. Fibrates for primary prevention of cardiovascular disease events. Cochrane Database Syst Rev 2016;11:CD009753.
[45] Miettinen TA, Gylling H. Plant stanol and sterol esters in prevention of cardiovascular diseases: a review. International journal of clinical pharmacology and therapeutics 2006;44:247-250.
[46] Buchwald H, Varco RL, Matts JP, Long JM, Fitch LL, Campbell GS, et al. Effect of partial ileal bypass surgery on mortality and morbidity from coronary heart disease in patients with hypercholesterolemia. Report of the Program on the Surgical Control of the Hyperlipidemias (POSCH). N Engl J Med 1990;323:946-955.
[47] Kakaei F, Nikeghbalian S, Kazemi K, Salahi H, Bahador A, Dehghani SM, et al. Liver transplantation for homozygous familial hypercholesterolemia: two case reports. Transplantation proceedings 2009;41:2939-2941.

[48] Ford I, Murray H, McCowan C, Packard CJ. Long-Term Safety and Efficacy of Lowering Low-Density Lipoprotein Cholesterol With Statin Therapy: 20-Year Follow-Up of West of Scotland Coronary Prevention Study. Circulation 2016;133:1073-1080.
[49] Miedema MD, Nauffal VD, Singh A, Blankstein R. Statin therapy for young adults: A long-term investment worth considering. Trends Cardiovasc Med 2019.
[50] Collins R, Reith C, Emberson J, Armitage J, Baigent C, Blackwell L, et al. Interpretation of the evidence for the efficacy and safety of statin therapy. Lancet 2016;388:2532-2561.
[51] Desai NR, Sabatine MS. PCSK9 inhibition in patients with hypercholesterolemia. Trends Cardiovasc Med 2015;25:567-574.
[52] Sabatine MS, Giugliano RP, Keech AC, Honarpour N, Wiviott SD, Murphy SA, et al. Evolocumab and Clinical Outcomes in Patients with Cardiovascular Disease. N Engl J Med 2017;376:1713-1722.
[53] Cohen J, Pertsemlidis A, Kotowski IK, Graham R, Garcia CK, Hobbs HH. Low LDL cholesterol in individuals of African descent resulting from frequent nonsense mutations in PCSK9. Nat Genet 2005;37:161-165.
[54] Cohen JC, Boerwinkle E, Mosley TH, Jr., Hobbs HH. Sequence variations in PCSK9, low LDL, and protection against coronary heart disease. N Engl J Med 2006;354:1264-1272.
[55] Mayne J, Dewpura T, Raymond A, Bernier L, Cousins M, Ooi TC, et al. Novel loss-of-function PCSK9 variant is associated with low plasma LDL cholesterol in a French-Canadian family and with impaired processing and secretion in cell culture. Clin Chem 2011;57:1415-1423.
[56] Chretien M, Mbikay M. 60 YEARS OF POMC: From the prohormone theory to pro-opiomelanocortin and to proprotein convertases (PCSK1 to PCSK9). Journal of molecular endocrinology 2016;56:T49-62.
[57] Benjannet S, Rhainds D, Essalmani R, Mayne J, Wickham L, Jin W, et al. NARC-1/PCSK9 and its natural mutants: zymogen cleavage and effects on the low density lipoprotein (LDL) receptor and LDL cholesterol. J Biol Chem 2004;279:48865-48875.
[58] Chorba JS, Shokat KM. The proprotein convertase subtilisin/kexin type 9 (PCSK9) active site and cleavage sequence differentially regulate protein secretion from proteolysis. J Biol Chem 2014;289:29030-29043.
[59] Chorba JS, Galvan AM, Shokat KM. Stepwise processing analyses of the single-turnover PCSK9 protease reveal its substrate sequence specificity and link clinical genotype to lipid phenotype. J Biol Chem 2018;293:1875-1886.
[60] Garvie CW, Fraley CV, Elowe NH, Culyba EK, Lemke CT, Hubbard BK, et al. Point mutations at the catalytic site of PCSK9 inhibit folding, autoprocessing, and interaction with the LDL receptor. Protein science : a publication of the Protein Society 2016;25:2018-2027.
[61] Humphries SE, Neely RD, Whittall RA, Troutt JS, Konrad RJ, Scartezini M, et al. Healthy individuals carrying the PCSK9 p.R46L variant and familial hypercholesterolemia patients carrying PCSK9 p.D374Y exhibit lower plasma concentrations of PCSK9. Clin Chem 2009;55:2153-2161.
[62] Mayne J, Ooi TC, Raymond A, Cousins M, Bernier L, Dewpura T, et al. Differential effects of PCSK9 loss of function variants on serum lipid and PCSK9 levels in Caucasian and African Canadian populations. Lipids in health and disease 2013;12:70.

[63] Zaid A, Roubtsova A, Essalmani R, Marcinkiewicz J, Chamberland A, Hamelin J, et al. Proprotein convertase subtilisin/kexin type 9 (PCSK9): hepatocyte-specific low-density lipoprotein receptor degradation and critical role in mouse liver regeneration. Hepatology 2008;48:646-654.
[64] Cunningham D, Danley DE, Geoghegan KF, Griffor MC, Hawkins JL, Subashi TA, et al. Structural and biophysical studies of PCSK9 and its mutants linked to familial hypercholesterolemia. Nat Struct Mol Biol 2007;14:413-419.
[65] Piper DE, Jackson S, Liu Q, Romanow WG, Shetterly S, Thibault ST, et al. The crystal structure of PCSK9: a regulator of plasma LDL-cholesterol. Structure 2007;15:545-552.
[66] Benjannet S, Saavedra YG, Hamelin J, Asselin MC, Essalmani R, Pasquato A, et al. Effects of the prosegment and pH on the activity of PCSK9: evidence for additional processing events. J Biol Chem 2010;285:40965-40978.
[67] Qian YW, Schmidt RJ, Zhang Y, Chu S, Lin A, Wang H, et al. Secreted PCSK9 downregulates low density lipoprotein receptor through receptor-mediated endocytosis. J Lipid Res 2007;48:1488-1498.
[68] Pena F, Jansens A, van Zadelhoff G, Braakman I. Calcium as a crucial cofactor for low density lipoprotein receptor folding in the endoplasmic reticulum. J Biol Chem 2010;285:8656-8664.
[69] Strom TB, Tveten K, Leren TP. PCSK9 acts as a chaperone for the LDL receptor in the endoplasmic reticulum. Biochem J 2014;457:99-105.
[70] Dubuc G, Chamberland A, Wassef H, Davignon J, Seidah NG, Bernier L, et al. Statins upregulate PCSK9, the gene encoding the proprotein convertase neural apoptosis-regulated convertase-1 implicated in familial hypercholesterolemia. Arteriosclerosis, thrombosis, and vascular biology 2004;24:1454-1459.
[71] Jump DB, Tripathy S, Depner CM. Fatty acid-regulated transcription factors in the liver. Annu Rev Nutr 2013;33:249-269.
[72] Brown MS, Goldstein JL. The SREBP pathway: regulation of cholesterol metabolism by proteolysis of a membrane-bound transcription factor. Cell 1997;89:331-340.
[73] Grefhorst A, McNutt MC, Lagace TA, Horton JD. Plasma PCSK9 preferentially reduces liver LDL receptors in mice. J Lipid Res 2008;49:1303-1311.
[74] Tavori H, Fan D, Blakemore JL, Yancey PG, Ding L, Linton MF, et al. Serum proprotein convertase subtilisin/kexin type 9 and cell surface low-density lipoprotein receptor: evidence for a reciprocal regulation. Circulation 2013;127:2403-2413.
[75] Raal F, Panz V, Immelman A, Pilcher G. Elevated PCSK9 levels in untreated patients with heterozygous or homozygous familial hypercholesterolemia and the response to high-dose statin therapy. Journal of the American Heart Association 2013;2:e000028.
[76] Benjannet S, Rhainds D, Hamelin J, Nassoury N, Seidah NG. The proprotein convertase (PC) PCSK9 is inactivated by furin and/or PC5/6A: functional consequences of natural mutations and post-translational modifications. J Biol Chem 2006;281:30561-30572.
[77] Sun H, Samarghandi A, Zhang N, Yao Z, Xiong M, Teng BB. Proprotein convertase subtilisin/kexin type 9 interacts with apolipoprotein B and prevents its intracellular degradation, irrespective of the low-density lipoprotein receptor. Arterioscler Thromb Vasc Biol 2012;32:1585-1595.

[78] Tavori H, Giunzioni I, Linton MF, Fazio S. Loss of plasma proprotein convertase subtilisin/kexin 9 (PCSK9) after lipoprotein apheresis. Circ Res 2013;113:1290-1295.
[79] Sabatine MS, Underberg JA, Koren M, Baum SJ. Focus on PCSK9 Inhibitors: From Genetics to Clinical Practice. Postgraduate medicine 2016;128 Suppl 1:31-39.
[80] Shapiro MD, Miles J, Tavori H, Fazio S. Diagnosing Resistance to a Proprotein Convertase Subtilisin/Kexin Type 9 Inhibitor. Ann Intern Med 2018;168:376-379.
[81] Shapiro MD, Tavori H, Fazio S. PCSK9: From Basic Science Discoveries to Clinical Trials. Circ Res 2018;122:1420-1438.
[82] Sullivan D, Olsson AG, Scott R, Kim JB, Xue A, Gebski V, et al. Effect of a monoclonal antibody to PCSK9 on low-density lipoprotein cholesterol levels in statin-intolerant patients: the GAUSS randomized trial. JAMA 2012;308:2497-2506.
[83] Arrieta A, Page TF, Veledar E, Nasir K. Economic Evaluation of PCSK9 Inhibitors in Reducing Cardiovascular Risk from Health System and Private Payer Perspectives. PLoS One 2017;12:e0169761.
[84] Ray KK, Landmesser U, Leiter LA, Kallend D, Dufour R, Karakas M, et al. Inclisiran in Patients at High Cardiovascular Risk with Elevated LDL Cholesterol. N Engl J Med 2017;376:1430-1440.
[85] Seidah NG, Prat A, Pirillo A, Catapano AL, Norata GD. Novel strategies to target proprotein convertase subtilisin kexin 9: beyond monoclonal antibodies. Cardiovasc Res 2019;115:510-518.
[86] Dana H, Chalbatani GM, Mahmoodzadeh H, Karimloo R, Rezaiean O, Moradzadeh A, et al. Molecular Mechanisms and Biological Functions of siRNA. International journal of biomedical science : IJBS 2017;13:48-57.
[87] Landlinger C, Pouwer MG, Juno C, van der Hoorn JWA, Pieterman EJ, Jukema JW, et al. The AT04A vaccine against proprotein convertase subtilisin/kexin type 9 reduces total cholesterol, vascular inflammation, and atherosclerosis in APOE*3Leiden.CETP mice. Eur Heart J 2017;38:2499-2507.
[88] Maki KC. The ODYSSEY Outcomes trial: Clinical implications and exploration of the limits of what can be achieved through lipid lowering. Journal of clinical lipidology 2018;12:1102-1105.
[89] Korman MJ, Retterstol K, Kristiansen IS, Wisloff T. Are PCSK9 Inhibitors Cost Effective? Pharmacoeconomics 2018;36:1031-1041.
[90] Seidah NG, Prat A. The biology and therapeutic targeting of the proprotein convertases. Nat Rev Drug Discov 2012;11:367-383.
[91] Giunzioni I, Tavori H. New developments in atherosclerosis: clinical potential of PCSK9 inhibition. Vasc Health Risk Manag 2015;11:493-501.
[92] Wang Y, Huang Y, Hobbs HH, Cohen JC. Molecular characterization of proprotein convertase subtilisin/kexin type 9-mediated degradation of the LDLR. J Lipid Res 2012;53:1932-1943.
[93] Poirier S, Mayer G, Benjannet S, Bergeron E, Marcinkiewicz J, Nassoury N, et al. The proprotein convertase PCSK9 induces the degradation of low density lipoprotein receptor (LDLR) and its closest family members VLDLR and ApoER2. J Biol Chem 2008;283:2363-2372.

[94] Canuel M, Sun X, Asselin MC, Paramithiotis E, Prat A, Seidah NG. Proprotein convertase subtilisin/kexin type 9 (PCSK9) can mediate degradation of the low density lipoprotein receptor-related protein 1 (LRP-1). PLoS One 2013;8:e64145.
[95] Demers A, Samami S, Lauzier B, Des Rosiers C, Ngo Sock ET, Ong H, et al. PCSK9 Induces CD36 Degradation and Affects Long-Chain Fatty Acid Uptake and Triglyceride Metabolism in Adipocytes and in Mouse Liver. Arterioscler Thromb Vasc Biol 2015;35:2517-2525.
[96] Stoekenbroek RM, Lambert G, Cariou B, Hovingh GK. Inhibiting PCSK9 - biology beyond LDL control. Nature reviews Endocrinology 2018;15:52-62.
[97] Lai Q, Giralt A, Le May C, Zhang L, Cariou B, Denechaud PD, et al. E2F1 inhibits circulating cholesterol clearance by regulating Pcsk9 expression in the liver. JCI insight 2017;2.
[98] Le May C, Kourimate S, Langhi C, Chetiveaux M, Jarry A, Comera C, et al. Proprotein convertase subtilisin kexin type 9 null mice are protected from postprandial triglyceridemia. Arterioscler Thromb Vasc Biol 2009;29:684-690.
[99] Le May C, Berger JM, Lespine A, Pillot B, Prieur X, Letessier E, et al. Transintestinal cholesterol excretion is an active metabolic process modulated by PCSK9 and statin involving ABCB1. Arterioscler Thromb Vasc Biol 2013;33:1484-1493.
[100] Ooi TC, Krysa JA, Chaker S, Abujrad H, Mayne J, Henry K, et al. The Effect of PCSK9 Loss-of-Function Variants on the Postprandial Lipid and ApoB-Lipoprotein Response. The Journal of clinical endocrinology and metabolism 2017;102:3452-3460.
[101] Sharotri V, Collier DM, Olson DR, Zhou R, Snyder PM. Regulation of epithelial sodium channel trafficking by proprotein convertase subtilisin/kexin type 9 (PCSK9). The Journal of biological chemistry 2012;287:19266-19274.
[102] Berger JM, Vaillant N, Le May C, Calderon C, Bregeon J, Prieur X, et al. PCSK9-deficiency does not alter blood pressure and sodium balance in mouse models of hypertension. Atherosclerosis 2015;239:252-259.
[103] Haas ME, Levenson AE, Sun X, Liao WH, Rutkowski JM, de Ferranti SD, et al. The Role of Proprotein Convertase Subtilisin/Kexin Type 9 in Nephrotic Syndrome-Associated Hypercholesterolemia. Circulation 2016;134:61-72.
[104] Mikolasevic I, Zutelija M, Mavrinac V, Orlic L. Dyslipidemia in patients with chronic kidney disease: etiology and management. International journal of nephrology and renovascular disease 2017;10:35-45.
[105] Le QT, Blanchet M, Seidah NG, Labonte P. Plasma Membrane Tetraspanin CD81 Complexes with Proprotein Convertase Subtilisin/Kexin Type 9 (PCSK9) and Low Density Lipoprotein Receptor (LDLR), and Its Levels Are Reduced by PCSK9. J Biol Chem 2015;290:23385-23400.
[106] O'Neill LA. How Low Cholesterol Is Good for Anti-viral Immunity. Cell 2015;163:1572-1574.
[107] Arama C, Diarra I, Kouriba B, Sirois F, Fedoryak O, Thera MA, et al. Malaria severity: Possible influence of the E670G PCSK9 polymorphism: A preliminary case-control study in Malian children. PLoS One 2018;13:e0192850.
[108] Festi D, Colecchia A, Sacco T, Bondi M, Roda E, Marchesini G. Hepatic steatosis in obese patients: clinical aspects and prognostic significance. Obes Rev 2004;5:27-42.

[109] Wree A, Broderick L, Canbay A, Hoffman HM, Feldstein AE. From NAFLD to NASH to cirrhosis-new insights into disease mechanisms. Nat Rev Gastroenterol Hepatol 2013;10:627-636.
[110] Francque SM, van der Graaff D, Kwanten WJ. Non-alcoholic fatty liver disease and cardiovascular risk: Pathophysiological mechanisms and implications. J Hepatol 2016;65:425-443.
[111] Ipsen DH, Lykkesfeldt J, Tveden-Nyborg P. Molecular mechanisms of hepatic lipid accumulation in non-alcoholic fatty liver disease. Cell Mol Life Sci 2018;75:3313-3327.
[112] Buzzetti E, Pinzani M, Tsochatzis EA. The multiple-hit pathogenesis of non-alcoholic fatty liver disease (NAFLD). Metabolism 2016;65:1038-1048.
[113] Angulo P, Kleiner DE, Dam-Larsen S, Adams LA, Bjornsson ES, Charatcharoenwitthaya P, et al. Liver Fibrosis, but No Other Histologic Features, Is Associated With Long-term Outcomes of Patients With Nonalcoholic Fatty Liver Disease. Gastroenterology 2015;149:389-397 e310.
[114] Ying I, Saposnik G, Vermeulen MJ, Leung A, Ray JG. Nonalcoholic fatty liver disease and acute ischemic stroke. Epidemiology 2011;22:129-130.
[115] Bosy-Westphal A, Petersen S, Hinrichsen H, Czech N, M JM. Increased plasma homocysteine in liver cirrhosis. Hepatology research : the official journal of the Japan Society of Hepatology 2001;20:28-38.
[116] Bravo E, Palleschi S, Aspichueta P, Buque X, Rossi B, Cano A, et al. High fat diet-induced non alcoholic fatty liver disease in rats is associated with hyperhomocysteinemia caused by down regulation of the transsulphuration pathway. Lipids in health and disease 2011;10:60.
[117] Musso G, Gambino R, De Michieli F, Biroli G, Faga E, Pagano G, et al. Association of liver disease with postprandial large intestinal triglyceride-rich lipoprotein accumulation and pro/antioxidant imbalance in normolipidemic non-alcoholic steatohepatitis. Annals of medicine 2008;40:383-394.
[118] Ouweneel AB, Van Eck M. Lipoproteins as modulators of atherothrombosis: From endothelial function to primary and secondary coagulation. Vascular pharmacology 2016;82:1-10.
[119] Alkhouri N, Tamimi TA, Yerian L, Lopez R, Zein NN, Feldstein AE. The inflamed liver and atherosclerosis: a link between histologic severity of nonalcoholic fatty liver disease and increased cardiovascular risk. Digestive diseases and sciences 2010;55:2644-2650.
[120] Guillot A, Tacke F. Liver Macrophages: Old Dogmas and New Insights. Hepatology communications 2019;3:730-743.
[121] Vonghia L, Magrone T, Verrijken A, Michielsen P, Van Gaal L, Jirillo E, et al. Peripheral and Hepatic Vein Cytokine Levels in Correlation with Non-Alcoholic Fatty Liver Disease (NAFLD)-Related Metabolic, Histological, and Haemodynamic Features. PloS one 2015;10:e0143380.
[122] Austin RC. The unfolded protein response in health and disease. Antioxid Redox Signal 2009;11:2279-2287.
[123] Ruggiano A, Foresti O, Carvalho P. Quality control: ER-associated degradation: protein quality control and beyond. The Journal of cell biology 2014;204:869-879.

[124] Colgan SM, Hashimi AA, Austin RC. Endoplasmic reticulum stress and lipid dysregulation. Expert Rev Mol Med 2011;13:e4.
[125] Yoshida H. ER stress and diseases. FEBS J 2007;274:630-658.
[126] Vincenz-Donnelly L, Hipp MS. The endoplasmic reticulum: A hub of protein quality control in health and disease. Free radical biology & medicine 2017;108:383-393.
[127] Lin JH, Walter P, Yen TS. Endoplasmic reticulum stress in disease pathogenesis. Annual review of pathology 2008;3:399-425.
[128] Schonthal AH. Endoplasmic reticulum stress: its role in disease and novel prospects for therapy. Scientifica 2012;2012:857516.
[129] Ghemrawi R, Battaglia-Hsu SF, Arnold C. Endoplasmic Reticulum Stress in Metabolic Disorders. Cells 2018;7.
[130] Mogami H, Gardner J, Gerasimenko OV, Camello P, Petersen OH, Tepikin AV. Calcium binding capacity of the cytosol and endoplasmic reticulum of mouse pancreatic acinar cells. J Physiol 1999;518 (Pt 2):463-467.
[131] Carreras-Sureda A, Pihan P, Hetz C. Calcium signaling at the endoplasmic reticulum: fine-tuning stress responses. Cell calcium 2018;70:24-31.
[132] Vandecaetsbeek I, Vangheluwe P, Raeymaekers L, Wuytack F, Vanoevelen J. The Ca2+ pumps of the endoplasmic reticulum and Golgi apparatus. Cold Spring Harbor perspectives in biology 2011;3.
[133] Luciani DS, Gwiazda KS, Yang TL, Kalynyak TB, Bychkivska Y, Frey MH, et al. Roles of IP3R and RyR Ca2+ channels in endoplasmic reticulum stress and beta-cell death. Diabetes 2009;58:422-432.
[134] Coe H, Michalak M. Calcium binding chaperones of the endoplasmic reticulum. General physiology and biophysics 2009;28 Spec No Focus:F96-F103.
[135] Michalak M, Robert Parker JM, Opas M. Ca2+ signaling and calcium binding chaperones of the endoplasmic reticulum. Cell calcium 2002;32:269-278.
[136] Zhu G, Lee AS. Role of the unfolded protein response, GRP78 and GRP94 in organ homeostasis. Journal of cellular physiology 2015;230:1413-1420.
[137] Krebs J, Agellon LB, Michalak M. Ca(2+) homeostasis and endoplasmic reticulum (ER) stress: An integrated view of calcium signaling. Biochem Biophys Res Commun 2015;460:114-121.
[138] Blond-Elguindi S, Cwirla SE, Dower WJ, Lipshutz RJ, Sprang SR, Sambrook JF, et al. Affinity panning of a library of peptides displayed on bacteriophages reveals the binding specificity of BiP. Cell 1993;75:717-728.
[139] Yang J, Nune M, Zong Y, Zhou L, Liu Q. Close and Allosteric Opening of the Polypeptide-Binding Site in a Human Hsp70 Chaperone BiP. Structure 2015;23:2191-2203.
[140] Lebeau P, Al-Hashimi A, Sood S, Lhotak S, Yu P, Gyulay G, et al. Endoplasmic Reticulum Stress and Ca2+ Depletion Differentially Modulate the Sterol Regulatory Protein PCSK9 to Control Lipid Metabolism. J Biol Chem 2017;292:1510-1523.
[141] Kang S, Dahl R, Hsieh W, Shin A, Zsebo KM, Buettner C, et al. Small Molecular Allosteric Activator of the Sarco/Endoplasmic Reticulum Ca2+-ATPase (SERCA) Attenuates Diabetes and Metabolic Disorders. J Biol Chem 2016;291:5185-5198.

[142] Mandl J, Meszaros T, Banhegyi G, Csala M. Minireview: endoplasmic reticulum stress: control in protein, lipid, and signal homeostasis. Mol Endocrinol 2013;27:384-393.
[143] Carlson J. Endoplasmic reticulum storage disease. Histopathology 1990;16:309-312.
[144] Teckman JH, Perlmutter DH. Retention of mutant alpha(1)-antitrypsin Z in endoplasmic reticulum is associated with an autophagic response. Am J Physiol Gastrointest Liver Physiol 2000;279:G961-974.
[145] Lin L, Schmidt B, Teckman J, Perlmutter DH. A naturally occurring nonpolymerogenic mutant of alpha 1-antitrypsin characterized by prolonged retention in the endoplasmic reticulum. J Biol Chem 2001;276:33893-33898.
[146] Beuret N, Rutishauser J, Bider MD, Spiess M. Mechanism of endoplasmic reticulum retention of mutant vasopressin precursor caused by a signal peptide truncation associated with diabetes insipidus. J Biol Chem 1999;274:18965-18972.
[147] Birk J, Friberg MA, Prescianotto-Baschong C, Spiess M, Rutishauser J. Dominant pro-vasopressin mutants that cause diabetes insipidus form disulfide-linked fibrillar aggregates in the endoplasmic reticulum. J Cell Sci 2009;122:3994-4002.
[148] Gilbert A, Jadot M, Leontieva E, Wattiaux-De Coninck S, Wattiaux R. Delta F508 CFTR localizes in the endoplasmic reticulum-Golgi intermediate compartment in cystic fibrosis cells. Experimental cell research 1998;242:144-152.
[149] Kim PS, Lee J, Jongsamak P, Menon S, Li B, Hossain SA, et al. Defective protein folding and intracellular retention of thyroglobulin-R19K mutant as a cause of human congenital goiter. Mol Endocrinol 2008;22:477-484.
[150] Takahashi K, Adachi K, Yoshizaki K, Kunimoto S, Kalaria RN, Watanabe A. Mutations in NOTCH3 cause the formation and retention of aggregates in the endoplasmic reticulum, leading to impaired cell proliferation. Hum Mol Genet 2010;19:79-89.
[151] Ron D, Walter P. Signal integration in the endoplasmic reticulum unfolded protein response. Nat Rev Mol Cell Biol 2007;8:519-529.
[152] Calfon M, Zeng H, Urano F, Till JH, Hubbard SR, Harding HP, et al. IRE1 couples endoplasmic reticulum load to secretory capacity by processing the XBP-1 mRNA. Nature 2002;415:92-96.
[153] Hetz C, Martinon F, Rodriguez D, Glimcher LH. The unfolded protein response: integrating stress signals through the stress sensor IRE1alpha. Physiol Rev 2011;91:1219-1243.
[154] Schuck S, Prinz WA, Thorn KS, Voss C, Walter P. Membrane expansion alleviates endoplasmic reticulum stress independently of the unfolded protein response. The Journal of cell biology 2009;187:525-536.
[155] Back SH, Schroder M, Lee K, Zhang K, Kaufman RJ. ER stress signaling by regulated splicing: IRE1/HAC1/XBP1. Methods 2005;35:395-416.
[156] Tang CH, Chang S, Paton AW, Paton JC, Gabrilovich DI, Ploegh HL, et al. Phosphorylation of IRE1 at S729 regulates RIDD in B cells and antibody production after immunization. The Journal of cell biology 2018;217:1739-1755.
[157] Cinaroglu A, Gao C, Imrie D, Sadler KC. Activating transcription factor 6 plays protective and pathological roles in steatosis due to endoplasmic reticulum stress in zebrafish. Hepatology 2011;54:495-508.

[158] Brown MS, Goldstein JL. A proteolytic pathway that controls the cholesterol content of membranes, cells, and blood. Proc Natl Acad Sci U S A 1999;96:11041-11048.
[159] Rozpedek W, Pytel D, Mucha B, Leszczynska H, Diehl JA, Majsterek I. The Role of the PERK/eIF2alpha/ATF4/CHOP Signaling Pathway in Tumor Progression During Endoplasmic Reticulum Stress. Curr Mol Med 2016;16:533-544.
[160] B'Chir W, Maurin AC, Carraro V, Averous J, Jousse C, Muranishi Y, et al. The eIF2alpha/ATF4 pathway is essential for stress-induced autophagy gene expression. Nucleic acids research 2013;41:7683-7699.
[161] Santi-Rocca J, Smith S, Weber C, Pineda E, Hon CC, Saavedra E, et al. Endoplasmic reticulum stress-sensing mechanism is activated in Entamoeba histolytica upon treatment with nitric oxide. PLoS One 2012;7:e31777.
[162] Bertolotti A, Zhang Y, Hendershot LM, Harding HP, Ron D. Dynamic interaction of BiP and ER stress transducers in the unfolded-protein response. Nature cell biology 2000;2:326-332.
[163] Carrara M, Prischi F, Nowak PR, Kopp MC, Ali MM. Noncanonical binding of BiP ATPase domain to Ire1 and Perk is dissociated by unfolded protein CH1 to initiate ER stress signaling. eLife 2015;4.
[164] Shen J, Chen X, Hendershot L, Prywes R. ER stress regulation of ATF6 localization by dissociation of BiP/GRP78 binding and unmasking of Golgi localization signals. Dev Cell 2002;3:99-111.
[165] Credle JJ, Finer-Moore JS, Papa FR, Stroud RM, Walter P. On the mechanism of sensing unfolded protein in the endoplasmic reticulum. Proceedings of the National Academy of Sciences of the United States of America 2005;102:18773-18784.
[166] Kimata Y, Kohno K. Endoplasmic reticulum stress-sensing mechanisms in yeast and mammalian cells. Curr Opin Cell Biol 2011;23:135-142.
[167] Zhou J, Liu CY, Back SH, Clark RL, Peisach D, Xu Z, et al. The crystal structure of human IRE1 luminal domain reveals a conserved dimerization interface required for activation of the unfolded protein response. Proc Natl Acad Sci U S A 2006;103:14343-14348.
[168] DuRose JB, Tam AB, Niwa M. Intrinsic capacities of molecular sensors of the unfolded protein response to sense alternate forms of endoplasmic reticulum stress. Molecular biology of the cell 2006;17:3095-3107.
[169] Yoshida H, Matsui T, Hosokawa N, Kaufman RJ, Nagata K, Mori K. A time-dependent phase shift in the mammalian unfolded protein response. Dev Cell 2003;4:265-271.
[170] Maiuolo J, Bulotta S, Verderio C, Benfante R, Borgese N. Selective activation of the transcription factor ATF6 mediates endoplasmic reticulum proliferation triggered by a membrane protein. Proc Natl Acad Sci U S A 2011;108:7832-7837.
[171] Lebeau P, Byun JH, Yousof T, Austin RC. Pharmacologic inhibition of S1P attenuates ATF6 expression, causes ER stress and contributes to apoptotic cell death. Toxicology and applied pharmacology 2018;349:1-7.
[172] Yadav RK, Chae SW, Kim HR, Chae HJ. Endoplasmic reticulum stress and cancer. Journal of cancer prevention 2014;19:75-88.
[173] Avril T, Vauleon E, Chevet E. Endoplasmic reticulum stress signaling and chemotherapy resistance in solid cancers. Oncogenesis 2017;6:e373.

[174] Nishitoh H. CHOP is a multifunctional transcription factor in the ER stress response. J Biochem 2012;151:217-219.
[175] Li Y, Guo Y, Tang J, Jiang J, Chen Z. New insights into the roles of CHOP-induced apoptosis in ER stress. Acta biochimica et biophysica Sinica 2014;46:629-640.
[176] McIlwain DR, Berger T, Mak TW. Caspase functions in cell death and disease. Cold Spring Harbor perspectives in biology 2013;5:a008656.
[177] Szegezdi E, Logue SE, Gorman AM, Samali A. Mediators of endoplasmic reticulum stress-induced apoptosis. EMBO Rep 2006;7:880-885.
[178] Pinton P, Giorgi C, Siviero R, Zecchini E, Rizzuto R. Calcium and apoptosis: ER-mitochondria Ca2+ transfer in the control of apoptosis. Oncogene 2008;27:6407-6418.
[179] Ozcan U, Cao Q, Yilmaz E, Lee AH, Iwakoshi NN, Ozdelen E, et al. Endoplasmic reticulum stress links obesity, insulin action, and type 2 diabetes. Science 2004;306:457-461.
[180] Puri P, Mirshahi F, Cheung O, Natarajan R, Maher JW, Kellum JM, et al. Activation and dysregulation of the unfolded protein response in nonalcoholic fatty liver disease. Gastroenterology 2008;134:568-576.
[181] Lake AD, Novak P, Hardwick RN, Flores-Keown B, Zhao F, Klimecki WT, et al. The adaptive endoplasmic reticulum stress response to lipotoxicity in progressive human nonalcoholic fatty liver disease. Toxicol Sci 2014;137:26-35.
[182] Platko K, Lebeau PF, Byun JH, Poon SV, Day EA, MacDonald ME, et al. GDF10 blocks hepatic PPARgamma activation to protect against diet-induced liver injury. Molecular metabolism 2019.
[183] Maiers JL, Malhi H. Endoplasmic Reticulum Stress in Metabolic Liver Diseases and Hepatic Fibrosis. Seminars in liver disease 2019;39:235-248.
[184] Ozcan U, Yilmaz E, Ozcan L, Furuhashi M, Vaillancourt E, Smith RO, et al. Chemical chaperones reduce ER stress and restore glucose homeostasis in a mouse model of type 2 diabetes. Science 2006;313:1137-1140.
[185] Lebeaupin C, Vallee D, Hazari Y, Hetz C, Chevet E, Bailly-Maitre B. Endoplasmic Reticulum stress signaling and the pathogenesis of Non-Alcoholic Fatty Liver Disease. J Hepatol 2018.
[186] Dara L, Ji C, Kaplowitz N. The contribution of endoplasmic reticulum stress to liver diseases. Hepatology 2011;53:1752-1763.
[187] Donnelly KL, Smith CI, Schwarzenberg SJ, Jessurun J, Boldt MD, Parks EJ. Sources of fatty acids stored in liver and secreted via lipoproteins in patients with nonalcoholic fatty liver disease. J Clin Invest 2005;115:1343-1351.
[188] Han J, Kaufman RJ. The role of ER stress in lipid metabolism and lipotoxicity. J Lipid Res 2016;57:1329-1338.
[189] Natarajan SK, Rasineni K, Ganesan M, Feng D, McVicker BL, McNiven MA, et al. Structure, Function and Metabolism of Hepatic and Adipose Tissue Lipid Droplets: Implications in Alcoholic Liver Disease. Current molecular pharmacology 2017;10:237-248.
[190] Song Z, Xiaoli AM, Yang F. Regulation and Metabolic Significance of De Novo Lipogenesis in Adipose Tissues. Nutrients 2018;10.
[191] Reimold AM, Etkin A, Clauss I, Perkins A, Friend DS, Zhang J, et al. An essential role in liver development for transcription factor XBP-1. Genes & development 2000;14:152-157.

[192] Zhang K, Wong HN, Song B, Miller CN, Scheuner D, Kaufman RJ. The unfolded protein response sensor IRE1alpha is required at 2 distinct steps in B cell lymphopoiesis. J Clin Invest 2005;115:268-281.
[193] Zhang K, Wang S, Malhotra J, Hassler JR, Back SH, Wang G, et al. The unfolded protein response transducer IRE1alpha prevents ER stress-induced hepatic steatosis. EMBO J 2011;30:1357-1375.
[194] Oyadomari S, Harding HP, Zhang Y, Oyadomari M, Ron D. Dephosphorylation of translation initiation factor 2alpha enhances glucose tolerance and attenuates hepatosteatosis in mice. Cell Metab 2008;7:520-532.
[195] Xiao G, Zhang T, Yu S, Lee S, Calabuig-Navarro V, Yamauchi J, et al. ATF4 protein deficiency protects against high fructose-induced hypertriglyceridemia in mice. J Biol Chem 2013;288:25350-25361.
[196] Rutkowski DT, Wu J, Back SH, Callaghan MU, Ferris SP, Iqbal J, et al. UPR pathways combine to prevent hepatic steatosis caused by ER stress-mediated suppression of transcriptional master regulators. Dev Cell 2008;15:829-840.
[197] Yamamoto K, Takahara K, Oyadomari S, Okada T, Sato T, Harada A, et al. Induction of liver steatosis and lipid droplet formation in ATF6alpha-knockout mice burdened with pharmacological endoplasmic reticulum stress. Mol Biol Cell 2010;21:2975-2986.
[198] Zeng L, Lu M, Mori K, Luo S, Lee AS, Zhu Y, et al. ATF6 modulates SREBP2-mediated lipogenesis. EMBO J 2004;23:950-958.
[199] Horton JD, Shimomura I, Ikemoto S, Bashmakov Y, Hammer RE. Overexpression of sterol regulatory element-binding protein-1a in mouse adipose tissue produces adipocyte hypertrophy, increased fatty acid secretion, and fatty liver. The Journal of biological chemistry 2003;278:36652-36660.
[200] Koonen DP, Jacobs RL, Febbraio M, Young ME, Soltys CL, Ong H, et al. Increased hepatic CD36 expression contributes to dyslipidemia associated with diet-induced obesity. Diabetes 2007;56:2863-2871.
[201] Wilson CG, Tran JL, Erion DM, Vera NB, Febbraio M, Weiss EJ. Hepatocyte-Specific Disruption of CD36 Attenuates Fatty Liver and Improves Insulin Sensitivity in HFD-Fed Mice. Endocrinology 2016;157:570-585.
[202] Pagadala M, Kasumov T, McCullough AJ, Zein NN, Kirwan JP. Role of ceramides in nonalcoholic fatty liver disease. Trends in endocrinology and metabolism: TEM 2012;23:365-371.
[203] Li Y, Ge M, Ciani L, Kuriakose G, Westover EJ, Dura M, et al. Enrichment of endoplasmic reticulum with cholesterol inhibits sarcoplasmic-endoplasmic reticulum calcium ATPase-2b activity in parallel with increased order of membrane lipids: implications for depletion of endoplasmic reticulum calcium stores and apoptosis in cholesterol-loaded macrophages. J Biol Chem 2004;279:37030-37039.
[204] Fu S, Yang L, Li P, Hofmann O, Dicker L, Hide W, et al. Aberrant lipid metabolism disrupts calcium homeostasis causing liver endoplasmic reticulum stress in obesity. Nature 2011;473:528-531.

[205] Zhang J, Li Y, Jiang S, Yu H, An W. Enhanced endoplasmic reticulum SERCA activity by overexpression of hepatic stimulator substance gene prevents hepatic cells from ER stress-induced apoptosis. American journal of physiology Cell physiology 2014;306:C279-290.
[206] Halbleib K, Pesek K, Covino R, Hofbauer HF, Wunnicke D, Hanelt I, et al. Activation of the Unfolded Protein Response by Lipid Bilayer Stress. Mol Cell 2017;67:673-684 e678.
[207] Basseri S, Austin RC. ER stress and lipogenesis: a slippery slope toward hepatic steatosis. Dev Cell 2008;15:795-796.
[208] Jo H, Choe SS, Shin KC, Jang H, Lee JH, Seong JK, et al. Endoplasmic reticulum stress induces hepatic steatosis via increased expression of the hepatic very low-density lipoprotein receptor. Hepatology 2013;57:1366-1377.
[209] Yao S, Miao C, Tian H, Sang H, Yang N, Jiao P, et al. Endoplasmic reticulum stress promotes macrophage-derived foam cell formation by up-regulating cluster of differentiation 36 (CD36) expression. J Biol Chem 2014;289:4032-4042.
[210] Werstuck GH, Lentz SR, Dayal S, Hossain GS, Sood SK, Shi YY, et al. Homocysteine-induced endoplasmic reticulum stress causes dysregulation of the cholesterol and triglyceride biosynthetic pathways. J Clin Invest 2001;107:1263-1273.
[211] Colgan SM, Tang D, Werstuck GH, Austin RC. Endoplasmic reticulum stress causes the activation of sterol regulatory element binding protein-2. Int J Biochem Cell Biol 2007;39:1843-1851.
[212] Ruscica M, Ferri N, Macchi C, Meroni M, Lanti C, Ricci C, et al. Liver fat accumulation is associated with circulating PCSK9. Annals of medicine 2016;48:384-391.
[213] Rutishauser J, Spiess M. Endoplasmic reticulum storage diseases. Swiss medical weekly 2002;132:211-222.
[214] Seidah NG, Abifadel M, Prost S, Boileau C, Prat A. The Proprotein Convertases in Hypercholesterolemia and Cardiovascular Diseases: Emphasis on Proprotein Convertase Subtilisin/Kexin 9. Pharmacol Rev 2017;69:33-52.
[215] Saklayen MG. The Global Epidemic of the Metabolic Syndrome. Current hypertension reports 2018;20:12.
[216] Wang WA, Liu WX, Durnaoglu S, Lee SK, Lian J, Lehner R, et al. Loss of Calreticulin Uncovers a Critical Role for Calcium in Regulating Cellular Lipid Homeostasis. Sci Rep 2017;7:5941.
[217] van den Boogert MAW, Larsen LE, Ali L, Kuil SD, Chong PLW, Loregger A, et al. N-Glycosylation Defects in Man Lower LDL-Cholesterol Through Increased LDL Receptor Expression. Circulation 2019.
[218] Ding M, Bhupathiraju SN, Satija A, van Dam RM, Hu FB. Long-term coffee consumption and risk of cardiovascular disease: a systematic review and a dose-response meta-analysis of prospective cohort studies. Circulation 2014;129:643-659.
[219] Turnbull D, Rodricks JV, Mariano GF, Chowdhury F. Caffeine and cardiovascular health. Regulatory toxicology and pharmacology : RTP 2017;89:165-185.
[220] Zhou A, Hypponen E. Long-term coffee consumption, caffeine metabolism genetics, and risk of cardiovascular disease: a prospective analysis of up to 347,077 individuals and 8368 cases. Am J Clin Nutr 2019;109:509-516.

[221] Lievremont JP, Rizzuto R, Hendershot L, Meldolesi J. BiP, a major chaperone protein of the endoplasmic reticulum lumen, plays a direct and important role in the storage of the rapidly exchanging pool of Ca2+. J Biol Chem 1997;272:30873-30879.
[222] Rojo-Ruiz J, Rodriguez-Prados M, Delrio-Lorenzo A, Alonso MT, Garcia-Sancho J. Caffeine chelates calcium in the lumen of the endoplasmic reticulum. Biochem J 2018;475:3639-3649.
[223] Targher G, Day CP, Bonora E. Risk of cardiovascular disease in patients with nonalcoholic fatty liver disease. The New England journal of medicine 2010;363:1341-1350.
[224] Lakoski SG, Lagace TA, Cohen JC, Horton JD, Hobbs HH. Genetic and metabolic determinants of plasma PCSK9 levels. The Journal of clinical endocrinology and metabolism 2009;94:2537-2543.
[225] Lebeau PF, Byun JH, Platko K, MacDonald ME, Poon SV, Faiyaz M, et al. Diet-induced hepatic steatosis abrogates cell-surface LDLR by inducing de novo PCSK9 expression in mice. J Biol Chem 2019;294:9037-9047.
[226] Khera AV, Qamar A, Reilly MP, Dunbar RL, Rader DJ. Effects of niacin, statin, and fenofibrate on circulating proprotein convertase subtilisin/kexin type 9 levels in patients with dyslipidemia. Am J Cardiol 2015;115:178-182.
[227] Murphy BA, Tadin-Strapps M, Jensen K, Mogg R, Liaw A, Herath K, et al. siRNA-mediated inhibition of SREBP cleavage-activating protein reduces dyslipidemia in spontaneously dysmetabolic rhesus monkeys. Metabolism: clinical and experimental 2017;71:202-212.
[228] Baigent C, Keech A, Kearney PM, Blackwell L, Buck G, Pollicino C, et al. Efficacy and safety of cholesterol-lowering treatment: prospective meta-analysis of data from 90,056 participants in 14 randomised trials of statins. Lancet 2005;366:1267-1278.
[229] Gauthier MS, Awan Z, Bouchard A, Champagne J, Tessier S, Faubert D, et al. Posttranslational modification of proprotein convertase subtilisin/kexin type 9 is differentially regulated in response to distinct cardiometabolic treatments as revealed by targeted proteomics. Journal of clinical lipidology 2018;12:1027-1038.
[230] Seidah NG, Sadr MS, Chretien M, Mbikay M. The multifaceted proprotein convertases: their unique, redundant, complementary, and opposite functions. J Biol Chem 2013;288:21473-21481.
[231] Dorner AJ, Wasley LC, Kaufman RJ. Overexpression of GRP78 mitigates stress induction of glucose regulated proteins and blocks secretion of selective proteins in Chinese hamster ovary cells. EMBO J 1992;11:1563-1571.
[232] Reddy RK, Mao C, Baumeister P, Austin RC, Kaufman RJ, Lee AS. Endoplasmic reticulum chaperone protein GRP78 protects cells from apoptosis induced by topoisomerase inhibitors: role of ATP binding site in suppression of caspase-7 activation. J Biol Chem 2003;278:20915-20924.
[233] Kammoun HL, Chabanon H, Hainault I, Luquet S, Magnan C, Koike T, et al. GRP78 expression inhibits insulin and ER stress-induced SREBP-1c activation and reduces hepatic steatosis in mice. J Clin Invest 2009;119:1201-1215.
[234] Ji C, Kaplowitz N, Lau MY, Kao E, Petrovic LM, Lee AS. Liver-specific loss of glucose-regulated protein 78 perturbs the unfolded protein response and exacerbates a spectrum of liver diseases in mice. Hepatology 2011;54:229-239.

[235] Chen WT, Tseng CC, Pfaffenbach K, Kanel G, Luo B, Stiles BL, et al. Liver-specific knockout of GRP94 in mice disrupts cell adhesion, activates liver progenitor cells, and accelerates liver tumorigenesis. Hepatology 2014;59:947-957.
[236] Lebeau P, Platko K, Al-Hashimi AA, Byun JH, Lhotak S, Holzapfel N, et al. Loss-of-function PCSK9 mutants evade the unfolded protein response sensor GRP78 and fail to induce endoplasmic reticulum stress when retained. J Biol Chem 2018;293:7329-7343.
[237] Choosing the right statin for you. All statin drugs are not created equal. Your doctor will prescribe the best one to achieve your target LDL level. Heart Advis 2007;10:6.